THE STABILITY OF SHALLOW STOPES OF HARD ROCK MINES

BY

MARC C. BÉTOURNAY

DEPARTMENT OF MINING AND METALLURGICAL ENGINEERING

McGill University, Montreal

March, 1995

A Thesis submitted to the Faculty of Graduate Studies and Research
in partial fulfilment of the requirements of the
degree of Doctor of Philosophy

ISBN 0-612-05671-6

To my parents. To whom I owe
so much and the life-long desire to learn.

ABSTRACT

Canadian hard rock mine extraction practices have commonly created shallow stopes, 12% of which have caved to surface, from instabilities originating from stope hangingwalls, crowns or footwalls. To date, however, mine operators have applied few of the availabie data gathering and design tools to strike a balance between maximum economic excavation dimension and stope viability. The preference has been to use personal mining experience.

Several common rock mass environments are surveyed as well as the various ways in which shallow stopes have failed. It has been found that these rock masses develop gravity-induced movement in the form of plug failures, ravelling of rock blocks, strata failures, chimneying disintegration, and rock mass block caving.

The literature surveyed pertaining to shallow stopes deals essentially with descriptions of case studies rather than the development of design methods dedicated to these environments. The mine operator in the past has had to turn, by-and-large, to conventional rock mechanics analytical and numerical design methods which are inadequate to represent complex mechanical behaviours related to shallow stopes. Some limited analytical and empirical means have recently been specifically developed but not applied.

New failure-specific analytical equations are developed here for these common failure mechanisms. They address the mechanics of the failure process and incorporate the capability to arrive at the ultimate failure outline, for comparison to the location of the bedrock surface.

Six case studies are reviewed with regards to the application of the developed analytical equations, conventional numerical modelling, and empirical methods. In this fashion, the suitability of each method as a design tool for planned stope design and as a predictive tool to review known failures is examined. The case studies were selected to reflect the range of common Canadian hard rock mine geological environments, potential failure mechanisms, nature of planned shallow stope activity, and importance of historical cave-ins.

This research has shown that: plug failures occur along steep, uninterrupted discontinuities bounding large blocks. Plug failure potential reduces substantially with confining compressive stress, discontinuity inclination, the absence of low friction surfaces and shearing of intact rock interrupting the discontinuity. Ravelling requires little peripheral confining stress for stabilization and prevention of block falls or slides. However, inherent conditions such as shallow dipping or vertically dipping joints can cause block falls to develop to surface. Low confining stresses, resulting from multiple stope extraction in orthogonal horizontal directions, would offer conditions suitable for plug and ravelling failures. Strata failures are caused by excessive stope spans, but the limited loading received from above strata is such, that the failure cavity created is of limited vertical extent, some 25% of the stope width. Chimneying disintegration occurs in weak rock masses with low cohesion, over narrow openings that can be as deep as 275 m. The onset of chimneying disintegration can be created by compressive stresses, but develops as a result of mobilization of the rock mass by gravity in active shear. Block caving requires large spans to develop, and stabilizing could be overcome from arching stresses overcoming bulk arching strength. Controlling instability elements are tabulated for these failure mechanisms. A limit equilibrium correlation between span and cohesion for chimneying disintegration is presented, and the controlling limits between the occurrence of chimneying disintegration and block caving is discussed. Ravelling and chimneying disintegration are the most expected failure mechanisms for shallow stopes of hard rock mines. Although failure of the shallow stope may start around its periphery, stope failure to surface would likely occur in or close to the surface crown pillar.

Although the analytical equations developed require input of in situ stresses defined by numerical modelling in order to yield a precise answer, conventional numerical modelling or empirical methods are shown to be unable to predict stope failures as the analytical equations have. The development of the case studies has also shown that extensive laboratory and field data gathering work is required to obtain the required parameters and their potential variation in order to perform a design taking into consideration various failure modes anticipated, and that timely ground support with respect to the prevention of the development of gradual failures (ravelling, strata, chimneying disintegration and block caving failures) is essential. A step-by-step stability analysis procedure is presented, incorporating rockmass environment, expected failure mechanism(s), and applicable data gathering and anlytical methods.

RÉSUMÉ

L'exploitation canadienne des gisements en roc dur a couramment créé des chantiers peu profonds qui ont subit des effondrements dans 12% des cas. Ceux-ci ont débuté à partir des épontes supérieures, inférieures et des couronnes. Jusqu'à date cependant, les opérateurs miniers ont peu utilisé les méthodes de collectes de données et de conception disponibles pour équilibrer la dimension économique optimale du chantier et sa stabilité. L'outil de préférence a été l'expérience personnelle.

Plusieurs massifs rocheux communs ont été identifiés de même que les divers mécanismes de rupture encourus. Ces derniers se sont propagés par l'action de la gravité, notamment en: ruptures en bouchon, égrainage de blocs, ruptures des strates, désintégration en cheminée et foudroyage du roc.

Les ouvrages de références consultés sur le sujet des chantiers peu profonds s'en tiennent aux études de cas plutôt qu'au développement de méthodes de conception dédiées à ces milieux. L'opérateur de mine a dû, jusqu'à maintenant, utiliser des méthodes de mécanique des roches conventionnelles analytiques et numériques, qui sont inadéquates pour représenter les comportements complexes propres aux ouvertures peu profondes. Des méthodes analytiques et empiriques d'application limitée ont récemment été mises au point mais non utilisées.

De nouvelles équations, spécifiques au mécanismes de ruptures, ont été créés. Elles décrivent la mécanique du processus de rupture et permettent de calculer la forme ultime de la rupture pour fin de comparaison à la limite du socle rocheux.

Six cas d'études sont élaborés vis-à-vis l'application de ces équations analytiques, de la modélisation numérique conventionnelle et des méthodes empiriques. De cette façon, la convenance de chacune de ces méthodes fut évaluée pour la conception des chantiers et la prédiction d'effondrements connus. Les cas d'études furent choisis afin de représenter: les divers milieux géologiques canadiens de roc dur, les possibilités de mécanismes de rupture, le genre d'extraction planifié, de même que l'importance des effondrements déjà encourus.

Les résultats de cette recherche ont démontré que: les effondrements en bouchons se développent dans des blocs définis par des discontinuités ininterrompues à pendages élevés. La possibilité de telles ruptures diminue considérablement avec une augmentation de contraintes de confinement, une réduction du pendage, l'absence de surfaces à basses friction et l'advenance de cisaillement de roc situé au travers des discontinuités. L'égrainement de massif peut être stabilisé avec peu de contraintes. Cependant, des conditions pré-existentes telles des diaclases à faibles pendages ou des diaclases verticales peuvent permettent l'égrainage à se propager jusqu'en surface. De basses contraintes causés par l'extraction de chantiers dans deux directions horizontales orthogonales, offriraient des conditions propices aux effondrements en bouchon et par égrainage. Les ruptures de strates sont causées par des portées excessives de chantiers. Les strates inférieures reçoivent des charges limitées des strates supérieures, ainsi réduisant la limite ultime verticale de rupture qui est quelque 25% de la portée du chantier. Les ruptures par désintégration en cheminée se produisent dans les massifs faibles à basse cohésion, au dessus d'ouvertures à faibles portées mais aussi profondes que 275 m. Le déclenchement de ces ruptures pait être aidé par des contraintes compressives, mais la rupture se mobilise par gravité à cause de déplacements en cisaillement actif. Le foudroyage nécessite des chantiers à grandes portées pour se produire. La stabilisation peut être empêchée par une résistance en masse de l'arche stabilisatrice plus basses que les contraintes imposées. Les éléments d'instabilités pour ces mécanismes de rupture sont énumérés. Une corrélation d'équilibre limite pour la désintégration en cheminée entre la portée et la cohésion est présentée, et la limite entre le développement de la désintégration en cheminée et le foudroyage est discutée. L'égrainage en bloc et les ruptures par désintégration en cheminée sont les plus attendus des mécanismes de rupture. Bien que l'effondrement du chantier peu profond peut débuter aux parois, son développement jusqu'en surface se fera dans ou aux abords du pilier de surface.

Même si les équations analytiques nécessitent l'inclusion des contraintes calculées par la modélisation numérique, la modélisation numérique conventionnelle ou les méthodes empiriques sont incapables de prédire les effondrements identifiés par les équations analytiques. Cependant, la définition des cas d'études a démontré qu'une conception requiert une campagne approfondie d'essais en laboratoire et sur le terrain, qui définirait les paramètres impliqués et tiendrait compte des divers mécanismes de rupture anticipés. De plus, ces cas d'études ont démontré que la prévention du développement de ruptures graduelles (égrainage en bloc, ruptures de strates, ruptures en cheminée et foudroyage) nécessite l'apport immédiat de soutènement du massif. Un processus d'analyse de stabilité par étapes est présenté. Il incorpore le milieu géologique considéré, de même que le(s) mécanisme(s) de rupture anticipé(s) et les méthodes de collectes de données et d'analyses.

ACKNOWLEDGEMENTS

The author of this thesis would like to express considerable gratitude to his thesis supervisors, Dr. H. Mitri and Dr. F. Hassani. Their guidance, encouragement and enthusiastic support throughout the course of this research was helpful in addressing this new and important aspect of rock mechanics.

The writer wishes to thank the Canada Centre for Mineral and Energy Technology (CANMET) for the financial help and support that was provided to complete this program. In particular, Dr. J.E. Udd and Mr. G.E. Larocque are thanked for their strong support and encouragement. I also extend sincere appreciation for the helpful discussions and moral support provided by Messrs. M. Gyenge, R. Boyle, Y. Yu and Drs. N. Billette, T. Aston, and R. Wan of CANMET, and Mr. C. Mirza of Strata Engineering.

I would like to thank most sincerely Miss J. Byford and Mrs. J. Folta for their help in typing and drafting diagrams for this thesis.

The operators of the Pierre Beauchemin, Niobec, Dumagami, and Belmoral Mines are sincerely acknowledged for their cooperation in providing site access and samples, and for their interest in this research.

The work presented in this thesis has benefited greatly from discussions and encouragements from fellow McGill University Mining Engineering graduate students.

Finally, I am indebted to my wife Patricia, to whom I owe the unending patience, support and understanding that made the completion of this thesis possible. For my children, Cédric, Geneviève and Adrien who patiently waited for their father to finish this thesis and who encouraged me in many different ways, I am grateful.

CONTRIBUTION TO ORIGINAL KNOWLEDGE

The subject of this thesis falls within an emerging branch of rock mechanics: the study of rock mass behaviour around shallow underground openings of hard rock mines. The research forms the first systematic and comprehensive development, application and evaluation of dedicated design methods which would address the wide-ranging and complex rock mass mechanics of those environments. Furthermore, generic empirical and numerical methods are evaluated with regards to their usefulness versus these dedicated methods.

The geological settings for Canadian hard rock mines have been catalogued with respect to relationships to rock quality. Common failure mechanisms of these settings and their level of occurrences have been established.

From this development of behavioural knowledge, analytical methods were created to describe the mechanics of these failures. The methods are elaborated to provide an indication of rock, or rock mass, strength versus imposed stress. In this fashion, equations providing levels of confidence against failure now exist where no such dedicated design tools existed before.

Apart from this evaluation of inception of failure, methods to calculate the extent of zones of instabilities have also been developed. This now provides the means to evaluate the extent of expected failure in the rock mass around shallow stopes for comparison to the location of surface elements which may affect worker safety or disruption of infrastructure function.

Conventional numerical, empirical and rock mechanics methods have been shown to have limited or no applicability as design methods of shallow stopes of hard rock mines. However, they can be used to generate values of parameters (precise stress and deformation from numerical modelling, approximate strength and mechanical parameters from empirical means) that are used in the derived analytical equations.

Based on the analytical equations developed and case studies reviewed, critical stability parameters, as well as their inter-relationships, for the common Canadian hard rock environments have been enumerated. The likelihood of failure mechanisms occurring in a wide ranging variety of geological environments, stope geometries and stope dispositions is treated. Development of the case studies and expected extent of failure types has also indicated for the first time, that although failure may start around the periphery of a shallow stope, its development to surface will most likely occur in the surface crown pillar.

Several different failure cases have been classified and explained geomechanically for the first time through back analysis using developed analytical equations.

The first step-by-step procedure to evaluate the stability of shallow stopes is presented.

TABLE OF CONTENTS

TABLES

FIGURES

LIST OF SYMBOLS

SINGLE TERMS:

A	Area of block surface
A_L	Thrust arch length
C_l	Circumferential length of rupture arc
C_s	Scaled surface crown pillar span
E	Rock material modulus of elasticity
E_m	Rock mass modulus of elasticity
E_b	Bending rock material modulus of elasticity
F_s	Factor of safety
H	Thrust resultant from linear arch loading
H_c	Failure cavity height
I	Moment of inertia for rock beam cross section
K	Ratio of horizontal to vertical natural ground stress
L	Stope span, length of spanning structure
M	Moment of a force at a point
Q	NGI rock mass quality index
R	Reaction
T_s	Material tensile strength
V	Resisting shear force
W	Weight
Z	Depth

b	Beam width; width of block
c	Material cohesion
d	Distance from abutment to top of stratum failure
e	Location of linear arch thrust resultant, from neutral axis
f_c	Imposed compressive thrust
h	Height of a slice within active pressure shear failure analysis
i	Inclination angle of asperities on rock discontinuity surface
k	Discontinuity surface stiffness
m	Hoek and Brown material constant
n	Load to stratum depth ratio, linear arch loading
p	Total load on lowest spanning stratum
q	Load on beam, plate, per unit length
r	Radius
s	Width of a slide within active pressure shear failure; Hoek and Brown material constant
t	Thickness
$\dot{w}$	Total load on stratum
Γ	Amplification of imposed moment
$\alpha, \beta, \zeta, \eta, \omega$	Geometrical angles
γ_r	Unit weight of rock
ε	Imposed strain; eccentricity of flow ellipsoid
θ	Dip of strata, plate
μ	Plate stress coefficient

ν	Material Poisson's ratio
ξ	Slope of normal-shear displacement curve
ρ	Material density
σ	Imposed stress
σ_c	Rock unconfined compressive strength
τ	Imposed shear stress
ϕ	Material internal angle of friction
ϕ_r	Discontinuity internal angle of friction
ψ	Dip of discontinuity

SUBSCRIPTS:

a, b	Plate smallest and longest dimension respectively
c	Compression
f	Field
h	Horizontal
i, j	Sequence numbers
m	Rock mass; summation number count
n	Normal; summation number count
s	Sliding surface; shear
t	Tension
v	Vertical
w	Water
x, y, z	Cartesian coordinates, direction

CHAPTER 1

INTRODUCTION

1.1 GENERAL

Canada is one of the world's most active countries in extracting various metal bearing ores. Mining for such ore has primarily centered around extraction from underground stopes in hard rock environments. Because Canadian metalliferous orebodies usually extend to the limit of bedrock, shallow stopes have been routinely created at the boundary to overburden, bodies of water, and surface infrastructures.

Mining operators must therefore strike a balance between maximum economic excavation dimension and the stability for worker safety and overlying infrastructure viability. It is the hazard to human life and effects on mining activity that a failure to surface could engender which underscores the necessity to have stable shallow openings and to avoid the consequences of stope failures. The stability of shallow underground mine extraction was brought into focus with the Belmoral mine accident of May 21, 1980. A shallow stope cave-in which reached overburden allowed the inflow of some 100,000 tons of wet overburden into the underground workings. This mining catastrophe resulted in 8 mine worker fatalities and a lengthy cessation of operations. Belmoral represents one of several Canadian operations that have recently begun extracting ore from particularly weak rock mass environments.

It has also been learned that several other shallow stope failures in active mines have taken place over the last 50 years. Such failures continue to occur, as witnessed by

INCO's Casa Berardi Mine failure of April 1992. Furthermore, failures of shallow stopes of abandoned mines are also commonplace.

Mining operators must also recognize the limitations of their design and the safety of extraction when rock environments are difficult to stabilize. Despite the advancements in the field of rock mechanics, shallow stopes remain complex environments to design for. A variety of geological terrains with different types of rock mass quality and disposition of discontinuities exists. The nature of the mining extraction method may also adversely affect the rock competence, as may the geometry and size of the opening. The geotechnical maxim "each case is a unique case" is applicable here. But unlike other engineering disciplines, the design engineer is forced to work with materials he cannot change and loads he cannot alter. In such circumstances, a successful design must satisfactorily address the range of possible behaviours so that the best design methods are used and that results become meaningful.

Given the lack of dedicated design methods for shallow stopes, it was felt that there existed a need for design techniques addressing specific stope threatening instabilities. These techniques, although detailed enough to represent the problems to be solved, could be used by, and be intelligible to, practitioners in industry, who do not have sufficient knowledge or understanding of the complex rock mechanics issues involved.

1.2 DEFINITION OF PROBLEM

Shallow stopes are defined as the underground mine extraction openings closest to surface, usually within 30 m of the bedrock limit [1]. Depending on the shape of the orebody and distribution of ore grade, various stope configurations are used for extraction, Figure 1.1. Unlike deeper stopes, where mine extraction takes place surrounded by rock, shallow stopes are situated at or very near overburden and/or bodies of water.

The design of shallow stopes takes on a wider scope than that of deeper openings. Stability in this case implies

i) protection of workers from rock, soil, or water movements

ii) prevention of interference with surface activity

iii) requirement of long-term ground support.

The basis for design is also different. Natural ground stresses may not be sufficient to prevent gravity failures. Unless a rock material is very weak, failure by exceeding rock strength is not expected. Rock mass instabilities originate with geological discontinuities and rock fabric (bedding, foliation, etc.).

Gravity movements can occur in the rock mass at any point around the opening. Therefore, the integrity of the opening does not necessarily and uniquely depend on the rock above the top of the stope (known as a surface crown pillar).

One of the goals of preventing shallow stope failures is to stop ground instabilities from reaching surface at which point disastrous consequences can occur. The challenge of designing in these circumstances is to stop any size of failure opening from reaching surface and allowing wet soil or water inflow. For shallow stopes, small size instabilities, as small as 3 meters wide, to large features tens of meters in dimension, have been known to occur [2][3][4].

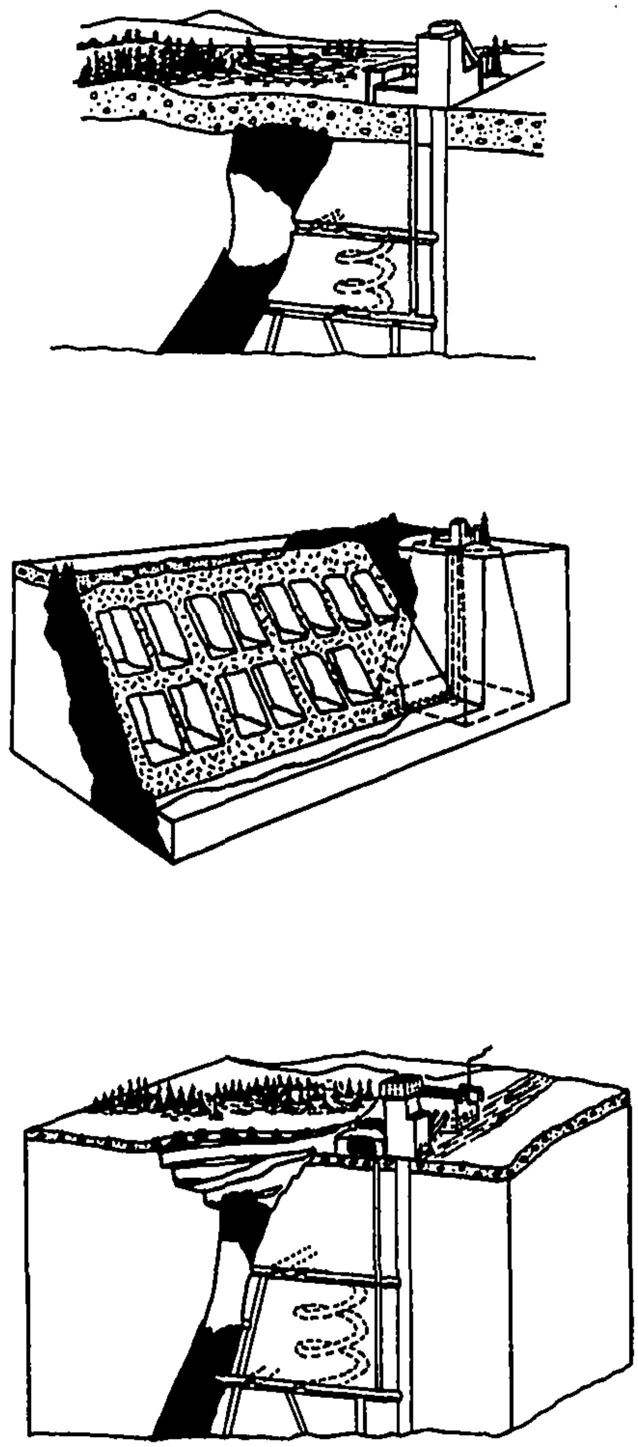

Figure 1.1 Common shallow stope configurations in hard rock mines.

1.2.1 Literature Review

A study of existing information was carried out to provide an understanding of the stability issues and corresponding design aspects related to shallow stopes of hard rock mines. It also served as the foundation for the development of the subject carried out in this research program.

The starting point of this literature review was the examination of the Roche [2] report. The purpose of this report was to establish the state of knowledge regarding the stability of shallow hard rock mine stopes, following the Belmoral mine accident. It was the first such survey performed. A comprehensive literature search was carried out. As well, this, and the Roche [3] survey, contained a total of twenty-four case studies of mines where on-site investigations of shallow stopes were carried out. Examination of these two surveys showed that up to then

i) there was little information on the occurrence or type of shallow stope failure

ii) there was no information on design methods to use for stope creation, or to estimate stope stability

iii) there was no systematic design or problem-solving approach scientifically developed, or used by mine operators

iv) there was little information which could be recommended to consider in developing the subject.

Further research for this thesis found that before 1985 only subsidence over soft rock mines (coal, evaporites) had been seriously treated. A few international incidents of failures reaching surface were briefly documented by Allen [5] and Rice [6].

A breakdown of the 24 Roche case studies was performed by Bétournay [1] and Bétournay et al [7]. Table 1.1 and Figure 1.2 present the summary of these analyses.

Table 1.1 summarizes the basic geological and mining characteristics encountered at these sites. Steep dipping orebodies of limited lateral extent (veins and tabular orebodies) predominate. These, overlain by considerable overburden, contain hangingwall/footwall of little competence located within host rock containing portions of pronounced alteration. Two or three joint families and faults usually transect the rock mass. No preferred mining method was found, and backfill as permanent stope stabilizer was only used half the time.

Other information, geophysical and geomechanical field work on the condition of shallow rock masses at hard rock mines [8][9][10], has indicated that the top 2 to 8 m of bedrock is often seriously weakened by alteration and contains a higher degree of fissuration, with enlarged joint apertures.

The approaches used to create shallow stopes at the study sites are analysed in Bétournay and Bétournay et al in regards to the geomechanical data collection stage (which provides the input values for the application of design methods), and the design formulation and application stage (which forms the basis for the creation of the stope).

Basic data collected for analysing potential stability problems usually consists of lab tests and field tests [1]. In addition to describing the site geology and the existing soil and rock units, field tests are performed to provide quantification of rock mass behaviour, such as deformation, natural ground stresses and distribution of rock quality, as well as soil tests to evaluate their potential stand-up or flow capabilities. Lab tests are required to help identify the strength characteristics of rock and rock masses.

Table 1.1 Summary of Site Characteristics for Shallow Stopes of Hard Rock Mines [1]

MINE	1	2+	3+	4	5	6	7	8	9	10+	11	12	13	14	15	16	17	18+	19	20	21	22	23	24
Items																								
- BODY OF WATER (m)			3	(3)	-	-	-	7.6	-	0	0	-	20	-	-	-	-	-	11	-	-	-	13	-
- OVERBURDEN (m)	(8)	(7)	27	36	4	15	5	20	17	16	20	15	3	5	30	9	1.5	(2)	5	-	45	N	19	(9)
Substantial clay deposits			·	·				·	·		·	·		·									·	
- FORM OF THE DEPOSIT																								
- tabular	·				·												·				·		·	
- single vein			·	·				·	·	·	·		·		·			·						
- multiple veins		·				·	·							·					·	·		·		
- mass												·				·								·
- Pronounced alterations	·			·	·			·						·			·		·		·		·	
- Walls of low competence	·	·	·		·			·					·	·	·	·			N	N	N	N	·	·
- Walls of high competence						·	·			·									N	N	N	N		
DIP (degree)	70	70	65	45	72	80	80	90	45	70	80	85	45	85	75	75	33	70	70	60	50	75	30	
IMPORTANT FAULT (s)		·	·	·		·		·	N	·	·	·	·		·	·		·	N	N	·	·	N	·
NUMBER OF WELL DEFINED JOINT FAMILIES	N	2	3	N	2	2	3	N	N	N	N	N	N	2	N	N	1	3	N	N		N	N	3
- MAIN MINING METHOD - Stope and Pillars																	·							
- Shrinkage stoping					·	·	·		·													·		
- cut-and-fill			·					·					·						·		·		·	
- blasthole stoping	·	·		·						·		·		·	N	·		·		·				
- Surface installations on pillar (s)						·	·			·							·				·			

N not retrieved, or not available
( ) removed
(+) pillars(s) separating open pit from underground opening
- not applicable

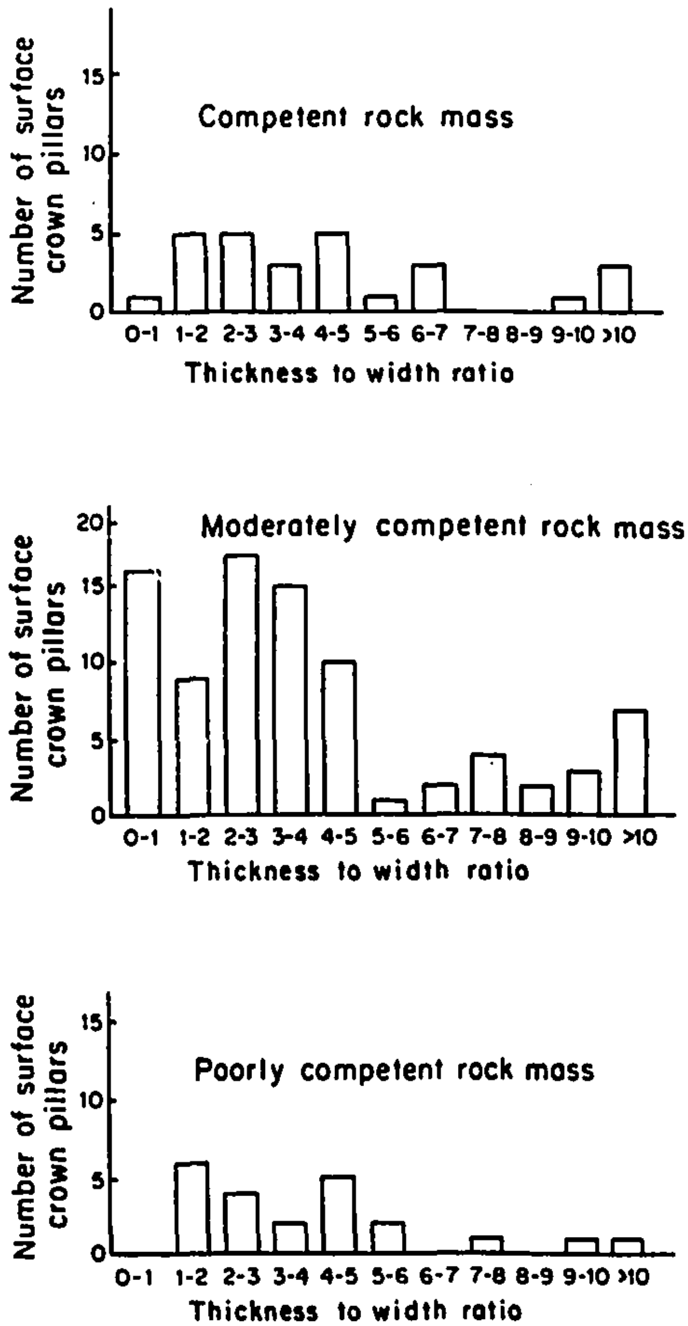

Figure 1.2 Thickness to width ratio used in designing shallow stopes of Canadian hard rock mines [7].

Of the field tests performed, the most common, yet not always carried out, was the measurement of natural ground stresses; unfortunately, this was not carried out at shallow stope depths. Location of weak zones and rock mass deformation properties were rarely addressed. Some form of discontinuity mapping was usually done, as was a restricted range of lab strength tests. Even so, no analysis of the data was done in order to classify surrounding conditions and define potential problems.

When performing the design, 46% of the mines precluded the use of existing methods (e.g. theoretical elastic solutions, numerical modelling, etc.), preferring to use "personal experience" in selecting stope geometry, size and methods of ground control. In other cases, 29% used an empirical method based on rock mass classification, e.g. the NGI system [11], 17% used numerical modelling, and 8% used conventional theoretical calculations (not related to shallow openings). Only 1 of 24 mines used more than 1 design method. The empirical and theoretical applications only considered the integrity of the surface crown pillar of the opening, rather than all of the rock mass around it. The thickness (top of bedrock to stope roof) to width (smallest stope wall to wall dimension) ratio as a selection for surface crown pillar dimensions was the preferred design choice based on personal experience. A total of 75% of such pillars surveyed were designed with a ratio less than five. The application of this non-scientific approach, when examined, reveals that no matter what rock mass condition existed in the pillars, Figure 1.2, little difference in the selected ratio existed. A thickness to width ratio less than five was used for all rock mass conditions, competent to incompetent.

The choice method of ground support was the application of conventional mechanical bolts. Backfill was used in stopes where one or several ground problem elements occurred. In certain cases, grout was used to render the mass impermeable at the contact with overburden. Monitoring of stopes was performed in 62% of the cases. Visual evaluation predominated, but was often paired with measuring instruments. In 32% of the cases, neither monitoring nor backfill was used.

Since 1985, in part because of the Roche surveys, more publications have become available on the subject. New cases were studied, [12][13][14][15][16][17][18][19], where site characteristics have been well defined and application of conventional rock mechanics and numerical modelling have been performed.

Some publications dealt with the development and application of data-gathering techniques such as improved diamond-drilling sampling for incompetent near-surface rock masses [20], three-dimensional geotomography using seismicity and radar [8][9], and the application of rock mass modulus measurements [10].

The Golder Associates [4] survey of privately existing information on shallow stope failures has provided numerous other examples of abandoned and active stopes, and focused on the sensitivity of various geomechanical parameters on the back-analysis of failures. An empirical classification scheme for evaluating the stability of surface crown pillars was developed.

Two publications presented the development of new analytical design methods for the surface crown pillars of shallow stopes. Hoek [21] introduced a limit equilibrium analysis in the case of plug type failures, based on shear resistance of the rock mass. Gill et al [22] developed a 2-D limit equilibrium analysis to evaluate the stability of block elements within a pillar.

Various other publications have examined the design process [1] and the importance or kind of parameters involved at various design stages [23][24]. Bétournay [24] outlines the three generations of design methods currently being used. The first, the rudimentary experience, is limited to the application of personal experience in selecting stope outline and ground control means (artificial support and surface crown pillars) with little scientific information or other considerations such as stability of the entire opening; limited effectiveness is achievable. The second consists of applying conventional rock mechanics methods (finite element analysis, general elastic methods, general failure estimation) which use a limited proportion of the key elements influencing the stability of shallow stopes on a small number of stress overcoming strength failure possibilities (mechanisms) given the geological contexts of these openings. The third generation would incorporate dedicated analytical, empirical, and numerical tools for the failure mechanisms anticipated; it is now taking shape with the previously mentioned dedicated methods and numerical modelling with "block codes", but has yet no analytical methods developed.

Back-analysis of failures [4] has shown that a small variation in natural ground stress has a profound influence on allowing or preventing gravity failures to occur. Published results of stress measurements in Canada relate to depths below 80 m [25][26], leaving extrapolations to be performed for in situ stresses existing at shallow levels. Severe limitations might accompany the application of conventional measuring methods as shallow depth [27]. Measurements applying hydraulic fracturing require high ground stresses to confine the rock mass in order to avoid seepage along discontinuities, a condition not existing in a near-surface segmented rock mass. Furthermore, the method assumes a value of the vertical stress and depends on fracturing orientation to determine the horizontal stresses. Overcoring with the U.S.B.M. deformation gauge might introduce more measurement error than the necessary accuracy for small rock deformations. The relatively new borehole slotter has had difficulties [28] and is more suitable for fine grained rock. There has been to date no clear examination of in situ stress conditions near surface, although field tests are presently under way [29]. These confirm the extrapolations and indicate significant levels of horizontal stress. In these tests overcoring was performed in vertical holes driven from surface, using doorstopper cells. In order to obtain repeatable results, this method requires consideration of a bonding agent and installation tool for water filled holes. The cell is sufficiently sensitive to capture the micro deformation anticipated, but these must be factored for temperature and other measuring variations. Thus reliability of results become questionable unless great expertise and evaluation of results is applied. The values obtained may not represent the level of confidence usually associated with strain cell measurements at deeper levels. A more satisfactory approach could be to use strain cells in upward dipping holes underground to shallow depths [29], requiring accessibility underground and a relatively undisturbed shallow rock mass which, as mentioned, is not always available.

The estimate of general and fractured nature of the rock mass, by measuring the variation of modulus of elasticity, has become important. The data is used to quantify the extent of rock mass competence indicated by the RQD drill core. Instruments such as the dilatometer [10] are used to supply these measurements, which can also be used as input to improve numerical modelling precision.

This and the application of diagnostic geophysical methods such as geotomography [8][9] outline the variations of rock mass integrity in 3 dimensions which can be used in defining the anticipated failure mechanism(s). The additional potential benefit of geotomography is to locate the trace of the major joints in the rock mass around the stope. This has not been entirely successful due to the highly fissured nature of the upper bedrock hindering full application of seismic signal velocity and frequency variation techniques [8].

1.3 ANALYSIS OF CONDITIONS

The common rock mass environments extracted from a review of the case studies of shallow stopes of hard rock mines are presented in Figure 1.3. These can be summarized as consisting of one or more of three geological conditions (massive to blocky rock, foliated rock, weak [fissured/altered] rock) in different relationships as hangingwall, footwall, and orebody.

For the purpose of this research, failure is defined as rock mass movement that starts from the shallow stope and reaches surface. This has been commonly referred to as caving. Thus, caving regroups all the different mechanisms of failures.

The effects of mining, such as caving, on lowering the ground surface is called subsidence. Depending on the extent of caving two types of subsidence are possible [30] [31], continuous and discontinuous. Common over broad extraction such as coal mining, continuous subsidence involves the formation of a smooth dipping surface profile that has no abrupt changes. Discontinuous subsidence involves localized large surface

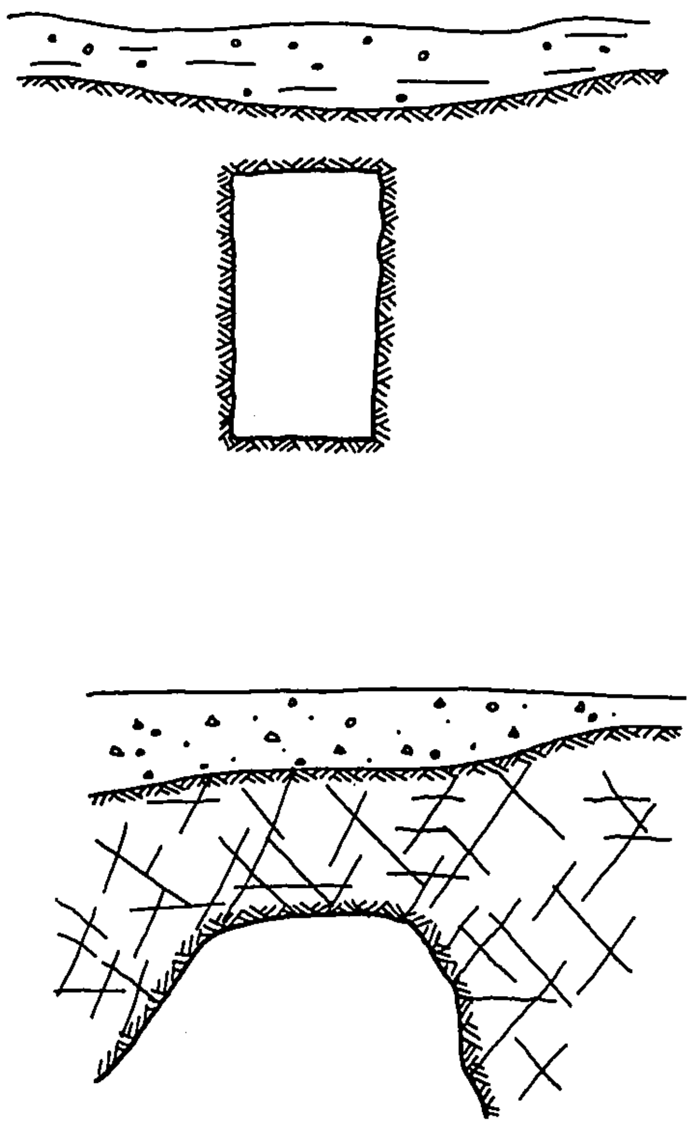

Figure 1.3 Common rock mass environments of shallow stopes of hard rock mines.
a) poorly jointed rock, b) jointed and blocky rock mass.

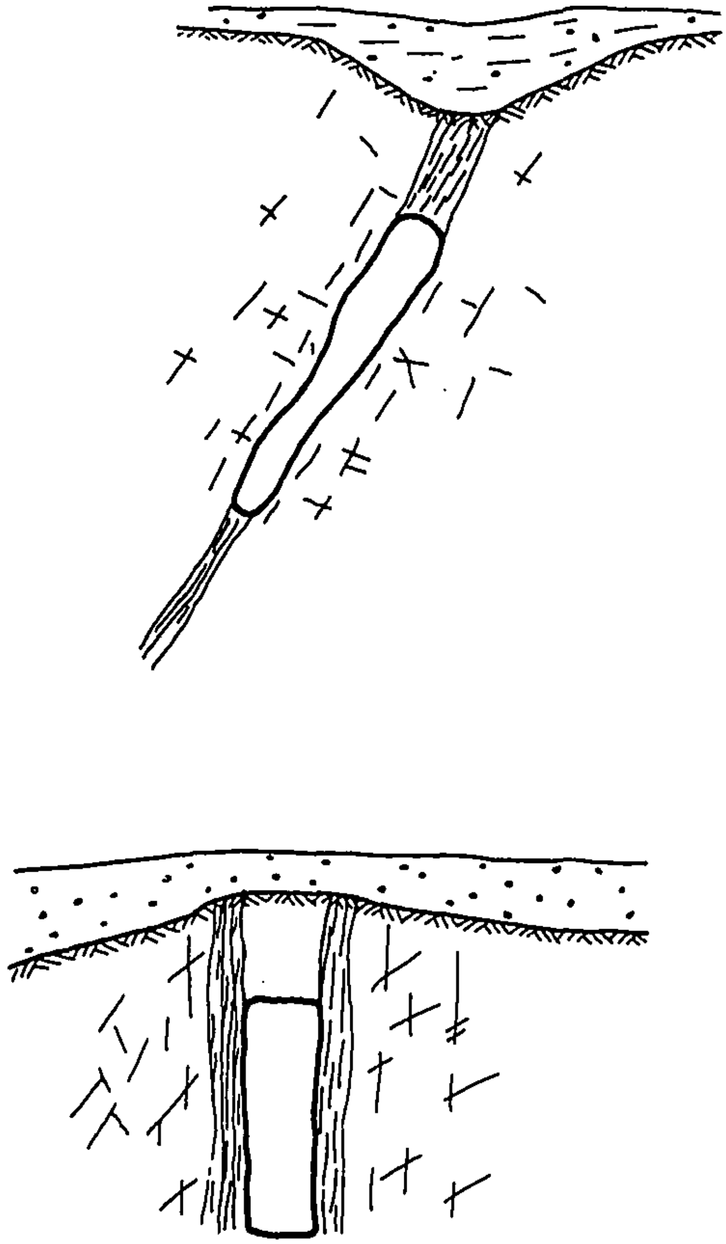

Figure 1.3 Common rock mass environments of shallow stopes of hard rock mines. c) weak, schistose orebody, competent walls, d) massive orebody, weak, schistose walls.

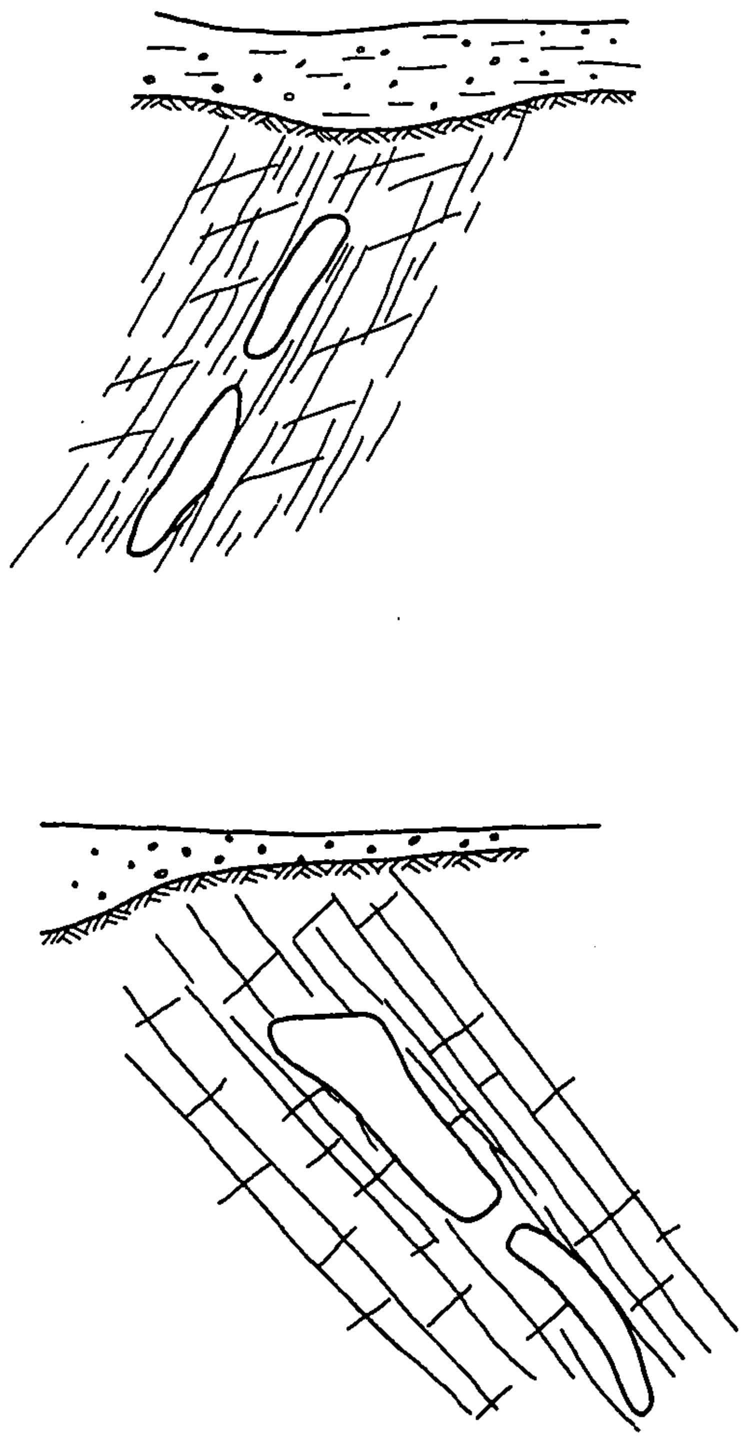

Figure 1.3 Common rock mass environments of shallow stopes of hard rock mines. e) generally foliated, slaty, f) well developed stratification.

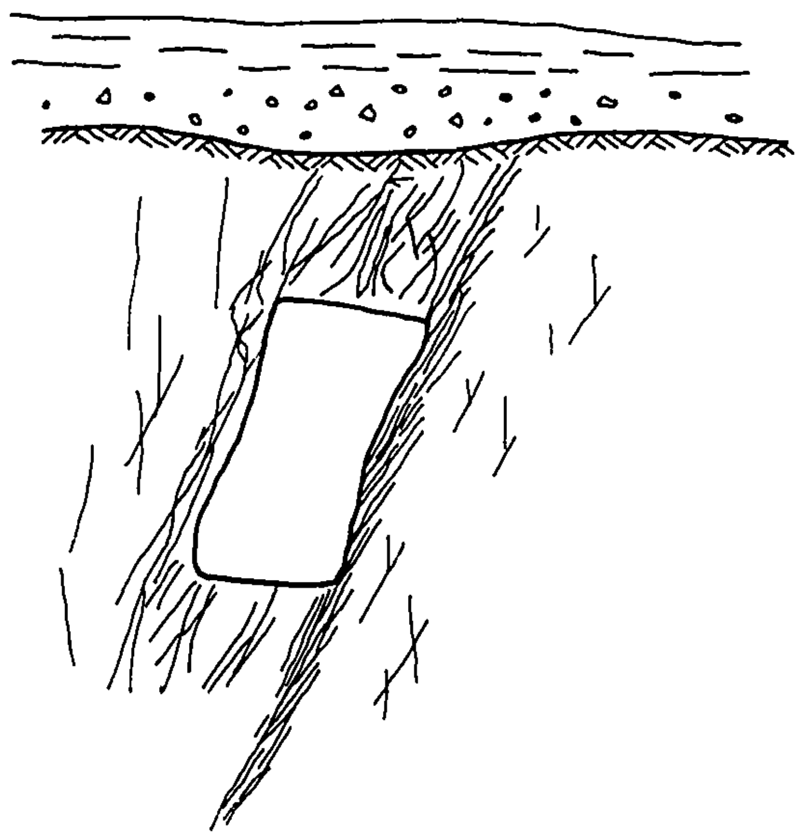

Figure 1.3 Common rock mass environments of shallow stopes of hard rock mines.
g) fault weakened, altered rock mass.

displacements. Failures, or caving, of shallow stopes are commonly of the discontinuous type, Figure 1.4. Shown there are the common failure types identified by examining the literature; each of them is taken to be causative and have distinct mechanics of failure. They are: plug failures, block ravelling failures, destratification failures, chimneying disintegration, and block caving. Some authors [30] refer to several different types of failure by a generic name such as chimneying. The final shape of the failure for some or all of these mechanisms may be chimney-like. Thus plug failure, chimneying by disintegration, and piping through caved material are described there as chimney caving.

The nomenclature of these failures used here is based on their mechanical behaviour to avoid confusion with terminology related to the shape of the failure and to allow for a more basic approach for scientific communication.

Table 1.2 makes the link between the host rock mass environments and types of failures. Possible root causes, affected portion(s) of the rock mass around the opening, and progression of failure are also presented.

Because orebody emplacement is often related to and contains faults, potential failure conditions may exist. By virtue of their extensive dimensions, such discontinuities seriously weaken the rock mass and contribute to the mobilization of large or small rock blocks that can use these surfaces to slide or move upon, as is the case for the large scale plug or the smaller scale rock block.

By virtue of the zone of damage imposed by their creation and movement, faults can be related to and adjoin extensive and continuous zones of weaker rock that contain more fragmented rock, even rock material that has been physically and chemically altered resulting in significantly lower strength. In these cases, faults create natural paths along

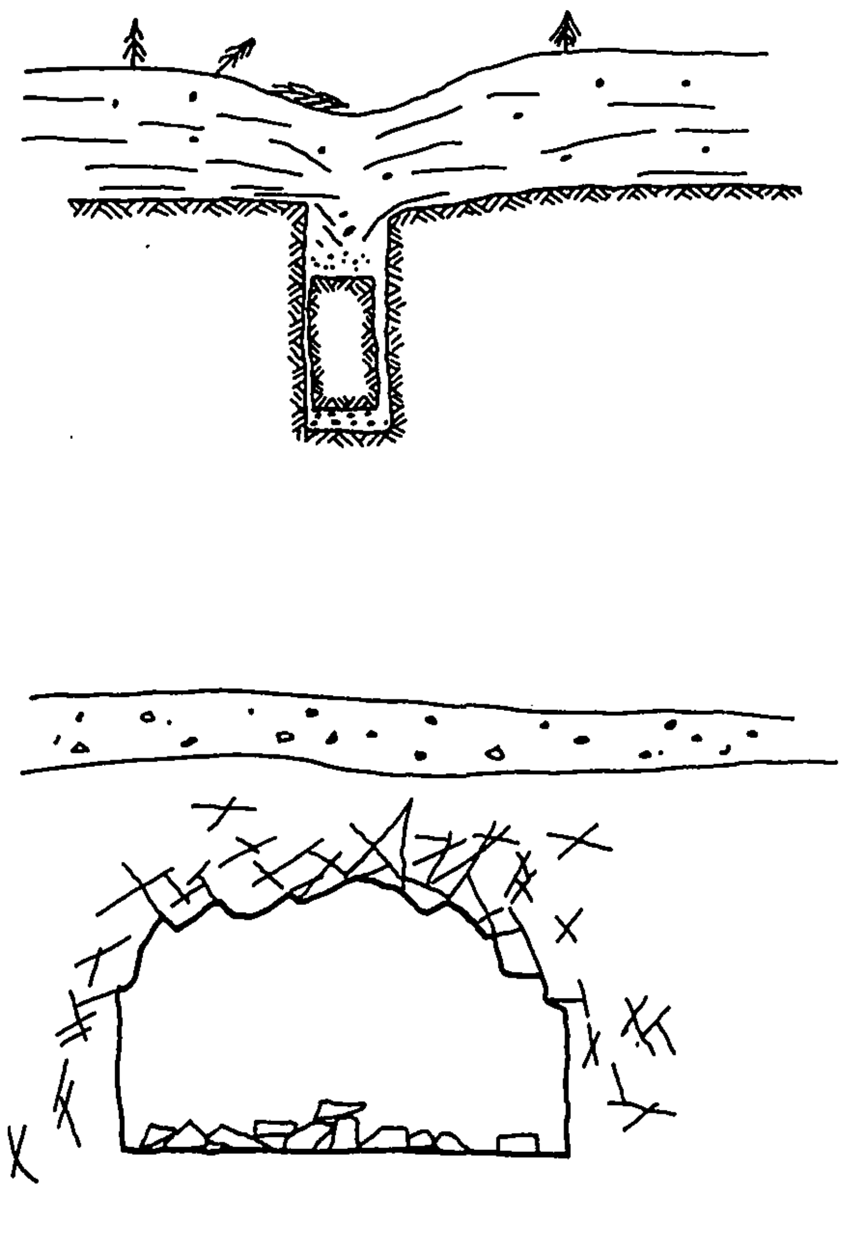

Figure 1.4 Common failure mechanisms of shallow stopes of hard rock mines.
a) plug failure, b) ravelling failure.

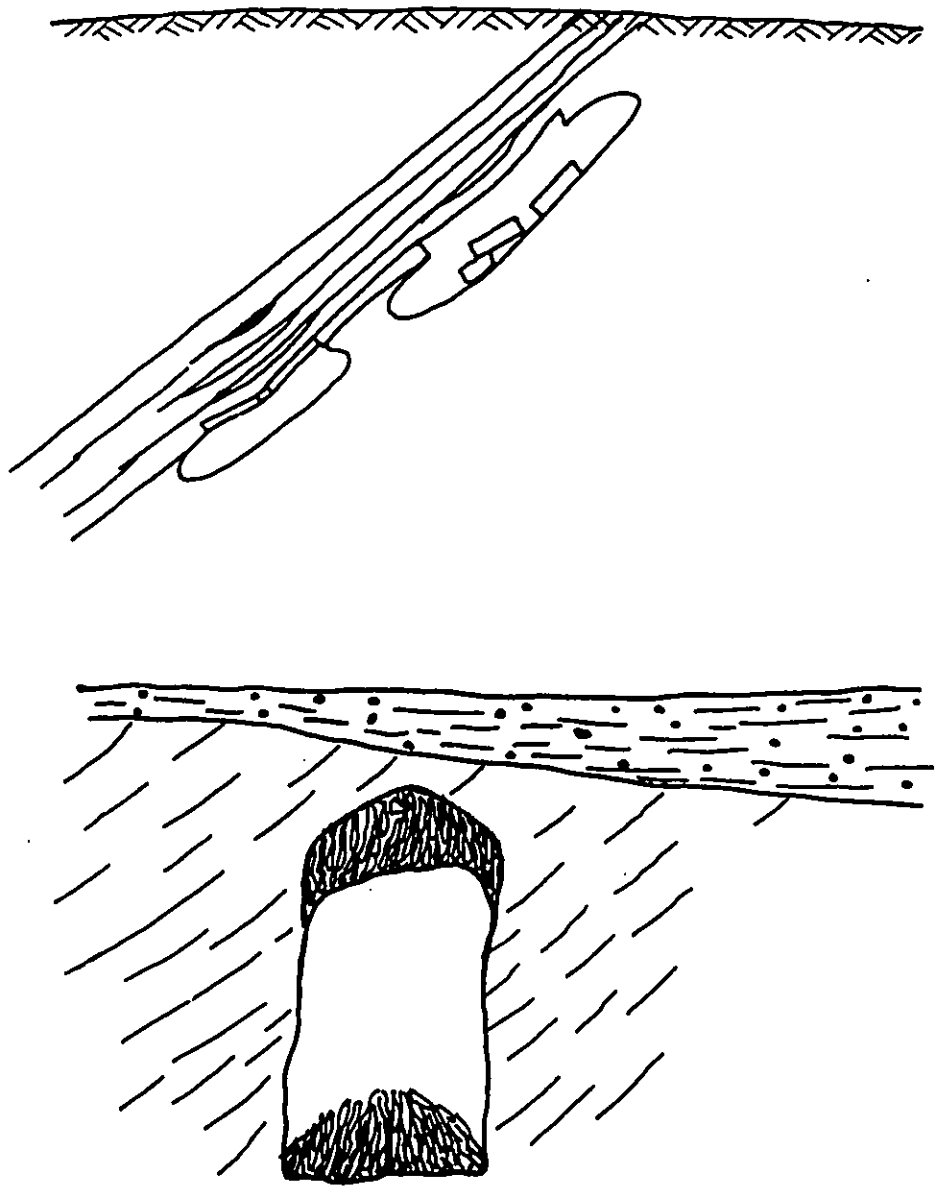

Figure 1.4 Common failure mechanisms of shallow stopes of hard rock mines.
c) strata failures, linear arching, d) chimneying disintegration failure.

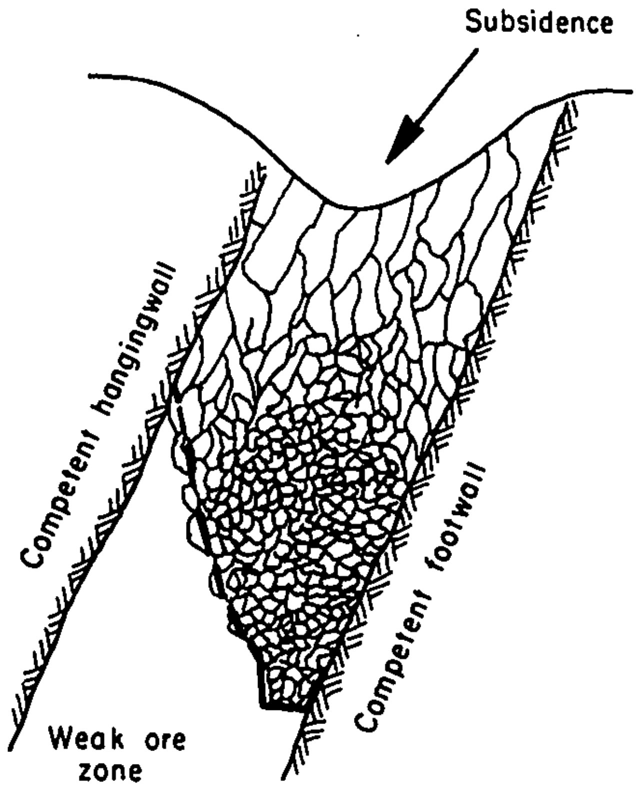

Figure 1.4 Common failure mechanisms of shallow stopes of hard rock mines.
e) block caving failure.

Table 1.2 Catalogue of Failure Mechanisms

Type of Failure (+)	Mining Environment (Figure 1.3)	Mobilized Rock Mass (*)	Possible Lack of Ground Stress Clamping	Possible Instability Elements
Plug failure m, r	d, e, f	CR	Yes	Large-scale steeply dipping discontinuities
Ravelling p, s	b, e, f	FW, CR, HW	Yes	Well-developed and continuous jointing
Strata failure p, s	e, f	CR, HW	No	Persistent parallel joints
Chimneying disintegration p, s	c, d, e, g	CR, HW	Yes	Weak material
Block caving p, s	b, e, g	CR, HW	Yes	Discontinuities or material weak in tension

(*)
CR = Crown
HW = Hangingwall
FW = Footwall
(+)
m = Massive
p = Piecewise
r = Fast
s = Gradual

which weak failure types such as chimneying disintegration and block caving can easily develop.

The failure mechanisms outlined reinforce the need for a design approach that considers the entire stope surroundings. The usual question "how much of a surface crown pillar should be left between the stope and overburden/surface?" (on which the justification to use the thickness to width ratio is based) should thus be rephrased "what portion of the rock mass around the stope is mobilized in potential failure by the creation of the opening?" Furthermore, any weak bedrock in contact with the overburden must be discounted from providing resistance to failure.

Table 1.3 presents an accounting of known Canadian shallow stope failures, their geological environment, and presumed failure mechanisms. It summarizes the information gathered from the Roche and Golder Associates surveys as well as the available literature. Generally weak (altered, numerous weak zones) and faulted rock masses are the most prone to complete failure, followed by blocky ground and generally foliated rock masses. Massive and poorly fissured rock masses have not recorded complete failures.

1.3.1 Plug Failures

The case of large blocks ("plugs"), the height of the surface crown pillar, collapsing down into the shallow stope has occurred on well-defined, continuous joints such as foliation and fault planes. A few of the plug failures have occurred at depths less than 30 m [4][32], but Allen [5] reported that a 600 m high block dropped down the stope height of some 20 m, along geological planes of weakness defined by subvertical dykes in a Michigan mine. Other plug failures have been recorded in areas with numerous

Table 1.3 Summary of Failed Canadian Shallow Stopes of Hard Rock Mines

Geological Setting	Massive	Blocky	Weak Orebody/ Massive Walls	Massive Orebody/Weak Walls	General Foliation	Well Developed Stratification	Faulted, Weak
Number of Failed Stopes	0	6	3	5	11	3	4
Mode of Failure (Figure 1.4)	-	b, e	d	a, d	a, b, c, d, e	a, c	b, d, e
Total Number of Stopes	25	31	63	44	67	28	9
Failure Percent	0	20%	5%	11%	17%	11%	44%

interspersed shallow stopes [32] such as the Sullivan Mine, British Columbia.

In such cases, an initial underground void must exist for this mechanism to occur. The mechanism seems to develop on discontinuity surfaces with low shear strength, without encountering break-up of the plug.

1.3.2 Ravelling Failures

When left unsupported, gradual failure of the periphery from unfavourably oriented rock blocks and subsequent enlargement of an opening is commonplace when the span exceeds self-support capabilities. Commonly, the blocks of the rock mass fail sequentially without the remainder of the rock mass mobilizing on a large scale, unless a stable, self-supported arch cavity is formed, which transfers the rock load from the unsupported span to the opening sides. This general arch shape locally takes on the jagged profile of the rock blocks that have fallen.

Depending on the severity of span versus self-support capabilities, progression of ravelling can reach the top of bedrock before stabilization occurs.

These observations have been reported generally for some failed and unfailed cases [4].

1.3.3 Strata Failures

Behaviour of stratified rock masses takes on particular dimensions when they are located around shallow underground excavations of hard rock mines. Canadian hard rock mine settings can present surface crown pillars or hangingwalls/footwalls in which continuous parallel joints predominate, such as gneissic fabric, or even sedimentary bedding joints. These dominant rock structures extend continuously over the mine site, effectively separating the rock into strata. Strata thickness may vary from site to site, typically from a few to tens of centimetres.

Strata failures occur by several mechanisms. Intact strata fail when gravity is sufficient to impose flexure leading to tensile failure, or impose load causing shear failure at the wall contacts.

Failure of horizontal strata in surface crown pillars is known to have occurred, such as at the Niobec Mine [33]; but because most stratiform structures in Canadian mines are dipping, flexure and shear are expected in the hangingwalls of shallow stopes.

1.3.4 Chimneying Disintegration Failures

Chimneying by disintegration is a mining induced failure which refers to the formation of isolated holes or "chimneys" in weak rock extending in an upward fashion from an underground opening towards surface either following a vertical path in a homogeneous mass or up dip in a weak unit bounded by competent rock. In the former setting, failure occurs by progressive collapse of a locally disintegrating rock mass which leaves behind intact steep walls which have similar dimensions as the opening from which the failure originates. Over the height of the chimney, its cross-sectional area usually remains the same. In the latter setting, failure can progress up dip in the weak unit or between the bounding rock.

The progression of this degradation of the rock mass can develop quickly. Rice [6] describes such a development over an opening with horizontal dimensions of 4.3 x 8.5 m in a relatively incompetent graphitic slate dipping at 60°. In this instance, a cave was initiated for the purpose of obtaining material for cut-and-fill stoping. In about one year, the chimneying had worked through to surface, vertically, a distance of 275 m cutting diagonally through the slate bedding.

Supplementary cases of chimneying disintegration have been reported by Picciaccia [34] and Bétournay [35] who observed and discussed with mine personnel such failures in the hangingwalls of the Bousquet 1 and Belmoral Mines, respectively. In both cases, the rock was schistose and weak. In the latter case, it was reported that such chimneying, which was seen to have reached the contact with overburden, commonly occurred from depths of up to 250 m with quick development. The Belmoral mine accident of 1980 is presumed to have occurred as a result of a chimneying disintegration [36].

Chimneying disintegration has also occurred in other environments, such as a rock mass altered to weak kaolinized rock, at the Selbaie Mine from the crown of a near-surface opening to the overburden [37]. This chimney continued in the dense till-like overburden until it reached surface. Such failures have also been witnessed above roadways in a Nova Scotia coal mine, Figure 1.5, and in English ironstone mines, where subsequent to the failure of the stratified roof beam, a weak mudstone would disintegrate and chimney, Figure 1.6 [31].

At the Bousquet and Belmoral Mines, some amount of debris was removed, allowing the chimneying to continue before it choked itself off; at Selbaie the failed material fell in a large stope also allowing the failure to continue. However, these sorts of materials are not expected to have a high bulking factor (the amount of supplemental volume occupied by a broken and caved material compared to its initial volume) once the

Figure 1.5 Chimneying disintegration in shale above Nova Scotia coal mine accessways.

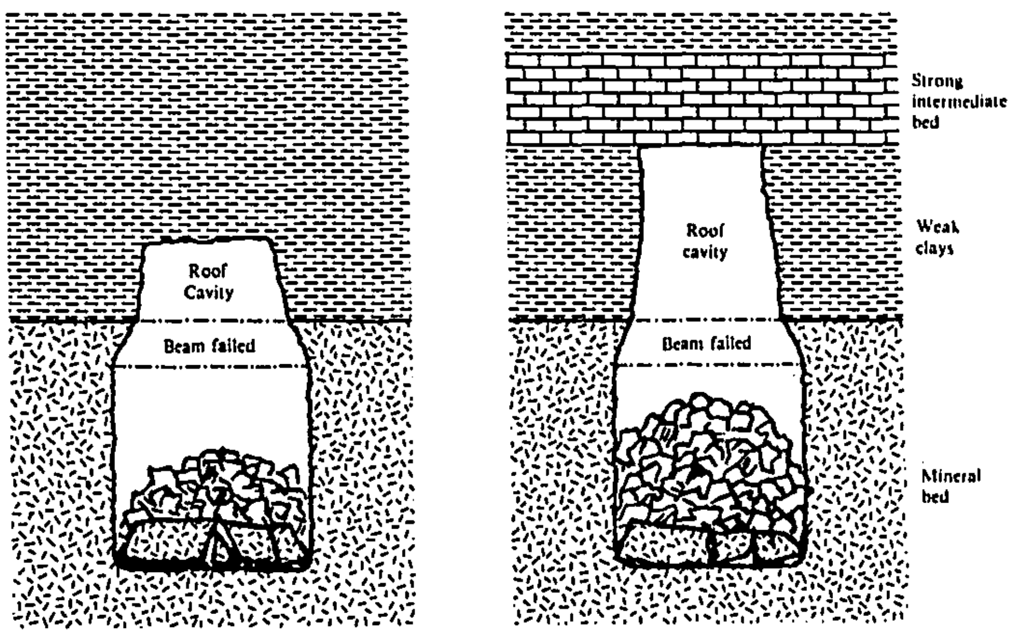

Figure 1.6 Characteristics of chimneying disintegration over a preliminary beam failure, [31].

rock/soil mass breaks down.

Both block ravelling and chimneying disintegration are mechanisms which involve a progressive limited portion of the rock mass, and can stabilize themselves when rock mass quality improves. These must be compared with block caving which involves the general gravitational flow of a broken down, extended mass into the upper portion of an underground opening. This is stopped if arching occurs within the loosened rock mass, or if the rock mass conditions vary.

1.3.5 Block Caving Failures

Although rock block displacements can start the block caving process, it is assumed that in the latter the blocks are moving relative to one another over a large volume of the rock mass, unlike block ravelling which predominantly affects the periphery of the opening. Several caving failures have been alluded to in the Golder [4] survey of failures, but no definite identification of such a failure mechanism as an unplanned event has been measured or reported during actual mine practice or abandoned mine failure.

1.4 REVIEW OF EXISTING DESIGN METHODS

The methods used in designing the shallow stopes of reviewed mine case studies belong to established rock mechanics practice. No method dedicated to specific or general stability of shallow underground openings issues has yet been applied. Nor, by and large, has the integrated design approach been used, i.e. using more than one method and framing the application of design with respect to limitations of each method.

New rock mechanics problems, such as instabilities related to shallow stopes, are usually first approached by using pre-existing, conventional methods. In the case of shallow stopes, various conventional methods have been used, which can be classified as:

i) analytical equations

ii) empirical methods

iii) block caving prediction

iv) numerical procedures.

The use of the Hoek [21] and Gill et al [22] methods (for surface crown pillars only) has not been reported. They are presented in this Chapter.

1.4.1 Analytical Formulas

Historically, the first approach to designing shallow stopes has been to use general analytical equations such as

i) beam theory

ii) plate theory

iii) arching formulas

iv) imposed redistributed stress.

All of these approaches pre-suppose that the rock material is continuous, isotropic, homogeneous and behaves in a linear elastic fashion. Some variants exist to adjust these equations to consider simple types of discontinuities. They will also be reviewed. However, these approaches contrast with the segmented and variable quality rock masses normally found at each site.

The advantage of applying these equations lies in their simplicity to use and interpret, where an imposed stress (from the self weight of the rock with/without consideration of imposed ground stress) can be compared to available rock strength. The analysis, except for plates, is 2-dimensional (plane strain) which simplifies the expectation of failure location. Failure is expected to lead to complete collapse of the surface crown pillar or hangingwall, tensile resistance of the continuous material being surpassed by stress.

In the cases studied, the entire pillar has been considered a beam or a plate. This in most cases is larger than the limiting thickness to span ratio of 0.5 above which the beam begins to behave more like a thick beam (where shear failure may be predominant over tensile failure at the abutments) requiring a complex and particular solution from the theory of elasticity.

The beam theory assumes that the structural element is very long in the third dimension, thereby only considering its thickness and span. The cross-section of the beam is essentially uniform, and a double-cantilever (fixed at both ends) situation is expected to exist (rock is continuous between the beam and the stope walls). The general formula to specify induced stresses at any point along the span is

$$\sigma_{induced} = \frac{My}{I} \tag{1.1}$$

where

$\sigma_{induced}$ = imposed stress at any point in the beam

M = moment at that point

y = distance from the beam neutral axis to that point

I = moment of inertia for the beam cross section

It is maximum at the beam ends with

$$\sigma_{Induced} = \frac{qL^2}{2t^2} \tag{1.2}$$

where

t = thickness of the member

L = beam span

q = load, per unit length

At this location the tension found at the top of the beam and compression at the bottom can be compared to the rock material tensile and compressive strength.

Elastic plate theory can be used where the spanning dimensions are similar (one is less than twice the other) but much greater than the plate thickness [38]. The stability of a stratum as a single plate involves the derivation of complex equations.

Timoshenko and Woinowski-Krieger [38], based on the theory of elasticity, developed a solution for induced stresses in a fully restrained plate. The maximum moment occurs at the centre of the longest edge b. Figure 1.7 shows moment values calculated by Timoshenko and Woinowski-Krieger for various plate geometries. The general formula to calculate the maximum stress (at mid-span of the longest dimension) is

$$\sigma_{Induced} = \frac{6\mu q a^2}{t^2} \tag{1.3}$$

where

μ = coefficient which varies with the span ratio

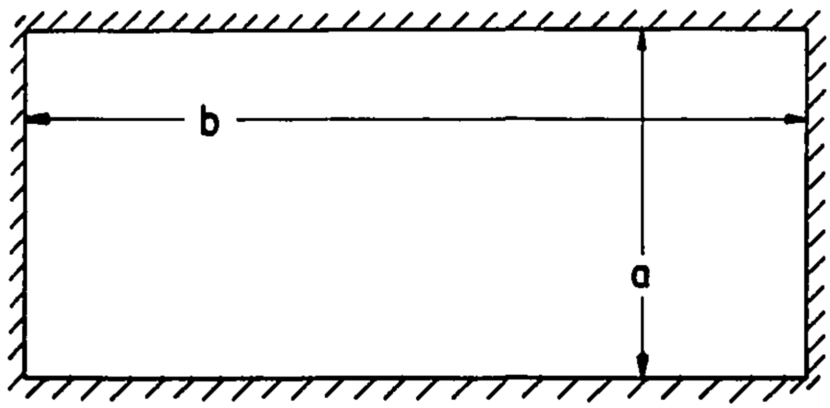

b/a	$(M_x)_{x=b/2,y=o}$	$(M_y)_{x=o,y=a/2}$	$(M_x)_{x=o,y=o}$	$(M_y)_{x=o,y=o}$
1.0	$-0.0513qa^2$	$-0.0513qa^2$	$0.0231qa^2$	$0.0231qa^2$
1.1	$-0.0581qa^2$	$-0.0538qa^2$	$0.0264qa^2$	$0.0231qa^2$
1.2	$-0.0639qa^2$	$-0.0554qa^2$	$0.0299qa^2$	$0.0228qa^2$
1.3	$-0.0687qa^2$	$-0.0563qa^2$	$0.0327qa^2$	$0.0222qa^2$
1.4	$-0.0726qa^2$	$-0.0568qa^2$	$0.0349qa^2$	$0.0212qa^2$
1.5	$-0.0757qa^2$	$-0.0570qa^2$	$0.0368qa^2$	$0.0203qa^2$
1.6	$-0.0780qa^2$	$-0.0571qa^2$	$0.0381qa^2$	$0.0193qa^2$
1.7	$-0.0799qa^2$	$-0.0571qa^2$	$0.0392qa^2$	$0.0182qa^2$
1.8	$-0.0812qa^2$	$-0.0571qa^2$	$0.0401qa^2$	$0.0174qa^2$
1.9	$-0.0822qa^2$	$-0.0571qa^2$	$0.0407qa^2$	$0.0165qa^2$
2.0	$-0.0829qa^2$	$-0.0571qa^2$	$0.0412qa^2$	$0.0158qa^2$
∞	$-0.0833qa^2$	$-0.0571qa^2$	$0.0417qa^2$	$0.0125qa^2$

Figure 1.7 Moment values for a fully clamped plate [38].

a = shortest span dimension

These beam and plate formulations do not take into consideration the variability between rock compression and tension modulus of elasticity [39] which locate the neutral axis away from the beam mid-height position assumed by the elastic behaviour of a member of one material.

When stratum failure involves tensile cracking, the elastic beam approach requires that, by the bending moments imposed and mechanics of stratum movement, the stratum breaks at its centre with parallel cracking developing at the abutment contacts. This could result in the formation of blocks supported at mutual contact points, at the upper part of the beam midspan, and at the abutments, Figure 1.8. Provided rock strength at the contact points is sufficient to resist the compressive and shear stress imposed, the block system will stay in place. This block system has been called a "linear arch" or "voussoir beam" by several authors [40][41][42] who showed that linear arching was possible in two or more blocks making up a beam. However, no information has been found on the analytical representation of a linear arch system of more than two blocks.

The physical description of the problem has been made by Evans [40] who analysed the force distribution for a linear arch condition of two blocks with the following assumptions:

1) The rock behaves elastically, under compressive stress.
2) There is no tensile stress operating due to the breaks in the undermined strata.
3) Sufficient shear strength for stability is generated by the frictional resistance due to the horizontal compressive force acting across the breaks.
4) The segmented beam is at the same level as the initial stratum horizon.

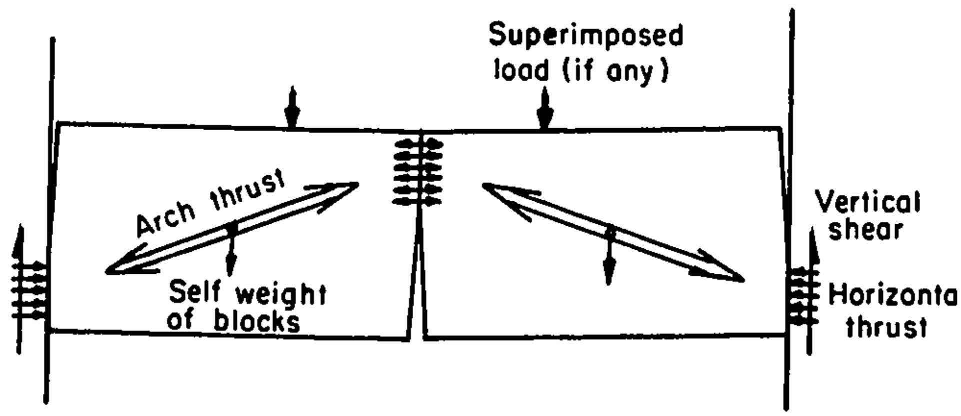

Figure 1.8 Linear arch behaviour.

5) Elastic strain of the abutments under horizontal compressive stress is negligible.

6) No horizontal pre-stress is present in the beam.

To these can be added the following assumptions, also implicitly made by other authors [30][42]:

7) The original beam has failed at mid-span to form the linear arch.

8) The magnitude and distribution of compressive thrust is the same at mid-span as at the abutments (Figure 1.9).

9) Failure is by imposed stress exceeding material strength (location of failure not indicated).

Linear arch failure has been defined in three ways: crushing at the contact points when imposed stresses are greater than material strength, buckling due to eccentricity from beam slenderness, or shearing at the abutments caused by block weight.

To evaluate the potential for crushing, Evans equated the maximum allowable (F_s=1) block thickness for a given span to the distribution of block compressive thrust (triangular shape) from block weight moments, Figure 1.9 (half-beam analysis).

$$\sigma_c t^2 \left(\frac{n}{2} - \frac{n^2}{3}\right) = \frac{\gamma_r \, t L^2}{8} \tag{1.4}$$

where

f_c=σ_c = imposed compressive stress equal to compressive strength of rock

t = thickness of failed strata

L = opening span

γ_r = unit weight of rock

n = load to depth ratio

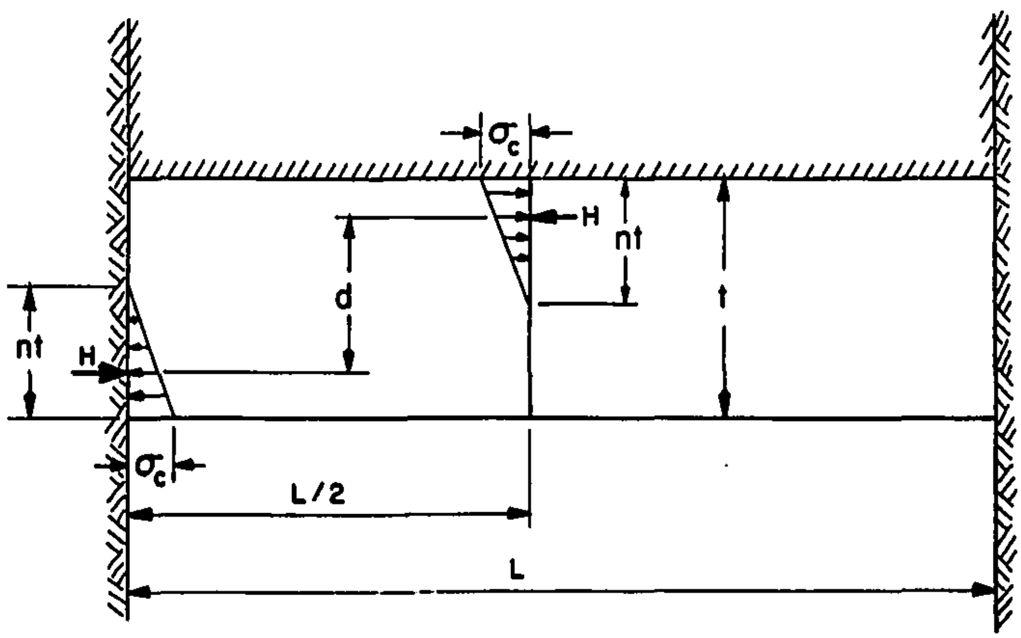

Figure 1.9 Distribution of stresses in a linear arch system [41].

The solution to calculate the maximum value of an imposed triangular compression thrust at the contact points was outlined by Beer and Meek [42] and expanded by Brady and Brown [30]. The latter publication suggested the particular solution path to obtain the imposed normal contact block stress. It proceeds by iteration of several formulas (relaxation technique) to calculate the actual n value, using sequentially

$$z_o = t\left(1-\frac{2n}{3}\right) \tag{1.5}$$

$$f_c = \frac{1}{4}\frac{\gamma_r L^2}{nz_o} \tag{1.6}$$

$$f_{av} = \frac{1}{2}f_c\left(\frac{2}{3}+\frac{n}{2}\right) \tag{1.7}$$

$$A_L = L + \frac{16}{3}\frac{z_o^2}{L} \tag{1.8}$$

$$\Delta A_L = \frac{f_{av}}{E_m}A_L \tag{1.9}$$

$$z = \left[\frac{3L}{16}\left(\frac{16z_c^2}{3L} - \Delta A_L\right)\right]^{1/2} \tag{1.10}$$

$$n = \frac{3}{2}\,(1-\frac{z}{t}) \tag{1.11}$$

where

z = thrust arch height

L = beam span

f_c = imposed maximum compressive stress

f'_{av} = average imposed stress over height

γ_r = unit weight of rock

A_L = arch length

E_m = field modulus of elasticity

z_o = original value of z selected

z_c = z value from the previous computational cycle

n = load to depth ratio

t = beam thickness

The first equation returns a value of the moment arm z_o from an initial n, the second calculates the compression level, the third the average thrust compression across the arch in one block, the fourth determines the length of the arch, the fifth the elastic shortening due to the compression at the contact points (beam only), the sixth the arch height and lever arm, the final equation the recalculated depth ratio n. The iteration stops when the last calculated n converges with the previous input in the first equation. Brady and Brown suggest taking the final value of f_c for comparison to the unconfined compressive rock strength σ_c to obtain the factor of safety, F_s

$$F_s = \frac{f_c}{\sigma_c} \tag{1.12}$$

The Beer and Meek process to solve for maximum span is as follows. Based on the Evans equation, modified to include strata dip, Beer and Meek outlined an expression for moment equilibrium

$$\frac{\gamma_r}{8} t L^2 \cos\theta = \frac{f_c}{2} ntz \tag{1.13}$$

which here has been corrected by using unit weight rather than weight as prescribed by the authors. The relationship between lever arm and thrust zone is

$$z_o = t\left(1 - \frac{2}{3}n\right) \tag{1.14}$$

The compression arch between loading points is in a parabolic form, given by Brady and Brown, its length is

$$A_L = L + \frac{8}{3}\frac{z_o^2}{L} \tag{1.15}$$

The deformation of this parabolic arch from loading is

$$\Delta A_L = \frac{11}{24}\frac{f_c}{E_m}A_L \tag{1.16}$$

The new lever arm shortening is

$$z = \sqrt{\frac{3}{8}L\left(\frac{8z_o^2}{3} - \Delta A_L\right)} \tag{1.17}$$

Substitution of z into equation 1.13 gives a fourth order equation for L in terms of n and f_c:

$$L^4 + C_1 L^2 - C_2 = 0 \tag{1.18}$$

where

$$C_1 = 0.1718\frac{f_c A_L^2}{E_m}$$

$$C_2 = A_L^2 z_o^2\left(1 - \frac{11}{24}\frac{f_c}{E}\right)$$

$$z_o = t\left(1 - \frac{2}{3}n\right)$$

$$A_L = \frac{4nf_c}{\gamma_r \cos\theta}$$

θ = dip of strata

Finding the span is a function of n and f_c. Beer and Meek do not explain how n is to be calculated, only that by using different values of f_c, a value of L will first increase with a peak reached at a particular stress and then decrease. The largest value of L is the critical span and the imposed stress is the critical stress imposed. These values represent limit equilibrium of the linear arch system. For thin beams, f_{cr} is lower than the compressive strength of the rock and the stability is dependent on the eccentricity of the beam. For larger values of t, the stability may depend on the unconfined compressive strength of rock. At very large strata thickness, shear failure of the linear arch system occurs if the weight imposed exceeds shear resistance.

$$V < 0.5\ \gamma_r\ Lt \tag{1.19}$$

V = maximum shear resistance

A non-elastic analysis of jointed beams was proposed by Pender [43], Figure 1.10. This flat beam can contain a number of discrete blocks defined by vertical joints. The system of blocks retains its stability if, after consideration of axial thrust within the blocks and dilatant joint behaviour, tensile stresses are not introduced between the lower portion of the blocks that could allow blocks to slide out by gravity. When the following

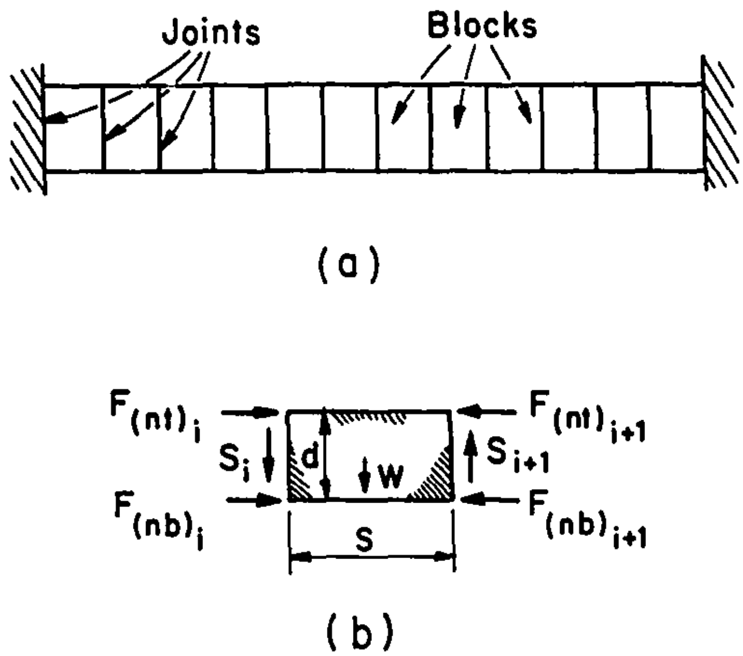

Figure 1.10 Distribution of forces on blocks of a jointed beam [43].

equation yields a negative value, sliding of blocks from the beam is expected:

$$(F_t)_{midspan} = \frac{wn}{8}\left[\xi\left(\frac{n+1}{n+2}\right)\left(\frac{k_n}{k_s}\right) - \frac{L}{2t}\right] \tag{1.20}$$

where

n = number of equal size blocks making up the beam

w = weight of each block

ξ = slope of normal-shear displacement curve

k_n = normal stiffness of the joint

k_s = shear stiffness of the joint

t = beam thickness

L = beam span

The stability of this beam can be compared to a surface crown pillar under study, if the pillar can be decomposed into several large vertical blocks.

The method cannot provide a comparison between imposed stress and strength available, for a factor of safety analysis. However, a modification of this approach could conceivably consider the effect of lateral ground stress.

The use of an arch shape has been considered a more stable structural member because of a more developed line of thrust it can accommodate. Rock load above an opening can be estimated to be distributed to the sides of the opening rather than completely imposed to the roof [44][45]. For a surface crown pillar, an elastic semi-circular arch is assumed to exist within the pillar to distribute the pillar load to the side of the stope, Figure 1.11a. The minimum thickness required for the surface crown pillar becomes the arch radius (stope half span) plus the radial thickness. The minimum radial

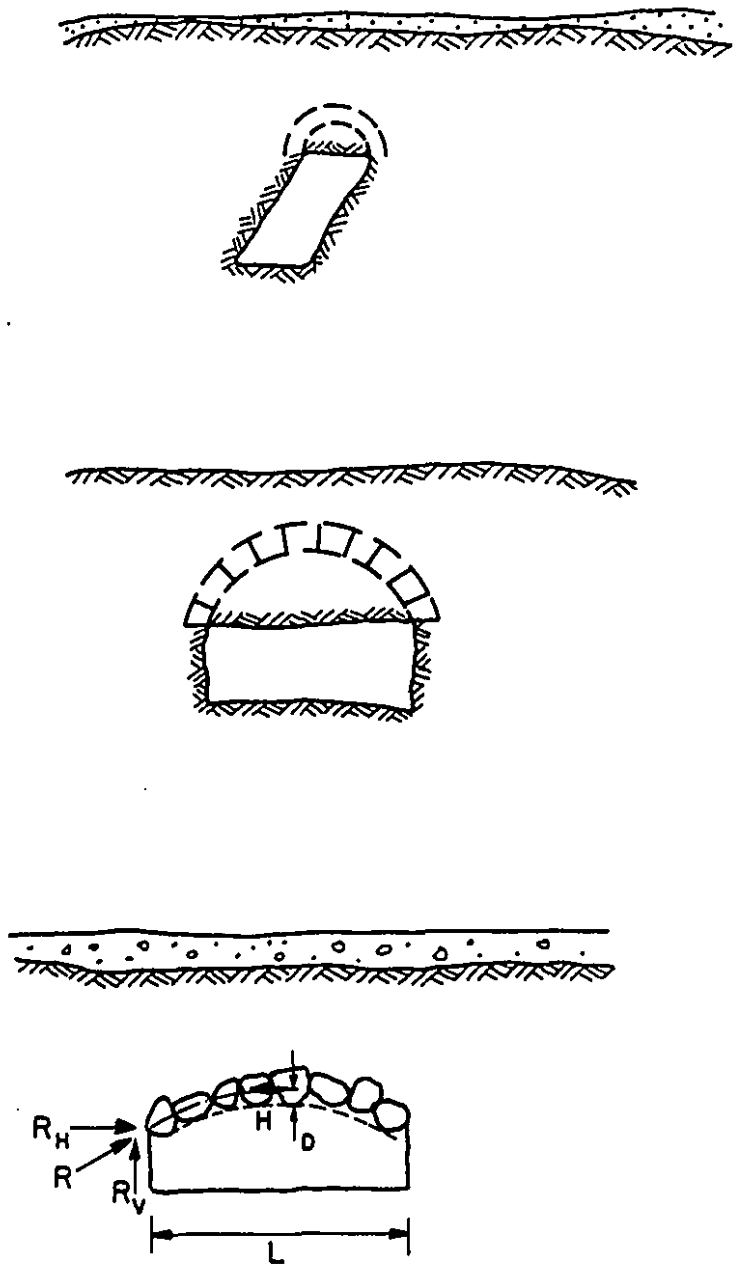

Figure 1.11 Approaches to the stability of a surface crown pillar as an arch shape.
a) elastic arch, b) masonry arch, c) boulder arch.

thickness for a circular arch is calculated from the ultimate load for an elastic arch [45]

$$W_{cr} = \gamma_c \frac{EI}{r^3} \tag{1.21}$$

where

γ_c = compressive force factor

r = arch radius

E = material modulus of elasticity

I = cross section moment of inertia

For an arch made up of interlocked blocks, as in the case of a masonry arch, Figure 1.11b, the required thickness to arch radius ratio for minimum stability is [46]

$$t/r = 1.06 \tag{1.22}$$

To demonstrate stability of such an arch, tensile stresses must be avoided between the blocks. The thrust lines must be constructed in equilibrium with all the loads acting on the arch and lying wholly within the masonry. The distributed load can be considered as a sum of several point loads around the circumference.

Another arch method has been formulated to analyse a broken rock mass consisting of boulders or untightly matched blocks [45], Figure 1.11c. Failure is expected to occur in one of three modes:

i) high loads opening the spaces between blocks permitting them to fall

ii) crushing of small areas leading to the possibility of freer movement

iii) blocks slipping out from low frictional resistance.

The horizontal reaction of this arch at each abutment is

$$R_h = \frac{WL^2}{8d} \qquad (1.23)$$

where

W = weight of the structure

L = span of the structure

d = rise of the line of thrust

When slip occurs, the vertical component R_v of the reaction is

$$R_v = R_h \tan \phi_r \qquad (1.24)$$

where

ϕ_r =angle of friction of the block surface

R_v is the shear strength that the abutment offers to resist the actual loading of half the arch, WL/2. If the actual loading is greater than the abutment resistance, failure will occur.

Various ground movement theories have been proposed to account for observed movements leading to arch formation in the back of underground openings. The general approach in the literature is to compare in two dimensions available strength to imposed stress to account for failure.

In the case of stratified rock masses Rziha and Fayal (in Hackett [47]) advanced theories stating that the overlying rocks are acted on by two forces only: cohesion and gravity. Only if gravity overcomes cohesion, collapse will occur. The collapse shape is a circular dome, related to the width of the excavation. Concepts also presented there relate to a limit of such failures with depth, i.e. the greater the depth the less likely the rock mass is to be affected.

Széchy [48] presents a historical review of approaches to estimate the location of one failure surface (leaving a stable cavity behind) from rock material expected to fail above an opening. It is worth noting that none of these look at the cavity shape as a load transferring mechanism.

Of the theories presented in Széchy, the Bierbaumer, Balla, and Ritter theories assumed a failure shape for the rupture of overlying rock masses. The first two assumed the rock failed in shear, Ritter assumed failure in tension. Ritter also derived the equation of his assumed parabolic shape based on a hydraulic radius approach, i.e. the failed weight of the material between opening and the failure surface was a maximum for the length of the perimeter of the parabola.

Terzaghi's rock pressure theory, developed originally for dry cohesionless soils [49], can be extended to cohesive soils and rock [48]. Once the opening is created, part of the rock mass is sliding down, bounded by vertical shear planes. Some of the rock load shearing on each plane is transferred laterally from these onto a stationary part, Figure 1.12. This means that only part of the rock load over the opening is being carried.

Rock loads from shearing stresses oriented at $45°+\phi/2$ are placed on the sides of the opening. If the unit weight of the material is γ_r and the lateral and vertical pressures are related by the constant K ($K = \sigma_H/\sigma_v$), then it can be shown that the vertical pressure at depth H is

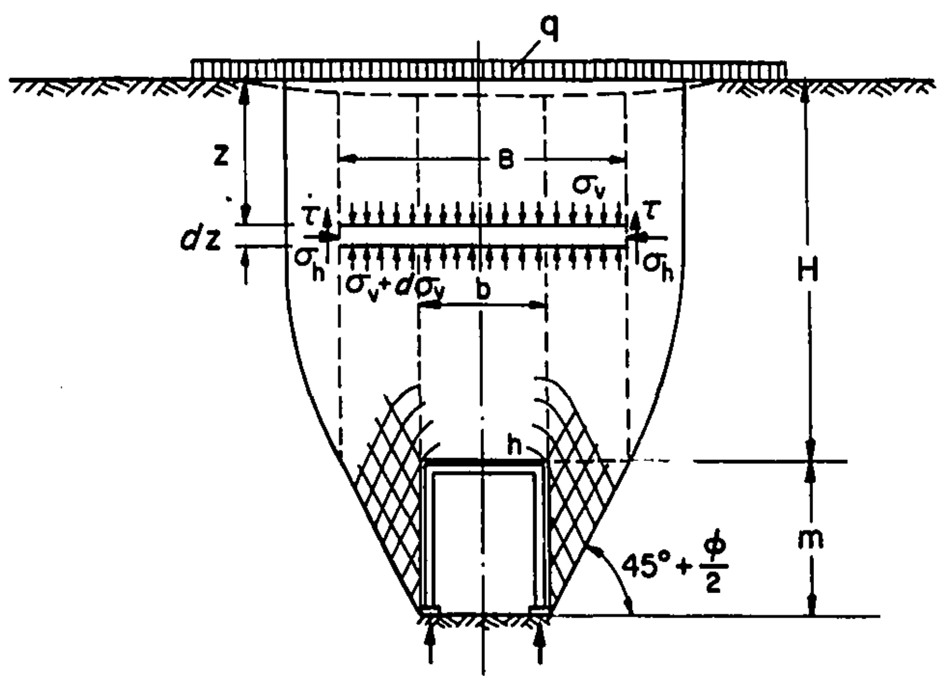

Figure 1.12 Terzaghi arch analysis, shallow case [48].

$$P_v = B\,\frac{\left(\gamma_r - \frac{2c}{B}\right)}{2K\tan\,\phi}\left(1 - e^{-K\tan\phi\frac{2H}{B}}\right) \tag{1.25}$$

where

B = opening width

c = material cohesion

ϕ = material internal angle of friction

No rock pressure will develop if B < $2c/\gamma_r$.

With openings at greater depth, arching action no longer extends to the ground surface. In his experiment Terzaghi found the value of the coefficient K to increase gradually from 1 to 1.5 over a height corresponding to B. Beyond heights greater than 2.5 B, the displacement of the lower areas did not affect stress conditions in the upper area. Rock pressure for a deeper opening can be separated into two terms, that which describes the zone of action and that of the rock load which acts on top of the active zone roof, Figure 1.13.

$$P_v = B\,\frac{\left(\gamma_r - \frac{2c}{B}\right)}{2K\tan\phi}\left(1 - e^{-K\tan\phi\,\frac{2H_2}{B}}\right) + \gamma_r H_1\, e^{-K\tan\phi\,\frac{2H_2}{B}} \tag{1.26}$$

With great depth the load term (with a height of H_2) becomes negligibly small.

Denkhaus [50] in his approach to roof failure at depth distinguishes between cohesive rock and insufficiently cohesive rock. The sufficiently cohesive approach has a separation of rock occurring in a dome shape, Figure 1.14, when the span of the opening (and therefore the dome) becomes too large. The weight of the dome exceeds the material's cohesive resistance, resulting in a sudden collapse of the dome. The limiting equation is given by

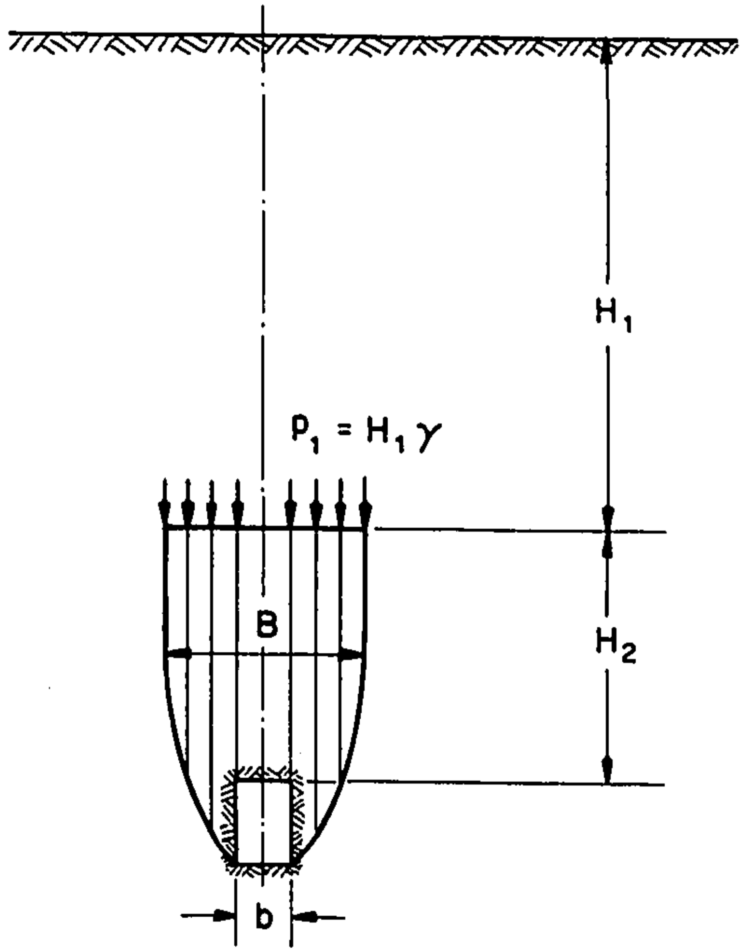

Figure 1.13 Terzaghi arch analysis, deep case [48].

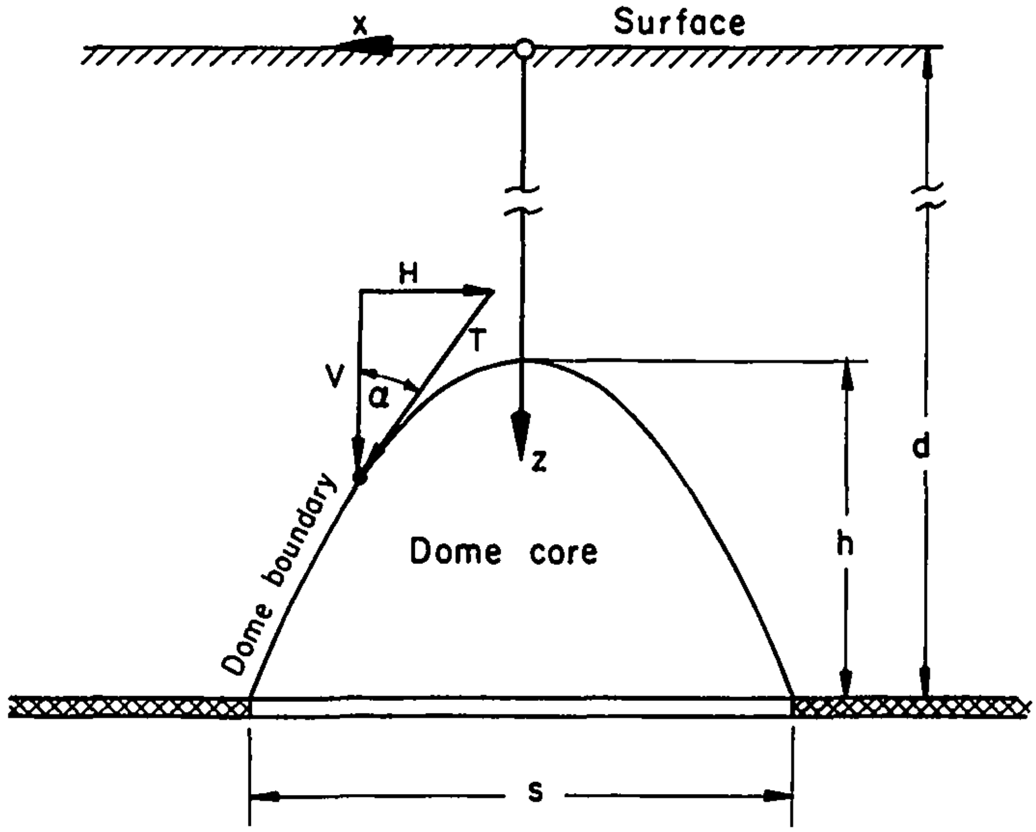

Figure 1.14 Denkhaus dome theory [50].

$$L = \sqrt{\frac{8\sigma_c d}{\gamma_r}\left(1 - \frac{h}{d}\right)} \tag{1.27}$$

$$h_{max} = 0.5d \tag{1.28}$$

$$L_{max} = \sqrt{\frac{2\sigma_c d}{\gamma_r}} \tag{1.29}$$

where

L = span of the dome

h = height of the dome

d = depth of cover above excavation

γ_r = unit weight of the rock

σ_c = uniaxial compressive strength of the rock

which does not relate directly to material cohesive or tensile resistance.

In the case of insufficiently cohesive rock material, portions will separate from the dome boundary gradually or at short intervals while the span is being increased. The relationship between the span and dome height is given by:

$$L = \sqrt{\frac{8\sigma_c d}{\gamma_r} (1-\frac{h}{d}) \log (1-\frac{h}{d})} \tag{1.30}$$

$$h_{max} = 0.63d \tag{1.31}$$

$$L_{max} = \sqrt{\frac{2.96\ \sigma_c d}{\gamma_r}} \tag{1.32}$$

The analytical solution to obtain a global description of imposed stresses around an underground opening is to apply the theory of elasticity in obtaining tangential, radial, and shear stresses around an opening. The theoretical solution to determine for an elastic, isotropic, homogeneous medium in which a circular opening is placed, is

$$\sigma_{tan} = \left(\frac{\sigma_x+\sigma_y}{2}\right)\left(1 + \frac{r^2}{r_d^2}\right) -$$

$$\left(\frac{\sigma_x - \sigma_y}{2}\right)\left(1 + \frac{3r^4}{r_d^4}\right)\cos 2\zeta \tag{1.33}$$

$$\sigma_{rad} = \left(\frac{\sigma_x+\sigma_y}{2}\right)\left(1 - \frac{r^2}{r_d^2}\right) +$$

$$\left(\frac{\sigma_x - \sigma_y}{2}\right)\left(1 - \frac{4r^2}{r_d^2} + \frac{3r^4}{r_d^4}\right)\cos 2\zeta \tag{1.34}$$

$$\tau_{rt} = -\left(\frac{\sigma_y-\sigma_x}{2}\right)\left(1 + \frac{2r^2}{r_d^2} - \frac{3r^4}{r_d^4}\right)\sin 2\zeta \tag{1.35}$$

where

σ_{tan} = tangential stress at a point, distance r from the centre of a circular opening of radius r

σ_{rad} = radial stress at a point, distance r_d from the centre of the opening

τ_{rt} = shear stress at a point, distance r_d from the opening centre

r = radius of circular opening

r_d = radial distance from center of opening to point

ζ = angle measured counterclockwise from the +x axis

The drawback with this approach pertains to the shape of shallow stopes which are not usually circular and, although closer to rectangular shape, can be of variable geometry. The elliptical and ovaloid shape has been used by Dhar et al [51] to get a closer stress distribution approximation for stopes. These solutions are for two-dimensional plane strain conditions, which may not be suitable for actual geometries under study.

Since the advent of numerical solutions, accurate approximations of stress distribution around underground openings with complex geometries in two or three dimensions has become possible, based on several rock mass behaviour assumptions (e.g. elastic, elasto-plastic) even allowing for such material behaviour as rock block movements within a rock mass. This is covered in detail in section 1.4.4.

In summary, although basic analytical formulas can be used to approximate elastic behaviour of the surface crown pillar and shallow stope surroundings, gravity failures (displacements from and within the rock mass) usually involved in destabilizing a shallow stope cannot be approximated nor quantified. Neither can the interaction effects between the pillar and the stope walls, or the surrounding rock be quantified.

Hoek [21] presented a limit equilibrium analysis to evaluate the potential for a rock block failure ("plug") defined by the entire surface crown pillar, Figure 1.15. The analysis was based on the ratio of rock mass shear strength available to induced shear stress:

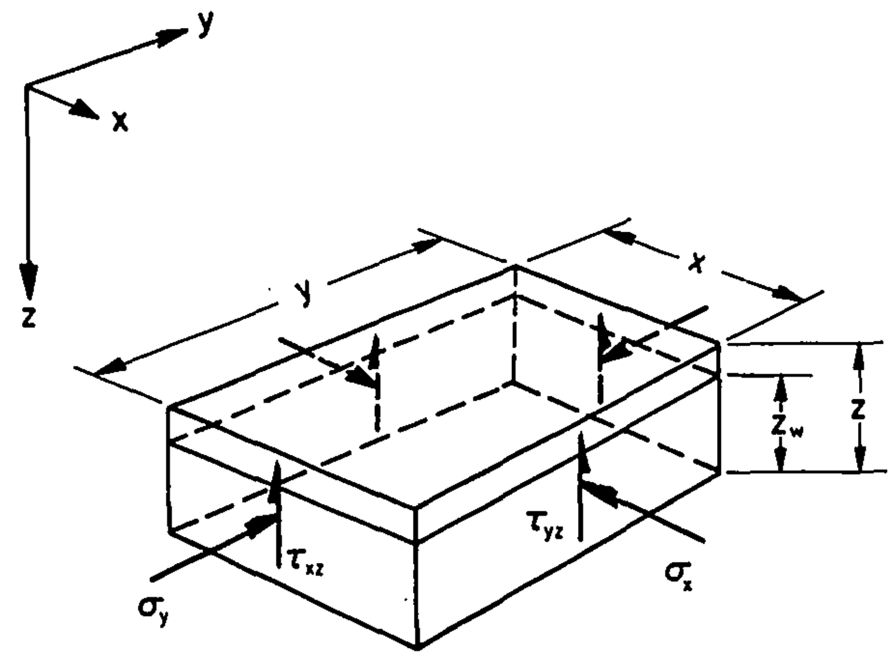

Figure 1.15 Hoek limit equilibrium analysis for plug failure [21].

$$F_s = \frac{2(\tau_{xz}(xz) + \tau_{yz}(yz))}{\gamma_r\ (xyz)} \tag{1.36}$$

where

x, y, z = the dimensions of the entire surface crown pillar spanning the shallow opening

τ_{xz}, τ_{yz} = the shear strengths on the xz and yz faces respectively

γ_r = the unit weight of rock

The shear strength of the rock mass is used as τ_{xz} and τ_{yz} inputs. It is obtained from the Hoek and Brown [52] failure criterion.

The procedure to calculate rock mass shear resistance begins with the Mohr failure envelope calculated for intact rock. This is obtained by using lab derived Mohr circles of the tensile test and compression tests with various levels of confinement. From the regression of results to generate the failure envelope is calculated an m value for the tested rock material; a value of s = 1 is given to lab tested material.

The basic equation relating the m and s parameters and Mohr circles is

$$\sigma_1 = \sigma_3 + \sqrt{m\sigma_c\ \sigma_3 + s\sigma_c^2} \tag{1.37}$$

where

σ_1 = major principal stress at failure

σ_3 = minor principal stress at failure

σ_c = unconfined compressive strength as calculated by the regression

These Mohr circles are tangent to a Mohr envelope given by σ, and τ the normal and shear stress that exist on the material failure surface at failure obtained by solving these equations

$$\tau = (\cot\phi - \cos\phi)\,\frac{m\sigma_c}{8} \tag{1.38}$$

$$\phi = \arctan\frac{1}{\sqrt{4h\cos^2\Theta - 1}} \tag{1.39}$$

$$\Theta = \frac{1}{3}\left(90 + \arctan\frac{1}{\sqrt{h^3-1}}\right) \tag{1.40}$$

$$h = 1 + \frac{16(m\sigma + s\sigma_c)}{3m^2\sigma_c} \tag{1.41}$$

where

h,Θ = solution constants

ϕ = material angle of friction

The slope of the tangent to the Mohr failure envelope at a normal stress of σ is given by ø. The corresponding cohesion c of the intercept of the tangent on the τ axis is

$$c = \tau - \sigma\tan\phi \tag{1.42}$$

By translating the laboratory "m" and the "s" value to field behaviour using the equations derived by Brown and Hoek [53] and rock mass quality

$$m_f = m_l\, e^{(RMR-100)/28} \tag{1.43}$$

$$s_f = s_l\, e^{(RMR-100)/9} \tag{1.44}$$

where

RMR = Bieniawski [54] rock mass quality rating

the rock mass Mohr failure envelope can be obtained by using equations 1.38 to 1.42.

The Hoek and Brown m and s constants are, respectively, very approximately analogous to the angle of friction (instantaneous indication of failure envelope slope) and failure envelope cohesive strength at that slope [55].

Lateral stresses which confine the plug are defined by the natural, pre-mining ground stresses distributed according to ratios between vertical stress (rock weight) and horizontal stress, from which the effect of groundwater pressure is subtracted

$$\sigma_x = \frac{\gamma_r Z K_x}{2} - \frac{\gamma_w Z_w^2}{2Z} \tag{1.45}$$

$$\sigma_y = \frac{\gamma_r Z K_y}{2} - \frac{\gamma_w Z_w^2}{2Z} \tag{1.46}$$

where

K_x and K_y = the ratios of horizontal to vertical stress in the x and y directions respectively

γ_w = the unit weight of water.

Z_w = the height of the water table

The Gill et al [22] method to evaluate block movements within a surface crown pillar rock mass is based on the block surfaces' stress-strain behaviour. The blocks are considered rigid. The method is two dimensional and considers the stability of a single block or the entire overlying surface crown pillar block assembly. In the case of the latter, the number of equilibrium equations to solve are the sum of those related to each of the constituent block sides. These relate to the sliding movements and consider shear and normal joint stiffness effects as well as possible pore pressure, seismic, and external loads. The method requires separating the surface crown pillar into a mesh representing individual blocks. The application of linear programming through computing is required. The method does not allow for block rotation or net block movements but can provide factors of safety for portions of the crown pillar as well as the required stabilizing force.

1.4.2 Empirical Methods

Empirical methods are based on information gathered and experience from other case studies, and are usually applied to conditions anticipated at a given site. The simplest empirical method used for shallow stopes has been the thickness to width ratio described in section 1.2. The more advanced methods have been based on large populations of ground stability conditions which, when classified under well-defined systems, can provide conditions similar to those considered for design/stability evaluation.

Two rock mass classification systems, which incorporate the Deere [56] approach to describe the broken nature (rock quality designation, RQD) of a rock mass, have been applied in designing shallow stopes.

The Bieniawski [55] or RMR system, utilizes six measurable parameters (strength of intact rock, drill core quality represented by the RQD, spacing of discontinuities, groundwater condition, condition of discontinuities, and orientation of discontinuities) to calculate a rock mass rating (Table 1.4) used in describing average stand-up time of unsupported openings, rock mass cohesion, and angle of friction. Each factor is weighted by its importance in affecting stability. The orientation of discontinuities to the extraction activity adjusts the calculated rating. The maximum rating is 100, indicating very good rock.

Table 1.4 Rock Mass Rating Empirical Evaluation System [51]

<table>
<tr><th colspan="4">PARAMETER</th><th colspan="7">RANGES OF VALUES</th></tr>
<tr><td rowspan="3">1</td><td rowspan="2">Strength of intact rock material</td><td colspan="2">Point load strength index</td><td>> 8 MPa</td><td>4 - 8 MPa</td><td>2 - 4 MPa</td><td>1 - 2 MPa</td><td colspan="3">For this low range - uniaxial compressive test is preferred</td></tr>
<tr><td colspan="2">Uniaxial compressive strength</td><td>> 200 MPa</td><td>100 - 200 MPa</td><td>50 - 100 MPa</td><td>25 - 50 MPa</td><td>10-25 MPa</td><td>3-10 MPa</td><td>1-3 MPa</td></tr>
<tr><td colspan="3">Rating</td><td>15</td><td>12</td><td>7</td><td>4</td><td>2</td><td>1</td><td>0</td></tr>
<tr><td rowspan="2">2</td><td colspan="3">Drill core quality RQD</td><td>90% - 100%</td><td>75% - 90%</td><td>50% - 75%</td><td>25% - 50%</td><td colspan="3">< 25%</td></tr>
<tr><td colspan="3">Rating</td><td>20</td><td>17</td><td>13</td><td>8</td><td colspan="3">3</td></tr>
<tr><td rowspan="2">3</td><td colspan="3">Spacing of joints</td><td>> 3m</td><td>1 - 3 m</td><td>0.3 - 1 m</td><td>50 - 300 mm</td><td colspan="3">< 50 mm</td></tr>
<tr><td colspan="3">Rating</td><td>30</td><td>25</td><td>20</td><td>10</td><td colspan="3">5</td></tr>
<tr><td rowspan="2">4</td><td colspan="3">Conditions of joints</td><td>Very rough surfaces
Not continuous
No separation
Hard joint wall rock</td><td>Slightly rough surfaces
Separation < 1 mm
Soft joint wall rock</td><td>Slightly rough surfaces
Separation < 1 mm
Soft joint wall rock</td><td>Slickensided surfaces
Gouge < 5 mm thick
or
Joints open 1-5 mm
Continuous joints</td><td colspan="3">Soft gauge > 5 mm thick
or Joints open > 5 mm
Continuous joints</td></tr>
<tr><td colspan="3">Rating</td><td>25</td><td>20</td><td>12</td><td>6</td><td colspan="3">0</td></tr>
<tr><td rowspan="5">5</td><td rowspan="4">Ground water</td><td colspan="2">Inflow per 10 m tunnel length</td><td colspan="2">None</td><td>< 25 litres/min</td><td>25-125 litres/min</td><td colspan="3">> 125 litres/min</td></tr>
<tr><td rowspan="2">Ratio</td><td>Joint water Pressure</td><td rowspan="2" colspan="2">0</td><td rowspan="2">0.0 - 0.2</td><td rowspan="2">0.2-0.5</td><td rowspan="2" colspan="3">> 0.5</td></tr>
<tr><td>Major principal stress</td></tr>
<tr><td colspan="2">General conditions</td><td colspan="2">Completely dry</td><td>Moist only
(interstitial water)</td><td>Water under
moderate pressure</td><td colspan="3">Severe water problems</td></tr>
<tr><td colspan="3">Rating</td><td colspan="2">10</td><td>7</td><td>4</td><td colspan="3">0</td></tr>
</table>

Table 1.4 (Continued)

B. RATING ADJUSTMENT FOR JOINT ORIENTATIONS

Strike and dip orientations of joints		Very favourable	Favourable	Fair	Unfavourable	Very unfavourable
Ratings	Tunnels	0	-2	-5	-10	-12
	Foundations	0	-2	-7	-15	-25
	Slopes	0	-5	-25	-50	-60

C. ROCK MASS CLASSES DETERMINED FROM TOTAL RATINGS

Rating	100 - 81	80 - 61	60 - 41	40 - 21	< 20
Class No	I	II	III	IV	V
Description	Very good rock	Good rock	Fair rock	Poor rock	Very poor rock

D. MEANING OF ROCK MASS CLASSES

Class No	I	II	III	IV	V
Average stand-up time	10 years for 5 m span	6 months for 4 m span	1 week for 3 m span	5 hours for 15 m span	10 min for 05 m span
Cohesion of the rock mass	>300 kPa	200-300 kPa	150-200 kPa	100-150 kPa	< 100 kPa
Friction angle of the rock mass	> 45°	40°-45°	35°-40°	30°-35°	< 30°

E. THE EFFECT OF JOINT STRIKE AND DIP ORIENTATIONS IN TUNNELLING

Strike perpendicular to tunnel axis				Strike parallel to tunnel axis		Dip 0° - 20° irrespective of strike
Drive with dip		Drive against dip				
Dip 45° - 90°	Dip 20° - 45°	Dip 45° - 90°	Dip 20°-45°	Dip 45° - 90°	Dip 20° - 45°	
Very favourable	Favourable	Fair	Unfavourable	Very unfavourable	Fair	Unfavourable

The NGI system (Barton et al [11]), also utilizes six measurable parameters (RQD, number of joint sets, joint roughness, joint alteration, ground stress levels, and groundwater condition) to calculate the quality Q index of rock mass quality (Table 1.5). The Q value is also used in calculating the need (versus no requirement) for support, the type and pressure of the support, for the roof or the sides of an opening reflecting various engineering purposes (the "ESR" value), Figure 1.16.

The equation

$$Q = \frac{RQD}{J_n} \times \frac{J_r}{J_a} \times \frac{J_w}{SRF} \tag{1.47}$$

where

RQD = rock quality designation

J_n = factor for the number of joints

J_r = factor for the roughness of joints

J_a = factor for the alteration of joint surfaces

J_w = factor for the water pressure on the joint surfaces

SRF = factor for the level of imposed ground stress

reflects a breakdown of the Q index into three main factors: size of rock mass blocks (RQD/J_n), resistance to block movement (J_r/J_a), and natural rock mass effects (J_w/SRF). The logarithmic scale for Q ranges from the very poor rock to the very good rock.

The database of both these classification systems originates for the most part from civil engineering projects located relatively deeper within a rock mass than shallow stopes. Furthermore, such cases have by-and-large been related to better ground conditions than shallow stopes of hard rock mines. Barton [57] undertook a careful examination of the Q system to determine the specific requirements necessary to ensure

Table 1.5 NGI Empirical Rock Mass Quality Evaluation System [11]

Description	Value	Notes
1. ROCK QUALITY DESIGNATION	RQD	
A. Very poor	0-25	1. Where RQD is reported or measured as 10 (including 0), a nominal value of 10 is used to evaluate Q.
B. Poor	25-50	
C. Fair	50-75	2. RQD intervals of 5, i.e. 100, 95,90 etc are sufficiently accurate.
D. Good	75-90	
E. Excellent	90-100	
2. JOINT SET NUMBER	J_n	1. For intersections use $(3.0 \times J_n)$
A. Massive, no or few joints	0.5-1.0	2. For portals use $(2.0 \times J_n)$
B. One joint set	2	
C. One joint set plus random	3	
D. Two joint sets	4	
E. Two joint sets plus random	6	
F. Three joint sets	9	
G. Three joint sets plus random	12	
H. Four or more joint sets, random, heavily jointed 'sugar cube' etc.	15	
J. Crushed rock, earthlike	20	
3. JOINT ROUGHNESS NUMBER	J_r	
a. Rock wall contact and		
b. Rock wall contact before 10 cms shear		
A. Discontinuous joints	4	
B. Rough or irregular, undulating	3	
C. Smooth, undulating	2	
D. Slickensided, undulating	1.5	1. Add 1.0 if the mean spacing of the relevant joint set is greater than 3m
E. Rough or irregular, planar	1.5	
F. Smooth, planar	1.0	2. $J_r = 0.5$ can be used for planar, slickensided joints having lineations, provided the lineations are orientated for minimum strength
G. Slickensided, planar	0.5	
c. No rock wall contact when sheared	1.0	
H. Zone containing clay minerals thick enough to prevent rock wall contact	1.0	

Table 1.5 (Continued)

4. JOINT ALTERATION NUMBER	J_a	ϕ_r (approx.)	
a. Rock wall contact			
A. Tightly healed, hard, non softening, impermeable filling	0.75		
B. Unaltered joint walls, surface staining only	1.0	(25°-30°)	1. Values of ϕ_r: the residual friction angle, are intended as an approximate guide to the mineralogical properties of the alteration products, if present.
C. Slightly altered joint walls non-softening mineral coatings, sandy particles, clay-free disintegrated rock, etc.	2.0	(25°-30°)	
D. Silty-, or sandy-clay coatings, small clay-fraction (non-softening)	3.0	(20°-25°)	
E. Softening or low friction clay mineral coatings, i.e. kaolinite, mica. Also chlorite, talc, gypsum and graphite etc., and small quantities of swelling clays. (Discontinuous coatings, 1-2 mm or less in thickness)	4.0	(8°-16°)	
b. Rock wall contact before 10 cms shear			
F. Sandy particles, clay-free disintegrated rock etc.	4.0	(25°-30°)	
G. Strongly over-consolidated, non-softening clay mineral fillings (continuous, < 5 mm thick)	6.0	(16°-24°)	
H. Medium or low over-consolidation, softening, clay mineral fillings, (continuous, < 5 mm thick)	8.0	(12°-16°)	
J. Swelling clay fillings, i.e. montmorillonite (continuous, < 5 mm thick). Values of J_a depend on percent of swelling clay-size particles, and access to water.	8.0-12.0	(6°-12°)	
c. No rock wall contact when sheared.			
K. Zones or bands of disintegrated or crushed L. rock and clay (see G, H and J for clay M. conditions)	6.0 8.0 8.0-12.0	(6°-24°)	
N. Zones or bands of silty- or sandy clay, small clay fraction, (non-softening)	5.0		
Q. Thick, continuous zones or bands P. of clay (see G, H and J for clay R. conditions)	 10.0-13.0 13.0-20.0	(6°-24°)	

Table 1.5 (Continued)

5. JOINT WATER REDUCTION FACTOR	J_w	approx. water pressure (Kgf/cm^2)	
A. Dry excavations or minor inflow, i.e. < 5 lit/min. locally	1.0	1.0	
B. Medium inflow or pressure, occasional outwash of joint fillings	0.66	1.0-2.5	1. Factors C to F are crude estimates. Increase J_w if drainage measures are installed.
C. Large inflow or high pressure in competent rock with unfilled joints	0.5	2.5-10.0	
D. Large inflow or high pressure, considerable outwash of fillings	0.33	2.5-10.0	2. Special problems caused by ice formation are not considered. Factors C to F are crude estimates. Increase J_w if drainage measures are installed.
E. Exceptionally high inflow or pressure at blasting, decaying with time	0.2-0.1	> 10	
F. Exceptionally high inflow or pressure continuing without decay	0.1-0.05	> 10	
6. STRESS REDUCTION FACTOR	SRF		
a. Weakness zones intersection excavation, which may cause loosening of rock mass when tunnel is excavated			1. Reduce these values of SRF by 25 - 50% if the relevant shear zones only influence but do not intersect the excavation
A. Multiple occurrences of weakness zones containing clay or chemically distintegrated rock, very loose surrounding rock (any depth)	10.0		
B. Single weakness zones containing clay, or chemically disintegrated rock (excavation depth < 50 m)	5.0		
C. Single weakness zones containing clay, or chemically disintegrated rock (excavation depth > 50 m)	2.5		2. For strongly anisotropic virgin stress field (if measured): when $5 \geq \sigma_1/\sigma_3 \leq 10$, reduce σ_c to $0.8\sigma_c$ and σ_t to $0.8\sigma_t$. When $\sigma_1/\sigma_3 > 10$, reduce σ_c and σ_t to $0.6\sigma_c$ and $0.6\sigma_t$, where σ_c= unconfined compressive strength, and σ_t = tensile strength (point load) and σ_1 and σ_3 are the major and minor principal stresses.
D. Multiple shear zones in competent rock (clay free), loose surrounding rock (any depth)	7.5		
E. Single shear zones in competent rock (clay free), (depth of excavations < 50 m)	5.0		
F. Single shear zones in competent rock (clay free), (depth of excavation > 50 m)	2.5		
G. Loose open joints, heavily jointed or 'sugar cube' (any depth)	5.0		3. Few case records available where depth of crown below surface is less than span width. Suggest SRF increase from 2.5 to 5 for such cases (see H)

Table 1.5 (Continued)

b. Competent rock, rock stress problems			
	σ_c/σ_1	σ_t/σ_1	SRF
H. Low stress, near surface	>200	>13	2.5
J. Medium stress	200-10	13-0.66	1.0
K. High stress, very tight structure (usually favourable to stability, may be unfavourable for wall stability)	10-5	0.66-0.33	0.5-2
L. Mild rock burst (massive rock)	5-2.5	0.33-0.16	5-10
M. Heavy rock burst (massive rock)	<2.5	<0.16	10-20
c. Squeezing rock, plastic flow of incompetent rock under the influence of high rock pressure			SRF
N. Mild squeezing rock pressure			5-10
O. Heavy squeezing rock pressure			10-20
d. Swelling rock, chemical swelling activity depending upon presence of water			
P. Mild swelling rock pressure			5-10
R. Heavy swelling rock pressure			10-20

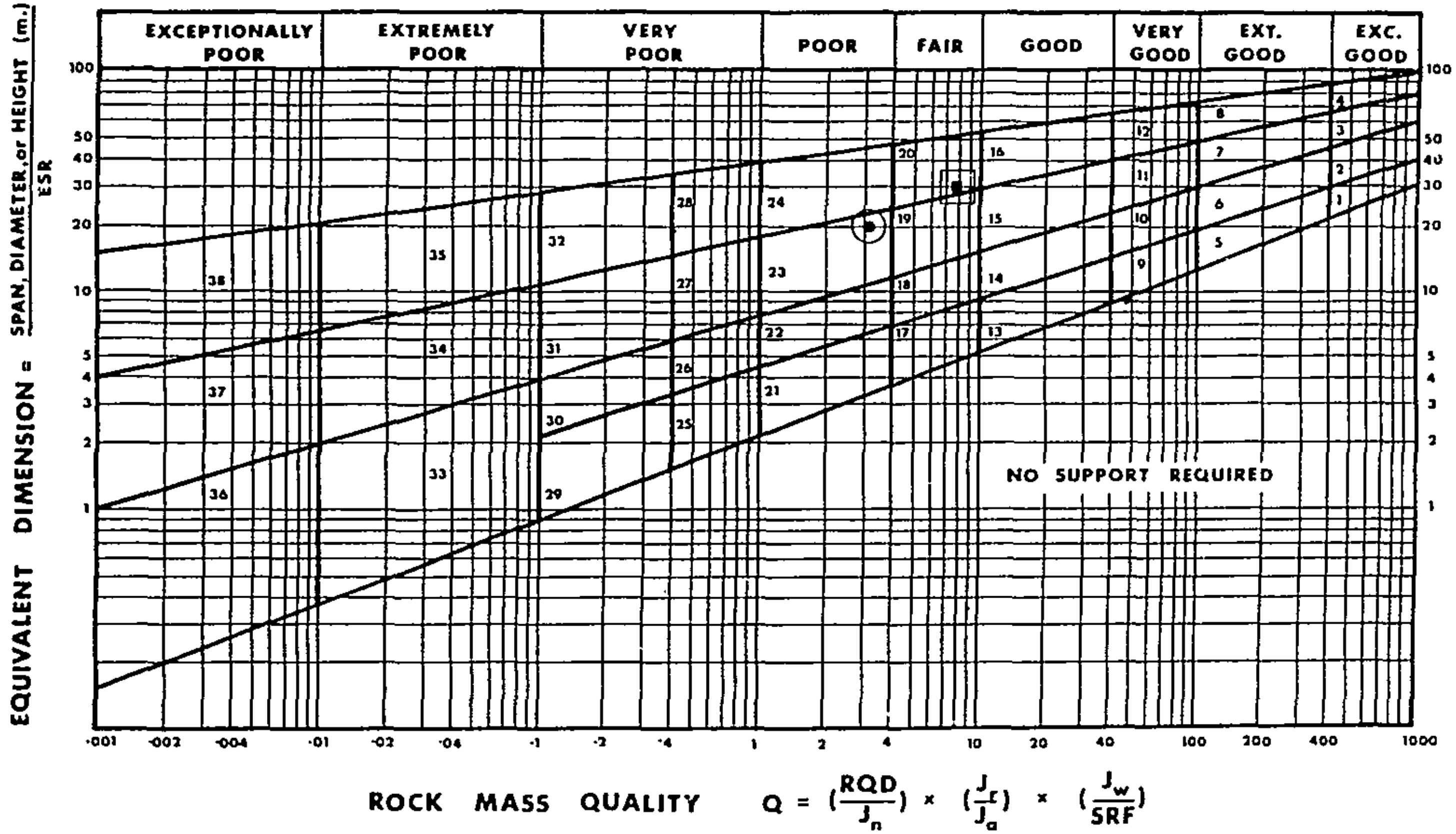

Figure 1.16 NGI tunnel support chart with categories of support [11]

that safe spans predicted could be achieved in practice.

These methods do not relate to the identification or design based on a particular failure mode, nor can they help select shallow opening geometry and proximity to surface. An opening affected by several geological materials is addressed based on the worst conditions. Furthermore, the problem is treated in two dimensions without considering the effect of the span in the third dimension. The NGI method allows the selection of stope dimensions (with or without support required), but the method has been shown to be conservative in regards to minimum critical span of surface crown pillars [58].

The ideal empirical method should be based on failed and unfailed shallow stopes of hard rock mines. Golder Associates [4] developed a three-dimensional empirical method for evaluating surface crown pillar self-stability. A relationship was derived representing stope span (L), stope strike length (S), pillar thickness (t), major discontinuity dip (ψ), and rock unit weight (γ_r) (tons/m^3). This scaled crown span expression (measured in meters) encompassing these parameters derived as

$$C_s = L \left[\frac{\gamma_r}{t\ (1 + L/S)(1 - 0.4\ \cos\psi)} \right]^{0.5} \tag{1.48}$$

was used to plot against rock mass quality, Figure 1.17, for 237 individual pillars.

From this distribution, a "critical span" relationship (between stable and unstable conditions) was obtained which is very similar to the NGI relationship

$$Critical\ Span = 3.3\ Q^{0.43}\ (\sinh^{0.0016}\ (Q)) \tag{1.49}$$

but not the 1976 review [57]:

$$Critical\ Span = 2\ Q^{0.66} \tag{1.50}$$

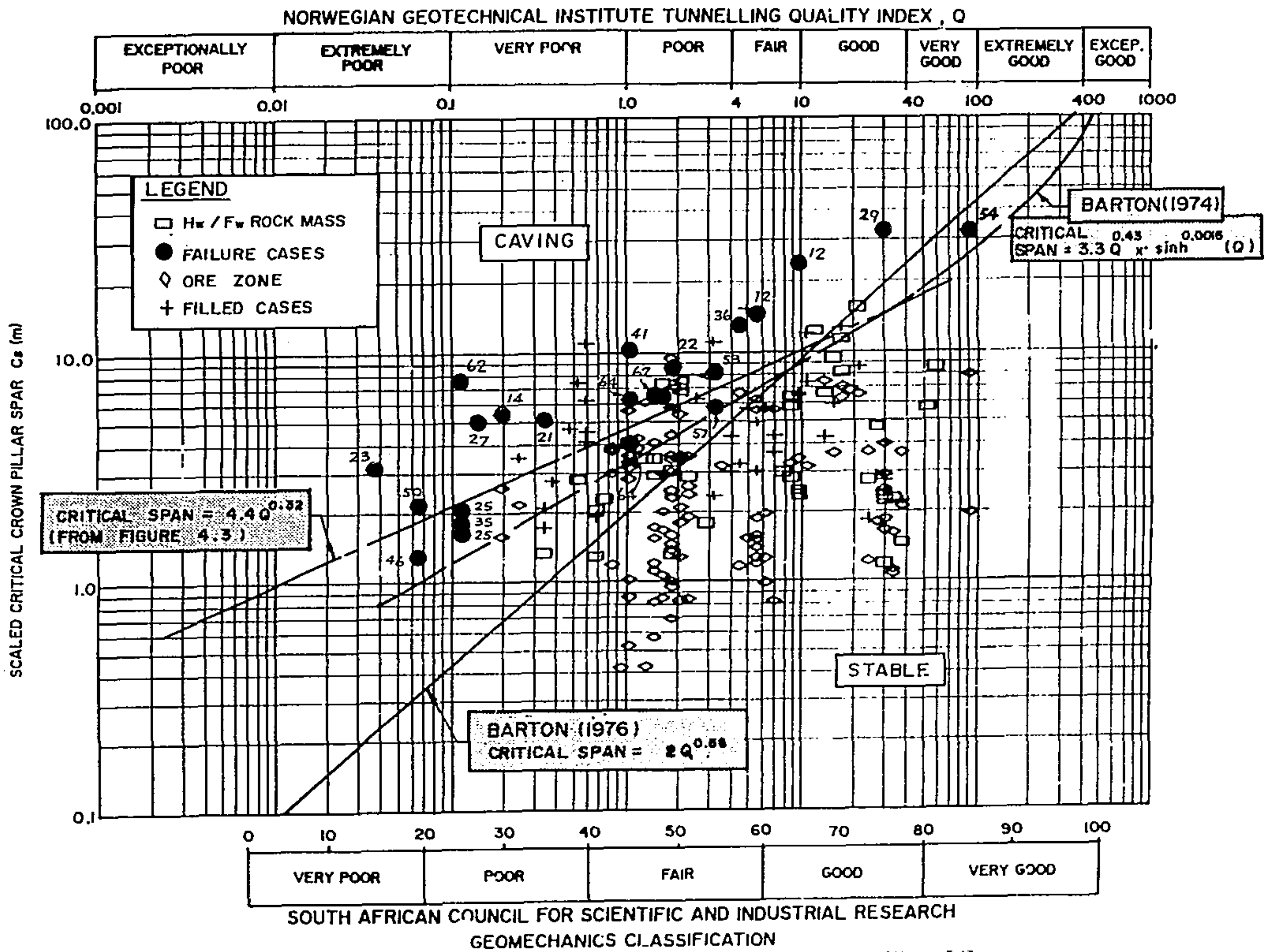

Figure 1.17 Critical empirical span for surface crown pillars [4]

The process to calculate a stable surface crown pillar is to use the chart or equation 1.49 to obtain C_s which is then used to calculate the required span or thickness using equation 1.48 (representing $F_s = 1$).

1.4.3 Block Caving Prediction

Caving can be defined as the uncontrolled break-up and gravitational flow movement of a portion(s) of a rock mass unable to support itself, towards and into an opening.

It becomes especially important to predict such a failure before an unstable opening is created to prevent the mobilization of a great portion of the rock mass over the opening which could lead to surface element such as water inflow from surface bodies of water or rain.

Although a number of authors have studied caving as a field induced process, none have outlined conditions or analytical equations leading to its inception, though it could be argued that minimum conditions to allow caving could be used as maximum conditions for maintaining an integral rock mass.

Coates [45], Bucky [59], and Kendorski [60] discuss field experience with induced caving from which the following parameters controlling caving were listed:

1) rock mass fracturing: caving depends on the effective existence of discontinuities. Blocks of similar shapes formed by persistent fracturing allow for unstable conditions compared to a rock mass composed of interlocked blocks formed by non-persistent fracturing that can key together, maintaining an interlocked rock mass, Figure 1.18.

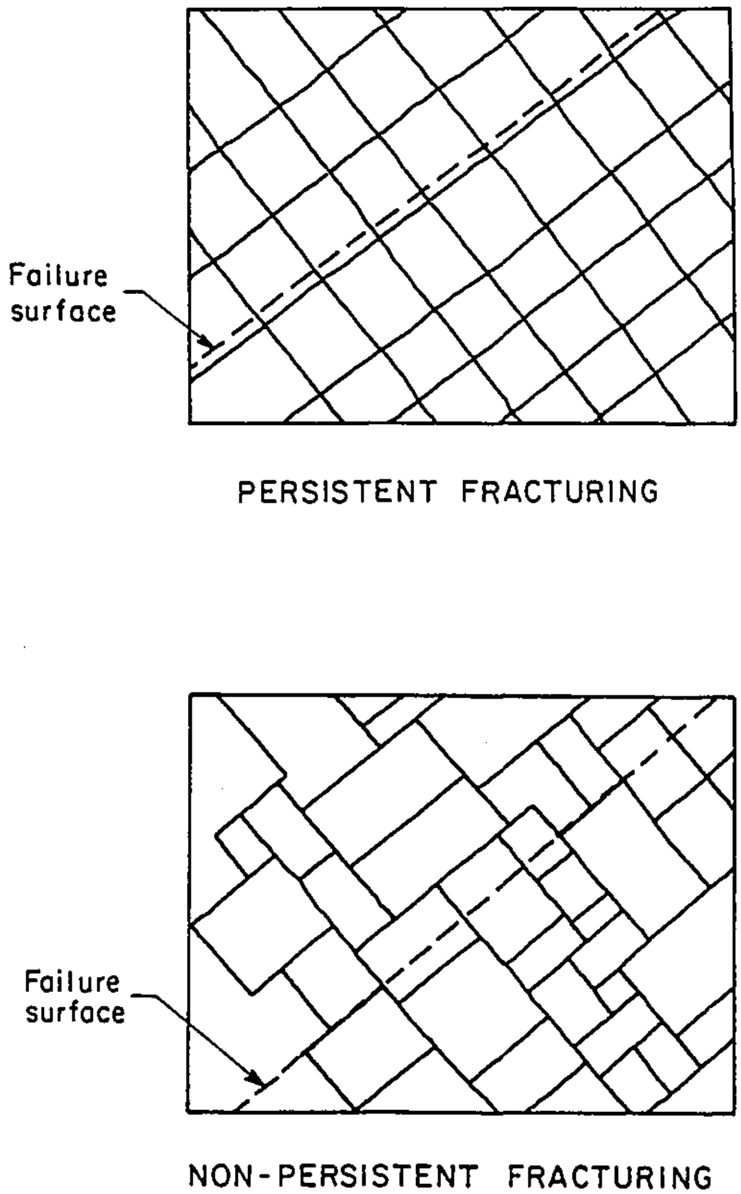

Figure 1.18 Joint continuity and its effects for caving [60].

2) block size: the larger the blocks created by discontinuities are, the better the resistance to caving onset and the better the chance for block interlocking and arching once the mass is mobilized.

3) rock strength: given the stresses imposed on rock blocks within a loosened rock mass, blocks are subjected to compression and shear stresses. Fragmentation of blocks to varying sizes becomes important, thereby depending on compressive strength. Movement of blocks during gravity flow is dependent on block surface cohesion and angle of friction.

4) ground stresses: high lateral stress will prevent general downward rock mass movement by confining rock blocks.

5) span of underground opening: a wider span will prevent effective arching action amongst blocks by forcing a greater tensile stress to a block arch.

Kendorski [60] attributes the start and continuity of caving to a well-developed low dip discontinuity joint set, which if not present, might mean that rock even if vertically jointed may have difficulty to cave.

The physical definition of the initiation of caving is not described in the literature. However, Mahtab and Dixon [61] and Coates [45] have concluded after elastic stress analysis of underground openings increasing in width, that caving may occur under the influence of increasing shear or tensile stress accompanying such larger spans.

No analytical formula for predictability of caving inception or stability of caving activity has been created. Empirical classifications on the other hand have been developed to evaluate the potential for caving based on rock mass quality [62][63].

Diering and Laubscher [63] created a chart to design stope geometries for caving extraction layouts, Figure 1.19. The limiting curves for self-support and caving are based on adjusted Rock Mass Rating values for variations in dip of the orebody and geological structure.

Model studies of sands and grains in silos [64] have found application in predicting the geometry of the flow pattern. This pattern consists of a limit ellipsoid beyond which material will not move and an interior ellipsoid of motion which limits the source of material falling into the stope, replaced by material within the limit ellipsoid, Figure 1.20.

Coates [45] describes the behaviour within the ellipsoid of motion as irrotational where material moves downwards without rotation. The material in the limit ellipsoid rotates as a result of rotation induced by shearing at the boundary of the ellipsoid of motion.

Such flow models, however, are based on flow of relatively uniform material. Therefore, the interlocking effects of blocks of various assortments of sizes might not make the flow ellipsoid concept valid.

The extent of the ellipsoid of motion is given in terms of its eccentricity [64]:

$$\varepsilon = \frac{1}{a}\sqrt{2 + b^2} = \sqrt{\frac{3L^2}{4h^2} - \frac{6V_e+1}{h^3}} \tag{1.51}$$

where

a = semi-major axes of the draw ellipsoid

b = semi-minor axes of the draw ellipsoid

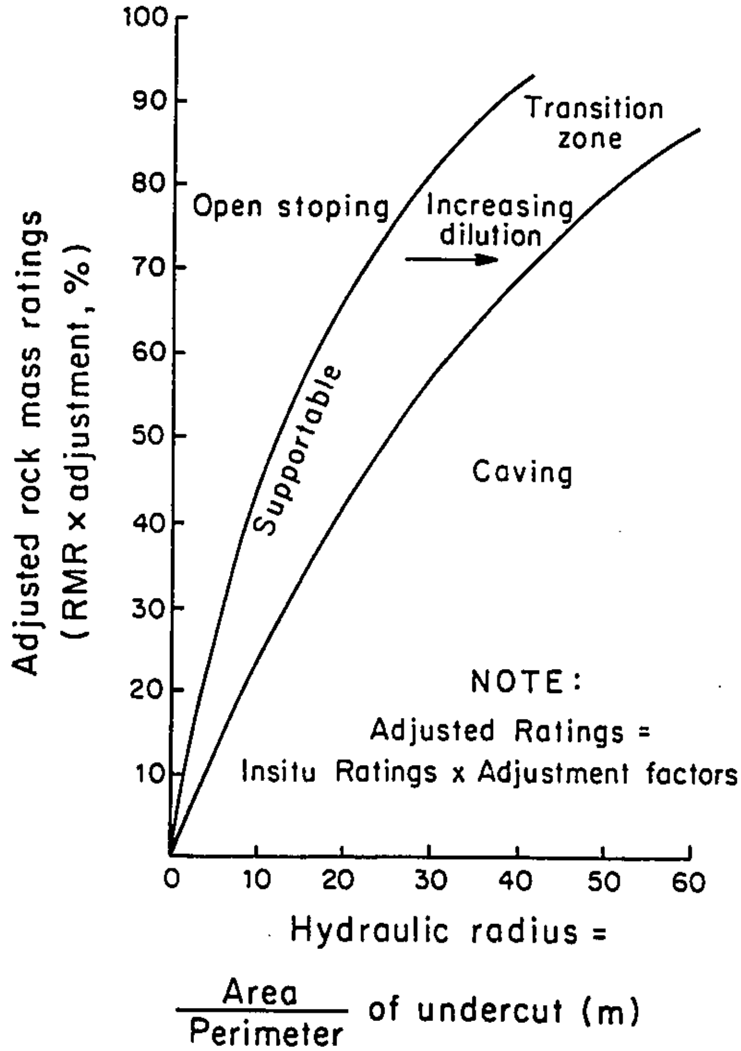

Dip of surface	Adjustment, %
0-30°	80
30-50°	85
50-70°	90
70-80°	95
80-90°	100

Figure 1.19 Caving chart and stability according to rock mass rating [63]

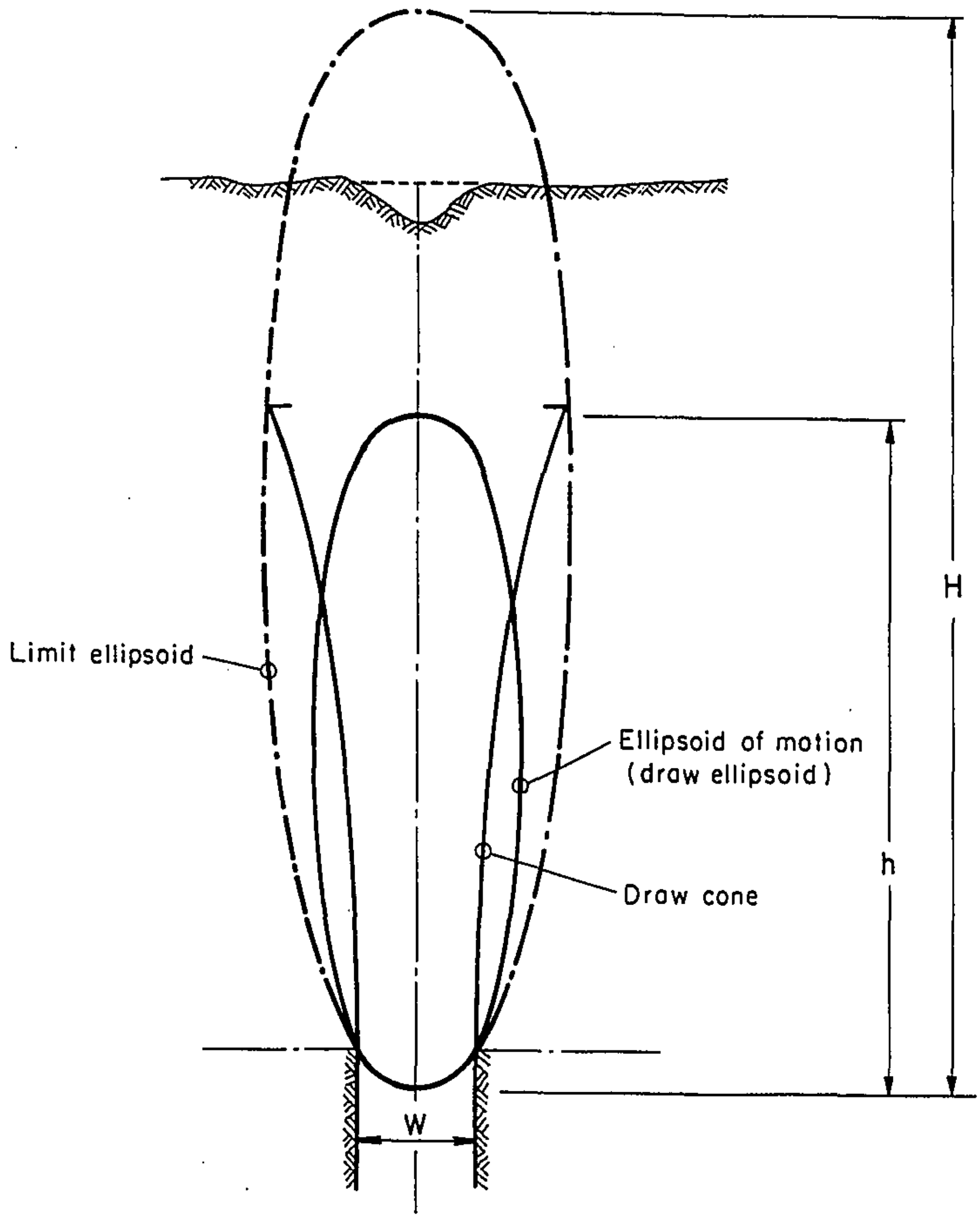

Figure 1.20 Ellipsoid drawing pattern for caved rock [4].

L = stope span

h = height of draw = 2a

V_e = volume of ellipsoid of motion = $\frac{4}{3\pi ab^2}$

1.4.4 Numerical Procedures

The delineation of stress conditions and expected displacements adjacent to and around shallow openings is now possible, given the increasing range of computer modelling programs available. However, few of the codes directly address the complex geometrical characteristics and behaviour modes related to shallow stopes of hard rock mines.

Linear elastic analysis, widely used in 2- and 3-dimensional finite element and boundary element computational codes, can only be considered relevant to provide general stress distribution around shallow openings located in a material(s) behaving in a linear elastic fashion. Tension, or shear failure from imposed stresses, rather than gravity movements, can be obtained given the application of a failure criterion such as the Drucker-Prager [65] or Hoek and Brown [52].

The Hoek and Brown criterion is an empirical approach based on the best fit curve of laboratory generated rock strength (expandable to field strength based on general rock mass quality). It considers major and minor principal stress imposed, and takes into account both compression and tensile modes of failure. The Drucker-Prager yield criterion takes into account triaxial stress conditions but fails to consider any tensile failure. Therefore, the application of this criterion may not be suitable, because of the probability of tensile failures in the near-surface environment.

In one application of finite elements for shallow stopes, results have been shown to be very sensitive to small changes in the m and s Hoek and Brown parameters when these are low, as is the case for rock masses of poor quality [16]. Application of linear elastic finite elements has been performed for shallow stopes, below the Kidd Creek Mine [66] and Thompson [12] open pits, and shallow stopes of variable dips such as the Pierre Beauchemin Mine stopes (45° dip) [67] and the Niobec Mine stopes (90° dip) [68]. A boundary element code has been used for stopes below the Ruttan Mine open pit [15].

Large strains imposed to rock leading to rock block movements or large rock mass strains occur during the failure of shallow stopes. Large displacements have been modelled for shallow stopes in blocky environments of abandoned mines by Golder Associates [4] and Picciaccia et al [69] for the Pamour Mine, using the UDEC distinct element code. Such codes allow for a 2- or 3-dimensional analysis of blocks making up a rock mass. Flexibility in selecting individual or generalized block geometry is possible. Application of the 2-dimensional version is usually not representative of complex 3-dimensional geometrical effects; however, many 3-dimensional programs are difficult to use for such cases. Multiple trials of 2-dimensional analysis are therefore usually relied on to provide indications of sequences of block movements.

Large strain models using the ADINA code have also been used to model movements in altered rock environments, at the Selbaie Mine [70] and the Gays River Mine [19].

1.5 OBJECTIVES

The general purpose of carrying out this research program is to improve the methods mine operators currently use to secure shallow stope mining activity and reduce future stope stability problems. This might ultimately enhance the safety of workers and the viability of mining.

Six specific objectives have been defined for this thesis. The first is to frame the situations in which failures of such stopes become possible, i.e. how and why failures occur. This entails establishing the rock environment types in which hard rock mine stopes are commonly located, classifying the variety of failure mechanisms which can and have occurred in each type, and identifying the geomechanical parameters associated with the development of the failure types.

The second objective is to contribute to rock mechanics knowledge by developing concepts and appropriate analytical equations hitherto non-existent for individual failure mechanisms common to shallow stopes of hard rock mines. These are meant to be practical and useable for the practitioners in industry. For the first time failure-specific, rather than global surrounding behaviour will be evaluated.

The third objective is to employ and evaluate numerical modelling as a design tool for shallow stopes of hard rock mines. Close simulation of the rock mass, mining geometry, and in situ loading conditions will be followed for the selection of particular numerical codes.

The fourth objective is to back-analyse well-known, but unresearched, failures of shallow stopes to identify the geomechanical conditions which led to failure, and rate the analytical, numerical and empirical design approaches according to their effectiveness in predicting the type of failure that occurred.

The fifth objective is to develop case studies of active mines that are planning to create or expand shallow stopes. This will address several different needs. It will complement the information obtained from known failure cases (which represent limit equilibrium). Supplemental rock masses of varying properties will afford a range of factors of safety for each type of failure analyses. In this sense a databank of cases becomes available to develop concepts and ranges of stability as well as failure for mine operators and future research. The opportunity will thus exist to measure the effects of particular rock mass parameters on the sensitivity of the various analyses. General conclusions about the geomechanical parameters controlling failure can be obtained.

The operators of each mine will have indications on the possible failure mechanism(s) anticipated and limitations to the extraction planned to avoid stope failure. Furthermore, some basis will exist for the selection of ground support and monitoring techniques.

Access to the site will allow the studying of existing conditions, quantifying of stability parameters and performing of laboratory and field measurements, to provide precise data to the analyses. Design will be based on an integrated approach, using the developed analytical equations, numerical modelling, and empirical methods. In this fashion, the suitability of each approach will be evaluated.

The final objective is to recommend design approaches for specific rock mass environments and expected failure mechanisms. The geometry and depth of stope would also be considered.

CHAPTER 2

DEVELOPMENT OF ANALYTICAL METHODS

This Chapter outlines mechanical representations of the common failure mechanisms identified in Chapter 1. Each mechanism is distinct from the other and represents an elementary form of failure. Each mechanical behaviour is formalized into a limit equilibrium equation. This follows the common geomechanical factor of safety approach to compare the influences of loads against the capacity of the rock mass to resist movement.

Although a limit equilibrium approach simplifies the problem to one of strength relationship without considering deformation, when properly defined, it can represent a rigorous analysis that is usually adopted as a norm in rock mechanics [30].

These analytical equations consider the redistributed ground stresses caused by and around the shallow stopes. This allows for their application to any particular situation. Numerical modelling is used to generate redistributed stress conditions from known natural stress distribution and stope geometry. This is a sophisticated method which provides not only a realistic stress distribution for any given problem, but also represents a good quantification of values which, when combined to the well-defined values for the other equation parameters, will yield an accurate representation of stability conditions. Current field and laboratory tests can provide equation parameters as accurate as the stress values returned by numerical modelling. It is left to the users of these equations to perform the appropriate in situ and lab tests to obtain the most representative and accurate parameters for application of the equations and numerical modelling. Major efforts in this direction is crucial for determining stability based on accuracy, completeness of data and range of parameter values.

The following broad lines of failure mechanisms and sub-types, presented in Chapter 1, will be developed analytically:

1) plug failure

2) ravelling failures (block falls; block slides)

3) strata failure

- intact strata (multiple and single layers)

- voussoir arching

4) chimneying disintegration

5) block caving

These analyses are outlined for self-supported openings, i.e. no artificial ground support is considered. This allows for a full comprehension of the mechanics of the problem, and for a proper consideration of the location and type of artificial ground support to be applied.

2.1 PLUG FAILURES

The plug failure mechanism affecting surface crown pillars of shallow underground openings involves the displacement of a large single block ("plug") downward during failure, driven by gravitational loading. Movement takes place on well-defined discontinuities bounding the block in three dimensions and extend from the opening upward to the top of bedrock.

The analytical equation developed here will consider the following issues:

1) The confinement stresses, σ_x' & σ_y', considered in Hoek's [21] approach are based on the linearly distributed natural, pre-opening ground stress values.

   A more representative consideration would be to use the redistributed stresses in the rock mass around the opening, once it has been created. These changes in direction and value from the natural ground stresses depend on the depth, size and geometry of the opening and relationship to others, the materials' moduli of elasticity, Poisson's ratio and unit weight as well as the properties of the natural stress field. The confinement stresses to be considered in the analysis must therefore be based on resultants of the redistributed stress field portion acting on the discontinuities where the block can potentially fail. It is conceivable that such resultants may in part be tensile (effectively adding no normal stress to the discontinuity) rather than only compressive which is anticipated by the Hoek analysis.

2) A potential failure block can originate within or as all of the surface crown pillar. This must be expected in light of the stress variations within the surface crown pillar and the presence of failure surfaces that can exist within it, not just at its boundary.

3) A block can fail on a number of large failure planes (if they exist or can be created by shearing), a minimum of three to define a three-dimensional block [30].

4) Plug failures commonly occur on continuous failure surfaces, usually defined by large-scale discontinuities such as faults, well-developed rock fabric (bedding, foliation, etc.) or large joints. It is unreasonable to expect that a rock mass of higher quality with few, if any, properly oriented weaknesses will fail in this fashion. Although a condition where some solid rock shearing is possible, shearing of large

quantities of intact rock is not representative of the problem as it usually presents itself.

A failure analysis should, however, be capable of considering both shearing on a discontinuity and rock bridges occurring across them. Strength properties of joint surfaces are not implicitly included in Hoek's [21] analysis, considered only qualitatively in the RMR rating employed. Specific and quantitative details, on fault and fabric shear strength and infilling properties for example, are worth considering.

Some of the commonly-used shear failure criteria, such as the Mohr-Coulomb

$$\tau = c + \sigma_n \tan \phi \tag{2.1}$$

where

ϕ = internal angle of friction of the rock material

σ_n = normal stress imposed on the sheared surface

τ = shear strength of the surface

c = cohesion of the discontinuity surface

the Newland and Allely [71],

$$\tau = c + \sigma_n \tan (\phi + i) \tag{2.2}$$

where

i = average angle that joint surface asperities make with the plane of the discontinuity

the Ladanyi and Archambault [72],

$$\tau = \frac{\sigma_n(1-a_s)V + \tan\phi + a_{sr}}{1-(1-d_s)\ V \tan\phi} \tag{2.3}$$

where

a_s = ratio of the sum of areas of sheared asperities to the total sample area

V = the rate of dilation at the instant of peak shear strength

a_{sr} = shear strength of the intact rock (asperities) and the Barton [73] criterion

$$\tau = \sigma_n \tan \left[JRC \log_{10} \left(\frac{JCS}{\sigma_n} \right) + \phi_r \right] \tag{2.4}$$

where

JRC = roughness of the joint, on a defined scale

JCS = compressive strength of the joint surface

ϕ_r = angle of friction of the joint surface defined by the basic internal angle of friction factored to reflect joint surface properties (asperity and infilling)

indicate that shearing strength of discontinuities is primarily influenced by the cohesion, the internal angle of friction, including the asperity (roughness) of the discontinuity surface.

Wide discontinuities which allow plug failures to occur must take into consideration the effects of joint properties, asperities, surface profiles, and infilling on strength of surfaces meters to tens of meters in size.

Barton and Bakhtar [74] in their review of the effects of joint properties on large scale strength of discontinuities concluded that small scale discontinuity topology has small effects on the very large size joint shear strength.

The roughness effects on joint shear strength decrease substantially as discontinuity size increases, according to Patton [75]. Small size irregularities are ignored when estimating the i value on a tens of centimetre scale; only the asperity angle of the larger irregularities is, Figure 2.1. This is also seen in tests to determine JCS and JRC for larger size joints, Figure 2.2. Therefore, the asperity component added to the basic angle of friction of the joint surface can be substantially reduced. On a scale of several meters involved in the shear strength of surfaces with potential plug failures, it is reasonable to

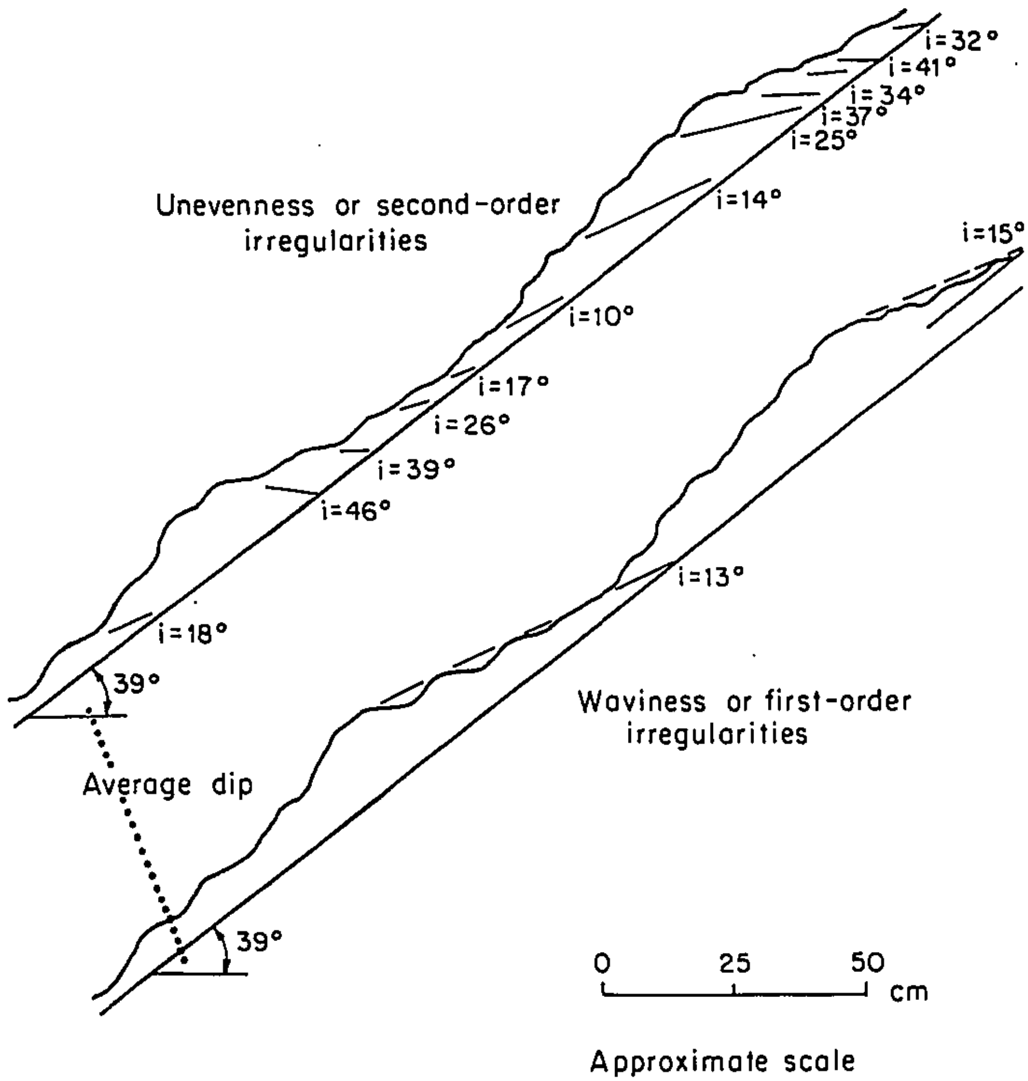

Figure 2.1 Reduction in asperity importance with larger scale [74].

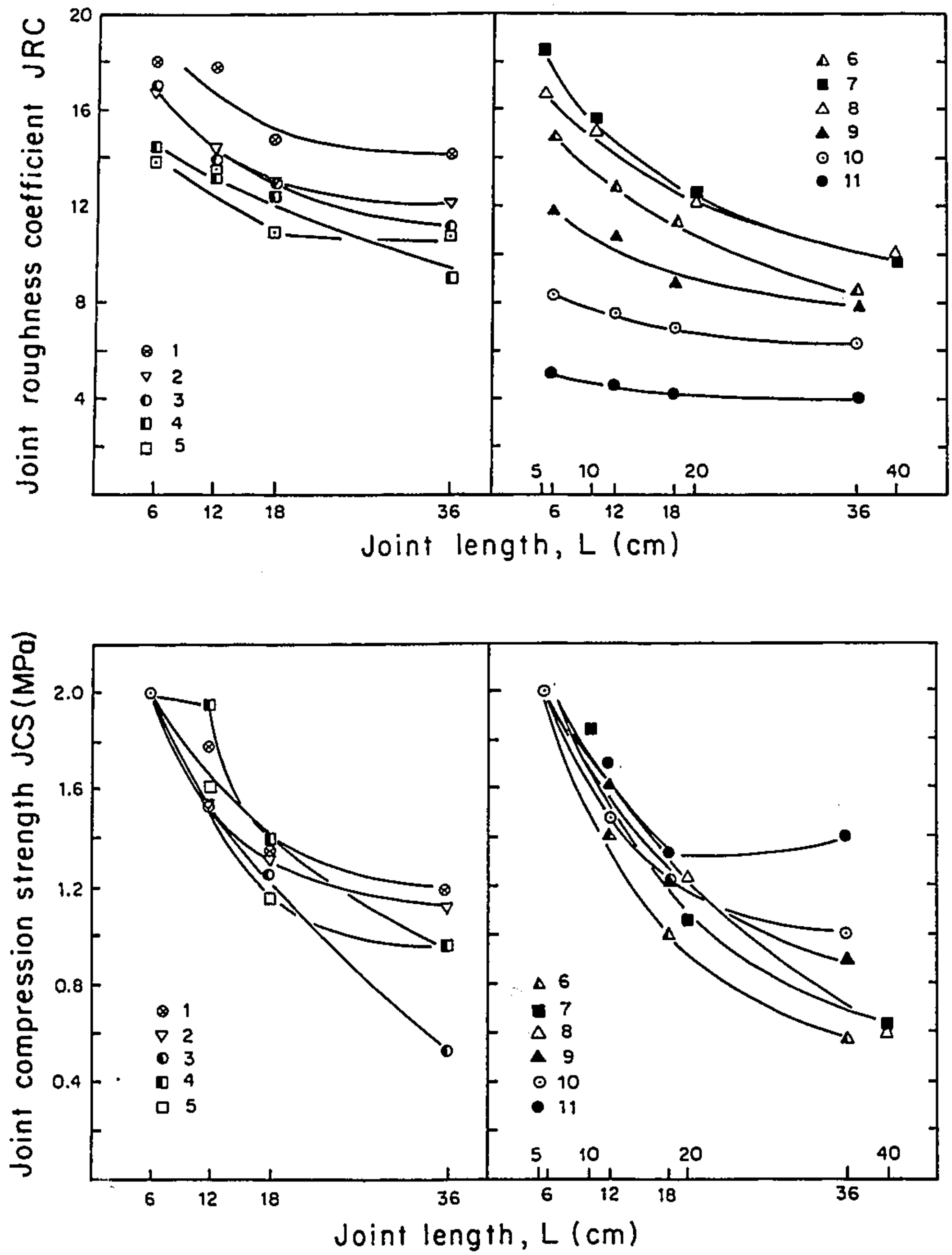

Figure 2.2 Larger scale effects on Barton shear criterion JCS and JRC [74].

discount the asperity component and adopt a simple shear failure criterion such as the Mohr-Coulomb criteria to describe the potential for plug failure which only relates cohesion and internal angle of friction of the discontinuity surface as direct shear strength parameters. The composite angle of friction for joint surface (including wall and coating) should be used to represent the discontinuity angle of friction value.

The equation to calculate the factor of safety against downward sliding by gravity of a block defined by vertical joints can be generally defined by

$$F_s = \frac{forces\ resisting\ movement}{forces\ inducing\ movement} \tag{2.5}$$

The components involved in calculating this factor are total shear resistance, total weight, and effects of groundwater in reducing shear resistance.

The shear resistance from each side of the plug defined by vertical sides is

$$c_i + \sigma_{ni} \tan \phi_{ri} \tag{2.6}$$

where

c_i = cohesion along the discontinuity forming the i^{th} side

σ_{ni} = normal stress on i^{th} side

ϕ_{ri} = angle of friction of the i^{th} discontinuity surface

This contributes to resisting the downward force of the plug given by its weight

$$W = V\rho g \tag{2.7}$$

where

V = volume of block

ρ = mass density

g = constant of gravity

Brady and Brown [30] have shown that groundwater pressure distribution on the i^{th} side between the top of the water table and the stope roof Z_i' follows a parabolic water pressure distribution, Figure 2.3.

The total pressure over this distance, for a 1 m wide side is

$$\frac{Z_i'^2 \gamma_w}{3} \tag{2.8}$$

or from the top of the block

$$\frac{(H_i - d)^2 \gamma_w}{3} \tag{2.9}$$

where

H_i = vertical distance from surface to the bottom of the i^{th} side

γ_w = unit weight of water

d = depth to the water table

The normal stress imposed on each block side can be obtained by using the actual, redistributed ground stresses which exist around the shallow stope. Numerical modelling can provide these stresses through the elements located at the exterior boundary of the block. Transformation of the principal stresses for each element will provide the normal component and shear component in contact with the block side; in two dimensions:

$$\sigma_{nj} = \left(\frac{\sigma_1 + \sigma_3}{2}\right) + \left(\frac{\sigma_1 - \sigma_3}{2}\right)\cos 2\alpha \tag{2.10}$$

$$\tau_{nj} = -\left(\frac{\sigma_1 - \sigma_3}{2}\right)\sin 2\alpha \tag{2.11}$$

where

σ_1, σ_3 = modelling element major and minor principal stresses respectively

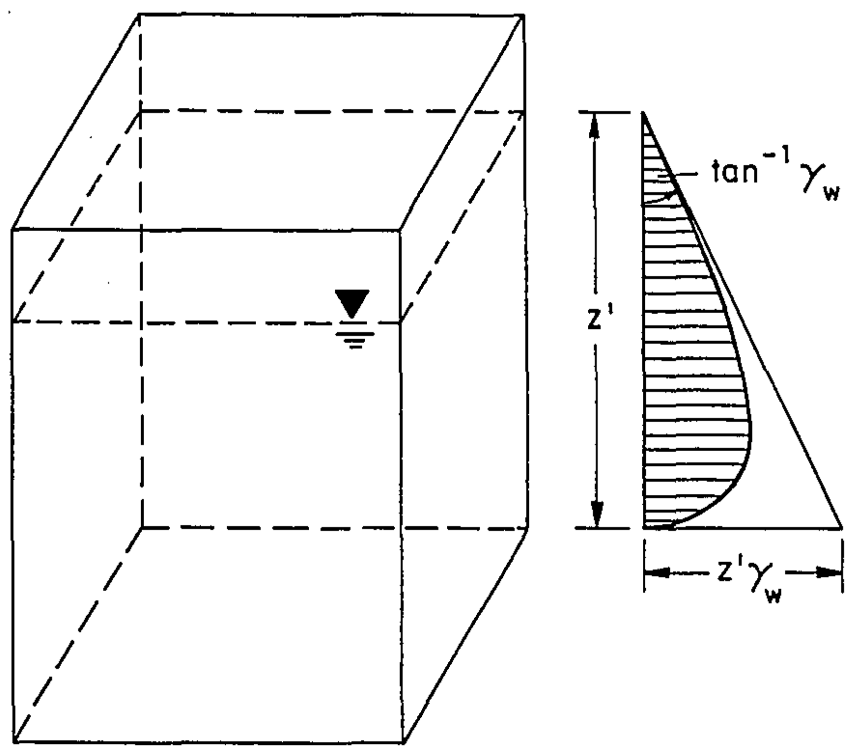

Figure 2.3 Parabolic water pressure distribution between surface and top of shallow stope [30].

σ_{nj} = stress normal to block surface

τ_j = shear stress parallel to block surface

α = angle between the plane on which σ_1 acts and the block surface, positive counterclockwise from the σ_1 plane.

Transformation of principal stresses in three dimensions to normal stress along one of the three axes used to define the model (e.g. y vertical, x and z horizontal) is performed using the direction cosines, l, m, and n, representing the cosine of an angle between a major principal stress direction and the direction along one of the three reference axes [76]:

$$\sigma_n = \sigma_1 \, l^2 + \sigma_2 \, m^2 + \sigma_3 \, n^2 \tag{2.12}$$

where

σ_n = resultant normal stress along reference axis x, y or z
σ_1, σ_2, σ_3 = modelling element major, intermediate and minor principal stresses
l = cosine of angle between x, y or z, and σ_1
m = cosine of angle between x, y or z, and σ_2
n = cosine of angle between x, y or z, and σ_3

The sign convention follows rock mechanics usage, compression is positive and positive shear stress produces a clockwise rotation about a point taken inside the infinitesimal stress element.

The normal component provides a resisting shear force which when added to the normal components of the other elements provides the total normal shear resistance for each side. This must also be added to the cohesion along the block side.

The normal force imposed by the in situ stress for each side is

$$\sum_{i=1}^{n} \left(\sum_{j=1}^{m} \sigma_{nj} \, A_j \right) \tag{2.13}$$

where

σ_{nj} = normal stress imposed for the j^{th} element of one block side

A_j = area of each model element (length times unit width for 2D)

j = j^{th} element of m elements for one side

i = i^{th} of n block sides

The equation to calculate the factor of safety against downward falling by gravity of a plug defined by vertical joints or joints dipping outward (giving the block a wedge shape) so that the block can fall into the stope, is composed of shear resistance provided by the imposed normal forces induced by the in situ stresses and the cohesion along the surface, divided by the driving force of the block, its weight plus the downward force provided by the force in the case of a block with non-vertical, dipping sides (Brady and Brown [30] in analysing the peripheral stability of a triangular block in this fashion include the downward vertical component of the normal force into the equation to satisfy equilibrium):

$$F_s = \frac{\sum_{i=1}^{n}\left(c_i A_i + \left(\left(\sum_{j=1}^{m} \sigma_{nj} A_j\right) - \frac{\gamma_w (H_i-d)^2 b_i}{3}\right)\tan\phi_{ri}\right)\sin\psi_i}{V\rho g + \sum_{i=1}^{m}\left(\left(\sum_{j=1}^{m} \sigma_{nj} A_j\right) - \frac{\gamma_w (H_i-d)^2 b_i}{3}\right)\cos\psi_i} \tag{2.14}$$

Where

ψ_i = dip of the i^{ith} block side

b_i = width of the i^{th} block side

When cohesion is zero and ϕ_r is greater than ψ_i the shear force component provided by the confining stress on this side will not be sufficient to contribute to resist the downward force [30]. This side then is not available for clamping and should not be included in the summation. Should two adjoining sides of a four sided block be subject to this condition, plug failure is assured.

The possibility that a plug may slide into a stope on an inclined surface must also be examined. In this case sliding can be assumed to occur only if the block side opposite the sliding side is of equal or lesser dip and the dip of the other sides are vertical or towards the stope periphery.

To avoid the geometric complications of resultants of 3D force vectors acting in one sliding direction, the sliding plug analysis will be limited to one sliding side, an opposite side with the same strike but lesser or equal dip, and two other sides, parallel, vertically dipping with strike orthogonal to the dipping sides.

The limit equilibrium equation of such a sliding plug becomes

$$F_s = \frac{c_s A_s + \left(\left(\sum_{j=1}^{m} \sigma_{nsj} A_{sj}\right) + V\varrho g \cos\psi_s - \frac{\gamma_w (H_s - d)^2 b_s}{3}\right) \tan\phi_{rs}}{V\varrho g \sin\psi_s + \left(\sum_{j=1}^{m} \sigma_{n2j} A_{2j} - \frac{\gamma_w (H_s - d)^2 b_s}{3}\right) \sin(\psi_s - \psi_2)} +$$

$$\frac{c_2 A_2 + \left(\left(\left(\sum_{j=1}^{m} \sigma_{n2j} A_{2j}\right) - \frac{\gamma_w (H_s - d)^2 b_2}{3}\right) \cos(\psi_s - \psi_2)\right) \tan\phi_{r2}}{V\varrho g \sin\psi_s + \left(\sum_{j=1}^{m} \sigma_{n2j} A_{2j} - \frac{\gamma_w (H_i - d)^2 b_2}{3}\right) \sin(\psi_s - \psi_2)} +$$

$$\frac{\sum_{i=3}^{4} \left(c_i A_i + \left(\left(\sum_{j=1}^{m} \sigma_{nij} A_{ij}\right) - \frac{\gamma_w (H_i - d)^2 b_i}{3}\right) \tan\phi_{ri}\right)}{V\varrho g \sin\psi_i + \left(\sum_{j=1}^{m} \sigma_{n2j} A_{2j} - \frac{\gamma_w (H_i - d)^2 b_i}{3}\right) \sin(\psi_s - \psi_2)} \qquad (2.15)$$

where

s = subscript indicating strength parameters of the side on which the block slides

ψ_s = dip of side on which the block slides

ψ_2 = dip of plug side opposite sliding side

If a two-dimensional approach is used, the elements are assumed to have unit thickness. In this instance the opening is very long in the 3rd dimension and plane-strain conditions assumed to exist. If this clamping force resultant on the failure surface in 2-D is sufficient, analysis may not require consideration of the third-dimension surfaces. When the block's plan dimensions are similar, a complete three-dimensional limit equilibrium analysis is necessary using 3-D modelling. In this case the three directional cosines of each model element of each plug surface must be used to calculate the normal stress imposed by each element and calculating the resultant over each surface as the normal stress component of equations 2.14 or 2.15.

The drawback of this plug failure approach is that it is computationally intensive in considering the conversion of stresses for each relevant mesh element to shear and normal stress effects. However, it affords a detailed analysis and close geometric representation of each plug failure problem and uses a representative problem-specific stress condition on potential block sliding surfaces. The equation can, however, be simplified by using the stress distribution preferred by the user.

2.2 BLOCK RAVELLING FAILURES

Field observations indicate that failures in the crown of underground openings (by ravelling or weak rock material failure) is commonplace when critical spans are exceeded.

Indeed, ravelling may even extend to the hangingwall and/or footwall, and lead to new cavities after continuous rock falls or block slides (from blocks defined by a minimum of three joints [30]).

Stable cavities imply that the rock mass is capable of sustaining compressive thrust through the peripheral blocks which effectively redistributes the weight of the blocks and imposed stresses to the sides of the openings, while resisting the shear stress between blocks. Continuous development of ravelling to surface can proceed if the material properties and/or lateral stresses are insufficient to stabilize it, leading to a possible failure of a shallow stope.

Effective weight transfer may not develop in rock masses that are sufficiently weak to cave, section 1.4.3, involving general flow of rock within the rock mass beyond the peripheral area of the opening. The weight transfer process becomes more efficient as the size of rock blocks increases, where in such rock masses larger unsupported spans are possible before ravelling leading to a stable cavity occurs [45].

To date no limit equilibrium method exists to calculate the factor of safety or expected cavity location and (dome) shape that can develop from block falls given the span of an opening, its rock mass properties, and the ground stress conditions. A limit equilibrium between forces has been outlined by Brady and Brown [30] but only for an isolated triangular block, falling from the periphery. This method does not calculate ultimate cavity growth for a rock mass based on imposed stresses, considers restraining forces rather than existing stresses, and does not consider other block shapes.

As well, the mechanics of sliding blocks at the periphery of a rock mass has not been addressed. In the approach used here, the physical development of crown and periphery ravelling involves the progression of parallelepiped block falls and/or slides from the immediate stope surroundings until the state of ground stress is such to provide a limit equilibrium to each block, i.e. the block weight is supported by clamping from the ground stress. Regardless of the geometry of a block, it will remain in place when the component of the shear resistance mobilized at the sides of the block exceeds the block's weight imposed shear stress.

The approach to limit equilibrium is based on the sum of the forces in the direction the weight is acting, written in factor of safety form

$$F_s = \frac{\Sigma V}{W} \tag{2.16}$$

where

W = block weight

ΣV = sum of shear force resistance in the same line of action as block weight

In this approach, the tangential stress at the stope periphery is used as the clamping stress that may or may not be sufficient to allow a block to fall or slide from the periphery. Block falls and block slides were defined by Brady and Brown [30] and Hoek and Brown [52] using stereographic projections. The former occur when blocks are defined by discontinuities which enclose a vertical line (center of the projections), Figure 2.4a, Figure 2.5. In this case the block drops out of the rock mass without sliding. If this line lies outside the intersecting discontinuities, a block may slide if its sliding surface or intersection of surfaces dips more than the block surface's angle of friction ϕ_r, Figure 2.4b, Figure 2.5.

The analyses developed here to obtain a stable cavity outline is two-dimensional. Only two joint families making up the block will be used, in a given plane, to analyze the

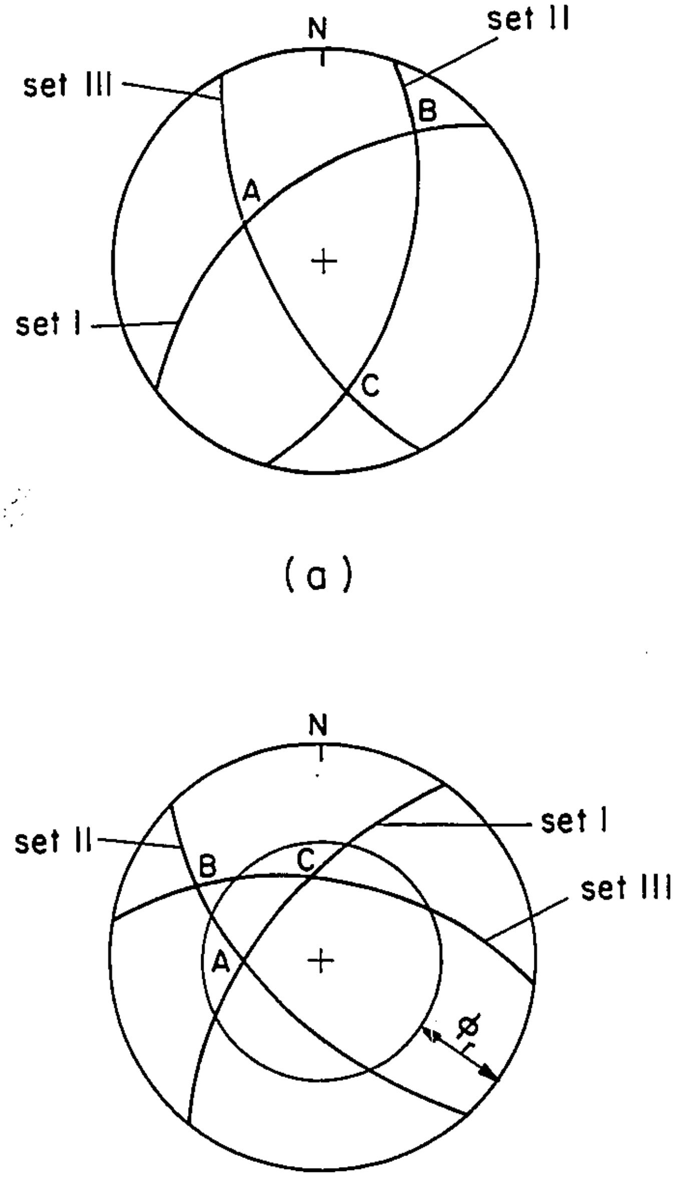

(b)

Figure 2.4 Stereographic conditions for a block fall and block slide [30].

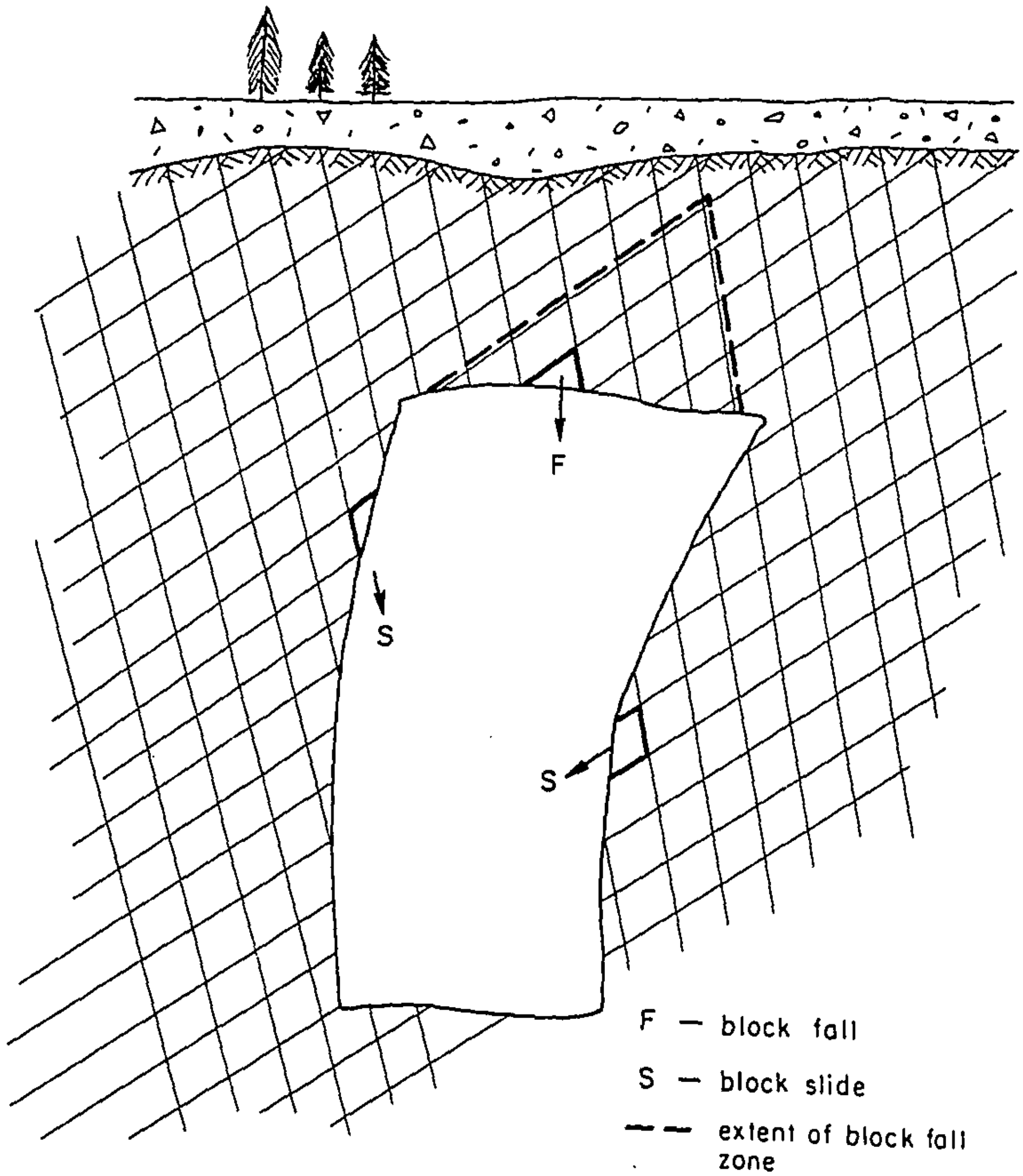

Figure 2.5 Disposition of block at stope periphery for ravelling analysis.

stability of a block, the third joint family assumed to be parallel to the plane of the problem at unit width spacing and offering no shear resistance. This simplified approach is therefore conservative but has been utilized commonly by other authors [30] [77] in analytical and numerical analysis. A three-dimensional analysis would increase complexities significantly and would not respect the objective to provide operators with simple methods of analysis.

This joint distribution implies that the rock mass is composed of parallelepiped blocks. The method could be expanded to include more joint families. By describing block geometry using representative joint family spacing, joint surface properties, and joint orientation, all geometrical and mechanical aspects are defined. The block is considered rigid (no deformations) and the block surfaces respect the Mohr-Coulomb failure criterion which for a tens of centimetre scale incorporates roughness and joint infilling effects represented by an angle of friction ϕ_r for the block surface, equation 2.4.

The procedure to calculate the extent of the cavity that will be produced by ravelling blocks is a process with two consecutive analyses. Since block falls would occur from the periphery before block slides (Figure 2.5), the procedure is to first analyze for block fall extent (if the conditions outlined in Figure 2.4a exist), then to analyze for block slides if falling blocks occur at the crown, and at the periphery.

It is conducted as follows:

1) The block weight is calculated from the spacing for each joint family to supply the block area which is multiplied by unit thickness; this will be multiplied by unit weight.

2) In the case of a block fall only the upper two of the block's four sides will be used as contact surfaces on which tangential stress acts, Figure 2.6. These are intersecting sides that are assumed to be in contact with the rock mass whereas the other two sides form part of the boundary surface.

3) In the case of a block slide, three surfaces in contact with the rock mass are used in the analysis, assuming one non-sliding surface forms part of the cavity boundary surface.

4) For ravelling to be continuous in the crown, block slides will occur after block falls, given that joints are not vertically oriented in which case only block falls occur.

5) The geometrical information is input in the limit equilibrium equation to represent the block ravelling type existing at that location of the periphery, and the value of the tangential stress at that location of the periphery necessary to provide support shear stress is calculated for a given location of stope boundary.

6) This value is compared to the tangential stress existing at the opening periphery, as returned by the numerical modelling which is run with the desired stope shape. Where this tangential stress is less than required, ravelling would occur. This will be the condition until sufficient stress levels exist to maintain an integral rock mass. The locations where compressive stress is just sufficient to clamp the blocks (F_s = 1) represent the expected stable cavity outline formed after ravelling. The final shape of this outline is compared to the bedrock boundary to evaluate for stope failure. In reality, numerical modelling should be redone progressively to confirm that tangential stresses with this expanded stope outline conform to the stress levels required. This is a process requiring computing time which is made easier by

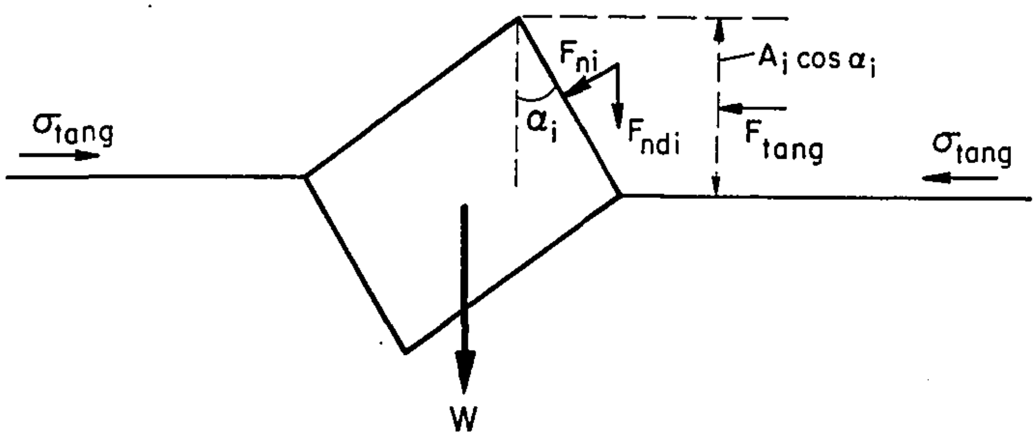

Figure 2.6 Stress distribution on ravelling, falling block.

constructing the modelling mesh in a fashion which can approximate the irregular periphery when elements are removed to represent ravelled blocks.

The analysis of a block fall is shown in Figure 2.6. The peripheral stress is first decomposed into a force acting on a vertical projection of the block side

$$F_{tang} = \sigma_{tang} A_i \cos\alpha_i \tag{2.17}$$

where

α_i = internal block angle between vertical and the i^{th} block face

σ_{tang} = tangential stress at the periphery of the opening

A_i = area of i^{th} side (length for 1 m unit width)

The component of that force normal to the block face is

$$F_{ni} = (\sigma_{tang} A_i \cos\alpha_i) \cos \alpha_i \tag{2.18}$$

The shear force resistance along a block face imposed by the tangential stress is, using the Coulomb criterion

$$c_i A_i + \sigma_{tang} A_i \cos^2\alpha_i \tan \phi_{ri} \tag{2.19}$$

where

c_i = cohesion on i^{th} block face

ϕ_{ri} = angle of friction of i^{th} block face

The vertical shear force component resisting block weight is

$$\sum_{i=1}^{2} V_i = \sum_{i=1}^{2} \left(c_i + \sigma_{tang} \cos^2\alpha_i \tan\phi_{ri}\right) A_i \cos\alpha_i \tag{2.20}$$

Brady and Brown [38] in analysing a triangular block in this fashion include the downward vertical component of the normal force

$$F_{ndi} = (\sigma_{tang} A_i \cos^2\alpha_i) \sin\alpha_i \tag{2.21}$$

in the equation to satisfy static equilibrium

$$W + \sum_{i=1}^{2} A_i\sigma_{tang}\cos^2\alpha_i\sin\alpha_i = \sum_{i=1}^{2} \left(c_i+\sigma_{tang} \cos^2\alpha_i\tan\phi_{ri}\right) A_i \cos\alpha_i \tag{2.22}$$

where

W = weight of the block

A_i = length of the block's i^{th} side (unit length, 3rd dimension)

n = number of sides considered in the analysis

from which minimum required tangential stress is obtained. But when cohesion is zero and $\alpha_i > \phi_{ri}$, the vertical shear force component provided by tangential stress on one side will not be sufficient to contribute to resist the downward force ($A_i\sigma_{tang} \cos^2\alpha_i \sin \alpha_i > A_i \sigma_{tang} \cos\alpha_i^2 \cos\alpha_i \tan \phi_{ri}$) in shear [38]. Because only two sides are available for clamping, the lack of clamping on one side guarantees failure. Therefore, a rock mass composed of such rock blocks will have blockfalls irregardless of the tangential stress value, unless support is provided. The result of such unsupported ground is to have a cavity created at the extent of block falls, Figure 2.5. Therefore modelling to yield peripheral stresses after all block falls occur and block slides take over around this new cavity, can start with a new stope periphery which incorporates this ultimate block fall cavity.

Examination of the discontinuities' orientation can lead to the geometric outline of this block fall cavity for modelling purposes and to examine if such a cavity would reach surface.

If the intersection of two limiting discontinuities drawn from the upper stope periphery corners lies inside the bedrock boundary, block falls will not reach the top of bedrock, Figure 2.5.

The ultimate cavity height created by such block falls alone, is given by its height from the highest of the stope corner involved:

$$h_r = \frac{L \sin(\psi_1 - \omega) \sin\psi_2}{\cos \omega \sin\left(180-(\psi_1 + \psi_2)\right)} \tag{2.23}$$

where

ω = dip of crown periphery

ψ_1 = dip of discontinuity in the same direction as the crown periphery

ψ_2 = dip of discontinuity in the opposite direction as the crown periphery

L = horizontal stope span

This can then be compared to the depth of this stope corner.

If sliding of blocks occur after block falls, then the cavity will have a different shape than that shown in Figure 2.5.

The analysis of sliding block equilibrium in the direction of the sliding motion can be performed by taking into consideration the dips of the joints and the angles made between a normal to the periphery and the block sides, Figure 2.7. It is assumed that the block will slide on the steepest dipping side with respect to the opening.

A sliding block (with sliding side dip of ψ_s) supports part of its weight normal to the sliding surface, W cos ψ_s, leaving the remainder of the weight W sin ψ_s to represent the failure driving force component of block weight.

The tangential stress provides a normal and equal force to each of the sides parallel to the directions of sliding, Figure 2.7:

$$F_{ns} = 2\,(\sigma_{tang}\, A_s \cos\alpha_{ns})\cos\alpha_{ns} \tag{2.24}$$

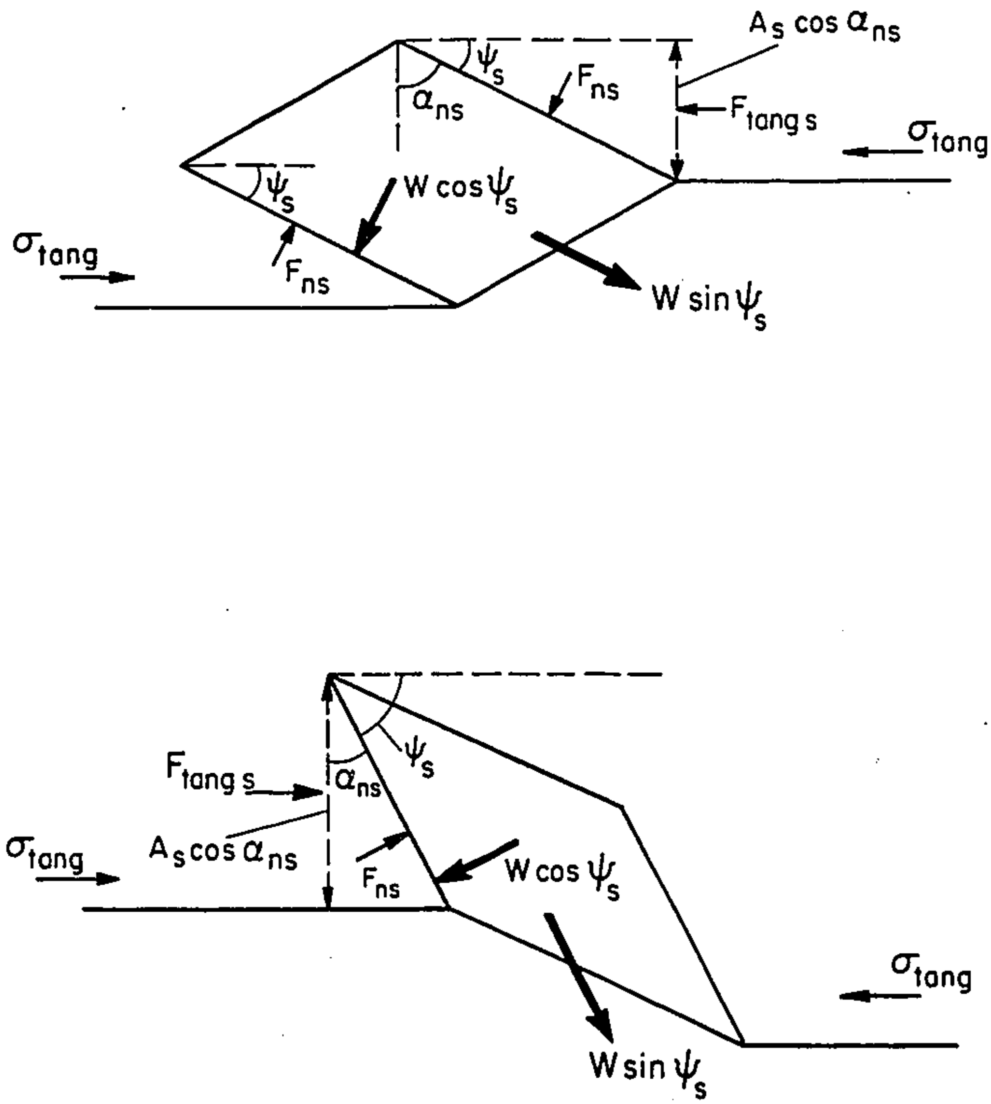

Figure 2.7 Stress distribution on ravelling, sliding, block.

where

α_{ns} = angle between normal to periphery and block sliding surface

This normal force, when added to the resisting weight component, provides the total resisting force

$$F_r = 2cA_s + (2\sigma_{tang}A_s\cos^2\alpha_{ns} + W\cos\psi_s)\tan\phi_{rs} \tag{2.25}$$

At limit equilibrium

$$W\sin\psi_s = 2cA_s + (2\sigma_{tang}\,A_s\,\cos^2\alpha_{ns} + W\,\cos\psi_s)\tan\phi_{rs} \tag{2.26}$$

In this fashion potential failures around the shallow stope are identified when the required tangential stress is compared to that provided by modelling for representative periphery geometry.

The block slide and block fall analyses should be performed for each rock mass sector that shows varying joint orientation and properties. In this fashion a representative final cavity outline of the entire rock mass can be obtained. Comparison of this cavity outline to the bedrock profile is used as verification against possible disruption of overburden and other surface elements. This analysis can include forces imposed on peripheral blocks to maintain them in place.

This analysis is simplified compared to the more sophisticated analysis of rock mass block movements afforded by discontinuum numerical codes such as the Block Spring Model [78] and other similar numerical block modelling codes. These allow for rotation as well as linear movement, while more sophisticated failure criteria than the Mohr-Coulomb criterion can be used.

However, the block code approach is still dependent on block geometry as input information. In both analytical and numerical approaches, even when an exhaustive geophysical, mapping, and rock core examination program is undertaken, the actual geometry and distribution of rock blocks around a shallow stope remains arbitrary, justifying a simple block geometry approach. The block codes are used to model simple block geometries and can indicate displacement and effect of ground support but will not provide factor of safety against ravelling. Furthermore, the analytical approach presented here will be faster in calculating ultimate block fall cavity height versus bedrock location.

The application of block codes for shallow stopes would seem more appropriate for large scale rock mass block mobilization such as caving. Progressive block ravelling from the periphery can be represented by this combined analytical and numerical approach.

2.3 STRATA FAILURES

Stratification of rock introduces distinct behaviour of rock masses. Because of low bonding at the strata interfaces, parting of the layers is easier than for intact rock. Failures are expected to originate, in part at least, from such weaknesses. The evaluation of performance of such environments requires different procedures than those applied in unstratified, but otherwise jointed rock masses.

The particular behaviours to design for are: slippage of strata leading to strata separation, stability of the lowest exposed stratum, stability of the stratum when it has failed but is self supporting through Voussoir action (linear arch).

If several strata fail, the extent of the failure zone around the stope has to be determined for comparison to possible break through to surface. Gravity loading is usually taken as the sole mechanism driving the failures, resisted by the shear, tensile or compressive strength of the rock strata. Lateral stress should be considered as an affecting agent, as should the reduction in gravity loading occurring in dipping strata. Depending on the longitudinal extent of an opening, the problem can be studied in either two or three dimensions.

2.3.1 Strata Separation

Movements leading to strata separation and deformation must first overcome the shear resistance between strata. A joint behaviour model, such as those described in section 2.1, can be used to establish strength against interbed shearing. In the simplest approach, the Coulomb model can use the imposed stresses, τ and σ_n, obtained from theoretical elastic stress analysis or from numerical modelling at points coinciding with the location of the bedding planes. Inter-strata shearing will occur when the shear stress imposed at the inter-strata joint boundary is greater than the shear bond strength. Once individual strata have separated, stability of single or stacked stratum must be examined.

2.3.2 Two-dimensional Strata Stability

Failure of a rock stratum by gravity involves complex loading mechanisms of one stratum or several strata on one another. If a less rigid stratum lies below a more rigid one, it will be only loaded by self-weight. When the lower stratum has more rigidity it will carry some of the upper load. Field observations indicate that metamorphic and sedimentary terrains associated with hard rock mining can occur in a stratified form with regular strata thickness and geomechanical properties [14][17][79]. On this basis, the analysis of strata behaviour considered in this research will be based on identical stratum overlying each other. In this section, the stability of a single stratum is treated. Loading of the lowest stratum by overlying stratum is outlined in the next section.

Elastic beam theory (where stratum thickness < 1/4 roof span) and plane strain conditions can be used to quantify the imposed stresses to a stratum under consideration in two-dimension situations (where the length of excavation is much greater than roof span).

The rock stratum can be considered as an elastic beam structure with both ends cantilevered. This reflects the continuity of the strata into the opening abutments.

The self load per unit length of one stratum is

$$q = \gamma_r \, t \tag{2.27}$$

where

γ_r = unit weight of rock

t = thickness of the strata

The induced stress considering a plane strain analysis is

$$\sigma_{induced} = \frac{My}{I} \tag{2.28}$$

where

M = moment applied to the beam by the load

y = distance from the beam neutral axes (half depth) to point of reference

I = moment of inertia of the beam cross-section

The gravity load q is used to calculate the imposed bending moment which, in the case of a double cantilever beam, is highest at the ends with a value of $M = q\,L^2/12$. At the strata centre $M = q\,L^2/24$.

For a perfectly elastic material the modulus of elasticity is the same in tension and compression resulting in the same level of imposed tension and compression. However, lab tests by Pandey and Singh [39] have shown that rock has a higher modulus of elasticity in compression than in tension. The rock type analyzed in their various tension and compression tests, a sandstone, displayed a compression modulus of 15 GPa, while the tensile modulus was 10 Gpa. This would produce differing levels of imposed tension and compression.

These authors locate the neutral axis of rock material subject to bending as

$$h_c = \frac{t}{1 + \sqrt{\dfrac{E_c}{E_t}}} \tag{2.29}$$

$$h_t = \frac{t}{1 + \sqrt{\dfrac{E_t}{E_c}}} \tag{2.30}$$

where

h_c = distance from the concave surface to the beam neutral axis

h_t = distance from the convex surface to the beam neutral axis

E_c = modulus of elasticity of rock in compression

E_t = modulus of elasticity of rock in tension

The beam of "two materials" can be transformed into one of equivalent material, Figure 2.8, for application of the elastic beam formula. In this case, the neutral axis coincides with the boundary between material in compression and tension, and is therefore known. Both materials have the same unit width. At the center span the upper portion with a modulus of elasticity E_c is under compression from bending, the lower portion is

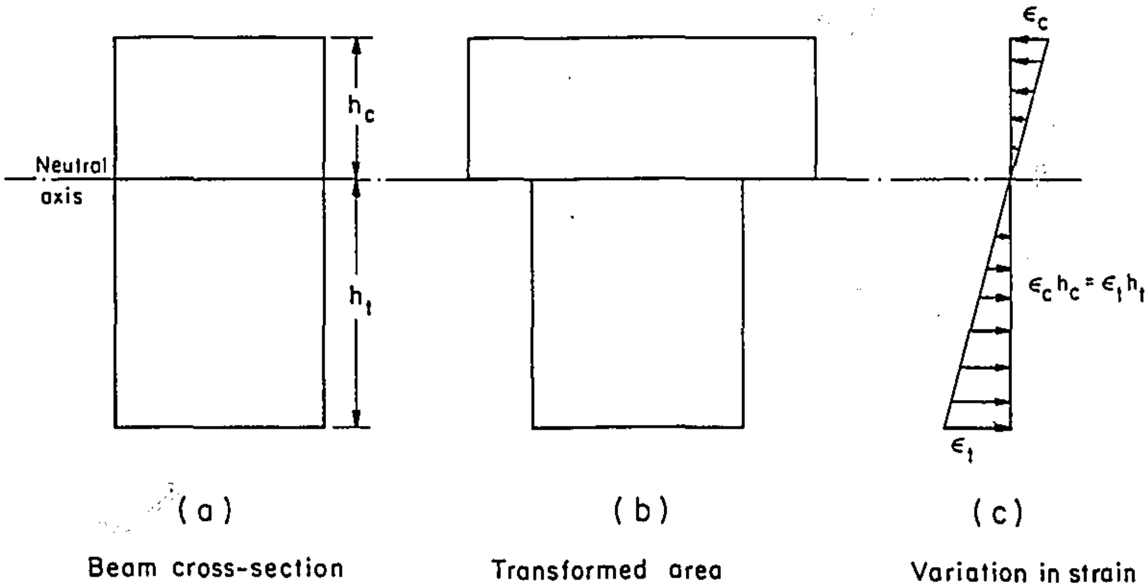

Figure 2.8 Transformation and stress distribution in a beam of "two materials".

in tension with a modulus of elasticity E_t. At the end of the beam the reverse occurs.

The basic deformation assumption used in the flexure theory remains valid, i.e. plane sections at right angles to the axis of the beam remain plane. Therefore, the strains must vary linearly from the neutral axis, Figure 2.8 (c). For this elastic case the stress is proportional to strain and the stress distribution for a higher modulus of elasticity in compression is also shown, in figures 2.9(a) following Hooke's law.

$$E = \frac{\sigma}{\varepsilon} \tag{2.31}$$

The transformation of the section is accomplished by changing dimension of a cross-section perpendicular to the neutral axes in the ratio of the elastic moduli of the materials. The transformed section is shown in Figure 2.8 (b).

The moment of inertia around the neutral axis is the sum of two rectangles about their base, which here is the neutral axis. Therefore, the moment of inertia is (transformed to the tension material)

$$I = \left(\frac{E_c}{E_t}\right)\frac{(b)\ h_c^3}{3} + \frac{(b)\ h_t^3}{3} \tag{2.32}$$

with b = unit width, therefore

$$I = \frac{1}{3}\left(\frac{E_c}{E_t}\ h_c^3 + h_t^3\right) \tag{2.33}$$

In the case of a double cantilever beam the highest imposed stress, at the beam ends, are at the top and bottom at a distance of h_c and h_t respectively for compression and tension.

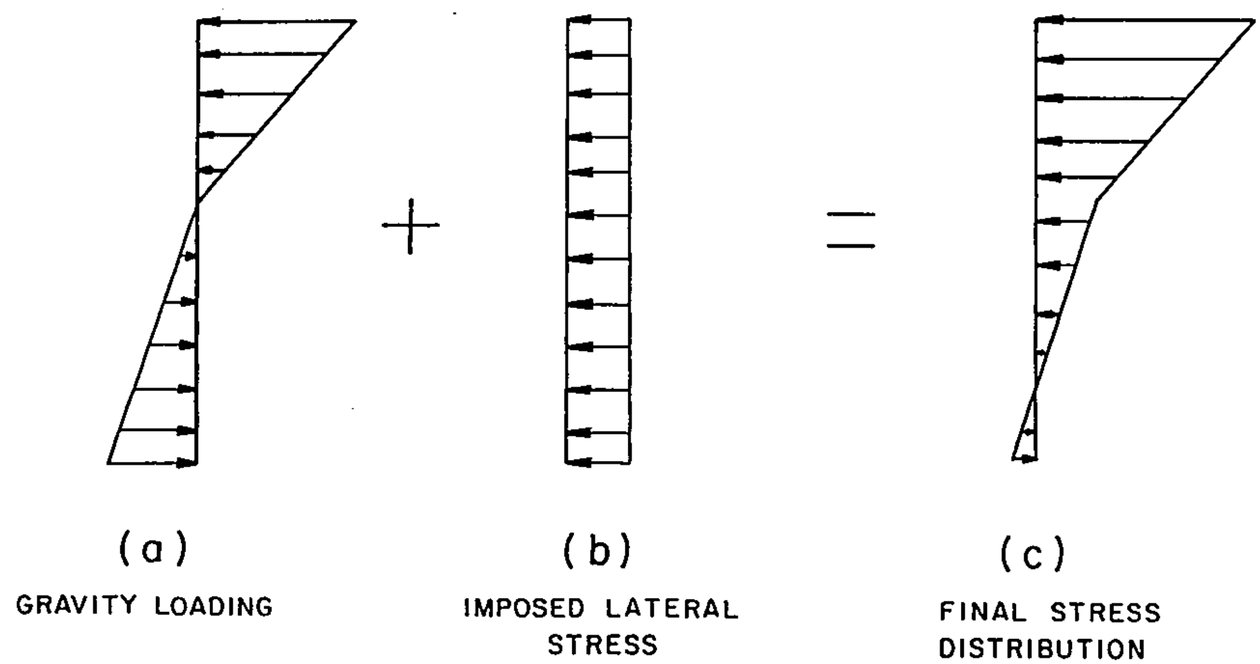

Figure 2.9 Effect of imposing lateral ground stress to a "two materials" rock beam.

This reduces equation 2.28 to

$$\sigma_c \max = \frac{Mh_c}{I}\frac{E_c}{E_t} = \frac{E_c}{E_t}\frac{qL^2 h_c}{4\left(\frac{E_c}{E_t}h_c^3 + h_t^3\right)} \tag{2.34}$$

$$\sigma_t \max = \frac{Mh_t}{I} = \frac{qL^2 h_t}{4\left(\frac{E_c}{E_t}h_c^3 + h_t^3\right)} \tag{2.35}$$

The maximum tensile and compressive stresses imposed should be compared to their respective strengths to obtain a factor of safety against failure. Using the sandstone moduli obtained by Pandey and Singh, a stratum 10 cm thick spanning a 10 m opening will be subjected to 10% less tensile stress than the stratum calculated with the elastic theory. As the rock takes on a higher modulus of elasticity, as for hard rock, this difference could increase.

The four point beam test prescribed by Pandey and Singh is simple to carry out, and given the potential difference in the calculation of imposed stresses, is worthwhile versus using the conventional elastic approach.

In the case of dipping strata the load q is reduced

$$q_\theta = q_{horizontal}\cos\theta \tag{2.36}$$

where

θ = dip of the strata

because part of the load is transferred to the lower abutment.

The presence of lateral ground stress imposes a load along the axis of the beam, Figure 2.9. This axial stress σ_a can be added directly to equations 2.34, 2.35, adding to the compressive stress, but lowering the tensile stress.

When the beam has a high slenderness aspect, amplification of the moment can occur by the action of a high axial stress (the moment is increased by a large value equal to the axial force times the beam deflection). Based on the theory of elasticity, the moment induced was calculated by Timoshenko and Goodier [80]. The amplification of the moments at the beam end, where it is highest, is

$$M_{end} = \frac{qL^2}{12}\ \Gamma \tag{2.37}$$

where

$$\Gamma = 3\left[\frac{(\tan\lambda\ -\ \lambda)}{\lambda^2\ \tan\lambda}\right]$$

$$\lambda = L\ \sqrt{\frac{3\sigma_a}{E\ t^2}}$$

L = beam span

t = beam thickness

σ_a = axial stress

E = the uniform modulus of elasticity for the material which can be replaced for rock. If E_b, the bending modulus of elasticity is used, its value is [34]

$$E_b = 4E_c\ /(1\ +\ \sqrt{E_c\ /E_t}\ ) \tag{2.38}$$

Verification of possible shearing of the beam at the abutment must also be performed. Shearing occurs commonly when the beam is very thick, equal to or greater than span. The shearing stress imposed for a 2-D case is

$$\tau = \frac{qL}{2t} \tag{2.39}$$

where

t = beam thickness

q = horizontal beam load

L = beam span

Comparison to the shear strength of intact rock will also yield a safety factor which can be compared to the safety factor against tensile or compressive failure in order to identify the most likely mode of failure.

The most important shortcomings of using elastic beam theory are

a) The roof must be continuous, with no discontinuities across its span.

b) The failure mode in rock beams depends on the geometry of the beam size. Wright and Bucky [81] and Stephansson [82] showed that "thin" or "slender" beams (less than half the thickness span) failed by tensile failure as expected by the beam theory, but that "thick" or "deep" beams (thickness greater than half the span) failed by an arch-shaped failure in the lower central beam area, Figure 2.10.

c) If the lowermost stratum is under some loading from above strata, there is actually a limit to the number of beds which actually impose load. The Fayol [83] experiment with identical beam stacking to confirm field behaviour showed that starting with the lowest beam, the deflection measured from each new stacked beam became progressively less until additional beams did not change the deflection of the lowest beam.

d) Sophisticated analysis of multilayered roofs of various geological material has been performed by Stephansson [82] and Shorey [84]. The former calculated deflections and moments at any point of individual stratum of layered systems with variable properties and included abutment compression, whereas the latter calculated deflections of strata in a double layer system using deep beam elastic analysis. They indicate that deformations continue into the opening abutments.

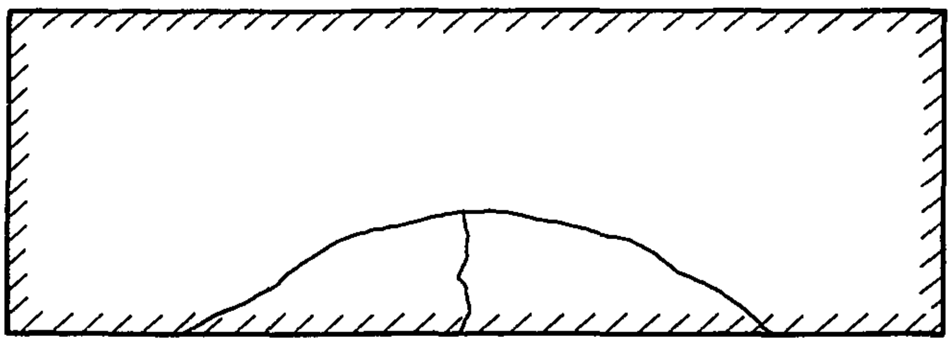

Figure 2.10 Failure mode for a "thick" or "deep" beam [81][82].

2.3.3 Extent of Failure Zone

If several poorly jointed strata have detached, increased loading of the lower stratum occurs. The ultimate bearing capacity of each of the lowest stratum is of interest in order to predict the cavity height that would be created if progressive rock stratum failures occur. Such a progression has been shown to be different than that predicted by the elastic beam theory [83], Figure 2.11. In the elastic case, failure of each stratum would be identical, involving strata breaking at the abutment. Field observations, however, indicate that strata fail at progressively shorter intervals, leaving behind a cavity shape over the opening [35][85].

The Fayol experiments [83] consisted of measuring the deflection of artificial beams as they were subjected to loading from progressive stacking. Starting with one double clamped beam, a deflection was measured under its own weight. The experiment was repeated with two similar beams stacked one on top of the other. The lower beam deflection was greater, and the upper beam less than that of a single beam. With each additional beam, the deflection imposed on the lowest beam decreased until any additional beam did not affect the deflection of the lowest beam. Furthermore, these additional beams did not themselves deflect, indicating that all or most of their load was transferred to lower beams. Load sharing of the upper beams to the lower beams is therefore in effect.

Delineation of the relative stability of each stratum under multiple identical strata loading must begin by identifying the load being distributed to each stratum.

In the case of hard rock mine stratification, each stratum can be assumed to have the same thickness and geomechanical properties (section 2.3.2), and each stratum is also

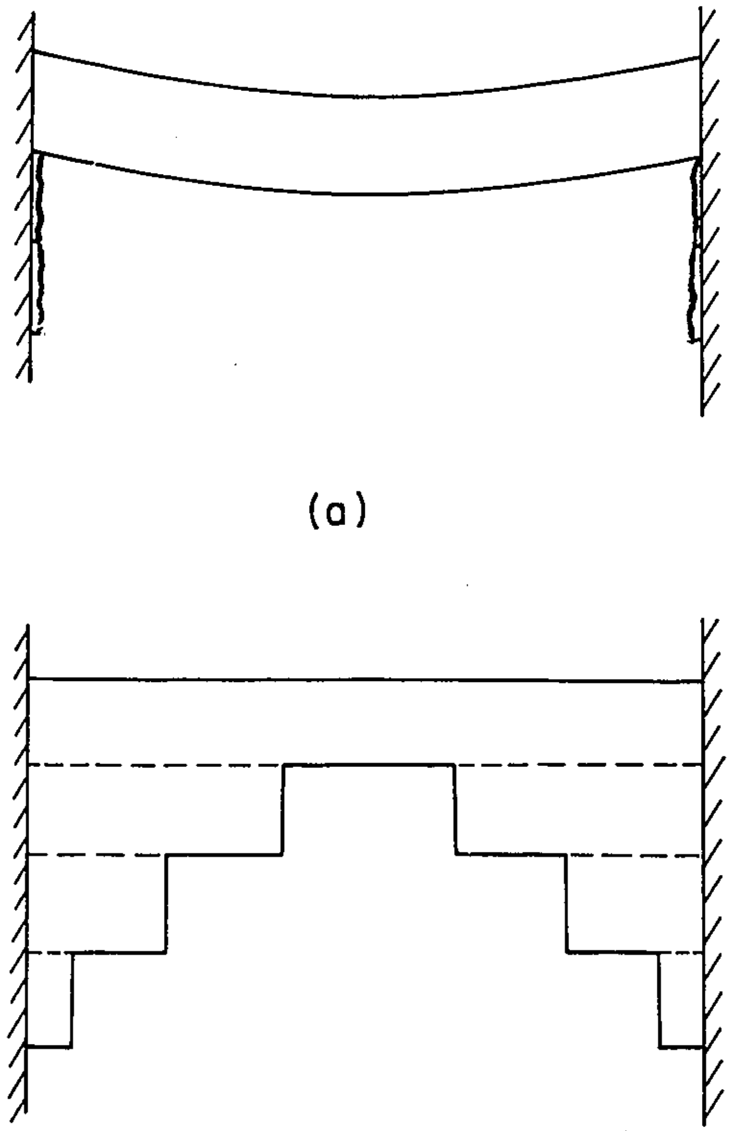

(a)

(b)

Figure 2.11 Simplified elastic beam behaviour (a) and actual field behaviour (b).

supported in the same way (double cantilever). The stacking of identical strata can be represented by a vertical column of springs with identical spring constants.

A solution is obtained if each stratum is considered as a spring loaded by its own weight. Because of the similarity, the load from each stratum will be divided equally between it and the lower strata, Figure 2.12. The total load on each stratum then becomes the sum of all the fractions of loads given by the overlying strata, as well as that of its own weight.

The total load imposed on the lowest (first) beam from itself and above loading strata, considering the dip of the strata, is

$$p_1 = \gamma_r t \cos\theta \sum_{i=1}^{n} \frac{1}{i} \tag{2.40}$$

where

γ_r = unit weight of rock
t = strata thickness
i = i^{th} stratum numbered from the lowest stratum
n = total number of strata loading lowest stratum

This series satisfy all of the Fayol observations: that the lowest stratum carries the highest load; that the strata from the bottom up are subjected to a decrease in load and therefore deformation; that given a high number of strata stacked, the effects on the lowest strata decrease; and that the upper stacked stratum carries very little of its own load.

If the lowest stratum fails, the second lowest stratum must now carry all of its own weight plus the load of the upper strata that the lowest strata was carrying, Figure 2.12.

In summation form, the load on the lowest stratum per unit length from itself and above strata after part or none of the n strata have failed is

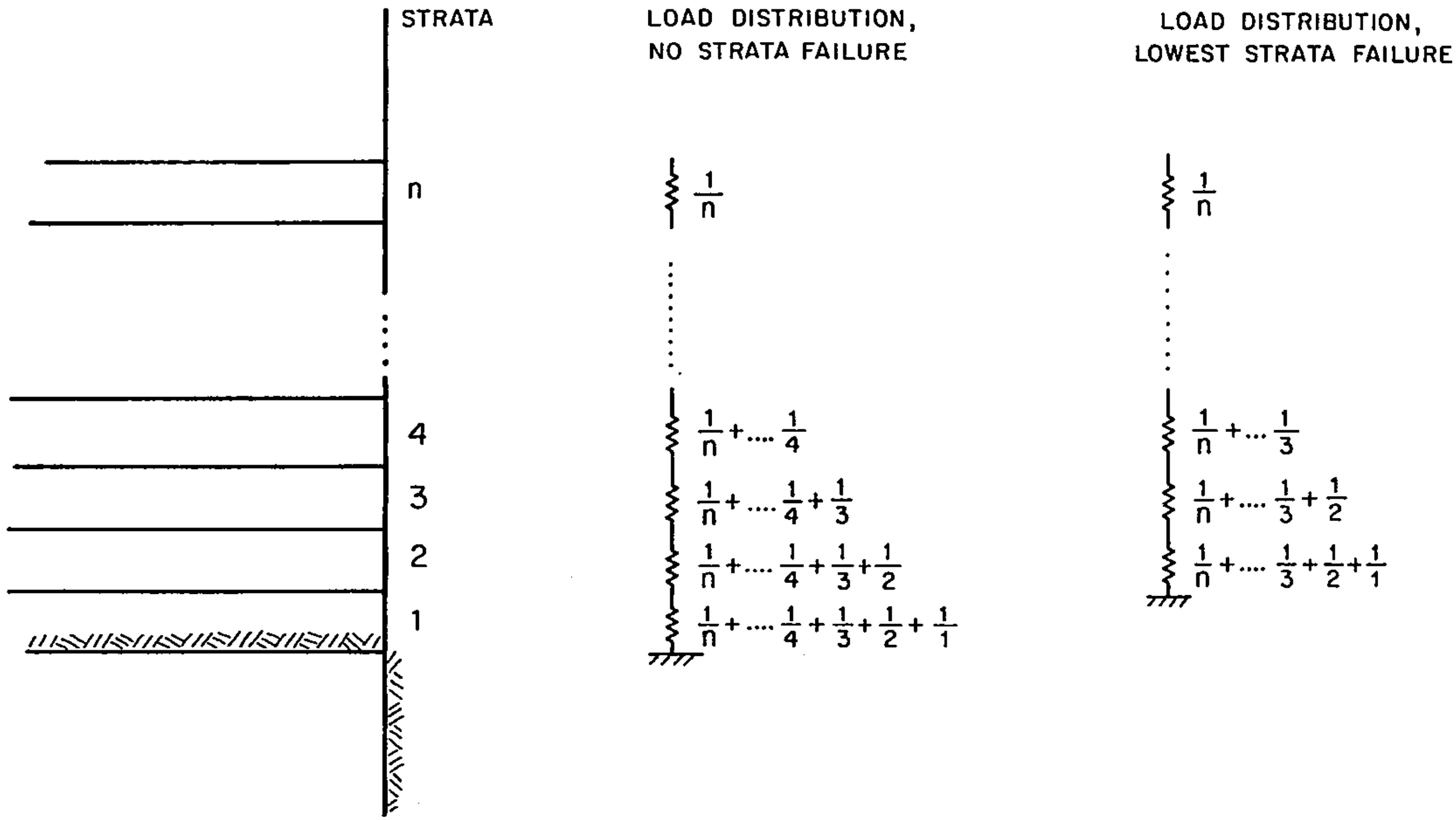

Figure 2.12 Consideration of strata loading.

$$p_{j+1} = \gamma_r \, t \cos\theta \sum_{i=1}^{n-j} \frac{1}{i} \qquad (2.41)$$

where

j = j^{th} strata that has failed ($j \geq 0$)

Figure 2.13 shows the behaviour of a loaded lower beam with friction table modelling. Although tension cracking at the upper portion of the beam end is shown, the lowest stratum fails by growth of a shear crack. This condition exists when the compression load placed at the bottom corner of the stratum exceeds the strength of the material.

The general development of stratum failure can be described as follows. When the tensile stress imposed by the load surpasses tensile strength, a vertical crack grows from the tip of the beam towards its neutral axis at the beam end. This reduction in effective beam thickness amplifies the imposed compressive stress at the bottom of the stratum, by a factor proportional to the inverse of the square of the available thickness, $1/t^2$. Because a rock stratum behaves as a beam of "two materials", equations 2.34, 2.35 and Figure 2.8, the value of the compression imposed for a given thickness will be higher than the tension. With a reduction in thickness the difference increases significantly and the compressive stress imposed quickly reaches the material's strength before tensile failure is complete. A shear failure in the bottom stratum at the abutment commences to grow and accelerates because the thickness of the stratum becomes smaller, until the shear crack reaches the top of the beam, Figure 2.13. In this case because the crack grows from the edge of the intact thickness, shear stress is zero as is vertical stress, leaving induced compressive stress acting parallel to stratification.

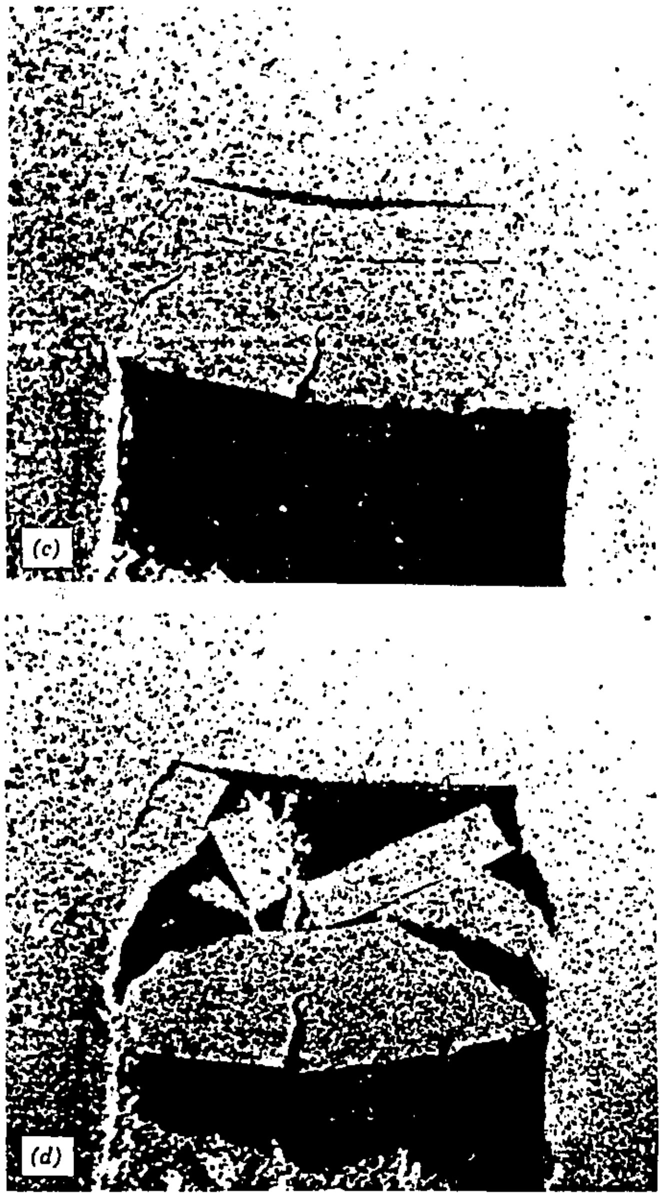

Figure 2.13 Loaded beam behaviour, friction table modelling [135].

The failure therefore occurs as an unconfined compression failure, oriented at 45° + $\phi/2$ to the plane on which σ_1 the induced compressive stress acts, respecting Mohr's strength theory. The failure is assumed to follow a linear path from the lower stratum corner to a distance of d_j from the end of the stratum:

$$d_j = (t) \tan (45° + \phi/2) \tag{2.42}$$

where

t = stratum thickness

Because of the acceleration of this shear failure due to compressive stress increasing to very high values, the tensile crack is assumed not to continue its growth.

The process of shear failure is therefore dependent on tensile cracking forming first. Tensile cracking will not occur when the total load on the lowest stratum is insufficient to begin the tensile rupture.

Tensile cracking will begin when the imposed stress equals that of tensile strength, from equation 2.35

$$T_s = \frac{p_{i+1} \, L_{j+1}^2 \, h_t}{4\left(\frac{E_c}{E_t} h_c^3 + h_t^3\right)} \cos \theta \, \Gamma - \sigma_a \tag{2.43}$$

where

T_s = material tensile strength

σ_a = imposed axial stress

Γ = amplification of imposed moment on slender beam (equation 2.37)

p_{j+i} = load on the lowest stratum

L_{j+1} = spanning length of the lowest unfailed stratum

= L -2(jd_j)

j = j^{th} stratum to have failed

θ = dip of strata

The span L_{j+1} can provide the cavity height created after the j^{th} strata has failed by shearing, as described above. The total cavity height normal to strata expected as a result of several strata failures will be made up of the sum of the thicknesses of the strata that have failed:

$$H_c = jt \tag{2.44}$$

where

j = j^{th} and last strata to fail

t = strata thickness

Therefore using equation 2.42

$$H_c = \frac{jd_j}{\tan\,(45° + \phi/2)}\ \frac{L - L_{j+1}}{2\ \tan\,(45° + \phi/2)} \tag{2.45}$$

This approach respects the field and experimental observations about strata failures. The disadvantage of such an approach is that it is two dimensional and therefore does not properly represent how the failure develops in the third dimension. Because some support exists in the third dimension the results calculated err on the conservative side. However, the calculation of such a failure for a plate (three dimensional stratum problem) requires very complex calculations to account for the neutral axis location away from center thickness [30]. This would not provide a simple design tool. The method does not indicate a lower limit for stratum thickness for this failure to be valid, i.e. can there be a minimum thickness below which tensile failure will proceed to fail the beam completely rather than allow for continued shear growth in this fashion? (the shear and tensile cracks coaloesce, or the tensile crack is too close to the strata bottom and forces a tensile failure before the shear crack failure).

2.3.4 Two-dimensional Linear Arch Performance

Once a stratum has failed, it can enter into a linear arch configuration. This configuration will be in equilibrium unless one of three failure conditions prevail: by shearing, (equation 1.36); by buckling within a block because of eccentricity of loading where thickness is much smaller than span (this occurs before the peak compressive material strength is reached); or by exceeding material compressive strength.

The compressive thrust generated by the linear arch has been historically assumed [30][40] to be triangular over a portion of the voussoir blocks, Figure 1.6. The vertical extent of the thrust zone is over a portion of the block height nt.

Sterling [41] examined through experimentation the likely value for n and the distribution, shape, and size of the contact compression distribution zone at failure of the linear arch. Several types of stress distribution zones were examined to compare to his test result findings. Figure 2.14 shows the distributions considered and the value of the parameter β which is representative of each distribution. This parameter is obtained by equating the value of the thrust distribution resultant H to its location e from the beam half-height, Figure 1.6. For a triangular distribution

$$H = 1/2(ntb\sigma_c) \tag{2.46}$$

$$e = t/2 - 1/3\ (nt) \tag{2.47}$$

where

b = beam width

If n from equation 2.46 is substituted in equation 2.47 and if

$$\beta = \frac{b\sigma_c}{2H}\left(\frac{t}{2} - e\right) \tag{2.48}$$

n yields $\beta = 0.33$ for the triangular distribution.

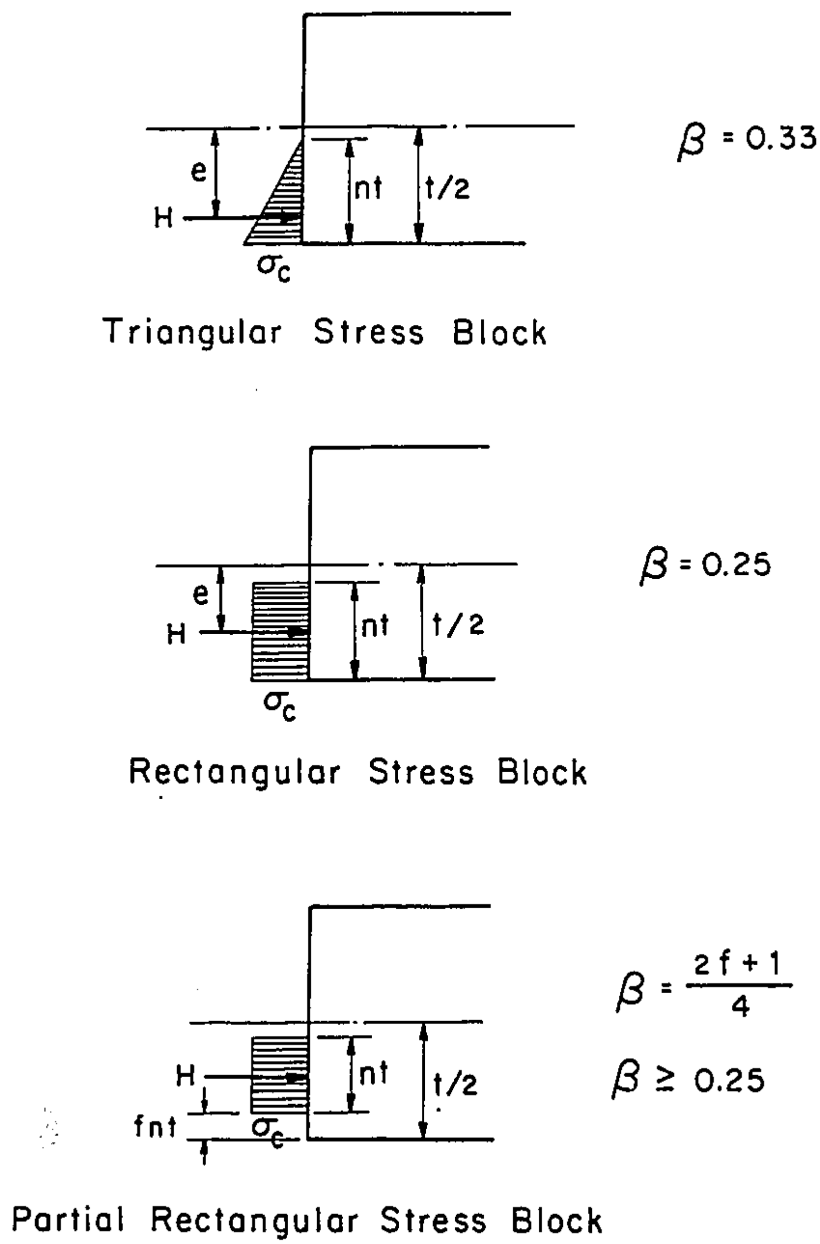

Figure 2.14 Stress distribution zones during linear arch testing [41].

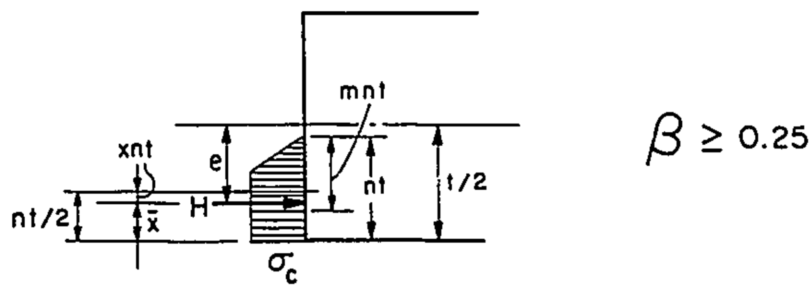

Triangular/Rectangular Stress Block

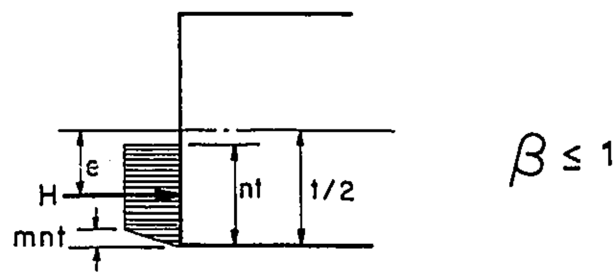

Rectangular/Triangular Stress Block

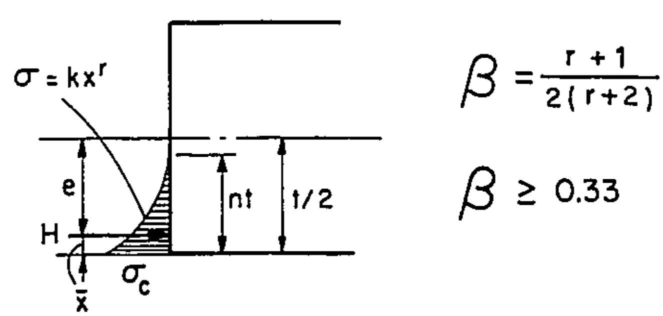

Power Distribution Stress Block

Figure 2.14 (Continued)

After monitoring the location and the thrust zone resultant from lab tests on linear arches of sedimentary rocks, Sterling registered a reduction from high to low β value without a change in the nt value, indicating a change from a power distribution to triangular distribution to rectangular distribution. At peak load application, the average β value was 0.23. This value fits closely the rectangular thrust distribution. After peak load, the sample went through a rectangular/triangular, then partial rectangular distribution, accompanying crushing of rock from the edge towards the stratum mid-height. Sudden diagonal cracking completes the collapse of the stratum.

The rectangular distribution reflects the lowest β value and represents a condition of plasticity over the height of thrust distribution, nt, at peak strength.

Based on Sterling's laboratory results and the fact that crushing failure requires a compression failure zone distributed over the height nt rather than a triangular distribution indicating compression failure limited to the edge of the block as indirectly assumed by the Beer and Meek [42] and Brady and Brown [30] triangular distribution, the rectangular thrust distribution offers a more representative consideration of failure conditions and indicates material has reached plasticity before failing as is normal in compression failures. The critical span based on compressive failure therefore must be calculated using the rectangular thrust zone.

The Beer and Meek solution can still be used to calculate the maximum compressive thrust for a given critical span. If this thrust is less than compressive strength, then stability depends on eccentricity of loading (buckling) or imposed shear stress versus block-abutment shear strength.

Previous authors have accepted that when compressive failure occurs, the material's unconfined compressive strength is surpassed. In reality, the block portion in contact with the abutment is subjected to compressive thrust and to shear from block weight. Shear stress has an increasing effect as the block thickness increases for a given span. Examined in a Mohr diagram, Figure 2.15, this stress condition indicates that the maximum compressive stress imposed at failure must be less than the unconfined compressive strength. The imposed stresses, thrust compression f_c, shear τ, and lateral ground stress σ_a, must be used to calculate the distribution of stress in the block at contact points, using Mohr stress equations with

$$\sigma_x = f_c + \sigma_a \qquad (\sigma_y = 0) \tag{2.49}$$

$$\sigma_1 = \frac{f_c + \sigma_a}{2} + \sqrt{\left(\frac{f_c + \sigma_a}{2}\right)^2 + \tau^2} \tag{2.50}$$

$$\sigma_3 = \frac{f_c + \sigma_a}{2} - \sqrt{\left(\frac{f_c + \sigma_a}{2}\right)^2 + \tau^2} \tag{2.51}$$

where

f_c = imposed compressive stress

which can then be compared to the Mohr strength envelope. Definition of the Mohr strength envelope can best be handled by using the Hoek and Brown [52] failure criterion to define the envelope

$$\sigma_1 = \sigma_3 + \sqrt{\sigma_c m \, \sigma_3 + s\sigma_c^2} \tag{2.52}$$

Because the option to use a field size rock strength envelope can be generated, the criterion is well known, and it offers a simple means to calculate maximum stress

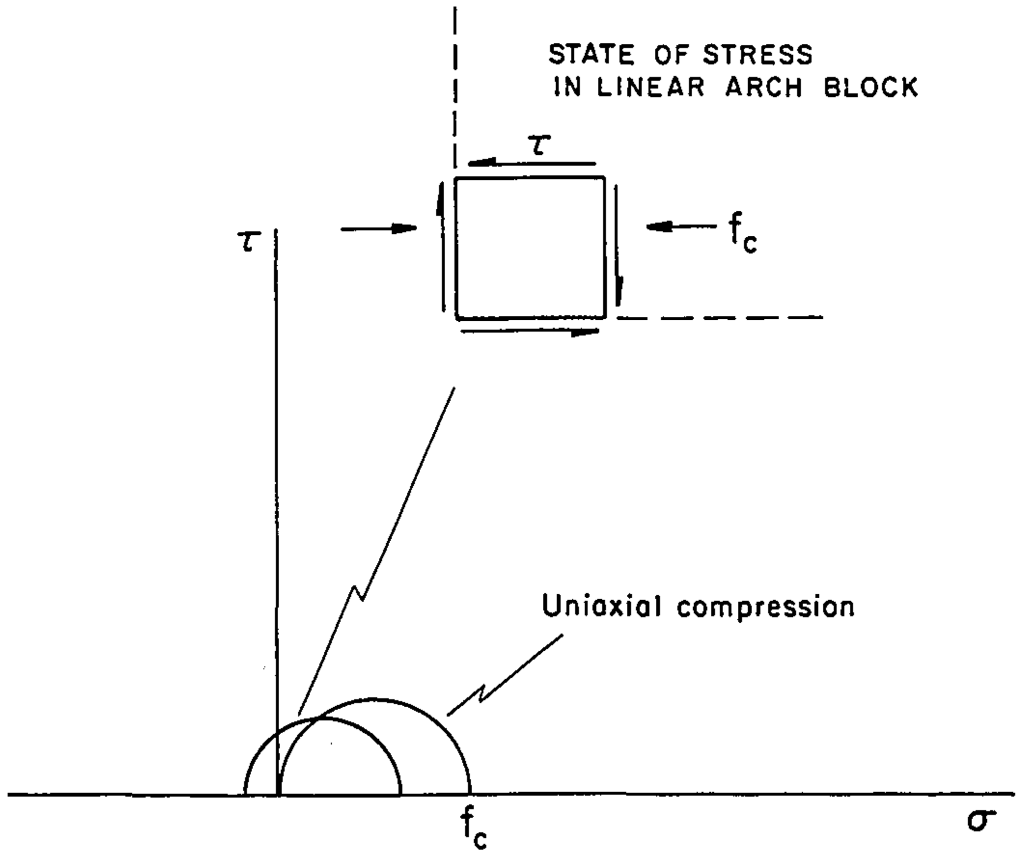

Figure 2.15 Stress condition at linear arch contact point.

allowable, Chapter 1.4. It provides a more flexible method.

The procedure to verify if imposed stress is greater than strength requires the comparison of σ_1 values obtained from equations 2.50 and 2.52. At the minor principal stress imposed (equation 2.51) a value of strength (σ_1) is returned from equation 2.52 using problem specific values of m and s. This value is compared to that of the imposed σ_1 stress, equation 2.50:

$$F_s = \frac{\sigma_1 \ strength}{\sigma_1 \ stress} \tag{2.53}$$

The values m and s can be selected to reflect field conditions, including weaknesses parallel to stratification.

To obtain f_c for peak strength based on the rectangular distribution, the substitution of z for a rectangular distribution must be used in equations 1.21 to 1.25:

$$z_o = t\ (1-n) \tag{2.54}$$

If the value of f_c for the rectangular thrust when input in equations 2.51 and 2.52 provide for a factor of safety greater than one, then the strata peak strength is not surpassed. If further verification against buckling, and shear, indicates satisfactory resistance to failure the linear arch is stable.

This linear arch approach represents a more conservative and realistic approach than that developed by other authors.

2.3.5 Three-dimensional Linear Arch Performance

The Brady and Brown and Beer and Meek solutions for the stability of three-dimensional linear arch systems adopts the approach for reinforced concrete plates having failed by plastic collapse along diagonal rupture lines, resulting in a diagonal linear arch configuration. This implies that plastic collapse occurs when the material is stressed beyond its elastic maximum, into the plastic zone. This creates a dilemma in the case of rock, since the tensile peak strength of rock coincides with yield strength; no plastic behaviour is possible. Plastic analysis, on this basis, does not appear to be representative.

In reality, rock strata are often weakened by existing or inherent discontinuities which make the anticipated behaviour different from that expected by theoretical considerations leading to yield lines. Furthermore, visual observations of strata plate failures indicate that transverse rather than diagonal failures [41][85] occur.

Such failures also fit the stress distribution of fully clamped plates, based on the maximum tensile stress imposed, Figure 1.5. If the rock fails along the location of highest tensile stress, cracking will start at the mid-point of the longest sides and progress along the length of these. The plate effectively becomes supported at the smaller sides only, and, because the load is now greater along these sides than that which caused failure to begin, the plate fails similarly to a beam condition leaving a linear arch with cracking having occurred parallel to the short sides, at the center.

The analysis, therefore, reverts back to applying equations representing a two-dimensional case.

2.4 CHIMNEYING DISINTEGRATION FAILURES

Chimneying disintegration occurs in weak rock (severely altered rock, sercitic or chlorite schists, graphitic slate) above openings, when upward (vertical) progressive failure by gravity without stoppage leads to the creation of vertically sided cavities ("chimneys"). These chimneys cut across rock fabric such as slatey cleavage and form above relatively small openings with spans of less than 5 m [6][18][34][35].

The mechanical conclusions that can be drawn from the observations of chimneying disintegration failures presented in Chapter 1.4 are:

a) the resisting strength of the rock mass above an opening is surpassed;

b) existing lateral ground stresses are not sufficient to prevent the rock mass from failing by gravity at the developing chimney front;

c) chimneying disintegration is unlike block caving; sufficient cohesion exists to maintain competent chimney walls. Block caving can be modelled by flow of granular materials [64];

d) lateral stresses are insufficient to force a failure resulting in a shape different than vertical walls;

e) the inherent fabric of the rock mass plays a role in failures, at least allowing movement and/or a partial breakdown to smaller rock mass particle size.

Chimneying disintegration therefore lies in between the bounds of block caving (flow) and a stable rock mass. A survey of the literature indicates that there has been no work carried out to formulate models or analyse for predicting the possible onset of chimneying disintegration, or that of block caving, based on physical or numerical studies, or field trials.

Chimneying occurs in weak rock, which can disintegrate but, in the cases visually observed (Chapter 1.4), with some degree of cohesion in order to maintain resistance to the vertical wall failure. This can be used as a basis for considering the rock as a c-ϕ

geotechnical material. For the development of analysis it will be assumed that failure at the top of the chimney is related to the mobilization of active earth pressure under gravity loading. In the active condition, shear strength opposes the effect of gravity [86] until it is surpassed by shear stress. This would explain the shearing of material fabric also noted.

Resistance in the horizontal plane to stresses is provided by the form of the chimney cross-section, which remains approximately that of the stope's plan dimensions. Imposed stress, obtained from simple elastic equations such as that for circular openings, or numerical modelling, can be compared to material resistance.

The formation of active stress induced ruptures in the stope roof is assumed to be developed in the following manner. Once an underground opening is created, its roof starts to deform. Due to this deformation, movements take place in the weak rock material. If these displacements are great enough, the shear strength of the material is mobilized, along active pressure rupture lines. For a homogeneous material, a first rupture line develops in the rock mass above the opening involving the fall of rock between it and the stope. Rupture lines continue to develop sequentially above the cavity created and material slides down, in a progressive fashion, from a new rupture line to the cavity below resulting in the upward growth of the cavity, Figure 2.16. Chimney development can be stopped near surface if the load is insufficient to activate a rupture line. Formation of a rupture line implies that material weight is sufficient to surpass the material's cohesion resistance provided along the rupture line.

To set up the problem mathematically, the most simple approximation of rupture lines is to use a 2-D circular shear slip surface, as has been assumed in active pressure

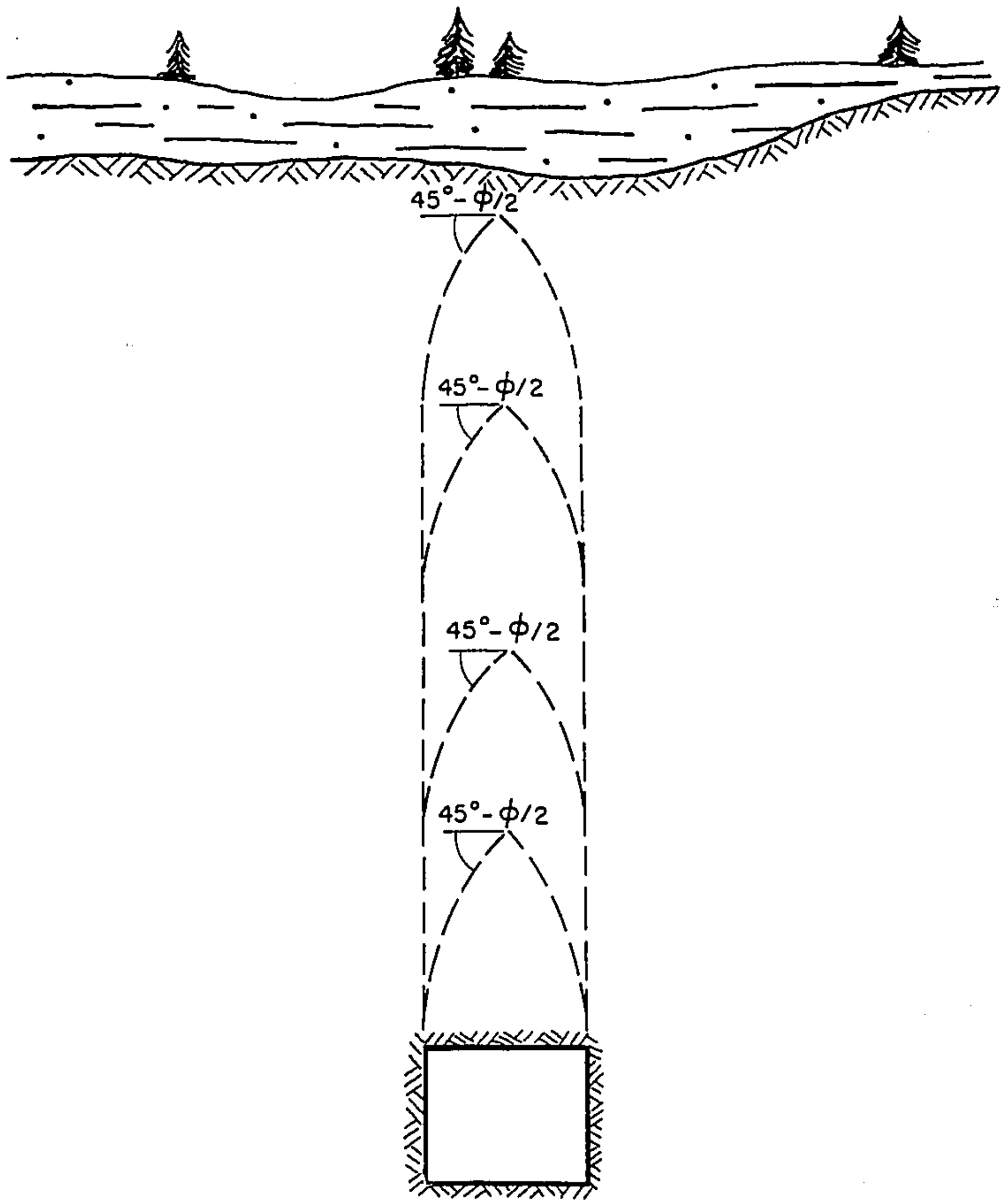

Figure 2.16 Assumed progression of a chimney failure by shear rupture, from mobilization of active earth pressure in homogeneous rock material.

shear failures in slopes of cohesive soils or slopes of weak rock material and even rock rubble [87]. This is an approximation to a 3-D situation, representing a more conservative, but simpler to use approach, which has also been used in slope stability issues. By its potential to breakdown to smaller particle size, such a material is able to develop failures approaching a circular shape. Geological features such as joints are no longer the single important feature to control failure. The failure surface is free to find the line of least resistance through the material. Rock mass cohesion is low, allowing the ease with which shearing can fail a broken down solid. Each rupture line is composed of two circular arcs each reflecting symmetry. Half the weight is distributed to each arc. The junction point of the arcs of the first rupture line and tunnel walls are tangents. The rupture line apex represents a point where passive earth pressure exists, i.e. where the material is being compressed in a horizontal direction as a result of the opposite components of shear resistance acting at this point.

Therefore, each rupture line limb is defined: circular arc segment drawn from a horizontal diameter, reaching a point where the slope of the circular arc is the sliding plane of passive earth pressure, $45°-\phi/2$. In order for this passive earth pressure condition to be respected, subsequently higher rupture lines must also have a $45°-\phi/2$ tangent at the apex, meaning that the rupture lines are parallel to the first one and that shearing also occurs vertically between arc segments, (Figure 2.16). This progression in effect creates vertical walls as the failure continues, which is representative of the vertical walls oberserved in cases of failure.

This chimneying progression assumes that material failure along the first rupture line must occur for the others to follow.

The problem of solving for the stability of the first rupture in a homogeneous material is best resolved by using the method of slices, which is commonly used to calculate the factor of safety related to mobilization of active pressure circular arc failures in slopes composed of soil and rock material [86][87][88].

Each slice mobilizes a vertical component of shear resistance that when added to the other components, resists the total weight acting in the opposite direction. The horizontal components of shear resistance for slices of both arcs of the rupture line are cancelled due to the symmetry of the problem. Since in a homogeneous material case each arc subtends half the weight, and resists equally to the other arc, the problem can be simplified by considering only one arc. When material properties vary so that the strength varies, both arcs should be used.

The general relationship to calculate the factor of safety in a method of slices is

$$F_s = \frac{\Sigma \; resistance \; for \; each \; slice}{\Sigma \; weight \; for \; each \; slice} \tag{2.55}$$

This reflects the approach that each slice has a weight and each slice has a vertical component of shear resistance. With a sufficient number of slices dividing the problem, the arc portion over each slice can be assumed to be straight.

For the first rupture line in a homogeneous material above the opening, the radius of the rupture arc can be obtained if it is assumed that the center lies on a horizontal line spanning the stope's upper boundary and if the angle it subtends over its height is known; for a circular segment Figure 2.17, the geometry of such an arc is [89]:

$$r = \frac{b}{[1 - \cos\,(\alpha/2)]} \tag{2.56}$$

where

$\alpha/2 \;=\; 45° + \phi/2$

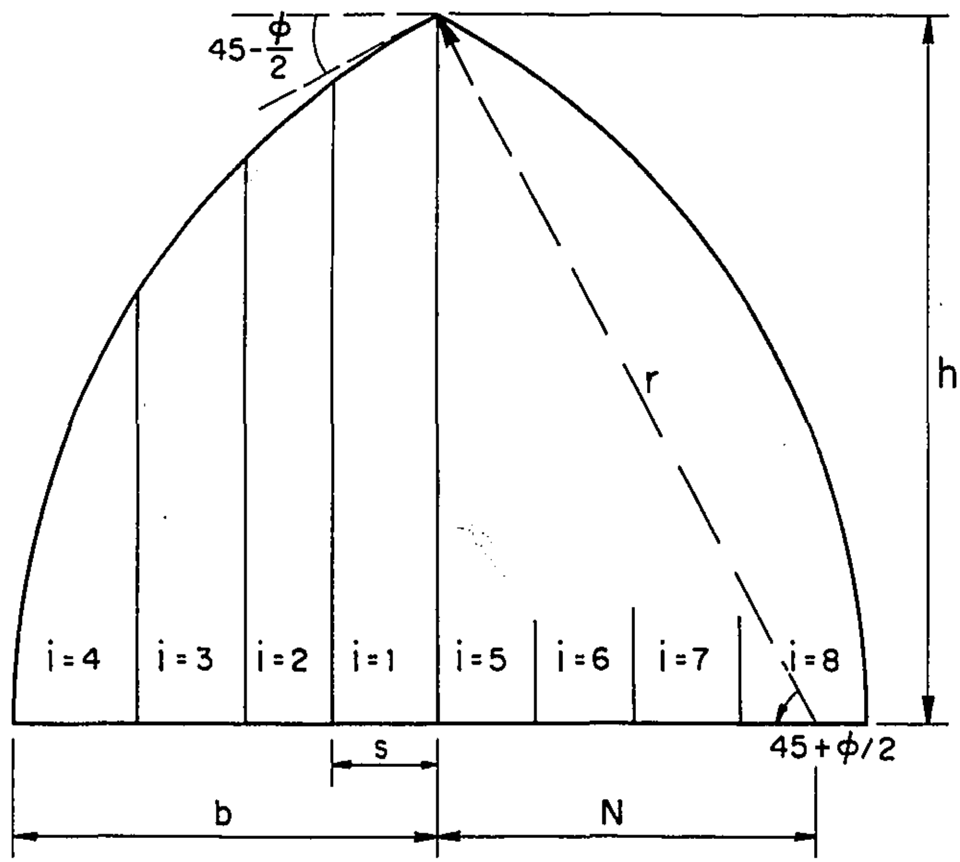

Figure 2.17 Chimneying rupture outline with arc and slice definitions.

ϕ = rock mass angle of friction

b = 0.5L

L = stope span

This radius is then used to calculate the height of each slice for a given slice width s.

The height of the line to the apex of such an arc is [89]

$$h = \sqrt{b\ (2r\ -\ b)} \tag{2.57}$$

and the circumferential length of the arc is

$$C_l = \frac{\alpha/2}{360}\ (2\pi r) \tag{2.58}$$

the area subtended by this arc is

$$A_T = \frac{(45^\circ\ +\ \phi/2)}{360}\ \pi r^2\ -\ \frac{hN}{2} \tag{2.59}$$

where

N = r - 0.5L

the weight under the arc is

$$W_T = A_T\ \gamma_r \tag{2.60}$$

The shear resistance c_m along each slice portion of the arc is rock mass cohesion which has one value in isotropic conditions or can use values representing resistance along each segment if anisotropism or inhomogeneities occur.

The vertical component of this resistance depends on the angle from horizontal the radius makes when it is at mid point of each slice, Figure 2.18.

If the highest side of the i^{th} slice is h_{ih}, then the angle through which the vertical component of shear resistance acts is

$$\beta_i = \tan^{-1}\left[\frac{(h_{ih}\ +\ h_{(i\ +\ 1)h})\ 0.5}{N\ +\ (i-\ \frac{1}{2})s}\right] \tag{2.61}$$

$$h_{ih} = \sqrt{l_i\ (2r\ -\ l_i)} \tag{2.62}$$

where

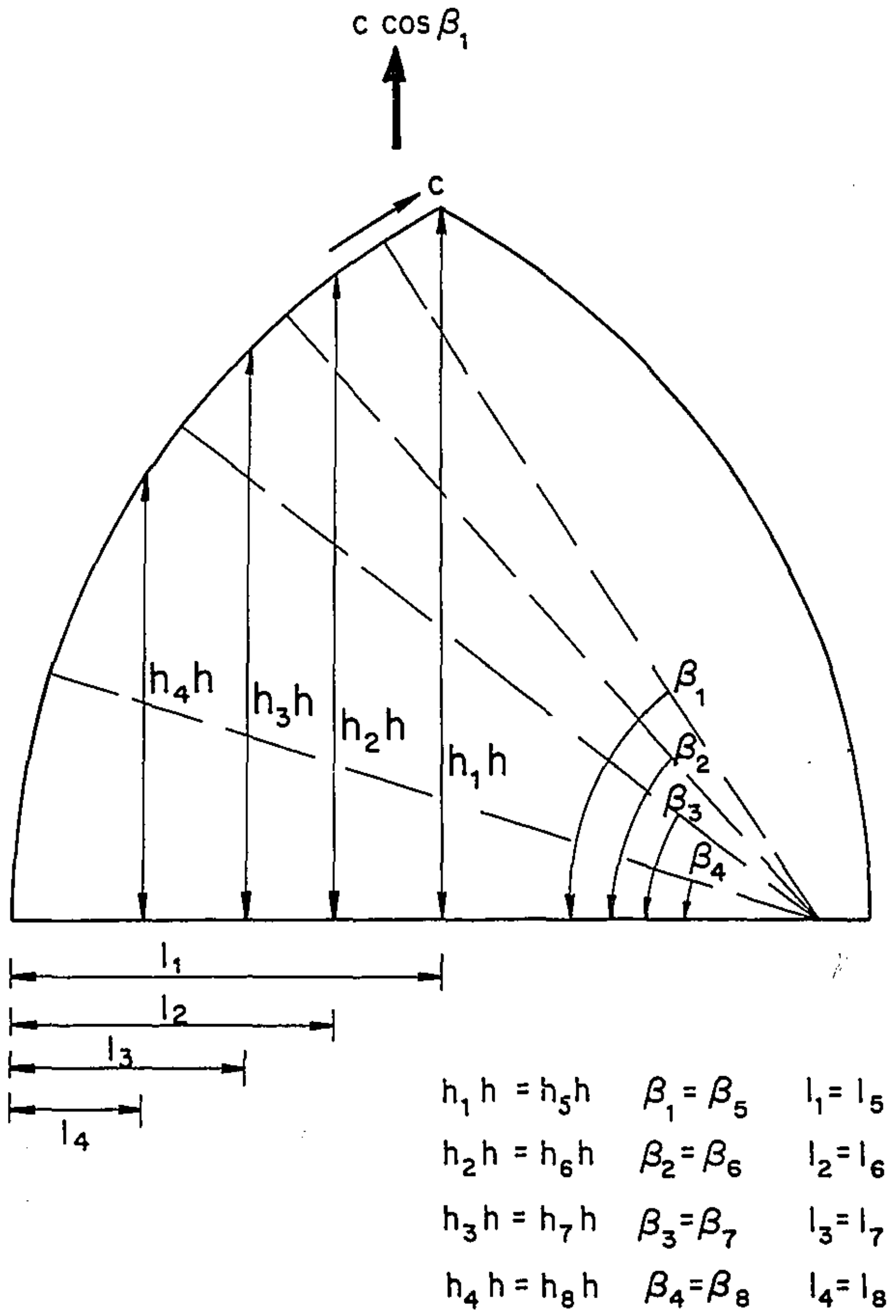

Figure 2.18 Chimneying rupture resistance per slice.

l_i = 0.5L - (i-1)s

i = i^{th} of n slices

s = width of each slice

Since the vertical component of this shear resistance is

$$c_m \cos \beta_i \tag{2.63}$$

and that it acts over an area of

$$\frac{s_i}{(\sin \beta_i)} \cdot 1m \tag{2.64}$$

then the vertical shear force resistance for each slice is

$$V_i = \frac{s}{\sin\left[\tan^{-1}\left(\frac{(h_{ih}+h_{(i+1)h})0.5}{N+(i-1/2)s}\right)\right]} c_m \cos\left[\tan^{-1}\left(\frac{(h_{ih}+h_{(i+1)h})\ 0.5}{N+(i-1/2)s}\right)\right] \tag{2.65}$$

The factor of safety against chimneying disintegration in homogeneous material is

$$F_s = \frac{1}{\gamma_r\left[\frac{(45° + \phi/2)\ \pi r^2}{360} - \frac{h_1 N}{2}\right]} \sum_{i=1}^{n} \frac{s}{\sin\left[\tan^{-1}\left(\frac{(h_{ih}+h_{(i+1)h})\ 0.5}{N+(i-1/2)s}\right)\right]} \cdot$$

$$c_m \cos\left[\tan^{-1}\left(\frac{(h_{ih}+h_{(i+1)h})\ 0.5}{N+(i-1/2)s}\right)\right] \tag{2.66}$$

When resistance within the rock mass varies, the analysis considers the materials under both arcs: the weight and shear resistance must be summated from each slice under both arcs of the rupture line.

The second and subsequent rupture lines will be parallel to the first and each will occur at some height, h_s, over the previous one when the subtended weight exceeds shear resistance. The same angle β_i is used for the same number of slices, to calculate the vertical rock mass shear resistance. At the vertical sides of subsequent rupture line, shearing over the height h_s occurs. The value of h_s is an unknown quantity which will be obtained through this limit equilibrium equation.

$$\gamma_r \, h_s \, \frac{L}{2} = h_s \, c_m + \sum_{i=1}^{n} \frac{s}{s \left[\tan^{-1} \left[\dfrac{(h_{ih} + h_{(i+1)h}) \, 0.5}{N + (i-1/2)s} \right] \right]} \, c_m \cdot$$

$$\cos \left[\tan^{-1} \left[\frac{(h_{ih} + h_{(i+1)h}) \, 0.5}{N + (i-1/2)s} \right] \right] \qquad (2.67)$$

This approach implies that the rupture mechanism is continuous once the first rupture level and ground fall has occurred. This is representative of the non-stop development of chimneying disintegration as seen in the field.

In the case of a weak, dipping homogeneous material bounded by competent rock, the development of chimneying must take into consideration that a vertical path is not possible. A known example was encountered at the Selbaie Mine [18] where only one of the two arcs of the rupture proceeded progressively up-dip to surface, Figure 2.19. This was demonstrated by physical, numerical modelling and field observations. In such a case the analysis to identify the possibility for the first failure to develop remains the same. Since sufficient weight can be mobilized for the second and subsequent rupture up dip then the process is again self-driving. The limitation to such a chimney disintegration up-dip will occur for the second rupture arc when the dip ψ of the weak zone is sufficiently shallow for the normal component of the weight on the footwall (W cos ψ) plus the resistance against tensile rupture of a rupture arc are sufficient to resist the driving force W sin ψ, Figure 2.20.

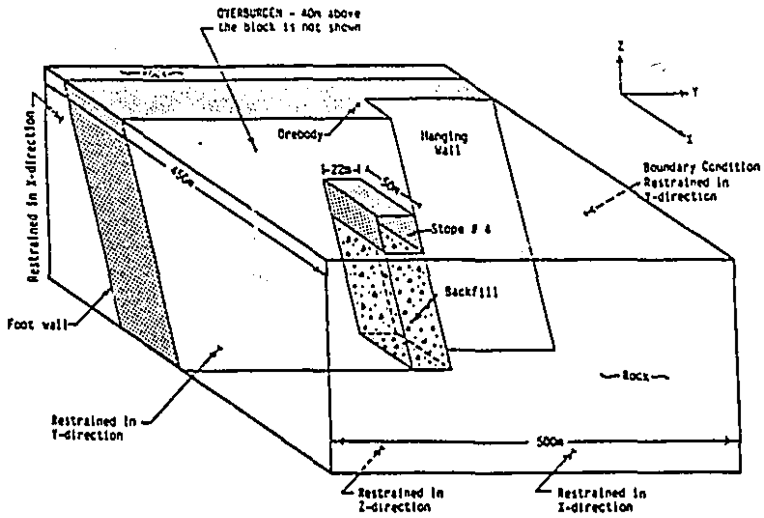

Model of 1983 Cave-in in Stope 4

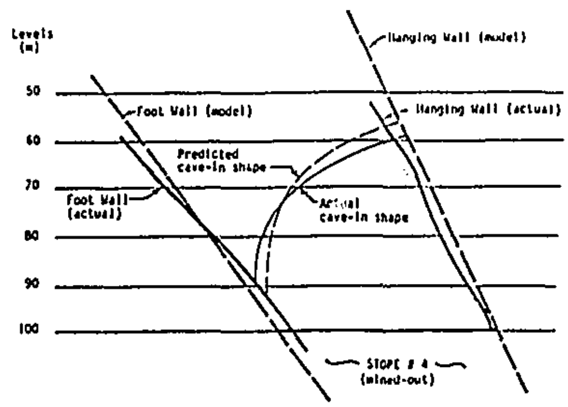

Figure 2.19 Development of chimneying failure at Selbaie Mines, numerical modelling and actual behaviour [18].

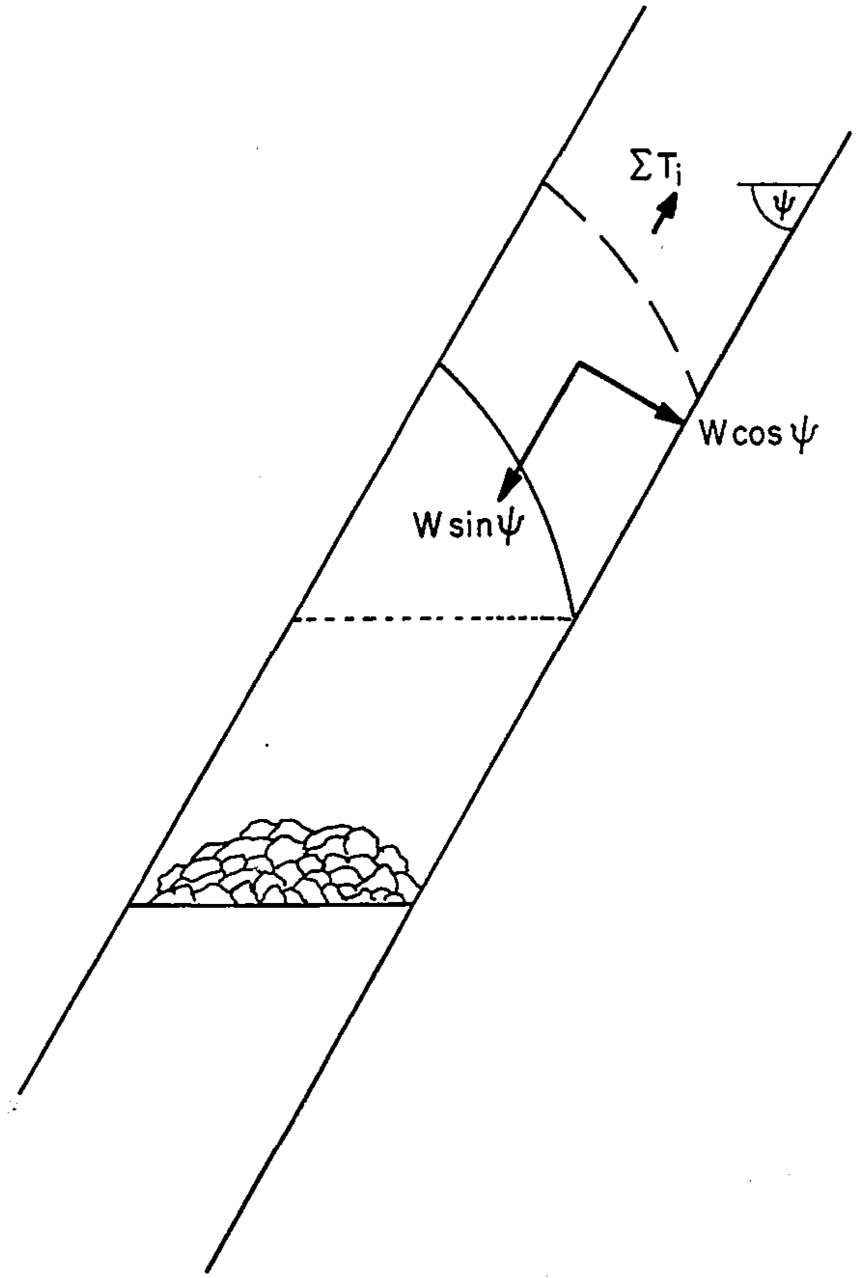

Figure 2.20 Up-dip potential for chimneying disintegration.

The limit condition for chimneying disintegration failure to continue up-dip is

$$1 = \frac{\Sigma\, T_i + W_T \cos\psi \tan\phi_r}{W_T \sin\psi} \tag{2.68}$$

where

ΣT_i = sum of the tensile resistance for all slices along an arc parallel to the first rupture arc.

ϕ_r footwall surface angle of friction

The lowest dip that chimneying disintegration failure will occur on is when the material has no tensile resistance, therefore, chimneying will occur when $\psi > \phi$. This does not take into consideration confinement effects that may be imposed to the weak zone from redistributed ground stresses, which may not be a factor if the hangingwall and footwall have reached their maximum displacement with mining and mobilization of the weak material.

2.5 BLOCK CAVING FAILURES

The main controlling parameters for the continuous gravity flow of disintegrated rock masses, block caving, have been outline in Chapter 1.4.5. These are block size, rock strength, block surface cohesion, opening span, and lateral ground stress. But given the large body of information existing on the subject and the numerous studies that have been made (Chapter 1.4.5) and the absence of dedicated analytical equations (only empirical, reflecting the difficulty of the problem), solutions to predict the onset of caving would require more intense studies than can be derived here. It can be expected, however, that identification of block falls and slides from the upper stope periphery, as described in Chapter 2.2, could lead to caving.

The approach used here to evaluate the propensity for caving is not the conditions that will initiate the caving process (mobilization and break up of the rock mass), but the mechanical action that would prevent caving from continuing. This is an arching action that effectively stops the caving process. The closest analogy to arching action in caving circumstances is that identified in vertical rough walled bins; this is similar to the outline of caving boundaries described theoretically by flow ellipsoids. In this case the boundary of the limit ellipsoid represents the bin walls.

Loosely placed material in these circumstances in which friction exists between material and wall are partially supported by friction of the vertical walls [45][90][91][92]. Krynine [91] in defining this friction showed that the usual flat arch element considered in soil arching, Figure 2.21, cannot have principal stresses acting orthogonal and parallel to bin walls. Vertical stresses at the wall are in fact shear stresses. Krynine resolved the distribution of stresses at the walls using the Mohr circle, Figure 2.22. Minor principal planes drawn through the Mohr circle poles show radiating major principal stress directions, whereas the trajectory of the minor principal stress defines a continuous compression arch that dips downward instead of upward. This argument requires that the material be in a state of plastic equilibrium and that the net movement must be vertically downward by randomized interparticle shear movements [88] (which occur in block caving). Moment equilibrium requires that the stresses be constant throughout the arch. If the element is of uniform density and thickness, the shape will be a catenary, by acting in a supportive role [92].

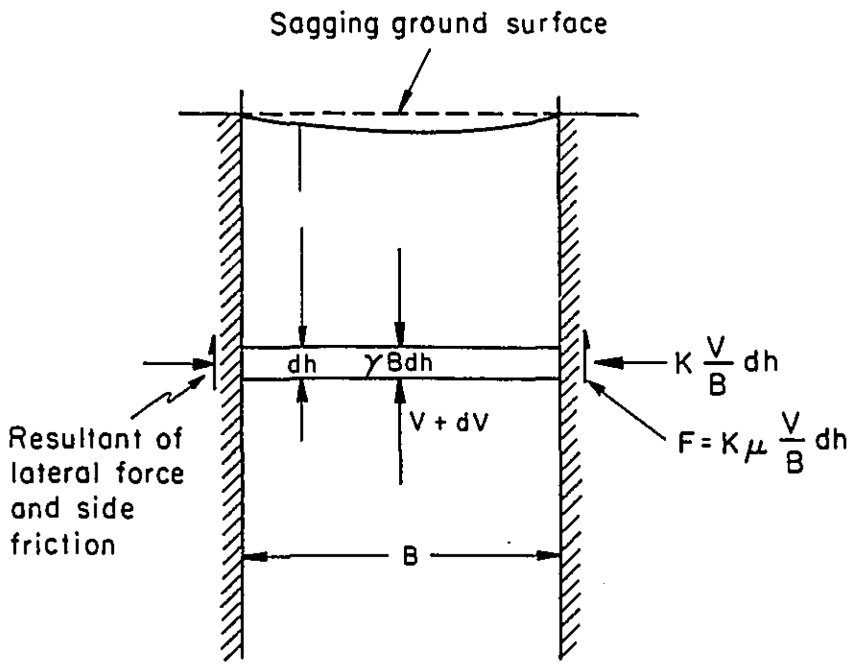

Figure 2.21 Conventional flat arch element defining soil arching [49].

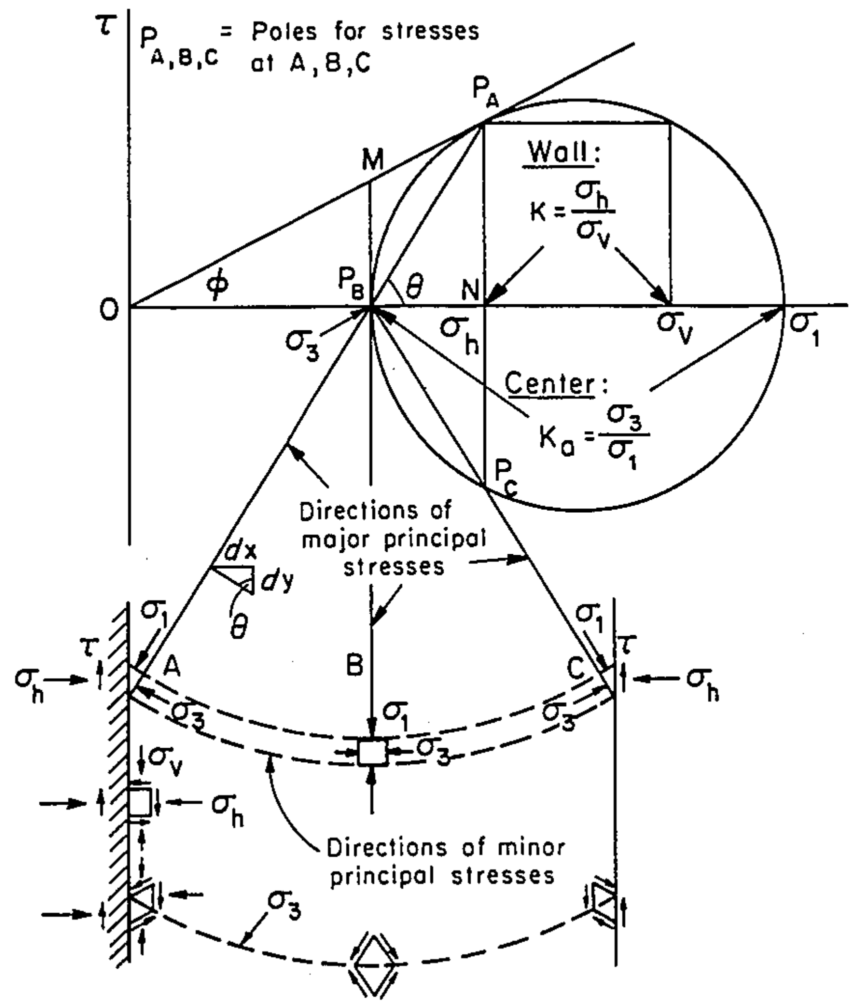

Figure 2.22 Distribution of stresses at bin walls using Mohr circle analysis [92].

The horizontal and shear stresses at the wall, where arching is occurring, from the force equilibrium on the triangular element of Figure 2.22 are:

$$\sigma_h = \sigma_1 \cos^2\theta + \sigma_3 \sin^2\theta \tag{2.69}$$

$$\tau = (\sigma_1 - \sigma_3) \sin\theta \cos\theta \tag{2.70}$$

where

σ_1 = major principal stress equal to the unit weight of rock times the depth, $\gamma_r Z$

σ_3 = minor principal stress related to σ_1 by the active stress ratio, K_a

θ = $45° + \phi_r/2$, indicating active earth pressure mobilized along a rough wall

ϕ_r = internal angle of friction of the rock material surface

Considering the soil to be in an active stress state against the bin walls

$$K_a = \frac{\sigma_1}{\sigma_3} = \frac{1 - \sin\phi_r}{1 + \sin\phi_r} \tag{2.71}$$

the catenary arch maintains its integrity through the compressive action of the minor principal stress. The principal stress σ_1 is known for any given depth, it is

$$\sigma_1 = \gamma_r Z \tag{2.72}$$

where

Z = depth from surface

γ_r = unit weight of rock

This approach has the following implications for the stability of the arch:

i) Arching is possible in all granular materials, irrespective of the material surface internal angle of friction, ϕ_r

ii) The arching shape is a catenary, which would be the shape expected of a linear arch composed of several blocks

iii) Arching is possible irregardless of span

iv) A limit equilibrium shear relationship exists at the wall contact

v) A certain thickness of arch exists to allow for the formation of lines of thrusts to transmit the loads to the walls.

vi) The arch is made up of fragments of cohesionless rock material.

Therefore failure can occur either from surpassing intact material compressive strength from stresses imposed through block contacts [45] or from exceeding the bulk compressive strength of the arch [93]. Rock blocks with cohesive surfaces would increase the bulk resistance of the arch and its ability to form and remain stable at the wall contacts.

The factor of safety to obtain the ability of the rock block within the catenary arch to resist compressive stress is

$$F_s = \frac{\sigma_c}{\sigma_1} \tag{2.73}$$

where

σ_c = unconfined compressive strength of a block.

From Figure 2.22 the highest imposed stress is expected in blocks within the arch subject to gravity loading, i.e. σ_1.

Jenike [93] postulates that gravity flow of a solid in a channel will take place provided the yield strength which the bulk solid develops as a result of the consolidating pressure is insufficient to support arching.

There is insufficient data in the literature to help define the strength envelope of gravity flow of large size bulk solids, resembling block caving situations. Wilkins [94] theorizes that strength is proportional to initial void ratio, number of contact points and number of particles broken. The strength relationship depends on contact stress point forces and orientation:

$$\frac{P}{Q} = \tan(\phi_r + \beta) \tag{2.74}$$

where

P = average force on a single stone in the direction of σ_1

Q = average force on a single stone in the direction of σ_3

β = angle made by tangent plane at point of contact with direction of σ_1

Therefore without specific lab or field tests to obtain such detailed data, it would be difficult to define the bulk strength envelope.

An alternate method could be to use approximate relationships developed by Hoek and Brown for rock masses [95] including "disturbed" rock mass situations, Table 2.1, under the material "waste rock with fines".

As per equation 2.52 in which the m field and s field values are used, a value of resisting σ_1 can be used to the σ_3 level for the required depth, presenting the factor of safety as per equation 2.53.

2.6 EFFECTS OF DYNAMIC LOADING

Rock masses supporting mining activity are regularly subjected to dynamic loading originating with blasting activity. In certain cases, seismic activity from earthquakes can also be imposed. Wave effects on rock masses are numerous. They include imposition of stress, rock mass deformation and physical damage. Their response will depend on the nature and location of the source as well as the dynamic compliance.

Table 2.1 Approximate Relationship Between Rock Mass Quality and Material Constants [95]
Disturbed rock mass m and s values Undisturbed rock mass m and s values

EMPIRICAL FAILURE CRITERION $\sigma_1 = \sigma_3 + \sqrt{m\sigma_c\sigma_3 + s\sigma_3^2}$ σ_1 = major principal effective stress σ_3 = minor principal effective stress σ_c = uniaxial compressive strength of intact rock, and m and s are empirical constants		CARBONATE ROCKS WITH WELL DEVELOPED CRYSTAL CLEAVAGE dolomite, limestone and marble	LITHIFIED ARGILLACEOUS ROCKS mudstone, silstone, shale and slate (normal to cleavage)	ARENACEOUS ROCKS WITH STRONG CRYSTALS AND POORLY DEVELOPED CRYSTAL CLEAVAGE sandstone and quartzite	FINE GRAINED POLYMINERALLIC IGNEOUS CRYSTALLINE ROCKS andesite, dolerite, diabase and rhyolite	COARSE GRAINED POLYMINERALLIC IGNEOUS & METAMORPHIC CYRSTAL-LINE ROCKS - amphibolite, gabbro gneiss, granite, norite, quartz-diorite
INTACT ROCK SAMPLES						
Laboratory size specimens free	*m*	*7.00*	*10.00*	*15.00*	*17.00*	*25.00*
from discontinuities	*s*	*1.00*	*1.00*	*1.00*	*1.00*	*1.00*
CSIR rating: RMR = 100	m	7.00	10.00	15.00	17.00	25.00
NGI rating: Q = 500	s	1.00	1.00	1.00	1.00	1.00
VERY GOOD QUALITY ROCK MASS						
Tightly interlocking undisturbed rock	*m*	*2.40*	*3.43*	*5.14*	*5.82*	*8.56*
with unweathered joints at 1 to 3 m.	*s*	*0.082*	*0.082*	*0.082*	*0.082*	*0.082*
CSIR rating: RMR = 85	m	4.10	5.85	8.78	9.95	14.63
NGI rating: Q = 100	s	0.189	0.189	0.189	0.198	0.189
GOOD QUALITY ROCK MASS						
Fresh to slightly weathered rock,	*m*	*0.575*	*9.821*	*1.231*	*1.395*	*2.052*
slightly disturbed with joint at 1 to 3 m.	*s*	*0.00293*	*0.00293*	*0.00293*	*0.00293*	*0.00293*
CSIR rating: RMR = 65	m	2.006	2.865	4.298	4.871	7.163
NGI rating: Q = 10	s	0.0205	0.0205	0.0205	0.0205	0.0205
FAIR QUALITY ROCK MASS						
Several sets of moderately weathered	*m*	*0.128*	*0.183*	*0.275*	*0.311*	*0.458*
joints spaced at 0.3 to 1 m	*s*	*0.00009*	*0.00009*	*0.00009*	*0.00009*	*0.00009*
CSIR rating: RMR = 44	m	0.947	1.353	2.030	2.301	3.383
NGI rating: Q = 1	s	0.00198	0.00198	0.00198	0.00198	0.00198
POOR QUALITY ROCK MASS						
Numerous weathered joints at 30-500 mm,	*m*	*0.029*	*0.041*	*0.061*	*0.069*	*0.102*
some gouge. Clean compacted waste rock	*s*	*0.000003*	*0.000003*	*0.000003*	*0.000003*	*0.000003*
CSIR rating: RMR = 23	m	0.447	0.639	0.959	1.087	1.598
NGI rating: Q = 0.1	s	0.00019	0.00019	0.00019	0.00019	0.00019
VERY POOR QUALITY ROCK MASS						
Numerous heavily weathered joints spaced	*m*	*0.007*	*0.010*	*0.015*	*0.017*	*0.025*
<50 mm with gouge. Waste rock with fines	*s*	*0.0000001*	*0.0000001*	*0.0000001*	*0.0000001*	*0.0000001*
CSIR rating: RMR = 3	m	0.219	0.313	0.469	0.532	0.782
NGI rating: Q = 0.01	s	0.00002	0.00002	0.00002	0.00002	0.00002

Both of these dynamic sources emit p and s type seismic waves. In the case of earthquakes, the seismic front is taken to move parallel to surface in a planar fashion. Owing to the high intensity and frequency distribution of origin, the attenuation of the wave occurs over several hundreds of kilometres. Blasting waves attenuate over several hundreds of meters and approach a particular point in a rock mass from its source around the mine in a spherical wave front. References on dynamic behaviour of rock masses [30][96][97] use p wave effects from orthogonal incidence of these waves. Shear wave effects are not discussed with respect to the stability of openings.

As a conservative approach, the impact of the seismic source can be based on its intensity at the source, acting normal to the surface examined. This does not take into consideration the attenuation imposed by the rock mass between source and point of interest nor the angle of incidence which may occur.

The spalling of rock mass blocks from the periphery of an underground opening is often registered after blasts [30][97]. There are four mechanisms induced by dynamic loading which can be responsible for such occurrences [30][96][97].

(1) added thrust towards an underground opening imposed by the seismic wave front which adds to the block-failing forces,
(2) spalling at free-face (stope periphery) because of the action of internally reflected waves,
(3) the successive wave direction changes,
(4) effects on discontinuities (between blocks) from the wave stress imposed.

During the propagation of the elastic wave, each material particle executes transient motion. This velocity is associated with a dynamic state of stress which is superimposed on any static stress existing in the material. Therefore the component of this stress in the direction having failure (down dip and towards an opening) will change the limit equilibrium equation by adding a force to the sum of destabilizing forces. This loading has the most influence on block slides and falls, and strata failures from hangingwall or crown. The intensity of the effects depends on the location of the seismic source and the wave peak particle velocity.

When a compressive wave is reflected at a free face (such as the periphery of a stope) a tensile wave is generated and internally reflected within the rock mass. As this wave sweeps past the original oncoming wave there will be a moment and also a distance from the free surface where the resulting stress will become tensile [30][97]. This can effectively open rock mass joints that are nearly parallel to the periphery. But the role of such a reflected tensile pulse is limited in space due to joint separation, trapping the wave near the free face.

With respect to failures from block or strata, secondary action of dynamic waves can continue to weaken the rock mass from successive shocks incorporating reversals in motion, and from internal reflections within the rock mass from free surfaces and open discontinuities. Roof blocks that can potentially fall are supported only by lateral clamping stress and may be affected by such tensile stress when it is sufficient to reduce the effect of the clamping stress. Successive changes of wave direction or reduction in clamping stress leading to insufficient block support are other, if temporary, effects on block or plug failures. In this case the ground motion may come and go before the block (s) has (have) travelled very far from their position or the duration of the stress reduction sufficient to prevent a return to the static stress clamping thereby allowing total block slippage. Thus successive block movement with a series of destabilizing events can occur (temporary and partial mobilization on failure surfaces) or even allow the largest of blocks to slip-out totally (full failure plane mobilization).

The fourth effect relates to the loss of strength at the failure plane due to dynamic loading. Tests reported by Barton and Bakhtar [74] show that even at low normal stresses (e.g. < 2 MPa) the first (less so for subsequent) cycles of loading significantly reduces joint aperture by destroying asperities and therefore reducing shear resistance, affecting small block surfaces more. A further loss of shearing strength along a potential failure plane can arise if dynamic loading can build up pore pressure along the failure surface. i.e. the joint not being able to drain effectively during the application of load. In this case the dynamic load adds directly to the pore water pressure. This case is more representative of a long plug failure surface(s) because smaller blocks around the periphery of the opening have no water pressure imposed, Figure 2.3. Barton and Bakhtar summarize that typical joint permeability at low normal stress (< 2 MPa) is of the order of .01 to .001 m/sec which, over the lengths of plug discontinuities of several tens of meters may not allow significant drainage even after several dynamic wave impacts.

Reduction of vibrations which can affect the integrity of a shallow stope can be done in two fashions. Blast damage can be used to monitor the effect of the location (periphery and failure type) and energy of blasting activity. In this case, reduction in the powder factor should be balanced between production efficiency and damage. In weak rock masses, reduction in the powder factor can reduce the break-up of the mass, inception of shear rupture and mobilization of chimneying disintegration. Seismic monitoring could indicate peak particle velocity values for comparison to blast damage and for input values to calculate the reduction in stabilizing forces.

CHAPTER 3

THE PIERRE BEAUCHEMIN MINE CASE STUDY

3.1 GENERAL GEOLOGY

The Pierre Beauchemin Mine is located in Quebec, 20 km north-west of Rouyn-Noranda, Figure 3.1. The site is situated in the Superior Province of the Precambrian Shield.

The host rocks are tonalite and diorite, portions of the Flavian Pluton. It is 17 x 18 km in extent, the largest of regional intrusives, Figure 3.2. The diorite, the youngest rock type, cuts older ones such as the tonalite. The mineralization consists of a series of small lenses, striking Northeast-Southwest and dipping approximately 38° Southeast. The gold is finely disseminated, found in the tonalite country rock as well as the diorite intrusive, and believed to have been concentrated by the action of, and along, a wrench fault [98]. The ore grades 6.4 g of gold and 1.03 g of silver per ton of ore.

Several structural geology elements are present at the mine site. Two major discontinuities, faults, are located close to the orebody, Figure 3.3. One is found in the footwall, the second accompanies the orebody, located between the immediate hangingwall and footwall of the ore. Their strikes are similar to that of the orebodies, but the dip varies from 35-45°, and can be steeper locally.

The faulting, besides forming large scale weakness planes, is associated with surrounding zones of alteration and schistosity. The alteration products in diorite are carbonate stringers paralleling the schistosity and the fault. In tonalite, the surrounding

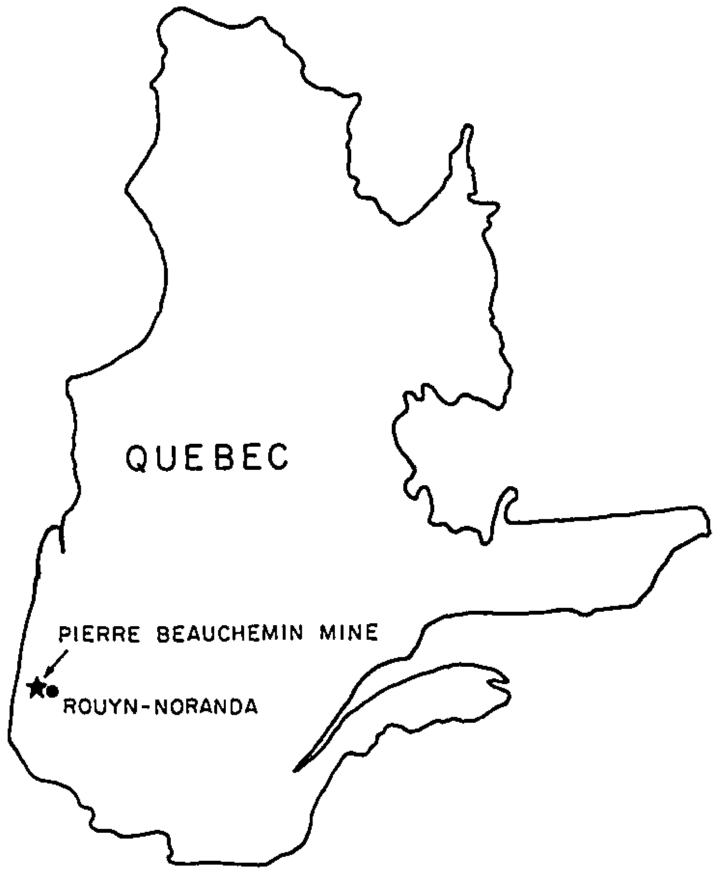

Figure 3.1 Location of the Pierre Beauchemin Mine.

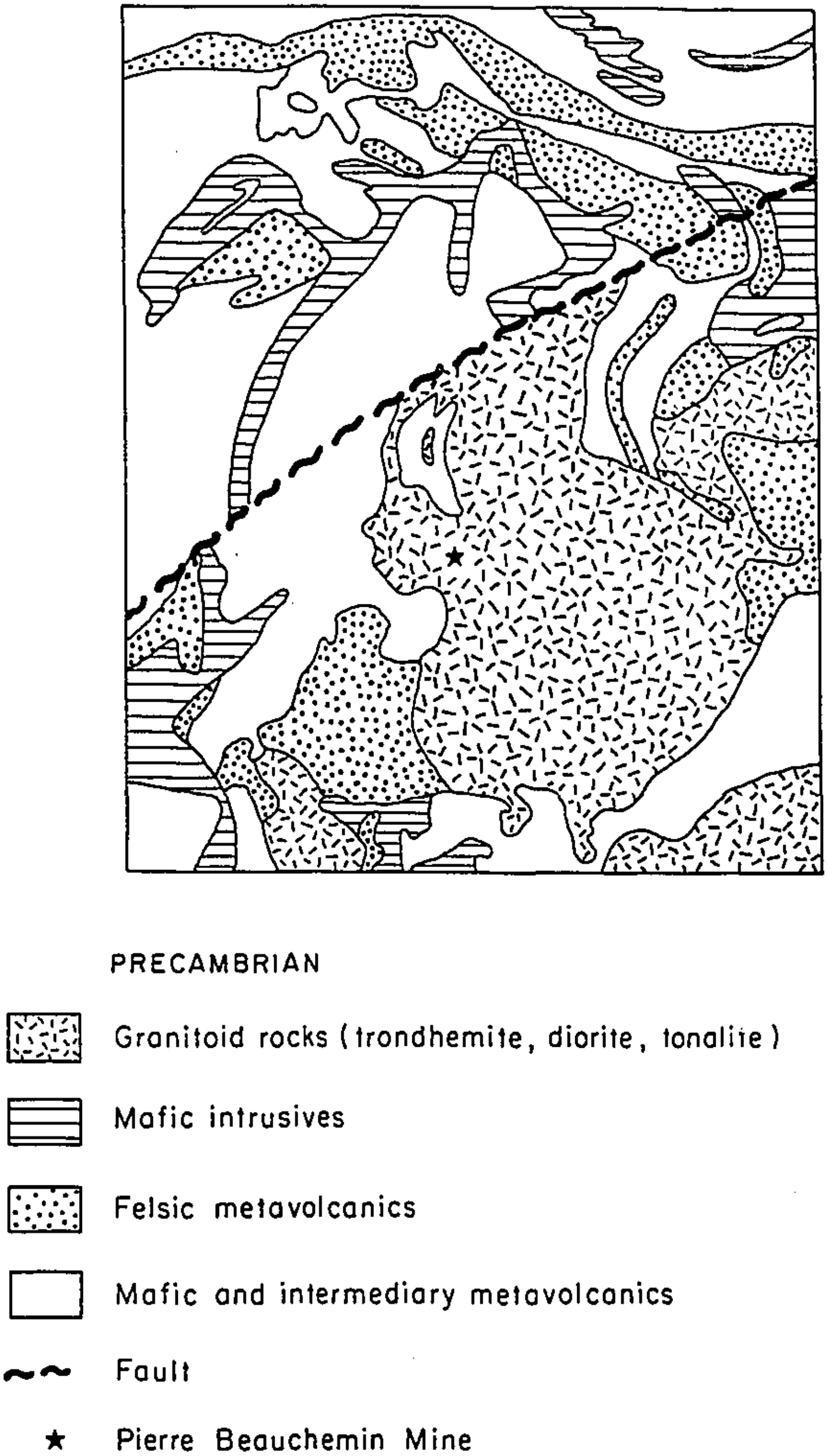

Figure 3.2 Regional geology, Pierre Beauchemin Mine.

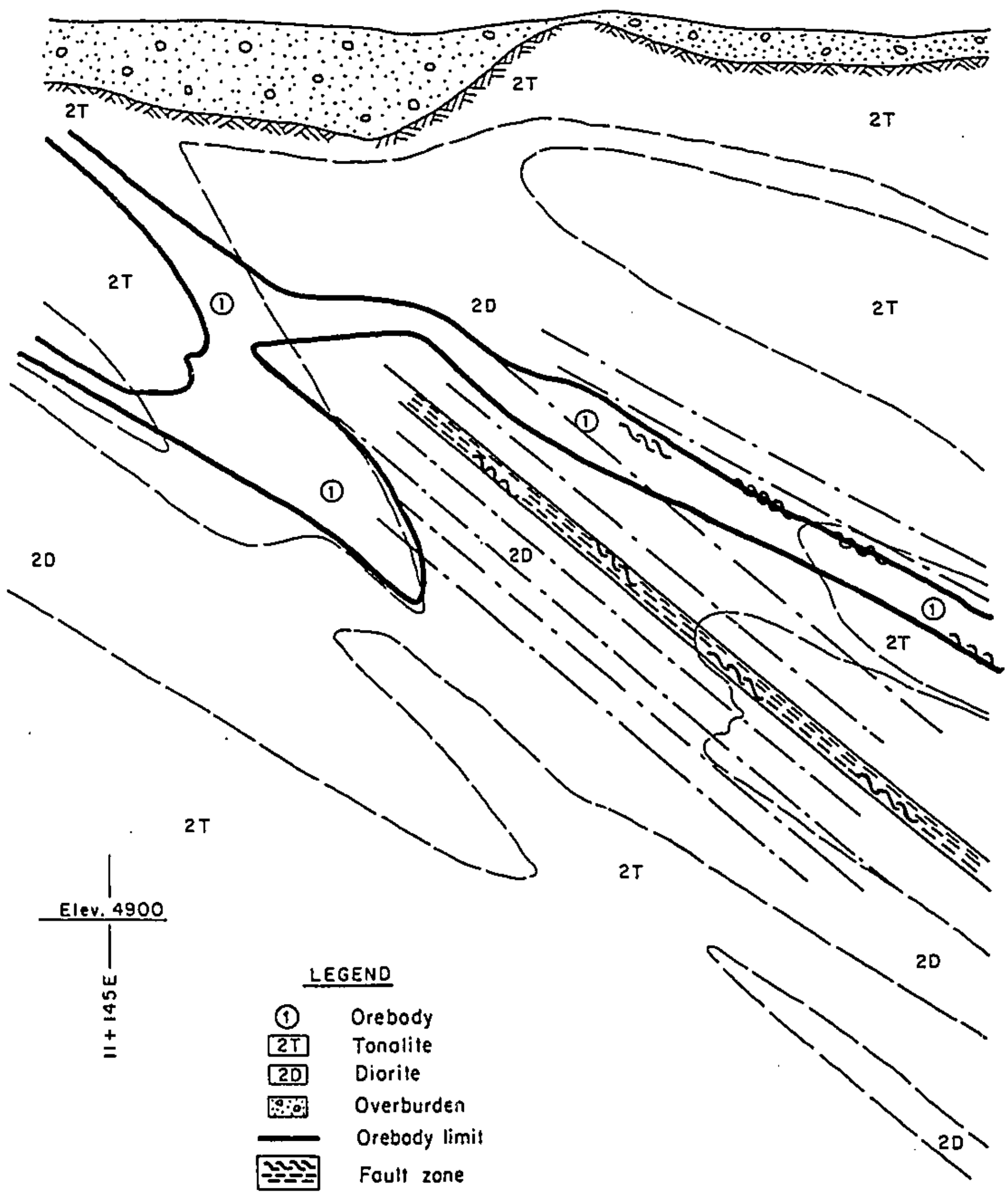

Figure 3.3 10+50N mine cross-section, Pierre Beauchemin Mine.

rock is silicified and moderately hematized. Gouge, up to 45 cm thick, is located on the fault traces. It has high plasticity and a low water content. The gouge is surrounded by hard schistose material which easily breaks. The total thickness of the fault zone is usually 2 m but can extend to 5 m. For this research program the components of the fault zones were identified but could not be sampled undisturbed because of their weak nature.

The joints intersecting the openings in the vicinity of the shallow stopes are well defined. The structural survey performed for this thesis on rock core and drifts in the vicinity of ore zone indicated that four joint families exist. Three families are regularly present, Figure 3.4: S65E 85NE, N20E 50NW, N25E 45SE, with a fourth family S50E 60SW occurring randomly. The N25E 45SE joints are wide joints which effectively stratify the rock mass surrounding the shallow stopes.

The properties associated with these joints are summarized in Table 3.1. Water inflow was not seen during the in situ surveys. Except for the N25E 45SE family, the joint distribution is not regular. Spacing is usually greater than 30 cm. When the joint families intersect to form blocks, their sizes are at least 0.5 -1 m^3.

Figure 3.5 performs the block movement analysis described by Hoek and Brown [48] for the recognition of block roof falls and block slides using the stereographic method (Figure 2.4).

The Pierre Beauchemin joint surfaces are unaltered. Barton [11] prescribes an angle of 35° for slightly rough, unaltered joint surfaces; it is drawn in Figure 3.5. The joint relationship drawn there indicates that three block geometries can potentially fall and one type of block geometry slide is possible along the orebody cross-section, which coincides with the S65E 85NE joint family.

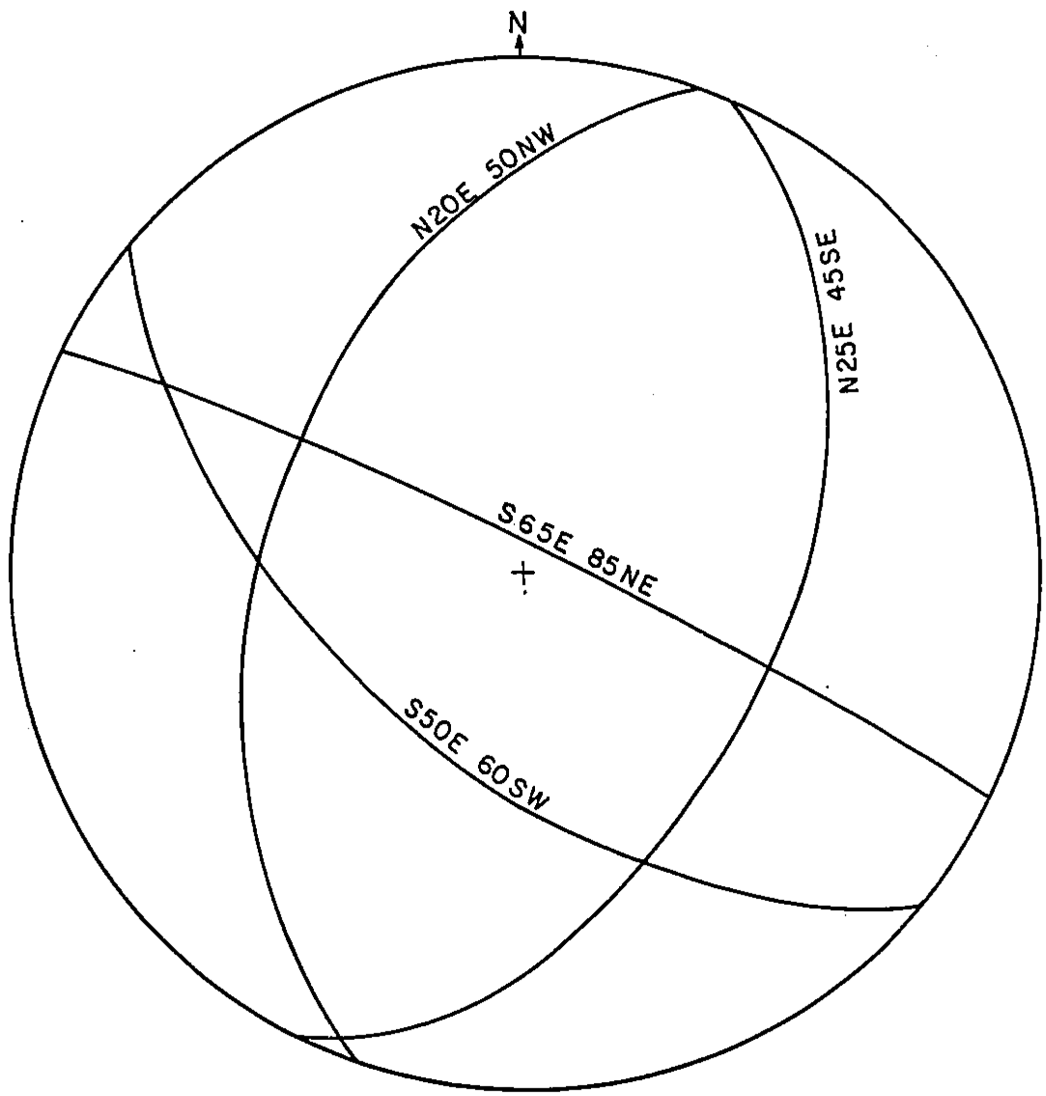

Figure 3.4 Stereographic projection of joint families around the 105N-1 shallow stopes, Pierre Beauchemin Mine.

Table 3.1 Properties of Pierre Beauchemin Mine Rock Joints

Joint Family		Spacing (m)	Average Joint Length (m)	Joint Condition
N25E	45SE	0.25	>40	Planar, slightly rough; no alteration
N20E	50NW	>1	>2	Planar, slightly rough; no alteration
S65E	85NE	>0.3	>5	Planar, slightly rough; no alteration
S50E	60SW	>2	>2	Planar, slightly rough; no alteration

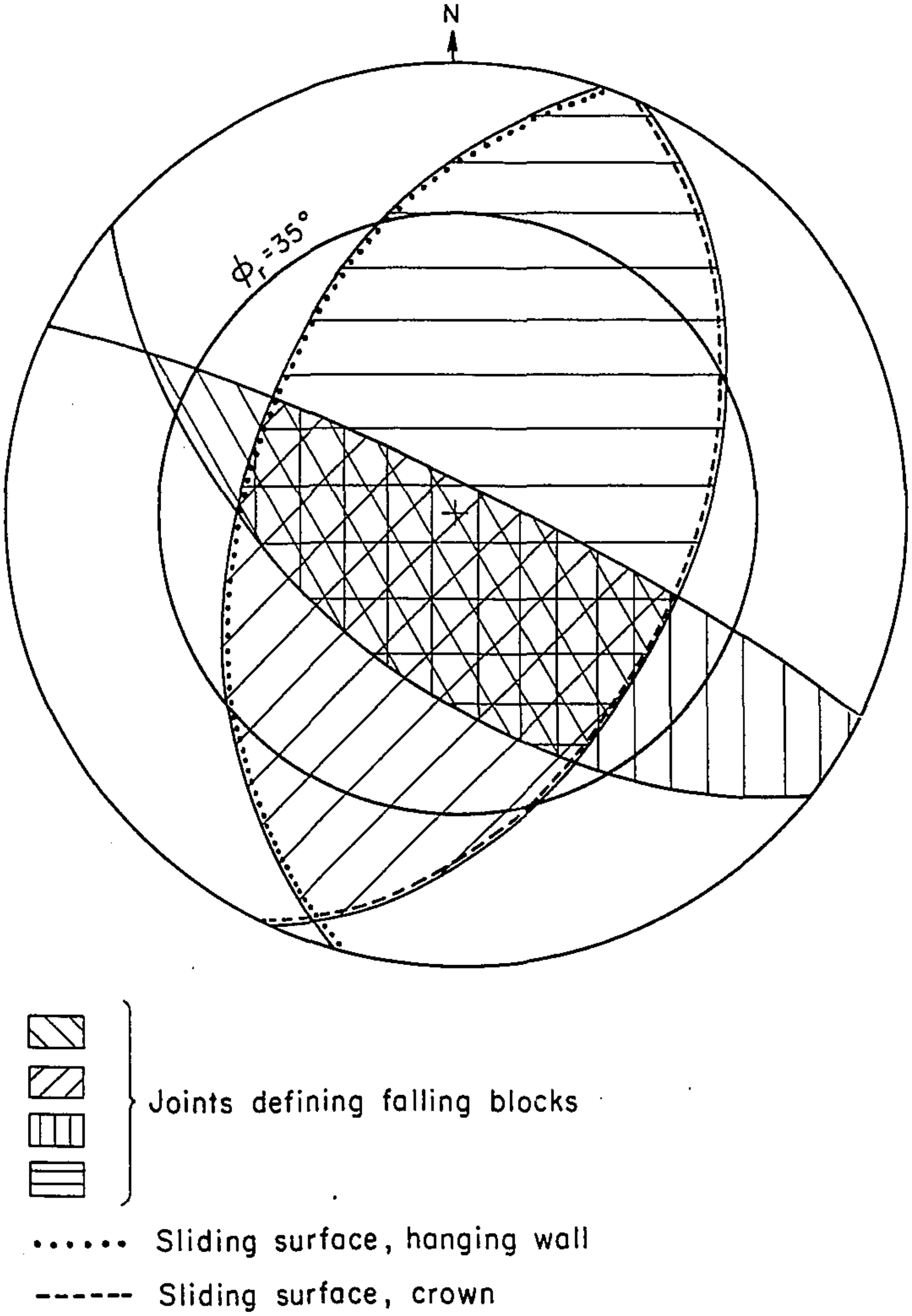

Figure 3.5 Analysis of potential joint-defined block movements around shallow stope 105N-1, Pierre Beauchemin Mine.

Because the family S50E 60SW randomly occurs, and because its strike is similar to the S65E 85NE family, the joint will not be considered in block movement analysis. One block form defined by the three other joints is capable of sliding from the crown or hangingwall, and falling from the crown.

3.2 MINING EXTRACTION

Between 1955 and 1962 a previous operator, Eldrich Mines Ltd., carried out underground mining to a depth of 300 m, creating several long drifts and open stopes. This included eight shallow stopes, each mined from the depth of approximately 30 m to a depth of about 130 m. These had a longitudinal span of 110 to 125 m. and footwall to hangingwall heights varying from 6 to 15 m.

In 1984, Mines Sullivan Inc. acquired the mining rights and, after a period of diamond drilling exploration, re-opened the mine to extend the shallow stopes closer to surface and mine a new and extensive zone situated deeper and to the east of the known lenses. In 1988, Cambior Inc. purchased Mines Sullivan Inc. and renamed the mine as the Pierre Beauchemin Mine.

Because fill has been considered uneconomical, bolting and pillars have been the only means of support. The general mining method is by longhole. Drill patterns are performed at a set distance along the dip of the stope, within the stope, Figure 3.6. After the ore is blasted, a scraper is used to bring the ore to an ore chute at the center of the bottom of the stope. In the case of the shallow stope extension up-dip, a two-bench approach was used where jack-leg drills and blast cycles would be performed on the upper

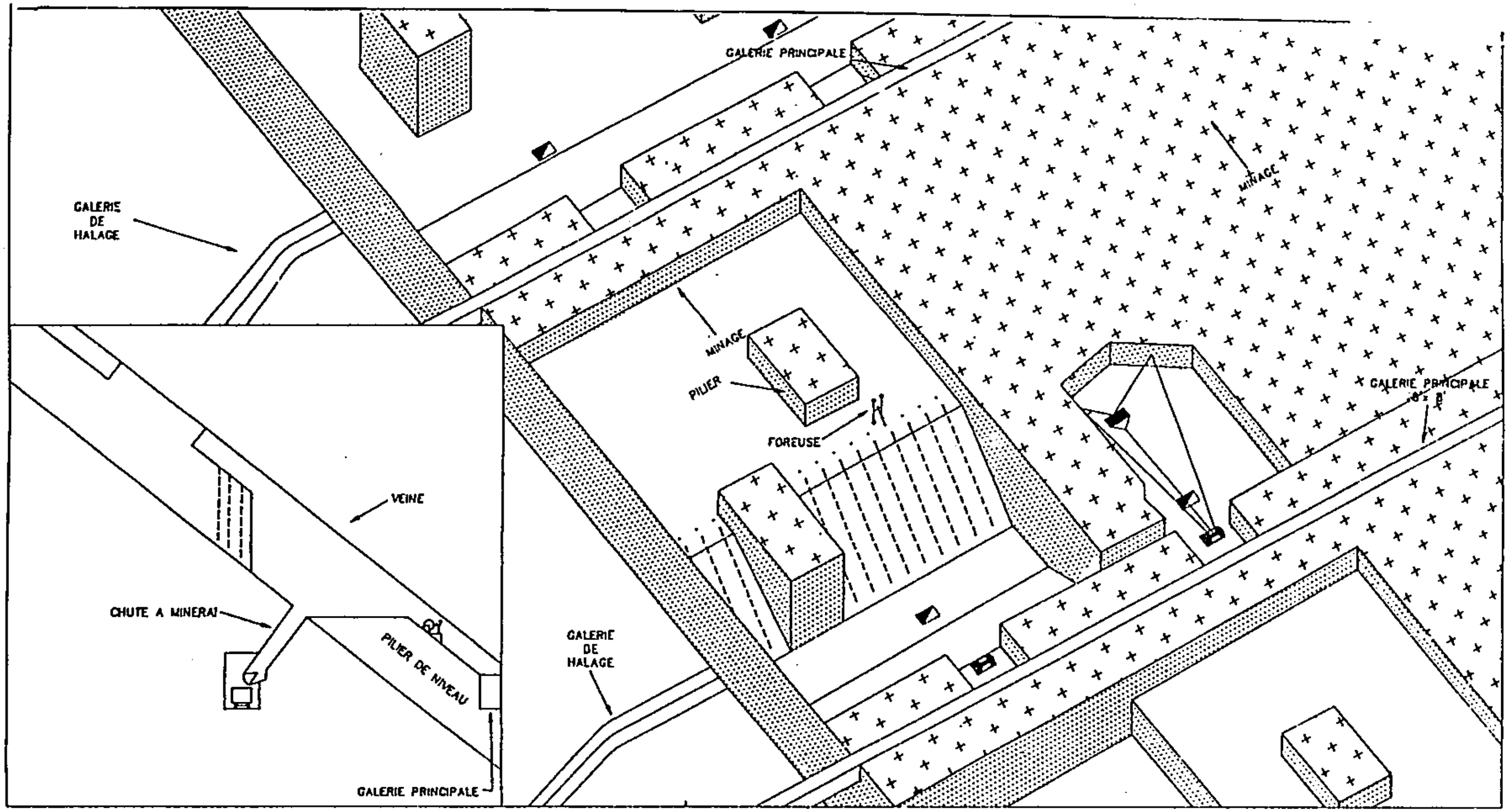

Figure 3.6 Pierre Beauchemin Mine, mining method (mine drawing).

bench followed by the lower bench.

3.3 SELECTION OF CASE STUDY

The Pierre Beauchemin Mine was selected as a case study for the following reasons. It is representative of the Canadian hard rock mine characteristics defined in Table 1.1: several joint families and faults transecting the rock mass, considerable overburden, and long stopes that are not backfilled. The case reflects a rock mass environment where well-developed hangingwall stratification exists. (Figure 1.3f). Furthermore, other joint families can combine to provide possible forms of block failures around the shallow stope periphery. Three types of failure mechanisms are therefore evident and could be designed for: ravelling from blocks formed by joint intersections, strata failure related to the wide joints existing throughout the rock mass but affecting the hangingwall, and also possibly allowing a plug failure.

These mechanisms can occur over the wide shallow stopes, representing a case where failure potential is high. Because the problem is geometrically (several stopes on dip) and geomechanically complex (several materials of varying properties), global analysis such as modelling is required to obtain representative stress and displacements affecting every opening. In this case modelling can possibly also indicate areas of failure. Comparison between the developed shallow stope analytical equations and modelling is therefore worthwhile.

The Pierre Beauchemin Mine is an active mine where the potential for failure becomes an important issue for worker safety. For the shallowest stope only 17 m separates saturated overburden (sand and gravel overlying low plasticity clay), conditions similar to the Belmoral soil inflow which followed the collapse of a shallow stope. Therefore, further mining extraction towards surface must be carefully evaluated. The work performed under this thesis would supply the mine operators with information that would have a bearing on further shallow stope expansion that is currently planned. Because site access was possible, rock core available and in situ tests already performed, supplementary rock and rock mass property evaluations could be added which would well define the site geomechanically and provide representative results of analyses.

3.4 NUMERICAL MODELLING

3.4.1 Numerical Model Selection

Applications of numerical models in rock mechanics provide the possibility of obtaining approximate solutions to the behaviour of surface or underground excavations while considering a large number of influencing factors such as natural earth stresses, rock properties, ground support, geometry of opening, etc.

Modelling of solid materials such as rock masses can be divided into two approaches: one approximating the mass as a continuous medium, the other a discontinuous approach, regarding the mass as a group of independent blocks.

The differential type of continuum models, including boundary and finite element techniques, characterize the entire region of interest. Boundary element models, in two or three dimensions, feature discretization only along interior or exterior boundaries. The interface between different material types and discontinuities are treated as internal boundaries which must be similarly discretized. Boundary element procedures are most apt for modelling linear, homogeneous elastic systems, although certain forms of non-linearity can be treated. They provide economic means of two- and three-dimensional rock mass analysis.

The finite element method is well suited to obtain continuous stress distribution in two or three dimensions and carry out estimation of mining induced fracture and weakness zones adjoining openings, by utilizing suitable failure criteria. Mining induced displacements are calculated. Irregular geometries, non-uniform material, non-uniform loadings, and location of stopes close to surface can be addressed. Non-linear material behaviour can be modelled.

Discontinuum models feature numerical procedures involving the equations of motion of blocks. Distinct element analysis is an example of a discontinuum model. The response to applied load on these relatively large block systems are calculated in time steps taking into account block interactions. In this method, the solution process is based on a force-displacement law specifying the interaction between the blocks and a law of motion which determines displacements induced by out of balance forces. The blocks can be treated as rigid or endowed with the ability to deform. This method is restricted to two dimensions unless very large computers are used. As with continuum models, it is still necessary to compute using a pre-determined mesh, with precise location of all joints.

The selection of a particular numerical code therefore depends on a proper definition of the problem to be modelled. In examining the geometry of the opening(s) a 2-D or 3-D approach can be selected. A 2-D approach assumes that the openings, geological units and rock mass properties are infinitely continuous in a direction perpendicular to the 2-D section modelled. Openings which are very long can be so modelled with representative results; those that are not will have such modelling predict conditions, such as redistributed stresses and displacements, which may be more accentuated than the real case.

A continuum model can be used when the material in reality remains continuous after openings are created. Otherwise, a discontinuum model should be used where movements are sufficiently large to break down the continuity throughout the rock mass.

Treatment of the material load-deformation response is linear elastic when it follows a linear relation between the components of stress and strain, i.e. Hooke's law.

When irrecoverable strain is produced by stressing a material, non-linear behaviour must be considered.

Finally, geological materials must also be examined in regards to their mechanical properties in various directions. Isotropism reflects the same mechanical properties in all directions. Anisotropism, whereby mechanical properties of rock are expected to be different in various directions, should be considered in the model.

In the case of the Pierre Beauchemin mine the following material properties were used in selecting the type of numerical model and its material properties. Laboratory tests performed (section 3.4.2) indicated that the diorite and tonalite rocks behaved elastically and had no anisotropic behaviour. All samples tested, which were obtained from drill holes at different orientations, showed similar results. Visual inspection of the rock core also revealed no physical rock composition variations.

Inspection of the rock mass at the site, in access drifts and stopes, has revealed no disassociation of the rock mass before ground support was installed.

The shallow stopes of the mine are opened 110 - 125 m in the longitudinal direction. The Pierre Beauchemin shallow stopes can therefore be justifiably modelled using a 2-D linear elastic code. Ideally, this code should also be able to model the non-linear behaviour expected of the faults cutting the rock mass.

The SATURN code developed at McGill University is such a numerical code. It is a 2-D boundary element code, written to represent the rock behaviour as linear elastic. Faults can be considered as separate material, behaving in a linear elastic fashion (using the Coulomb or Goodman [99] discontinuity failure criteria) or non-linear fashion (using the Barton-Bandis [74] discontinuity failure criterion). The fault zone thickness at Pierre Beauchemin (approximately 2 m) would be sufficient to consider each as distinct geological units, capable of being stressed and showing representative strains for given stresses encountered (as opposed to a fault with only a thin weak zone which would always show large, unrepresentative strains). At this point in time, however, consideration of ground surface as a limiting plane had not been completed so that shallow stopes could not be properly modelled.

Instead, the MSAP2D numerical model was adopted. MSAP2D (Microcomputer Static Analysis Package for 2-Dimensional Problems) is a finite element numerical model developed at McGill University for use on personal computers equipped with mathematical coprocessor and fixed disk [100]. The system is composed of five modules. The first three modules--ZONE, PRESAP and MESH 2D--represent the preprocessor and the graphics interface of the system. The fourth module, program MSAP2D, is the core processor of the system. The fifth module, program POSTSAP, is an enhanced-graphics postprocessor. Screen or printer output are possible for the entire, or portion of, model mesh, element and node numbers, as well as vectorial nodal displacements, major and minor principal stresses of all elements. Moreover, the Coulomb, Hoek and Brown [52], and Drucker-Praeger [65] failure criteria are incorporated in order to allow for the calculation of the safety level of a problem.

The fault zones are sufficiently thick to have been considered as distinct geological units.

3.4.2 Geomechanical Properties

Input of geomechanical material properties as well as natural ground stress values was necessary for analysis with the analytical failure and empirical equations, as well as modelling with MSAP2D. In particular, the material weight, Young's modulus of elasticity, Poisson's ratio, and initial stress data in the model's x and y direction were required. Furthermore, the field value of the m and s parameters were also required, as input data into the Hoek and Brown failure criterion used to evaluate global rock mass stability around the mine openings modelled.

The Hoek and Brown failure criterion was selected because it can translate laboratory test intact strength values to field values, using rock mass quality, and allows a Mohr-Coulomb rock mass strength envelope to be generated. Furthermore, if laboratory or rock mass strength properties are not available, tables of approximate parameter values exist from which representative values can be selected (Table 2.1).

For this research the lab tests performed to supply model input parameters and material strength characteristics consisted of uniaxial and triaxial compression tests, and Brazilian indirect tensile tests, using rock core obtained from three diamond-drill holes used for dilatometer testing (located in the hangingwall of shallow stopes). As mentioned earlier, no visual evidence of rock fabric was evident. Lab test results showed no variation in strength results with samples originating from these holes.

The results showing the mean values of the compression strength results and the mean value of the Brazilian tensile strength are shown in Table 3.2. The intact rock cohesion intercept and angle of friction are also included, as is the calculated Hoek and Brown failure criterion laboratory m value. This represents the intact rock m value. It was calculated using the regression calculations prescribed by Hoek and Brown [52]. The s value is always equal to unity for intact rock. This failure criterion also allows the rock mass value of the m and s parameters to be calculated, based on rock mass quality developed by Bieniawski's Rock Mass Rating [55].

The Rock Mass Rating for tonalite and diorite was calculated after examination of the rock core (Appendix 1), and used to transform lab intact strength to rock mass strength, Table 3.3, as per Brown and Hoek [54], equations 1.43 and 1.44.

The geomechanical parameters of the fault zone were not measured directly, however, because undisturbed sampling of the weak fault zone material could not be performed by diamond drilling or manual sampling. Instead, representative values for the model input parameters were sought from references.

The fault is composed of two weak materials, the clay gouge on the fault discontinuity and the schist material surrounding it. Shear strength tests on fault gouge or fault gouge and surrounding material have been few, Table 3.4. The results show that in the low normal stress range tested (which is also the expected range for shallow openings) in situ cohesion varies from 0.1 to 0.24 MPa and angle of friction from 25°-45°.

Table 3.2 Pierre Beauchemin Mine Rock Material Laboratory Test Results

	Compressive Strength (MPa)		Tensile Strength (MPa)	Modulus of Elasticity (GPa)	Poisson's ratio	Cohesion (MPa)	Ø (degrees)	Hoek & Brown m value	Unit Weight MN/m^3
	Confinement	Peak Strength							
Tonalite	0 5 10 15 20	184.5 195.8 225.3 259.2 296.2	14.9	76.7	0.27	33	50	11.2	.0269
Diorite	0 5 10 15 20	58.8 88.0 100.2 116.0 138.8	12.8	72.2	0.28	18	46	4.7	.0272

Table 3.3 Pierre Beauchemin Mine Rock Mass Rating Parameters

	RQD	Rock Mass Rating (RMR)	Field	
			m	s
Tonalite	60	74	4.42	0.056
Diorite	77.6	75	1.83	0.06

Table 3.4 Shear Strength Parameters for Fault Materials (Tabulated in Barton and Bakhtar [74])

Faulted Material Type	Description of Filling	Type of Test	c'_m (MPa)	Ø' (degrees)	σ_n' (MPa)	References
Granite	Clay-filled faults	in situ direct shear test				
	(30% 5μ clay)		0.1	45	0.1-1	Rocha [98]
	(40% 5μ clay)		0.1	25	0.1-1	
Basalt	Clayey basaltic breccia: wide variation from clay to basalt content	in situ direct shear test	0.24	42	0-2.5	Ruiz et al [104]
Granite	Tectonic shear zone: schistose and broken granites, disintegrated rock and gouge	in situ direct shear test	0.26	45	0-4-0.7	Evdokimov and Sapegin [94]

The assembly of schist and gouge at Pierre Beauchemin is similar to the Evdokimov and Sapegin [101] value shown.

As for the m_{field} and s_{field} value to adopt for the fault material, neither Hoek [53] nor Hoek and Brown [95] which provide approximate relationships for fault zones and material constants discuss fault material values. Since the s value represents relative rock mass cohesion and m relative rock mass angle of friction [53], and since fault zone material could be classified in the lower rock quality RMR values, Table 2.1 was used to couple rock mass quality with Hoek and Brown m and s values. Assuming an RMR < 22 ("Poor" quality), an m = 0.2 and s = 0.0001 were chosen. The s value takes into consideration the plasticity of the fault gouge and zone shear strength, the m value the lower angle of friction provided by the schistosity planes. Calculation of the fault zone cohesion with these values (Appendix 1) using the Hoek and Brown equations 1.45 to 1.49 returns a value of $c_m \geq 0.25$ MPa, in the lower stress range, which is comparable to the Evdokimov and Sapegin values (Table 3.4).

In situ field tests carried out by private consultants for the mine have determined the rock mass modulus of elasticity using the Ménard pressuremeter in 7.5 cm size boreholes [102] at a depth of 10 m to 30 m. Also determined at this site were the direction and values of pre-mining ground stresses performed by CANMET [27]. In this case, the method of overcoring using CSIR triaxial strain cells ("Leeman cells") was used. Test measurements were carried out at a depth of 115 m, some 640 m laterally from the stope being modelled. Table 3.5 presents the in situ modulus of elasticity and natural ground stress values.

Table 3.5 Pierre Beauchemin Mine Summary of In Situ Geomechanical Field Parameters [26][102]

Average Modulus of Elasticy, E_m (GPa)		
Tonalite	20.0	
Diorite	12.6	
Natural Ground Stresses		
	Orientation (bearing/dip)	Value (MPa) (depth = 115 m)
Major Principal Stress	96°/12°	10.8
Intermediate Principal Stress	2°/20°	6.3
Minor Principal Stress	192°/66°	3.3

Dilatometer tests and lab tests were not carried out in the fault zone material. Reference to values obtained by other authors had to be made.

Cording et al [103] and Rocha [104] present values of 8 to 14 GPa for modulus of elasticity values of schists. A lower modulus value, 3 GPa, was chosen for a combined fault-schist value because of the lower schist integrity surveyed in the field. Similarly, 0.29 for Poisson's ratio was chosen as a combined value.

3.4.3 The Pierre Beauchemin Mine Numerical Model

The MSAP2D numerical modelling code was used to model a representative shallow stope of the mine. The model required input of the modulus of elasticity, Poisson's ratio and unit weight of each geological material, as well as in situ stress distribution in order to calculate displacements and stress redistribution.

Several lenses have been extracted leaving behind shallow stopes but one stope in particular would be advantageous to model. The 105N-1 stope, Figure 3.7, is the mine's shallow stope situated closest to surface, 17 m vertically from the top of bedrock. It is the uppermost of a series of stopes extracting ore from the 105N lenz. Furthermore, the mine was evaluating the possibility of advancing this stope closer to surface.

The current dimensions of the 105N-1 stope are: 43 m on a 45° dip, with a measured height of 5.4 m. The longitudinal dimension is 120 m. The modelling section is assumed to be located at longitudinal mid-span. The tonalite (material 1) forms the greater portion of the surrounding rock mass, whereas diorite (material 2) forms the immediate rock mass of the shallow stope. One fault (material 3) and associated weakness zone crosses the 105N-1 stope between the footwall and hangingwall, whereas

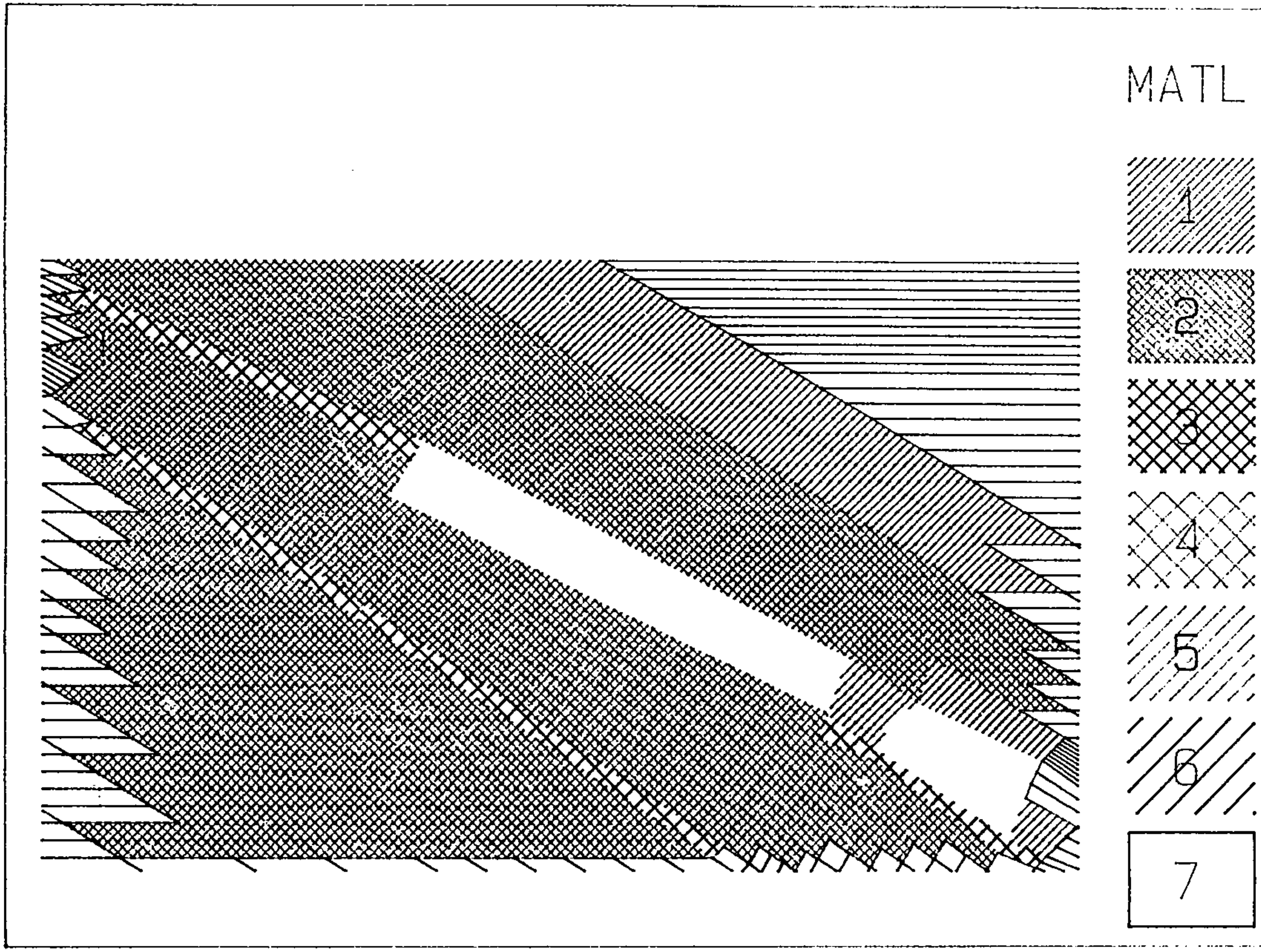

Figure 3.7 Enlargement of the Pierre Beauchemin numerical model: geology around the existing shallow stope. Materials: 1 - tonalite, 2 - diorite, 3 - fault zone.

the second fault zone is 20 m into the footwall, Figure 3.7.

Numerical modelling was carried in three runs to represent three mining steps: current stope size - 17 m from the overburden; mining extraction expanding the stope to 11 m, and to 6 m from surface, creating an on-dip stope span of 50 m and 57 m respectively for mining steps two and three.

In each case the model width was 780 m and the height, starting from surface, was 540 m deep. The mesh is composed of smaller elements, 1 m x 2 m on average, around the periphery of the shallow stope, especially the hangingwall and surface crown pillar in order to arrive at a good representation of the redistribution of stresses around the opening. In this fashion a better definition of critical and failure areas could be afforded with the model's failure criteria, and with the applications of the analytical equations which use distributed stress values as the input parameters. The first mining step was defined by a mesh of 2650 elements; the second, 2930; and the third, 2900 elements. Figure 3.8 shows the mesh for the outline of the current 105N-1 stope. Figures 3.9 - 3.10 show the mesh for the two planned expansions.

3.4.4 Modelling Results

Figure 3.11 is an enlargement of the displacements calculated to have occurred around the current shallow stope. The maximum displacement is 2.2 mm and occurs at the central periphery of the stope hangingwall. The pattern of rock mass displacements is similar for the next two mining steps. The hangingwall displacements remain unchanged, but the displacements in the surface crown pillars increase as extraction advances.

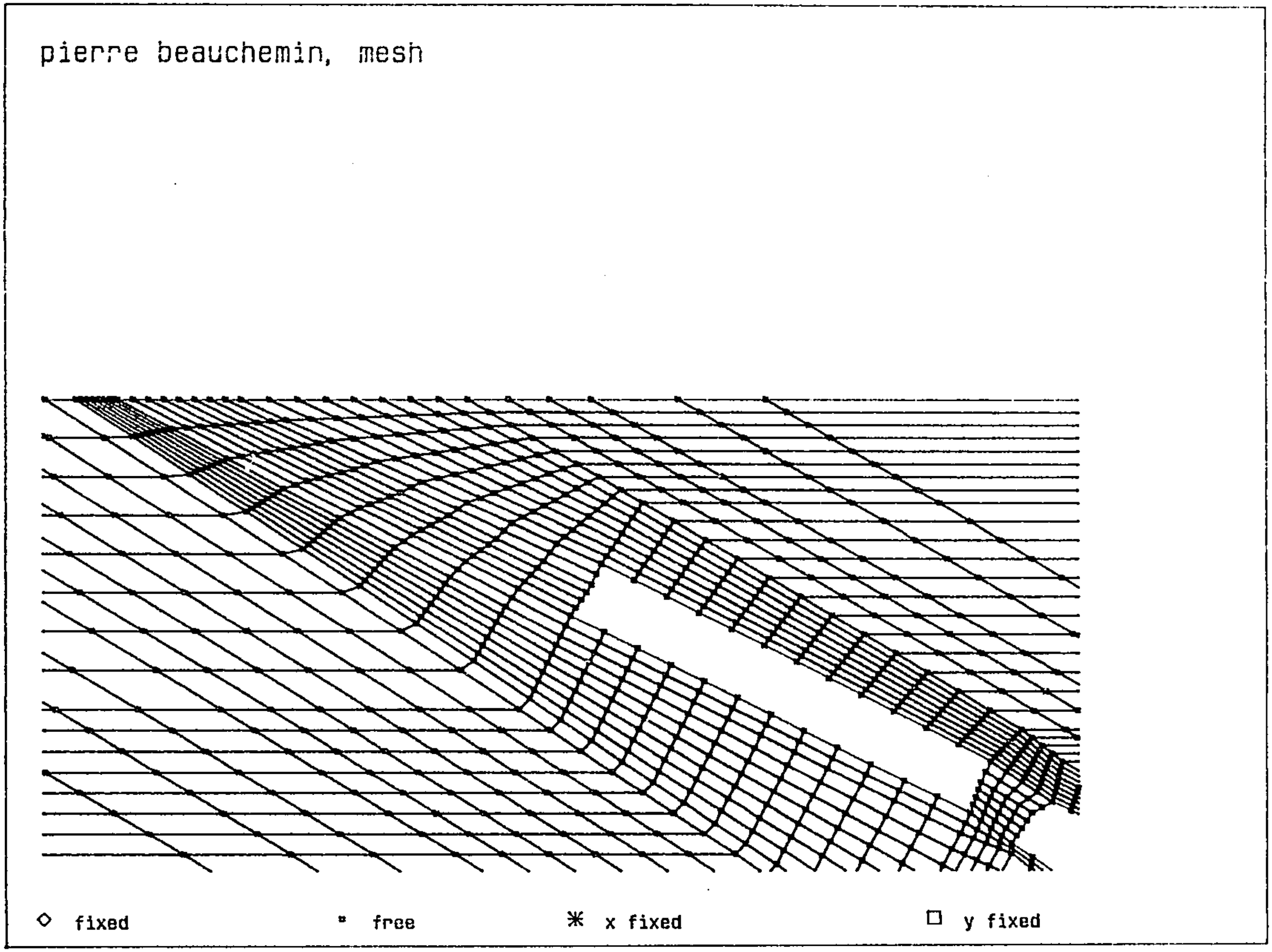

Figure 3.8 Enlargement of the Pierre Beauchemin Mine numerical model mesh around the shallow 105N-1 stope, current stope size (mining step one).

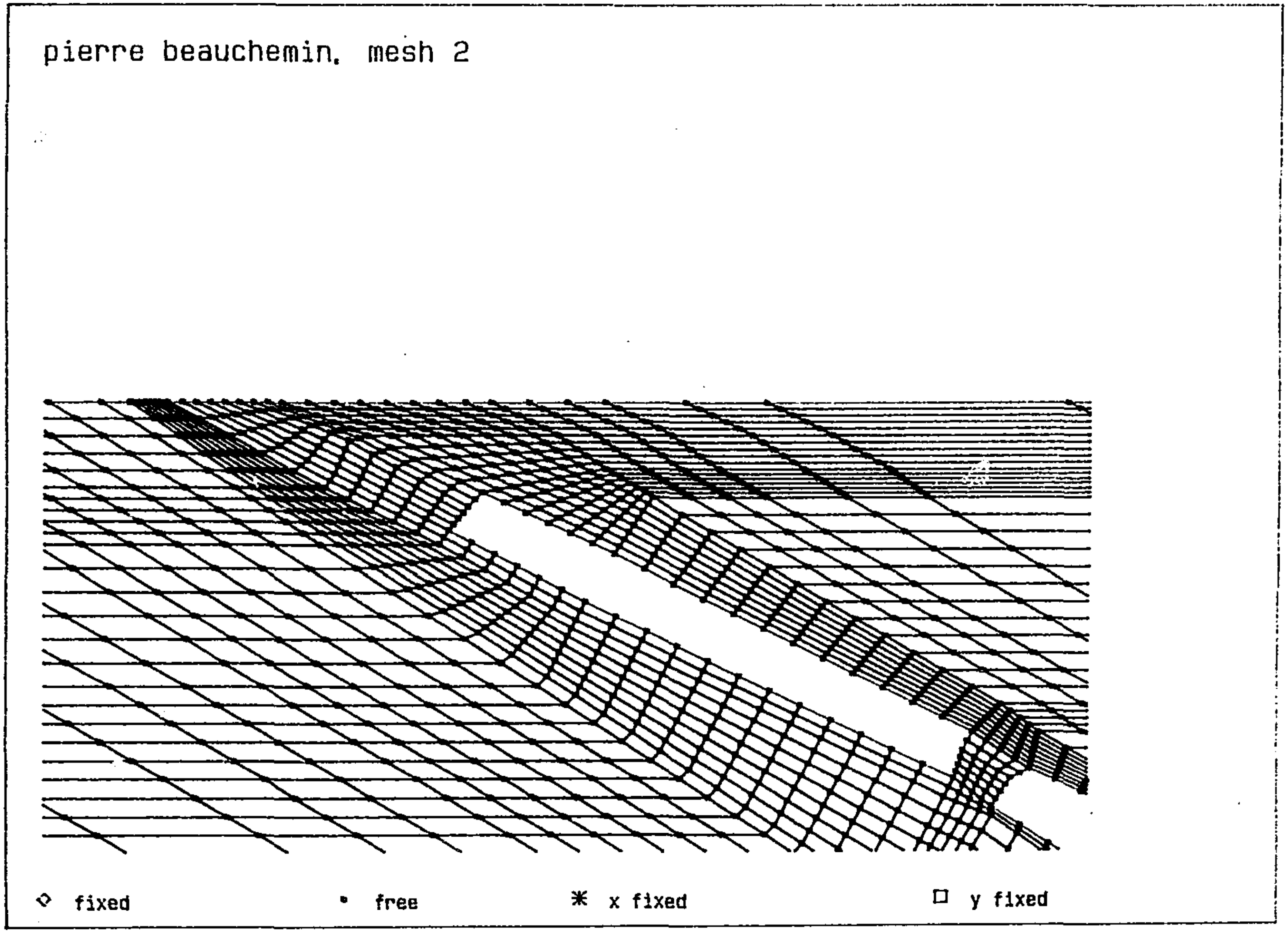

Figure 3.9 Enlargement of the Pierre Beauchemin Mine numerical model mesh around the 105N-1 shallow stope, first stope expansion (mining step two).

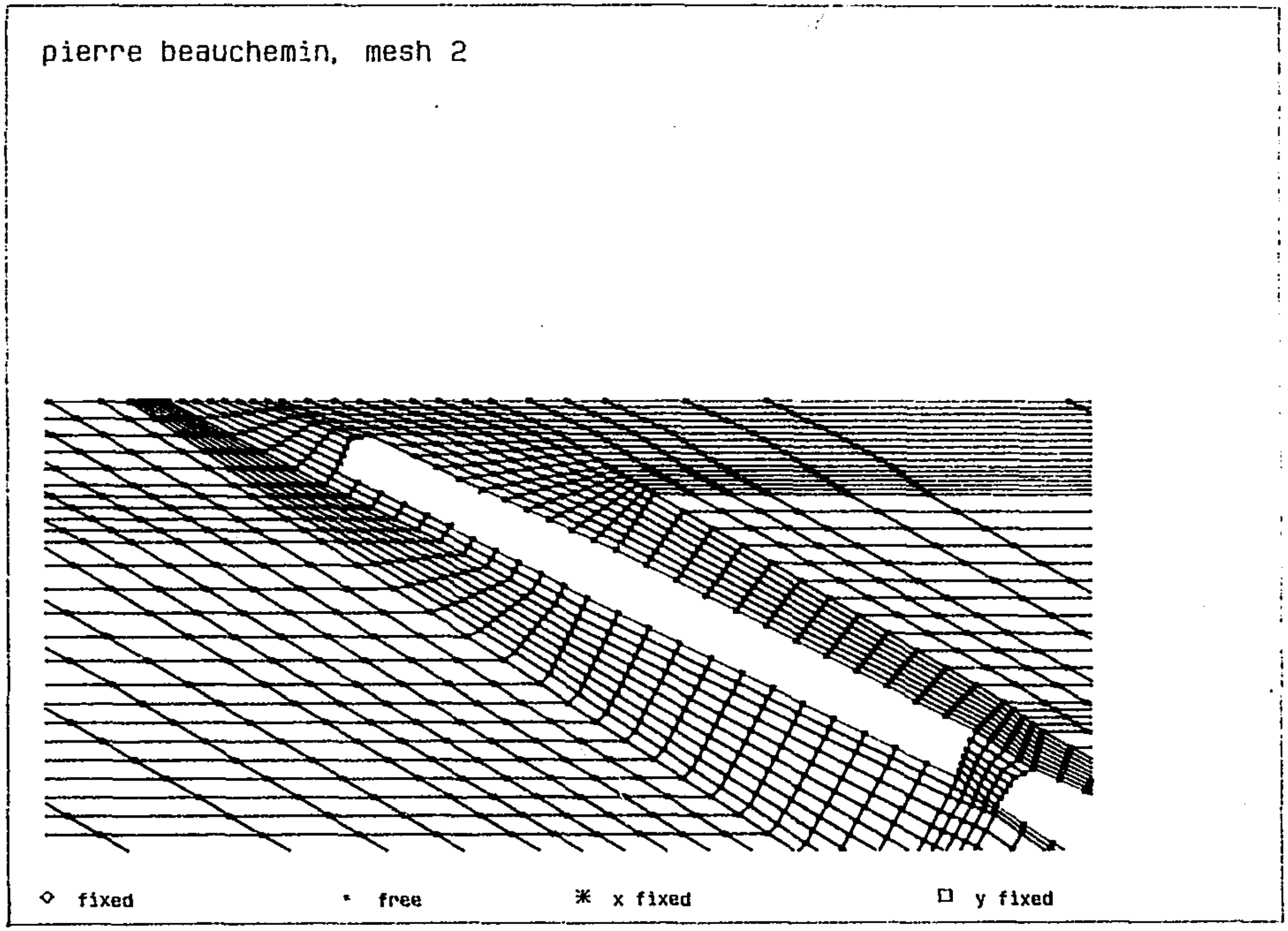

Figure 3.10 Enlargement of the Pierre Beauchemin Mine numerical model mesh around the 105N-1 shallow stope, second stope expansion (mining step three).

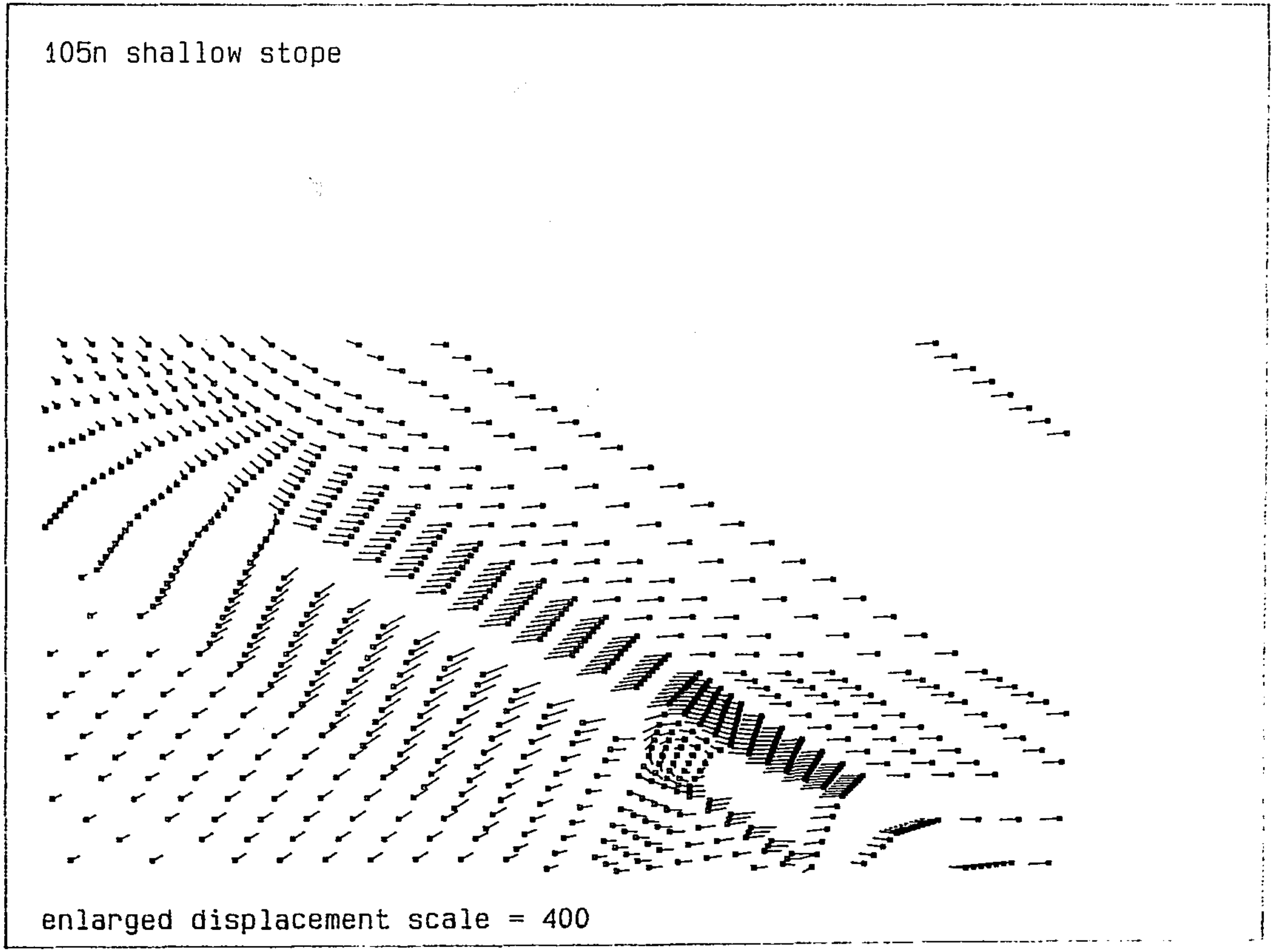

Figure 3.11 Pierre Beauchemin Mine, model displacements around shallow 105N-1 stope, mining step one.

The major principal stress at this site is horizontal in the plane of the section modelled and is 3.3 times the vertically oriented minor principal stress. This high ratio would account for the net horizontal displacements towards the shallow stope as well as the displacement trend above the shallow stope, towards surface. This trend becomes more evident with mining extraction, displacement toward surface reaching 1 mm at the third mining step.

Figures 3.12 to 3.14 show the stresses around the shallow stope for each mining step. The tensile stresses located at the surface crown pillar/upper footwall area increase in magnitude, and extend in the surface crown pillar area with each mining step, whereas tensile stresses in the hangingwall (radial) extend along the periphery and at depth but do not appreciably increase in magnitude with each mining step. A level of 0.45 MPa is reached with step three at a 12 m depth into the hangingwall.

The tangential stresses remain constant and compressive over most of the stope periphery, as the stope span is expanded. In the sill pillar between the first and second stope 11 MPa compressive is recorded; the surface crown pillar is subjected to up to 6.5 MPa compressive stress at its periphery. Tensile tangential stresses increase significantly in the upper footwall from 0.8 MPa for that first mining step to 2.1 MPa in the third step.

Application of the Hoek and Brown failure criterion incorporated in MSAP2D allowed for the relative estimation of failure given elastic behaviour of the material under the stress conditions imposed around the shallow stope. Based on material values outlined in Table 3.3, this is shown in Figures 3.15 - 3.17.

The diorite and tonalite are at a high safety level (safe: $F_s > 1.4$) with each mining step. Only two elements at the stope footwall fall below this category at the third mining

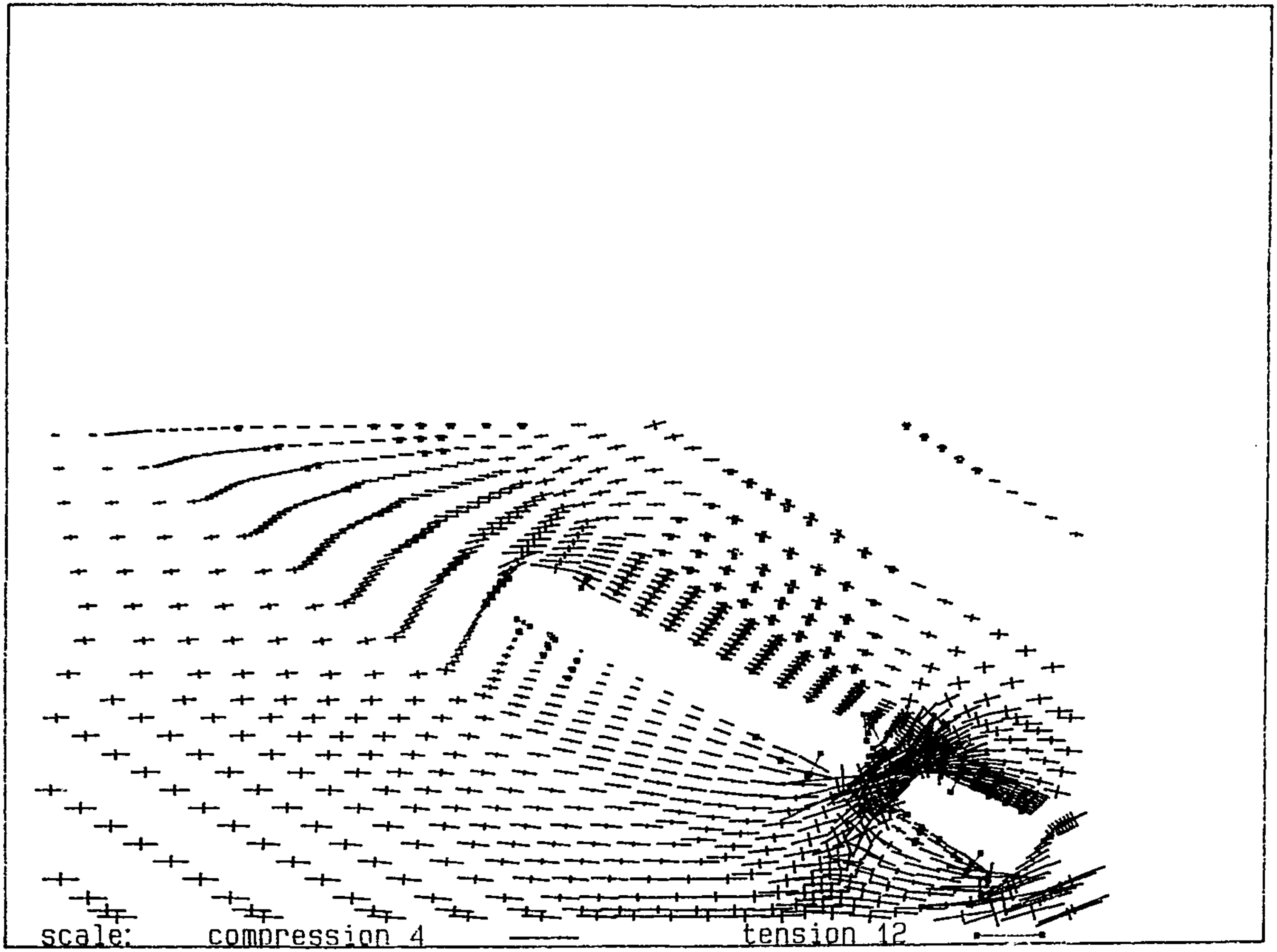

Figure 3.12 Numerical modelling results of imposed ground stresses, mining step one, around shallow stope 105N-1, Pierre Beauchemin Mine.

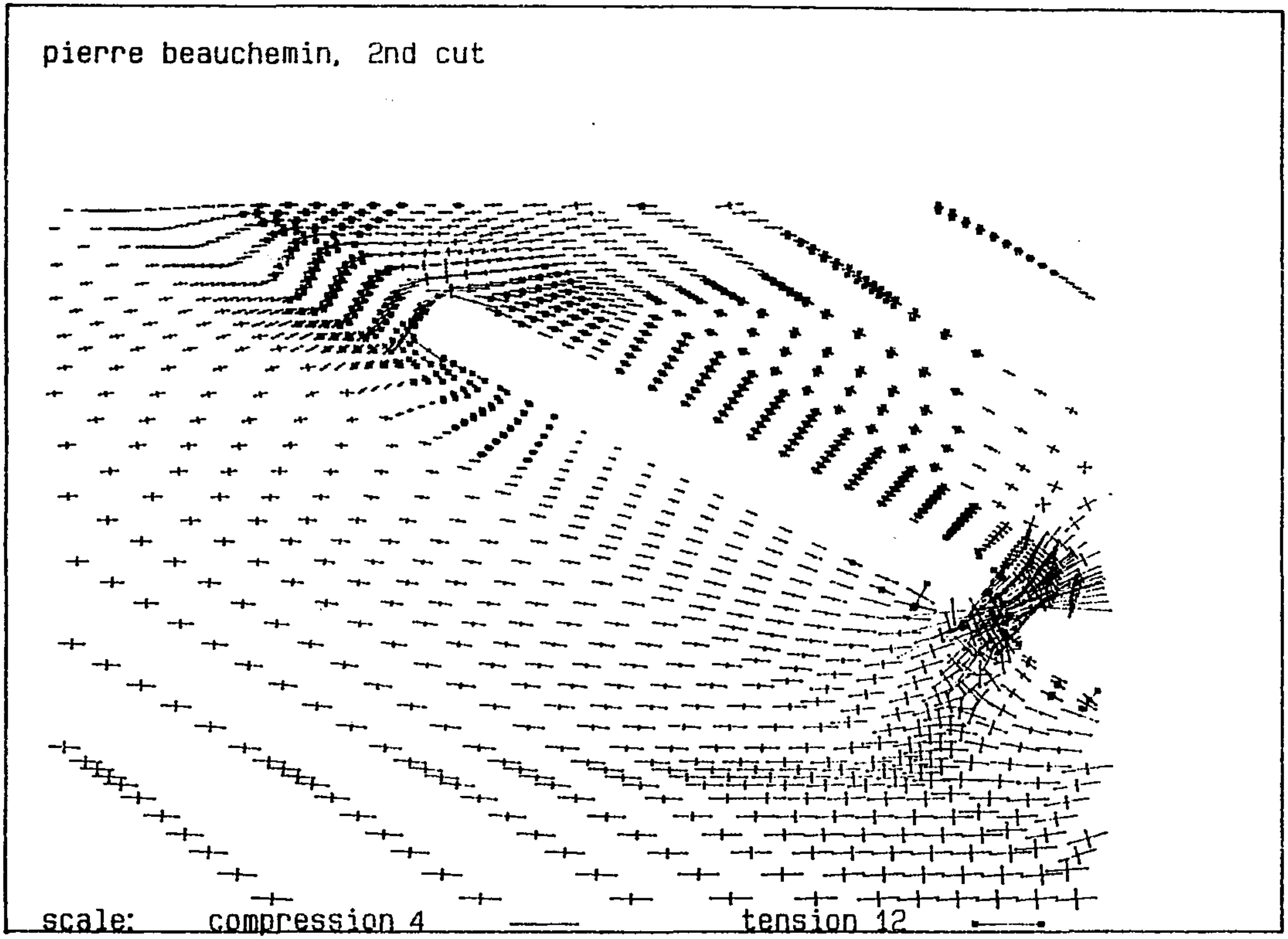

Figure 3.13 Numerical modelling results of imposed ground stresses, mining step two, around shallow stope 105N-1, Pierre Beauchemin Mine.

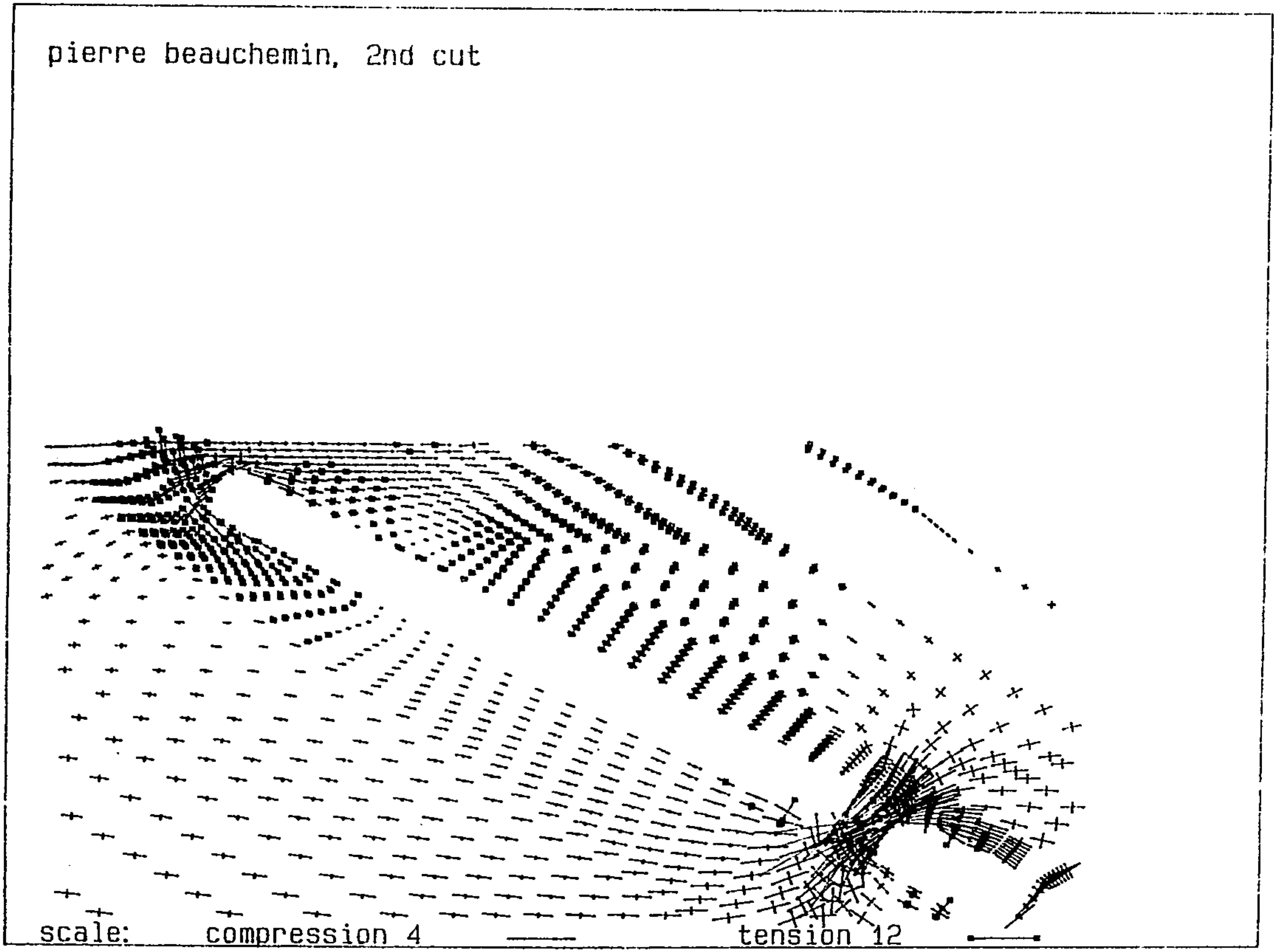

Figure 3.14 Numerical modelling results of imposed ground stresses, mining step three, around shallow stope 105N-1, Pierre Beauchemin Mine.

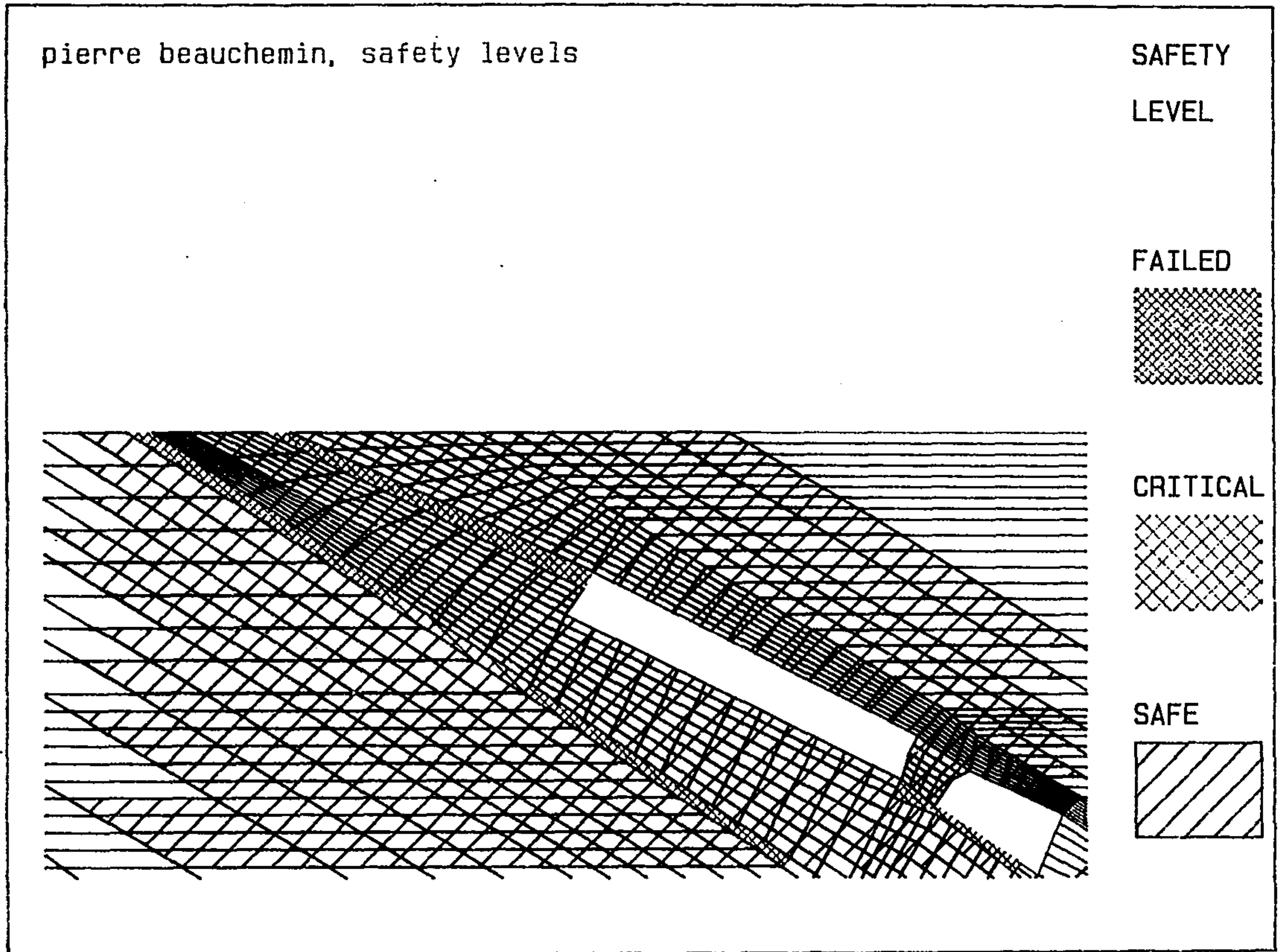

Figure 3.15 Hoek and Brown failure criterion safety levels for the rock mass around stope 105N-1, mining step one, Pierre Beauchemin Mine.

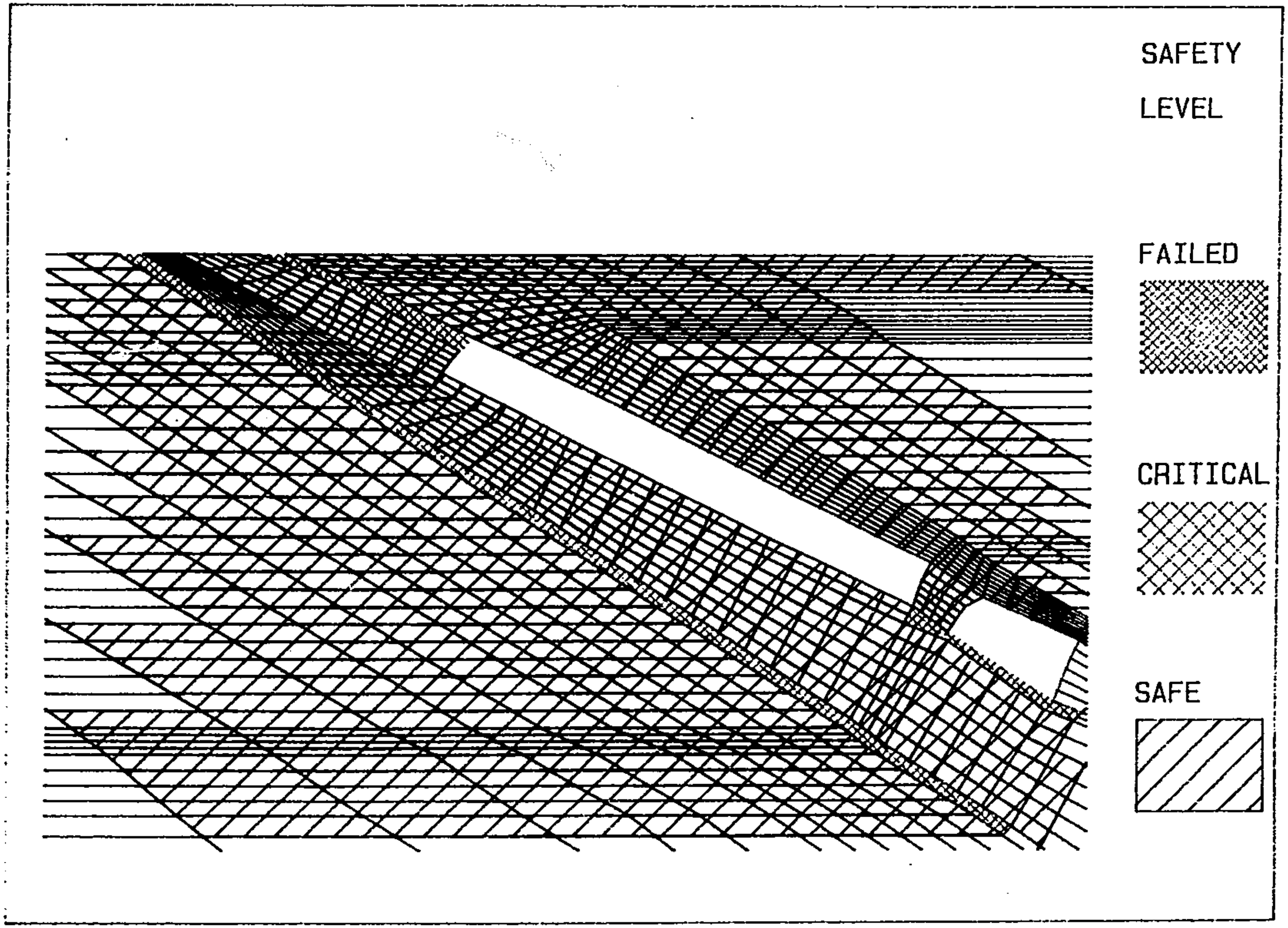

Figure 3.16 Hoek and Brown failure critierion safety levels for the rock mass around stope 105N-1, mining step two, Pierre Beauchemin Mine.

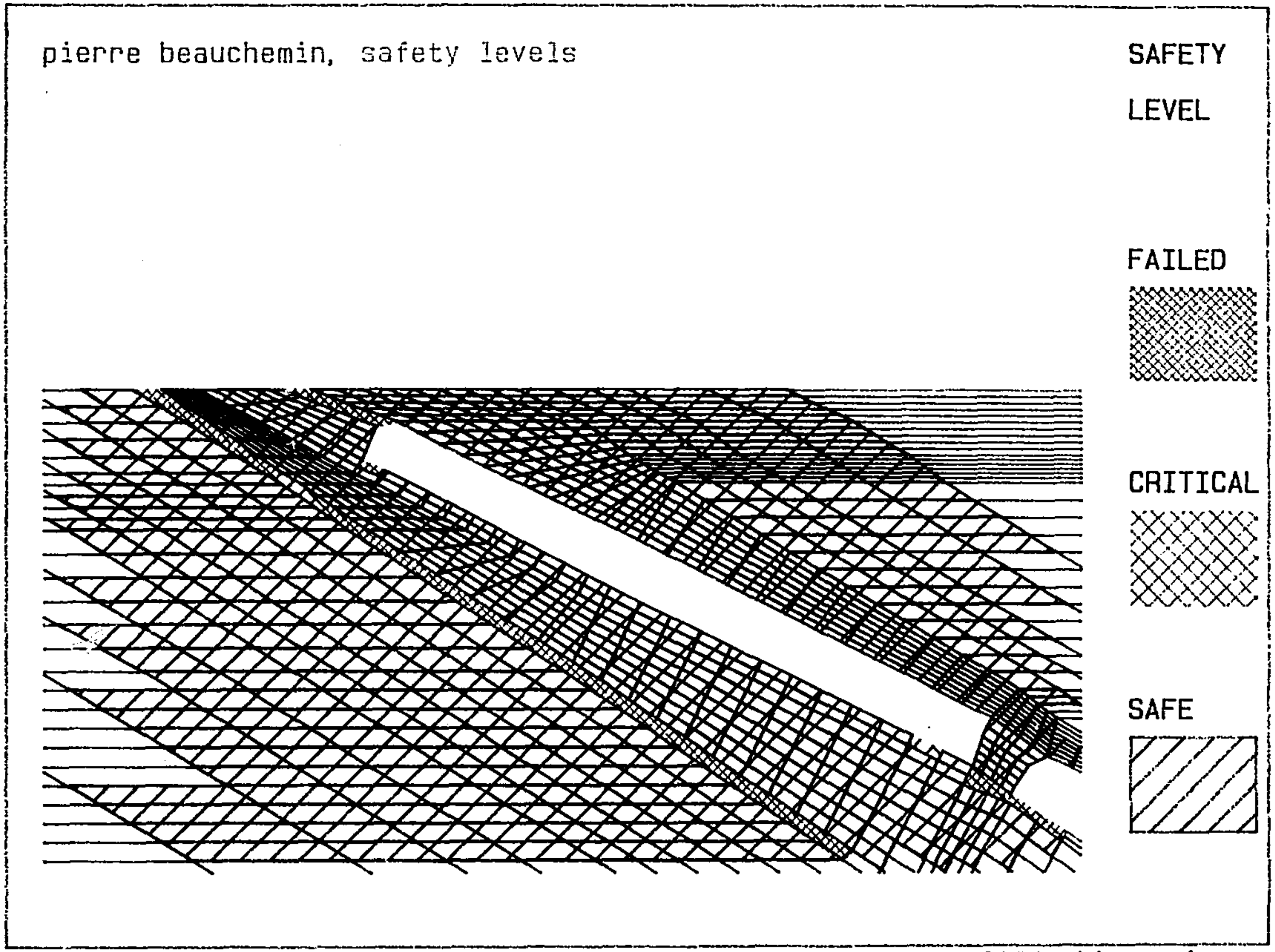

Figure 3.17 Hoek and Brown failure criterion safety levels for the rock mass around stope 105N-1, mining step three, Pierre Beauchemin Mine.

step due to the high tensile stress approaching or surpassing the diorite rock mass tensile strength of 2.0 MPa (Appendix 1).

The two fault zones are for the most part failed (F_s <1) in the first mining step and almost completely so by the third step.

3.5 APPLICATION OF ANALYTICAL EQUATIONS

As outlined in section 3.1, sufficient discontinuity families exist to create blocks, thereby requiring analysis for ravelling potential in the crown and hangingwall. Stratification is well developed, parallel to the stope hangingwall; strata failures are therefore possible. Furthermore, because the stratification joint family is so continuous, it is possible that it can form the boundaries of a long inclined block, within the surface crown pillar, which could fail as a plug.

Chimneying disintegration, which is known to occur in poor rock, may not readily occur in sound rock such as the diorite surface crown pillar but will nevertheless be examined as to its relative potential. Caving aspects will also be addressed, potentially important when the rock mass is well segmented by joints.

3.5.1 Plug Failure

The persistence of joint family N25E 45SE and the existence of cross joint S65E 85NE also of potentially influencing length (> 5 m) indicates that a plug could be formed within the surface crown pillar and slide on one of the N25E 45SE discontinuities.

Appendix I calculates the factor of safety against a plug failure defined by N25E 45SE joints forming the extension of the hangingwall and footwall into the pillar. Numerical modelling stress results are used as the imposed stress on the plug. Considering only the resistance from the N25E family (2-D analysis), the factor of safety against plug failure runs from 13.5 to 18.9 to 14.9 from mining step 1 to mining step 3. Therefore, a higher safety factor would be anticipated once the resistance along the S65E family is calculated.

3.5.2 Ravelling Failures

Block ravelling from the surface crown pillar or hangingwall is possible since block falls (when the crown periphery is horizontal, the mine has so far created an inclined periphery parallel to the dipping N20E 50NW family) and slides are expected. The joint orientations would not permit block slides from the footwall or block fall from the hangingwall. Of the four joint families occurring it is practical to consider two in the plane of the cross section of the shallow stope. Joint family S65E 85NE is nearly perpendicular to family N25E 45SE and parallel to the model cross- section. Therefore, it can be considered as the third joint family needed to form blocks. The other two families needed to represent the block condition in the section are the N25E 45SE and N20E 50NW families. The S50E 60SW family will not be considered because it occurs at random and has similar strike to S65E 85NE.

To obtain a true geometry of the block in the plane of the section, the apparent dip of N20E 50NW in the plane of S65E 85NE has to be obtained. By using the stereographic method the apparent dip is 49° NW. Similarly the apparent dip for N25E

45SE is 45° SE. The spacing between joints is outlined in Table 3.1.

Although joint intersections are not common, analysis of block behaviour will indicate stability as a worse case situation in areas where such intersections are common. Ravelling analysis will be carried out assuming the entire rock mass, except for the fault zones in the cross section plane, is cut by regularly spaced joints of these two families. The occurrence and joint properties outlined are the same for tonalite and diorite.

Application of equation 2.22 (in Appendix 1) indicates that because $\phi_{ri} < \alpha_i$, roof block falls would occur irregardless of stress conditions at the periphery. Calculation of the ultimate cavity height from block falls (equation 2.23) indicates that a cavity height of 3.8 m would occur from block falls. This is close to the depth of the stope, 6 m, after mining step 3. Applying equation 2.26 (Appendix 1), sliding of blocks from the crown will occur when 0.005 MPa compressive tangential stress or less occurs. The minimum tangential stress at the periphery of the crown occurs in mining step 1, it is 2.8 MPa compressive. Block slides from the crown are therefore not anticipated, and since block slides are required to permit ravelling to continue, failure to surface would not continue beyond block falls. Similarly, the tangential stress at the hangingwall periphery is compressive, having values of at least 0.4 MPa occurring in mining step 3, which is more than the required 0.021 MPa to prevent hangingwall block slides as calculated by equation 2.26 (in Appendix 1).

3.5.3 Strata Failures

Because the hangingwall of the mine is well stratified from the N25E 45SE joint family, and because cross-joints occur infrequently, strata failures are plausible.

Appendix 1 outlines the calculations performed to locate the ultimate failure cavity of the stratified hangingwall. Laboratory beam samples of diorite and tonalite were tested to obtain the bending properties outlined in Chapter 2.3.2.

As per the Pandey and Singh four-point beam test procedure [39], similar sized beams (~20 cm x 8 cm x 8 cm) with parallel sides were tested to provide the modulus of elasticity in tension which could then be used to calculate with the modulus of elasticity of compression the location of the neutral axis (equations 2.29, 2.30), and induced tensile stress, equation 2.35. The results of the lab tests indicated that the modulus of elasticity in tension for diorite is 42.6 GPa, for tonalite it is 38.2 GPa.

Using equations 2.41, 2.43, 2.44 and 2.45, Appendix 1, progressive stratum failure leading to an ultimate cavity outline was examined. Including the 45° dip of the same line strata, it was calculated that the maximum stable hangingwall on-dip span would be 9.4 m. The ultimate failure cavity would reach depths of 7.6 m, 9.0 m, and 10.5 m into the respective hangingwalls of mining steps one to three. This represents a vertical depth of 11.8 m, 9.2 m, and 6.4 m respectively from the top of bedrock for steps one to three. Therefore ultimate strata failure will not reach surface.

If the strata that are failing enter into a linear arch configuration, calculations show that, with a thickness of 0.25 m the diorite strata will fail by buckling rather than compressive thrust failure or block slippage, Appendix 1. The linear arch would be stable at a maximum span of 10.75 m.

This is more than the maximum 9.4 m expected for a loaded stratum. Stabilization by voussoir action however may be difficult if some other failed strata are loading the linear arch system.

3.5.4 Chimneying Disintegration Failure

Although the Pierre Beauchemin rock is sound and the rock mass is unlike the weak rock mass encountered in cases where chimneying disintegration has occurred, a chimneying failure analysis is performed to measure the degree of probability of such a failure.

A value of ϕ and c_m for rock mass conditions are applied to equation 2.66. These were selected based on the derivation of the rock mass failure envelope from the Hoek and Brown failure criterion (Appendix 1, Table 2). The calculations, Appendix 1, indicate that a factor of safety of 44.4 exists against chimneying disintegration.

3.5.5 Block Caving Failure

If the rock mass above the shallow stope mobilizes into a caving failure mechanism, calculations of caving pressures (Appendix 1) indicate that compression will be smaller than the required levels to force a block compression failure: the bulk strength expected of the caved material will be sufficient to resist imposed stress ($F_s = 1.20$). The imposed compression will also be insufficient to fail intact blocks within a stabilizing arch. Therefore the potential for caving stabilization exists.

3.6 APPLICATION OF EMPIRICAL METHODS

The critical spans provided by empirical methods can be compared against results obtained by numerical modelling and analytical equations. The NGI system and the Golder empirical calculation provide a maximum opening span for given rock mass properties. The Diering and Laubsher empirical chart will also be used to test for capability.

Design with the NGI system permits a more detailed evaluation of the rock mass and identification of stability elements. Furthermore, the application of the Golder empirical approach is based on the NGI Q value, and since more case studies have been examined compared to the RMR system, it will be used in the case studies. Figure 1.14 shows the NGI tunnel support chart [11] which is commonly used to estimate stability of openings and ground support required. The vertical axis calculates the ratio of span or height of opening to the Excavation Support Ratio (ESR). The recommended ESR ratio for permanent mine openings is prescribed as 1.6. For shallow stopes long-term stability is an important issue as water inflow must be prevented during the life of the mine at least, as must any subsidence that can affect surface infrastructure.

With a horizontal stope span of 7.0 m (in each of the 3 mining steps), the opening situated in diorite of Q = 3.88 (calculated in Appendix 1) plots slightly above the critical self support line, indicating support is recommended to avoid failure. The support category includes tensioned grouted bolting with shotcrete. The original NGI publication does not specify the treatment dipping of hangingwalls as spans or height. The approach used here is to accept, as a worse case situation, the hangingwall as a roof which would currently have a horizontal span of (43 m x cos (dip)) or 30.4 m. The span to ESR ratio versus Q for this diorite hangingwall also plots above the critical span line. More intensive ground support is prescribed compared to the previous smaller span, tension grouted bolts with mesh reinforced shotcrete. With the next two mining steps, the hangingwall span expands to 35.5 m and 42.5 m which would require progressively more intense ground support according to the NGI method.

For the diorite crown, the application of the scaled critical span equation (Appendix 1) yields a minimum pillar thickness of 4.7 m for a span of 8.4 m. If this chart was used to help identify the proximity to surface for stope expansion, the third mining step (planning 6 m of surface crown pillar thickness) would be close to failure.

The Diering and Laubscher procedure to evaluate block caving potential, Figure 1.19, will also permit unsupported spans to be evaluated as stable, in need of support, or prone to caving.

From the chart in Figure 1.19, the current shallow stope with a hydraulic radius of 2.63 (43 m x 6 m/(86 m+ 12 m)) and an adjusted RMR of 64 (75 x 0.85; 45° orebody dip) plots in the open stoping region. Mining step 2 would have a hydraulic radius of 3.06, the third of 3.49, which also fall in the 'no support required' category.

3.7 SUMMARY

An integrated design using numerical modelling and shallow underground empirical and analytical methods has been performed for a typical shallow stope of the Pierre Beauchemin Mine. Applications of the developed analytical equations indicate that the most likely mode of failures are block falls from the crown (if its periphery is horizontal) and strata failures in the hangingwall, and that neither will lead to complete failure to surface. Other types of failures are not anticipated.

Application of numerical modelling indicates that the unfaulted rock mass surrounding the current opening will not readily fail. Failure by exceeding rock mass strength is unlikely except for the fault zones.

Empirical methods indicate that the span for the surface crown pillar is very close to the critical stable line for self-support (and to failure for the largest expansion), but that the hangingwall requires ground support. Caving is not anticipated around the opening (applying empirical methods) but that if it occurs it may be able to form a stabilizing arch. Currently no bolting is used in the surface crown pillar.

Cónventional 2.1 m mechanical anchors on a 1.5 m spacing are usually applied shortly after each new excavation round and have been sufficient to maintain hangingwall integrity.

Observations on the current stope stability (mining step 1) confirm analytical equation, modelling and empirical results: i.e. that the 105N-1 stope periphery's is integral block falls are few, and block slides do not occur in the crown, and no indications exist of plug movement. Hangingwall strata failures but not block slides have occurred before bolting is performed. Rock mass strength has also not been exceeded.

Based on the field behaviour versus the application of these methods, mining step two can be carried out without ground control problems other than those already encountered, but mining step three would be at the limit of stability before failure is anticipated to surface because block falls would reach a depth of 2.2 m from surface. The empirical chart indicates a minimum pillar thickness of 4.7 m. Hangingwall support is required to prevent ground falls.

CHAPTER 4

THE NIOBEC MINE CASE STUDY

4.1 GENERAL GEOLOGY

The Niobec mine situated in Quebec, Figure 4.1, is in a portion of the St-Honoré carbonatite complex some 8 miles North-East of Chicoutimi, Figure 4.2. The complex, one of several regional intrusives, is located in the Precambrian Grenville Province of the Canadian Shield. The carbonatite and satellite rocks are capped by Palaeozoic limestone belonging to the Trenton group. Most likely related to the Saguenay graben movement parented by the St. Lawrence rift system, the complex is thought to be a plutonic or a hypabbysal event [105].

The St-Honoré complex is 3.2 km in diameter in a kidney shape showing well-differentiated lithological units. The central core is composed of coarse grained dolomitite carbonatite in which subvertical lenses rich in rare earth elements and niobium occur irregularly.

Site investigations for this research revealed that the limestone is composed of calcareous units (2 to 5 cm thick) with alternating shale bands (<1 cm thick). It is horizontal, even, regularly bedded, dense and of uniform composition. The stopes where limestone forms the roof provide an indication that this unit is unjointed. Similar lack of jointing exists in raises, drifts, ramps and rock core. Furthermore, the bedding does not easily part.

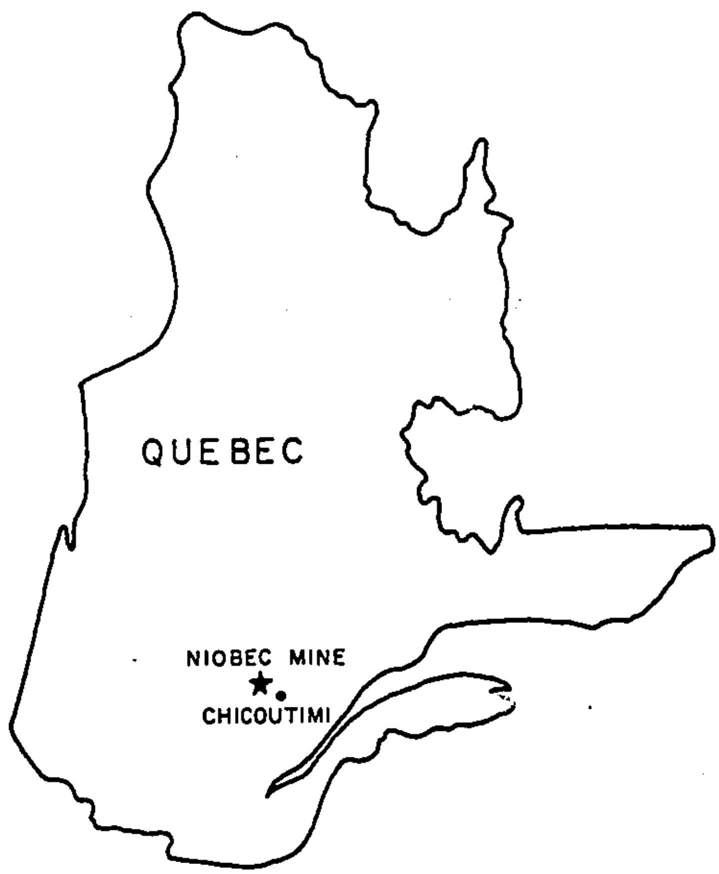

Figure 4.1 Location of the Niobec Mine.

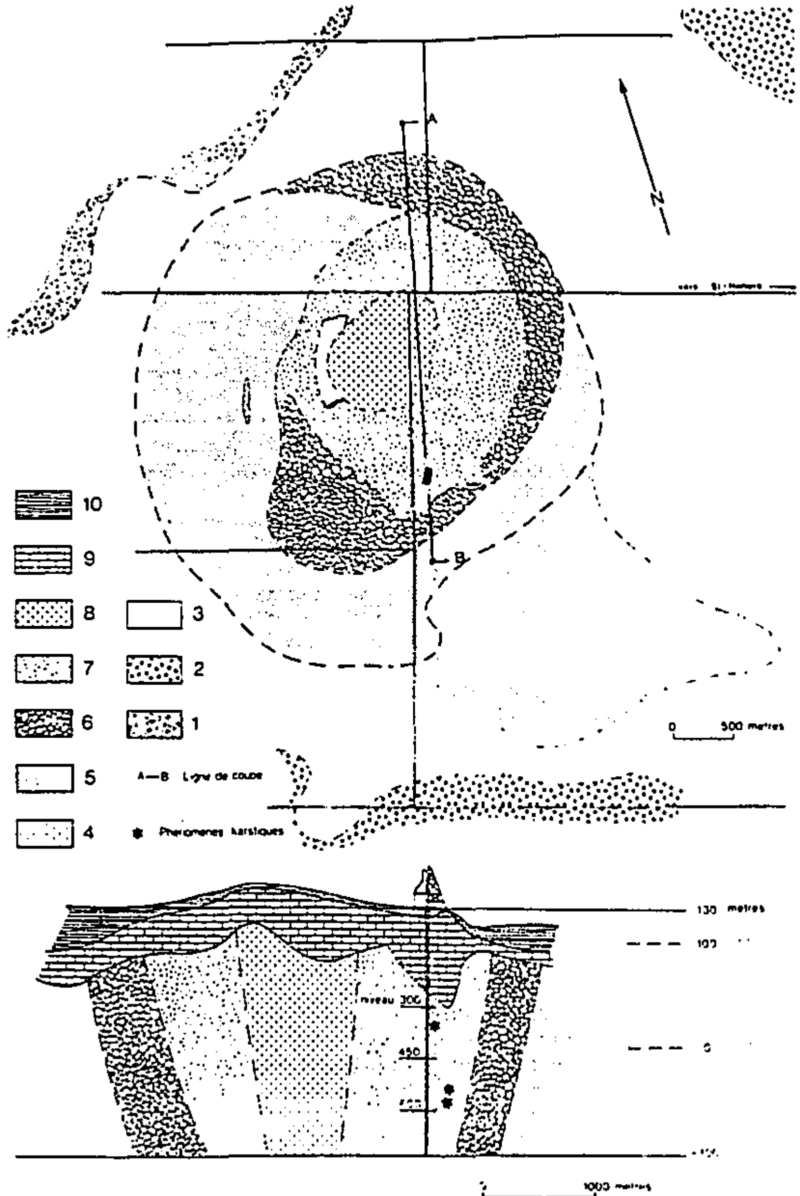

Figure 4.2 Niobec Mine geology: units 1 and 2, ultra-mafic; unit 3, fenetized rocks; units 4 and 5, syenites; units 6 to 8, carbonatite; unit 9, limestone; unit 10, overburden, cross section along A-B [106].

The carbonatite rock core examined contained two categories of structural discontinuities. The first consists of large extension joints >10 m (created by the stress/destressing activity of the intrusive [106]) with sub-horizontal and some vertical orientations. The second of small (<50 cm) joints oriented similar to the large joints. The small joints occur throughout the rock mass in a non-intersecting fashion. Few rock mass blocks were found on site. The stereographic plot of joint orientations surveyed on site is pictured in Figure 4.3. The large sub-horizontal joints predominate between 200 m and 300 m depth, the large sub-vertical joints occur at random throughout the mine. The intersection of large joints form "T" or "⊥" patterns.

The joints are generally smooth with large scale undulations. Alteration around sub-horizontal joints can be intense, but alteration of small scale joints is rare. No faulting has been revealed.

4.2 MINING EXTRACTION

The Niobec mining pattern follows the economical concentrations of niobium outlined in the sub-vertical lenses. The irregular distribution of these lenses results in an irregular stoping pattern, thereby creating several shallow openings and limestone surface crown pillars.

Mining is presently being performed at two levels. The upper level, where the stope roof (depth of 70-90 m) is the underside of the limestone surface crown pillar, has stopes opened to a depth of 180 m. The second level, separated from the first by a 30 m sill pillar, has stopes developed to the 300 m level. Most of the lower level stopes follow

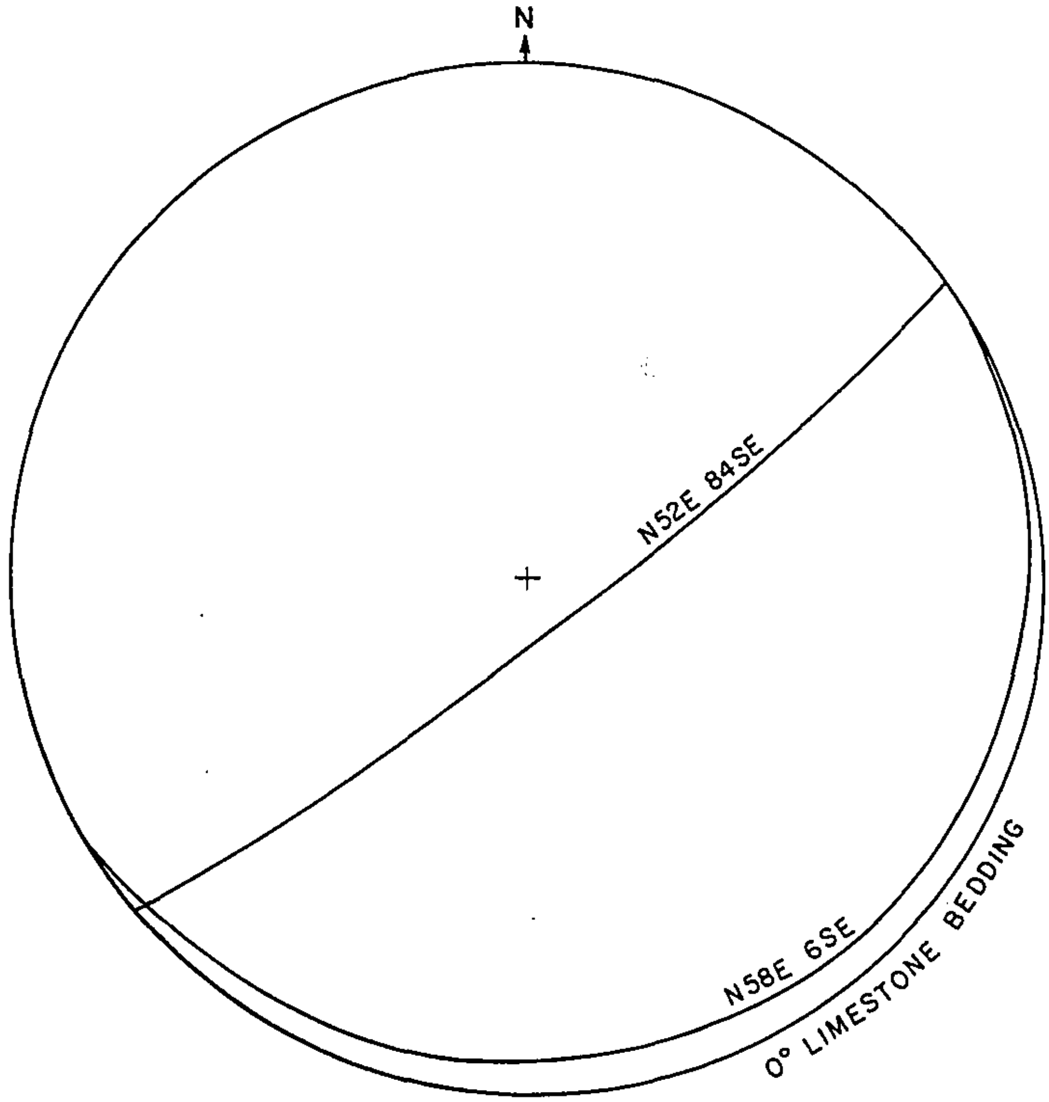

Figure 4.3 Stereographic projection of joint families, Niobec Mine.

the same lenses as the upper level, with some lateral shift due to the mineralization dip.

Mining was started on the first level and goes on concurrently with the second level. For economic reasons, backfill has not been used. The stopes, at least 90 m high and 25 m x 25 m wide, have been left opened since their excavation. Only the stope back is bolted, the stope walls are unsupported. Long term sloughing never exceeds 3-4% of original stope volume mined.

The mine uses large diameter blast hole stoping, Figure 4.4. Creation of the stope progresses by first blasting into a vertical raise, then by vertical slices into the existing void. Ore is retrieved by means of trackless equipment operating at draw points under the stope.

4.3 SELECTION OF CASE STUDY

The Niobec Mine represents two rock mass environments: well-developed stratification and massive, poorly jointed conditions, Figures 1.3 a,c. Furthermore, the very large stoping carried out would greatly affect natural ground stresses around these stopes. Consecutive open stoping might create low stresses in some of the stope peripheries. Such redistributed stresses could induce tensile stresses which might adversely affect rock mass integrity. This could also be seen in the light of the thick limestone cap and to what degree it would be affected. In this case numerical modelling would be an indispensable tool.

Owing to the large, open stope dimensions created at this mine, the limestone located in the surface crown pillars would represent a good opportunity to apply the

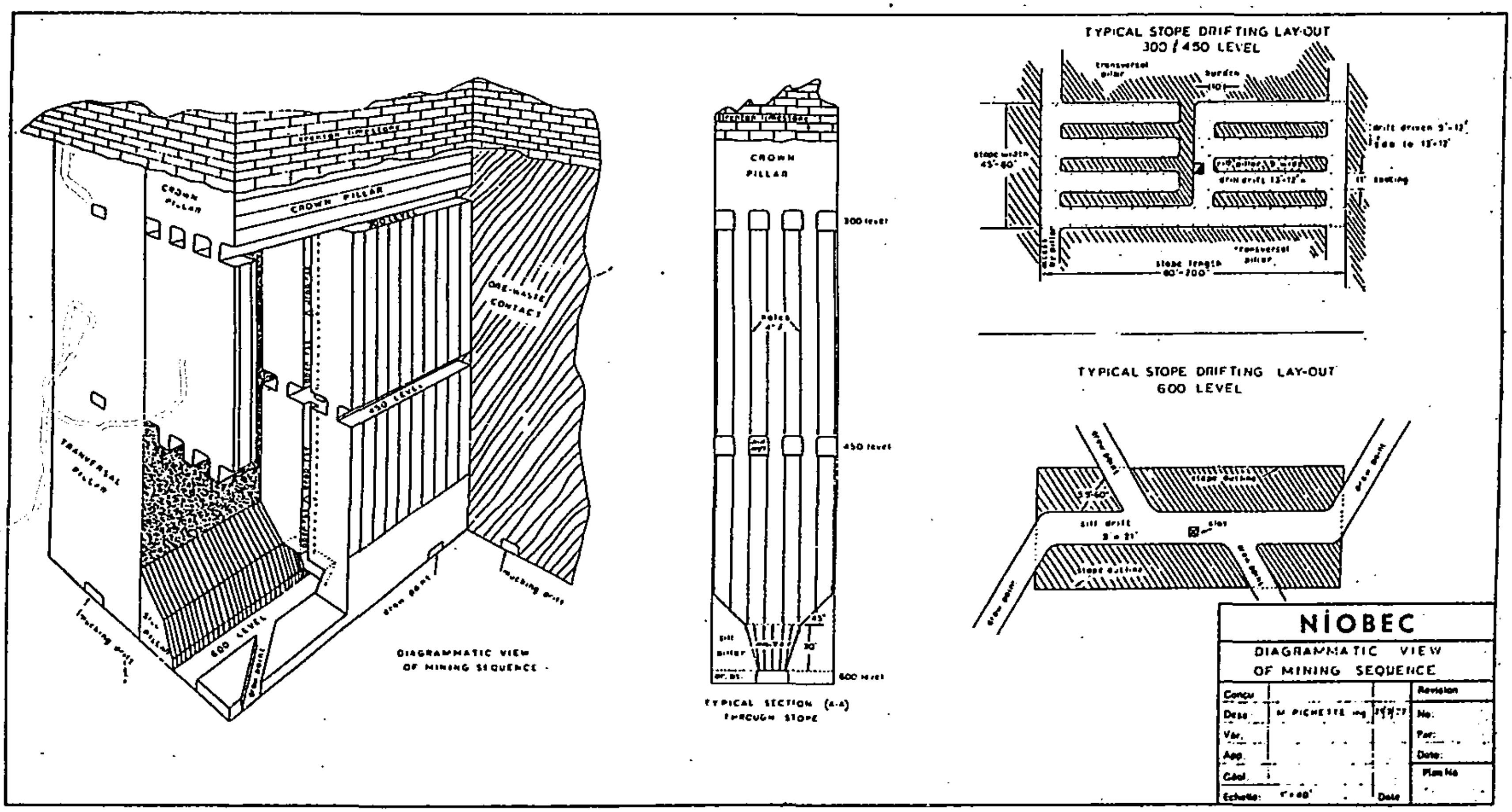

Figure 4.4 Niobec Mine ore extraction method (mine diagram).

analytical equation for realistic estimation of intact strata failure.

Furthermore, the lack of natural jointing would make the application of linear elastic considerations more relevant. Strata failures have occurred in stope roofs that were left unbolted, reaching a stable cavity configuration; this could be compared against analytical and modelling predictions. Even if failure occurs to surface, the overburden is thin (< 8 m), dewatered and no infrastructure exists above mine workings.

Site access was possible, to carry out rock mass evaluation, discuss previous shallow stope integrity with mine operators, and obtain rock samples for testing and rock quality evaluation. In situ stress measurements were available. The work performed would provide indications to the mine as to the effects of the size and positioning on shallow stope stability and would complement work already performed [68] [107].

The design performed here would supply mine operators with information that would have a bearing on the removal of support pillars between stopes, that is currently planned, leaving behind a very large shallow stope: 360 m long, 25 m wide and 90 m high.

4.4 NUMERICAL MODELLING

4.4.1 Numerical Model Selection

The numerical code to model the upper stopes of the Niobec mine was selected based on the geometry of the stopes and the rock mass behaviour.

The stope plan dimensions being similar, a 3-dimensional modelling code would provide more representative results and would model more closely the actual stope geometry rather than a 2-dimensional code which would assume the openings to be sufficiently long in the horizontal direction. The excellent rock mass quality of the limestone and carbonatite bordering on the massive shown in the field, responding elastically in the lab tests, and the absence of faults and weak zones around shallow openings justified the use of a code using linear elastic material behaviour.

The numerical code selected was the BMINES program. This finite element program developed for the U.S. Bureau of Mines [108] is capable of modelling complex geometries in 2 or 3 dimensions. Several geological materials can be considered with isotropy and linear or non-linear behaviour, although the latter option was not operational at CANMET. Geological material disposition can be vertical, horizontal or inclined. Gravity or initial state of stress can be considered. Mesh generation and mesh plotting is possible as well as the plotting of stress and factor of safety contours (Hoek and Brown, Drucker-Praeger or Mohr-Coulomb c-ϕ failure criteria). BMINES is currently designed to operate at CANMET on a SUN Sparc station. Various modelling projects other than shallow stopes have been performed for the Dumagami [109], Sigma [110], and Kidd Creek [66] mines with BMINES.

4.4.2 Geomechanical Properties

The material properties obtained from the zone 1 carbonatite and limestone are presented in Table 4.1. These comprise compressive strength (tested only at two confinement levels due to lack of samples supplied by the company), Brazilian tensile strength, modulus of elasticity, Poisson's ratio, cohesion intercept value, and angle of friction. The carbonatite represents the better portion of the rock mass which hosts most

Table 4.1 Niobec Mine Rock Material Laboratory Test Results

	Compressive Strength (MPa)		Tensile Strength (MPa)	Modulus of Elasticity (GPa)	Poisson's Ratio	Cohesion (MPa)	Ø degrees	Hoek & Brown m value	Unit Weight (MN/m^3)
	Confinement	Peak Strength							
Carbonatite	0	140.5	9.4	56.4	0.25	28	47	20	0.027
	14.1	295.0							
Limestone	0	92	5.6	30.0	0.20	14	40	16.3	0.027

of the zone 1 extraction.

Average values for the RQD and rock mass rating surveys performed were used to calculate Hoek and Brown rock mass parameters m and s with equations 1.43 and 1.44, Table 4.2. Ground stress measurement data performed for the mine by CANMET [27] is presented in Table 4.3. Although no in situ test of rock mass modulus of elasticity was performed at Niobec, the Serafim and Pereira [103] empirical equation returned values based on calculated rock mass rating values (Appendix 2). Application of the equation

$$E_{mass} = 10^{\frac{RMR-10}{40}} \tag{4.1}$$

returns a value of 28.2 GPa for the carbonatite and 63.1 GPa for the limestone. The carbonatite value appears reasonable versus the laboratory modulus (56.4 GPa) given its poorly jointed nature. The calculated field value for limestone is greater than the laboratory value (30.0 GPa) and is therefore not representative. A reduced value of field modulus is in order because of the existing discontinuities. A field modulus value of 50% lab value is often used for high quality rock masses [112] such as the Niobec limestone (RQD=92, RMR=82). Therefore, a value of 15 GPa will be used.

4.4.3 The Niobec Mine Numerical Model

Of the shallow openings existing at the mine, those located in the northern portion of the mine, "zone I", were selected for analysis. There, several consecutive stopes occur in the first mine level with openings situated immediately below them, Figure 4.5. These stopes are 90 m high and have horizontal dimensions ranging from 25 m x 25 m to 30 m

Table 4.2 Niobec Mine Rock Mass Rating Parameters

	RQD %	Rock Mass Rating (RMR)	Field	
			m	s
Carbonatite	87	68	6.4	0.03
Limestone	92	82	8.6	0.1

Table 4.3 Niobec Mine Summary of In Situ Geomechanical Field Parameters [26]

Modulus of Elasticity (GPa)		
Carbonatite	28.2*	
Limestone	15.0+	
*using equation 4.1	+ using a reduction of 50% from lab tests	
Natural Ground Stresses		
	Orientation (bearing/dip)	Value (MPa) (Depth 300 m)
Major Principal Stress	90°/05°	22.3
Intermediate Principal Stress	180°/0°	9.4
Minor Principal Stress	280°/85°	7.2

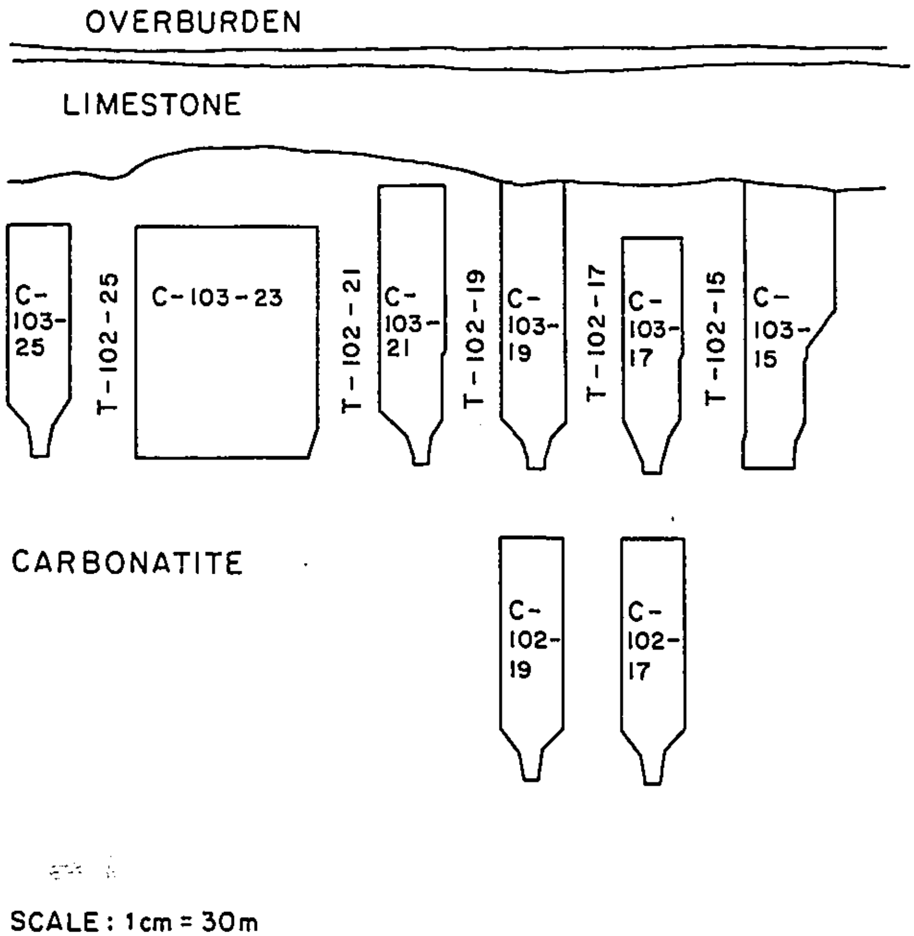

Figure 4.5 East-west longitudinal section of zone 1 stopes, Niobec Mine, looking north.

x 75 m. The sequence of stopes and pillars is located in part in altered carbonatite (up to 50%), which is of poorer quality. Because no other area in the mine would offer such stope proximity and numbers, this area would offer a "worse case" situation.

Two numerical modelling sequences were performed to simulate the events representative of current stope distribution and planned future pillar extraction, which would remove all rib (support) pillars but leave in place the sill (level) pillar between the two mining blocks. The resulting upper excavation would be 360 m long, the lower, 75 m long.

A 3-D mesh of 18,144 elements was used to model the extracted rock mass with pillars. A 3-D mesh of 15,552 elements was used to model the large openings created with pillars removed. Because of limitations on the number of elements used, the smallest dimension of elements was limited to 5 m, a series of which were used in the stope crown and hangingwall/footwall periphery, to arrive at a better representation of the redistributed stresses around the stopes. The model, with pillars in place was 1240 m high, 2350 m wide; the model with pillars removed was 1240 m high, 2339 m wide.

4.4.4 Modelling Results

Figures 4.6 and 4.7 respectively show the major and minor principal stresses in a longitudinal section of zone 1 with the pillars in place. This represents the current arrangement of stopes as seen in Figure 4.5. Figures 4.8 and 4.9 respectively show major and minor principal stresses on a cross section at mid-length of stope C-103-23. Figures 4.10 and 4.11 present the major and minor principal stresses on a cross-section at mid-length of stope C-103-19.

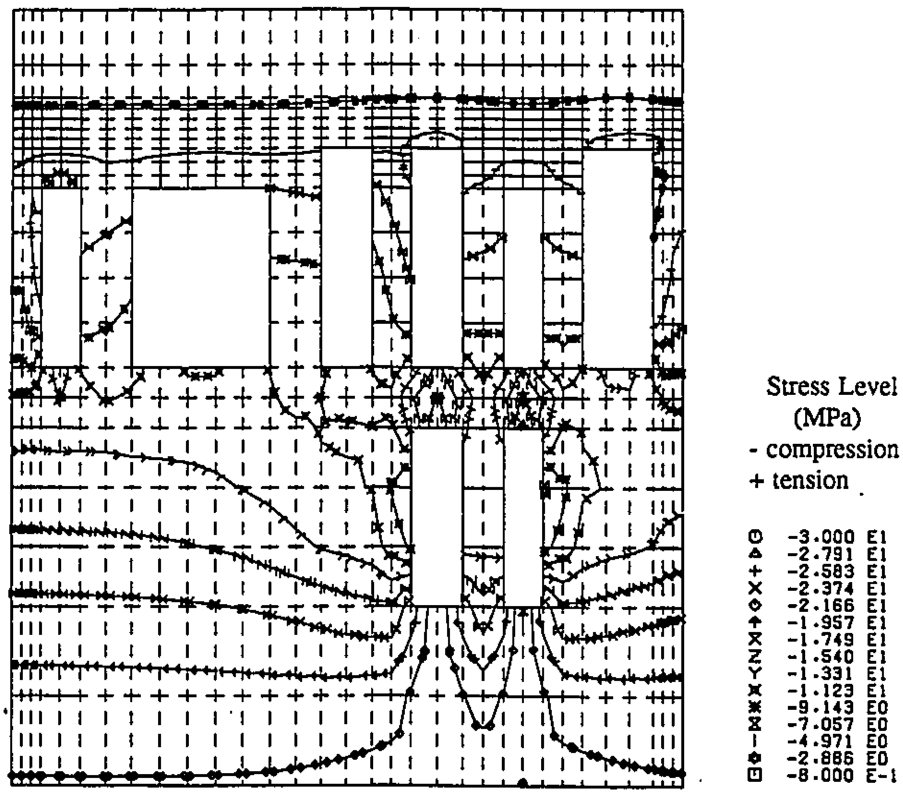

Figure 4.6 Major principal stresses, zone 1 with pillars in place, longitudinal section.

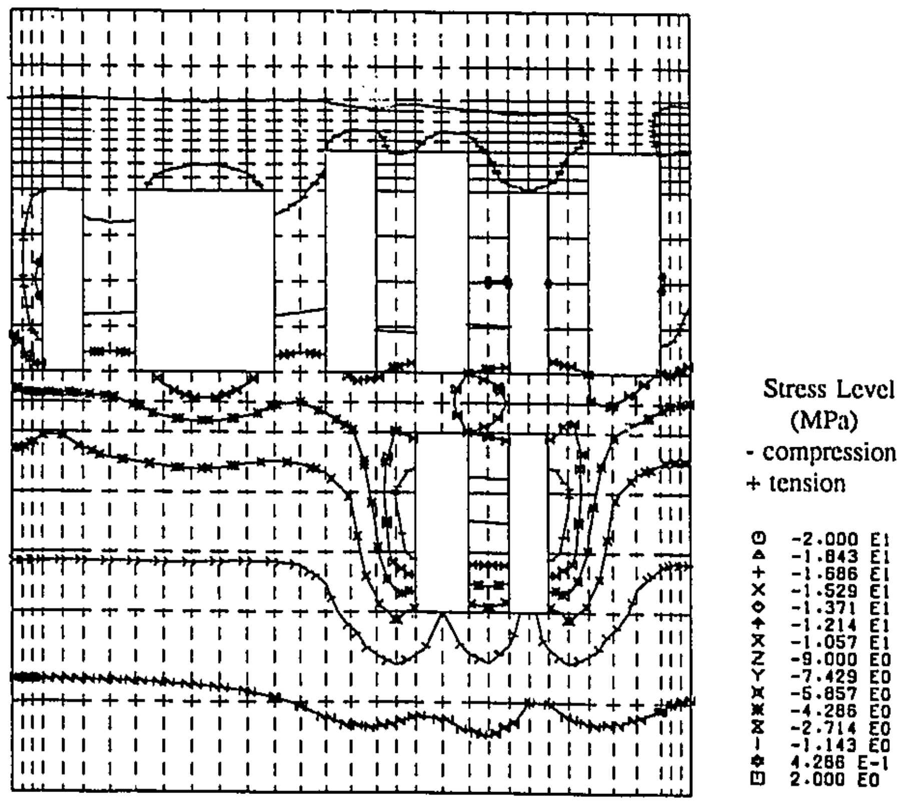

Figure 4.7 Minor principal stresses, zone 1 with pillars in place, longitudinal section.

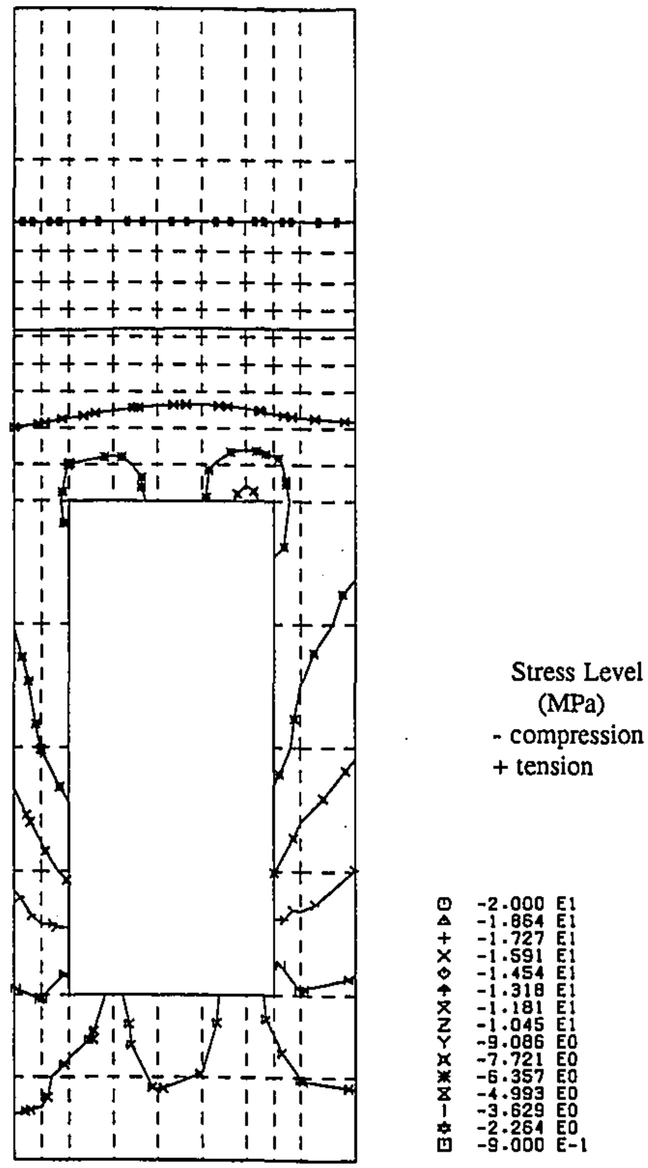

Figure 4.8 Major principal stresses, zone 1 with pillars in place, stope C-103-23 cross-section.

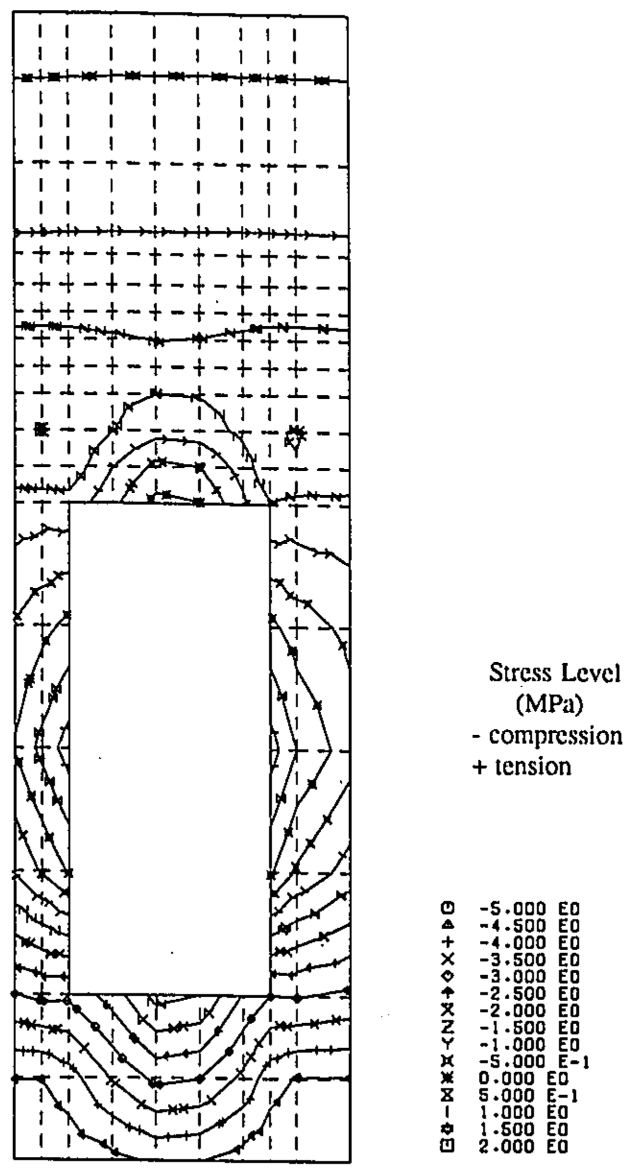

Figure 4.9 Minor principal stresses, zone 1 with pillars in place, stope C-103-23 cross-section.

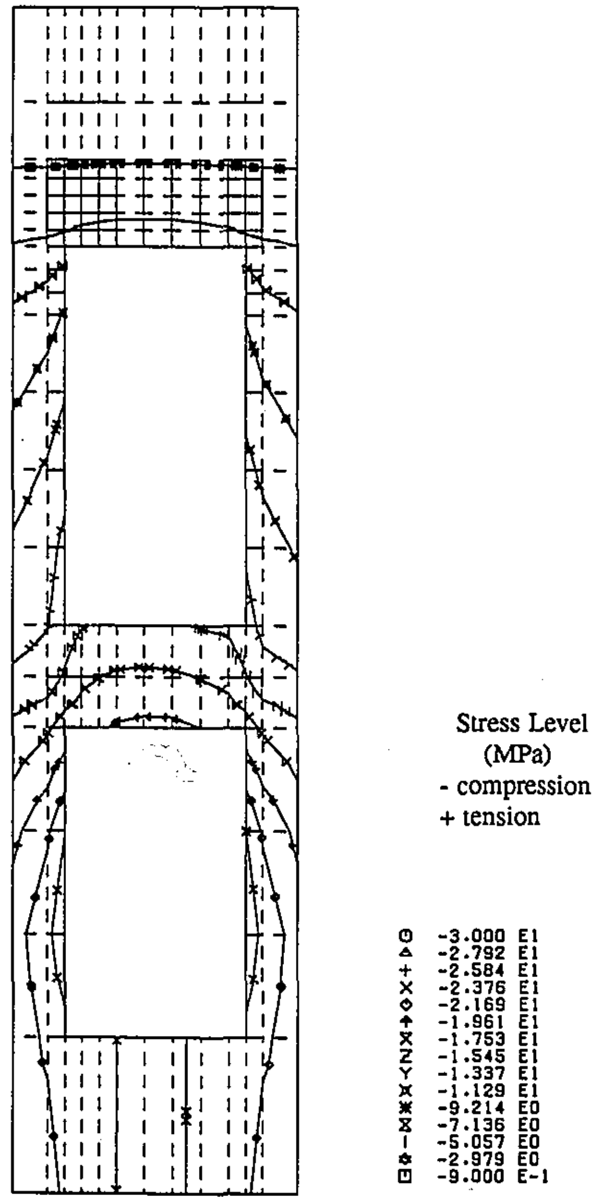

Figure 4.10 Major principal stresses, zone 1 with pillars in place, stope C-103-19 cross-section.

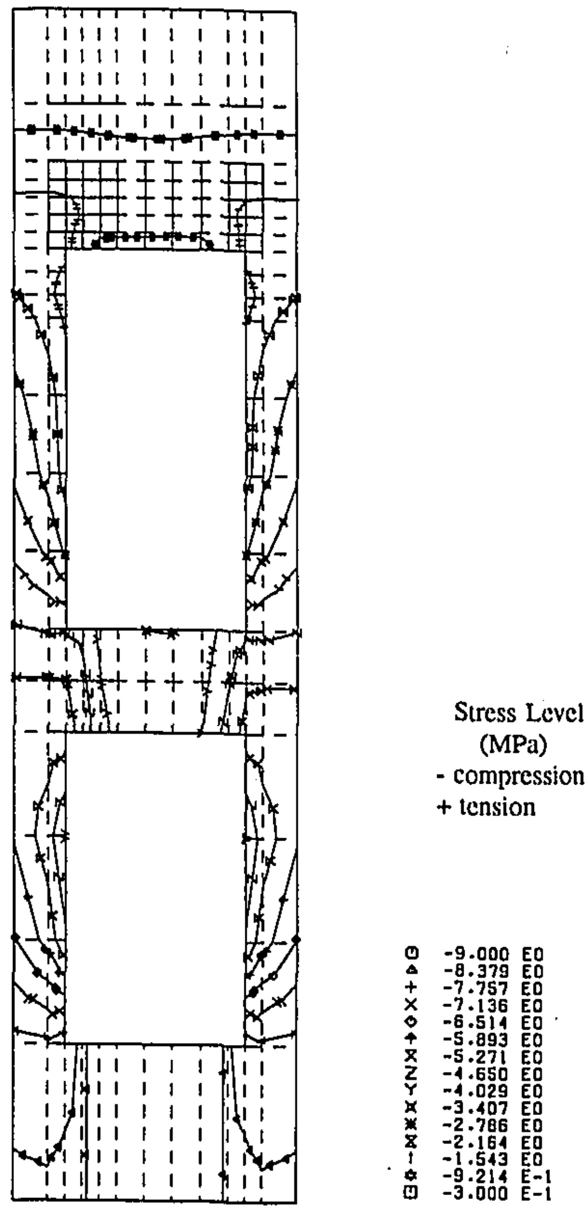

Figure 4.11 Minor principal stresses, zone 1 with pillars in place, stope C-103-19 cross-section.

The surface crown pillars of the upper stopes are subjected to very low compressive minor principal stresses, in the 0 to 1.1 MPa range, Figures 4.7, 4.9 and 4.11. In particular, the largest stope shows zero minor principal stresses. The stope crowns are subjected to compressive major principal stresses of the order of 5 to 7.1 MPa.

The pillars between the upper stopes, Figures 4.6, 4.7, are for the most part in compression, up to 11.2 MPa, except for small tensile areas (<0.43 MPa) at the western periphery of C-103-25 and between stopes C-103-19 and C-103-15.

The lower sill and support pillars are subjected to compressive stresses 1.1 to 19.6 MPa, Figures 4.6, 4.7, 4.10, 4.11. Figures 4.12 to 4.17 respectively show the modelling results of zone 1 with pillars removed: major and minor principal stresses on a central longitudinal section, major and minor principal stresses at the cross section previously located at the center of C-103-23, and major and minor principal stresses at the cross section previously located at the center of C-103-19.

The minor principal stress in the immediate surface crown pillar of the 360 m stope remains low, but compressive and higher than in the case with pillars in place, with a range of 0.6 to 1.6 MPa. The major principal stress there has a range of 5 to 15.5 MPa which is also higher than the condition with pillars.

The sill pillar between mining blocks is subjected to compressive stresses of the order of 0.4 to 17.5 MPa which is somewhat lower than the modelled stresses with pillars in place.

Application of the Hoek and Brown failure criterion incorporated in BMINES allowed for the relative comparison of strength versus imposed stress. The material values outlined in Table 4.2 and the geological distribution of Figure 4.5 yields the results

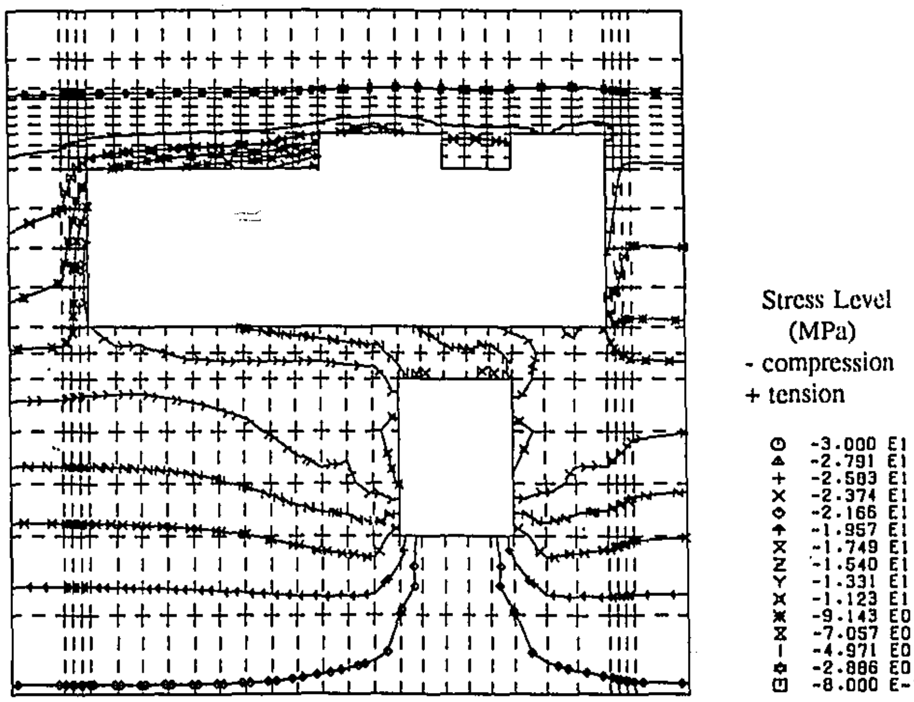

Figure 4.12 Major principal stresses, zone 1 with pillars removed, longitudinal section.

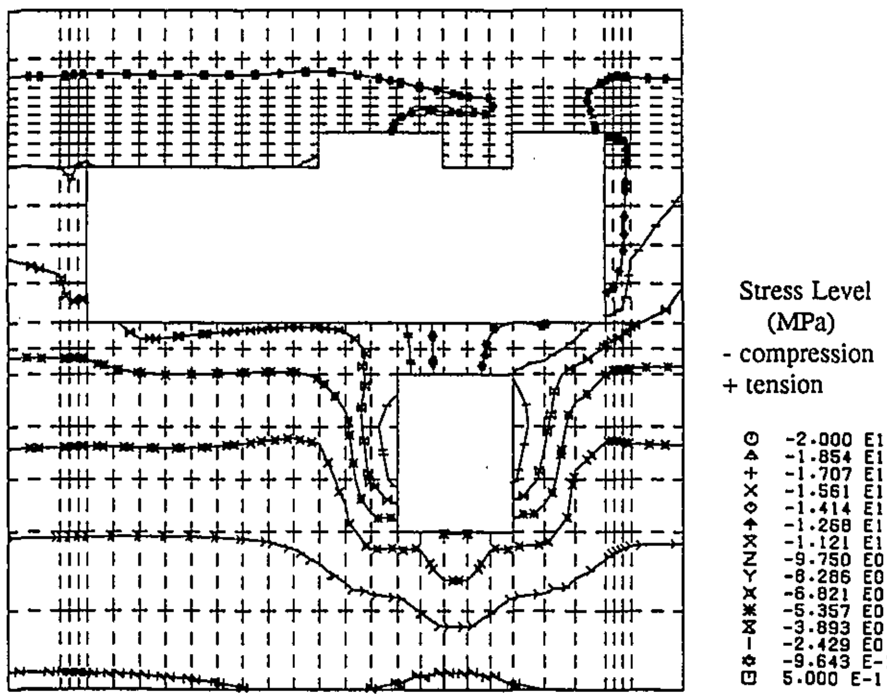

Figure 4.13 Minor principal stresses, zone 1 with pillars removed, longitudinal section.

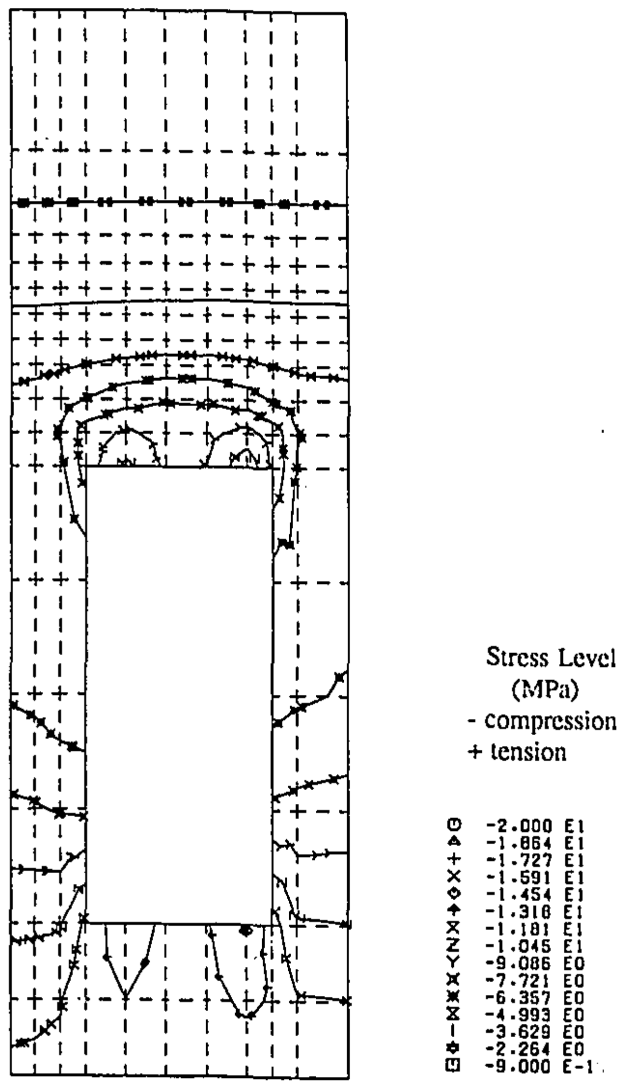

Figure 4.14 Major principal stresses, zone 1 with pillars removed, stope C-103-23 cross-section.

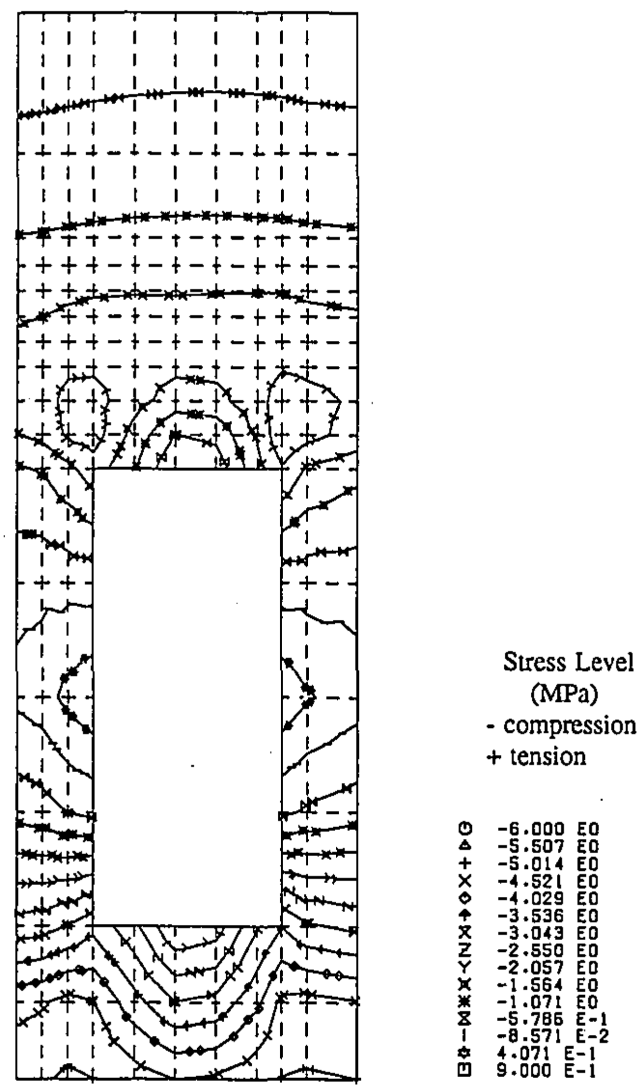

Figure 4.15 Minor principal stresses, zone 1 with pillars removed, stope C-103-23 cross-section.

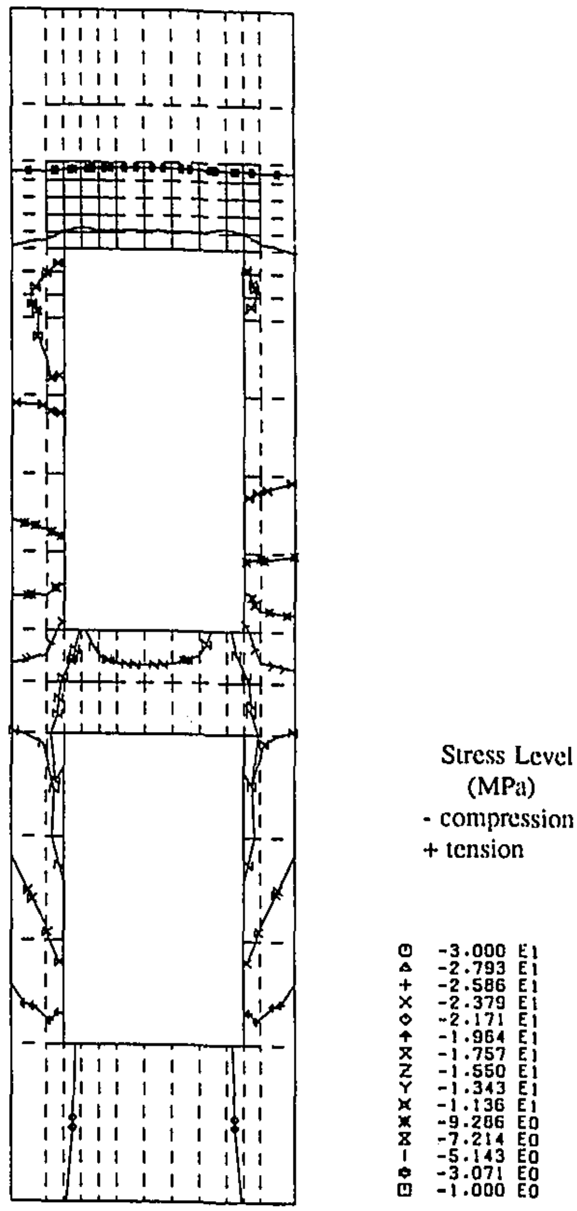

Figure 4.16 Major principal stresses, zone 1 with pillars removed, stope C-103-19 cross-section.

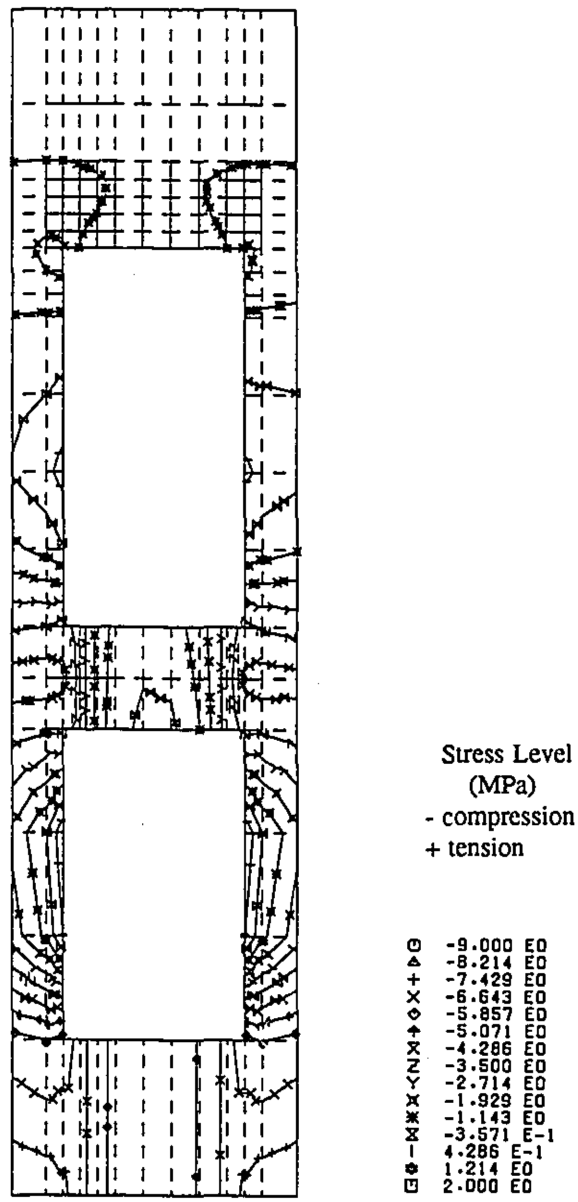

Figure 4.17 Minor principal stresses, zone 1 with pillars removed, stope C-103-19 cross-section.

shown in Figures 4.18 to 4.20 for the sections used earlier with pillars in place, 4.21 to 4.23 for sections used earlier with pillars removed.

The lowest factor of safety in the surface crown pillar is of the order of 3.4, above C-103-23. The lowest factor of safety once the pillars are removed is 3.14 occurring in the surface crown portion of the previous T-102-17 pillar.

The lowest value around the support pillars of the first level is 1.9 in the area underlined as being in tension. The sill and pillars of the second block rate at a factor of safety of at least 4.2. When the pillars are removed from the upper mining block, the lowest factor of safety, 1.7, occurs in the bottom of the sill pillar. The periphery to the fully opened lower block is at a factor of safety of at least 3.9.

4.5 APPLICATION OF ANALYTICAL EQUATIONS

Few discontinuities except bedding exist in the limestone surface crown pillar. Strata failures are therefore expected, while plug failures, ravelling and caving are not because blocks do not exist. Chimneying disintegration, which is known to occur in poor rock, may not readily occur in sound rock such as the limestone but will nevertheless be examined as to its relative potential.

4.5.1 Strata Failures

Because the crown of the shallow stopes are stratified from bedding, destratification is plausible.

Appendix 2 outlines the calculations performed to locate the ultimate failure cavity

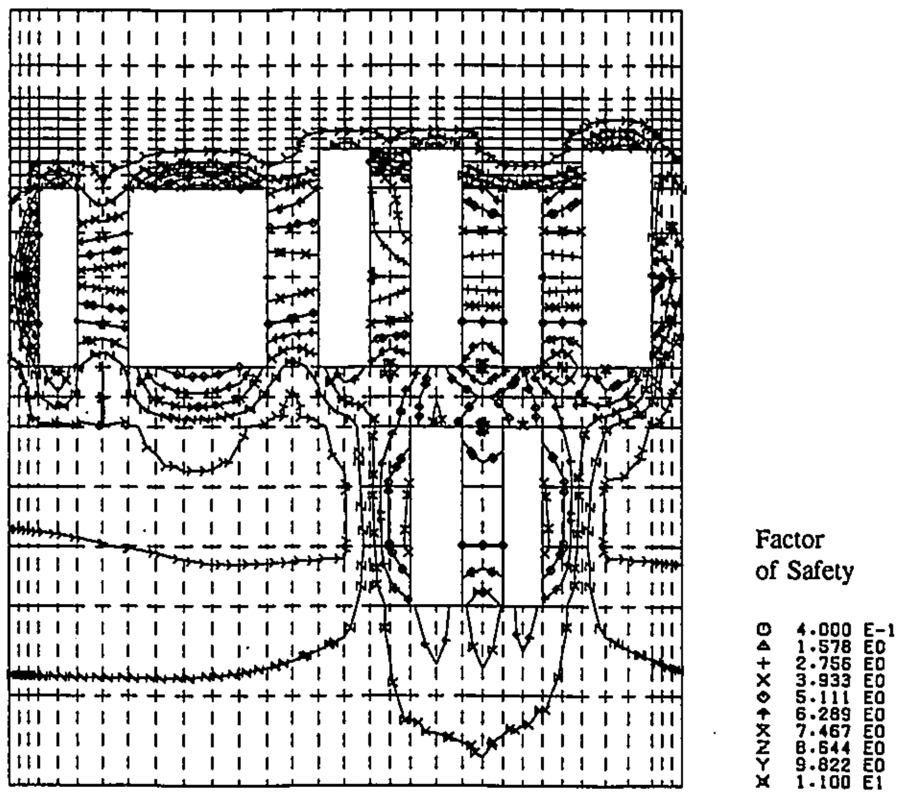

Figure 4.18 Application of the Hoek and Brown failure criterion, zone 1 with pillars in place, longitudinal section.

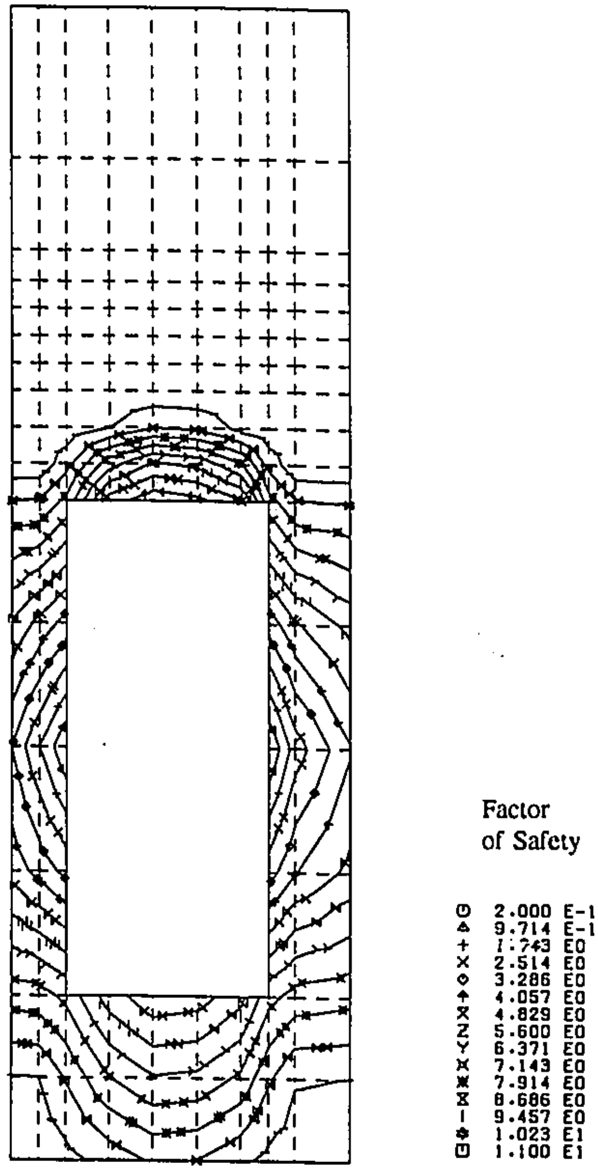

Figure 4.19 Application of the Hoek and Brown failure criterion, zone 1 with pillars in place, C-103-23 cross-section.

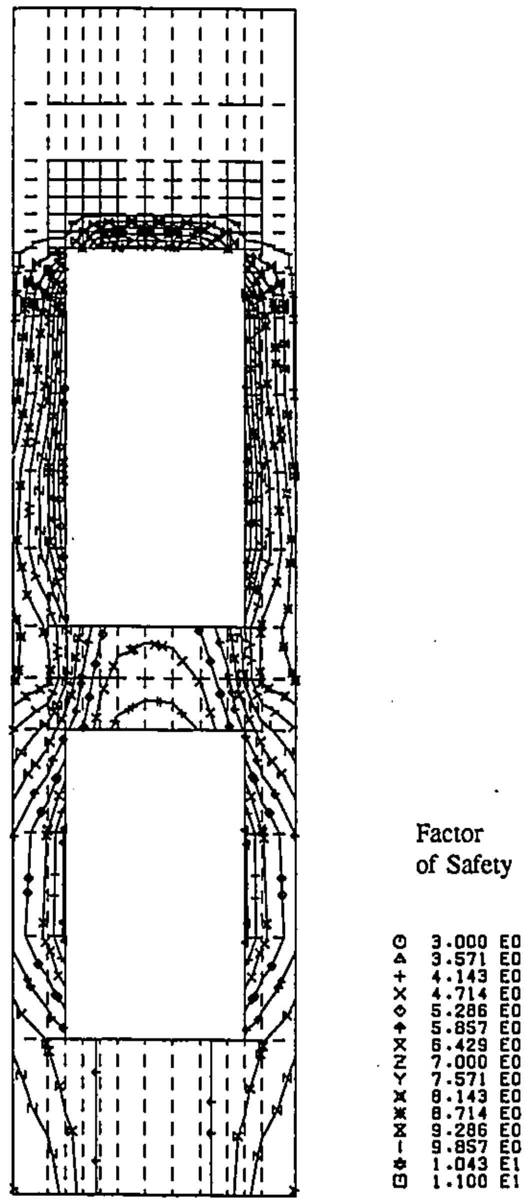

Figure 4.20 Application of the Hoek and Brown failure criterion, zone 1 with pillars in place, C-103-19 cross-section.

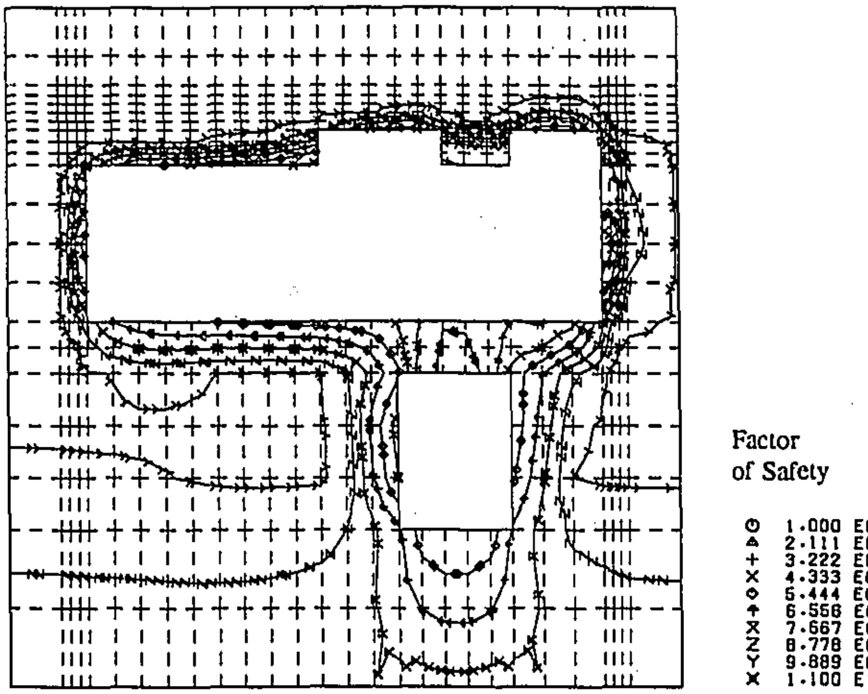

Figure 4.21 Application of the Hoek and Brown failure criterion, zone 1 with pillars removed, longitudinal section.

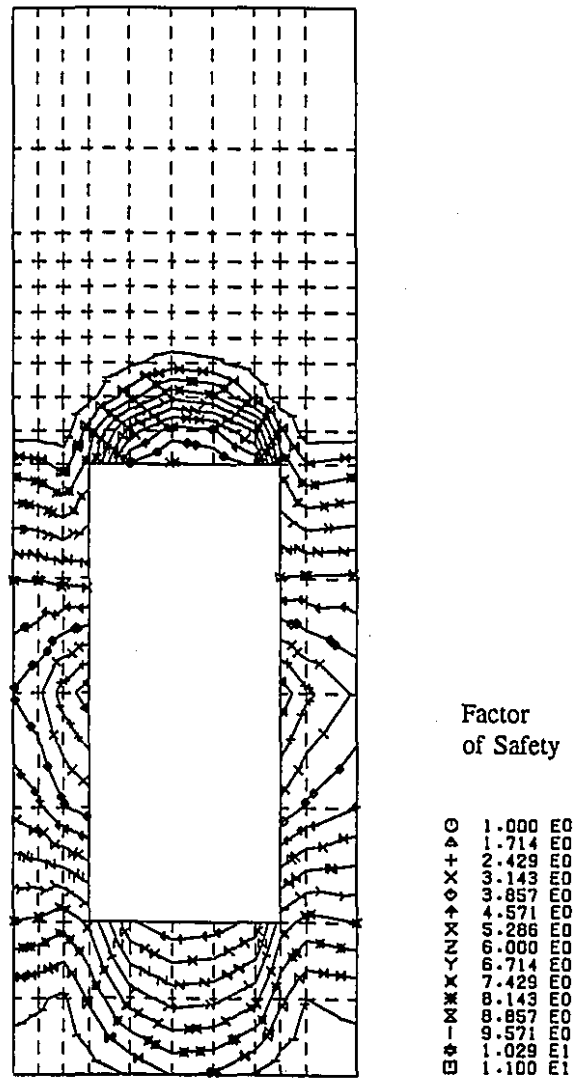

Figure 4.22 Application of the Hoek and Brown failure criterion, zone 1 with pillars removed, C-103-23 cross-section.

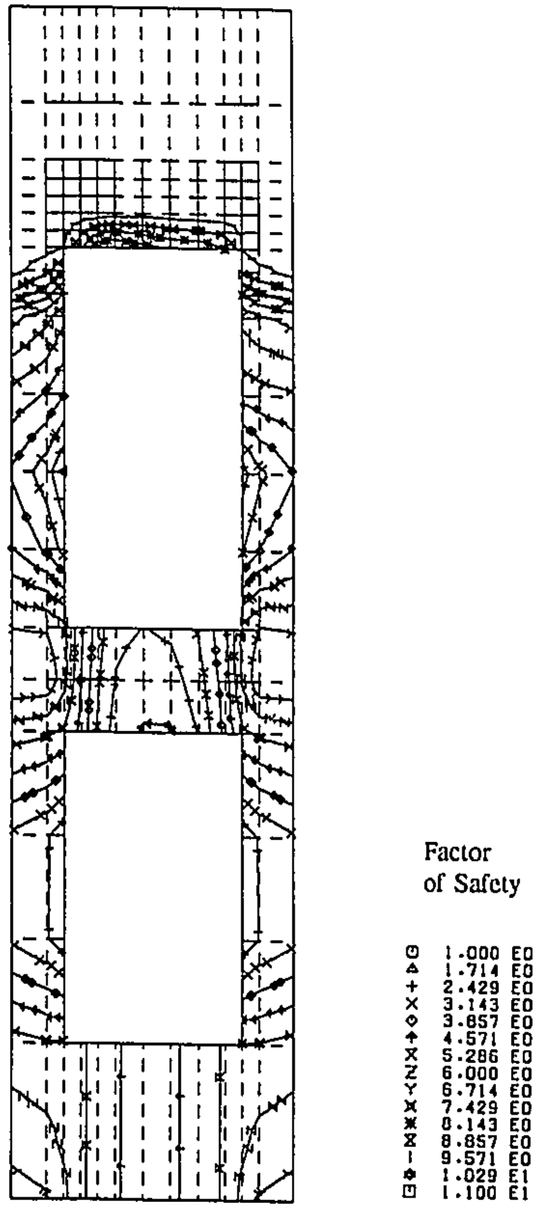

Figure 4.23 Application of the Hoek and Brown failure criterion, zone 1 with pillars removed, C-103-19 cross-section.

of the longest of the current stopes, C-103-23, Figure 4.5. The calculations are based on tensile strength from four-point beam tests of similar sized beams (~ 15 cm x 8 cm x 8 cm) with parallel sides. The results indicate a modulus of elasticity of 30.0 GPa in compression, 22.3 GPa in tension. With a span of 75 m strata failures are expected to a height of 17.0 m which will stop some 45 m away from surface. Two strata failures have occurred at Niobec [33], stope 209-27 and 202-12. The former had 25 m x 60 m plan dimensions. Failure (not measured) occurred over approximately 40 m in the center of the longest dimension and over the entire width of 25 m. The cavity height was 4 to 7 m. In the second stope of dimensions 25 m x 45 m, the failure (not measured) occurred over the entire crown to a cavity height of 4 to 7 m. It is not possible to conclude that failures in long stopes 60 m or more (the size of C-103-23 and the future 360 m long stope when pillars are removed) will be limited to some 40 m in length. However, the analytical equation predicts a cavity height of 10.0 m for a span of 45 m. The overestimation by the analytical equation may lie with this 2-D beam approach versus the actual dimensions being closer to those of a plate which offers better support.

If the strata that are failing enter into a linear arch configuration, calculations show that with a thickness of 0.06 m, the limestone beds will fail by buckling rather than compressive thrust or block slippage, Appendix 2. The linear arch would be stable at a maximum span of 3.53 m. This is more than the maximum 1.71 m expected for a loaded stratum. Stabilization by voussoir action, however, may be difficult if some other failed strata are loading the linear arch system.

4.5.2 Chimneying Disintegration Failure

The massive limestone surface crown pillar is unlike the weak rock mass environments where chimneying disintegration has occurred. However, a failure analysis was performed to measure the degree of probability of such a failure.

The selected ϕ and c_m for rock mass conditions were selected based on the derivation of the rock mass failures envelope from the Hoek and Brown failure criterion (Appendix 2, Table 2). The calculations, Appendix 2, indicate that a factor of safety of 30.7 exists against chimneying disintegration.

4.6 APPLICATION OF EMPIRICAL METHODS

The critical spans provided by the NGI and surface crown pillar methods can be compared against results obtained by numerical modelling and analytical equations.

The NGI system (Table 1.5, Figure 1.14) classifies the limestone at Q=61.3, "very good" rock quality (Appendix 2) which, with a span of 25 m for the smallest stope, 75 m for the largest current stope, and 360 m for the largest future stope, and an E.S.R. of 1.6, Chapter 3.6.1, all plot in the required support range. Untensioned grouted bolts for the smallest to tension grouted bolts for the largest opening is recommended. Conventional 2 m rock bolts on a 2.5 m pattern have been sufficient to support the stope crowns. The carbonatite stope walls, usually 90 m high, have a Q of 32.6, "good" rock quality. This plots into the support required area, tension-grouted bolts with chain-link mesh support prescribed. Field observations of the pillars left unsupported show no degradation.

The surface crown pillar empirical method returns (Appendix 2) a minimum pillar thickness of 2.2 m for a surface crown pillar spanning 25 m, (75 m longitudinally; 2.9 if the stope is 360 m longitudinally) with the quality on structural properties of the limestone rock mass.

4.7 SUMMARY

The Niobec case has provided the opportunity to examine several shallow stope stability aspects: the effect on stress distribution from several consecutive large stopes and vertical mining blocks and from the size of stopes, the level of stress from these conditions and its effects on the integrity of the poorly jointed rock mass, as well as destratification of the surface crown pillar.

Numerical modelling indicates that near-zero compressive minor principal stresses currently exist in the crowns of the consecutive slopes and that the levels will remain the same when the pillars are removed and a 360 m long 85 m wide and 90 m high opening is created above another large mining block. This can explain the reason for historical destratification but application of the Hoek and Brown failure criterion from modelling results did not indicate failure.

These stresses will not be sufficient to fail the massive rock in the limestone cap or hosting carbonatite, the factor of safety being at least 1.7. There is little evidence with this natural stress distribution (major principal stress parallel to the longitudinal direction) that longitudinally consecutive stopes result in significantly lower stresses over the central stopes.

However, alignment of the major principal stress with the east west distribution of zone 1 of stopes and the 360 m long planned stope once pillars are removed represents a better condition than if it was orthogonal to it [113].

The limestone bedding which parts with difficulty and the lack of other jointing in this unit reduces the anticipation of failure by destratification. Over the current 75 m C-102-23 stope span failure of the 0.06 m stratas would result in a 17 m high cavity using the analytical equation. Cases of failure at Niobec show that irrespective of span, failures in unsupported ground are limited to a span of 40-45 m and create cavities 4-7 m high. The cavity height predicted from the developed analytical equation for such a span is 10 m but reflects a conservative plane strain analysis versus actual plate conditions. Voussoir blocks from failed strata would only be stable over a stope a span of 3.5 m. Destratification failures would stop well before surface is reached, leaving some 45 m of rock above stopes.

Because of absence of more than one family of joints (bedding) the conditions for ravelling, plug failure and block caving are not present. An analysis for chimneying disintegration was nonetheless performed as a bench mark for the upper values of such an analysis in massive rock. The factor of safety against chimneying disintegration is 30.7.

The NGI empirical method indicates support is needed, which confirms the occurrence of failures, but recommends conservative ground control means. The surface crown pillar empirical chart required minimum thickness of the order of 2.3 m. This is well below the 4 to 7 m high failures recorded.

The massive carbonatite stope walls, which are dissected by two joint sets rather than three sets to form blocks, were not analysed for block slides. Observations of several shallow stopes in zones 1 and 2 indicate that the stopes are stable and that no failures are evident. This confirms the numerical modelling results. Conventional support of the stope crowns in limestone is sufficient to prevent destratification, the only expected failure mechanism.

Based on these results, planned retrieval of the support pillars can be carried out without shallow stope failure and that minimum degradation will occur if the stope crowns are supported as soon as they are created. Serious dilution is not expected from the limestone crown, or the carbonatite which is unsupported, as indicated by the modelling. The shallow stopes should therefore remain stable and no failures to surface are anticipated.

CHAPTER 5

THE DUMAGAMI MINE CASE STUDY

5.1 GENERAL GEOLOGY

The Dumagami Mine, a division of Agnico Eagle Mines Ltd., is located 60 km west of Val d'Or, Quebec, Figure 5.1.

The orebody of massive pyrite with disseminated gold averaging 7 g/ton is oriented east-west with a thickness of 5-15 m. The orebody has a longitudinal extent of about 300 m, a dip of 85° south and a plunge of 60° west. It is located in the Superior Province of the Precambrian Shield, in a geologic setting dominated by metavolcanic rock sequences, Figures 5.2, 5.3.

At depth, the plunging orebody crosses into the Bousquest no. 2 property, where Lac Minerals Ltd. also mines. A boundary separates the two properties, although current plans are to mine the orebody without leaving a boundary pillar.

The orebody is located in a sequence of fine to medium grained volcanoclastic rock sequence. The sequence of geological units from hangingwall to footwall can be generalized as follows, Figure 5.3: a mafic tuff becoming more foliated towards the ore zone; a 15 m wide highly foliated, sometimes sericitic tuff (with talc coated laminas 0.5-1 cm thick) at the contact with the orebody; a massive pyrite orebody; an immediate footwall 20 m wide of poorly to moderately foliated rhyolite with disseminated, or stringer, pyrite; a 15 m highly foliated schistose unit; and moderately foliated rhyolite.

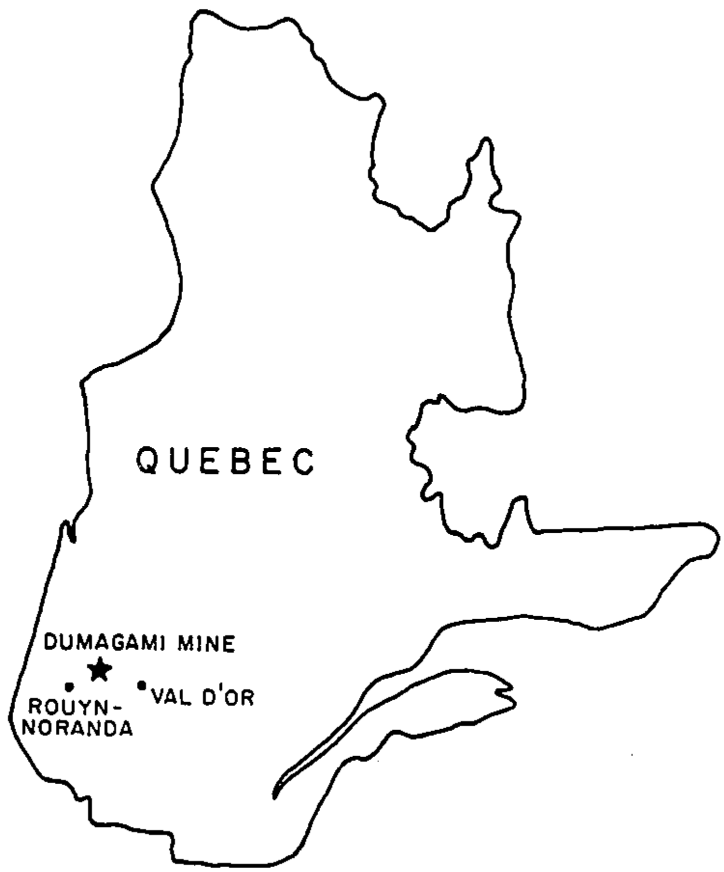

Figure 5.1 Location of the Dumagami Mine.

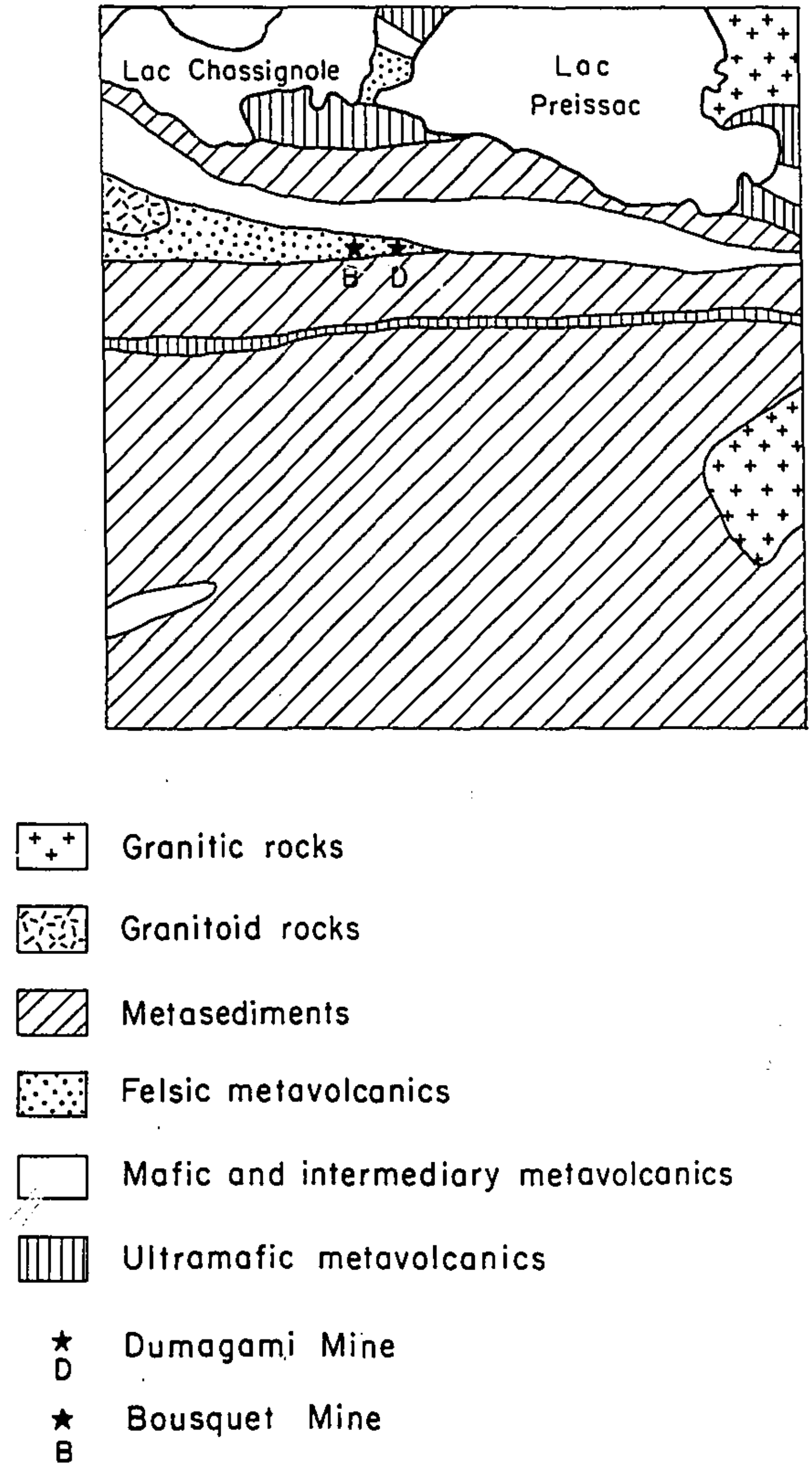

Figure 5.2 Regional geology, Dumagami Mine.

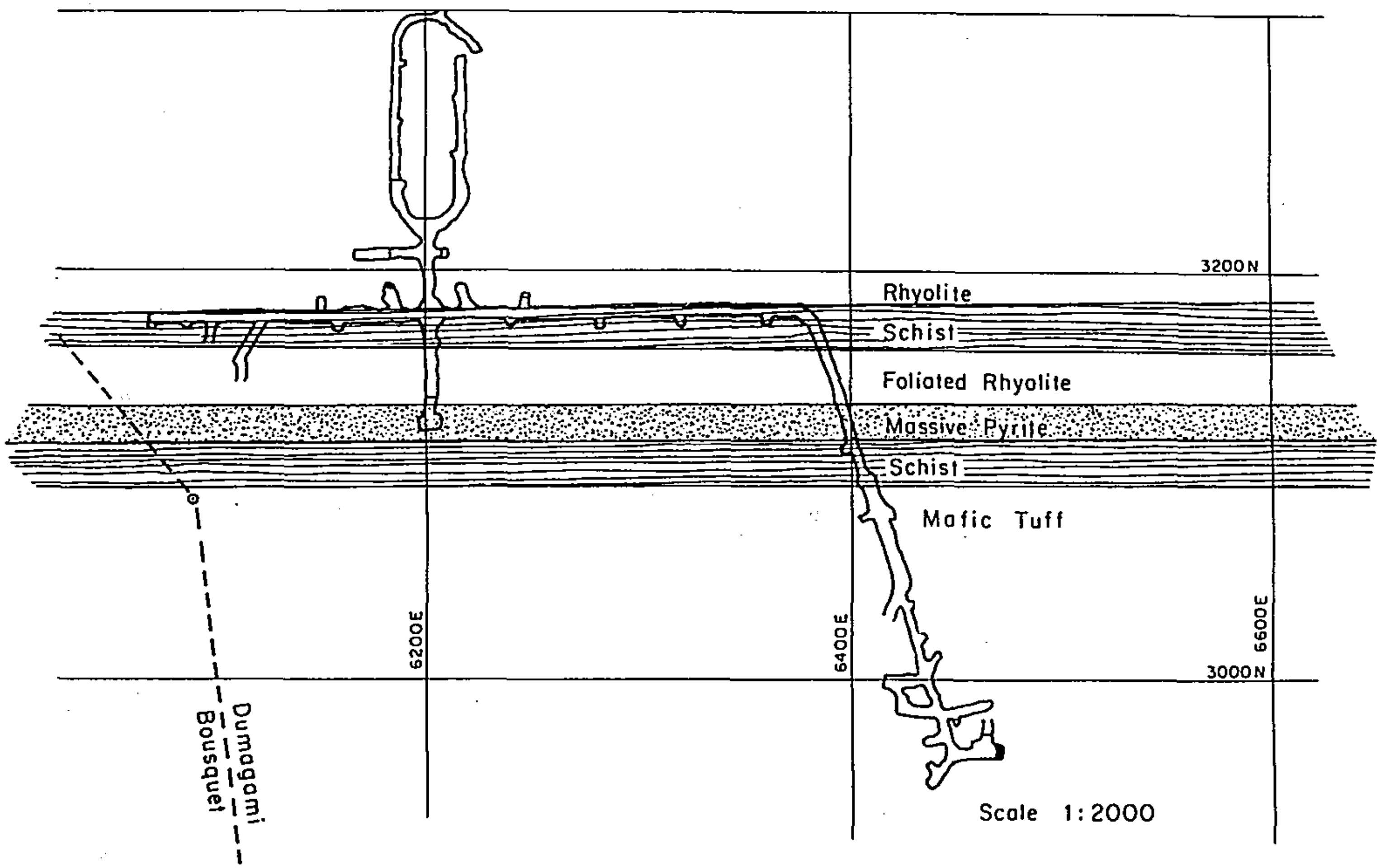

Figure 5.3 Sequence of geological units, Dumagami Mine, level 17.

Few structural geology elements have been identified while surveying the site. Figure 5.4. Rock core and field mapping for this research have shown that foliation/schistosity is the predominant type of discontinuity in the units. Some large sub-vertical joints orthogonally cross the orebody, spaced 0.8-3 m.

Sub-horizontally oriented joints, equally wide, occur in the massive pyrite with an average spacing of 2-5 m. The hangingwall ore boundary can be considered as a planar discontinuity over the extent of the orebody. On occasion, the massive pyrite is segmented by poorly developed east-west foliation; spacing is greater than 30 cm. Figure 5.5 indicates that blocks defined by the orebody boundary, by sub-vertical and sub-horizontal joints, can fall from the roof. However, field examination has shown only prismatic sliding blocks occur. If the N8W 85SW joint family extends to surface, plug failures could be possible bounded by this and the planar ore boundaries. Joint properties are shown in Table 5.1.

5.2 MINING EXTRACTION

The Dumagami Mine came into production in 1986, after diamond drilling exploration had delineated a gold bearing ore zone. Mining has followed a progressively deepening pattern. Extraction is complete between depths 140 m and 350 m.

The mining method used for this area has been blasthole mining practised in a multi-level sub-level retreat fashion, starting from the longitudinal extremities of the orebody and finishing at the stope center. This approach has reduced development costs, to a central cross cut and a drift located in the ore. Ore is removed from draw-points at

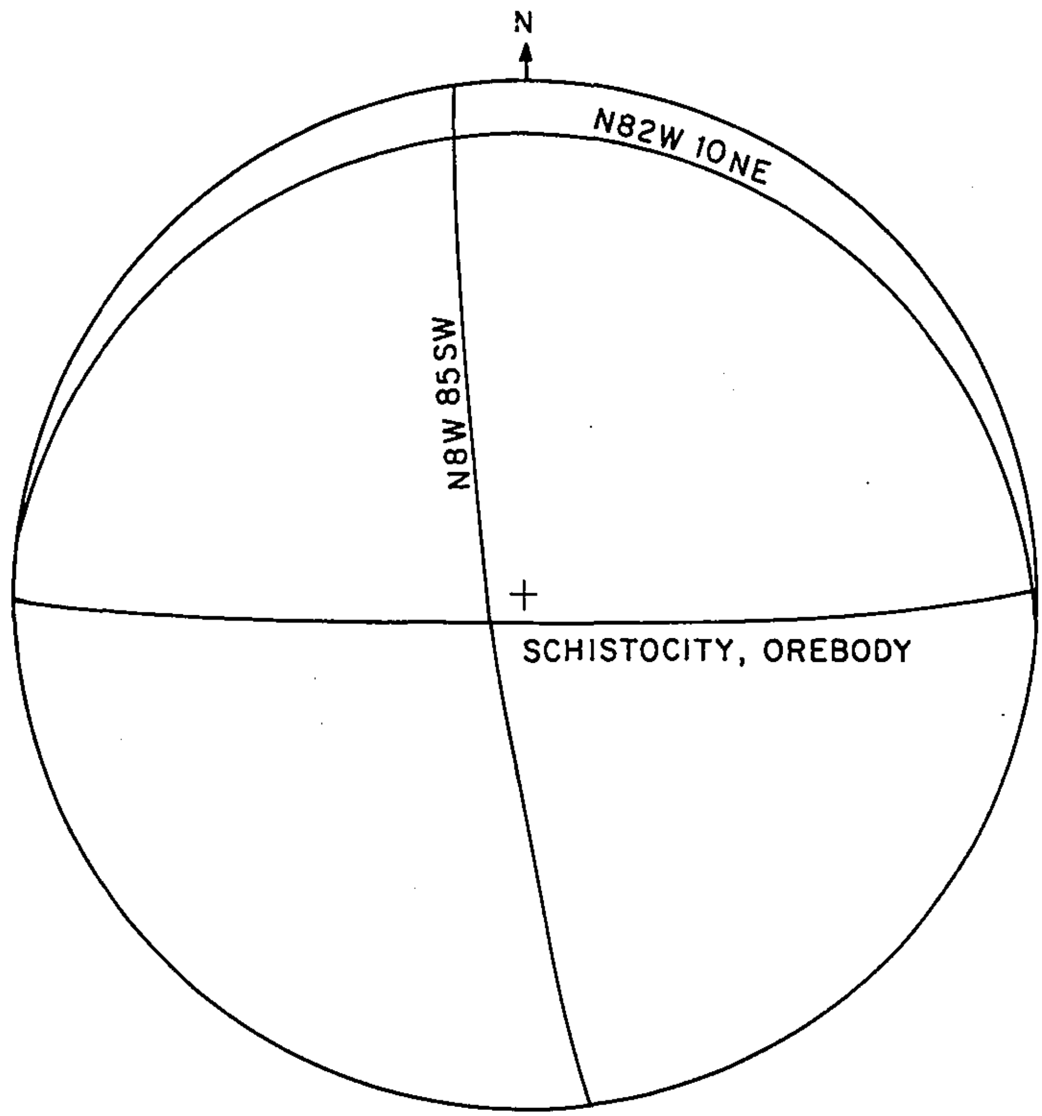

Figure 5.4 Stereographic projection of Dumagami Mine discontinuities.

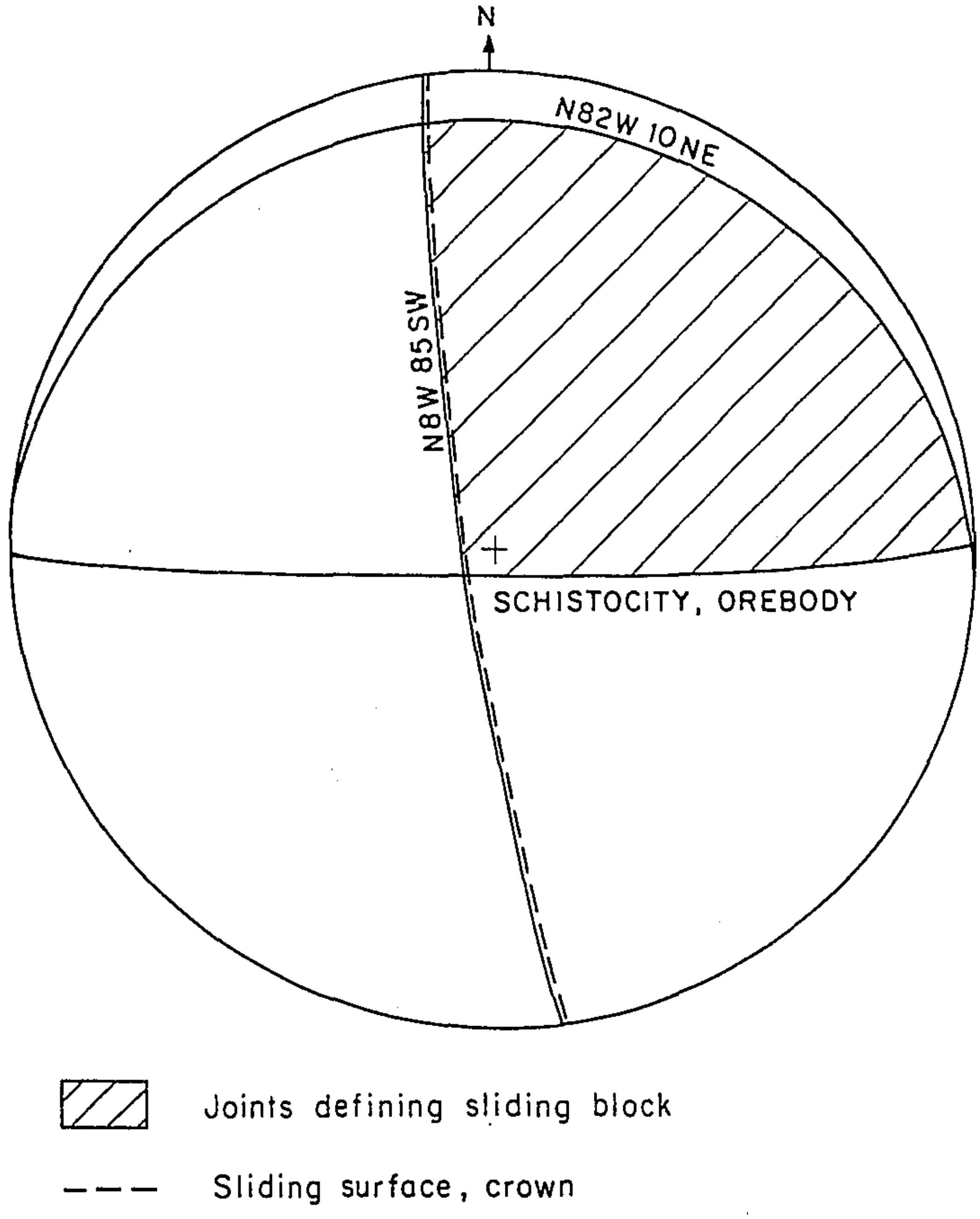

Figure 5.5 Block failure potential, stereographic analysis, Dumagami Mine.

Table 5.1 Properties of Dumagami Mine Rock Joints

Joint Family	Spacing (m)	Average Joint Length (m)	Joint Condition
N82W 10NE	2-5	> 9	Undulating, slightly rough, no alteration
N8W 85SW	0.8-3	> 9	Planar, slightly rough, no alteration
N90E 85S	> 0.3 (orebody) 0.01-0.02 (schist)	> 3 regional	Planar, smooth, talc covered (schist)

main levels with trackless loaders feeding ore to an ore pass system.

Mining is now being carried out at a depth of 680 m in an upward and retreat fashion away from the property boundary to reduce the effects of stress redistribution caused by the Bousquet 2 property extraction. Mining has progressed there from a depth of 800 m.

5.3 SELECTION OF CASE STUDY

The Dumagami Mine represents a rock mass environment of competent ore zone bounded by weak rock (on one side), Figure 1.3d. In this case the anticipated failure mechanisms are plug drop from the massive pyrite orebody, ravelling from the crown, and chimneying within the immediate hangingwall schist. Caving will also be examined. Without existing stratifications, strata failures are not expected. Stope walls are commonly affected by deformation of the schist into the opening which can affect the confinement of the crown. Saturated overburden and a small lake are located above the orebody. The stability of the shallow stope is therefore an important consideration.

This massive and vertical pyrite orebody is bounded by low friction boundaries and crossed by extensive, vertical joints which could form a plug. Plans are underway to mine a shallow stope that, with subsequent progressive expansion, will join a larger stope at depth, Figure 5.6. This progression might at some point adversely affect the stress distribution around the opening in regards to failures. Specialized modelling will be helpful in examining the potential failure of the current 210 m and future 330 m high schist hangingwall and whether this might continue to surface. The work performed

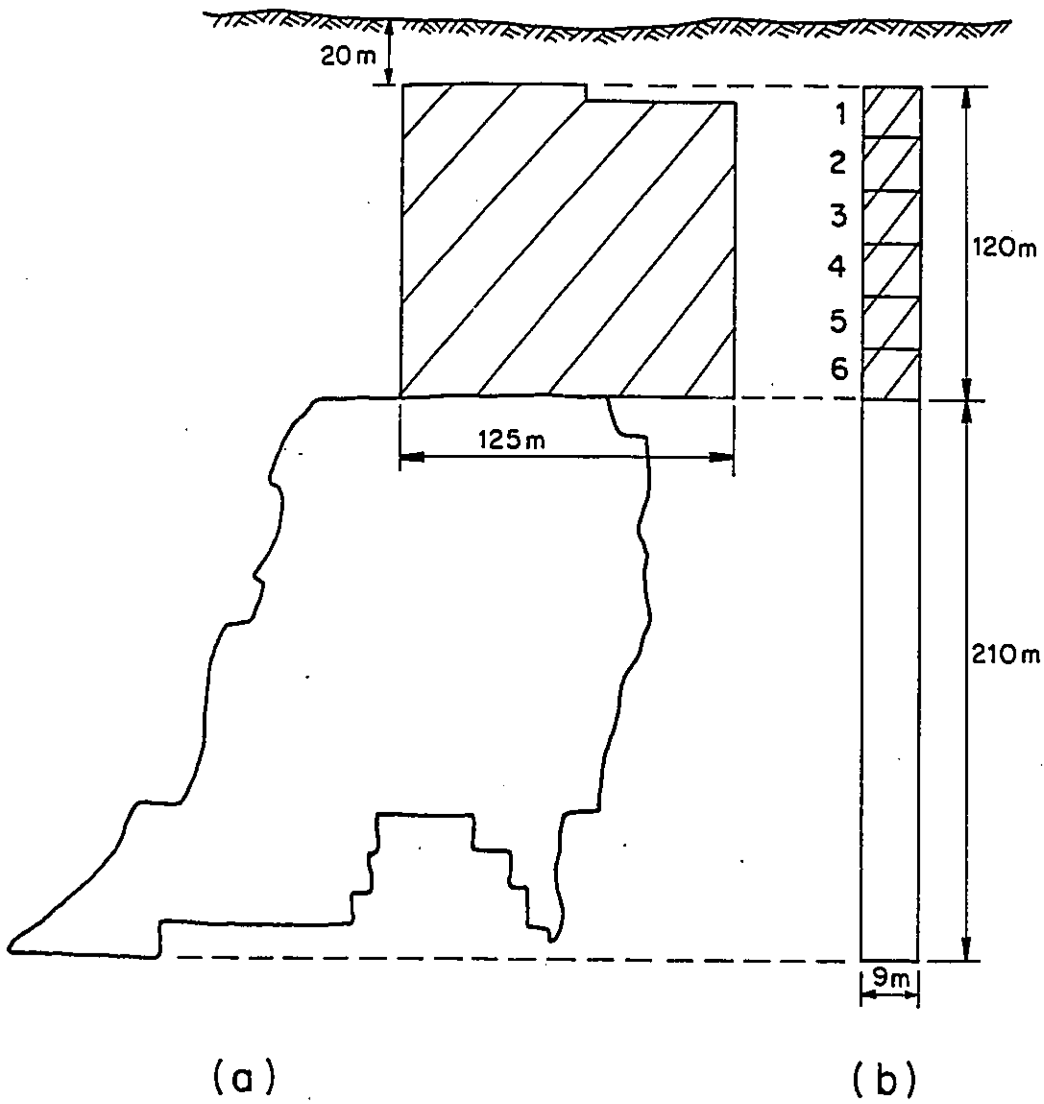

Figure 5.6 Longitudinal (a) and transversal (b) sections of the existing stope and planned (cross-hatched) shallow stope development. The sequence of shallow stope extraction is indicated.

under this thesis would supply the mine operators with information that would have a bearing on designing the shallow stope expansion. Because site access was possible, rock core available and in situ tests performed, supplementary rock and rock mass property evaluations could be added which would well define the site geomechanically and provide representative results of analysis.

The schistose material limiting the orebody is similar, but better in quality to that in which the Bousquet Mine chimneying disintegration occurred (chapter 1.3.4). Site observations when the Bousquet Mine was visited indicate that the schist material at that site is completely sericitic and disintegrates more rapidly and seriously than the Dumagami schist.

5.4 NUMERICAL MODELLING

5.4.1 Numerical Model Selection

The Dumagami rock mass is made up of two types of materials: material with expected linear elastic behaviour (ore zone, mafic tuff, rhyolite) because they are composed of sounder and homogeneous rock, and have shown elastic behaviour in the compression tests performed; and a material with distinct anisotropy (schist) which is composed of weak sericitic material which could exhibit more non-elastic (plastic) behaviour. This has been seen in the shallow and deep mine openings into which the schist has permanently deformed. In fact, sampling of this material only provided flakes or plates of rock, unsuitable for testing.

In order to obtain a representation of the behaviour of the schist zone, especially the hangingwall contact where chimneying is a possibility, a numerical model capable of handling non-linearity was used.

The program PCEPFE (Personal Computer Elastic Plastic Finite Element stress analysis program) developed at CANMET [114] is a static non-linear finite element program for analysis of two-dimensional structures (plane strain). Initial stresses, simulation of mining sequences (excavation and/or backfill), and arbitrary distributed loading, gravity loading as well as concentrated force loading can be handled by this program.

It assumes an elastic perfectly plastic material following a generalized Mohr-Coulomb yield criterion and incremental plasticity. Elements in plasticity are indicated as "failed" elements on the factor of safety plots and remain failed in subsequent mining steps. The model does not handle anisotropic material behaviour.

The two-dimensional feature of the model represents the longitudinal extent of the problem. Ideally a three-dimensional model would provide better stress distribution for a potential plug failure analysis. However, the three-dimensional non-linear model available (the CANMET BMINES) was not operational in the non-linear mode during the modelling stage of this research program.

5.4.2 Geomechanical Properties

The Dumagami Mine supplied rock core containing all of the site units except rhyolite. The core was obtained from a diamond drill hole driven orthogonal to foliation and the orebody for the purpose of carrying out in situ modulus of elasticity tests.

As part of this research all rock units supplied were tested, from rock core for intact strength and deformation properties, Table 5.1, except for the schist units, their highly segmented nature preventing such tests from being carried out. RQD was performed on the rock core. From these values and the rock mass rating (Appendix 3), the Hoek and Brown m and s field values were calculated using equation 1.43 and 1.44, Table 5.2. For the schist, representative field values of m and s were obtained by examining the Hoek and Brown recommended values [95], Table 2.1, and that calculated for the parent volcanic units. The unit is of very poor quality, RMR = 25. The parent rock material for the schist is volcanic rock (fine grained polymineralic rock). The tuff and rhyolite (similar to tuff in composition, RQD, joint properties and orientations) rate at m = 1.0 and s = 0.004. The more discontinuous schist will have a lower rock mass cohesion, whereas the angle of friction will also be lower due to the effect of talc covering the schist's plates. Therefore an m = 0.4 and s = 0.0001 were chosen. Since one joint family usually exists (foliation) and that the rock mass is divided into extensive but thin plates indicates that the m and s values were somewhat better than the worst rating given for that RMR, in Hoek and Brown.

Appendix 3 outlines the Hoek and Brown [95] calculations to obtain rock mass c and ϕ values, based on these m and s parameters. These were then used in the 2-D model to define the strength envelope. They are summarized in Table 5.3.

Although modulus of elasticity values were obtained from dilatometer tests, the orthogonal hole direction provided values parallel to schistosity. These field values shown in Table 5.3 are expected to be higher than test values in the weakest direction, tested from drill holes parallel to schistosity. Drill holes oriented parallel to schistosity caved

Table 5.2 Dumagami Mine Rock Material Laboratory Test Results

	Compressive Strength (MPa)		Tensile Strength (MPa)	Modulus of Elasticity (GPa)	Poisson's Ratio	Cohesion (MPa)	ϕ (degrees)	Hoek & Brown m Value	Unit Weight (MN/m^3)
	Confinement	Peak Strength							
Mafic Tuff	0 5 10 15 20 25	98 156.3 173.7 191.8 203.5 213.4	19.1	32	0.44*	30	43	5.7	0.0268
Hangingwall schist	-	-	-	-	-	-	-	-	0.027
Massive Pyrite	0 5 10 15 20 25	86.0 126.3 159.8 181.2 213.0 229.3	7.4	84	0.5*	17	54	14	0.05
Footwall Rhyolite	0 5 10 15 20 25	56.0 87.9 97.9 107.3 115.7 123.3	9.3	28	0.20	27	38	4.4	0.0274
Footwall Schist	-	-	-	-	-	-	-	-	0.0274
Rhyolite	-	-	-	-	-	-	-	5.7	0.0274

Table 5.3 Dumagami Mine Rock Mass Rating Parameters

	RQD	Rock Mass Rating (RMR)	Field			
			m	s	c_m (MPa)	ϕ (degrees)
Mafic Tuff	37	50	1.0	0.004	2.4	35
Hangingwall Schist	17	25	0.4	0.0001	0.8	25
Massive Pyrite	90	82	7.4	0.14	5.5	52
Footwall Rhyolite	76	54	0.9	0.006	2.0	32
Footwall Schist	8	25	0.4	0.0001	0.2	25
Rhyolite	50	50	1.0	0.004	2.4	35

readily and were not used. Only the massive pyrite values measured might be representative because, unlike the other units, foliation is not well developed. Table 5.3 therefore presents the other units' values adopted for modelling, based on the empirical Serafim and Pereira [111] approach, equation 4.1.

Natural ground stress orientation and values were obtained by CANMET [27] using overcoring of C.S.I.R. strain cells, Table 5.4, at a depth of 190 m.

5.4.3 The Dumagami Mine Numerical Model

Seven mining steps were run with PCEPFE, to simulate the currently existing shallow stope (step 1: 9 m wide, depth 140 to 340 m) and the progression for six consecutive openings that are planned to be created (each 20 m high) starting from a depth of 20 m and reaching the existing stope, Figure 5.6. The steps were carried out consecutively, i.e. the effects of a new mining step was based on the results of the previous one.

One finite element mesh was used from which elements were removed for each mining step. A model simulating a 3,000 m width and 1,000 m height was used because of the high opened stope existing at the site. Sufficient distance had to be provided for stresses and displacements to return to natural values before the model boundaries were reached. A total of 4620 elements made up the mesh before each mining step was created, Figure 5.7, representing the 5 geological materials (tuff, schist, ore zone, footwall rhyolite, rhyolite), Figure 5.8. Vertical stopes were used to approximate the 85° dip of the orebody.

Table 5.4 Dumagami Mine Summary of In Situ Geomechanical Field Parameters [26]

Modulus of Elasticity (GPa)		
Mafic Tuff	-	10.0*
Hangingwall Schist	15+	2.4*
Massive Pyrite	23+	23.0
Footwall Rhyolite	22+	12.0*
Footwall Schist	33.2+	2.4*
Rhyolite	-	10.0*
+ measured parallel to schistocity * using equation 4.1		
Natural Ground Stresses (depth = 190 m)		
	Orientation (bearing/dip)	Value (MPa)
Major Principal Stress	034°/06°	14.6
Intermediate Principal Stress	030°/12°	7.0
Minor Principal Stress	152°/76°	4.8

Dumagami

Figure 5.7 Sequence of extraction of the seven planned mining steps, Dumagami numerical model.

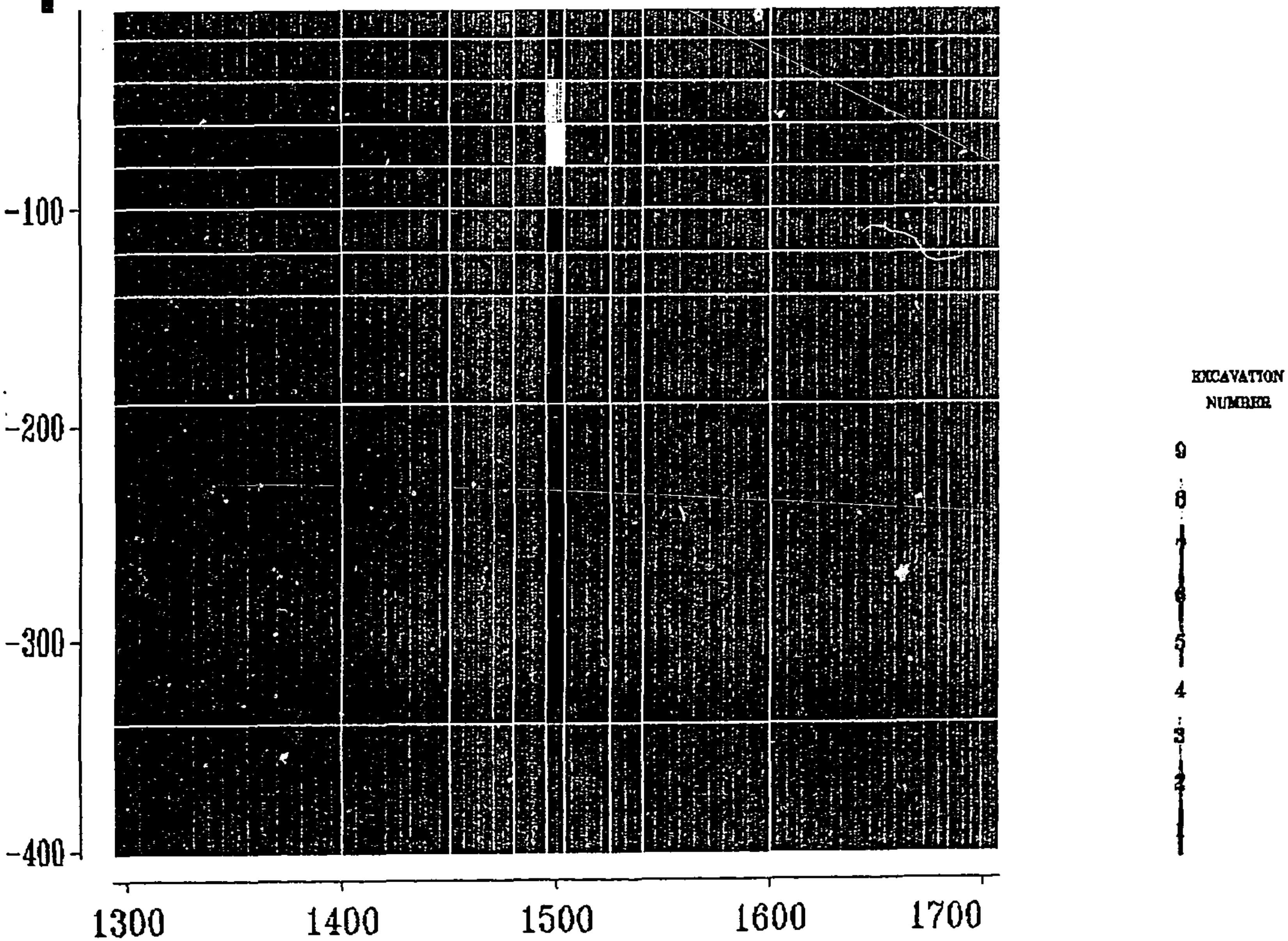

Dumagami

Figure 5.8 Dumagami model cross-section showing geological material distribution.

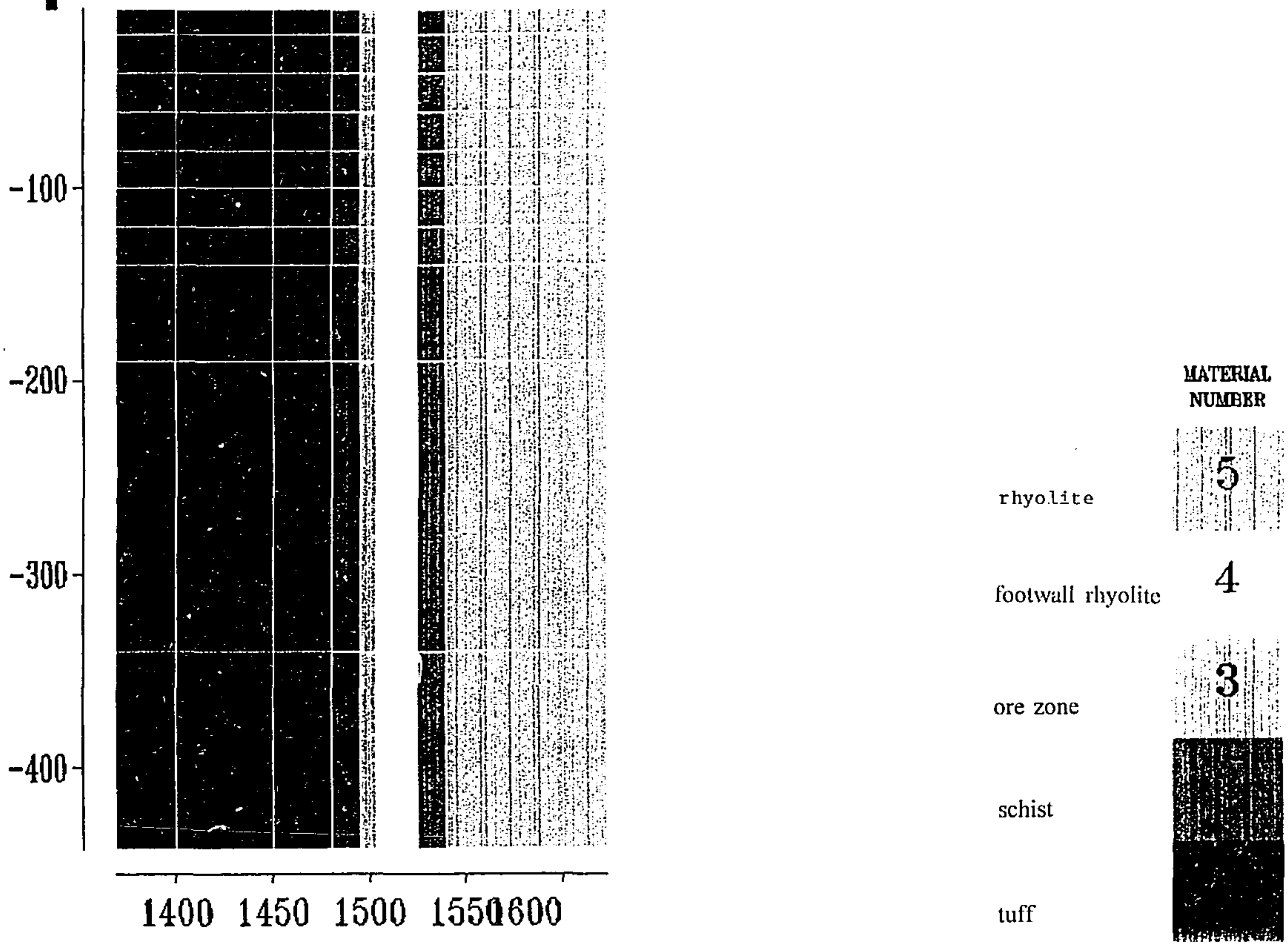

Only partially backfilled with loose rockfill, the current stope (mining step 1) and the planned mining extraction, which does not anticipate backfilling, were considered open in the modelling.

5.4.4 Modelling Results

Figures 5.9 - 5.28 present the displacements, stresses, and failed elements for mining steps one, two, six and seven, which represent important changes in conditions.

Displacements are highest in the schist hangingwall. Incremental mining steps would increase the displacements of the hangingwall in the new stope (step 2 to 7), from 14 cm to 28 cm. The crown and footwall periphery movements of this stope would never exceed 2 cm.

The hangingwalls and footwalls of the existing stope would generally be subjected to a reduction in stress with the creation and expansion of the shallow stope. The crown stresses above the existing stope would remain compressive and when the shallow stope comes closer and merges with the existing stope, values there would increase.

The surface crown pillar created in step 2 would be subjected to gradually increasing tangential compressive stresses, with subsequent stope expansion. These would be horizontal and start from 6 to 12 MPa, to reach 22 MPa before stopes merge. When this occurs, a significant increase to 40 MPa would be imposed. Radial stresses in the surface crown pillar would decrease to tensile values with expansion of the shallow stope.

Low tangential compressive stress values (0 to 2 MPa) would originally exist in the hangingwall and footwall of the shallow stope. Reductions to tensile values over the entire footwall would develop with each mining step, but the hangingwall would only

Dumagami

Figure 5.9 Rock mass displacements after mining step one, Dumagami model

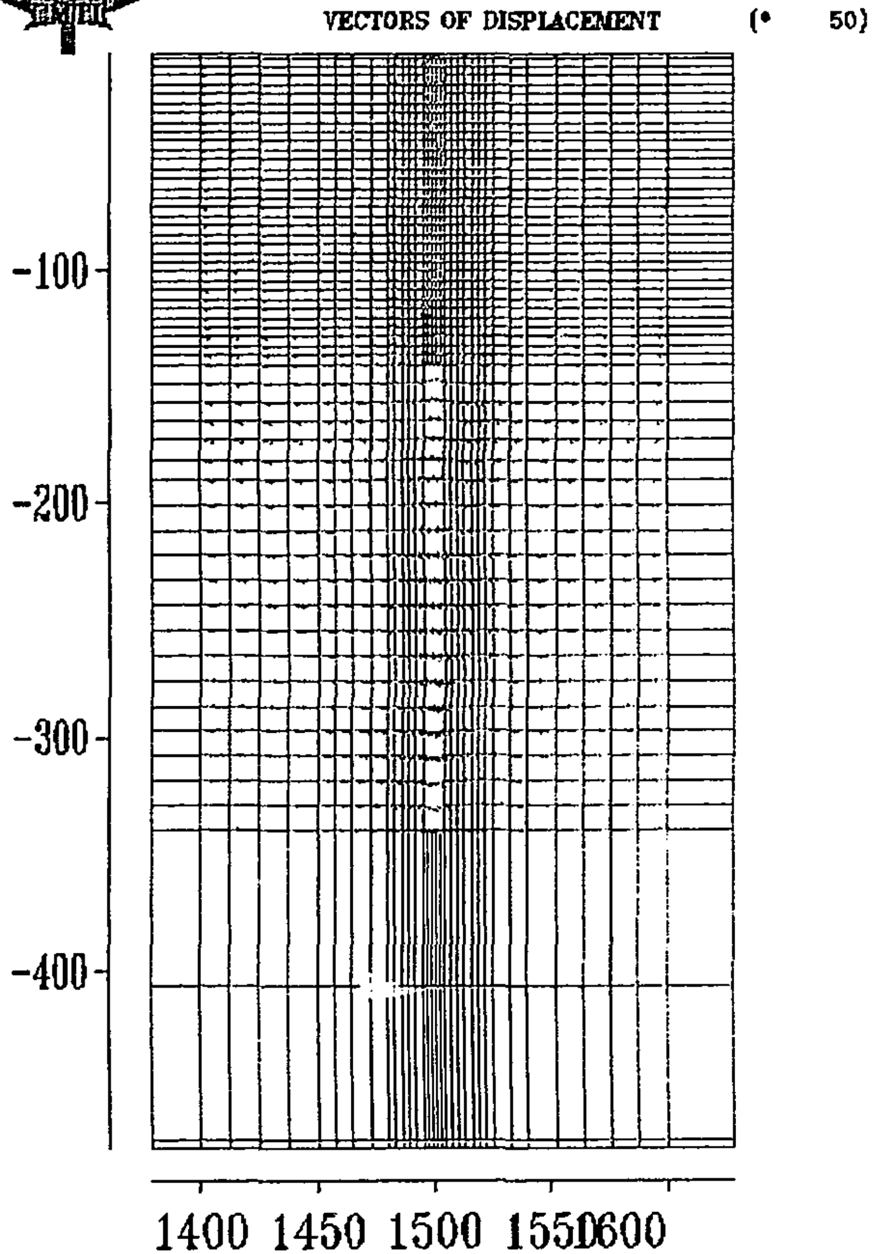

Dumagami

Figure 5.10 Stress orientation and intensity after mining step one, Dumagami model.

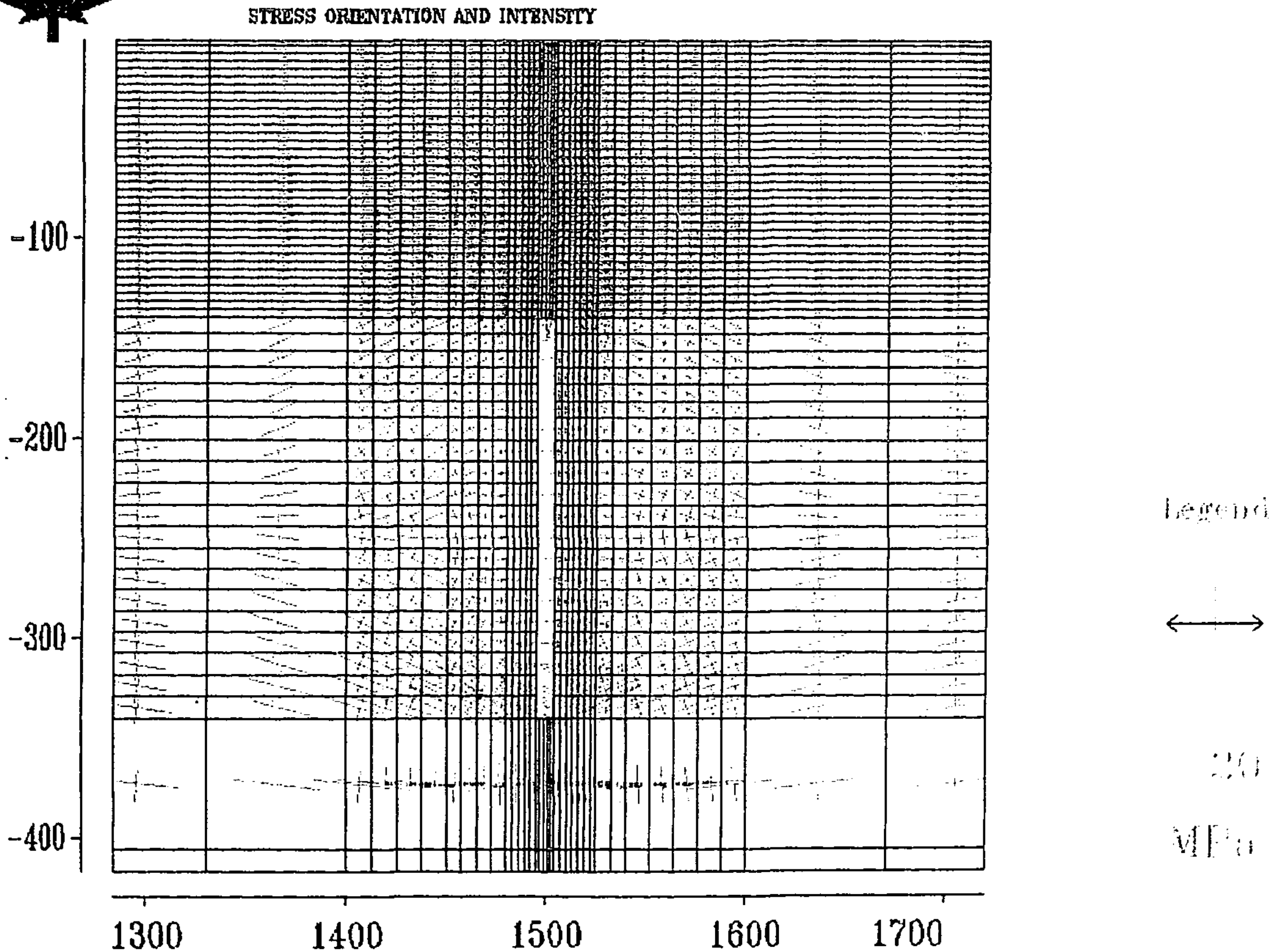

262

Dumagami Figure 5.11 Major principal stress levels after mining step one, Dumagami model

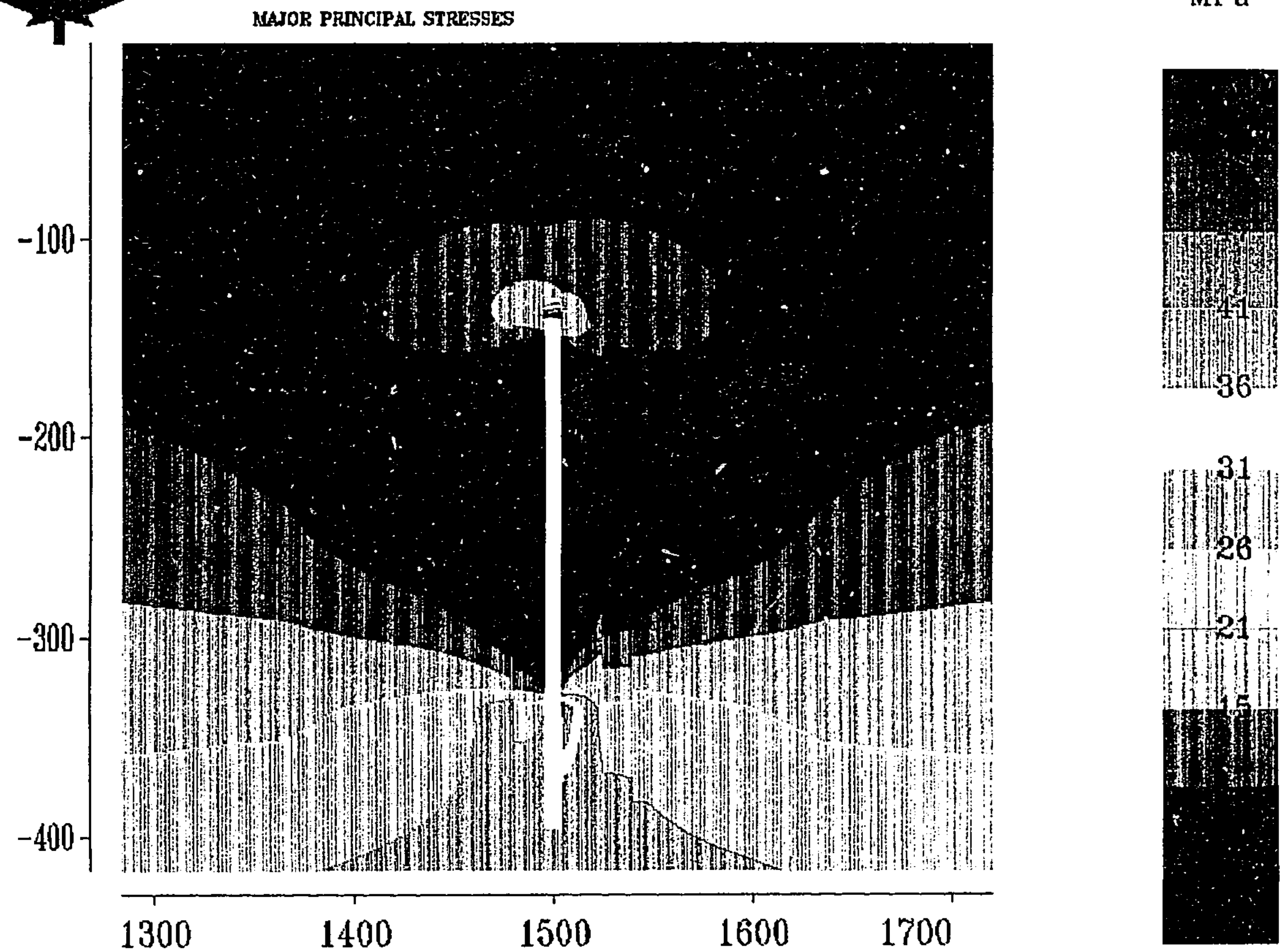

263

Figure 5.12 Minor principal stress levels after mining step one, Dumagami model.

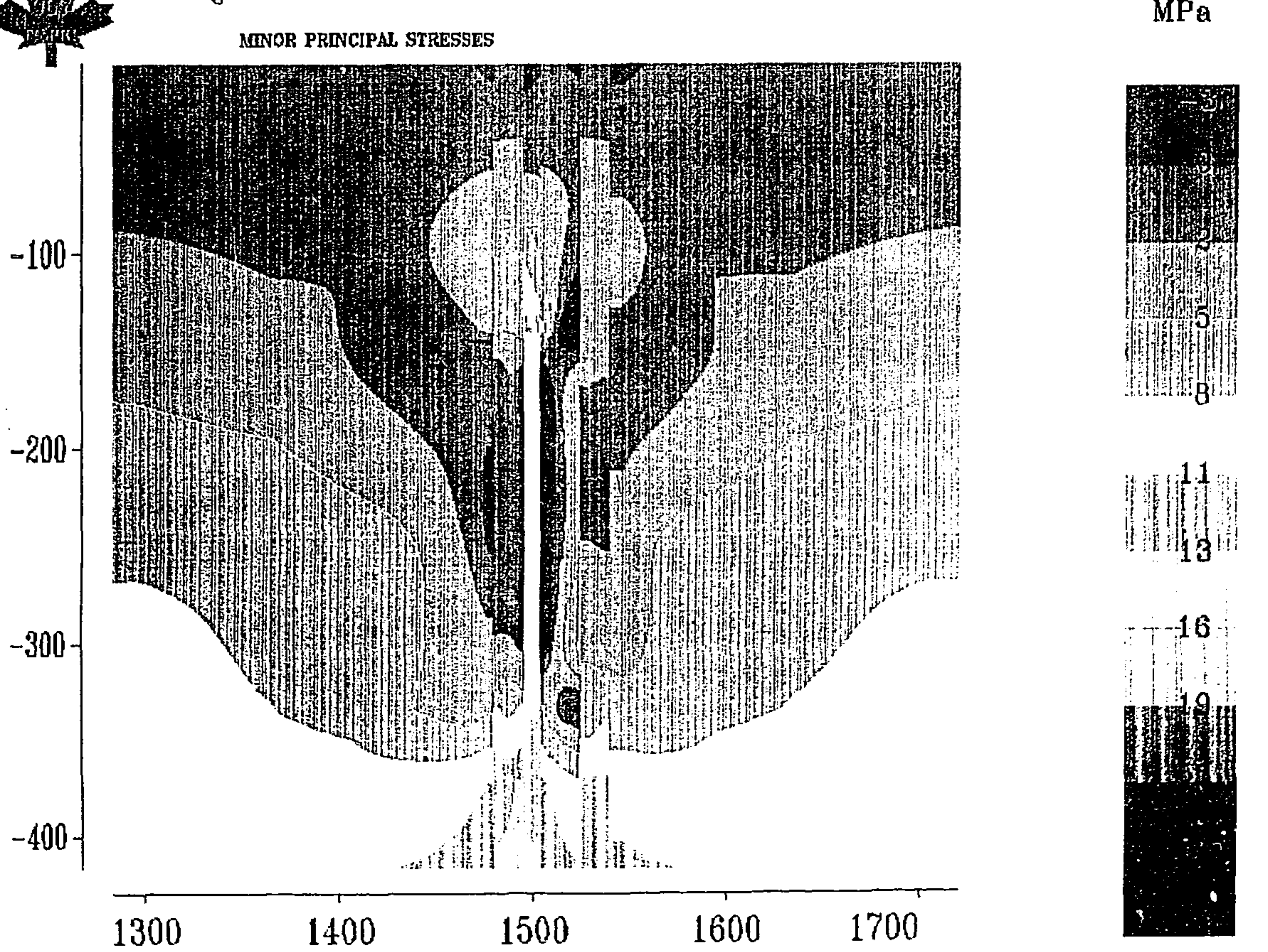

Dumagami Figure 5.13 Failed portions of the rock mass after mining step one, Dumagami model.

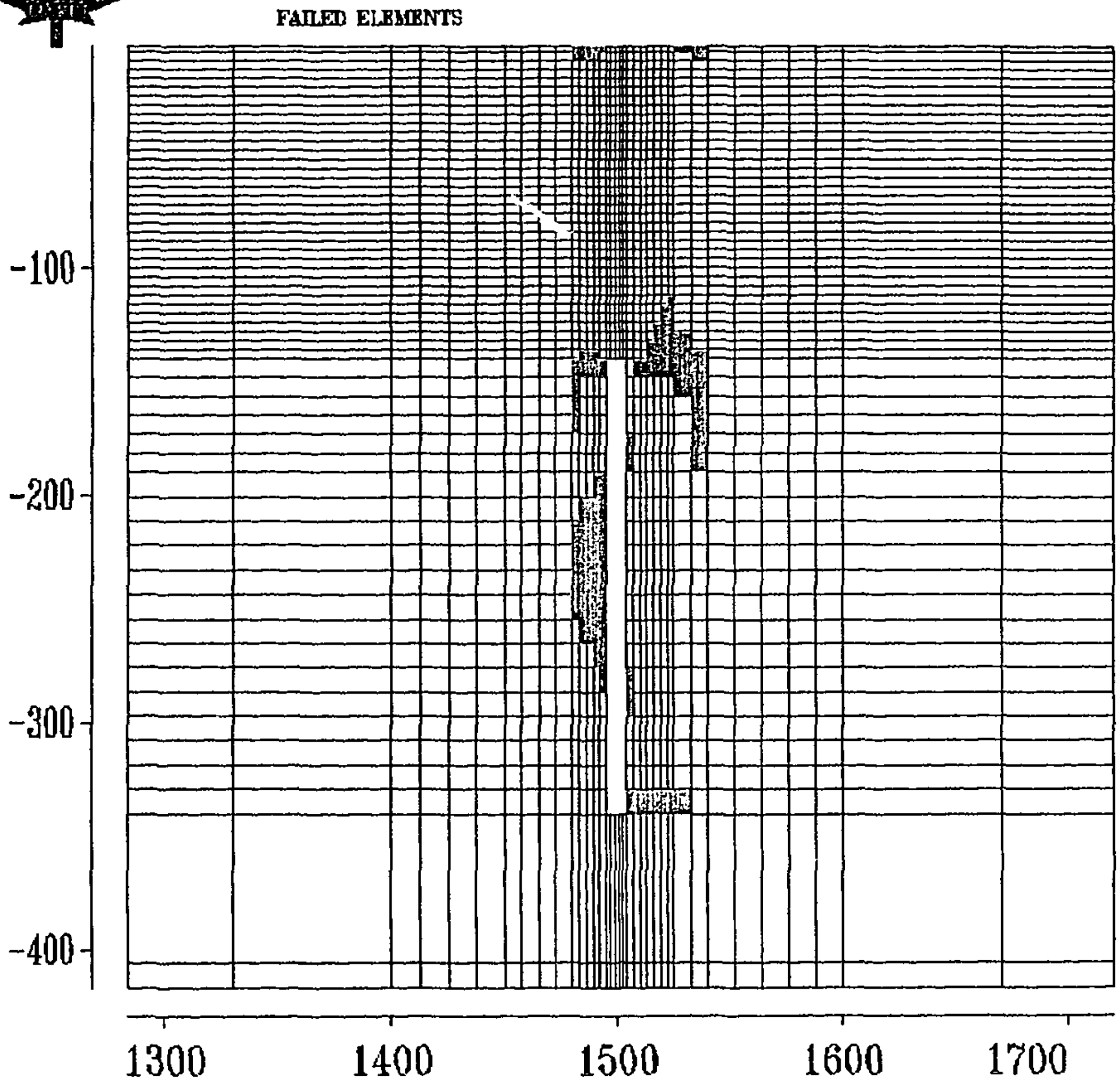

Dumagami Figure 5.14 Rock mass displacements after mining step two, Dumagami model.

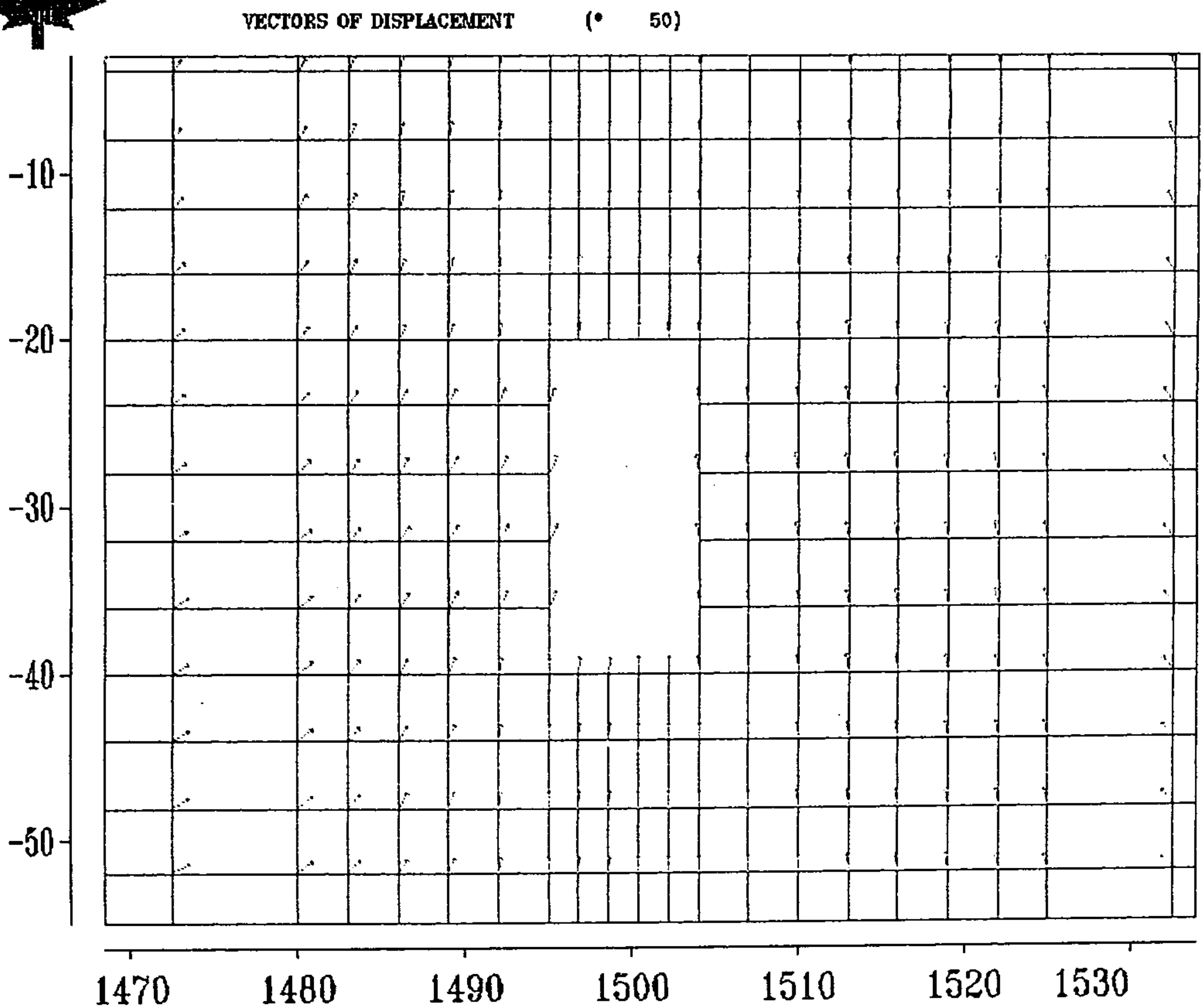

Dumagami

Figure 5.15 Stress orientation and intensity after mining step two, Dumagami model.

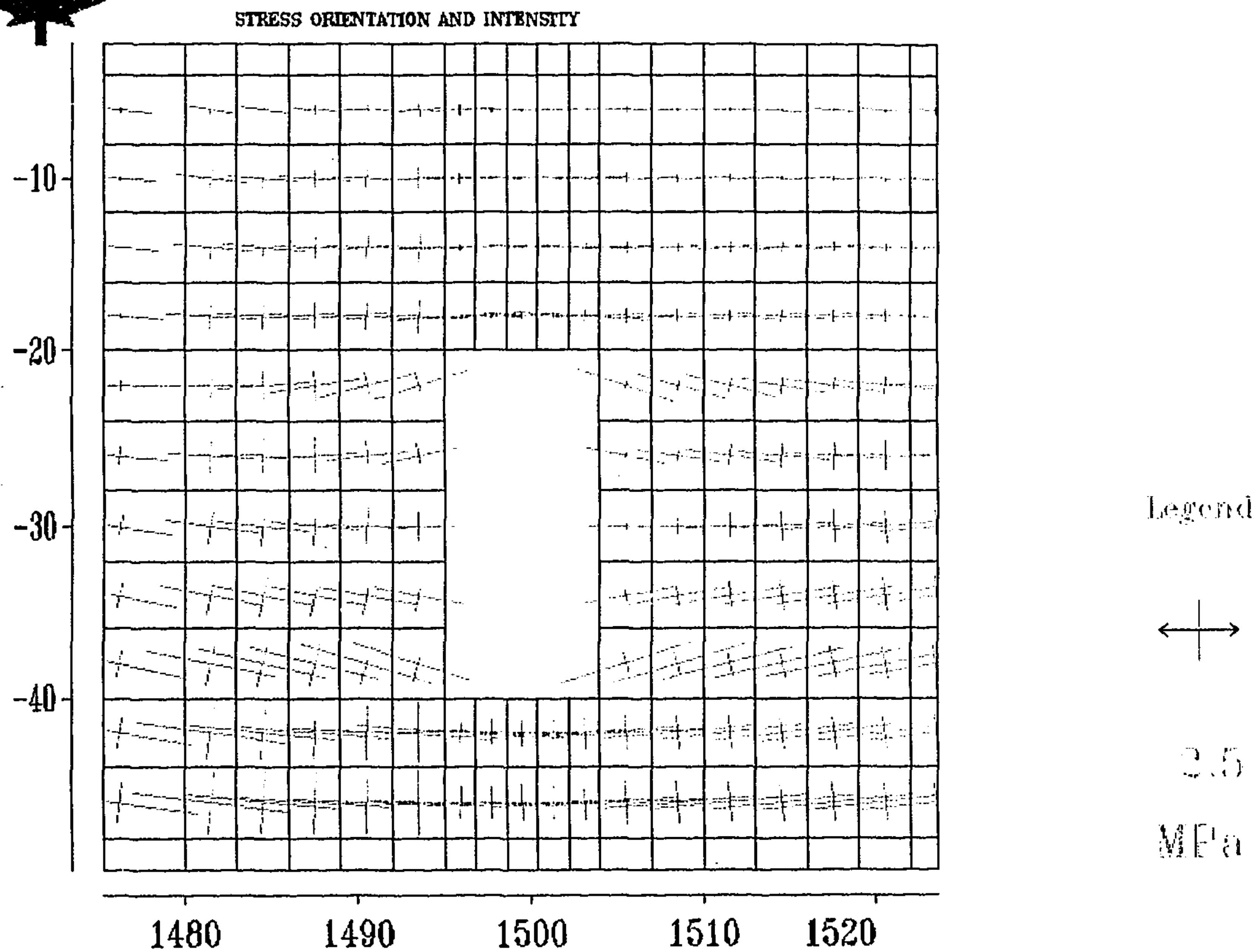

Dumagami

Figure 5.16 Major principal stress levels after mining step two, Dumagami model.

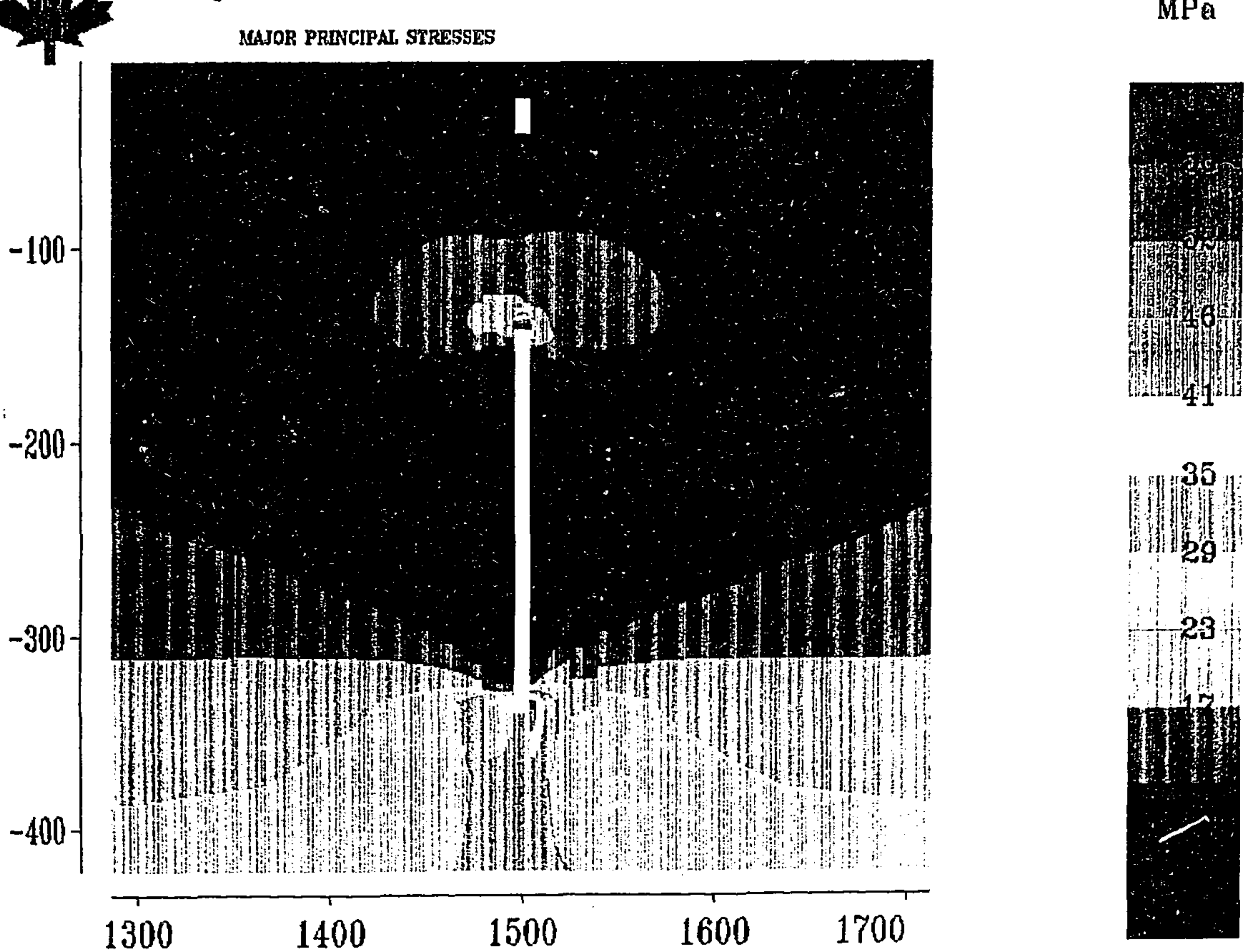

Dumagami Figure 5.17 Minor principal stress levels after mining step two, Dumagami model.

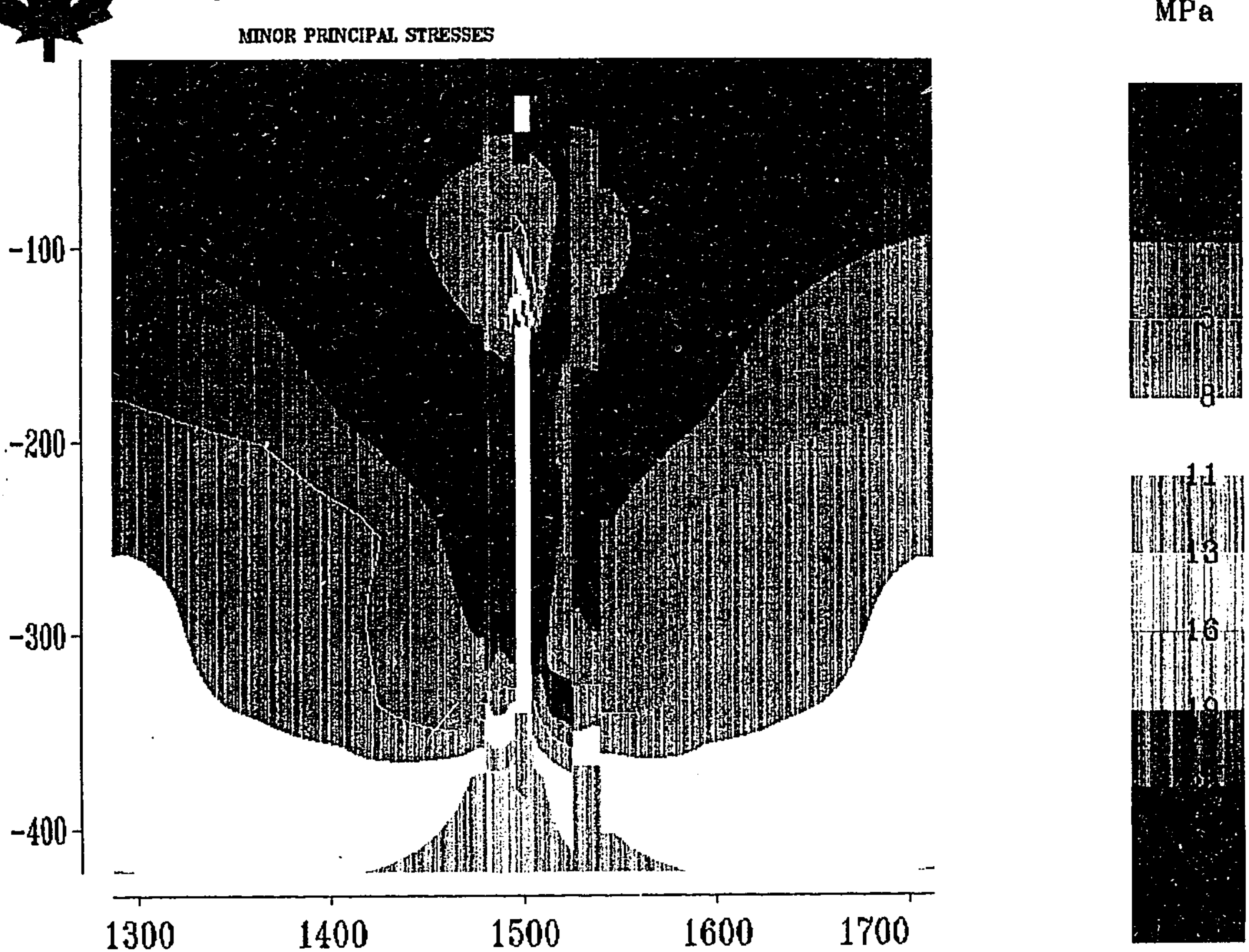

Dumagami

Figure 5.18 Portions of the rock mass after mining step two, Dumagami model.

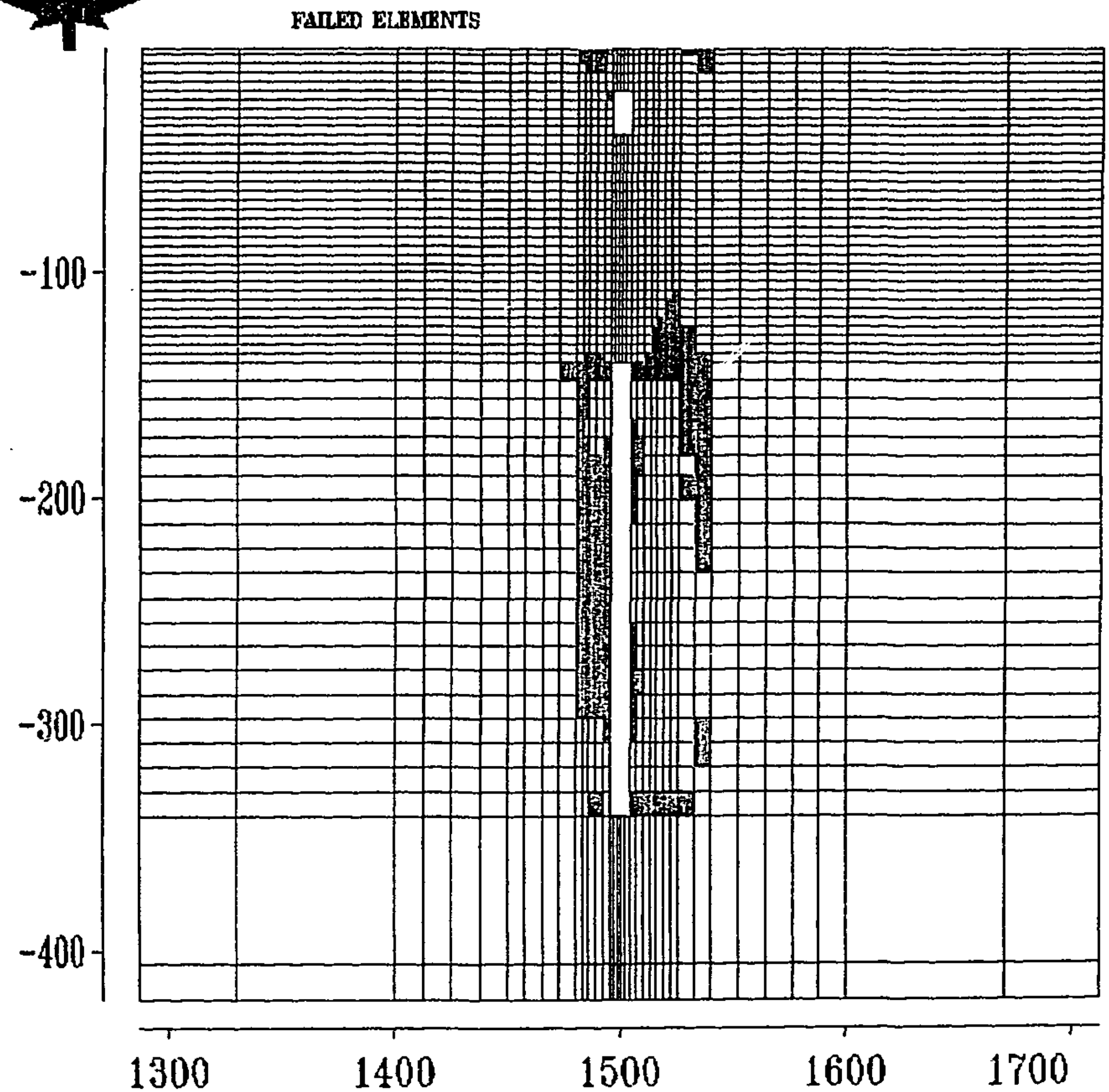

Figure 5.19 Rock mass displacements after mining step six, Dumagami model.

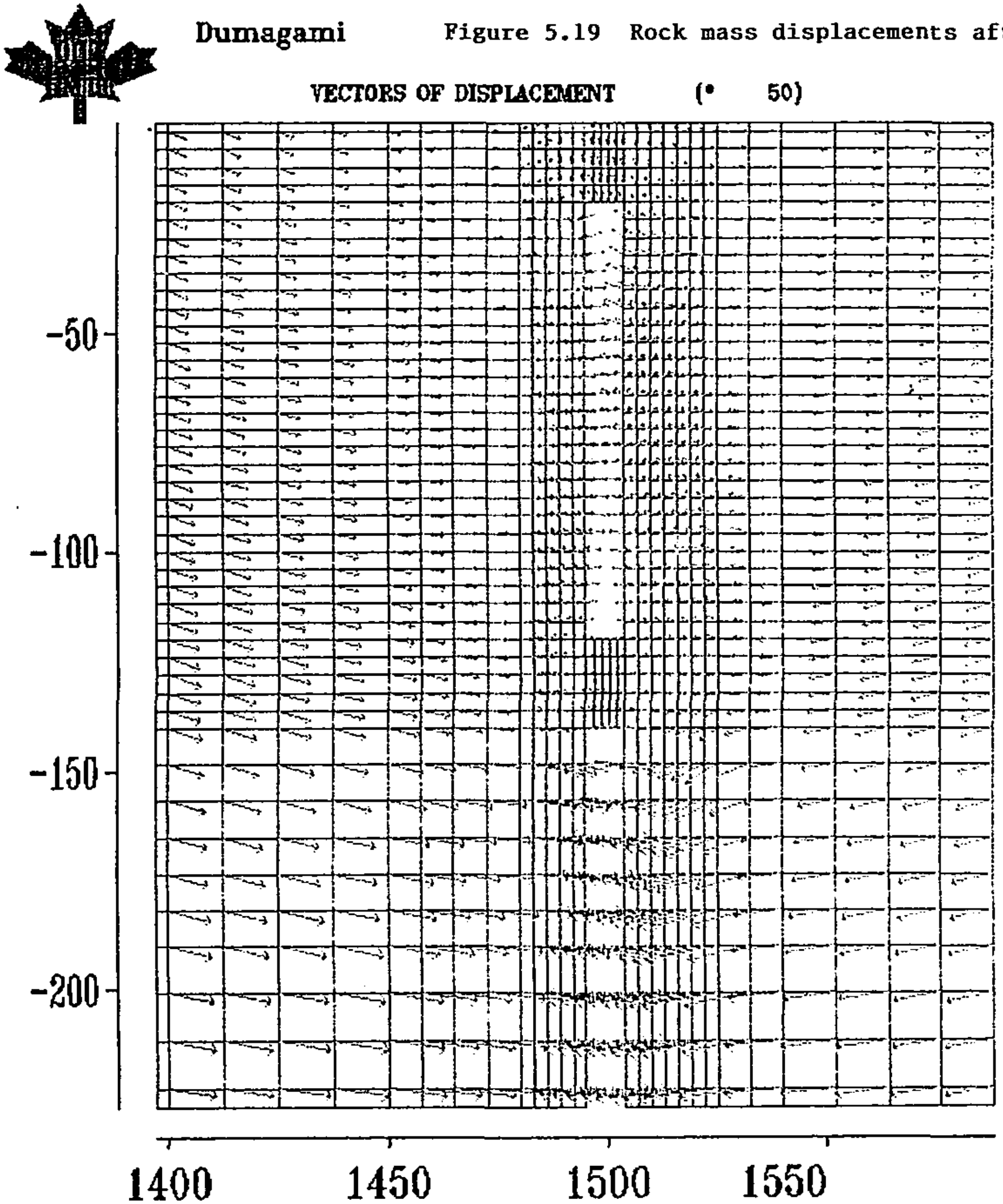

Dumagami

Figure 5.20 Stress orientation and intensity after mining step six, Dumagami model.

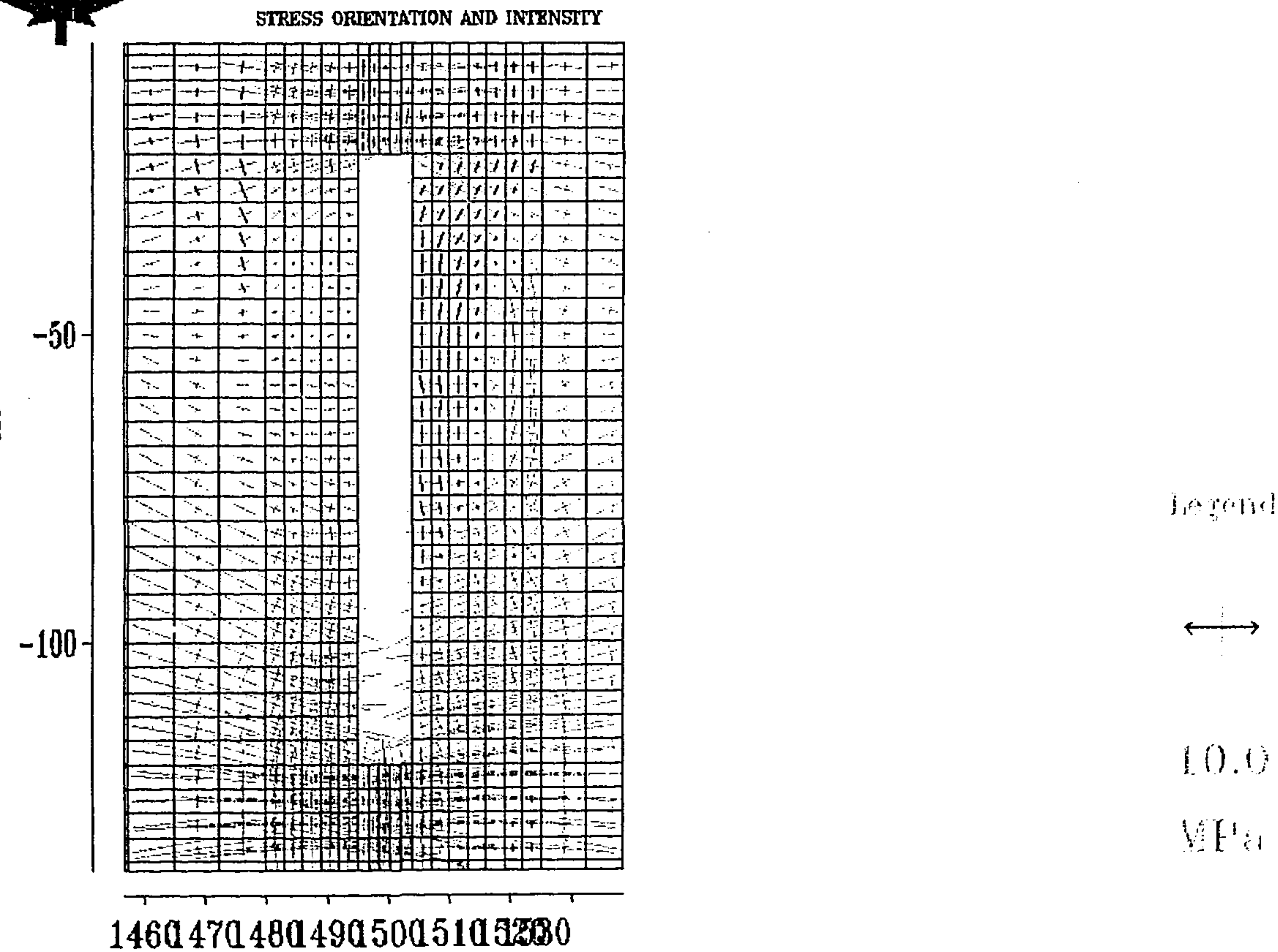

Figure 5.21 Major principal stress levels after mining step six, Dumagami model.

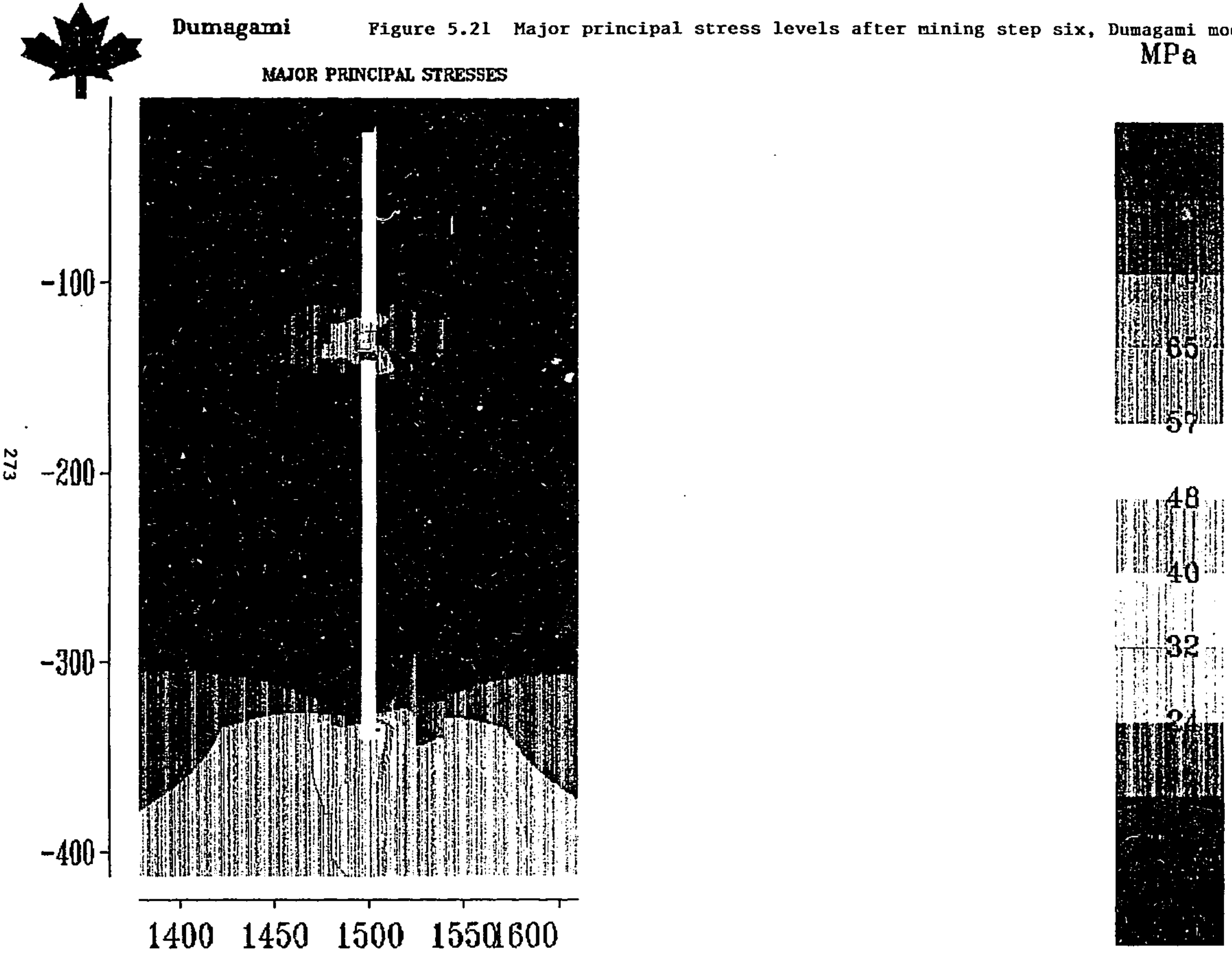

Dumagami Figure 5.22 Minor principal stress levels after mining step six, Dumagami model.

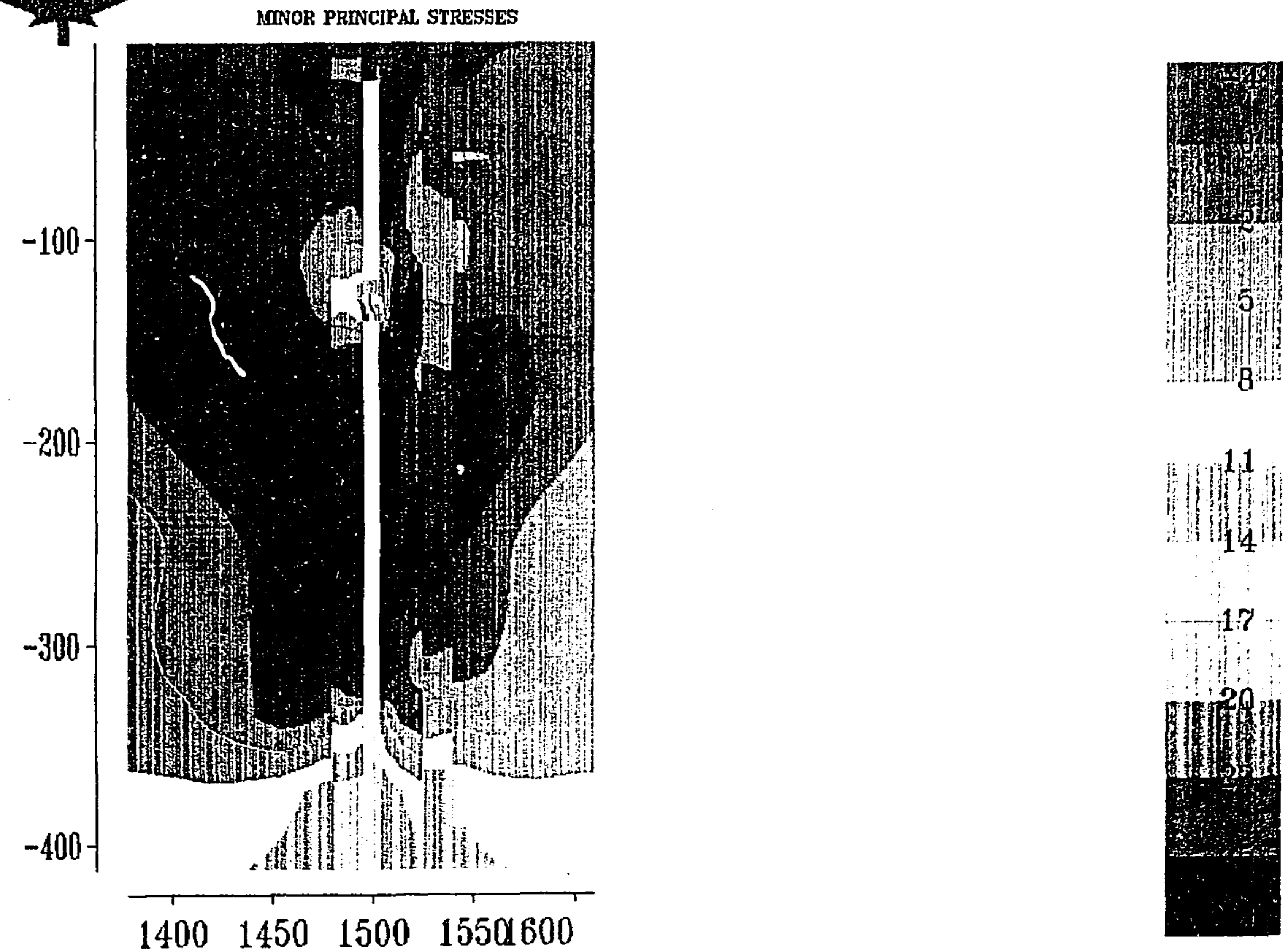

Dumagami Figure 5.23 Failed portions of the rock mass after mining step six, Dumagami model.

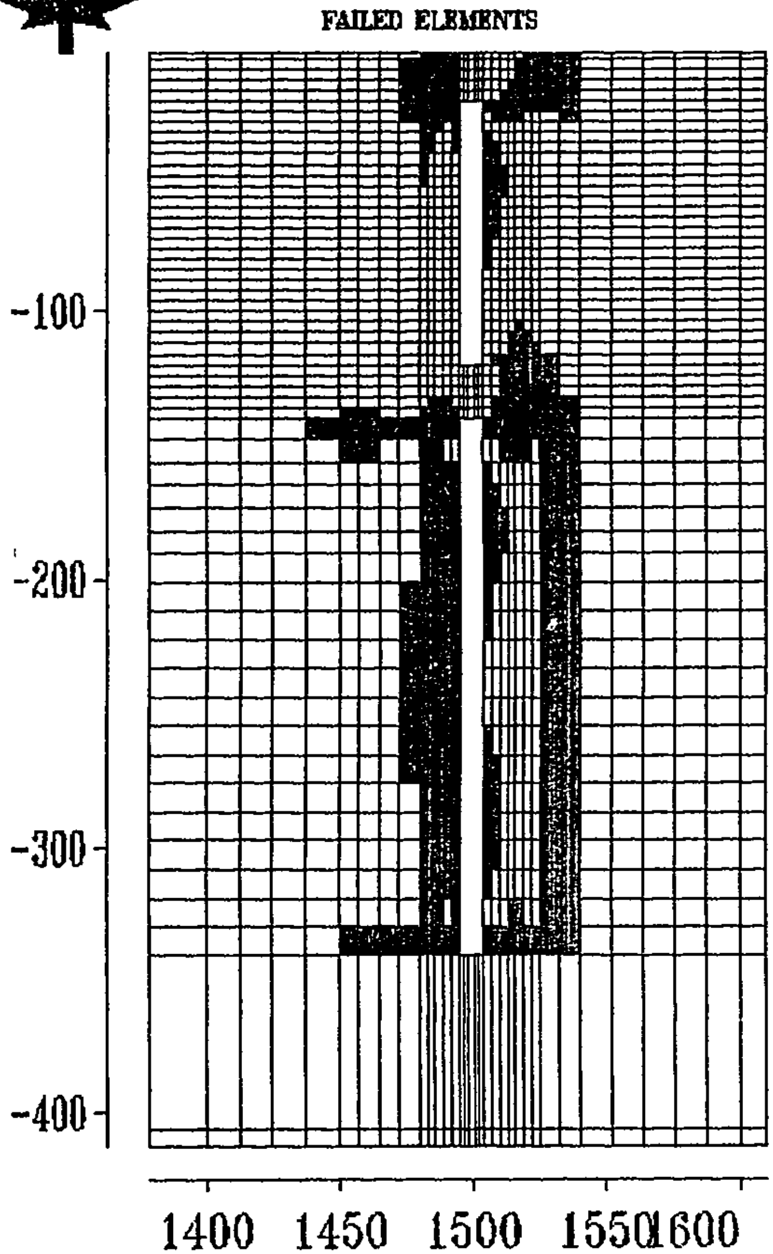

Dumagami Figure 5.24 Rock mass displacements after mining step seven, Dumagami model.

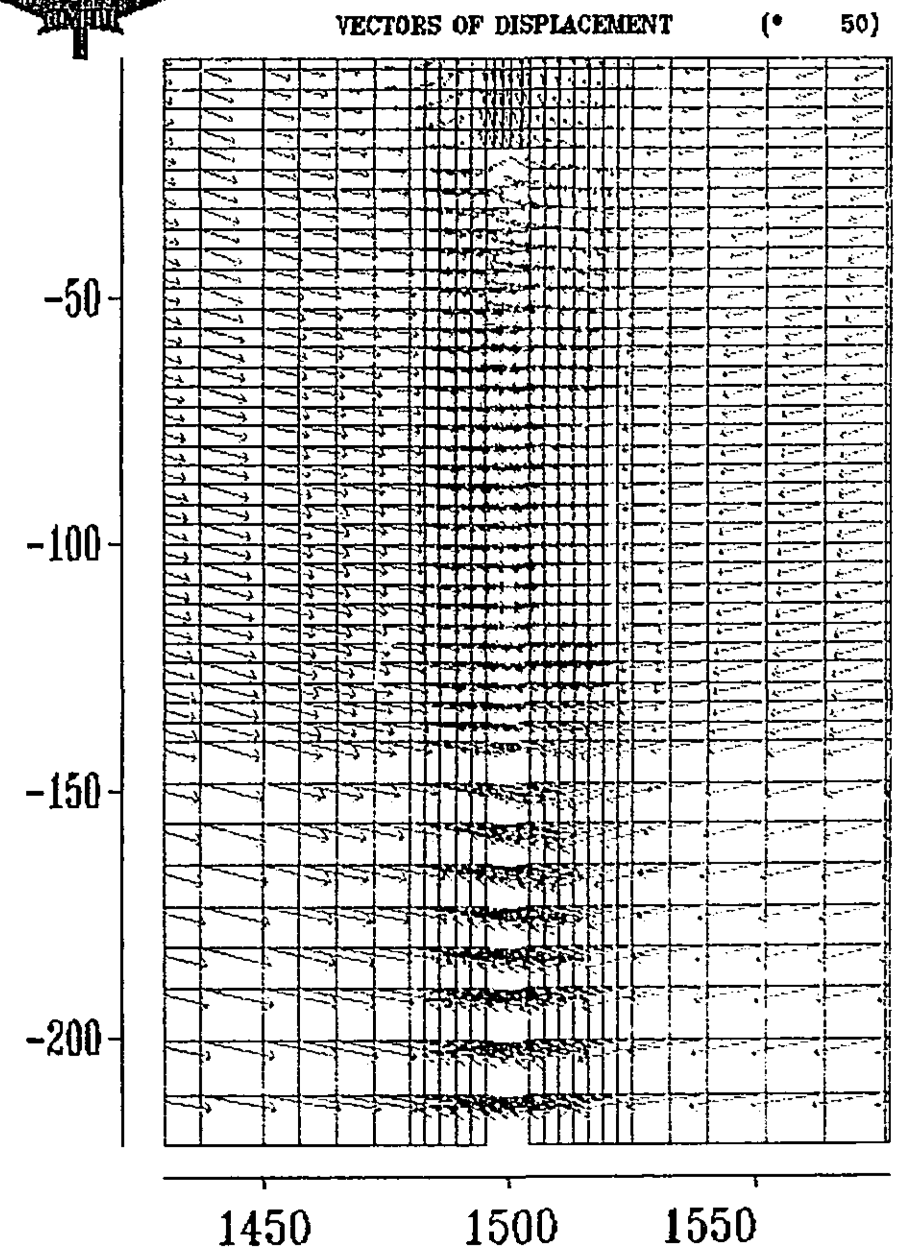

Dumagami

Figure 5.25 Stress orientation and intensity after mining step seven, Dumagami model.

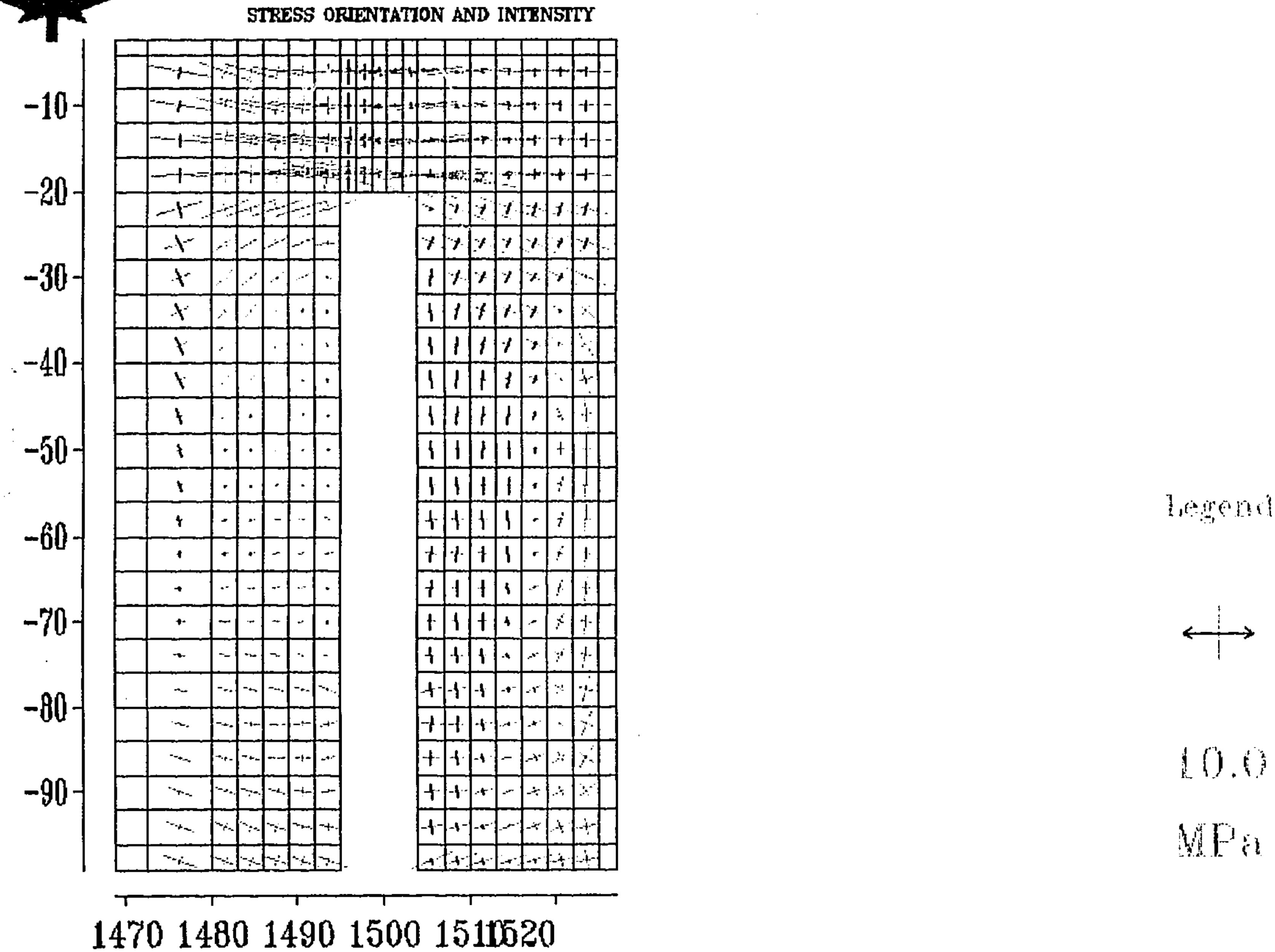

Dumagami Figure 5.26 Major principal stress levels after mining step seven, Dumagami model.

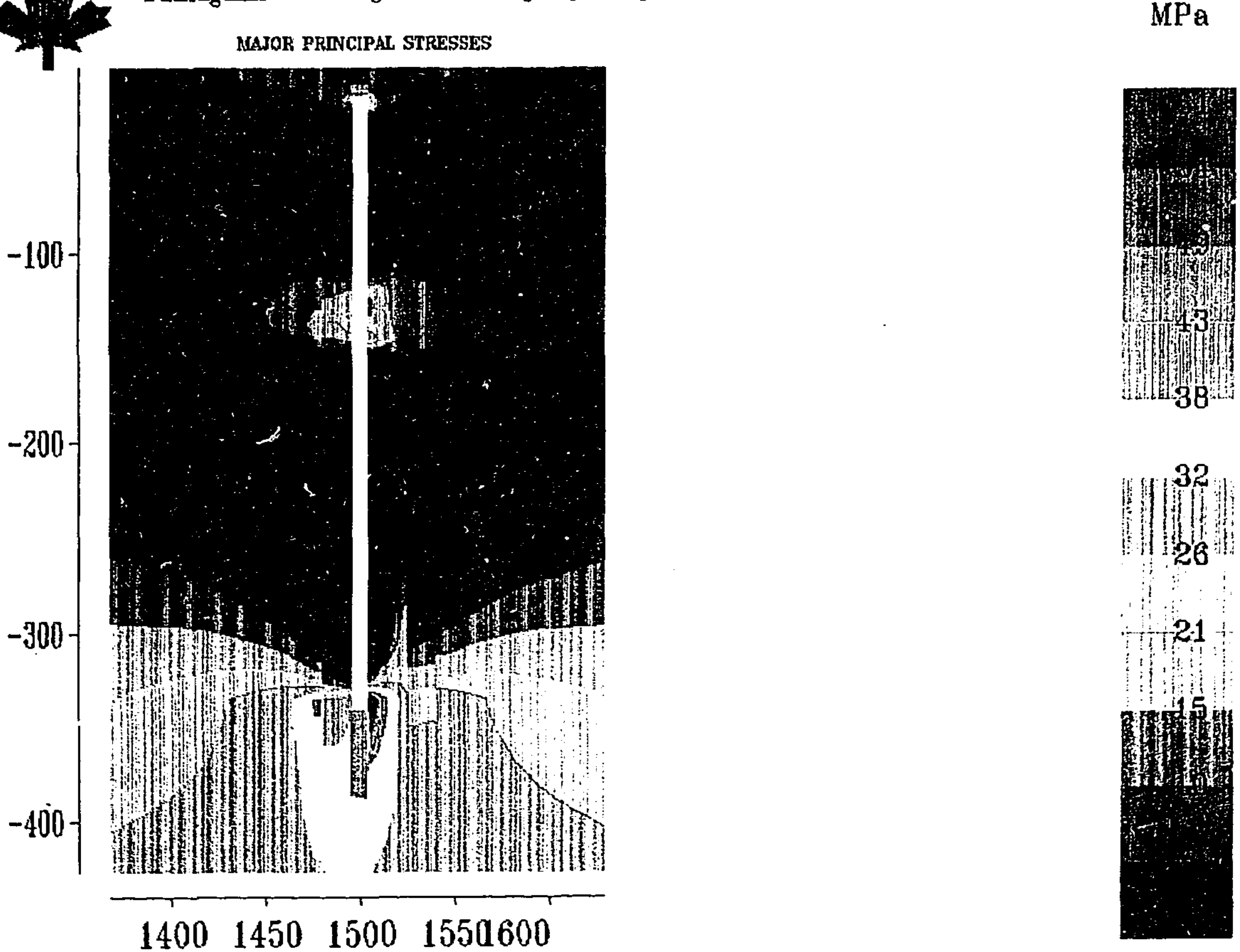

Dumagami Figure 5.27 Minor principal stress levels after mining step seven, Dumagami model.

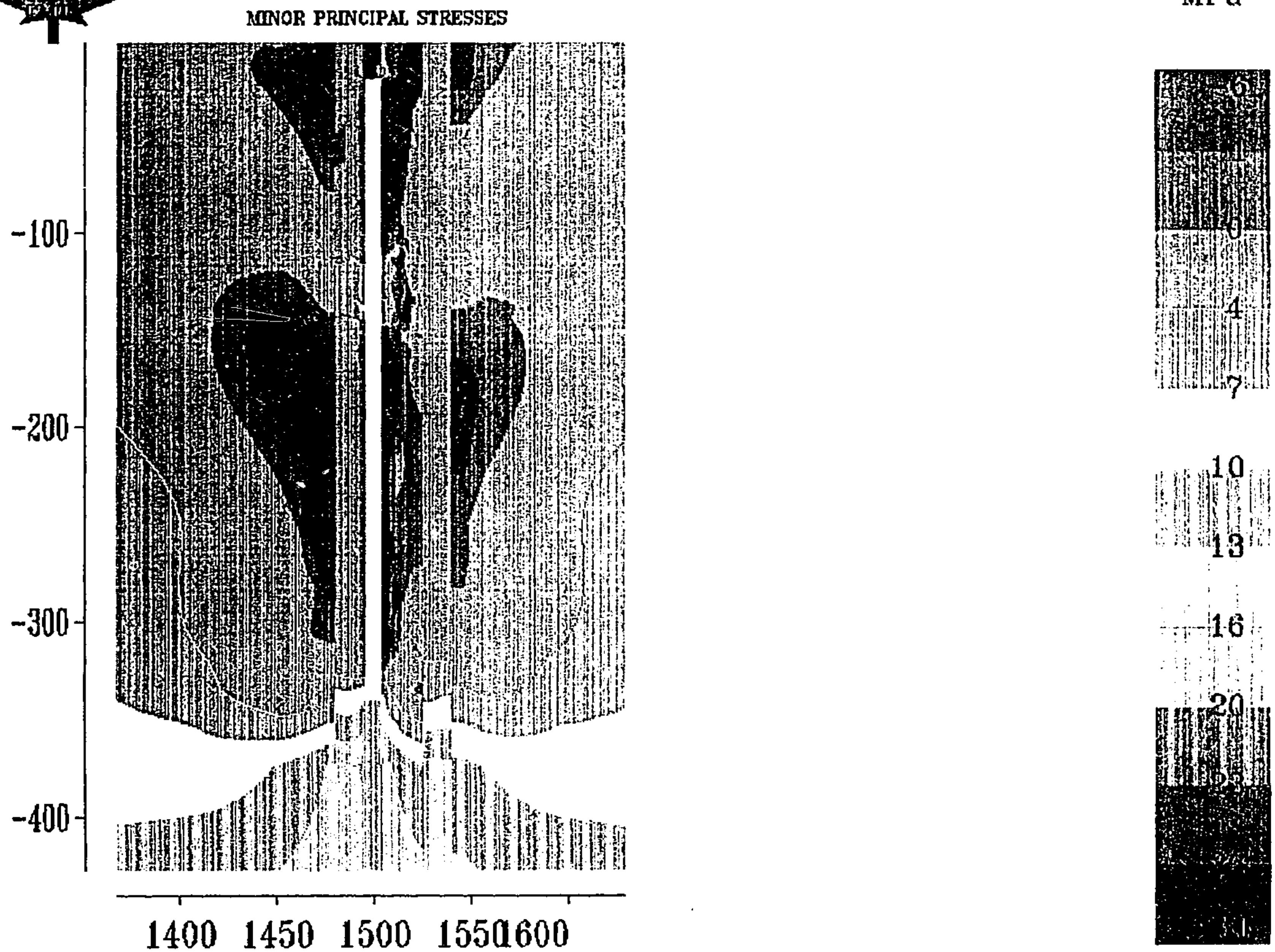

have a restricted tensile stress area. No tensile tangential or radial stresses would occur in the schist at the elevation of the surface crown pillar. Only compressive stresses would occur there.

In the first mining step (the existing deeper stope), failed elements occur in the upper footwall and hangingwall due to compressive stress exceeding strength. These regions would progressively develop more failed elements with the opening and expansion of the shallow stope.

Failed elements would occur near surface in the hangingwall and footwall schist as a result of compressive stress action. The failure of the upper portion of the hangingwall schist, above the shallow opening, extends with deepening of the shallow stope. The upper portion of footwall rhyolite also enters into failure although it fails from the high tensile stresses developed there. By the time the shallow stope merges with the deeper stope, all of upper hangingwall schist has failed. The massive pyrite surface crown pillar remains essentially intact.

5.5 APPLICATION OF ANALYTICAL EQUATIONS

5.5.1 Plug Failure

The persistence of the sub-vertical geological break between the orebody and schist on the hangingwall and orebody and foliated rhyolite on the footwall forms discontinuities on which a plug can fail. Given the persistence of the cross-cutting sub-vertical joint family, the geometry for a plug collapse is well defined. The near vertical nature of the joints also creates a worse case situation.

Appendix 3 calculates the factor of safety against a vertical plug failure using the numerical model results for a 2-D analysis. In reality a calculation including the third dimension stress would provide a higher factor of safety. The currently excavated opening has a high 2D factor of safety against plug failure for the 140 m high plug, it is 17.2. When the shallow stope is created, and a 20 m high plug can develop, the 2D factor of safety would drop to 4.5 (step 2) and increase with the expansion of the shallow stope to 21.8 when it merges with the deeper stope.

5.5.2 Ravelling Failures

Potential block falls were identified in Chapter 5.1 for the stope crown families from the three joint families occurring there. Because a poorly developed foliation is the predominant joint family in the footwall rhyolite and very few other joint families occur, block slides from this vertical periphery are not anticipated. The hangingwall schist is also dominated by the foliation with the occasional sub-horizontal joint, insufficient as to the number of joints and the dip needed to cause block slides.

The smallest value of tangential stress existing at the surface crown pillar periphery occurs in mining step 2 when the shallow stope is first created. It is 2.3 MPa, compressive. Very large blocks can be formed in the crown periphery, all of them more or less defined by near vertical and horizontal joints. The largest block can span the opening (9 m), have a height of 5 m and strike width of 3 m and the smallest block would be 0.5 m wide.

Appendix 3 calculates the required tangential stress to prevent block slides. Although a minimum of 0.93 MPa is required, for maintaining the largest block in place, this is well below the projected confining tangential stress existing at the periphery.

5.5.3 Chimneying Disintegration Failures

With the neighbouring mine, Bousquet, having been subjected to a schist chimneying disintegration failure, evaluation of such a failure at Dumagami needs examination. The Bousquet sericite schist is however qualitatively weaker, easier to break down.

The numerical modelling results show that at no time is the Dumagami hangingwall schist in tension, especially in the surface crown pillar area. However, the compressive stresses existing are sufficiently high to cause material failure. The failure increases in extent within the upper hangingwall with the enlargement of the shallow stope.

Appendix 3 provides the calculations for chimneying based on intact rock mass values. If failure occurs within the hangingwall into an access drift or cross-cut, with a span of 4 m, the factor of safety is 5.1. This drops to 2.5 for an opening that is 8 m wide. Current access cross-cuts are 3.5 m wide.

The 9 m wide pyrite orebody, because it has such a high rock mass quality and RQD (RQD = 82, RMR = 82, Q = 18, Appendix 3), would be less likely to chimney. Appendix 3 calculates a factor of safety of 21.6 against chimneying disintegration.

5.5.4 Block Caving Failure

The possibility exists that weak rock such as the schist can block-cave, after hangingwall failure has begun, although more efficient rock mass fragmenting (through imposed failure or with one more joint family to form 3-D shapes) is needed.

Appendix 3 presents the potential for cave arching with the current opening depth of 135 m, intact block compression failure in schist cave arching is not expected (F_s = 15.1) but bulk failure in the arch is (F_s = 0.9). Therefore, caving stabilization for schist at that depth would be difficult. At the depth of the new opening 20 m, stabilization could be achieved for caving in the schist. Factors of safety against intact compression and bulk failures rated at 103 and 114 respectively.

If the massive pyrite orebody was to block-cave, stable arching could develop at 135 m (intact block failure F_s = 22.1, bulk arch failure F_s 1.64) and 20 m depth (intact block failure F_s = 148.3, bulk arch failure F_s = 1.78).

5.6 APPLICATION OF EMPIRICAL METHODS

The NGI system (Table 1.5, Figure 1.14) classifies the massive pyrite orebody with Q = 27.3 as "good" rock quality (Appendix 3) which, with a span of 9 m and an E.S.R. of 1.6 (Chapter 3.6.1), plots slightly into the zone of required support. The system recommends untensioned grouted bolting at every 1.5 m. The hangingwall schist, rating of Q = 0.71 "very poor", plots well into the zone of required support for the heights encountered during the mining steps. Severe ground support is recommended at any height above 3 m. The footwall quality, Q = 2.75 "poor", is limited to an unsupported height of 4.8 m.

The surface crown pillar empirical method for a massive pyrite surface crown pillar span of 9 m yields a C_s of 12.0 m which when compared to its quality Q = 18 indicates that a minimum thickness of 2.8 m is required.

5.7 SUMMARY

Given the existing large stope and the extensive shallow stope development that is planned, stress distribution around the opening will be a key factor in influencing hangingwall schist stability as well as surface crown pillar viability.

Numerical modelling indicates that the current large stope at depth is, and will continue to be, subjected to stresses inducing failure in the schist hangingwall with the creation and expansion of the planned shallow stope. The stresses imposed to the massive pyrite will not cause failure. Field observations of this 210 m high wall corroborate the modelling results. The schist has massively moved into the opening, buckling to a depth of 5 m into the hangingwall. Such a condition is not anticipated in the hangingwall of the shallow stope planned.

The hangingwall schist from the stope crown to surface is expected however to become increasingly failed as a result of increasing compressive stresses with shallow stope creation and expansion.

Peripheral tangential surface crown pillar stresses will be sufficiently compressive to prevent block ravelling at any mining stage. Stresses on potential plug failure planes are also expected to be sufficient to prevent such a failure mechanism as it presents itself. No gravity failures are thus expected in the massive pyrite and neither is strength to be surpassed. If sub levels are created below the shallow stope, modelling should be performed to indicate any possible destressing around them that could eliminate the compressive stress required to prevent block slides. Massive block slides have occurred in sub levels near the base of the existing stope (mining step 1).

Caving is not expected in the pyrite because of its massive nature, nor in the schist because the schist has only one dominant joint orientation. In the case of the former arching would be possible to interrupt a block caving, but not in the schist.

The most likely mode of failure is in the hangingwall schist as a result of compressive failure, weakening rock mass resistance and perhaps allowing chimneying disintegration to occur. The factor of safety using intact schist strength varies from 5.1 for a 4 m opening to 2.5 m for an 8 m opening. Access cross-cuts or drifts located in the schist hangingwall at a depth of 0 to 30 m would be affected. Effective and immediate screening would prevent original rock mass degradation necessary for chimneying disintegration.

Although the surface crown pillar empirical method also evaluates the pyrite crown pillar as stable, it could not address schist stability. Only a thin surface crown pillar is deemed necessary with this approach; however, schist failure from as deep as 40 m into the hangingwall could occur if chimneying disintegration occurs. The NGI system confirmed the need for stope wall support and pyrite crown stability.

Based on these results planned mining extraction can be carried out provided support is applied to the hangingwall schist. Serious dilution is not expected in the developing shallow stope, but is in the existing stope.

CHAPTER 6

THE BELMORAL MINE CASE STUDY

6.1 GENERAL GEOLOGY

The Belmoral Mine is located approximately 10 km northeast of Val d'Or in northwestern Quebec, Figure 6.1. The area is in the southeast part of the Archean Abitibi greenstone belt; the mine is located within the Bourlamaque Batholith, a granodioritic intrusion cutting older Volcanic rocks.

A full site geology has been written by Vu et al. [115]. Gold-bearing quartz veins occur at the site in a shear zone which cuts the batholith. The host rock to the shear zone is massive, coarse granodiorite, Figure 6.2.

A typical cross-section would consist of the following units (Figure 6.3): sound granodiorite in the far-field hangingwall and far-field footwall; variable alteration and increase in fracture frequency, and schistosity within the immediate granodiorite hangingwall and footwall; and a shear zone of variable width consisting of chlorite schist inter-layered with quartz. Large scale quartz veins occur which carry gold, but the ore grade is highest when the quartz is intimately inter-layered with the schist, which is usually in the poorer quality schist sectors. The average grade of the deposit is 7.3 g/t of gold. Mineralization occurs randomly within the schist zone, but is about 3 to 4 m wide.

This shear zone is between 1 m and 15 m wide and has been traced for 2 km along strike and to a depth of 450 m. On average, the shear zone strikes N70E and dips

Figure 6.1 Location of the Belmoral Mine.

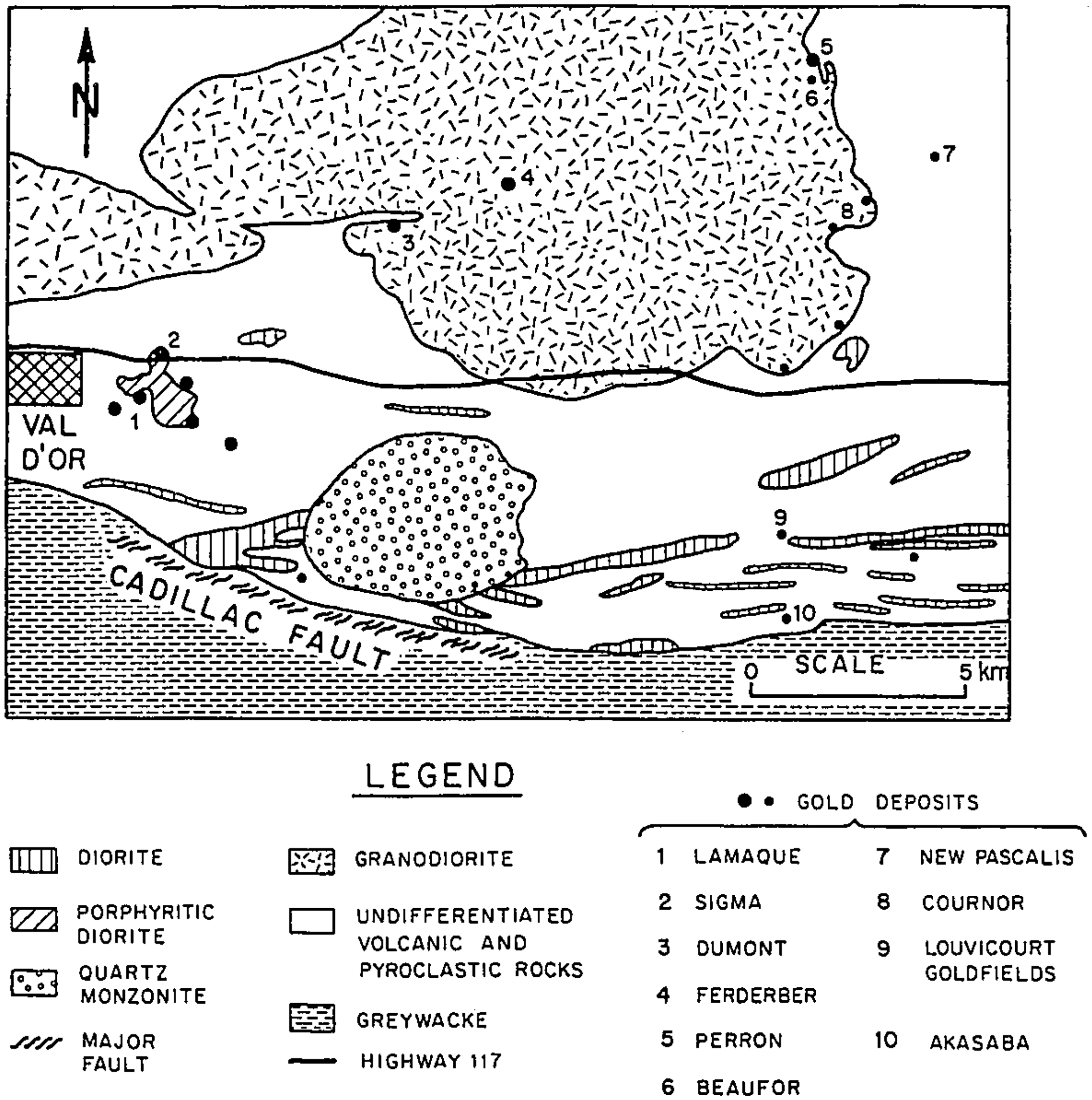

Figure 6.2 Regional geology, Belmoral Mine (Ferderber deposit) [115].

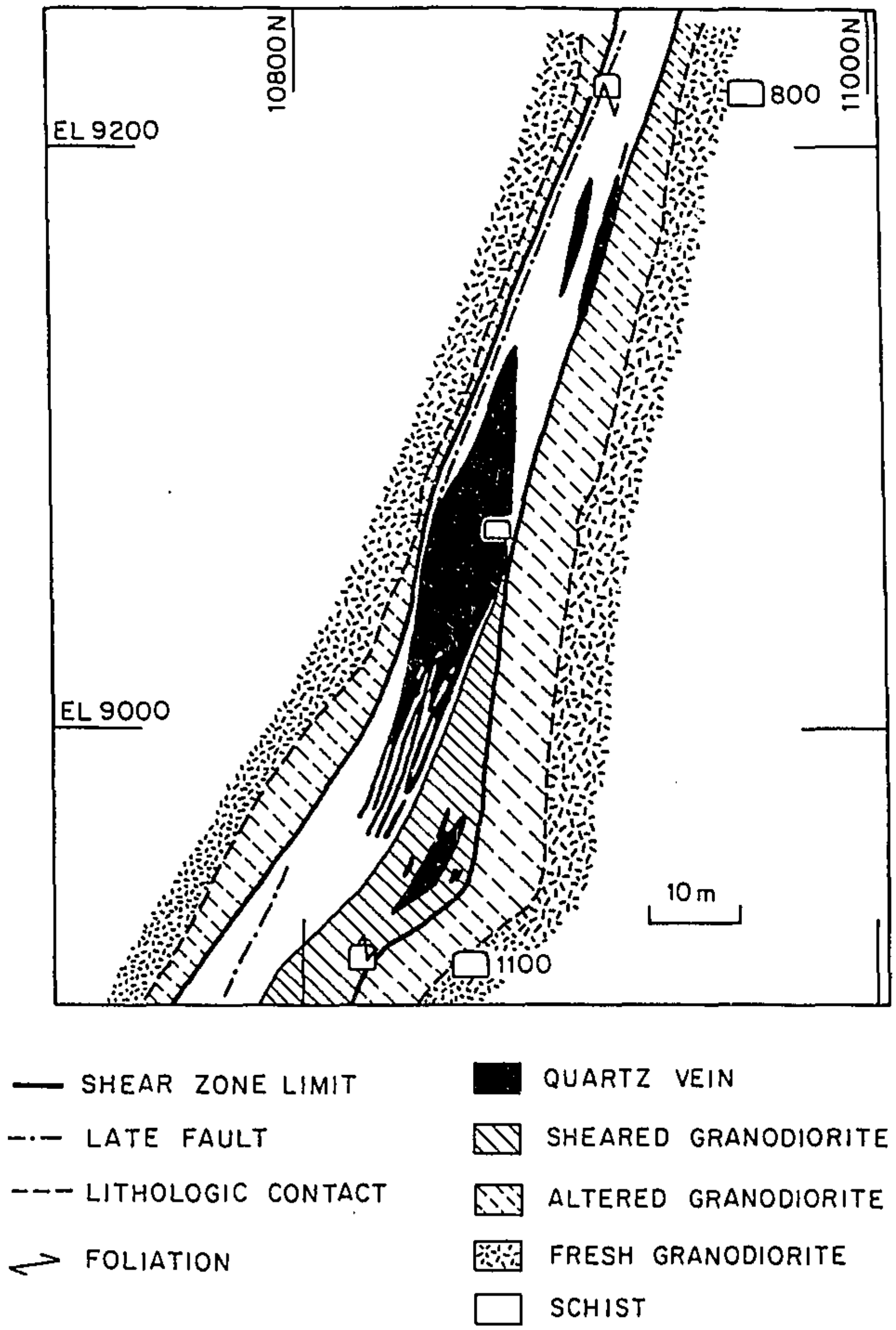

Figure 6.3 Generalized geological cross-section, Belmoral Mine [115].

65SE, however the strike varies locally from N50E to east-west and the dip decreases locally to 50°. The schist is fine grained and, besides its schistosity, has a foliation striking parallel to the shear zone but with varying dip. At shallow level, 0-200 m, the dip is vertical; at intermediate levels, 200 m - 350 m, the dip is 80SE; at deeper levels >350 m, the dip is parallel to the shear zone and schistosity.

Faults which created one or several gouge layers up to several centimeters in size are observed in many places cutting both the shear zone and the enclosing granodiorite close to the hangingwall contact. They strike N75E and dip 65SE. In many places they follow the margins of the shear zone but locally they cut the schist and quartz veins within it. Several joint families have been surveyed at Belmoral for this research, Figure 6.4. Few discontinuities, apart from the schistosity, occur in the mineralized zone. In the immediate granodiorite footwall and hangingwall, two families occur: N12W 44NE and S36W 70NW with a spacing of less than 50 cm. The same joint families occur in the far-field granodiorite but with a spacing of about 2 m.

Three random families also exist: S75W 81NW, N56W 60NE, S47E 65SW, with a spacing similar to the two main families. The joint properties are listed in Table 6.1. Joint configurations which will form blocks that can slide from the hangingwall are shown in Figure 6.5, using the joints orthogonal to the orebody and strike of the walls, S75W 81NW.

6.2 MINING EXTRACTION

The Belmoral Mine came into production in 1978 after sufficient grades were

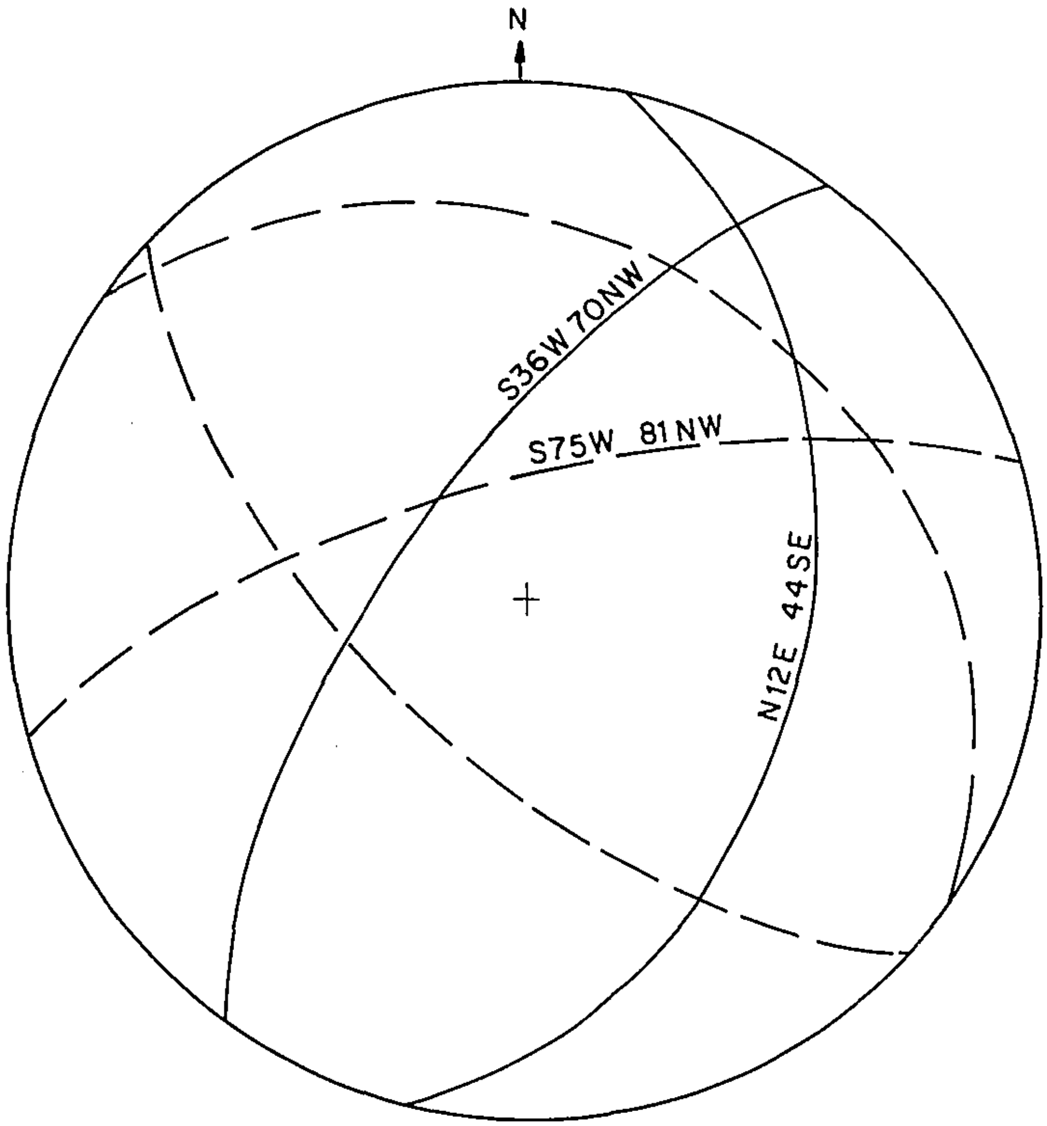

Figure 6.4 Stereographic projection of joint families, levels 6 and 8, Belmoral Mine.

Table 6.1 Properties of Belmoral Mine Discontinuities

Joint Family	Spacing (m)	Average Joint Length (m)	Joint Condition
N12E 44SE S36W 70NW	~ 2 (far field)	2 to 5	rough undular; chlorite covered; opened, < 2 mm
S75W 81NW N56W 60NE S47E 65SW	< 0.5 (immediate hangingwall/footwall)	1 to 2	
Schistosity	< 0.002		Smooth, interlayered with occasional gouge

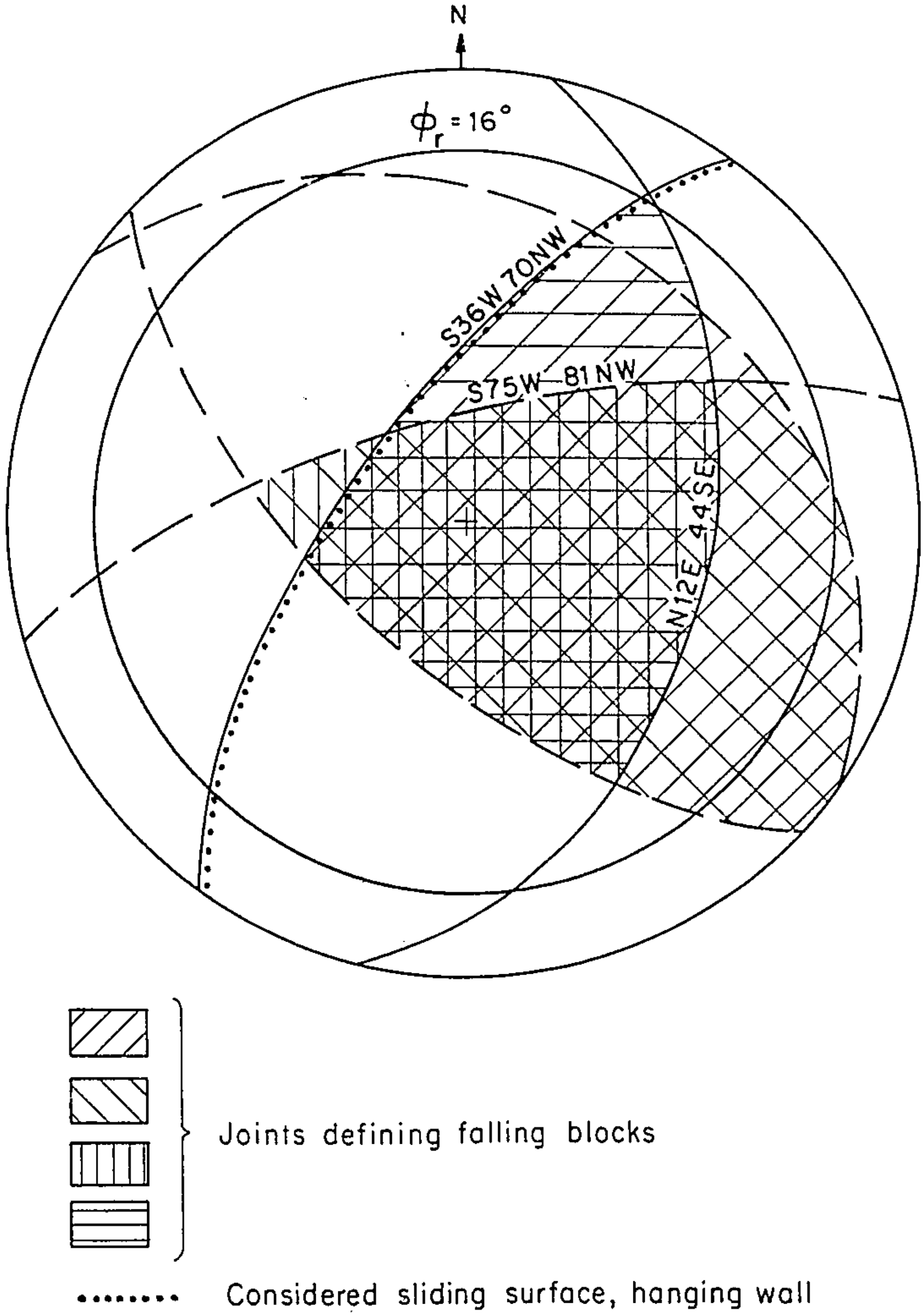

Figure 6.5 Block failure potential, stereographic analysis, Belmoral Mine.

indicated with diamond drilling exploration carried out between 1975 (the year of the discovery of the orebody) and 1976.

The orebody is covered by 20 - 40 m of overburden of variable compositions and characteristics [36]. The stratification from the bedrock upward is coarse gravel, fine sand, silty clay of low to moderate plasticity, and a varved clay of high sensitivity. The water content of these units was about 40% at the time of the 1980 shallow stope failure [36].

In the upper stopes shrinkage stoping was used. Cut-and-fill is now used at depth. The 2-7 stope, Figure 6.6, where the 1980 failure started, was 60 m longitudinally and 60 m deep. The width of the stope was 3.8 m, located in schist with altered granodiorite boundaries. The ore, accumulated by the progressive mining of horizontal overhand cuts, was recovered with draw-points at the base of the stope. It was kept partially filled for working and for support of stope walls. The ore was loaded onto haulage trucks which hauled each load to a stockpile located on surface.

6.3 SELECTION OF CASE STUDY

The Belmoral Mine represents Canada's most important failure of a hard rock mine shallow stope. Although it was related to great movements of overburden into the underground operations, the failure of the rock mass leading to soil inflow has never been back-analyzed. Either chimneying disintegration or hangingwall ravelling is alluded to in the report of the enquiry examining the disaster [36]. The rock mass environment is that of a weak ore zone, surrounded by competent rock, Figure 1.3c. Numerical

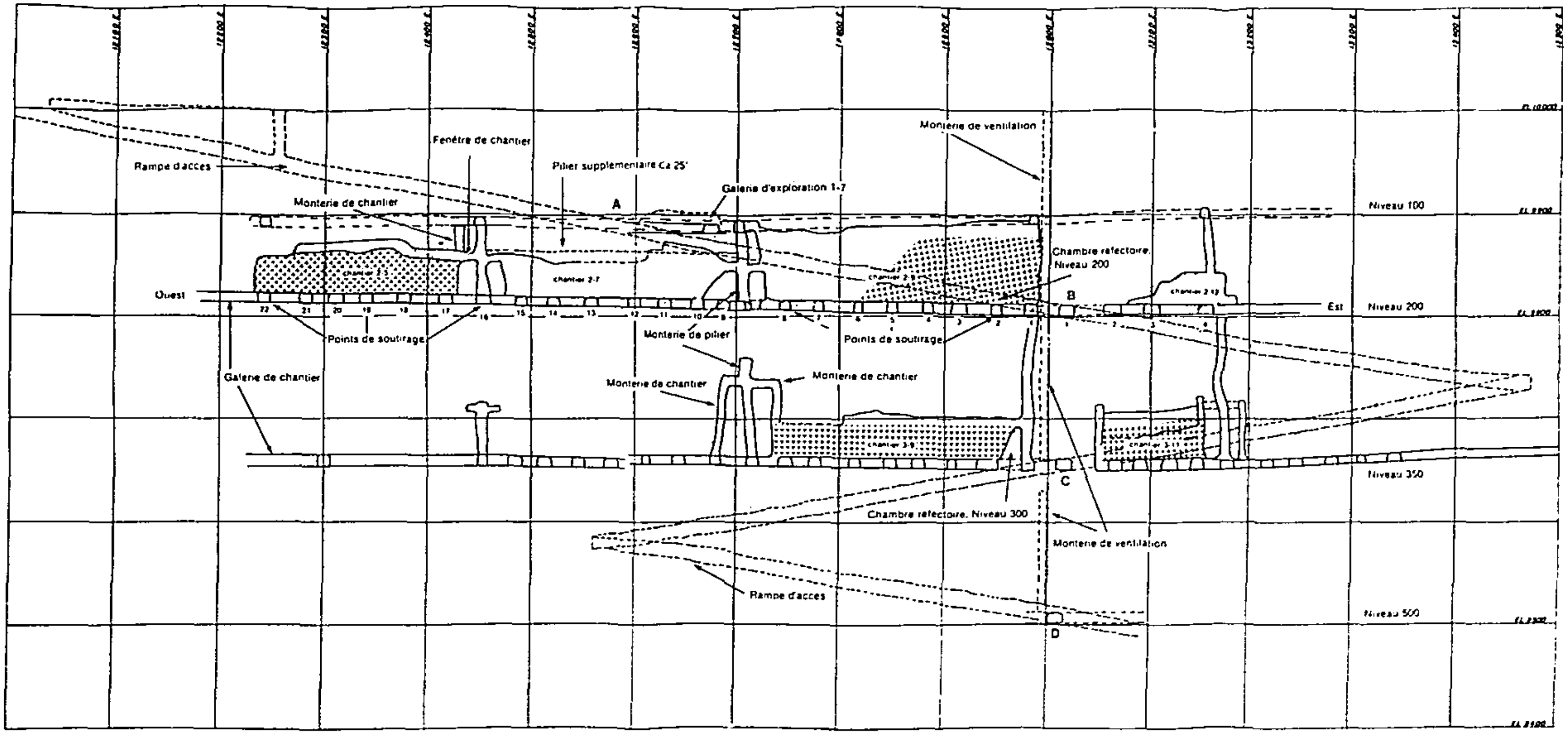

Figure 6.6 Longitudinal cross-section of the 2-7 stope, Belmoral Mine [36].

modelling in these environments would not only provide an indication of the nature of redistributed stresses but might be able to indicate material failure.

Belmoral is one of the Canadian mines with a weak rock mass environment that could have failed by chimneying disintegration. Such failures have already been registered at Bousquet [34] and Selbaie [37].

Belmoral mine operations, having started again in 1986, continue to work at shallow levels. Plans are underway to mine shallow stopes to the highest possible elevations. The back analysis of the 1980 shallow stope failure will provide mine operators indications of the stability elements and propensity for various failure mechanisms. This becomes important in the light of chimneying failures that have occurred since then, from levels as deep as 260 m [35]. Further mining extraction towards surface in this sense must be carefully evaluated.

Because site access was possible, rock core available and in situ tests performed, supplementary rock and rock mass property evaluations could be added which would well define the site geomechanically and provide representative results of analyses.

6.4 EVENTS LEADING TO FAILURE

The 1980 mine disaster occurred during mining of the gold bearing schist zone. From the record of testimonies and mining information provided to the Belmoral Mine accident enquiry, the following progression of events leading to failure is probable.

The progression of the instabilities leading to the 1980 shallow stope failure involved the 2-7 stope, extending from a depth of 35 m to 55 m and the exploration drift

1-7 located 5 m above this stope, Figures 6.7-6.11. The 1-7 drift was created after the 2-7 stope was well advanced.

Amongst the Belmoral Mine stopes, stope 2-7 had the reputation of being the worst. Mine inspectors reported that the rock mass had difficulty having enough "cohesion" to support its own weight. Severe dilution was observed. The stope hangingwall was composed of altered granodiorite. Exploration drift 1-7 was condemned soon after its creation due to roof failures.

Furthermore, in that sector, the hangingwall granodiorite was blocky, in part because of north-south joints that cross the orebody in that sector. Some geotechnical experts believed that the stope failure was related predominantly to a north-south fault intersecting the east-west orebody, where hangingwall ravelling occurred followed by massive schist failures. But based on other site observations taken during the excavations of these openings, the commission concluded that failure of the rock mass started above drift 1-7 followed by the sill pillar between drift 1-7 and stope 2-7, and progression from the merged single opening to overburden contact.

The removal of the blasted material stored in the stope from the draw-points allowed continuation of the failure which had begun earlier, and did not permit the caving process to choke itself off from bulking of failed material.

The second version of the failure mechanism is one in which weak granodiorite blocks would ravel to surface. The hangingwall failure version, however, does not explain the fact that the ore pulled from the stope one week before the ultimate failure was of high grade indicating that failure was occurring from the mineralized schist zone. This version was not found credible by the commission. Either version has also to

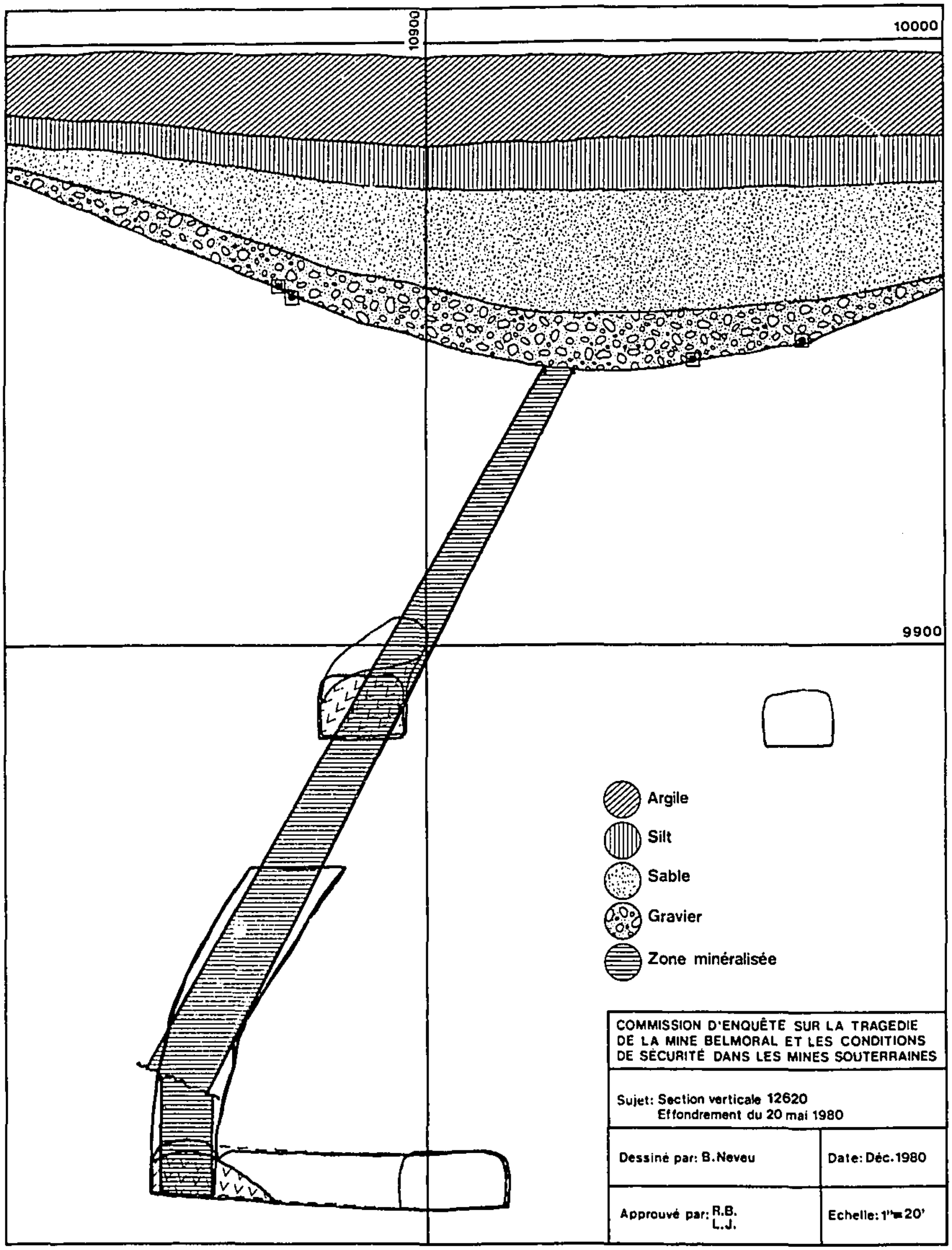

Figure 6.7 Beginning of schist zone failure, exploration drift 1-7, located above stope 2-7 [36]. Scale: 1 cm = 2.8 m.

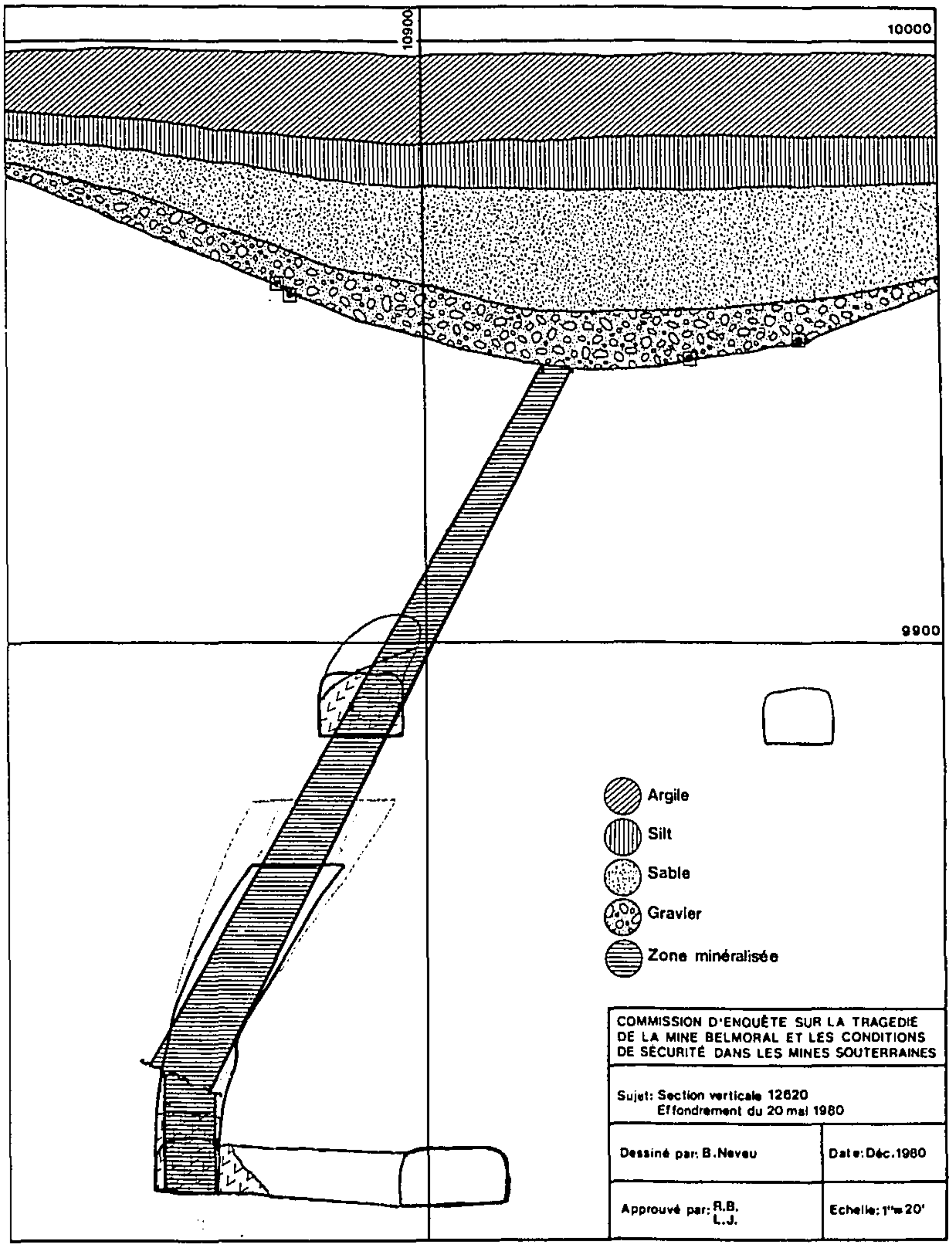

Figure 6.8 Progression of schist zone failure: beginning of stope 2-7 failure [36].

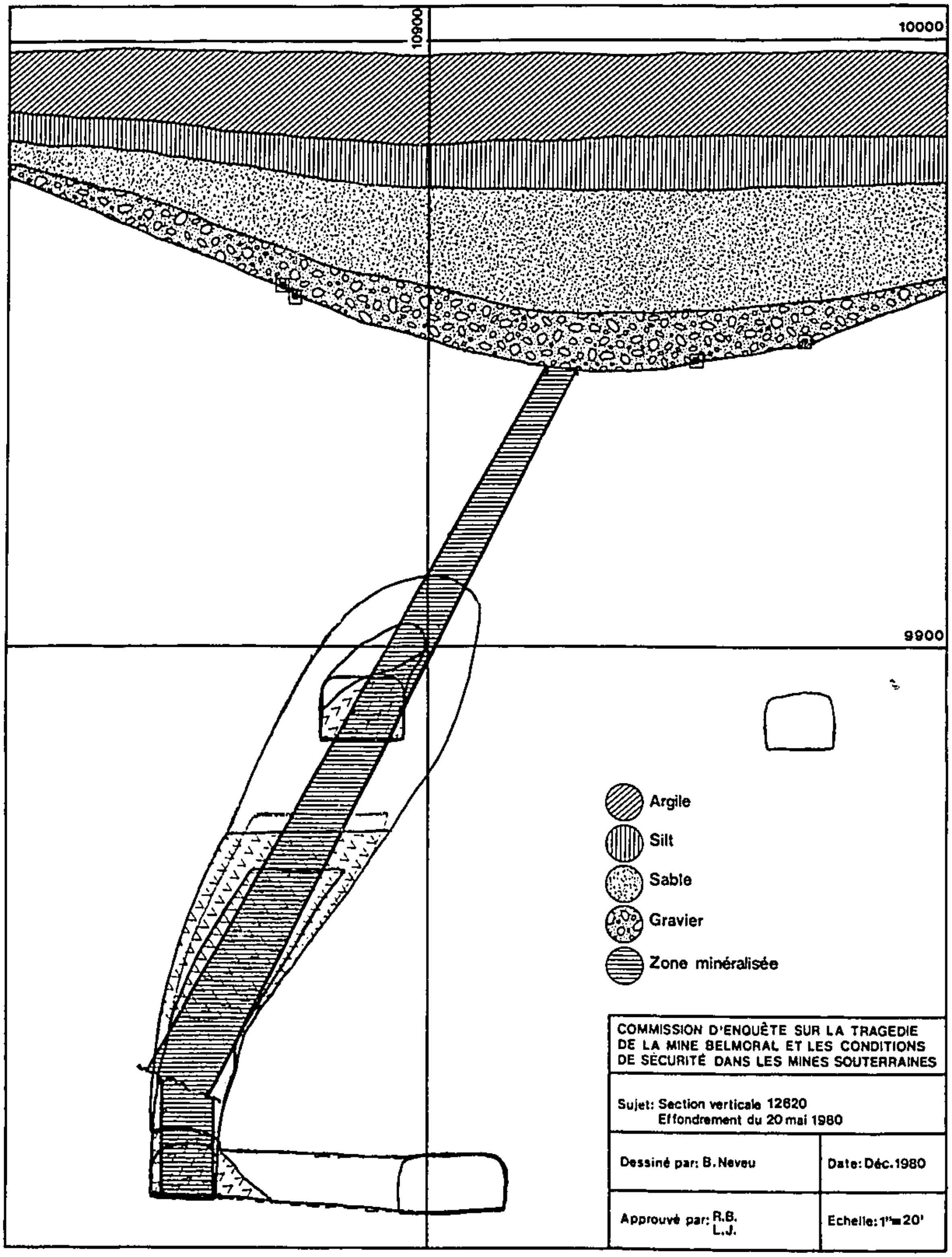

Figure 6.9 Progression of schist zone failure: enlargement to form one failure cavity [36].

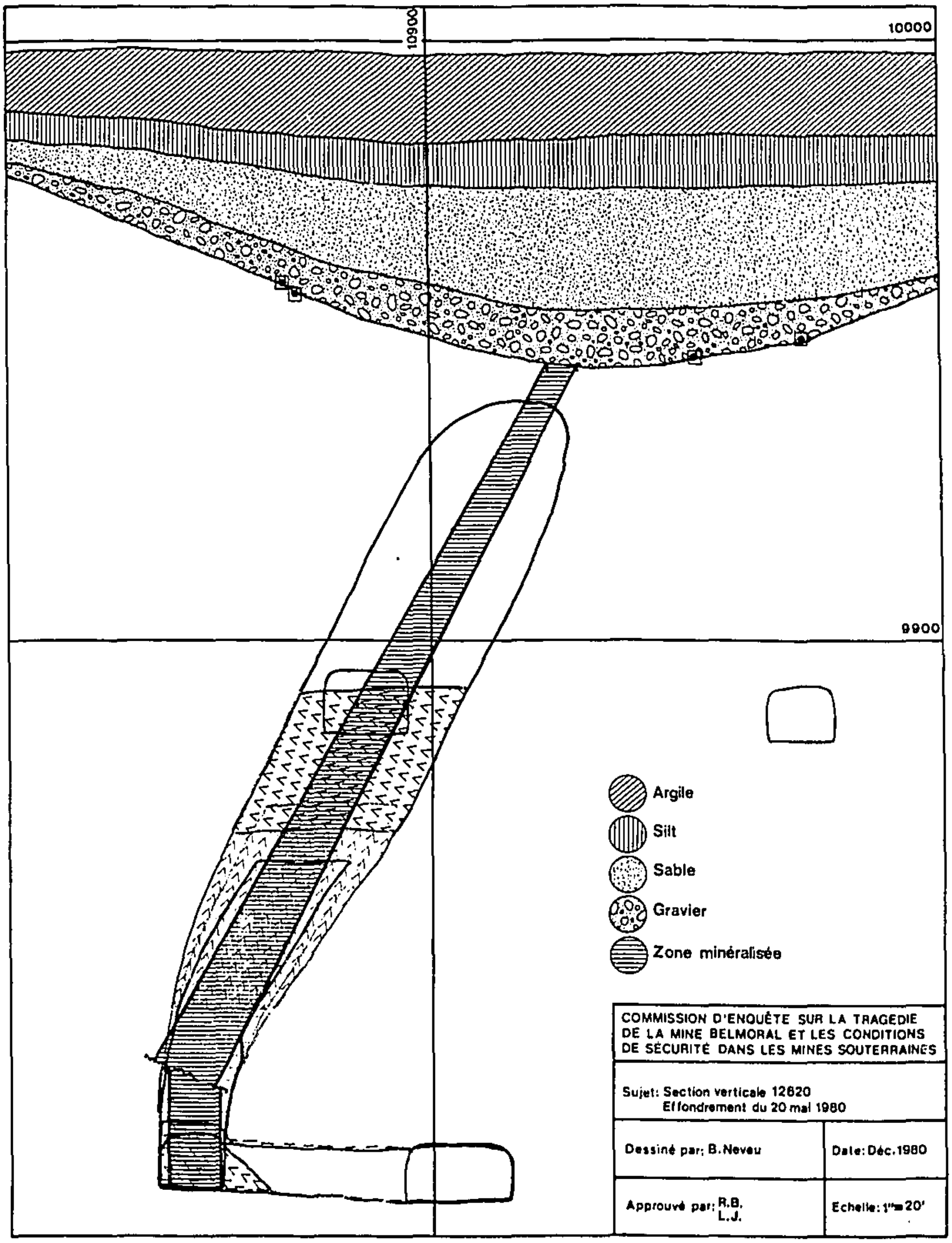

Figure 6.10 Progression of schist zone failure: enlargement of failure cavity towards surface [36].

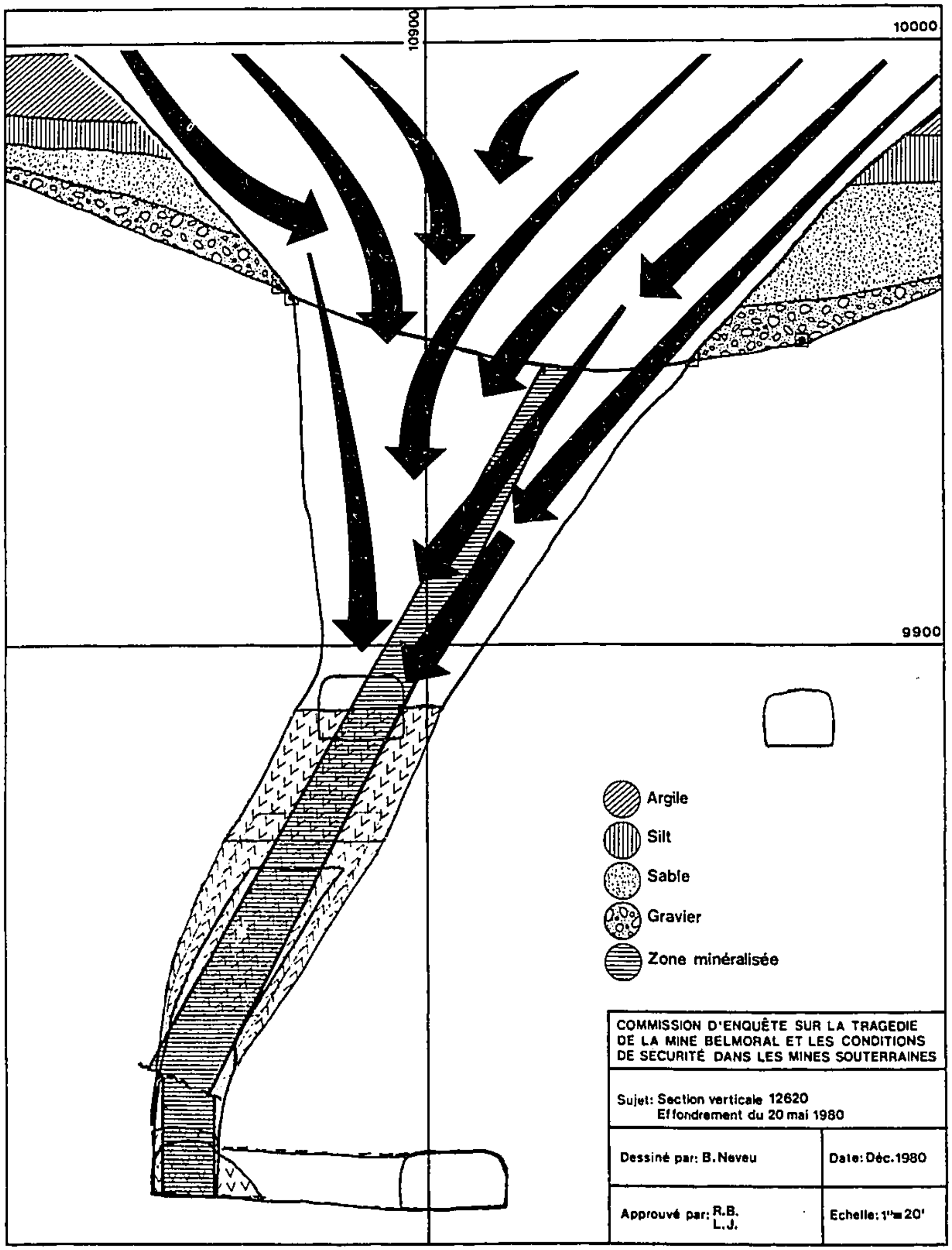

Figure 6.11 Progression of schist zone failure: failure to overburden and soil inflow [36].

account for the following. On the morning of the accident, muddy water was entering stope 2-7 and exiting at the draw-points. This would preclude a very wide opening at contact with the overburden at first (serious mud flow would have occurred otherwise).

6.5 NUMERICAL MODELLING

6.5.1 Numerical Model Selection

The Belmoral rock mass is made up of three types of material: granodiorite, altered and schistose granodiorite, and chlorite schist. It has been alluded to by the commission witnesses that the granodiorite was poorer at the hangingwall schist contact. The site geomechanical survey carried out for this research has indicated that the first 3 m of hangingwall and footwall granodiorite is often segmented into blocks that are formed by joints that are more closely spaced than the far-field granodiorite and that the granodiorite is more schistose.

The far-field granodiorite will be assumed to behave elastically, because the rock is sound, homogeneous and isotropic with large joint spacing and because it behaved elastically in compression lab tests. The immediate granodiorite was not tested in compression, however the alteration and schistosity were not so pronounced that it was expected to behave elastically. The far-field and immediate granodiorite will, however, be treated as geological units with different geomechanical properties.

The ore zone schist is weak, difficult to sample, and is composed of materials which may behave plastically when stressed (chloritic micaceous minerals interspersed with gouge). This will be treated as the third geological material.

The PCEPFE model described in Chapter 5.4.1 was used to model a 2-D cross-section of the 2-7 stope of the mine. The model assumes an elastic, perfectly plastic material following a generalized Mohr-Coulomb (c-ϕ) yield criterion and incremental plasticity. This would model the expected non-linear behaviour of the schist. The stope was 60 m long and separated longitudinally from stope 2-9 and stope 2-5 (also 60 m long with similar widths) by 3 m rib pillars, Figure 6.6.

Failure is presumed to have occurred over 40 m of the stope length. Ideally a 3-D non-linear code could be considered to give more representative stress and displacement fields around the failure zone. The combined length of all three stopes is of the order of 186 m, representative of a 2-D case. The non-linear, elasto-plastic approach is adopted to consider the behaviour of the schist zone. This material would be expected to retain an unrecoverable strain when stressed. With higher stresses, large permanent deformations occur which should not be calculated as elastic. A 3-D elasto-plastic code was not available for this research, therefore the 2-D PCEPFE was used.

6.5.2 Geomechanical Properties

Lab tests were performed on materials which could provide sufficient intact samples for representative testing. The far-field granodiorite was subjected to uniaxial and triaxial compressive stresses, and Brazilian indirect tensile tests, as input values for the calculation of Hoek and Brown [52] rock mass failure envelope. Rock core supplied by the mine was obtained from diamond drilling driven into bedrock from surface for the purpose of dilatometer testing to obtain rock mass modulus of elasticity [9].

The diamond drilling was unable to recover sufficient lengths of granodiorite schist (hangingwall and footwall rock) and ore zone schist for testing. However, some large intact blocks of schistose granodiorite were sampled manually, and then saw-cut into prismatic specimens, tested with a point load tester, which provided indirect tensile and compressive strength values using the International Society of Rock Mechanics (ISRM) suggested methods [116] and Hassani et al. [117] correlations for tensile strength. Table 6.2 provides the results of lab testing of Belmoral geological materials.

Rock mass quality RQD, RMR, and Q (Appendix 4) values were calculated from rock core, and haulage drifts and cross-cut exposures of the mine at the 200 level (same depth as the draw-points of stope 2-7). Values are presented in Table 6.3.

The field m and s properties were calculated using equation 1.43 and 1.44 which use the RMR as a basis for translation. From these values the Mohr failure envelope for the rock mass was generated (Appendix 4) and the c_m and ϕ values for modelling selected, Table 6.4. Where no value for the schist could be developed based on lab tests, Table 2.1 was used. Based on the RMR of 16 and a field evaluation of quality, an m of 0.35 and s = 0.00008 were selected.

The modulus of elasticity modelling input values were obtained from the dilatometer tests performed under a CANMET contract [10]. Results are shown in Table 6.5. In situ ground stress measurements have not been performed at Belmoral. The selection of natural ground stress orientation and values was performed on the following basis. Firstly, ground stress measurements in the Precambrian Shield have shown that the major principal stress is close to horizontal, perpendicular to the intermediate principal stress (also close to horizontal) and the minor principal stress (close to vertical)[26][27].

Table 6.2 Belmoral Mine Rock Material Laboratory Test Results

Rock Type	Compressive Strength (MPa)		Tensile Strength (MPa)	Modulus of Elasticity (GPa)	Poisson's Ratio	Cohesion (MPa)	ϕ (degrees)	Hoek and Brown m value	Unit Weight (MN/m^3)
	Confinement	Peak Strength							
Granodiorite	0	116.4	12.1	65.2	0.25	12	47	10.2	0.0274
	5	143.9							
	10	174.0							
	15	193.2							
	20	214.8							
Altered granodiorite	0	60.4	6.9	-	-	-	-	-	0.0274
Schist	-	-	-	-	-	-	-	-	-

Table 6.3 Belmoral Mine Rock Mass Rating Parameters

	RQD (%)	Rock Mass Rating (RMR)	Field	
			m	s
Far-field Granodiorite	83	79	4.8	0.1
Hangingwall Granodiorite	72	53	1.9	0.005
Schist	0 - 25%*	16	0.35	0.00008
* proportional to quartz content				

Table 6.4 Summary of Modelling Parameters, Belmoral Mine

	γ_r (MN/m^3)	υ	E_m (GPa)	c_m (MPa)	ϕ (degrees)
Far-field granodiorite	0.0274	0.24	10	5.9	52
Hangingwall/footwall granodiorite	0.0274	0.29	3	1.4	42
Schist	0.028	0.34	0.5	0.04	14

Table 6.5 Belmoral Mine Summary of In Situ Properties [10][26]

Average Modulus of Elasticity, E (GPa)		
Far-field granodiorite	10.0	
Hangingwall granodiorite	3.0	
Schist	0.5	
Natural Ground Stresses (adopted)		
	Orientation (bearing, dip)	Value (MPa/m)
Major Principal Stress	N20W/0°	0.065
Intermediate Principal Stress	N70E/0°	0.036
Minor Principal Stress	Vertical	0.0274

Furthermore, the major principal stress direction is usually oriented north-west to north-east. Secondly, the minor principal stress is 2.0 to 3.0 times smaller than the major principal stress and 1.4 to 1.7 times lower than the intermediate principal stress [118].

The closest stress measurements published were performed at Dumagami, some 85 km away along the same east-west Cadillac fault break structural region. Therefore, some degree of correlation could be made between the two. Table 6.5 shows the principal stress conditions adopted , reflecting these common shield values. Variations of the σ_1 to σ_3 and σ_2 to σ_3 values, from 2.0 to 2.5 and from 1.3 to 1.5, did not appreciably vary the level or distribution of stresses and failure zones around the openings modelled.

6.5.3 The Belmoral Mine Numerical Model

Two numerical modelling sequences were performed to simulate the events representative of the two versions of the development of failure described in the accident inquiry. These are the progressive ore zone failure and the progressive ravelling failure of the hangingwall. The "mining step" option of the PCEPFE program used allows to remove "failed" elements (yielding elements). Simulation of the progression of the failure of the material from the rock mass was done by removing the failed elements of a "mining step" and using this new excavation outline for the next step.

From a finite element mesh of 5286 elements, both sequences involved removal of rock material to create the next "mining step". In the case of the ore zone failure, Figure 6.12, seven steps were modelled. The sequence involves the development of the stope, the exploration drift, loss of sill pillar, and progression of failure to surface. In the

Belmoral Figure 6.12: Modelling mining steps to simulate schist zone failure progression.

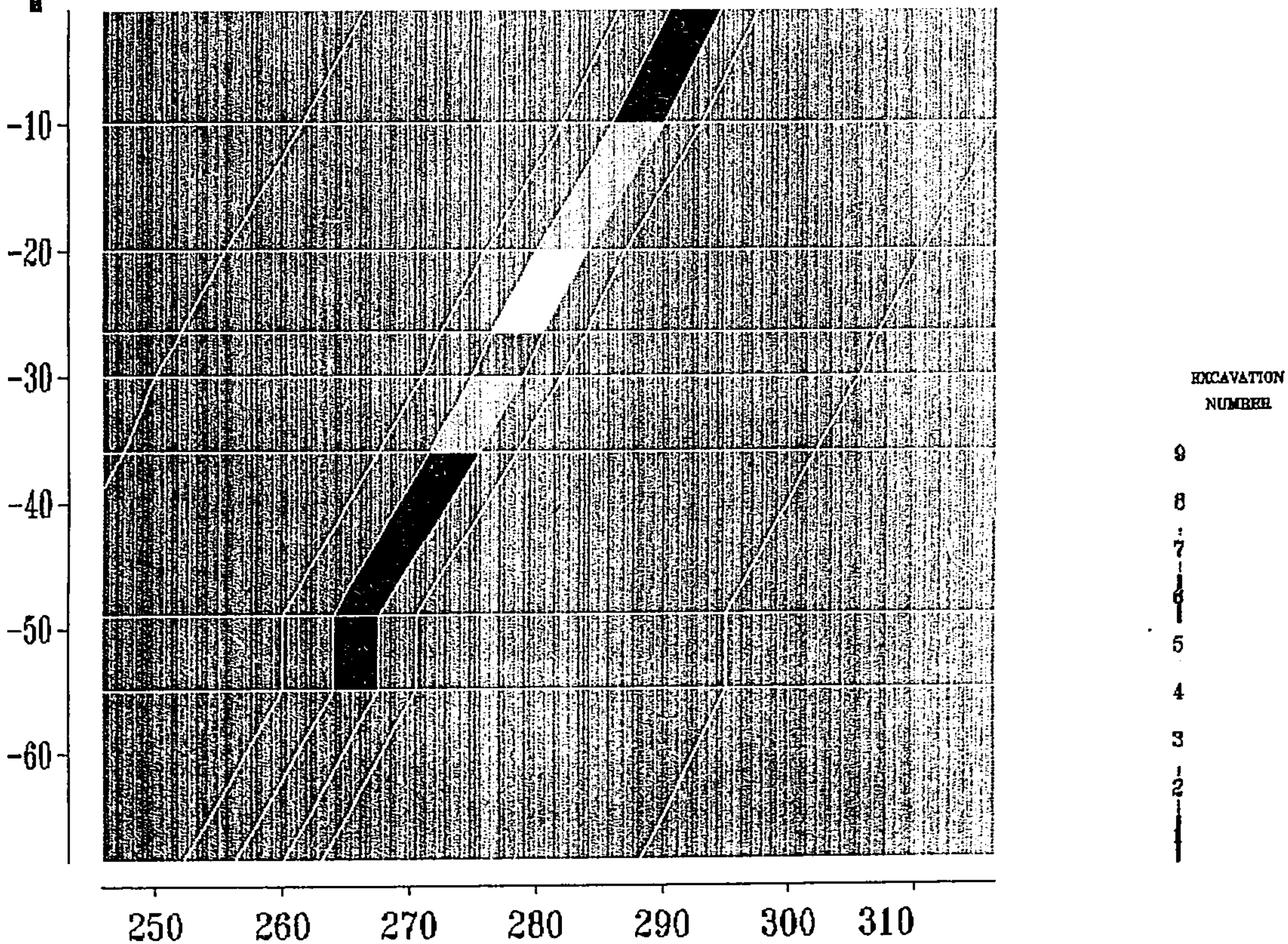

case of the hangingwall failure, eight steps were modelled, Figure 6.13, the first two being identical to the ore zone model, followed by the sloped portion of the 2-7 hangingwall (the bottom vertical hangingwall was not considered because blasted material would rest against it as reported to the commission, confining it from failure) and the remaining hangingwall progressively to surface.

It is possible that one type of failure might have caused or influenced the other. That possibility will be discussed based on results obtained from these basic failures.

The modelled section is assumed to be at the longitudinal center of the failure, (along mine section 12620). Material distribution is shown in Figure 6.14.

6.5.4 Modelling Results

The modelling results are presented in Figures 6.15 to 6.44 for the ore zone failure progression, 6.45 to 6.74 for the hangingwall failure progression showing only the hangingwall ravelling.

The creation of stope 2-7 has imposed compressive tangential stresses in the crown (up to 3.75 MPa) and the stope floor (up to 5.5 MPa), which are sufficient to bring the schist into failure. Failed elements occur to a depth of 2.4 m in this case, Figure 6.16.

Tensile tangential stresses occur in the footwall, starting at the contact between altered granodiorite and far-field granodiorite, reaching a value of 0.6 MPa at the stope periphery forcing failure in some elements. The upper altered granodiorite footwall has also failed.

Smaller values of tension (< 0.2 MPa) are registered at the hangingwall periphery and continue into the far-field granodiorite. These are sufficient to cause only localized

Belmoral Figure 6.13 Modelling mining steps to simulate hangingwall failure progression.

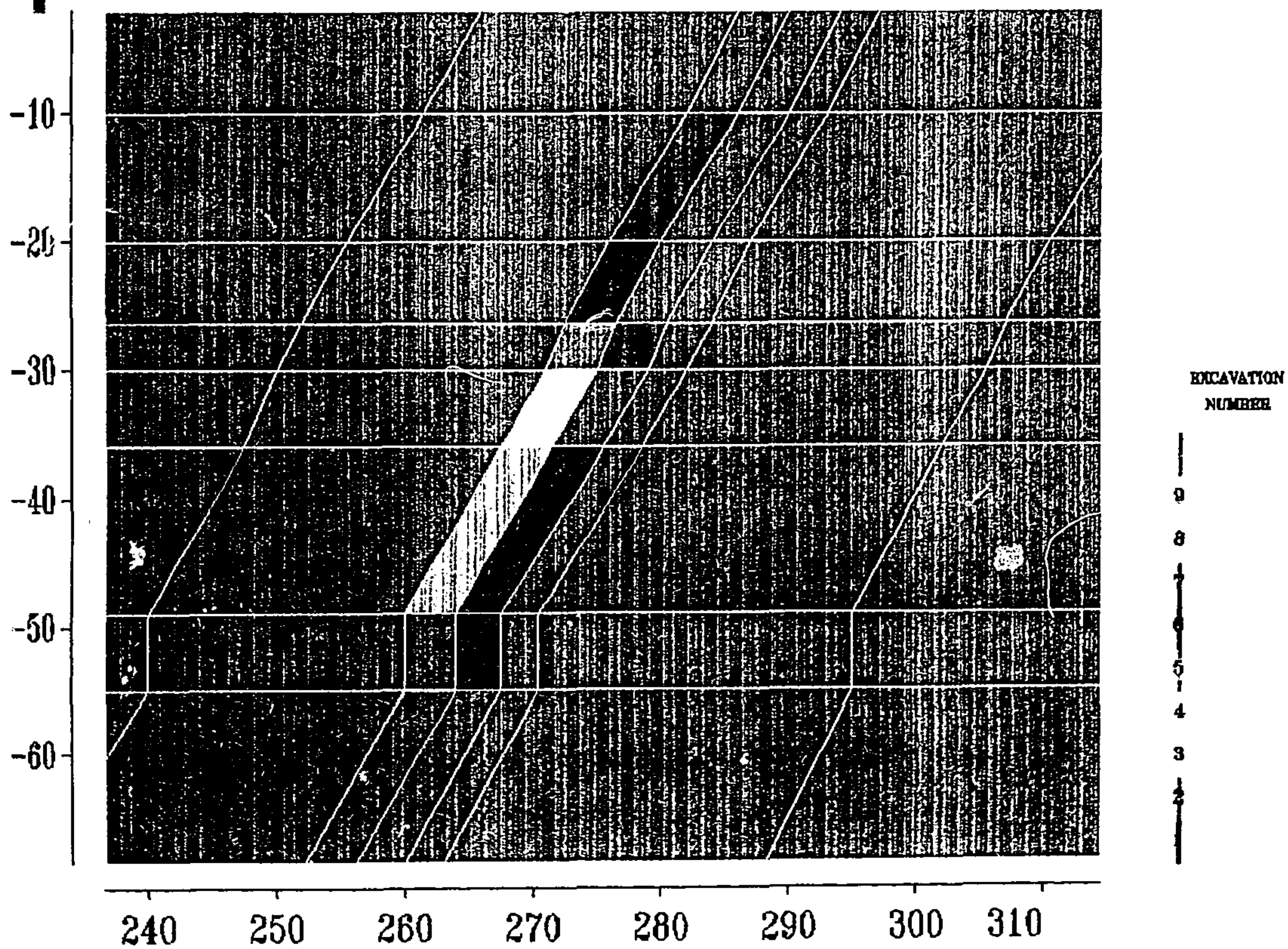

Figure 6.14 Geological cross-section of the Belmoral numerical model (Far-field granodiorite, material 1; peripheral altered granodiorite, material 2; schist, material 3).

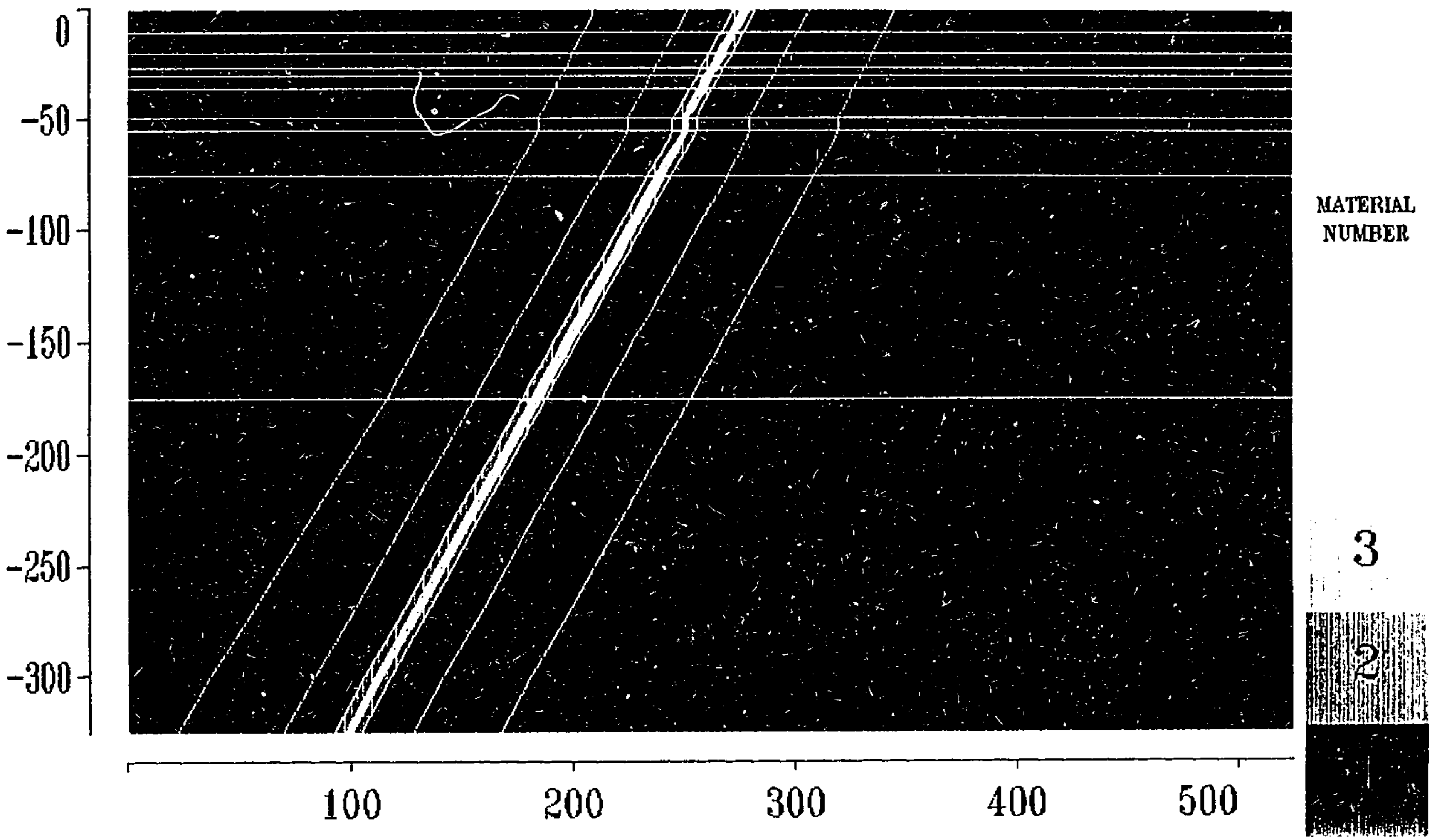

Belmoral

Figure 6.15 Rock mass displacements after mining step one, creation of stope 2 - 7, Belmoral Mine.

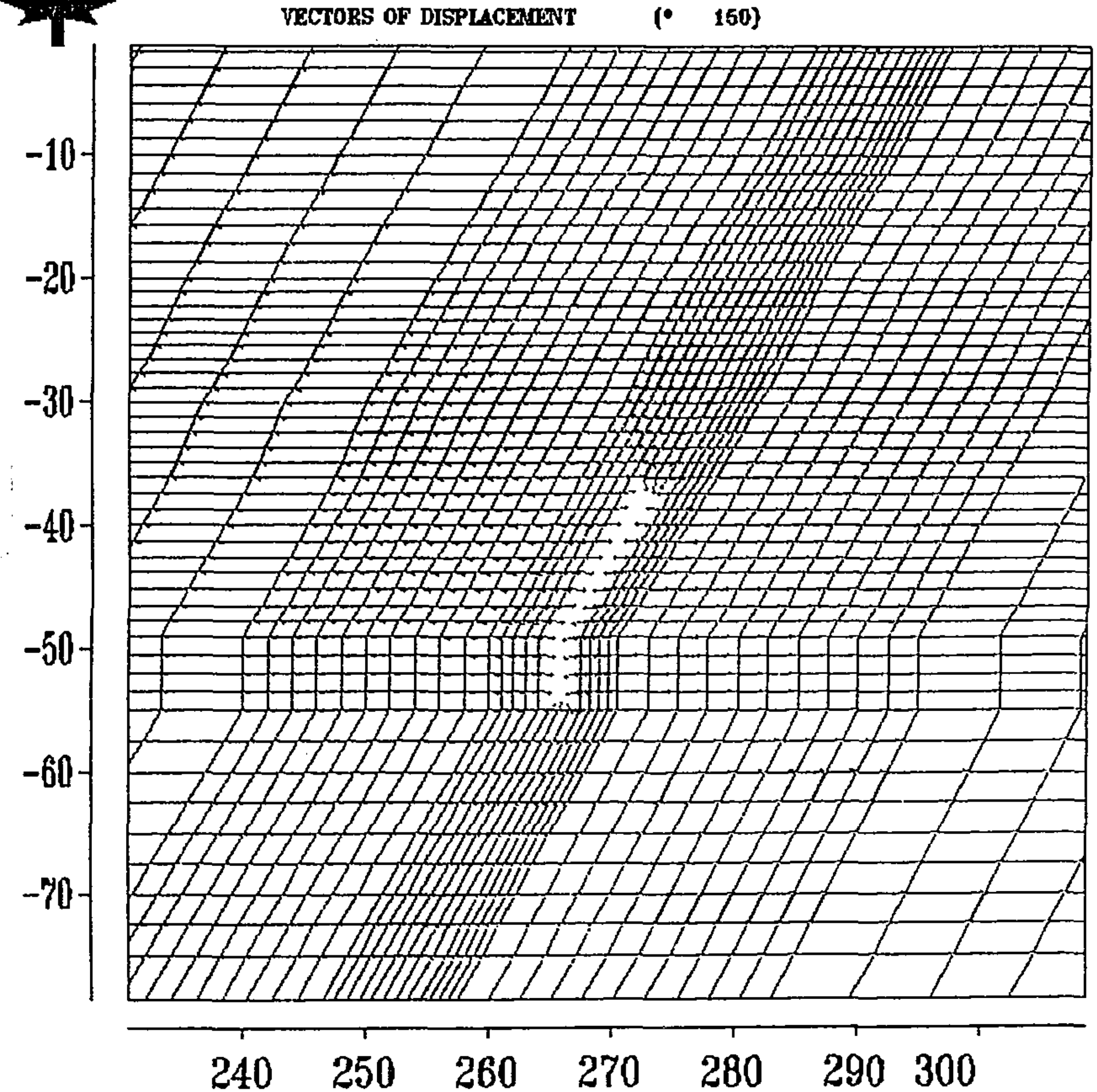

Belmoral Figure 6.16 Stress orientation and intensity after mining step one, creation of stope 2 - 7, Belmoral Mine.

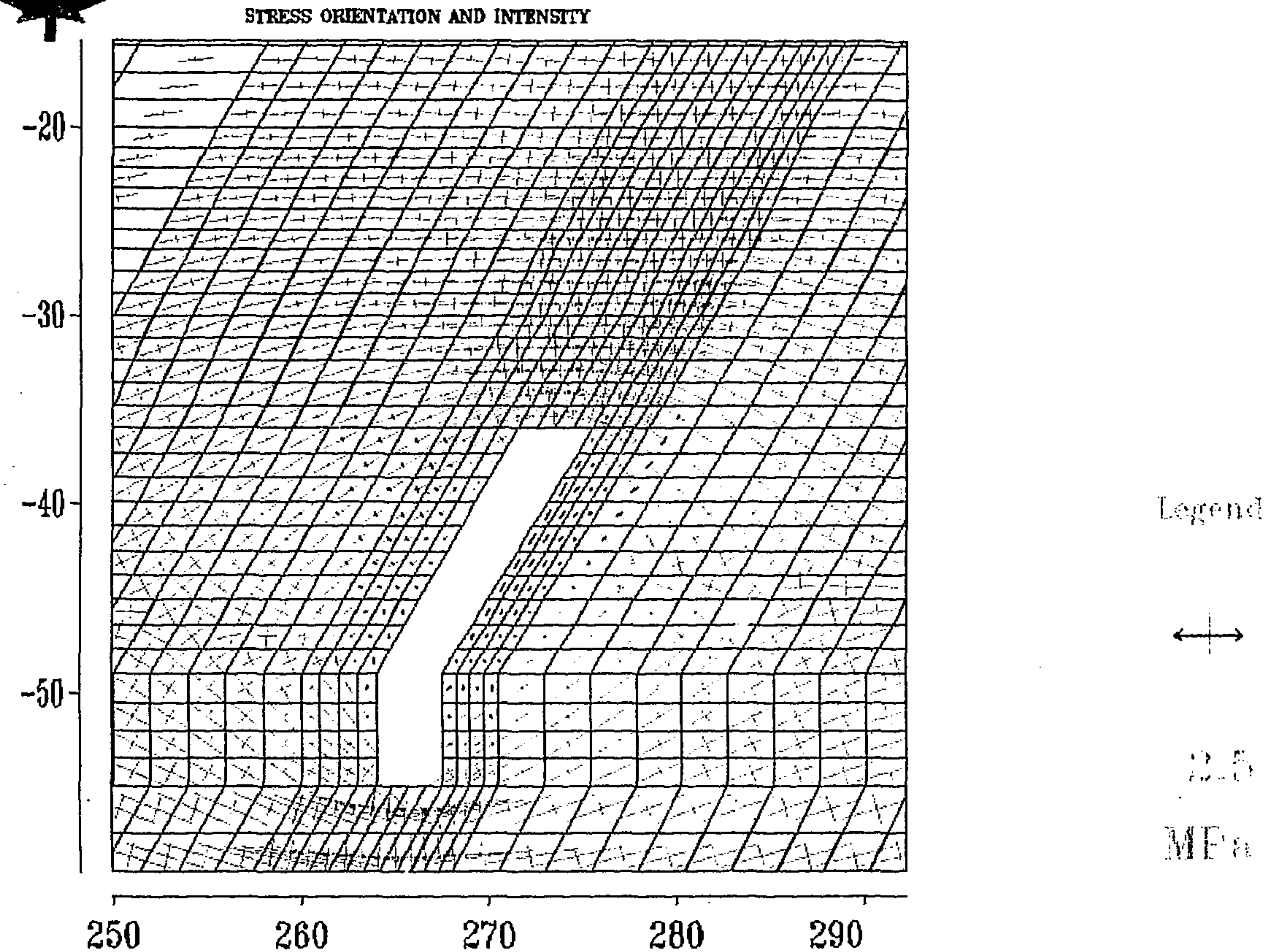

Figure 6.17 Major principal stress levels after mining step one, creation of stope 2 - 7, Belmoral Mine.

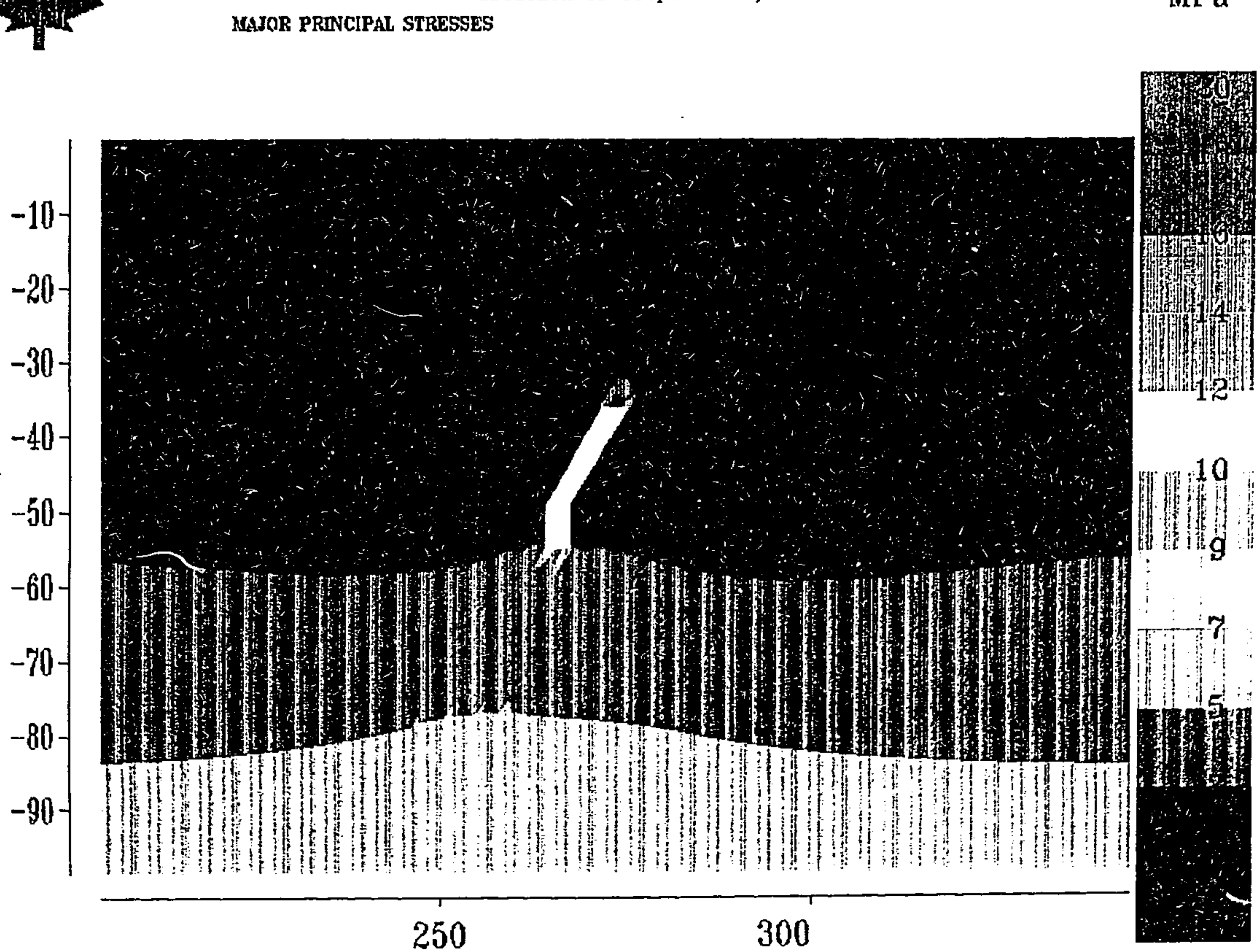

Belmoral

Figure 6.18 Minor principal stress levels after mining step one, creation of stope 2 - 7, Belmoral Mine.

MINOR PRINCIPAL STRESSES

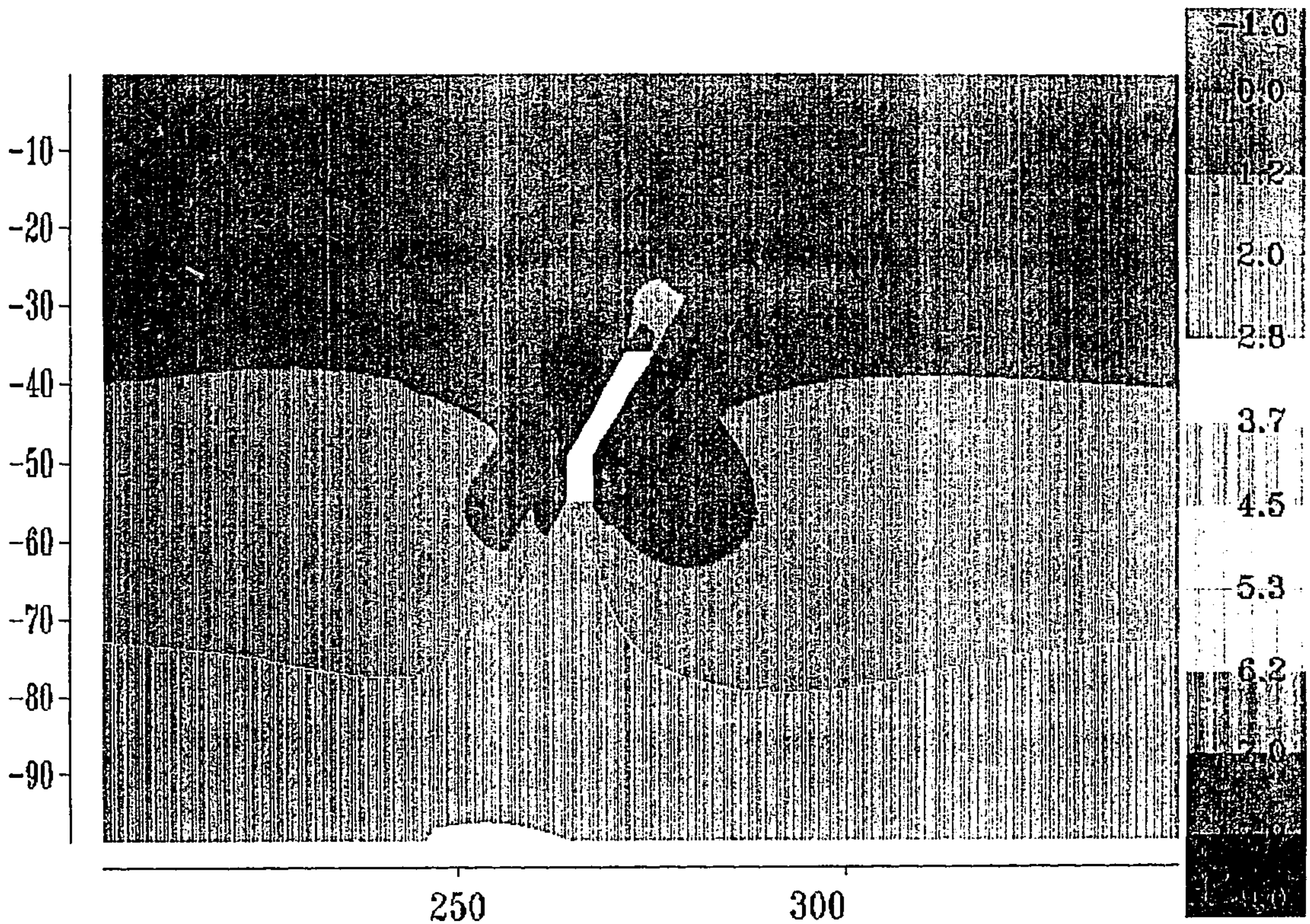

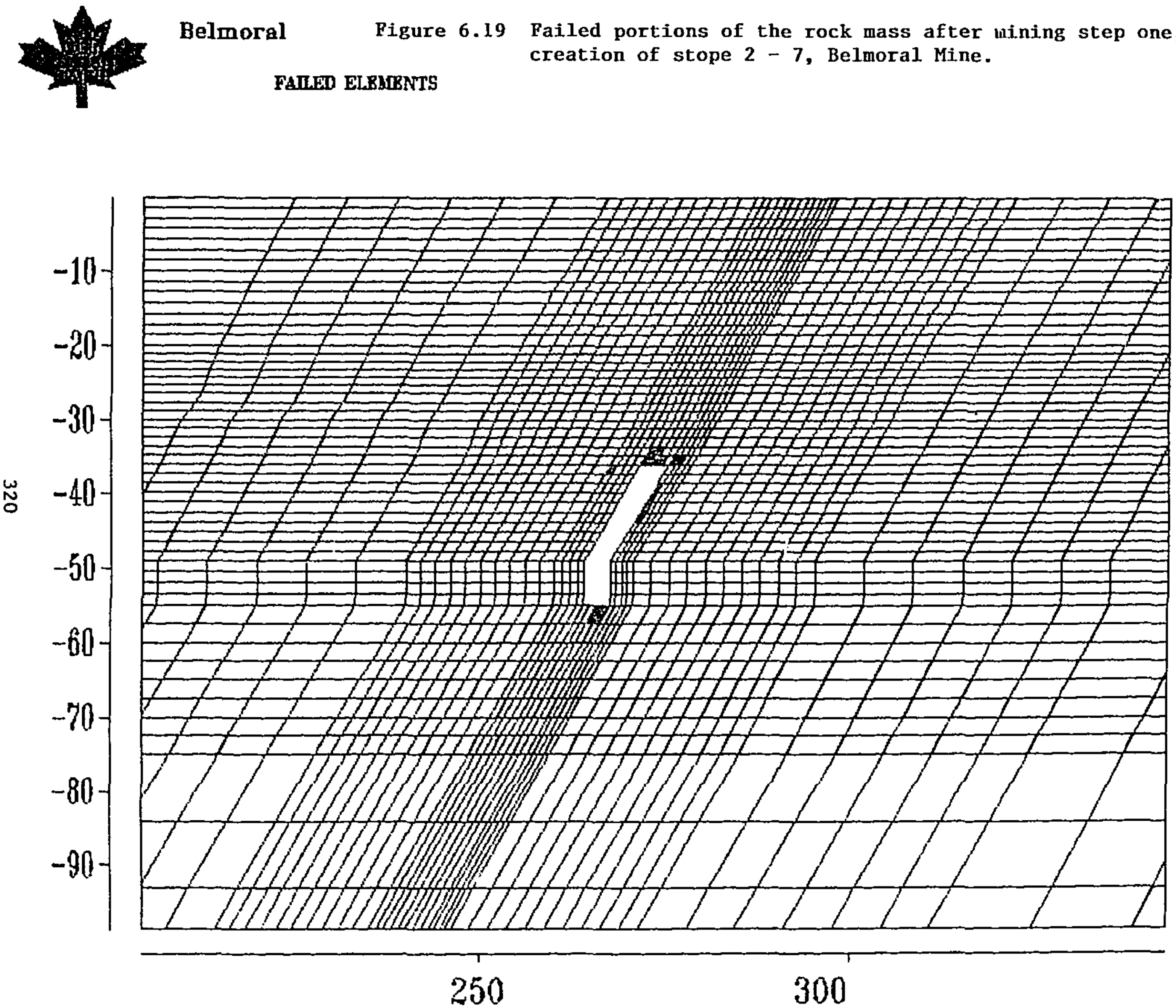

Figure 6.19 Failed portions of the rock mass after mining step one, creation of stope 2 - 7, Belmoral Mine.

Belmoral Figure 6.20 Rock mass displacements after mining step two, creation of drift 1-7, Belmoral Mine.

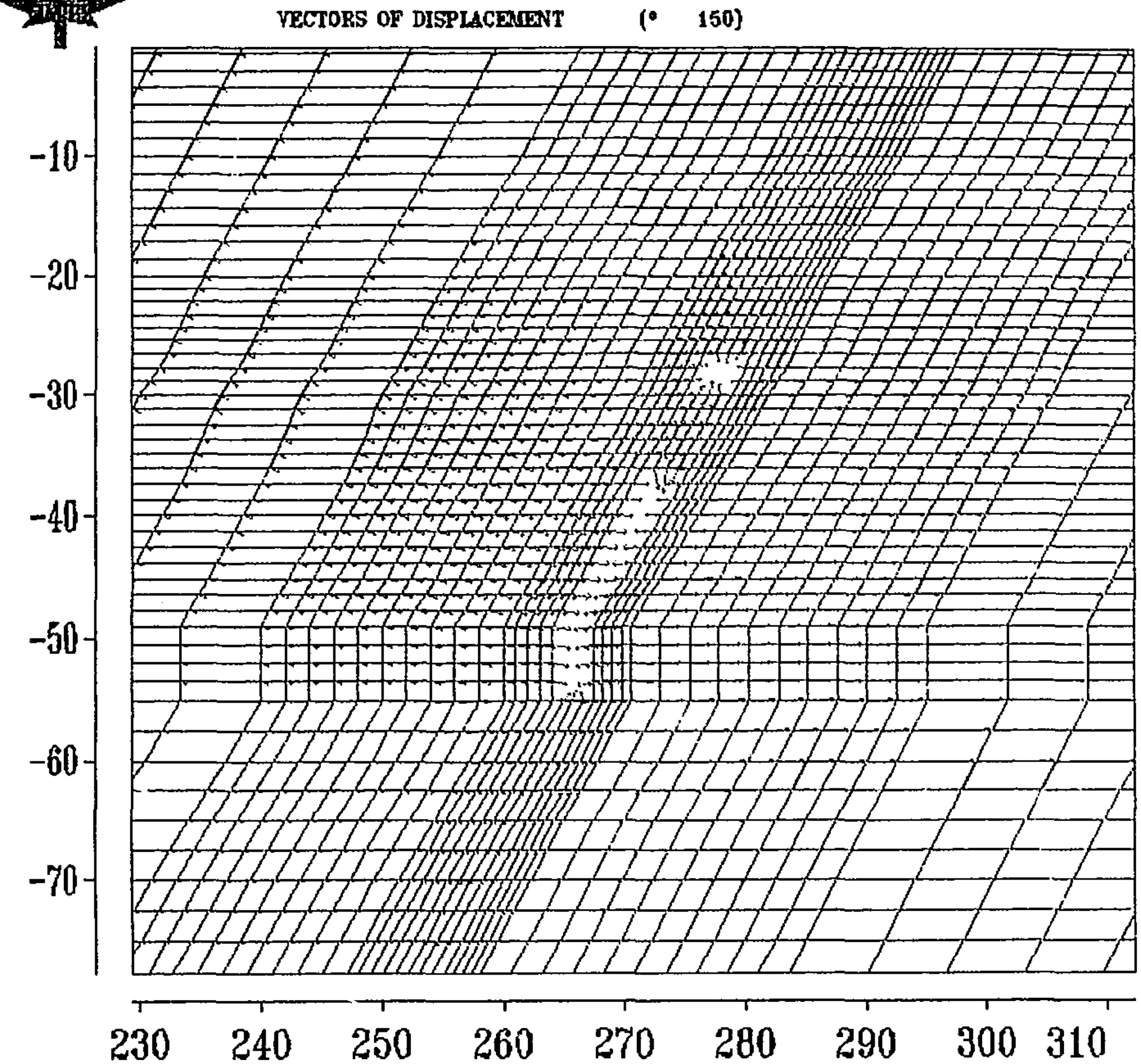

Belmoral

Figure 6.21 Stress orientation and intensity after mining step two, creation of drift 1-7, Belmoral Mine.

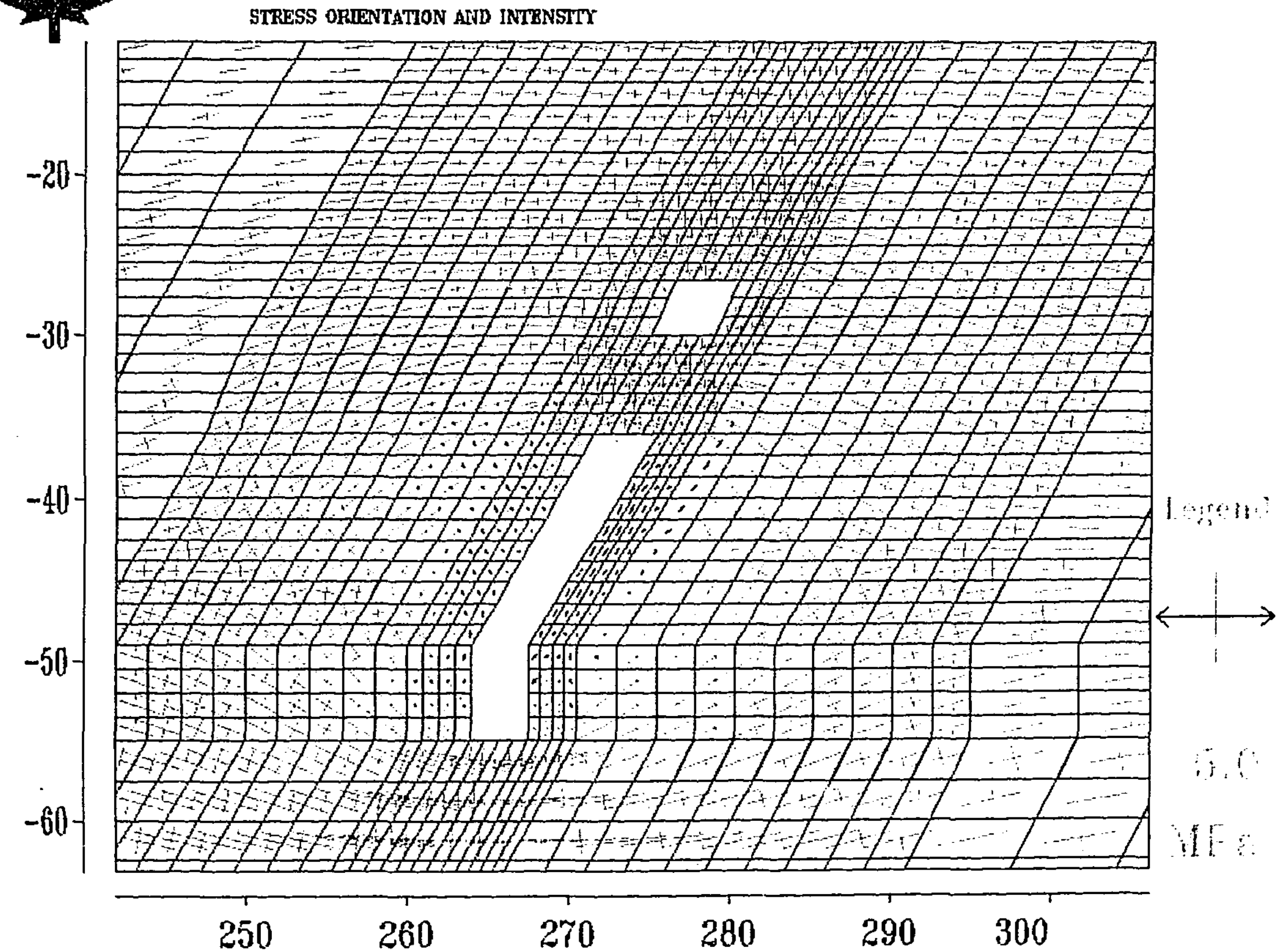

Belmoral Figure 6.22 Major principal stress levels after mining step two, creation of drift 1 - 7, Belmoral Mine.

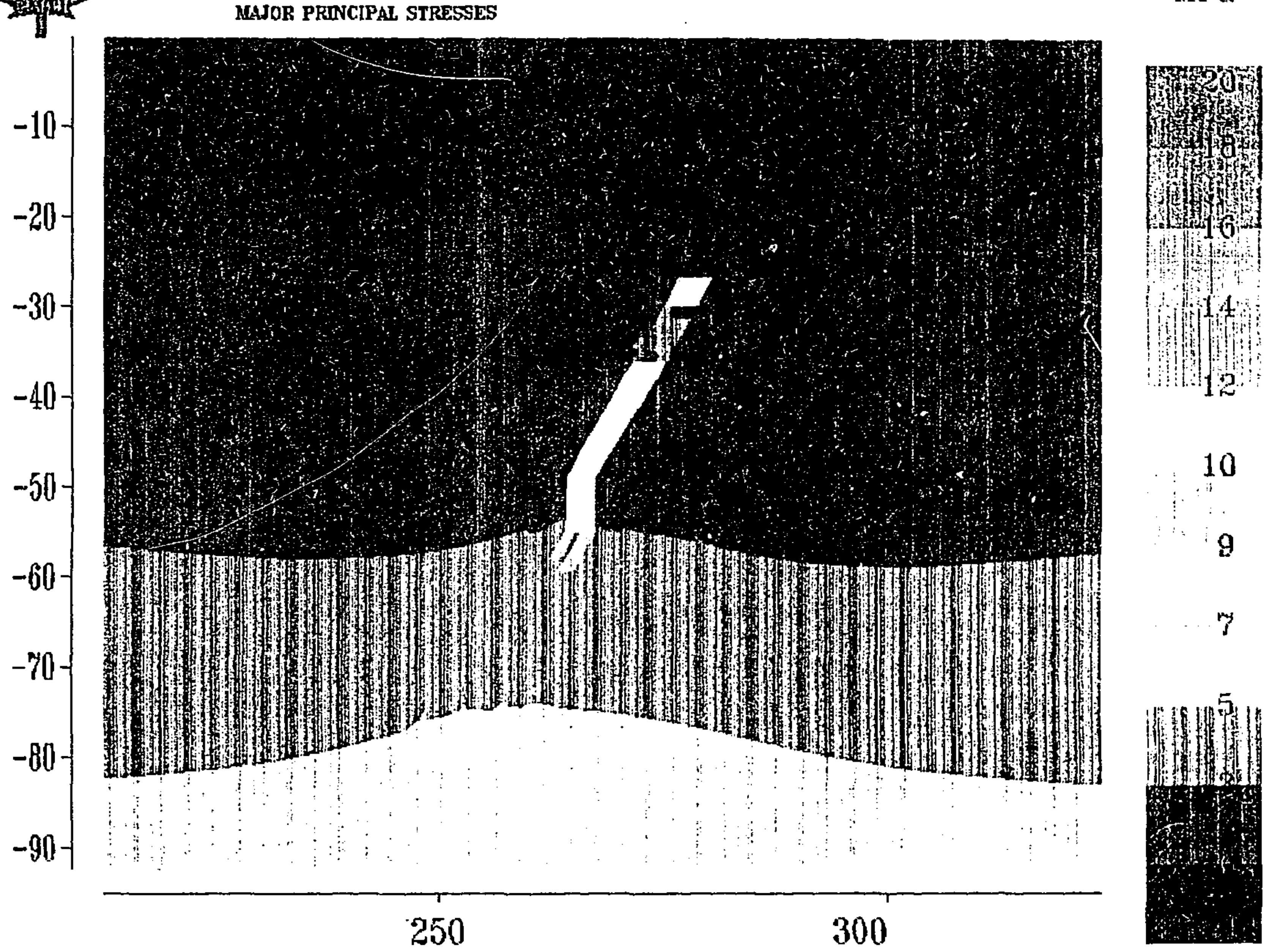

Belmoral

Figure 6.23 Minor principal stress levels after mining step two, creation of drift 1 - 7, Belmoral Mine.

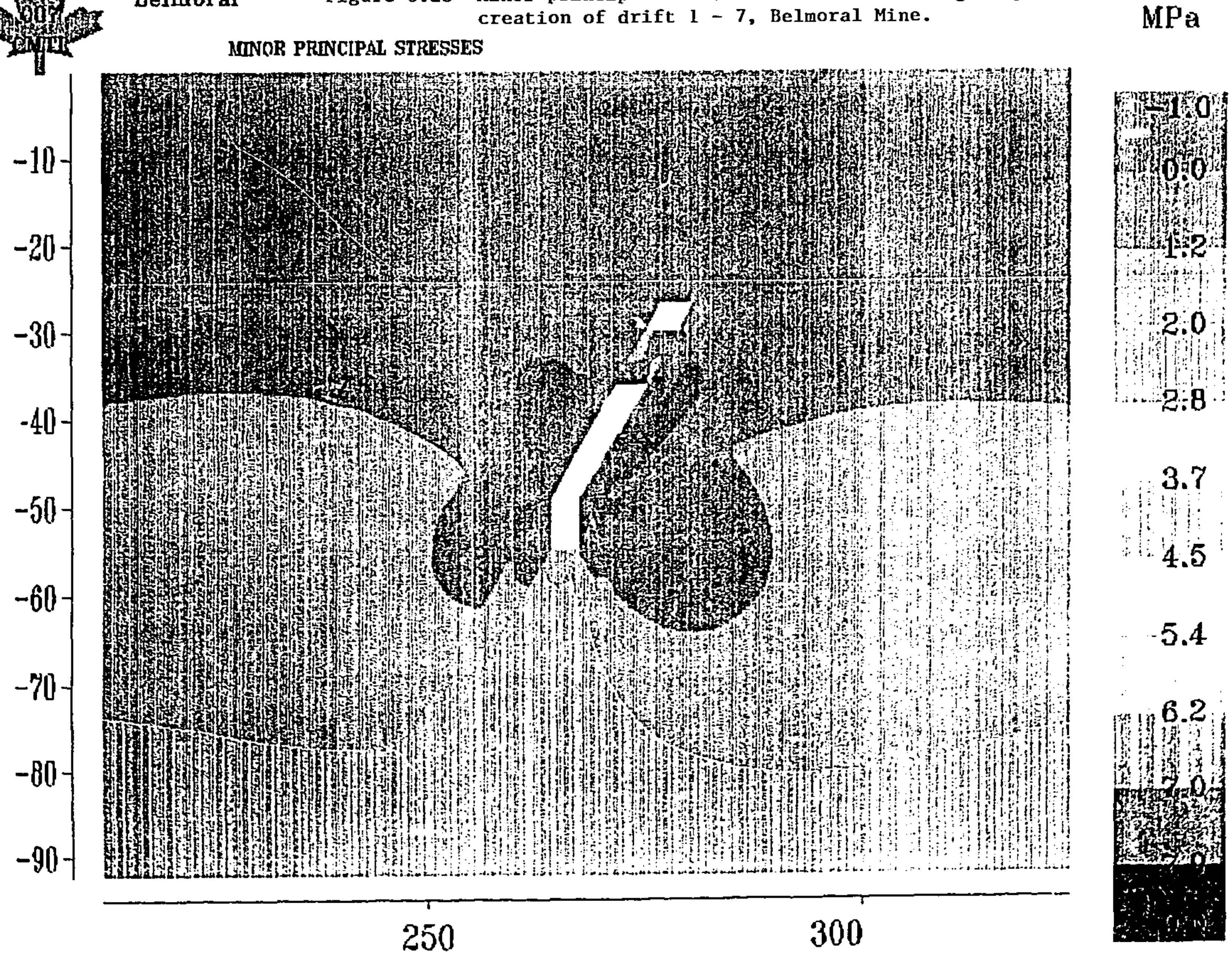

324

Belmoral Figure 6.24 Failed portions of the rock mass after mining step two, creation of drift 1 - 7, Belmoral Mine.

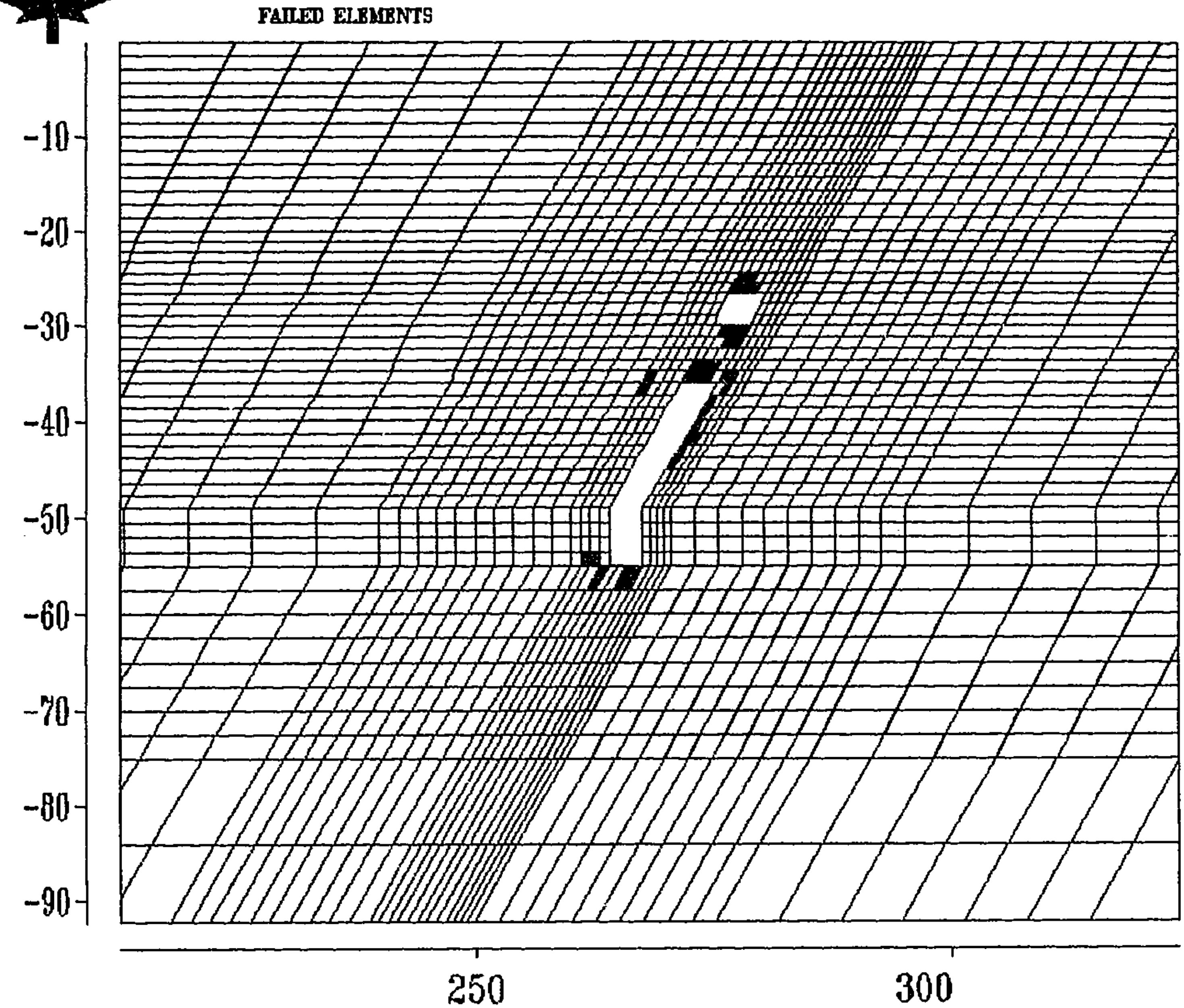

Belmoral

Figure 6.25 Rock mass displacements after mining step three, ore zone failure, Belmoral Mine.

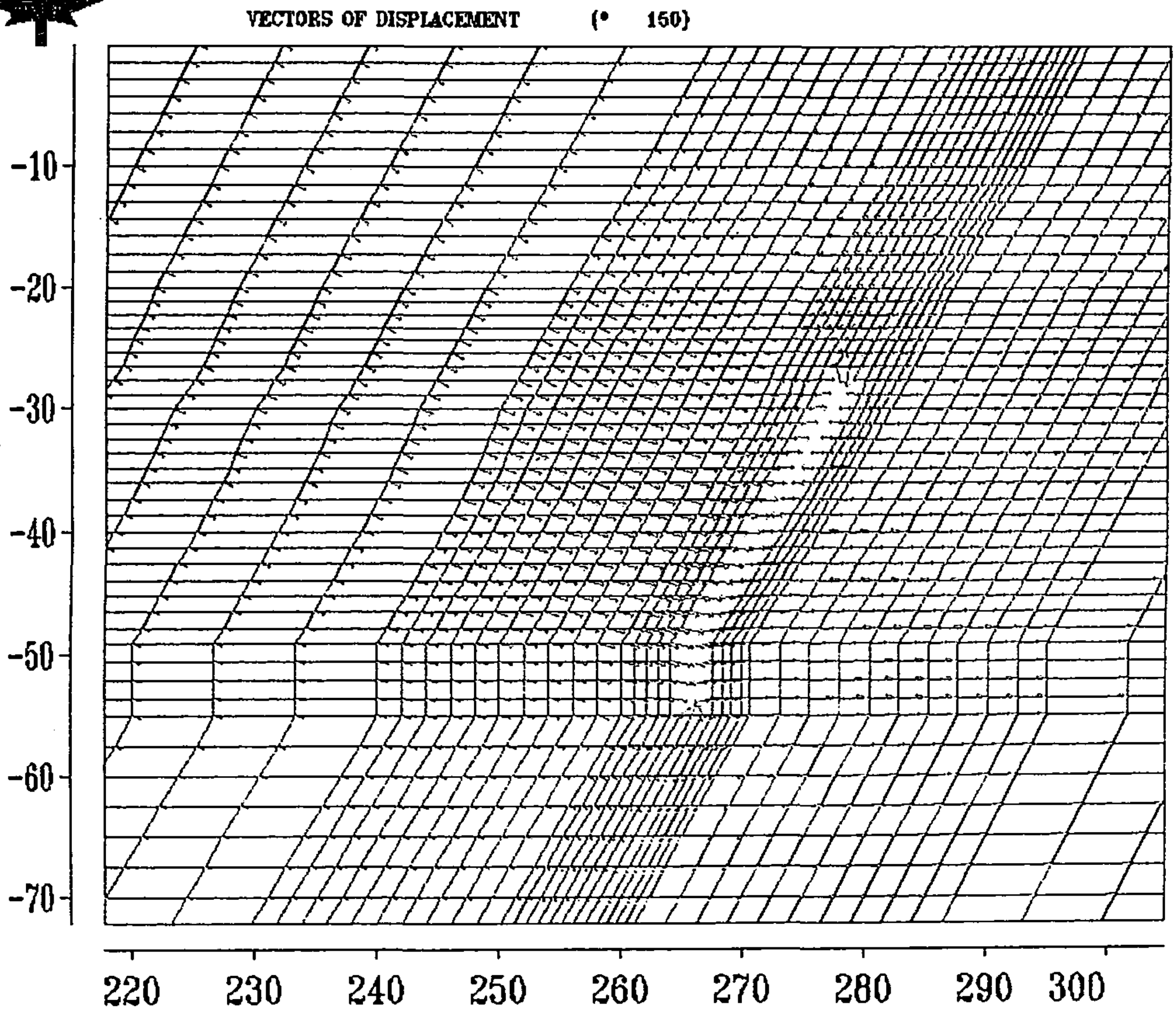

Belmoral

Figure 6.26 Stress orientation and intensity after mining step three, ore zone failure, Belmoral Mine.

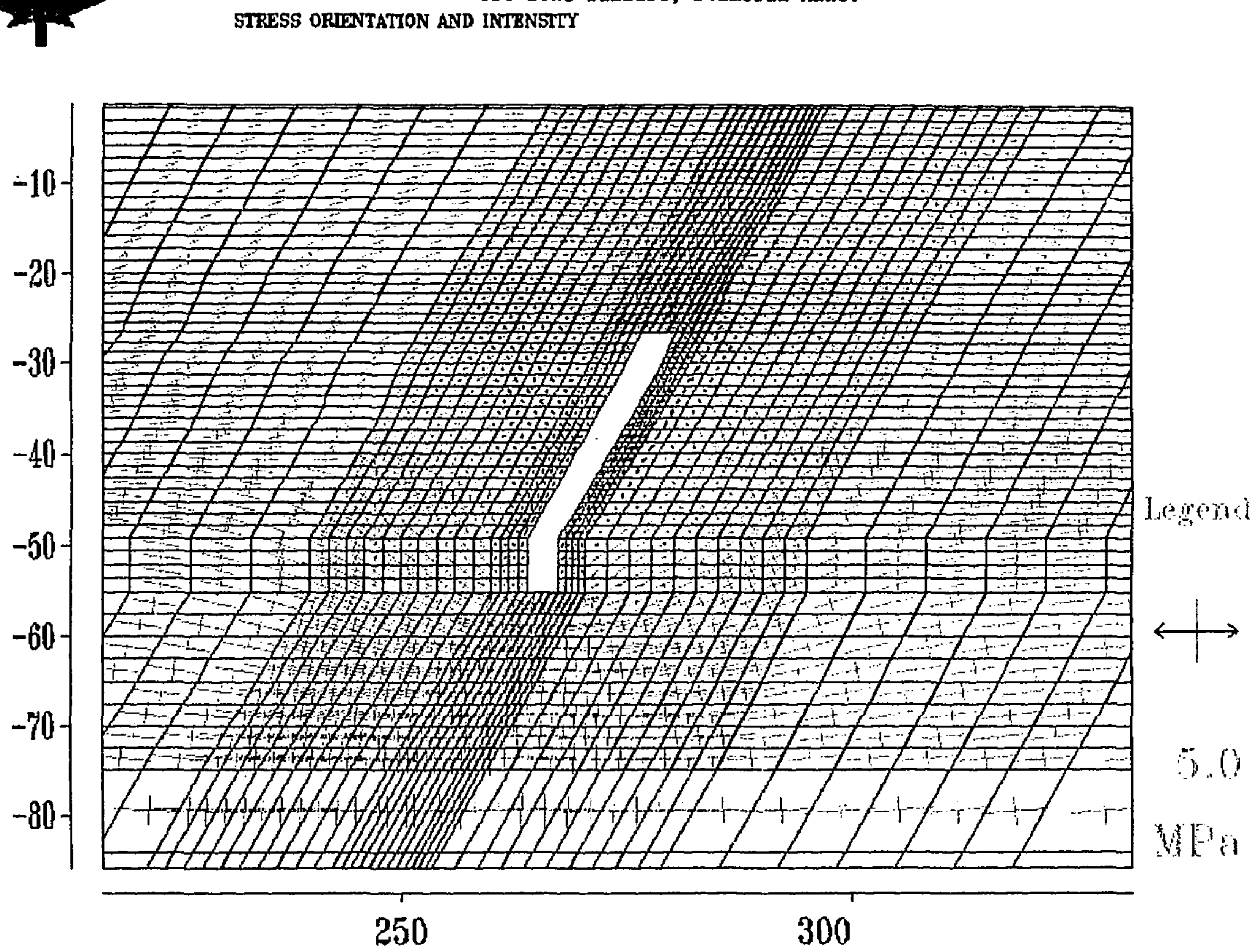

327

Figure 6.27 Major principal stress levels after mining step three, ore zone failure, Belmoral Mine.

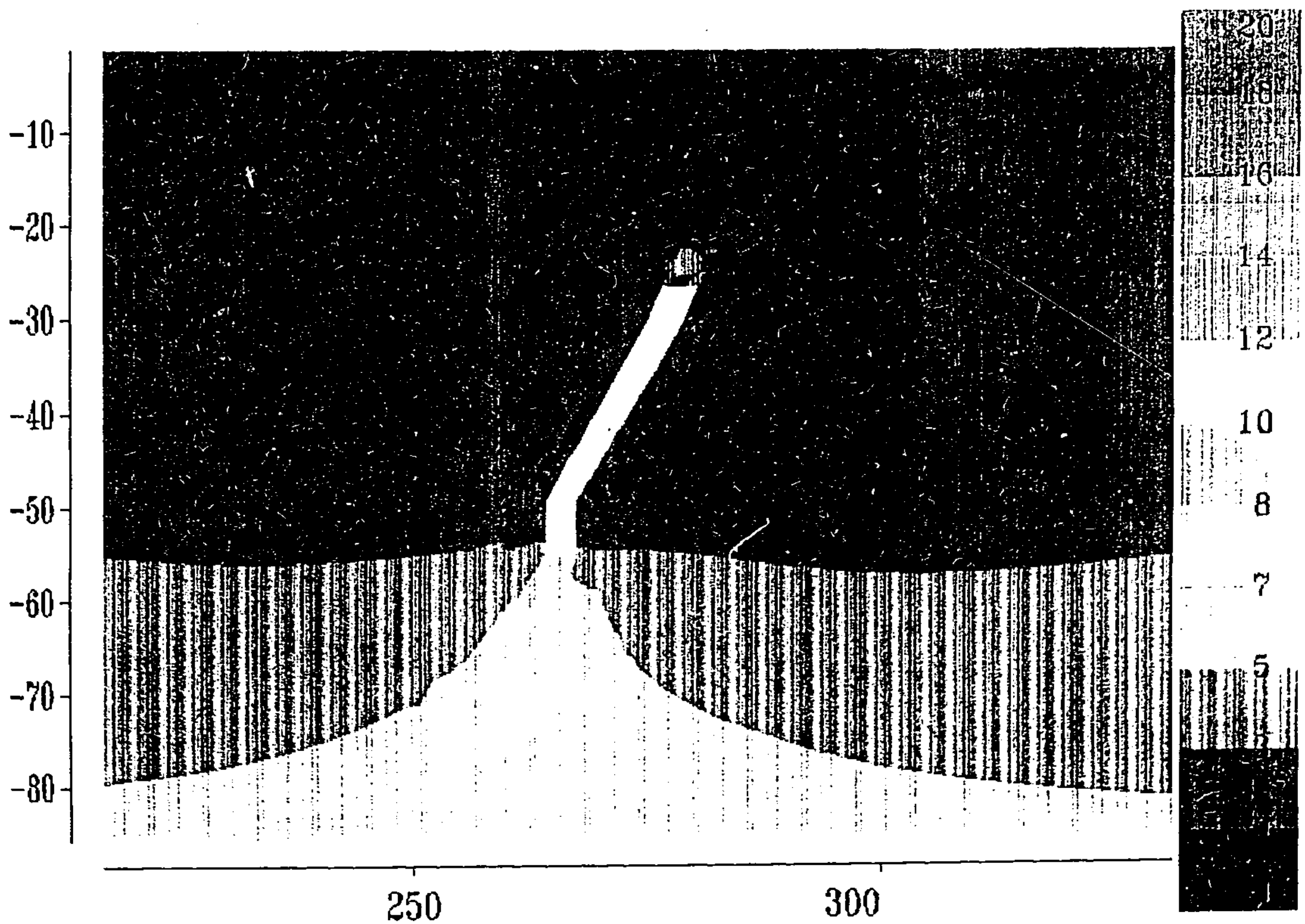

Belmoral

Figure 6.28 Minor principal stress levels after mining step three, ore zone failure, Belmoral Mine.

MINOR PRINCIPAL STRESSES

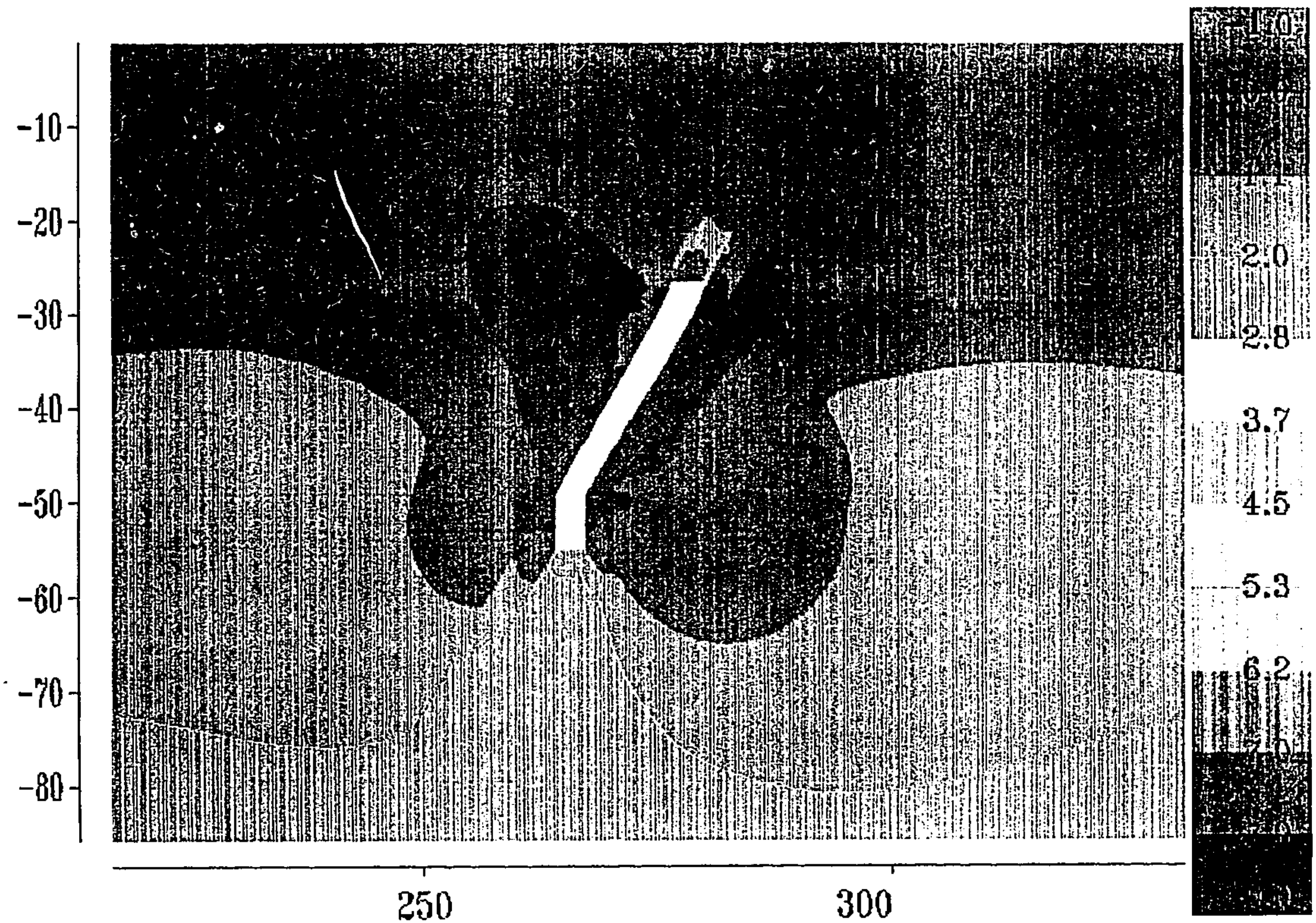

Belmoral Figure 6.29 Failed portions of the rock mass after mining step three, ore zone failure, Belmoral Mine.

FAILED ELEMENTS

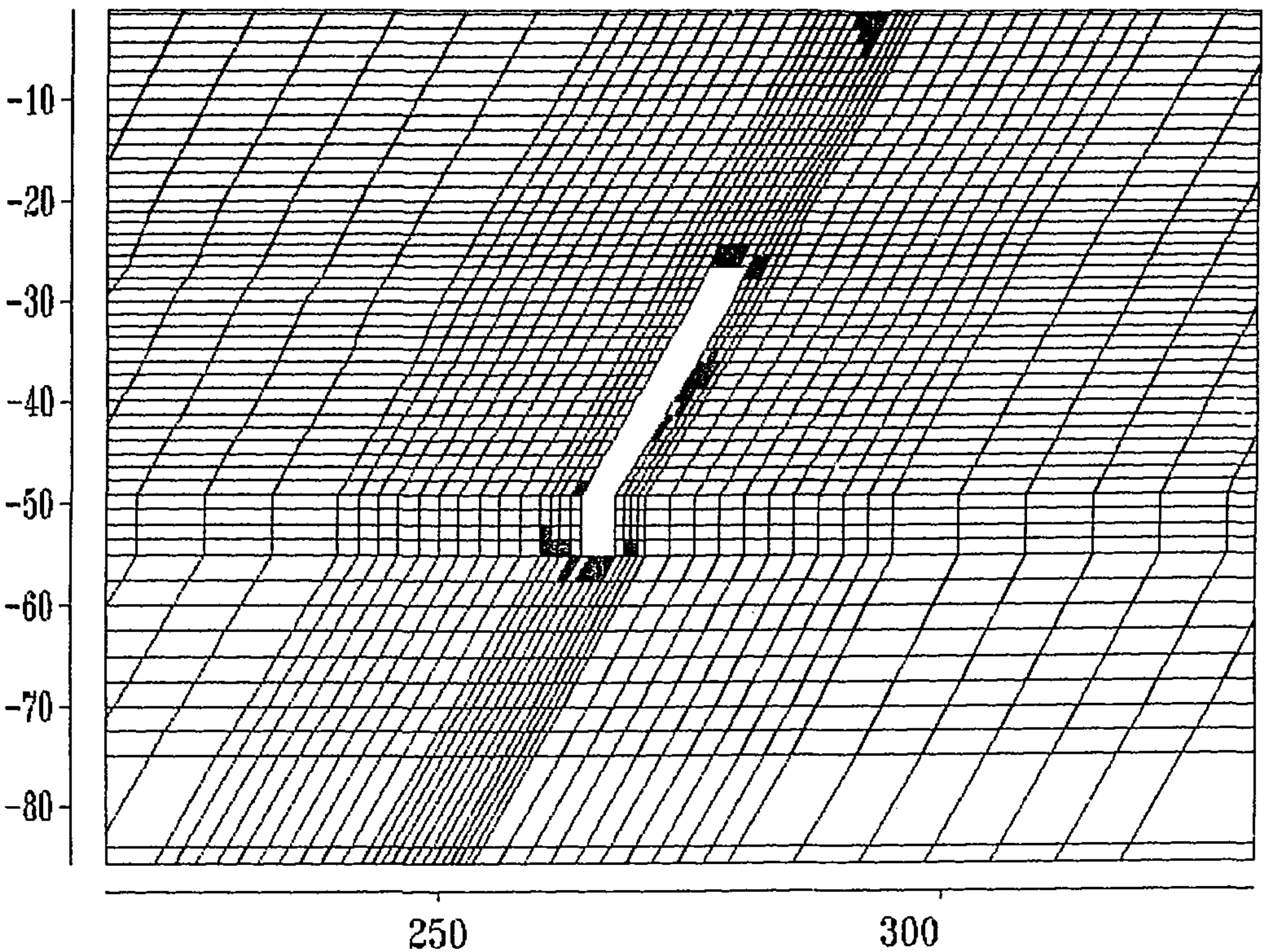

Belmoral Figure 6.30 Rock mass displacements after mining step four, ore zone failure, Belmoral Mine.

VECTORS OF DISPLACEMENT (* 150)

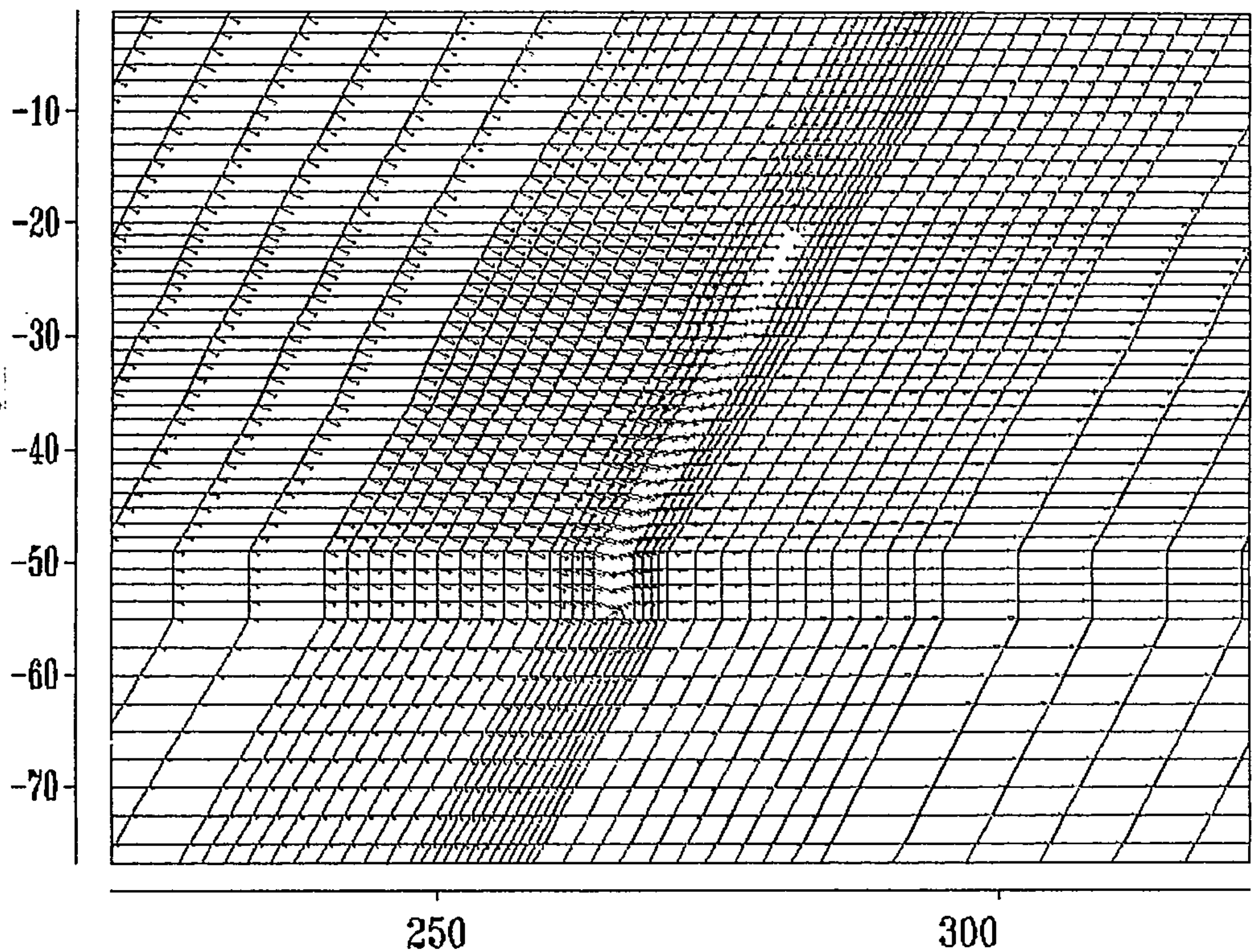

Figure 6.31 Stress orientation and intensity after mining step four, ore zone failure, Belmoral Mine.

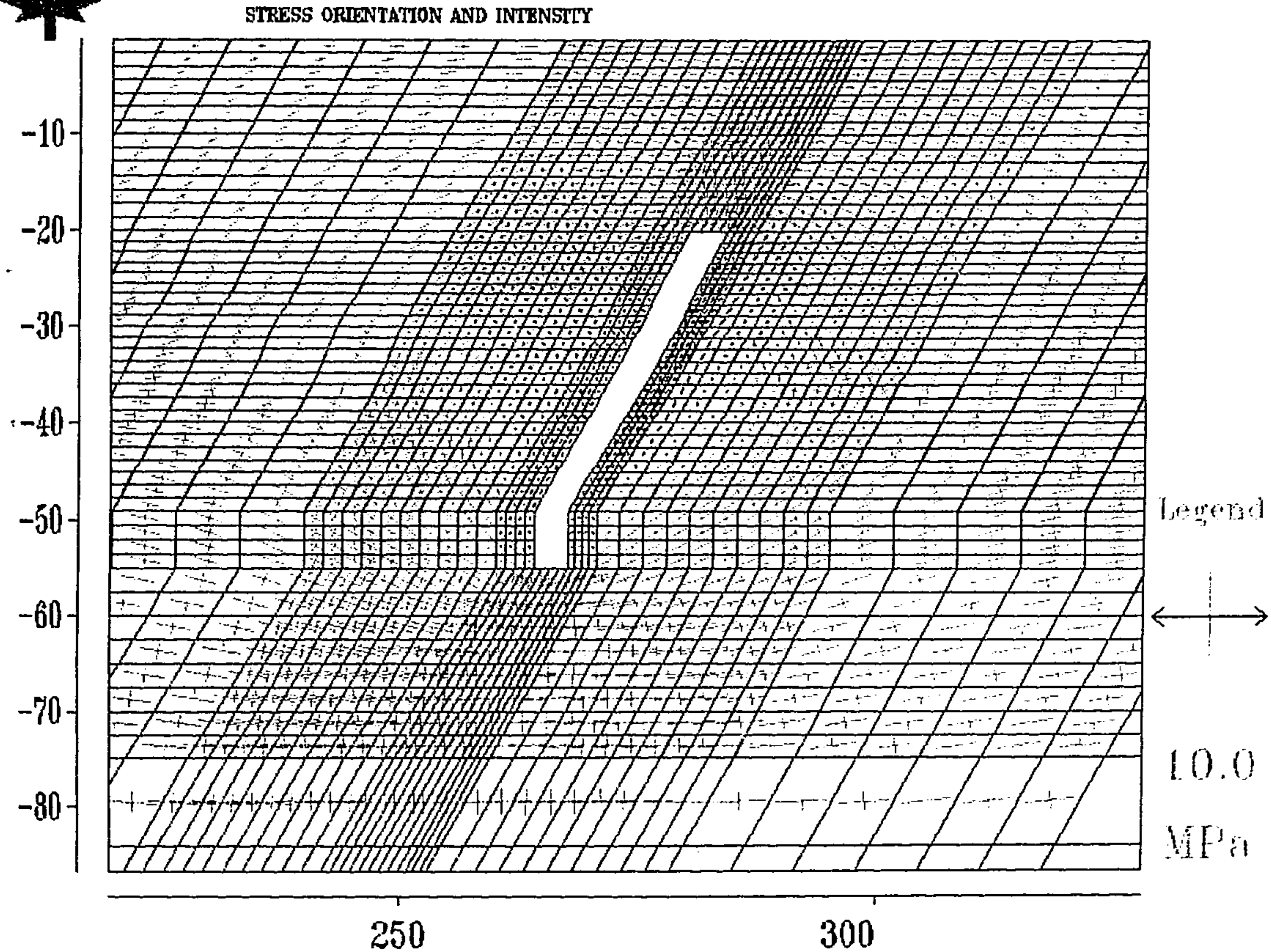

Belmoral Figure 6.32 Major principal stress levels after mining step four, ore zone failure, Belmoral Mine.

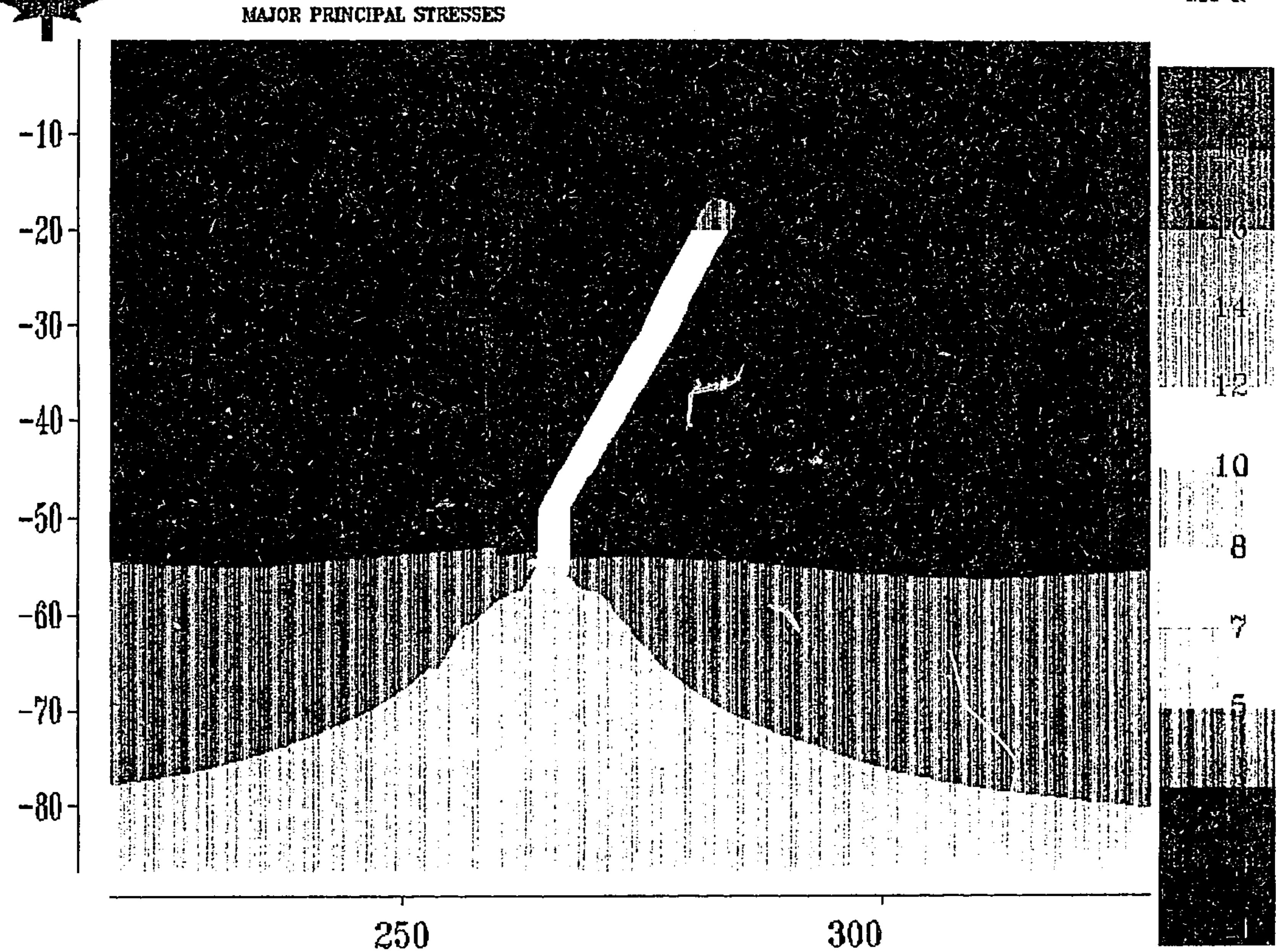

Figure 6.33 Minor principal stress levels after mining step four, ore zone failure, Belmoral Mine.

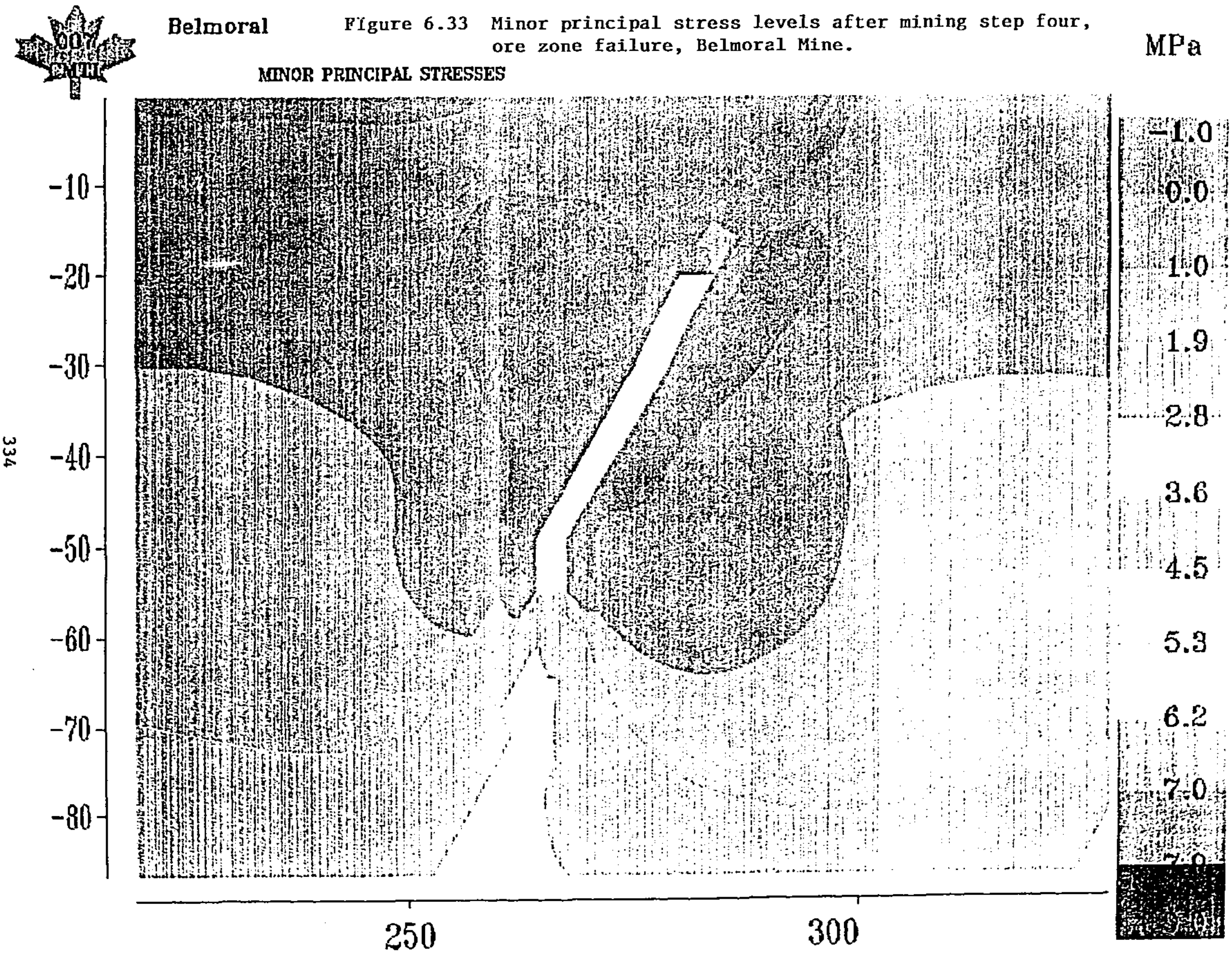

Belmoral Figure 6.34 Failed portions of the rock mass after mining step four, ore zone failure, Belmoral Mine.

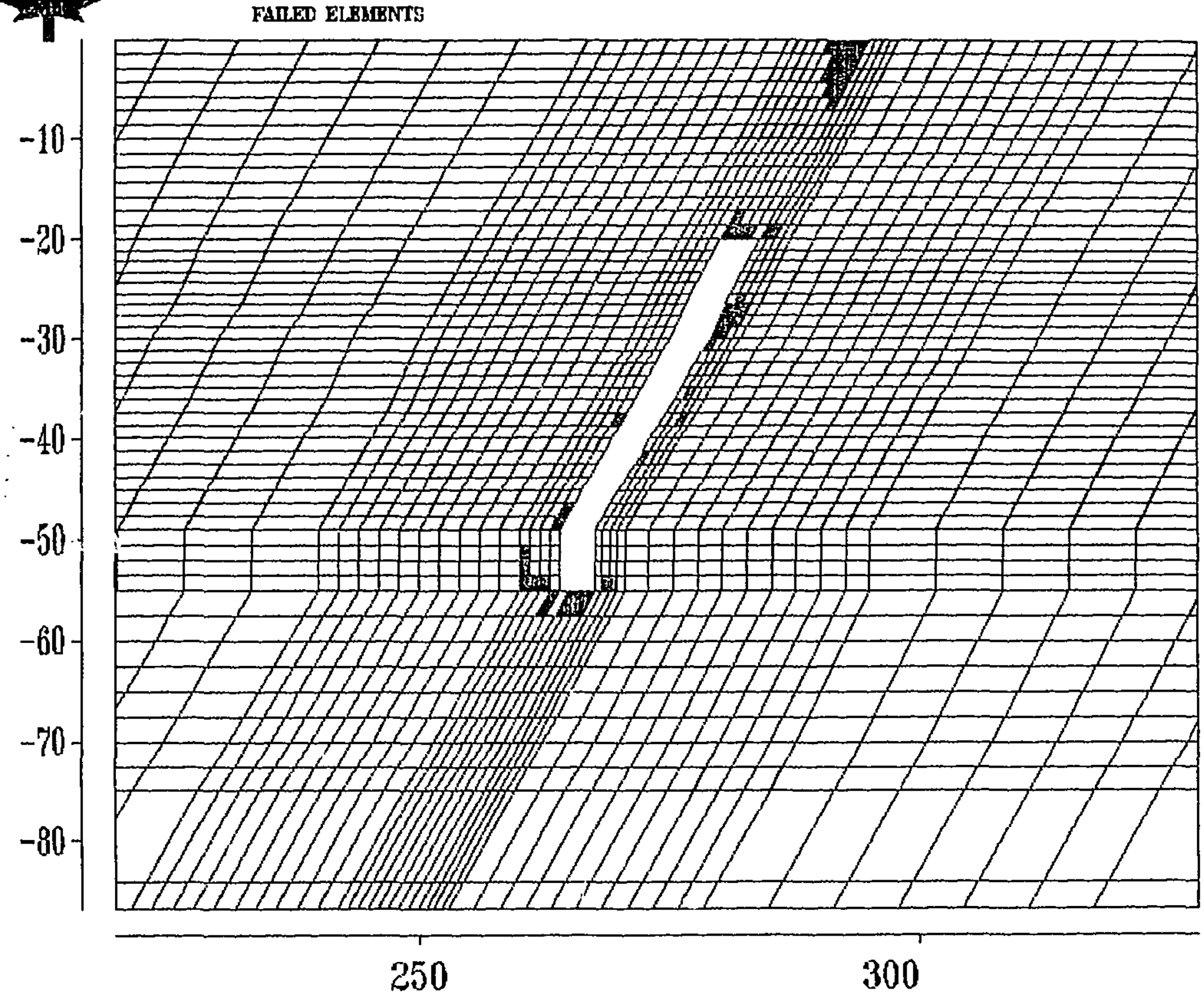

Belmoral

Figure 6.35 Rock mass displacements after mining step five, ore zone failure, Belmoral Mine.

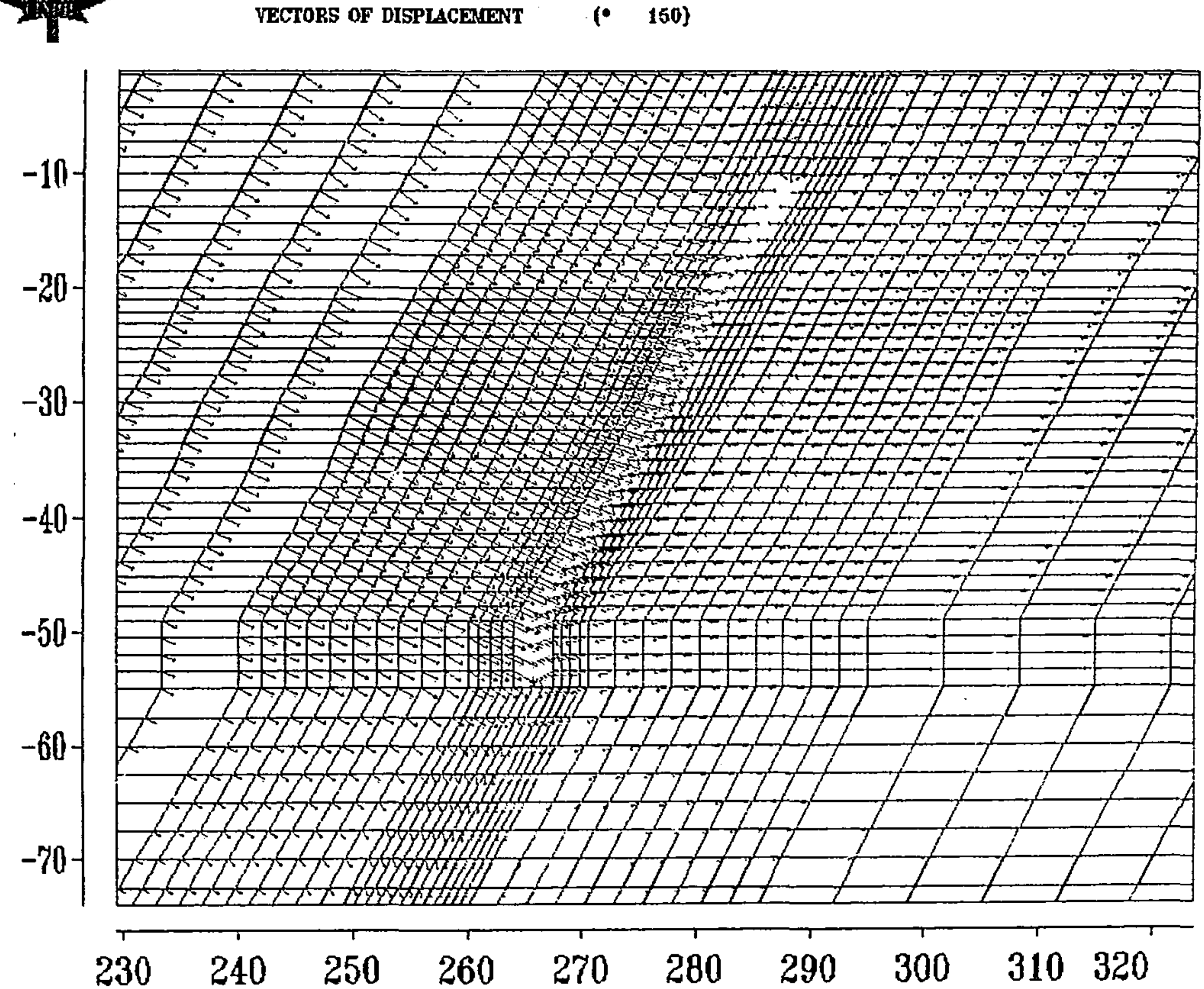

Belmoral Figure 6.36 Stress orientation and intensity after mining step five, ore zone failure, Belmoral Mine.

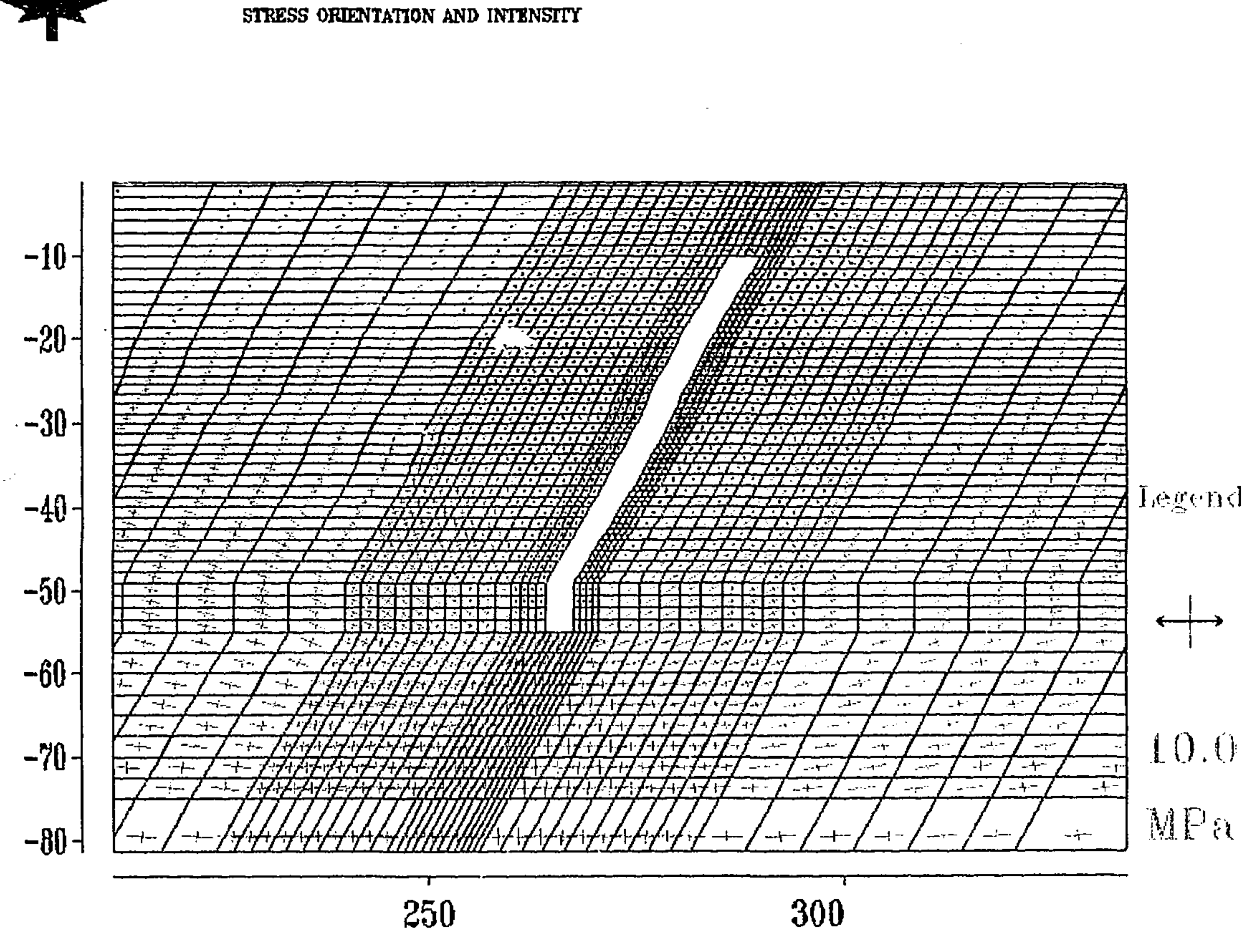

337

Belmoral

Figure 6.37 Major principal stress levels after mining step five, ore zone failure, Belmoral Mine.

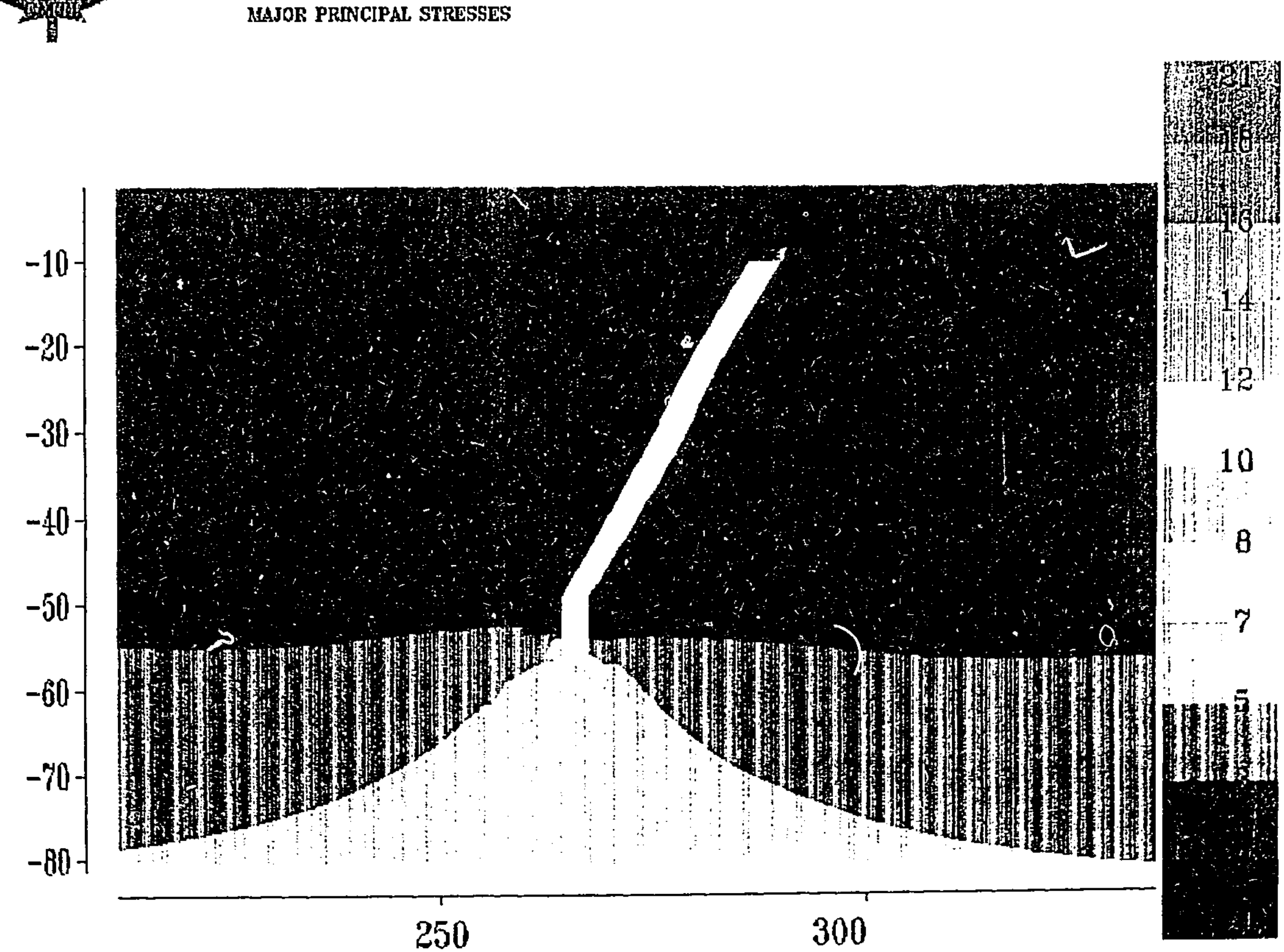

338

Belmoral Figure 6.38 Minor principal stress levels after mining step five, ore zone failure, Belmoral Mine.

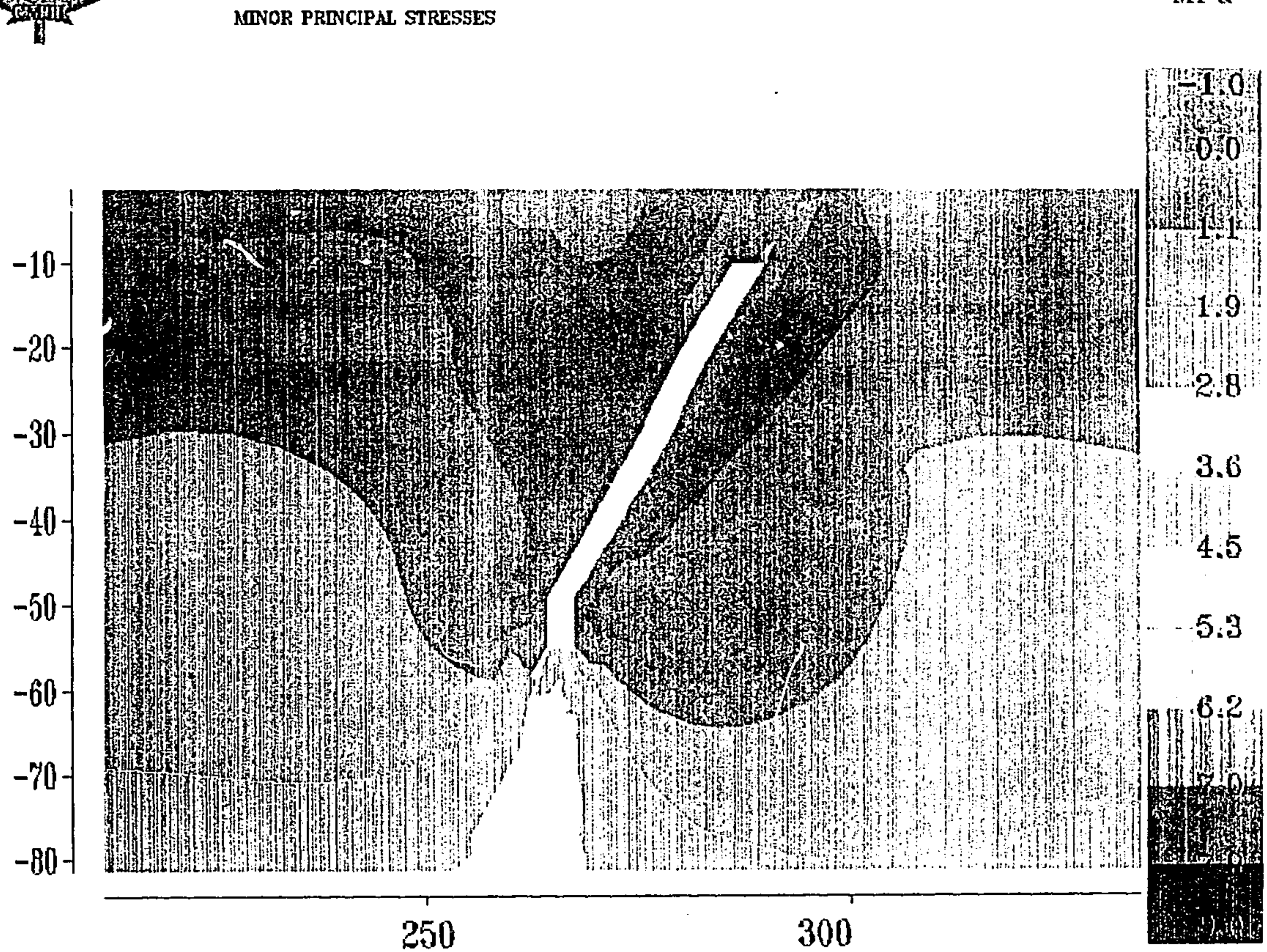

Belmoral

Figure 6.39 Failed portions of the rock mass after mining step five, ore zone failure, Belmoral Mine.

FAILED ELEMENTS

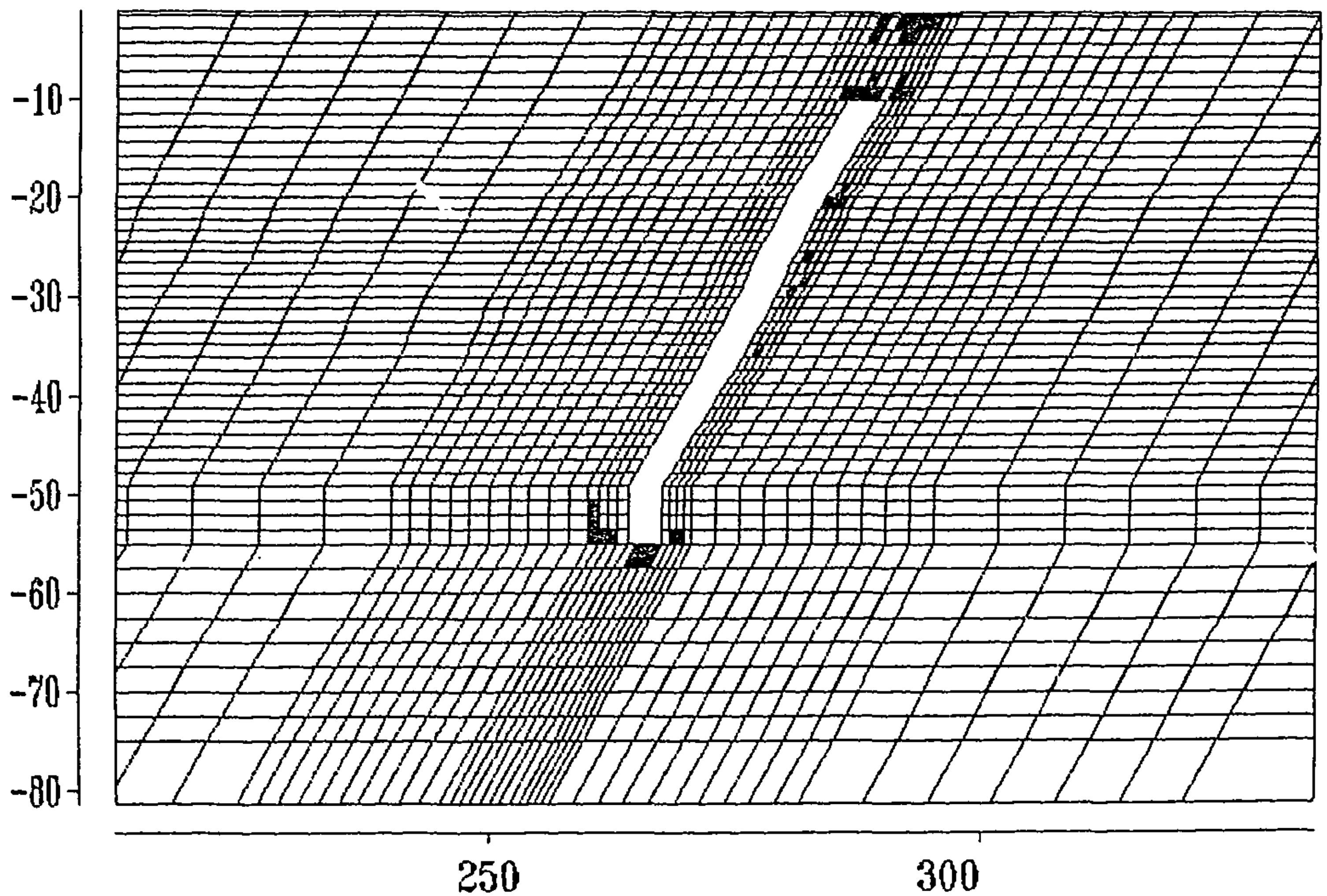

Belmoral Figure 6.40 Rock mass displacements after mining step six, ore zone failure, Belmoral Mine.

VECTORS OF DISPLACEMENT (* 150)

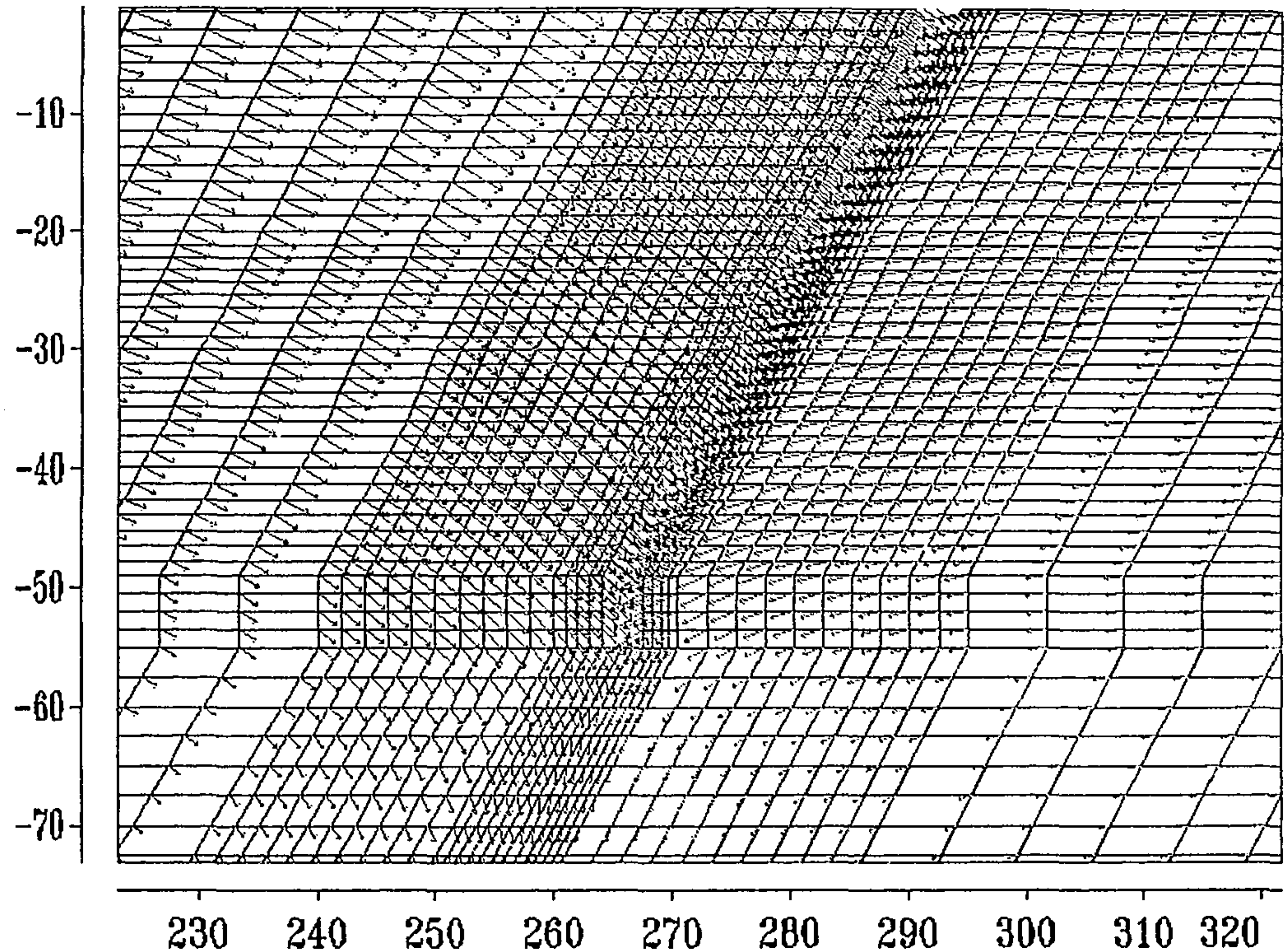

Figure 6.41 Stress orientation and intensity after mining step six, ore zone failure, Belmoral Mine.

STRESS ORIENTATION AND INTENSITY

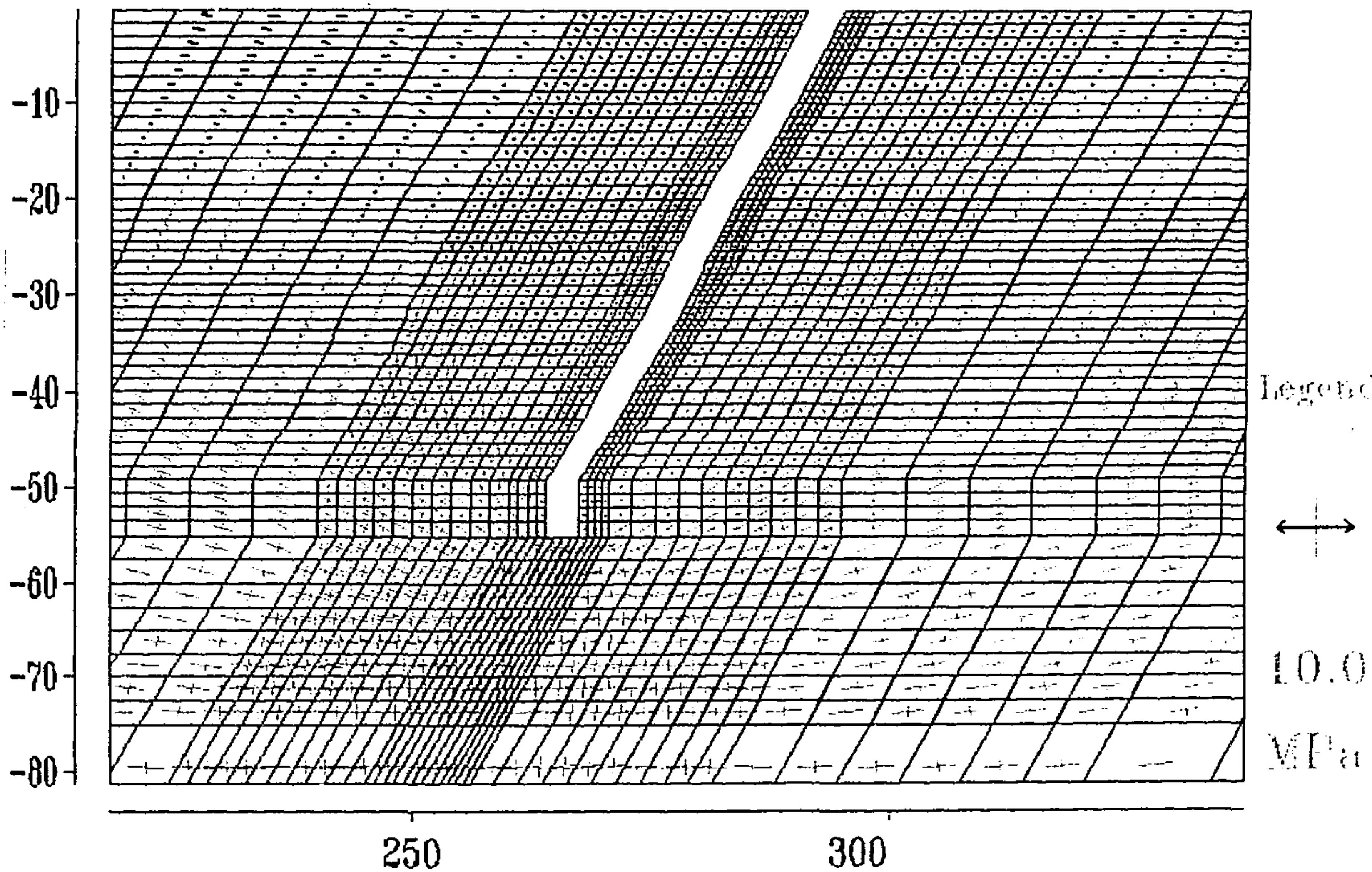

Belmoral

Figure 6.42 Major principal stress levels after mining step six, ore zone failure, Belmoral Mine.

MAJOR PRINCIPAL STRESSES

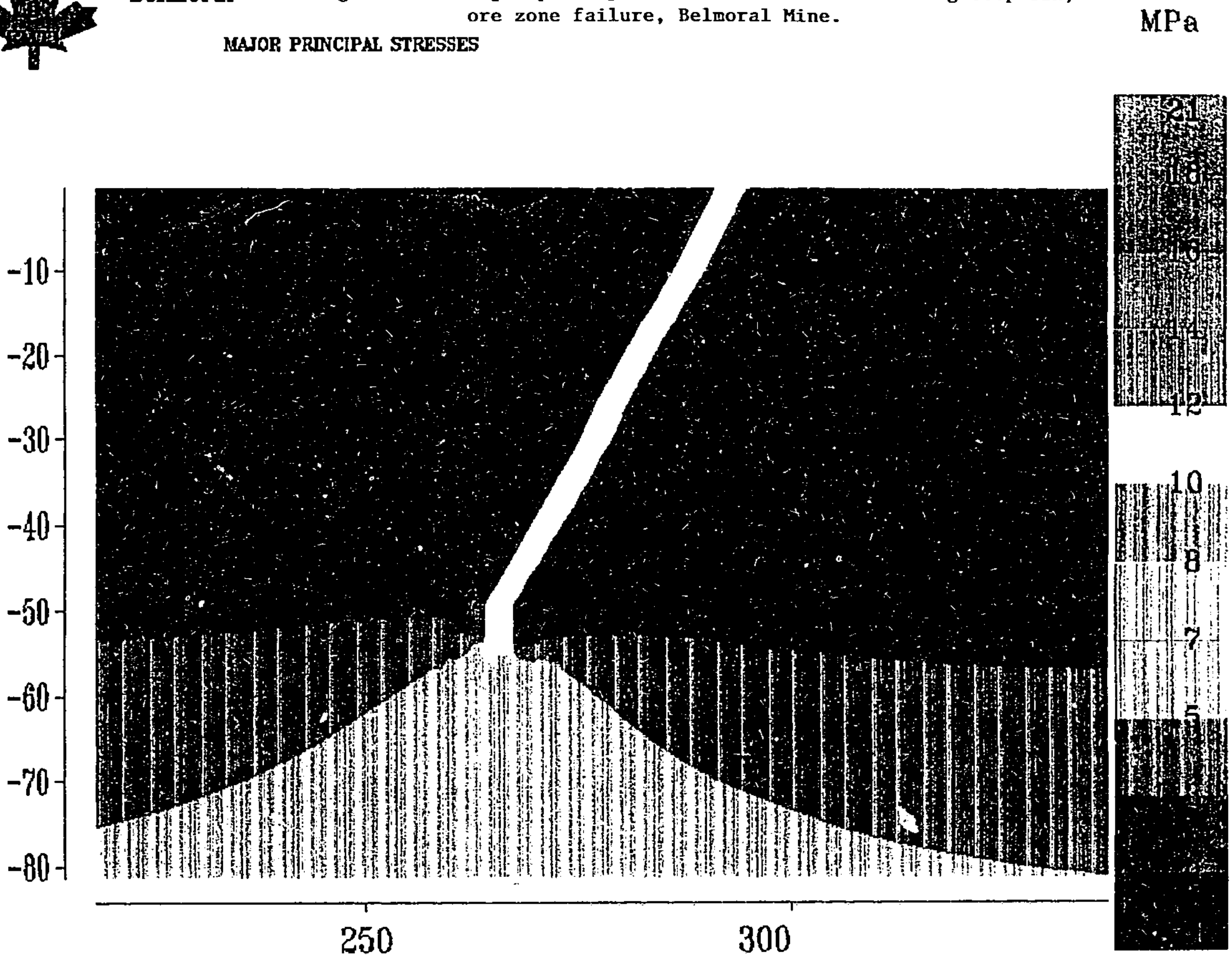

Belmoral Figure 6.43 Minor principal stress levels after mining step six, ore zone failure, Belmoral Mine.

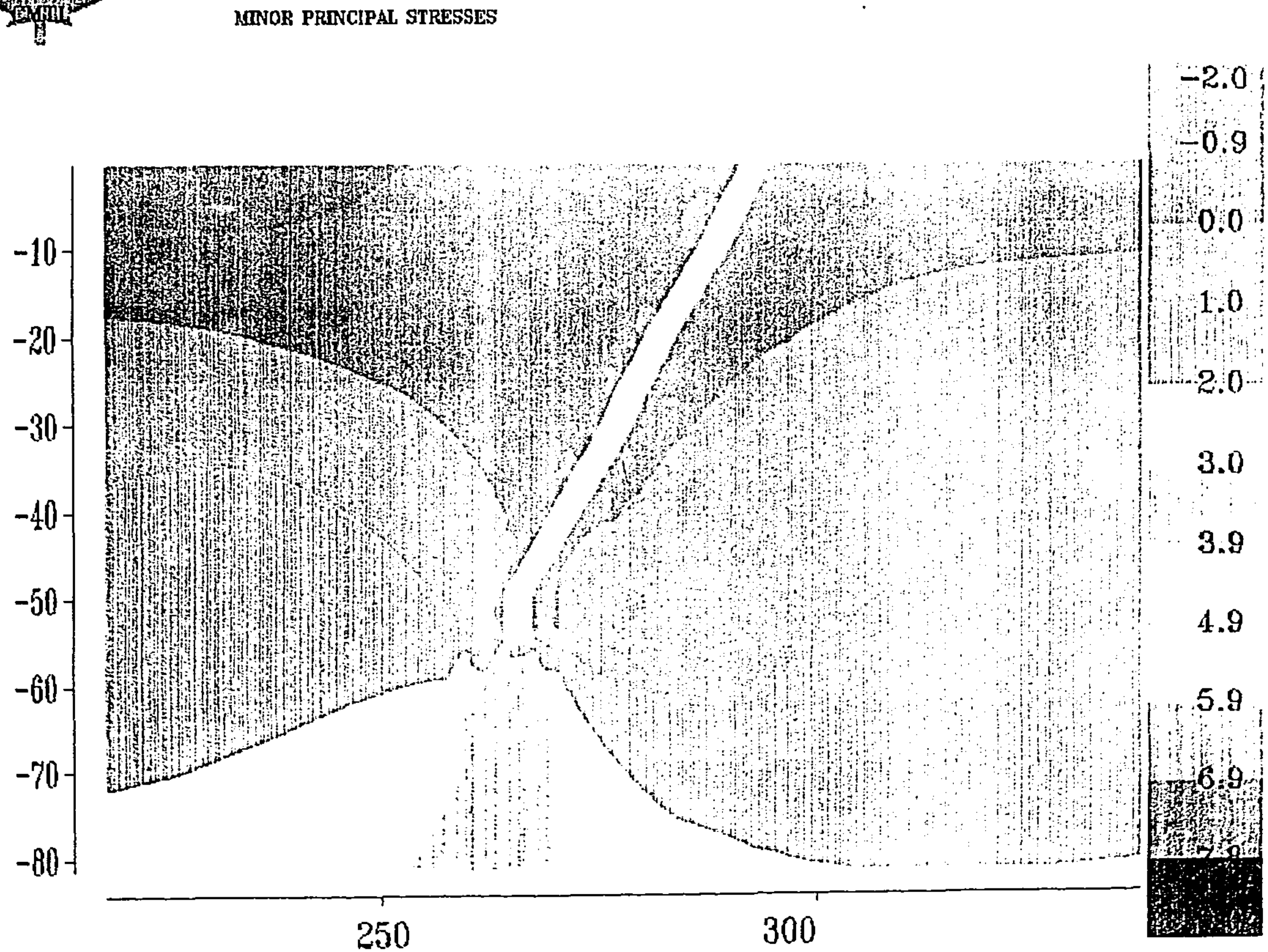

Figure 6.44 Failed portions of the rock mass after mining step six, ore zone failure, Belmoral Mine.

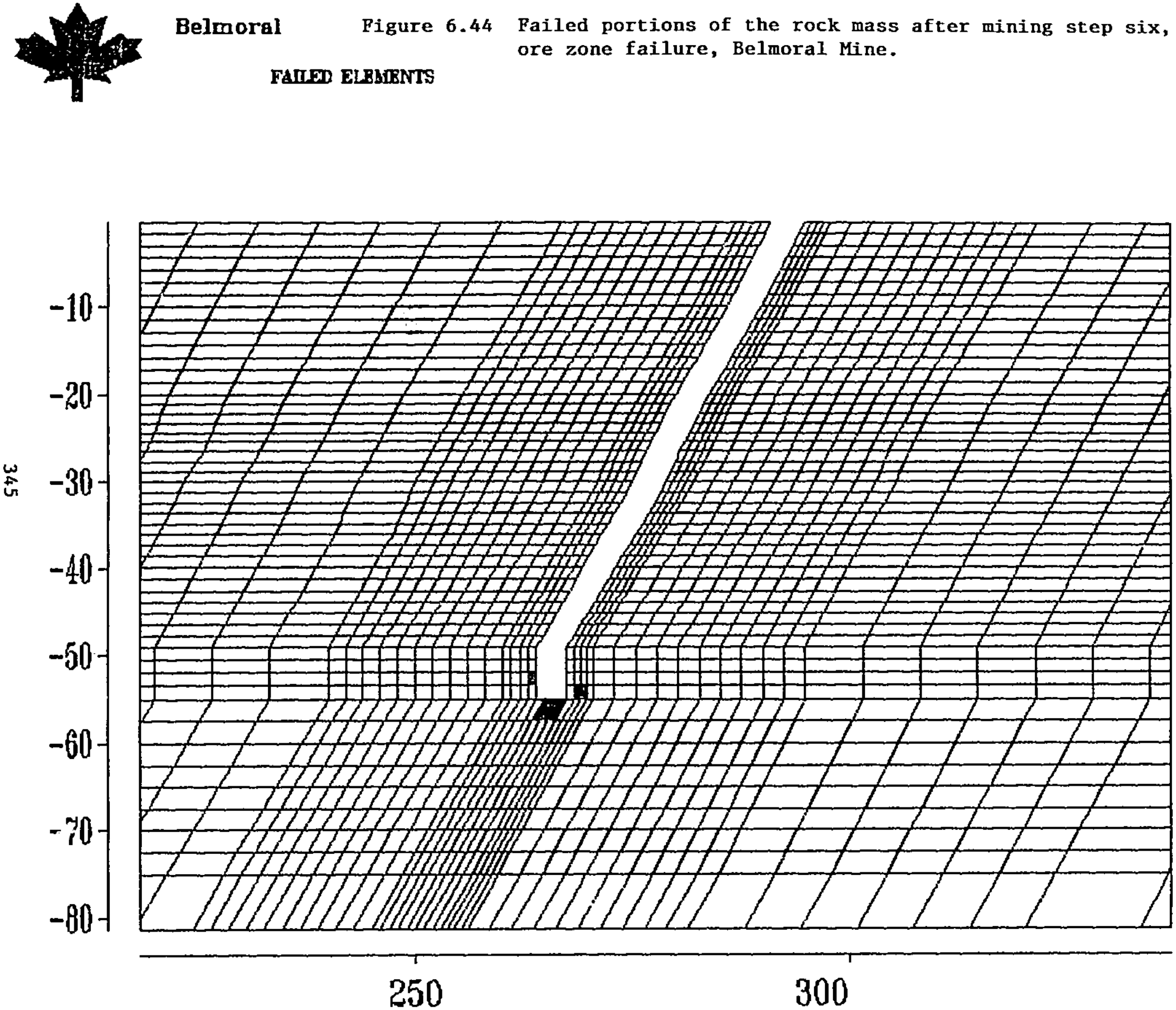

Belmoral

Figure 6.45 Rock mass displacements after mining step three, hangingwall failure, Belmoral Mine.

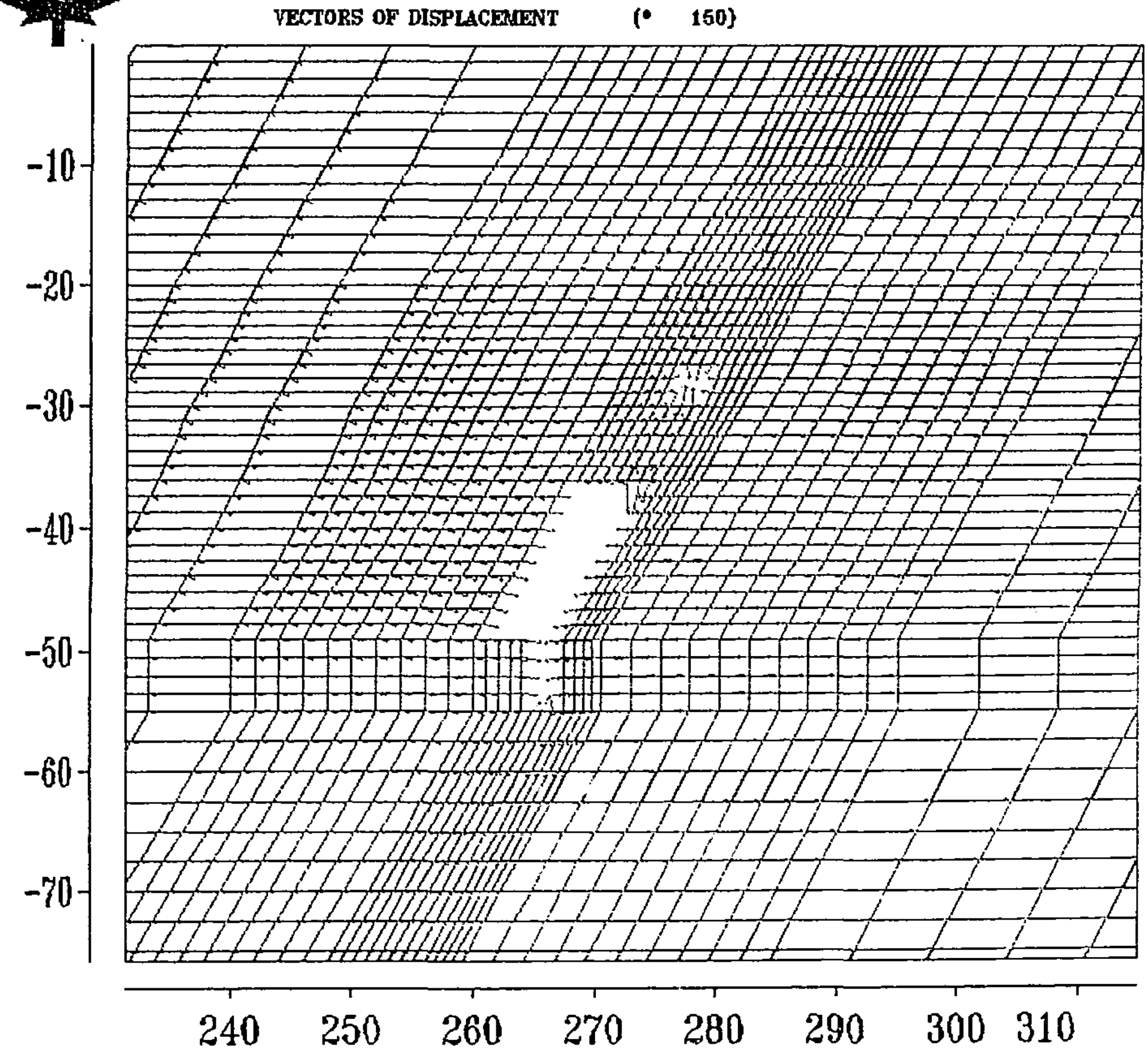

Belmoral Figure 6.46 Stress orientation and intensity after mining step three, hangingwall failure, Belmoral Mine.

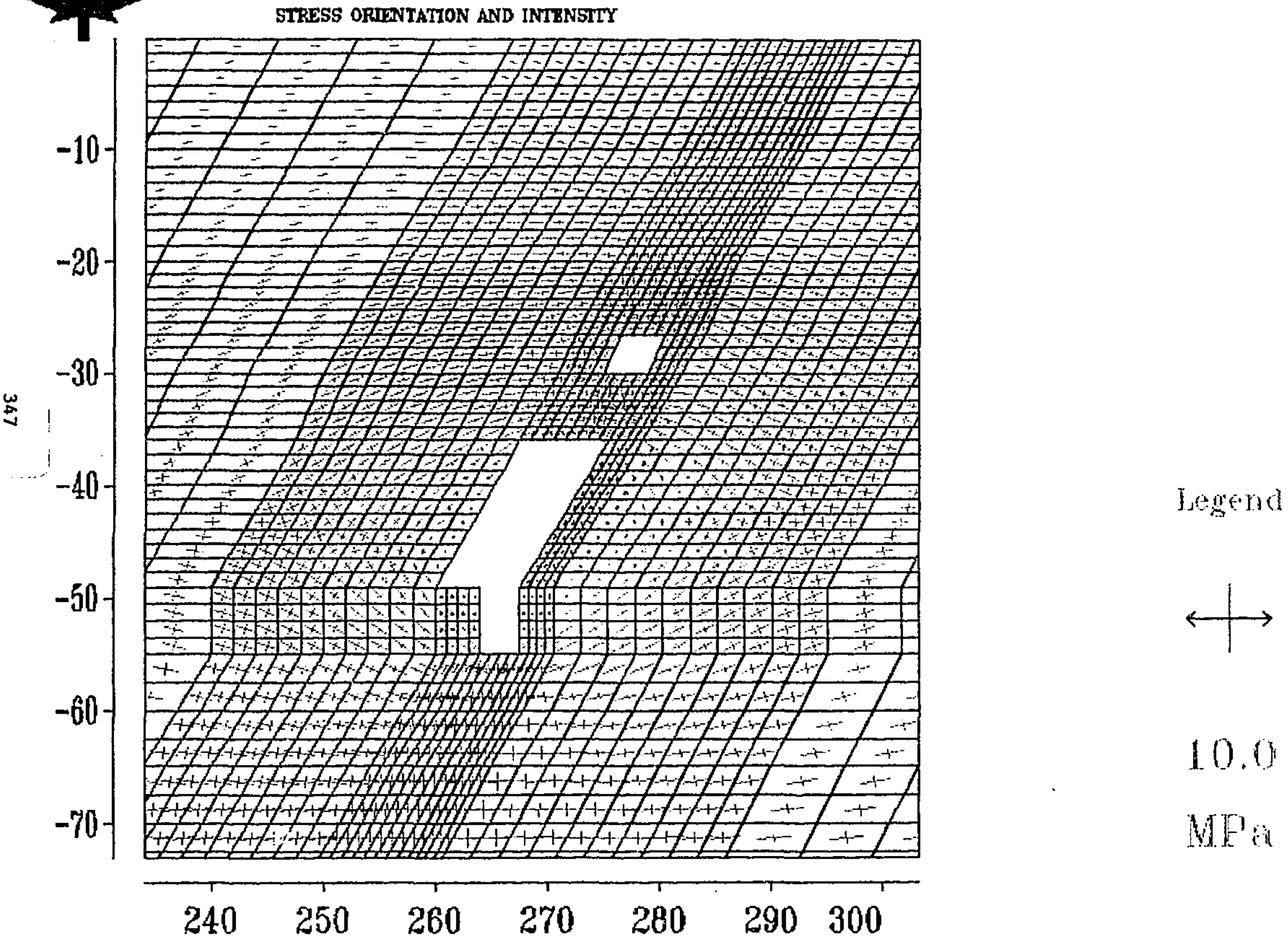

Belmoral

Figure 6.48 Minor principal stress levels after mining step three, hangingwall failure, Belmoral Mine.

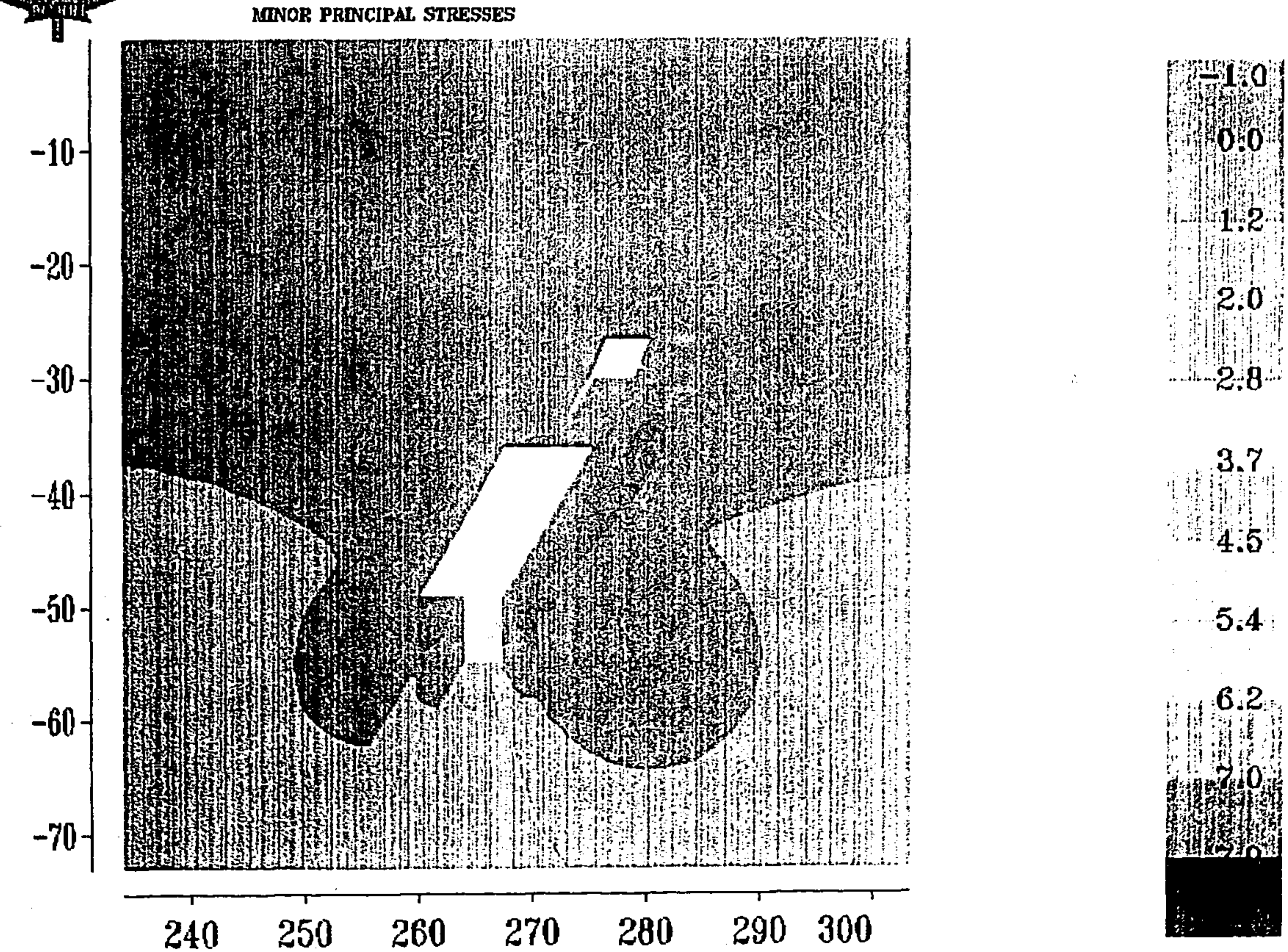

Belmoral Figure 6.49 Failed portions of the rock mass after mining step three, hangingwall failure, Belmoral Mine.

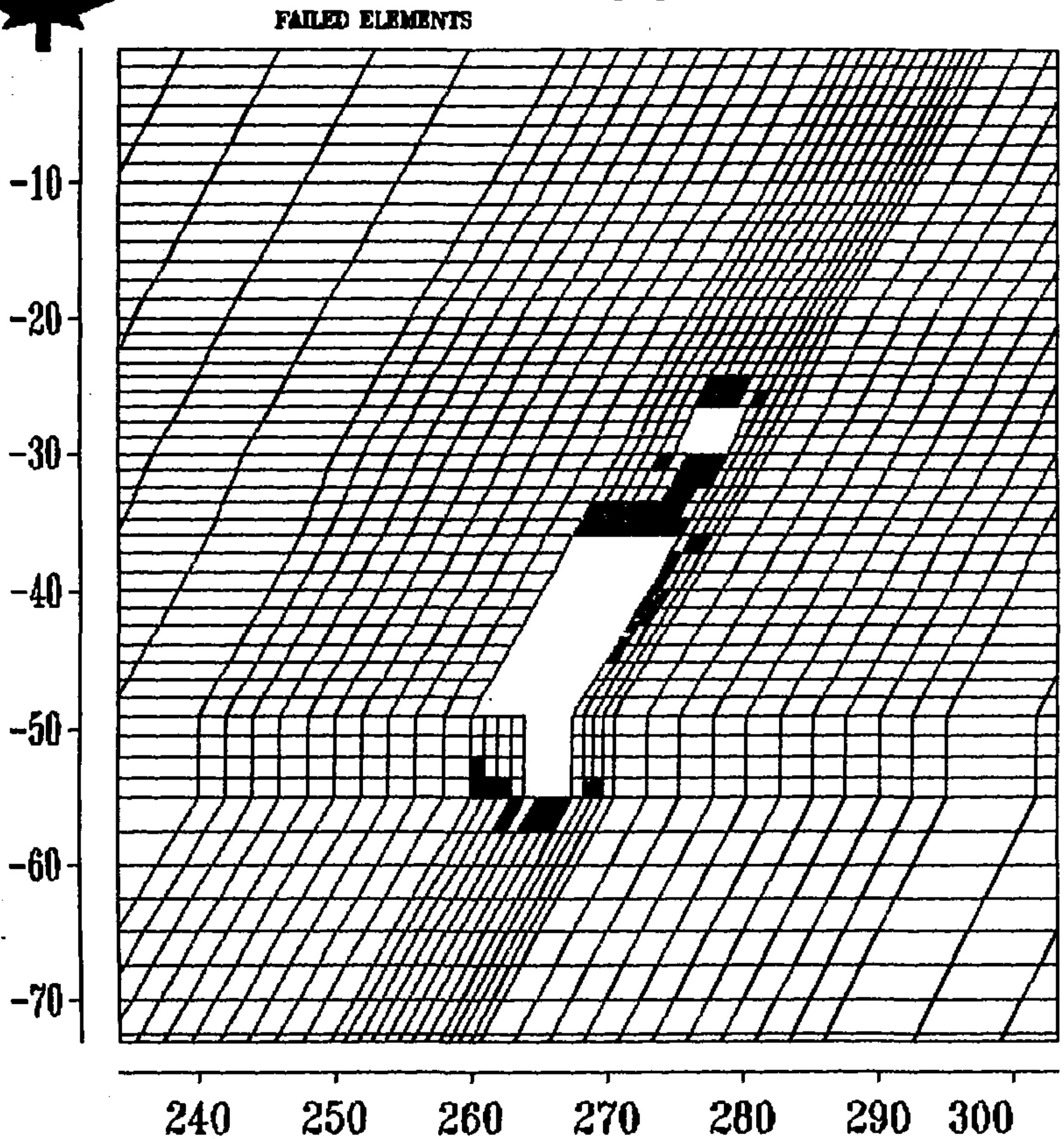

Belmoral

Figure 6.50 Rock mass displacements after mining step four, hangingwall failure, Belmoral Mine.

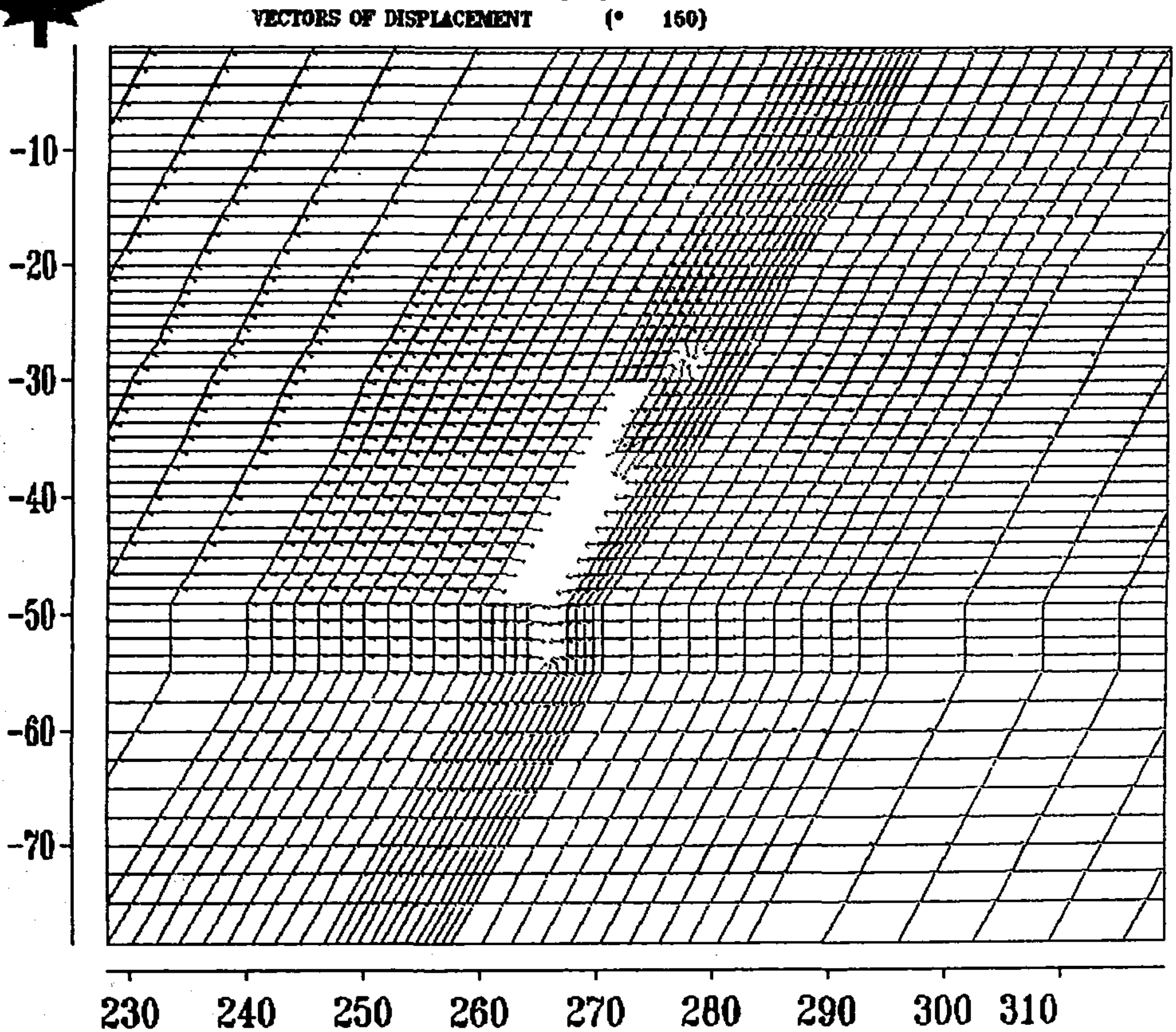

Belmoral Figure 6.51 Stress orientation and intensity after mining step four, hangingwall failure, Belmoral Mine.

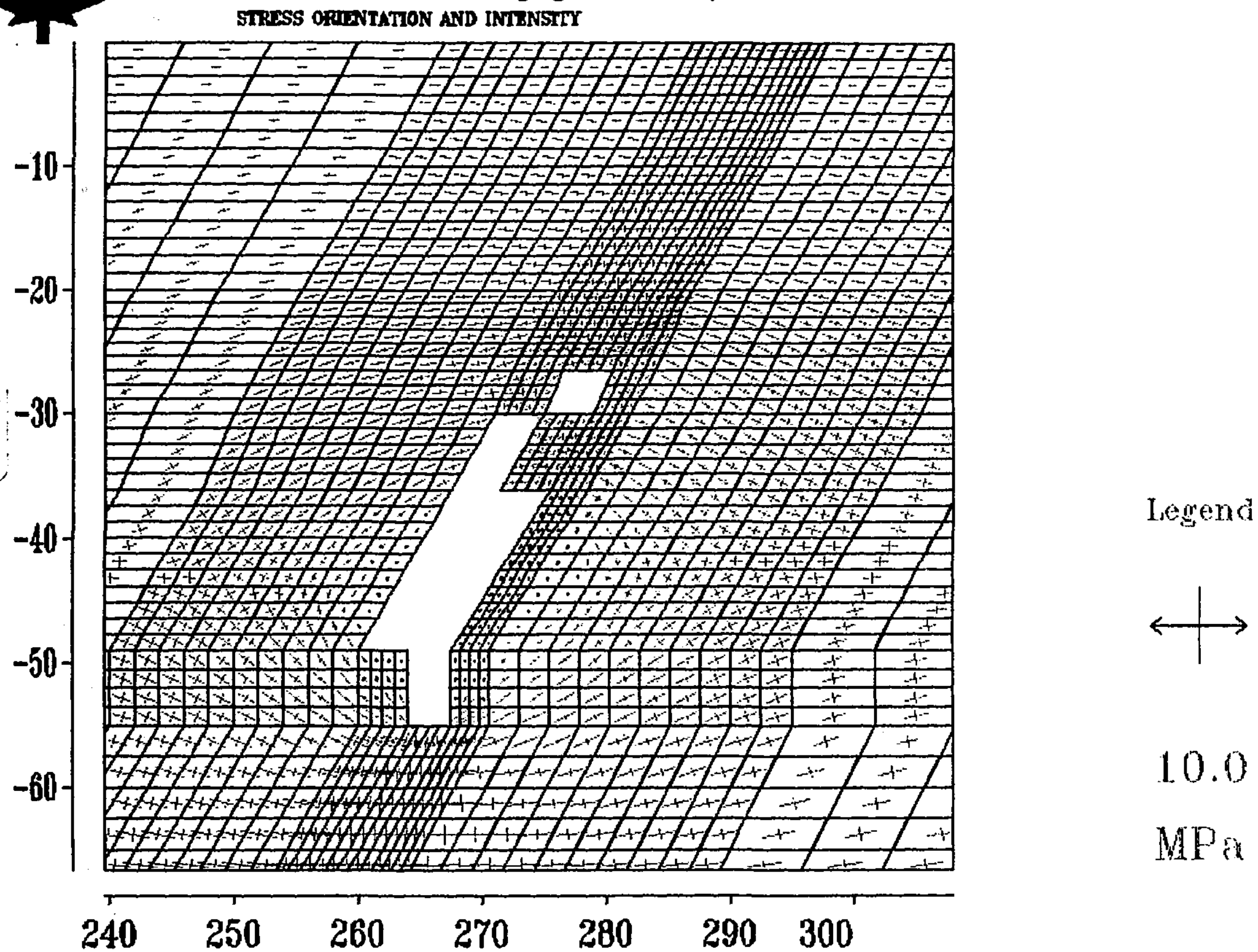

Belmoral Figure 6.52 Major principal stress levels after mining step four, hangingwall failure, Belmoral Mine.

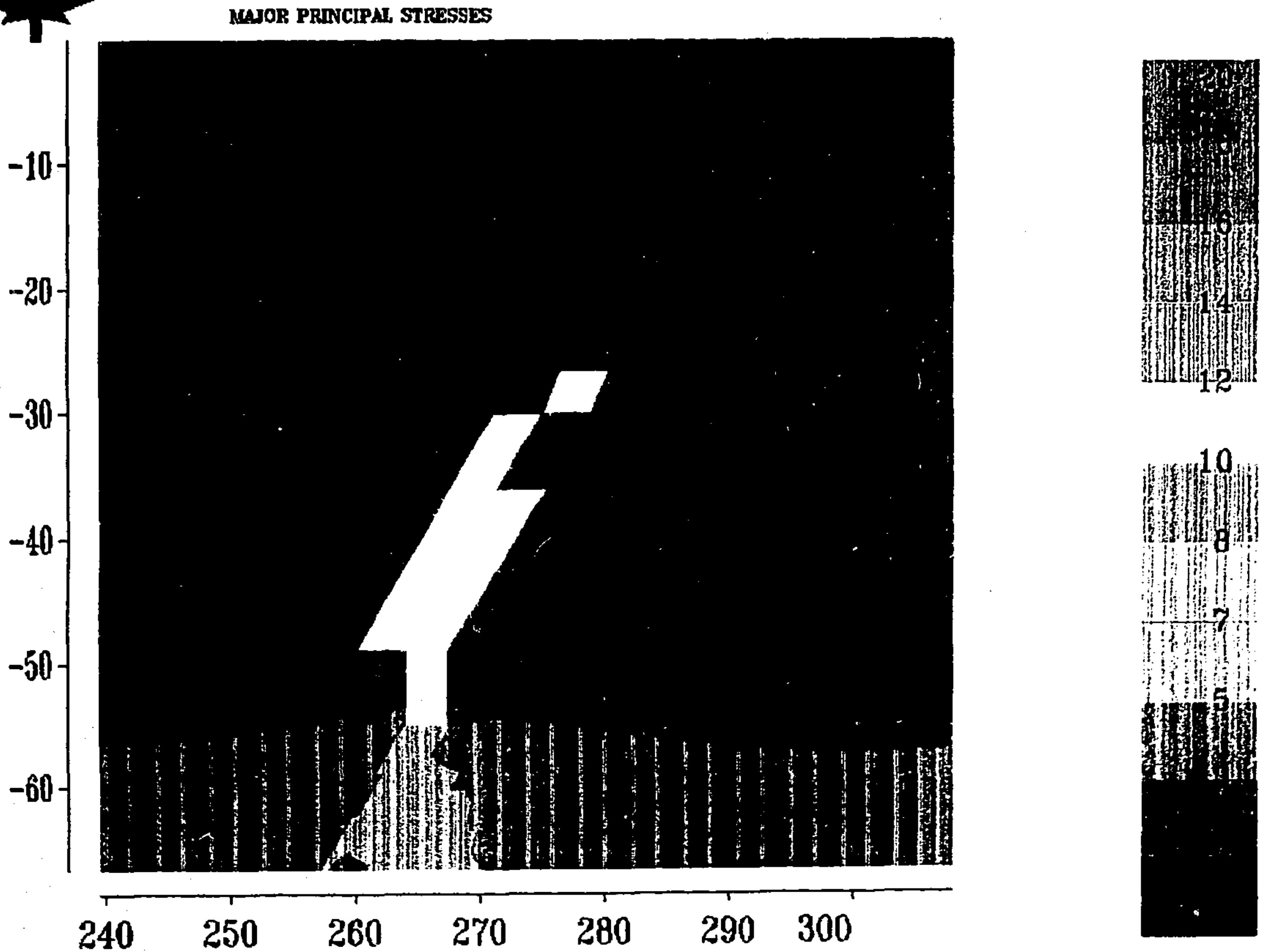

353

Belmoral

Figure 6.53 Minor principal stress levels after mining step four, hangingwall failure, Belmoral Mine.

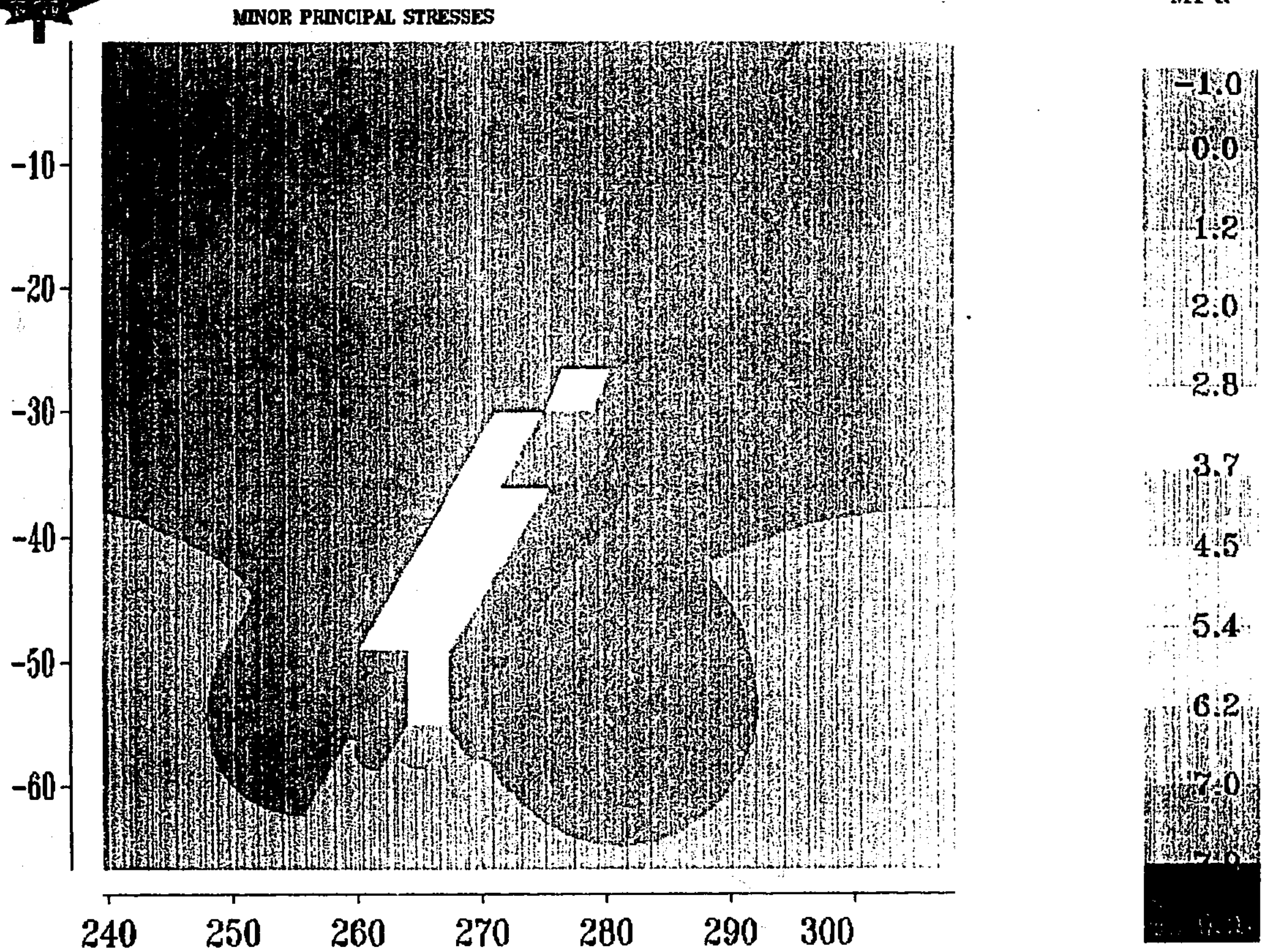

Belmoral Figure 6.54 Failed portions of the rock mass after mining step four, hangingwall failure, Belmoral Mine.

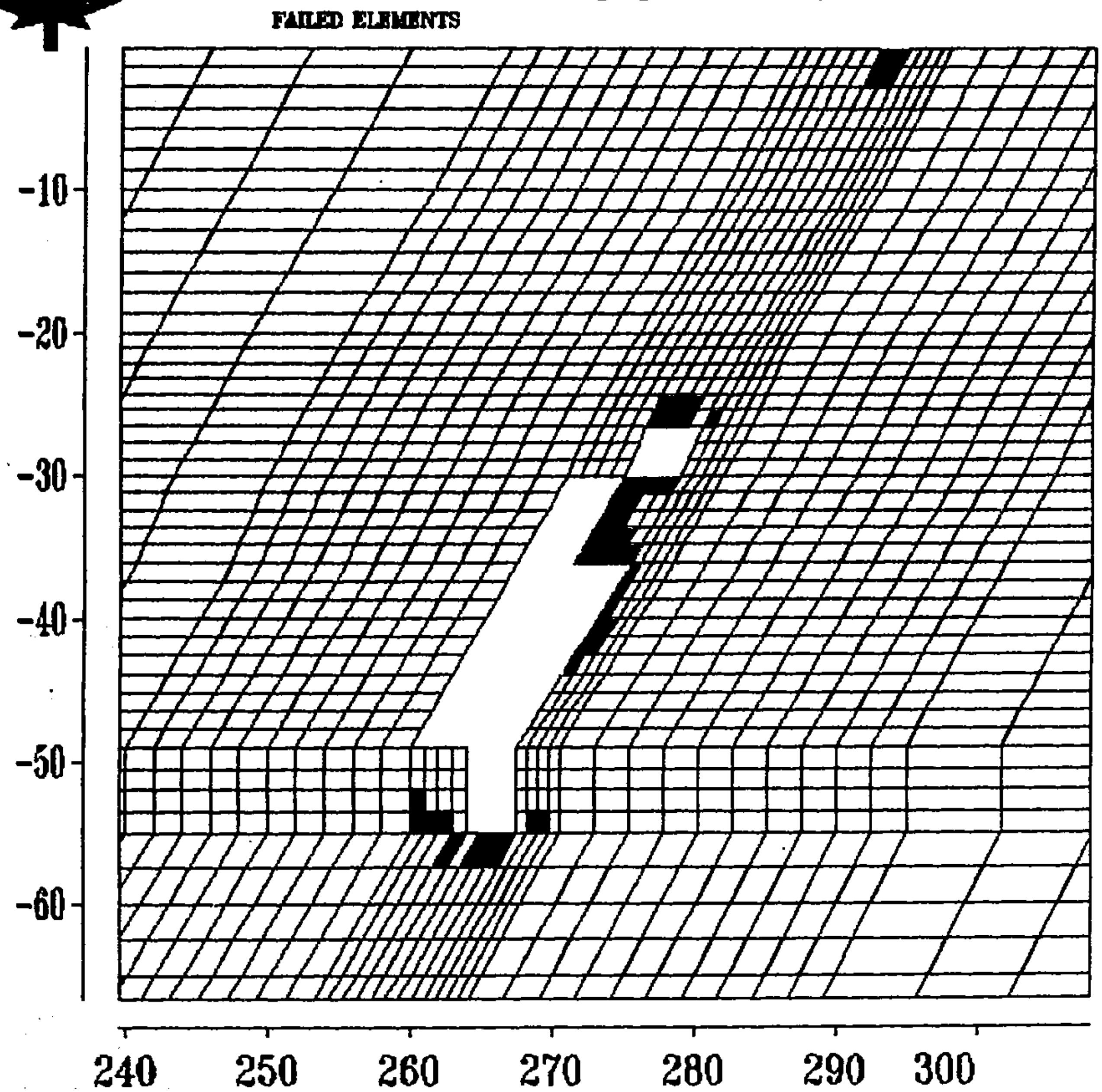

Belmoral

Figure 6.55 Rock mass displacements after mining step five, hangingwall failure, Belmoral Mine.

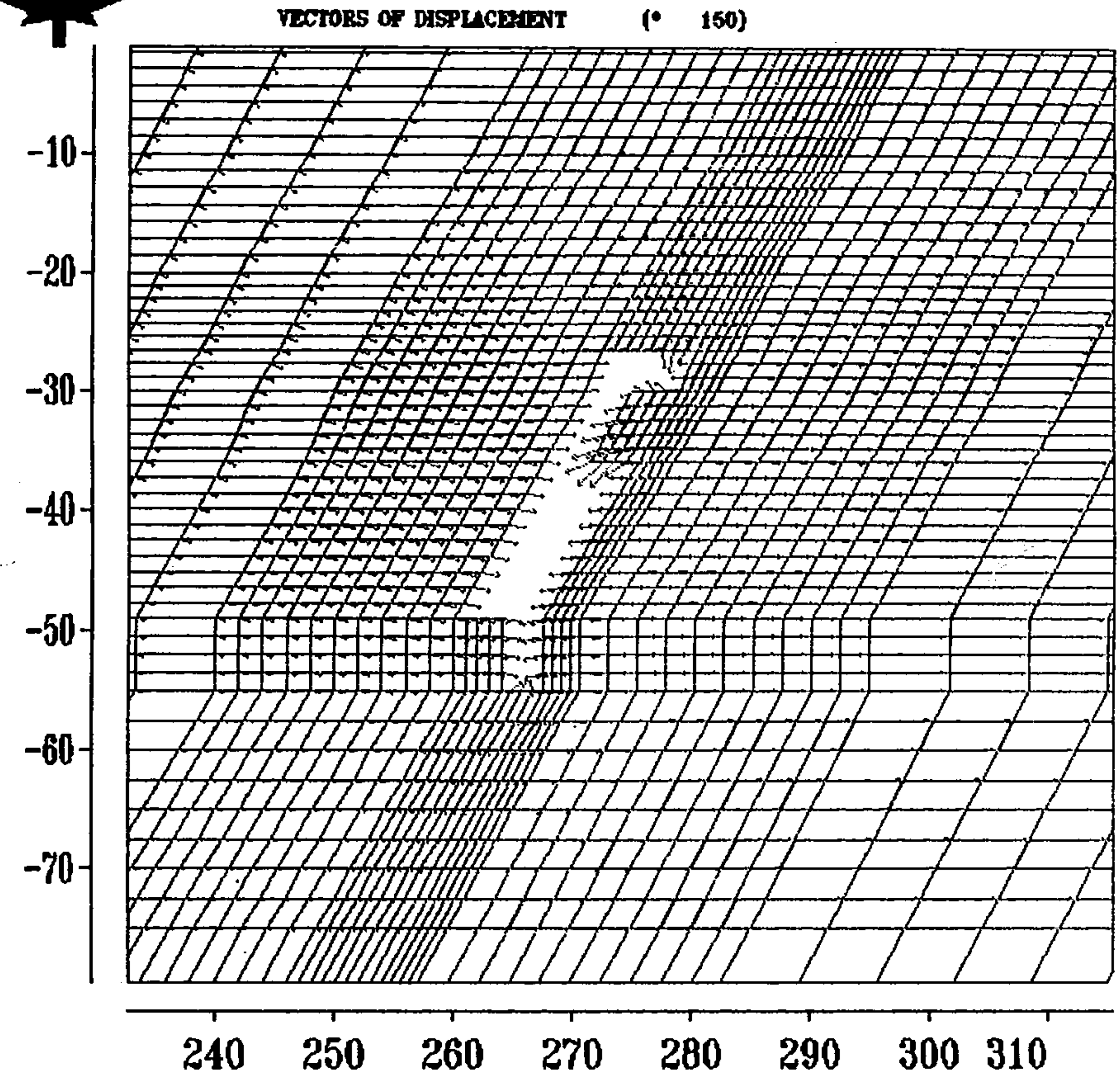

Figure 6.56 Stress orientation and intensity after mining step five, hangingwall failure, Belmoral Mine.

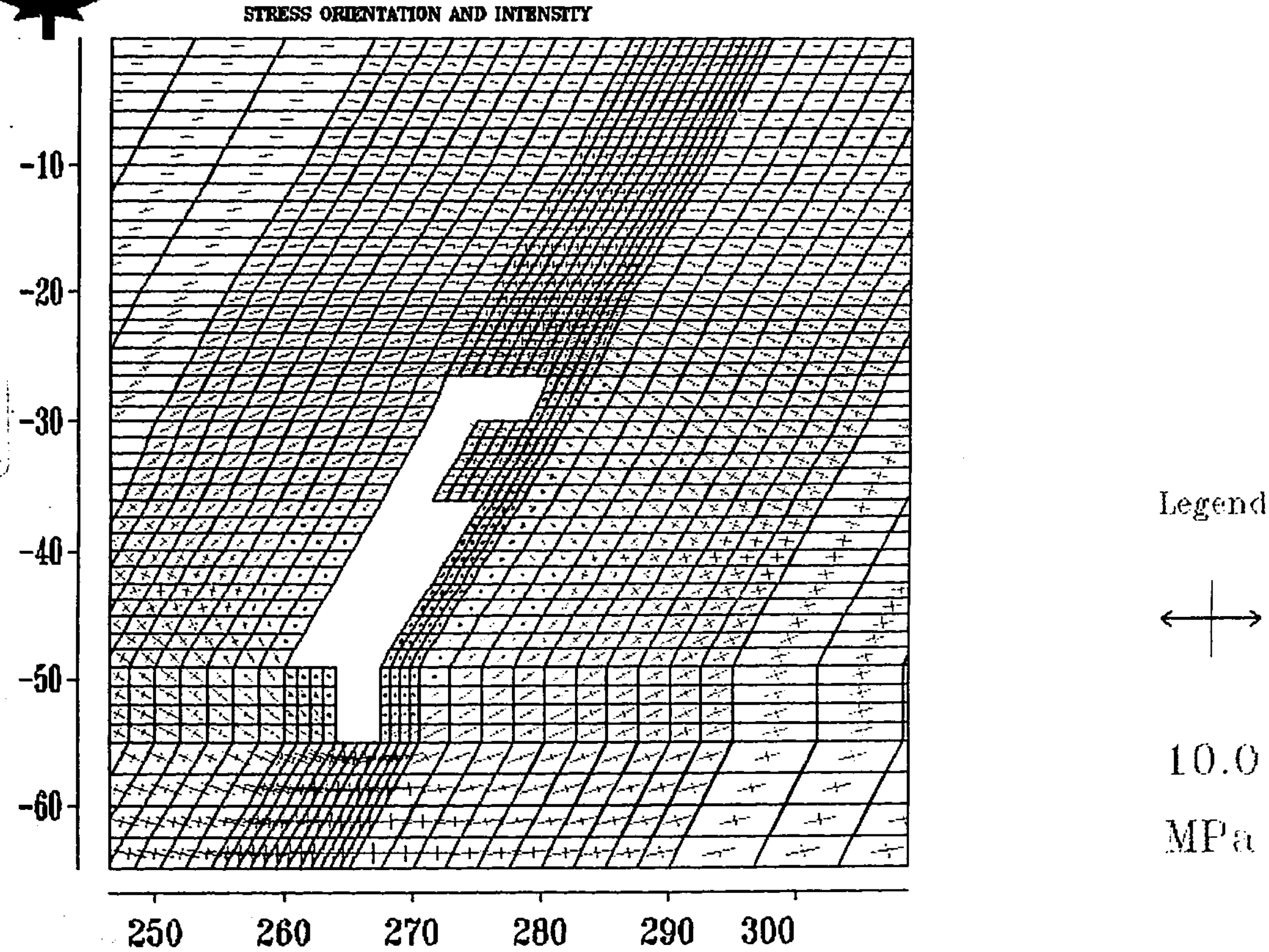

Belmoral

Figure 6.57 Major principal stress levels after mining step five, hangingwall failure, Belmoral Mine.

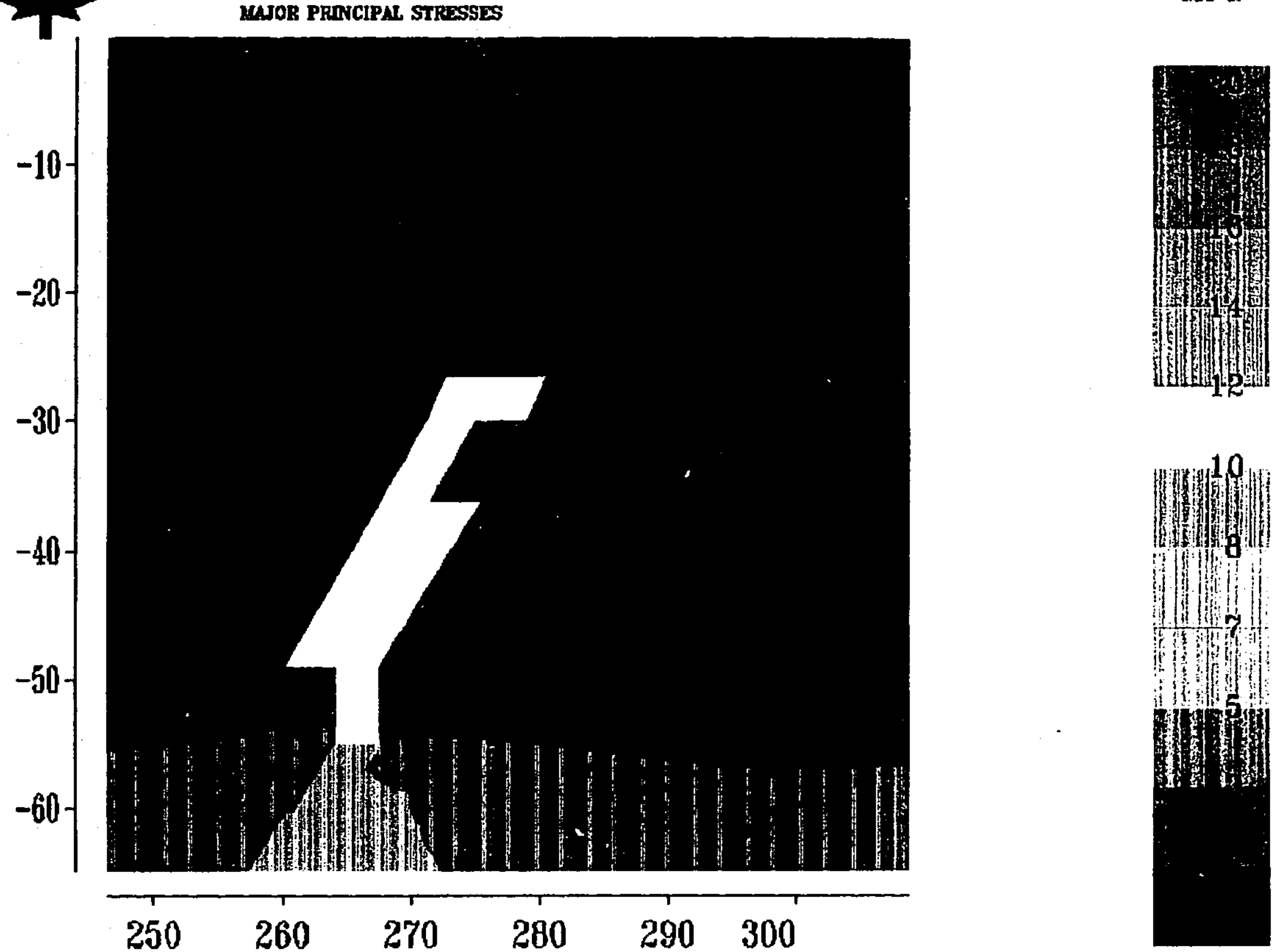

Belmoral

Figure 6.58 Minor principal stress levels after mining step five, hangingwall failure, Belmoral Mine.

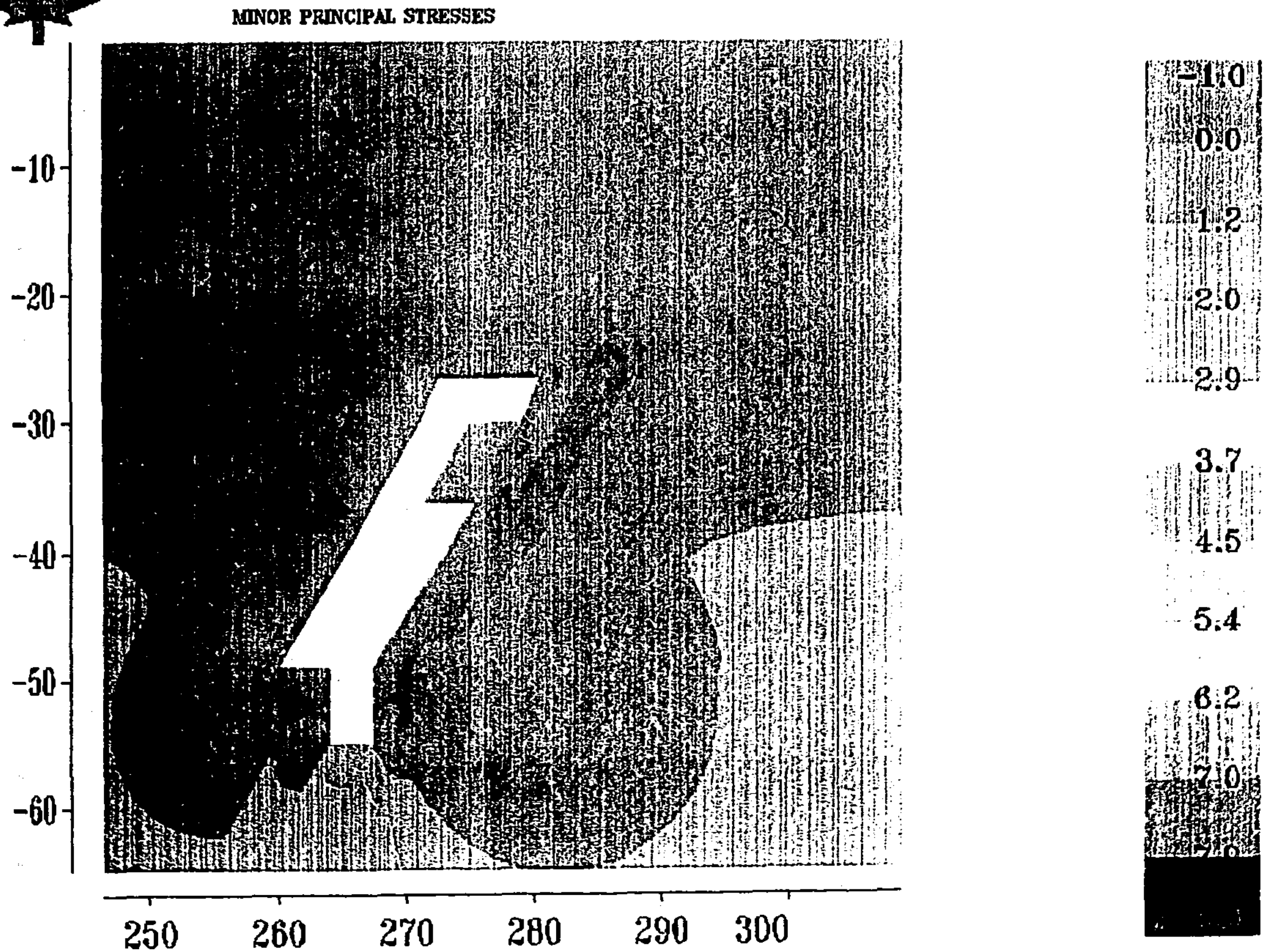

Belmoral Figure 6.59 Failed portions of the rock mass after mining step five, hangingwall failure, Belmoral Mine.

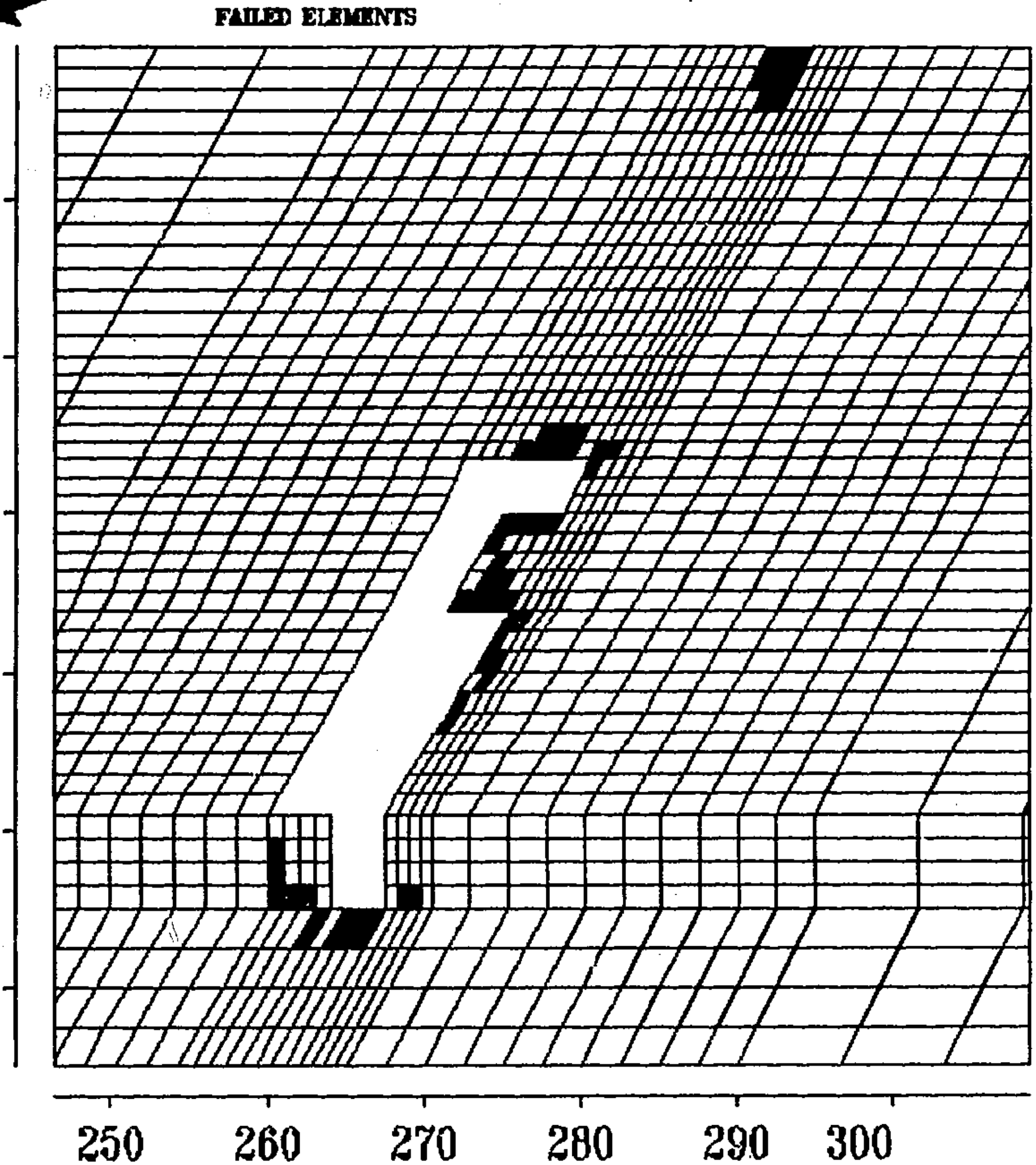

Belmoral

Figure 6.60 Rock mass displacements after mining step six, hangingwall failure, Belmoral Mine.

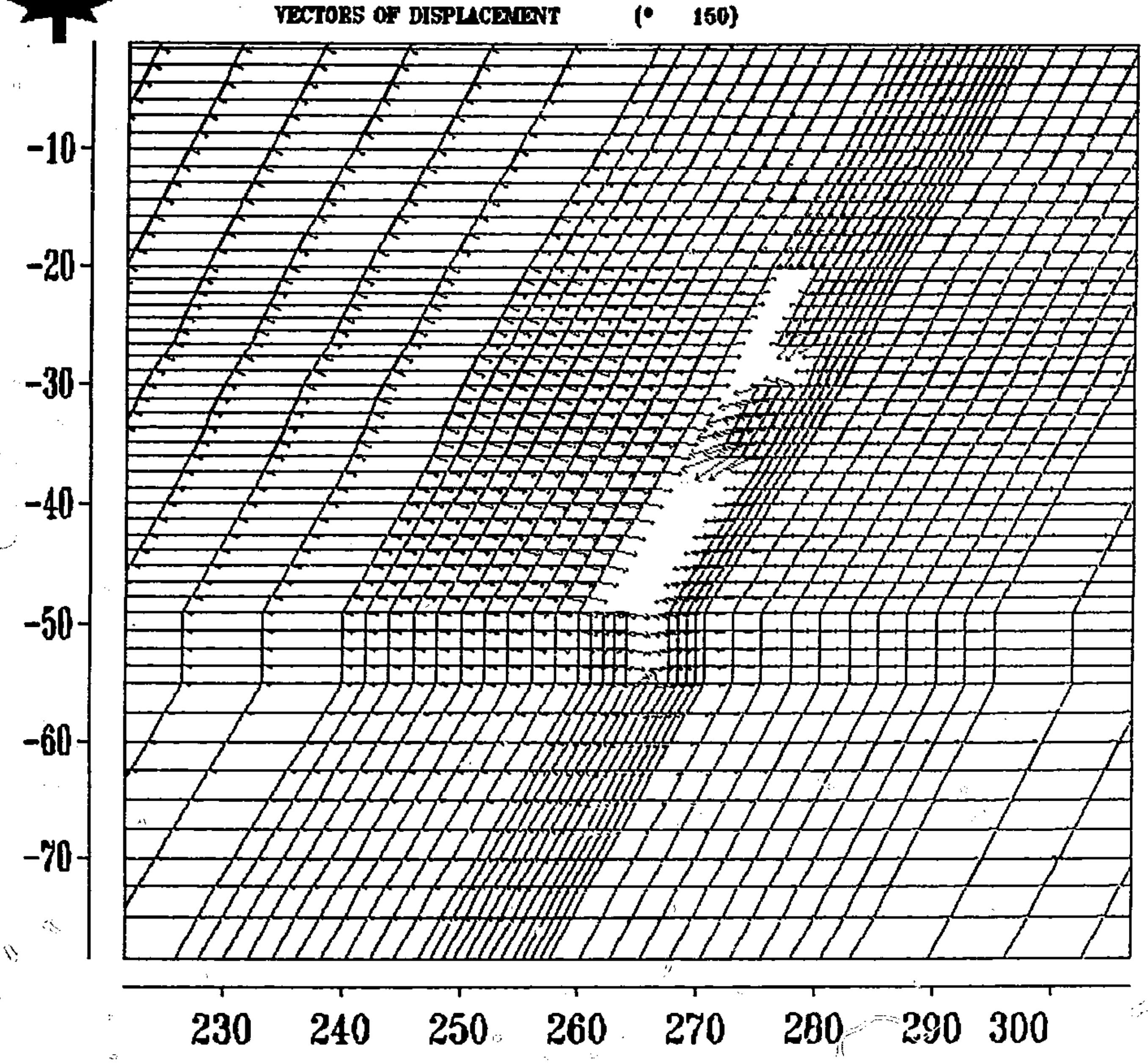

Belmoral

Figure 6.61 Stress orientation and intensity after mining step six, hangingwall failure, Belmoral Mine.

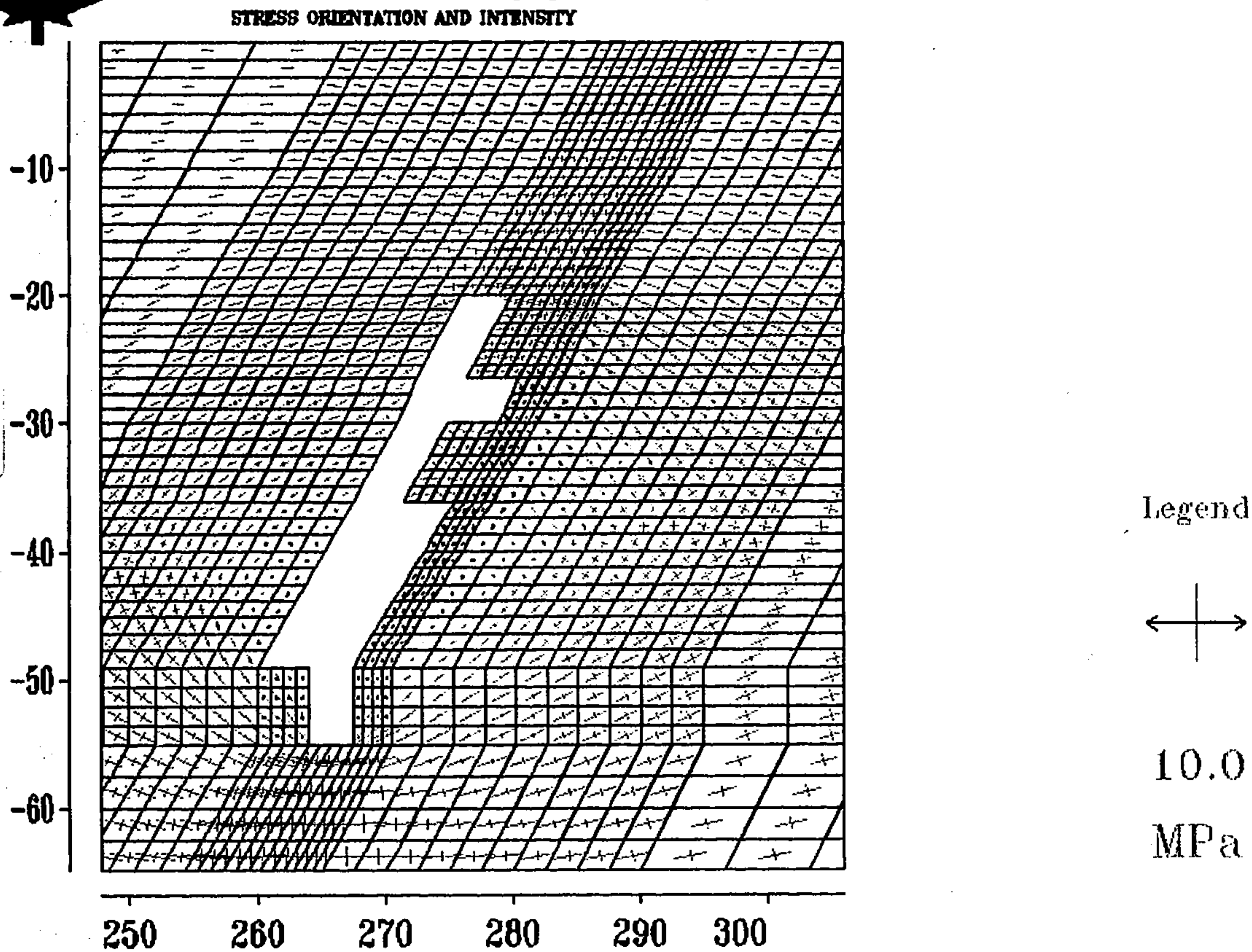

Belmoral Figure 6.62 Major principal stress levels after mining step six, hangingwall failure, Belmoral Mine.

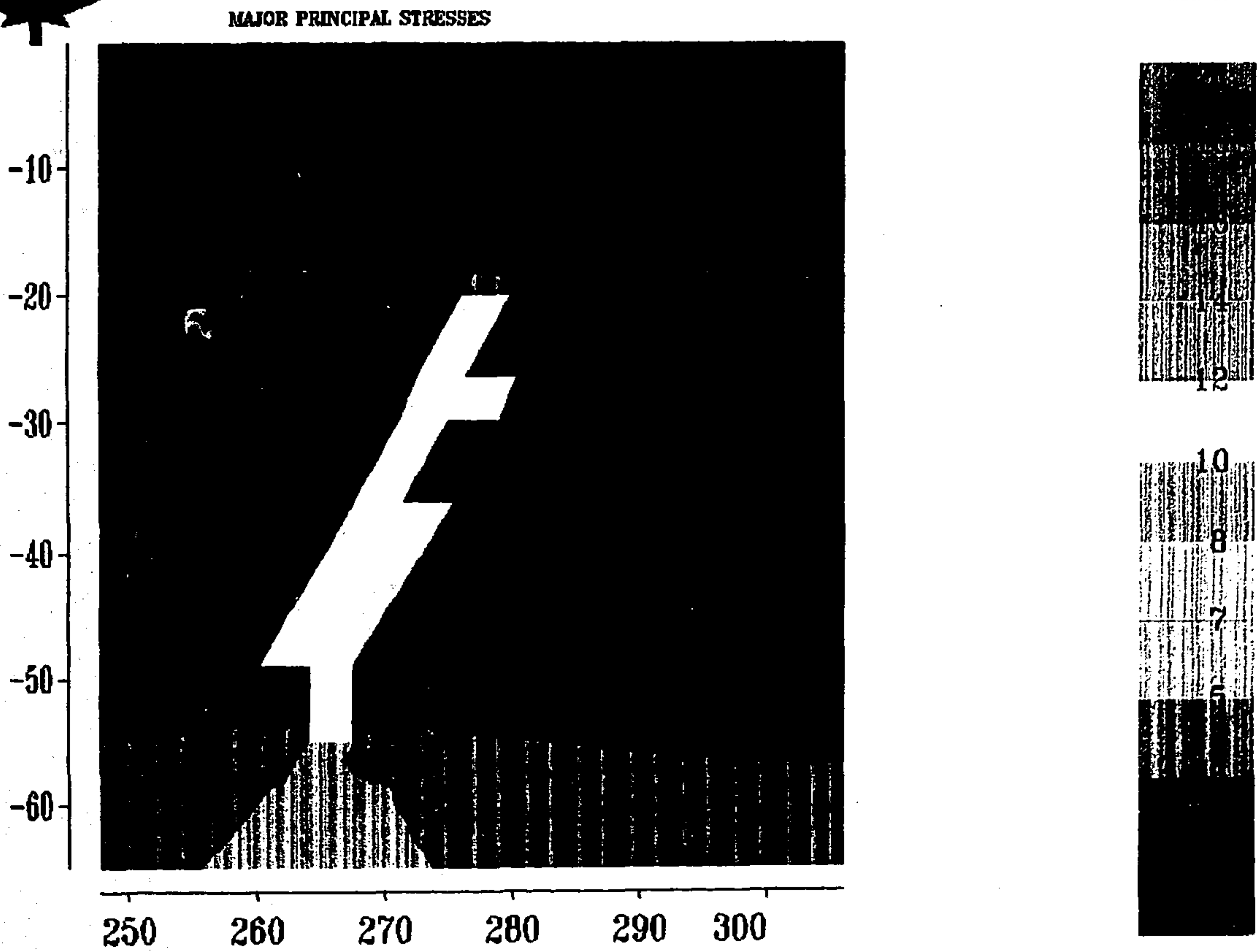

Belmoral

Figure 6.63 Minor principal stress levels after mining step six, hangingwall failure, Belmoral Mine.

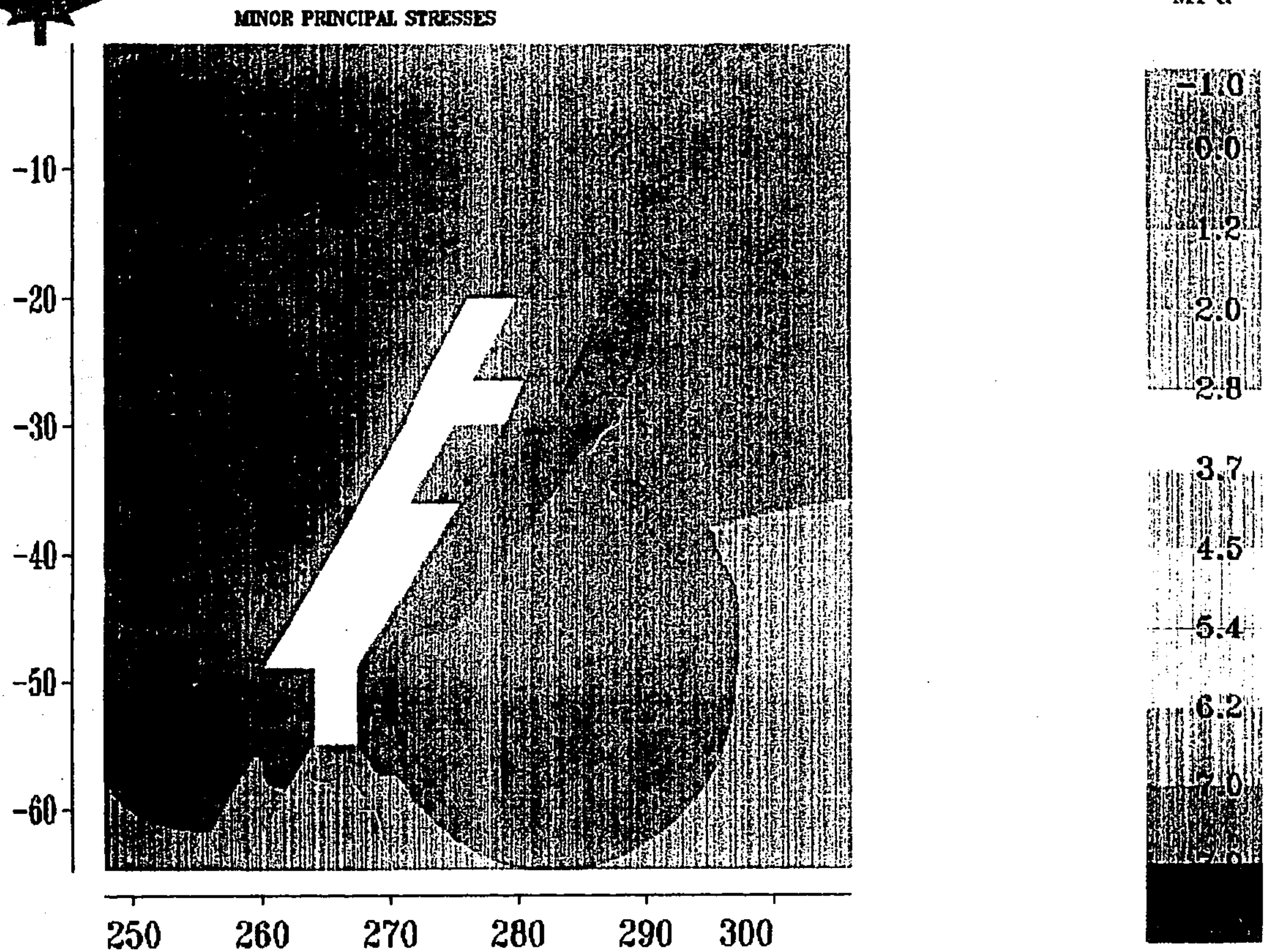

Belmoral Figure 6.64 Failed portions of the rock mass after mining step six, hangingwall failure, Belmoral Mine.

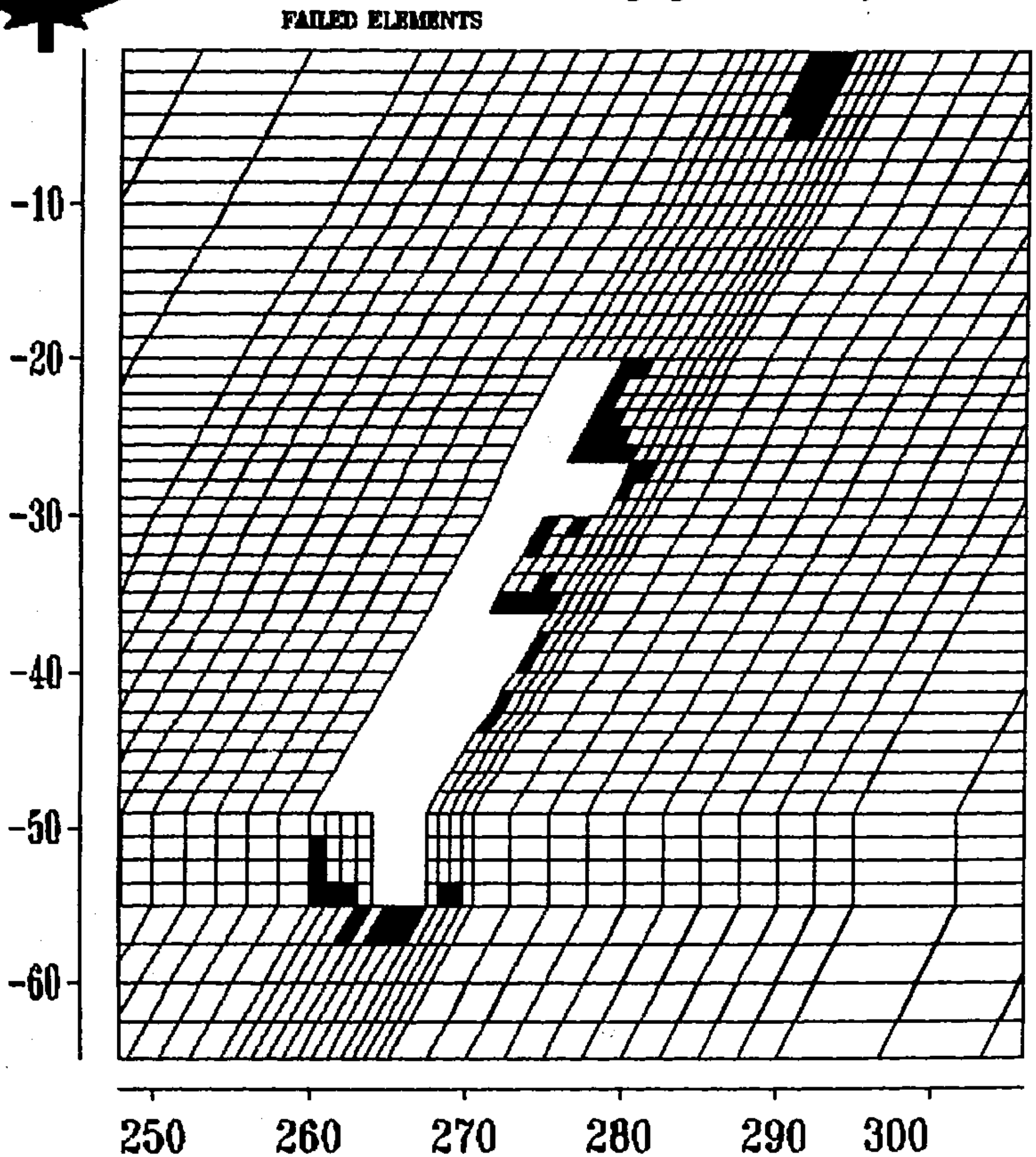

365

Belmoral Figure 6.65 Rock mass displacements after mining step seven, hangingwall failure, Belmoral Mine.

VECTORS OF DISPLACEMENT (* 150)

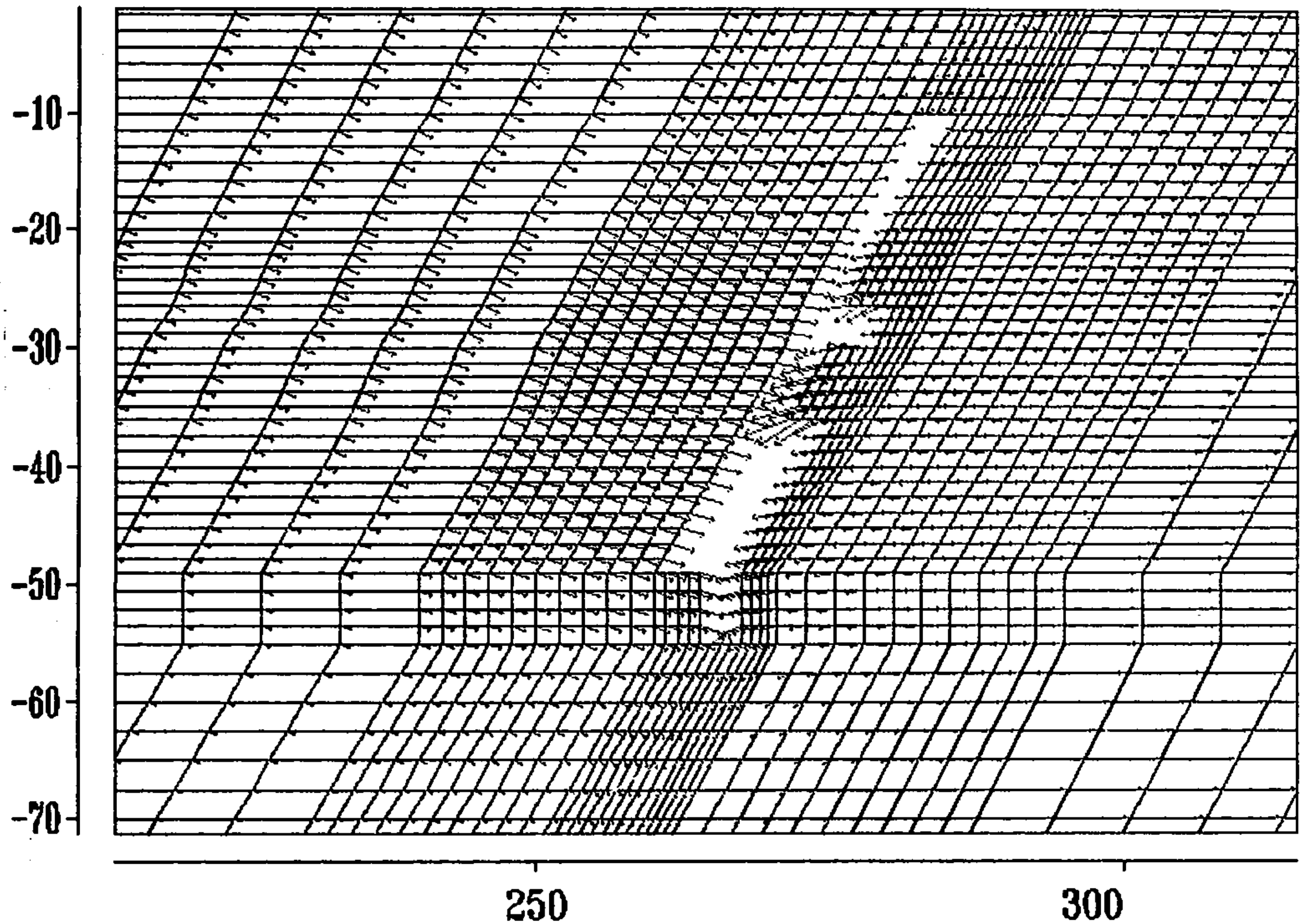

Belmoral Figure 6.66 Stress orientation and intensity after mining step seven, hangingwall failure, Belmoral Mine.

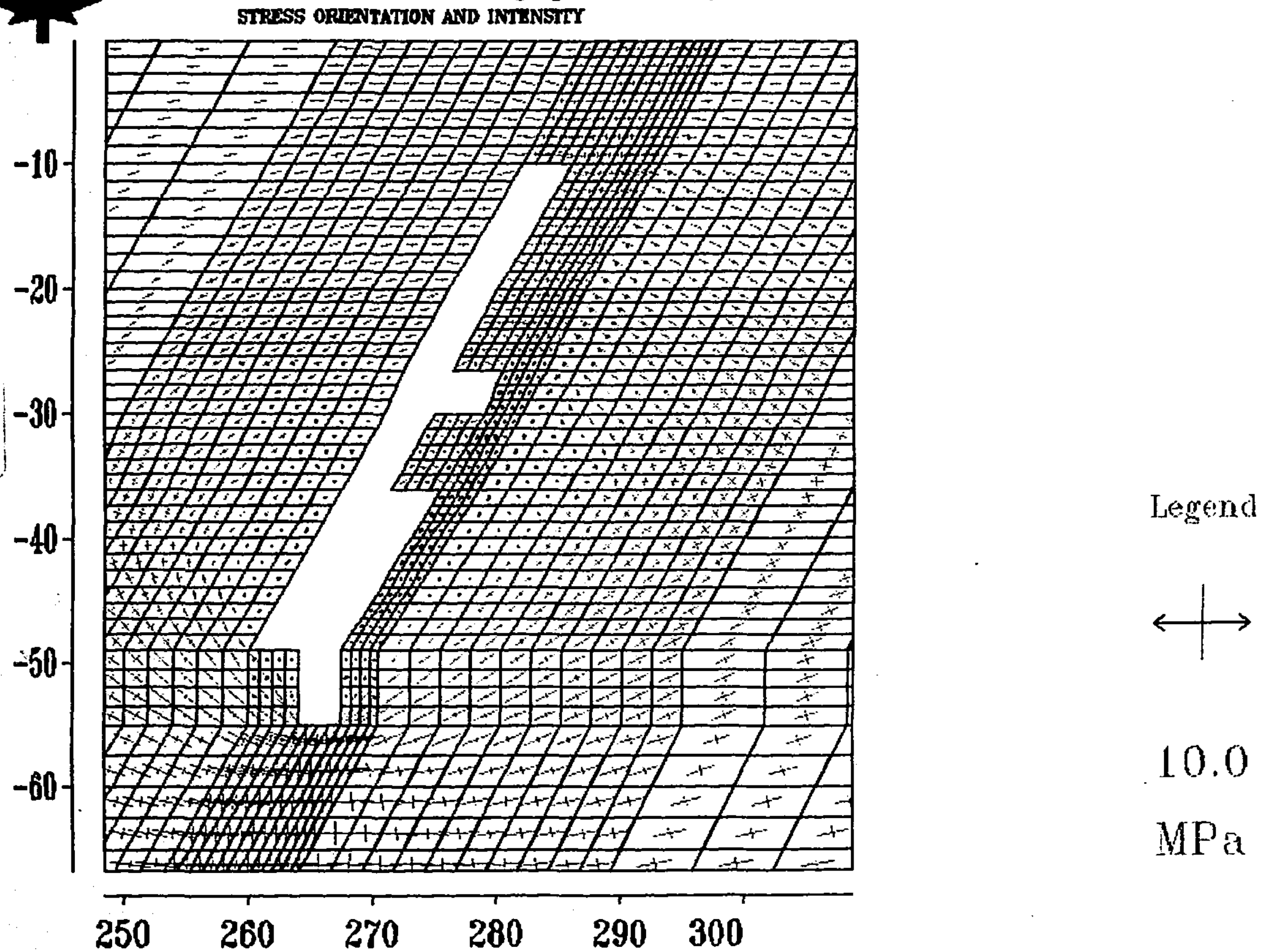

Belmoral Figure 6.67 Major principal stress levels after mining step seven, hangingwall failure, Belmoral Mine.

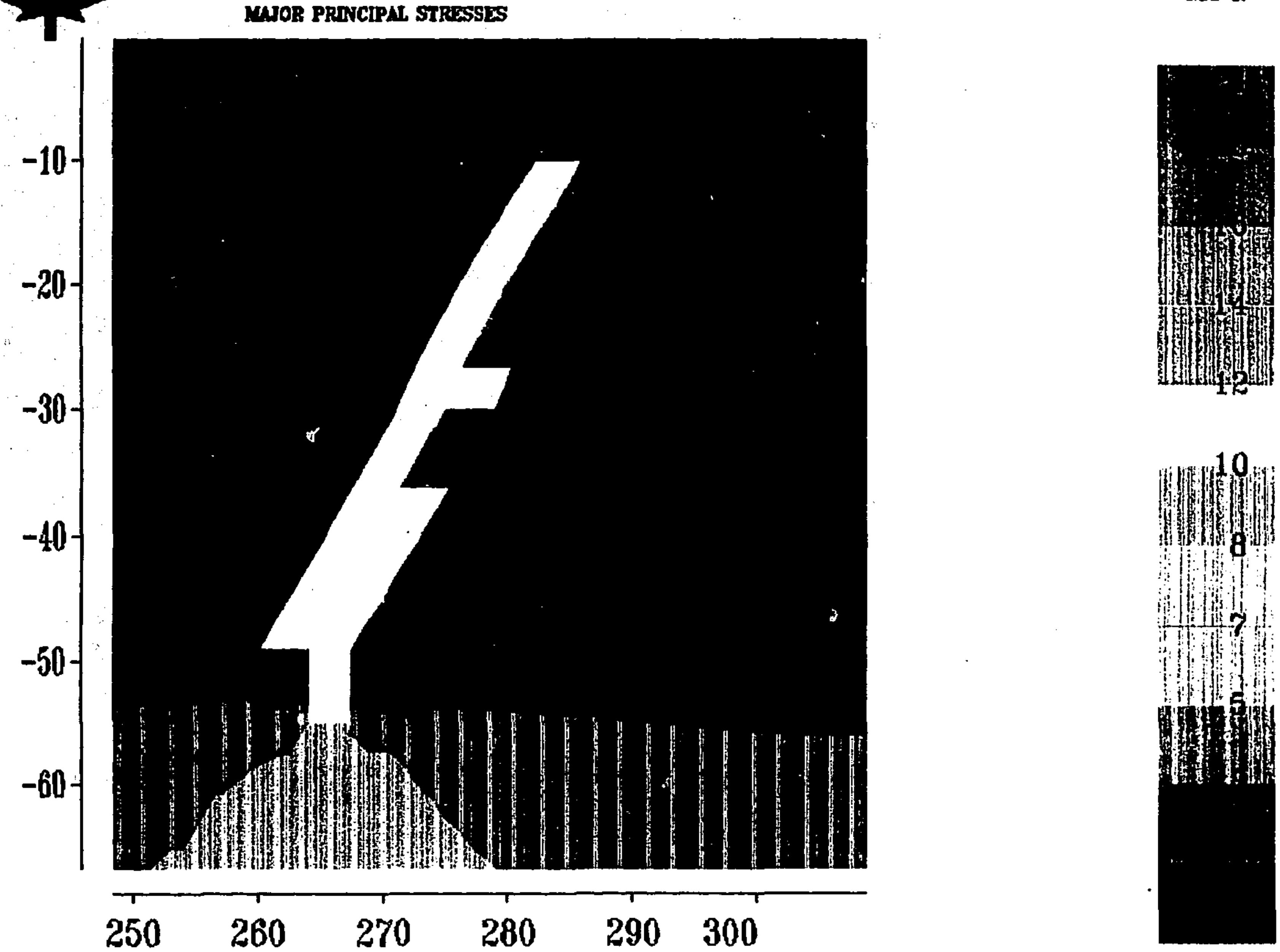

368

Belmoral

Figure 6.68 Minor principal stress levels after mining step seven, hangingwall failure, Belmoral Mine.

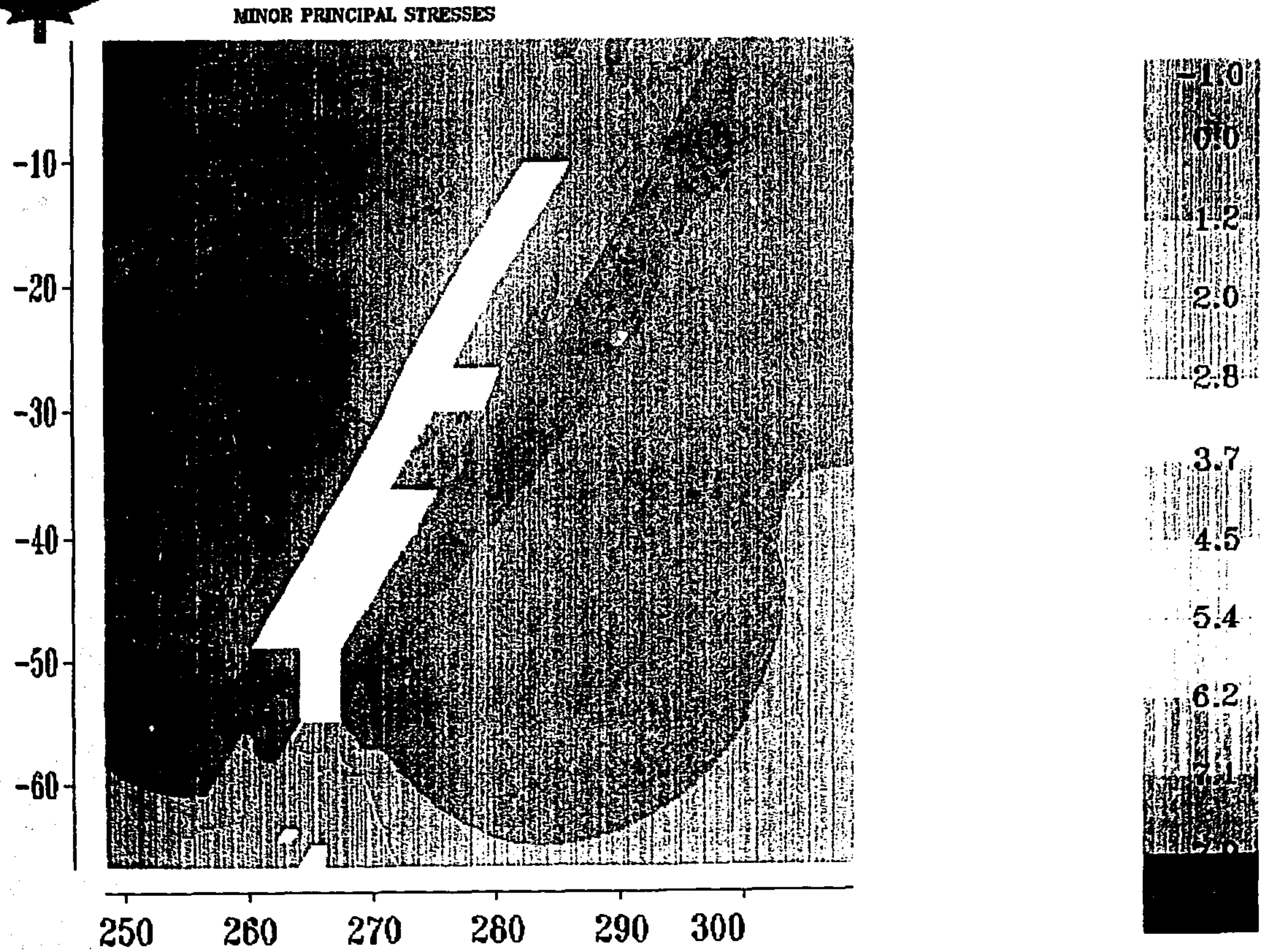

Belmoral Figure 6.69 Failed portions of the rock mass after mining step seven, hangingwall failure, Belmoral Mine.

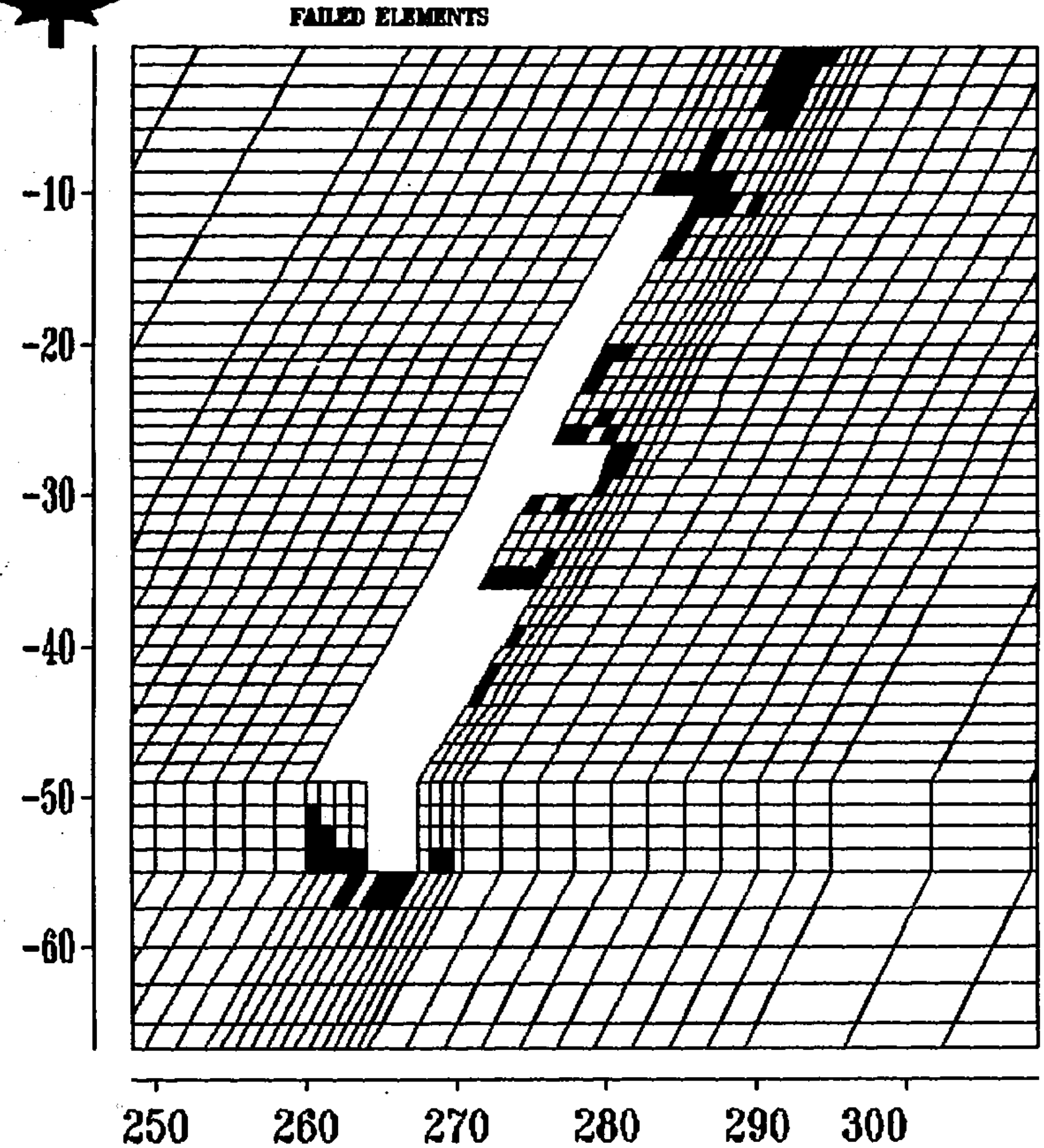

Belmoral

Figure 6.70 Rock mass displacements after mining step eight, hangingwall failure, Belmoral Mine.

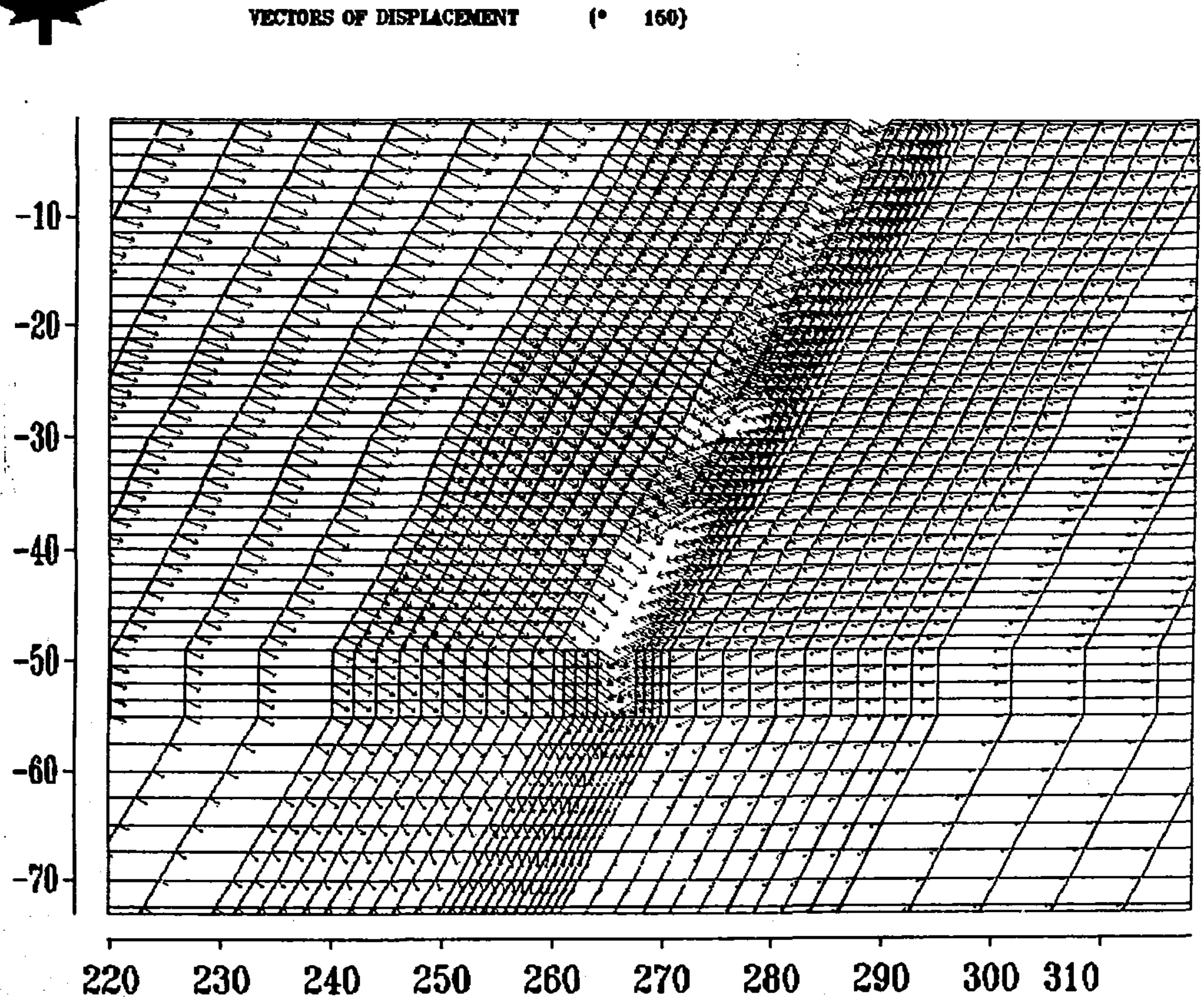

Belmoral Figure 6.71 Stress orientation and intensity after mining step eight, hangingwall failure, Belmoral Mine.

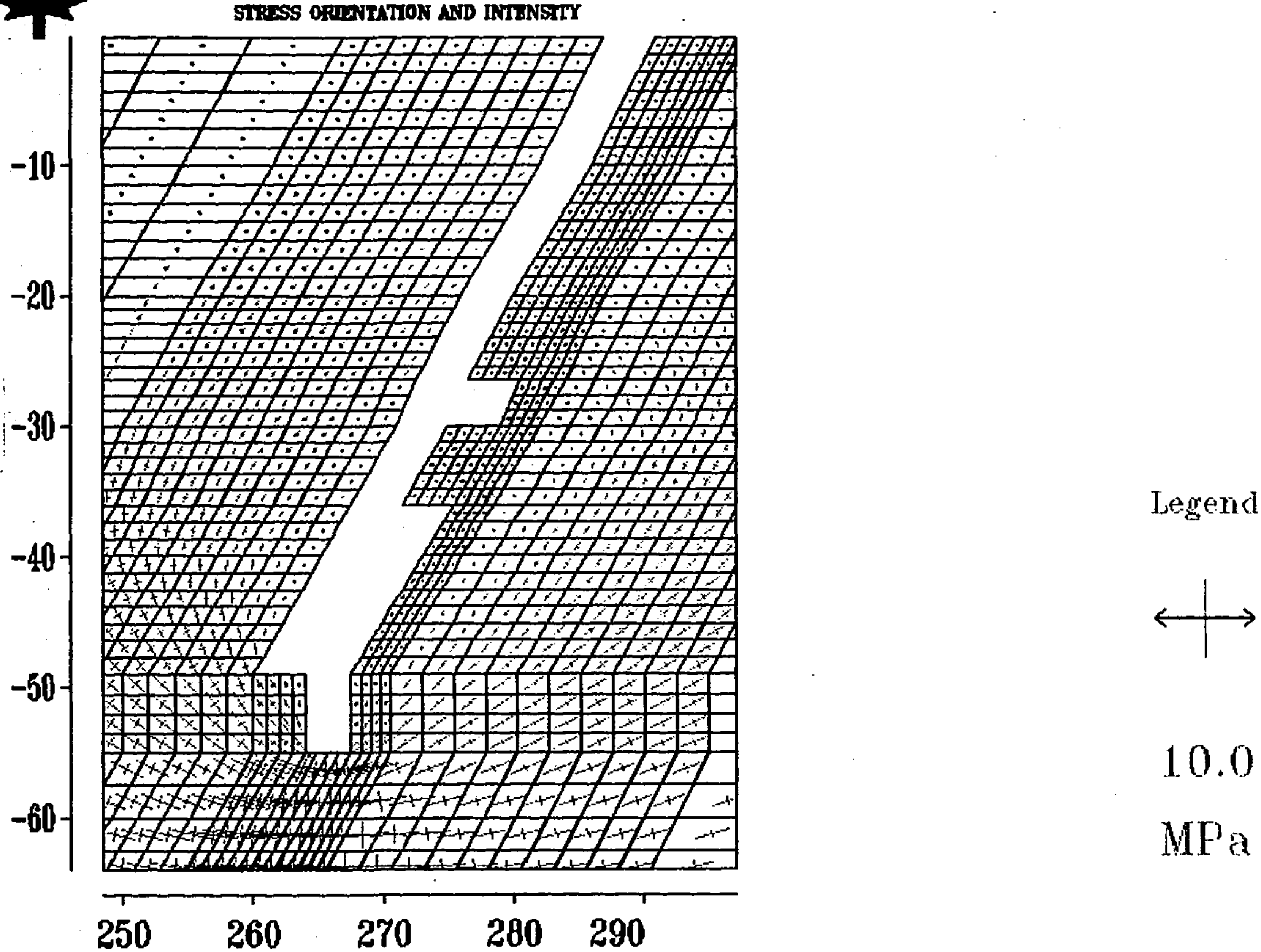

Belmoral Figure 6.72 Major principal stress levels after mining step eight, hangingwall failure, Belmoral Mine.

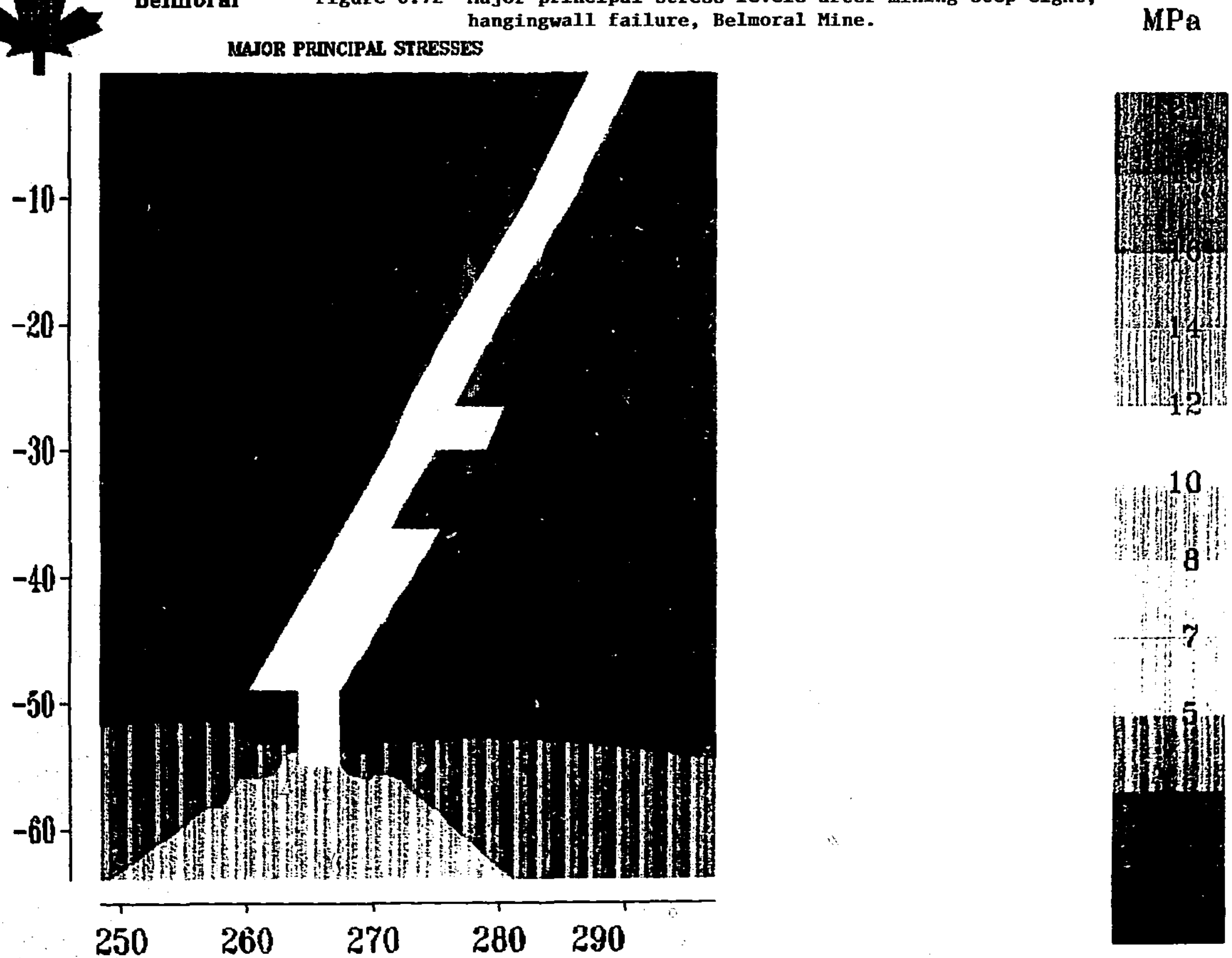

Belmoral

Figure 6.73 Minor principal stress levels after mining step eight, hangingwall failure, Belmoral Mine.

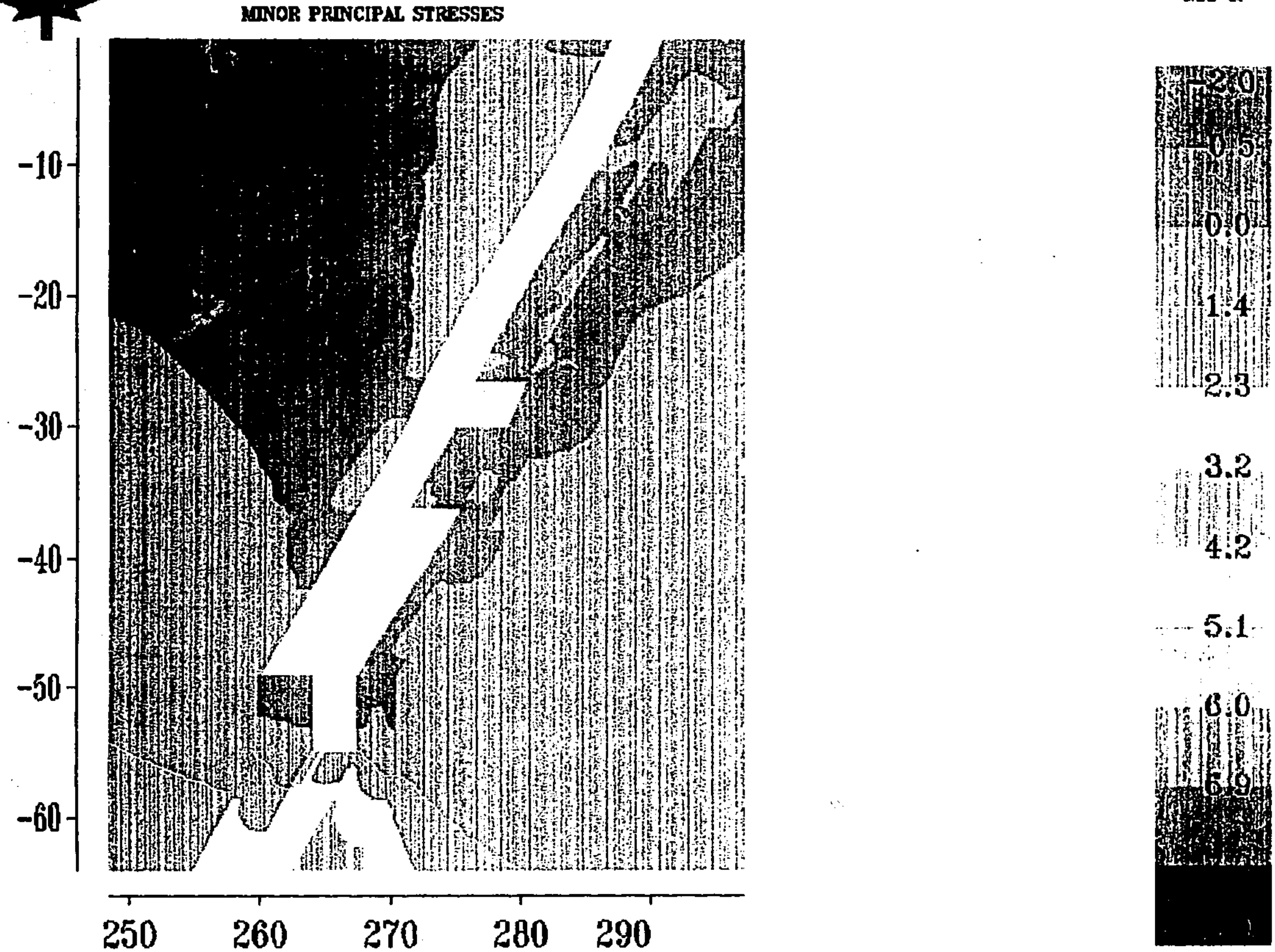

Belmoral Figure 6.74 Failed portions of the rock mass after mining step eight, hangingwall failure, Belmoral Mine.

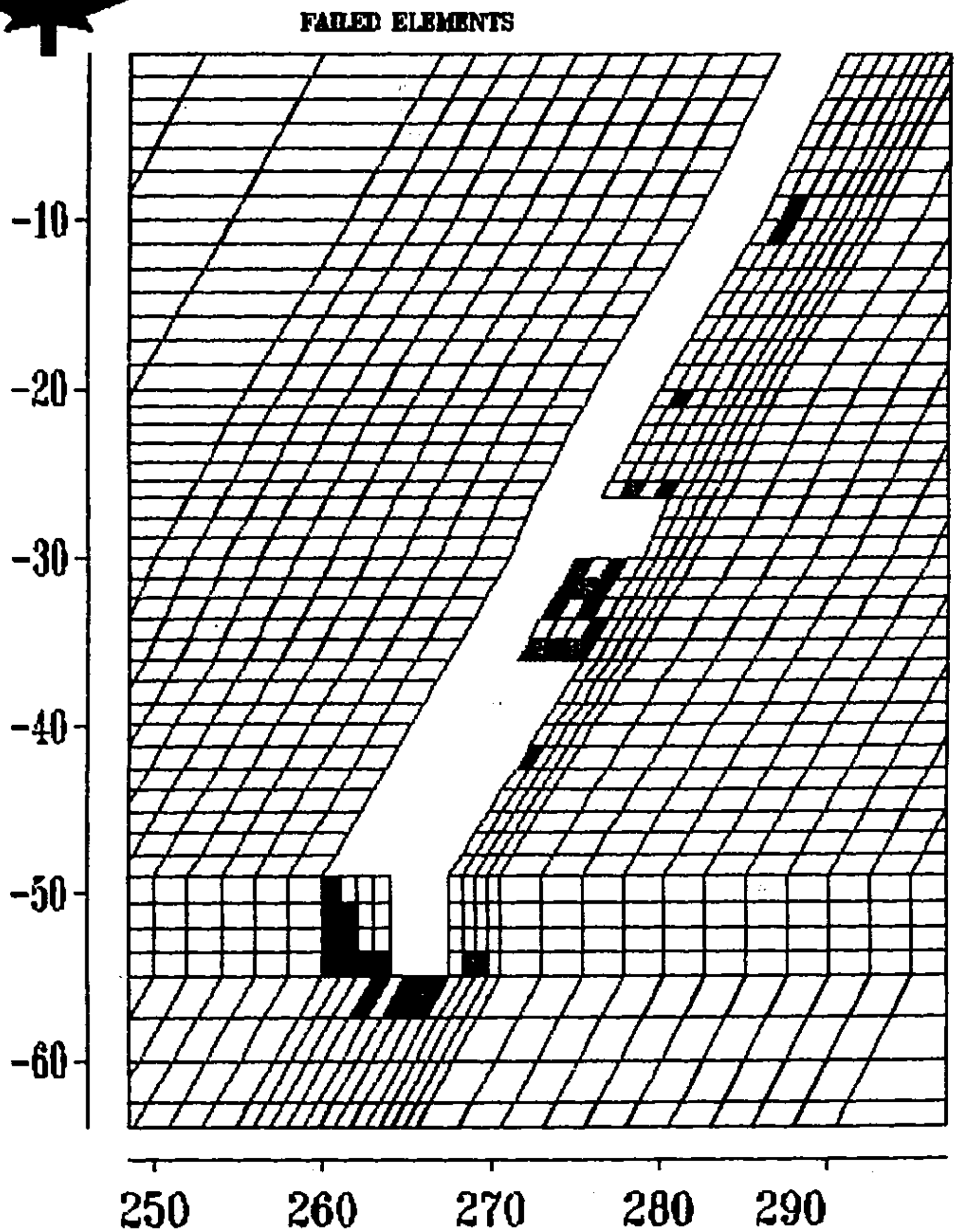

failure.

The creation of 1-7 exploration drift has imposed higher stresses in the crown above 2-7, leading to an increase in failed elements in the schist crown, Figure 6.21. Failed elements from compression are now registered in the lower stope hangingwall, but the tensile stresses remain small in the rest of the hangingwall and no failures are registered.

Most of the elements in the schist around drift 1-7 have failed, to a depth of 2.4 m. The schist between 2-7 and 1-7 has failed over 55% of its area, Figure 6.24.

Removal of the sill pillar in the third mining step has increased the number of elements failed above and around the crown of the old 1-7 drift, Figures 6.24 and 6.29. Compressive stresses there have increased to 5.0 MPa. The trend to increase the depth of the failed elements in the footwall and lower hangingwall with a larger opening has continued. The tensile stresses are distributed much deeper into the far field granodiorite hangingwall and over the entire height of the footwall altered granodiorite.

With subsequent and progressive removal of schist from the crown, compressive stresses remain constant or reduce somewhat in the crown. This then limits the extent of the failed elements to less than 2.4 m, Figures 6.24, 6.29, 6.34 and 6.39.

The tensile stresses expand deeper into the hangingwall and footwall, but are sufficiently low not to cause failure of the hangingwall altered granodiorite. Failure of elements in the footwall altered granodiorite does increase.

In the second modelling sequence, the development of ravelling within the hangingwall is represented by mining steps which progressively expand to the surface, after stope 2-7 and drift 1-7 have been created.

Removal of the altered granodiorite from the 2-7 hangingwall does not provoke any increase in tensile stress that existed in the original 2-7 footwall and far-field hangingwall, Figures 6.21 and 6.46. Compressive stresses in the 2-7 crown also remain at the same levels and the newly formed altered granodiorite portion of the crown is mainly in compression. The compression is sufficient to fail elements in the schist to a depth in the crown of 2.4 m, Figure 6.49. Removing the immediate 2-7 hangingwall increases the number of failed elements in the schist between 2-7 and 1-7.

The subsequent and progressive removal of the altered granodiorite to surface (mining steps 4 to 8) progressively increases the tensile stress zone in the far-field hangingwall granodiorite and in the immediate footwall granodiorite, Figures 6.51, 6.56, 6.61 and 6.66. This increase is not sufficient to cause expansion of failure areas in the hangingwall or footwall.

The crown of drift 1-7 remains fully in compression, at similar values. The crown in the hangingwall remains in compression, increasing only moderately, with each step. The mining steps between removal of the 2-7 hangingwall altered granodiorite and the penultimate mining step do not impose compressive stresses sufficient to exceed altered granodiorite hangingwall crown strength nor impose tensile stresses.

6.6 APPLICATION OF ANALYTICAL EQUATIONS

The testimony of consultants and mine personnel given at the inquiry into the Belmoral shallow stope failure point to a failure by ravelling of the hangingwall or the chimneying disintegration of the schist ore zone. These will be examined as well as the possibility of block caving and stabilization.

As the rock mass is not stratified into distinct strata, nor the weak schist ore zone composed of massive material or capable of moving as a plug on well-defined discontinuities, these will not be examined as potential failures.

6.6.1 Ravelling Failures

As per the hangingwall ravelling theory, the sequence of failure begins with the immediate 2-7 hangingwall followed by the progression of ravelling in the crown of this newly created cavity, Figure 6.13.

From the information in Table 6.1, the geometry of the ravelling blocks is as follows. The two principal families, along with one or more of the random sets that could provide block sides parallel to the plane of the analysis, would form the blocks that could ravel into the stope. The angles of joint families S36W 70NW and N12E 44SE that are made in a direction orthogonal to the orientation of the hangingwall are obtained by using stereographic nets. The former makes an angle 45° dipping NW, the latter one 45° dipping SE.

A joint spacing of 50 cm will be used as a worse case (heavier block) situation.

Barton [11] suggests using a low friction angle value (8° to 16°) for low friction coatings such as chlorite which cover the Belmoral joint surfaces. Given that the joint surfaces are undulating and slightly rough the higher value, 16°, will be used.

The initial block slides from the hangingwall require a minimum of 0.04 MPa compressive tangential stress, Appendix 4, to be prevented.

Modelling has shown that tensile tangential stresses exist at the lower portion of the hangingwall when stope 2-7 is created. More elements become in tension with the creation of drift 1-7. The conditions for hangingwall ravelling (blocks sliding out) to begin therefore exist.

Appendix 4 also indicates that once a cavity in the hangingwall has been initiated by blocks sliding out, blocks in the new cavity crown can fall because they cannot be stabilized by compressive tangential stress. Block falls are therefore expected from lack of effective clamping. As pointed out in Chapter 2, block slides would be necessary in the new cavity crown to continue the ravelling. Because compressive stresses are found in the crown of this cavity during hangingwall mining steps (4-7), and these are greater than the minimum 0.04 MPa required to prevent block slides, it is possible that under this sequence, hangingwall ravelling stopped long before surface was reached. The depth at which ravelling from block falls was expected to stop is at a distance of 1.8 m above the level of the opened hangingwall.

If, however, failure progresses first by chimneying disintegration in the schist ore zone, then block slides from the hangingwall can continue up to but not above the level of the highest opening in the schist.

6.6.2 Chimneying Disintegration Failure

The development of chimneying disintegration in the schist must take into consideration that a vertical path is not possible since the dipping altered and the unaltered granodiorite hangingwall lie in the path of such a development.

A prior example of a dipping, weak orebody surrounded by competent walls situation [18] was encountered with chimneying failures within the Selbaie Mine altered surface crown pillar where only one arc of the rupture line developed progressively to surface, Figure 2.19. This was demonstrated by physical, numerical modelling and field observations.

Therefore, the single rupture line arc analysis can be performed as a means to evaluate the schist zone failure scenario.

Appendix 4 indicates that for the approximate rock mass c_m and ϕ values calculated, a factor of safety of 0.98 exists against chimneying. The c_m and ϕ values reflect peak rock mass strength. A lower factor of safety would be obtained for a failed, residual strength rock mass, predicted by the numerical modelling.

Although the analytical approach for arching in caving stopes is based on cohesionless material, it should provide a conservative estimate of arching within this cohesive schist. Only bulk failure ($F_s = 0.8$) would be expected within a block caving of this schist.

6.7 APPLICATION OF EMPIRICAL METHODS

Application of empirical methods in the Belmoral case will be a good indication of their effectiveness as this is a known case of failure.

The schist is qualified as "extremely poor" rock in the NGI rating system, because of its Q = 0.01 rating. This plots well into the required support zone. The surface crown pillar chart, Figure 1.15, indicates that a Q of 0.01 returns $C_s = 0.45$ which calculates the pillar thickness at a minimum of 226 m for the 3.8 m stope span.

6.8 SUMMARY

Conditions existing at the Belmoral Mine at the time of the 1980 shallow stope failure provide sufficient information to back analyse mine stability conditions and make evaluations of stability. Quantification of geomechanical parameters through field and lab work complemented the description of the event leading to failure.

Numerical modelling, analytical equations and empirical methods indicate that failure around the Belmoral 2-7 stope was expected. However, only the analytical equations using as input numerical modelling stress data indicated how the failure to surface most likely happened.

Numerical modelling has indicated that stresses remain compressive in the schist surface crown pillar, and that the hangingwall is subjected to tensile stresses. Modelling only provides a limited view of the failure that occurred in that it fails to indicate the ultimate extent of the failure as it developed. Mining steps to remove the failed elements had to be carried out. Potential hangingwall ravelling was not indicated with this continuum code. Modelling established that at no time were tensile stresses imposed to the schist surface crown pillar and that compressive stresses were sufficient to exceed the strength of this weak material. It also indicated that as the opening was enlarged vertically in the schist, towards surface, tensile tangential stresses also moved up at the hangingwall periphery.

Analytical equations provided estimates of stability which were very representative of known or suspected failure events. This was the case for chimneying of the schist zone and ravelling of the hangingwall. In the case of the former, representative intact rock mass parameters were used. Using lower values to represent residual strength of the failed schist would have yielded a lower factor of safety, also in the failure range. In the case of the latter, numerical modelling stress distribution was required as an indication of lack of clamping action. Ravelling from the sloped hangingwall was indicated but would only carry on to a limited depth in the hangingwall before compressive stresses would maintain this rock mass integral. But once new portions of the hangingwall became exposed due to the schist failure, ravelling would continue.

The dedicated surface crown pillar empirical method could have indicated the failure that occurred there and those that occur to a depth of 226 m, but that a small change in C_s (based on rock mass quality which is difficult to quantify in the low range) yields significantly different critical pillar thickness (C_s = 0.45, t = 226 m; C_s = 0.5 t = 183 m). The known failures from level 260 m would not be predictable with this method.

Based on the analysis performed, the following failure scenario might explain the 1980 accident. Opening of the 2-7 stope caused shear failure from compressive stresses in the crown. Subsequent opening of the 1-7 drift above it precipitated compressive failure above both openings. This follows mine observations.

Complete failure of the pillar between openings occurred followed by chimneying disintegration above drift 1-7 to surface which was in part or in whole in failed schist rock. Hangingwall block slides, which may have started during the creation of 2-7, followed, but did not overtake, the chimneying development.

This would also explain the mine's observations [119] that both hangingwall and schist appeared to be opened at the bottom of the cone of failure in the overburden.

Design of any stope should take into consideration the mechanism of schist failure. Particularly long ground support must be used to anchor the schist beyond its zone of anticipated failure. Reduction or elimination of rock mass movement on active rupture lines must be minimized by installing ground support without delay and reducing blast damage, e.g. using perimeter blasting.

Plans to expand stopes to surface or creating any new shallow stopes extracting in this schist environment will be subjected to chimneying disintegration and hangingwall ravelling unless proper ground support is used to prevent mobilization of the rock mass. Occurrences of such failures to depths of 260 m indicates these precautions should be routinely taken.

CHAPTER 7

THE BRIER HILL MINE CASE STUDY

7.1 GENERAL GEOLOGY

The Brier Hill Mine is one of the State of Michigan iron mines found in the Menomenee Iron Range. It is situated in the northern Michigan peninsula near the town of Norway, Figure 7.1, near the border with the State of Wisconsin. It is located in a Precambrian Sedimentary formation [120] with an orebody consisting of alternating jasper-hematite, to hematite laminae, 0.5-3 cm thick.

It strikes N75W and dips 60° to 70° to the south, Figure 7.2. The orebody extends from a depth of 150 m to 450 m. Its thickness varies in cross section, 10 to 25 m, and reaches 200 m longitudinally at the 7th mine level.

The orebody is surrounded by jasper on the footwall and crown but its immediate hangingwall is a slate. The portion neighbouring the orebody is more graphitic and softer, tending to break into small pieces and having some gouge, 15-20 cm thick at the contact with the ore. The far-field footwall is also a slate formation. Overburden, 25 m to 35 m thick, is found above bedrock [6].

7.2 MINING EXTRACTION

The start of mining at Brier Hill has not been identified by the only reference for the case study [6], but by 1913 it appears there was sufficient mining completed to allow

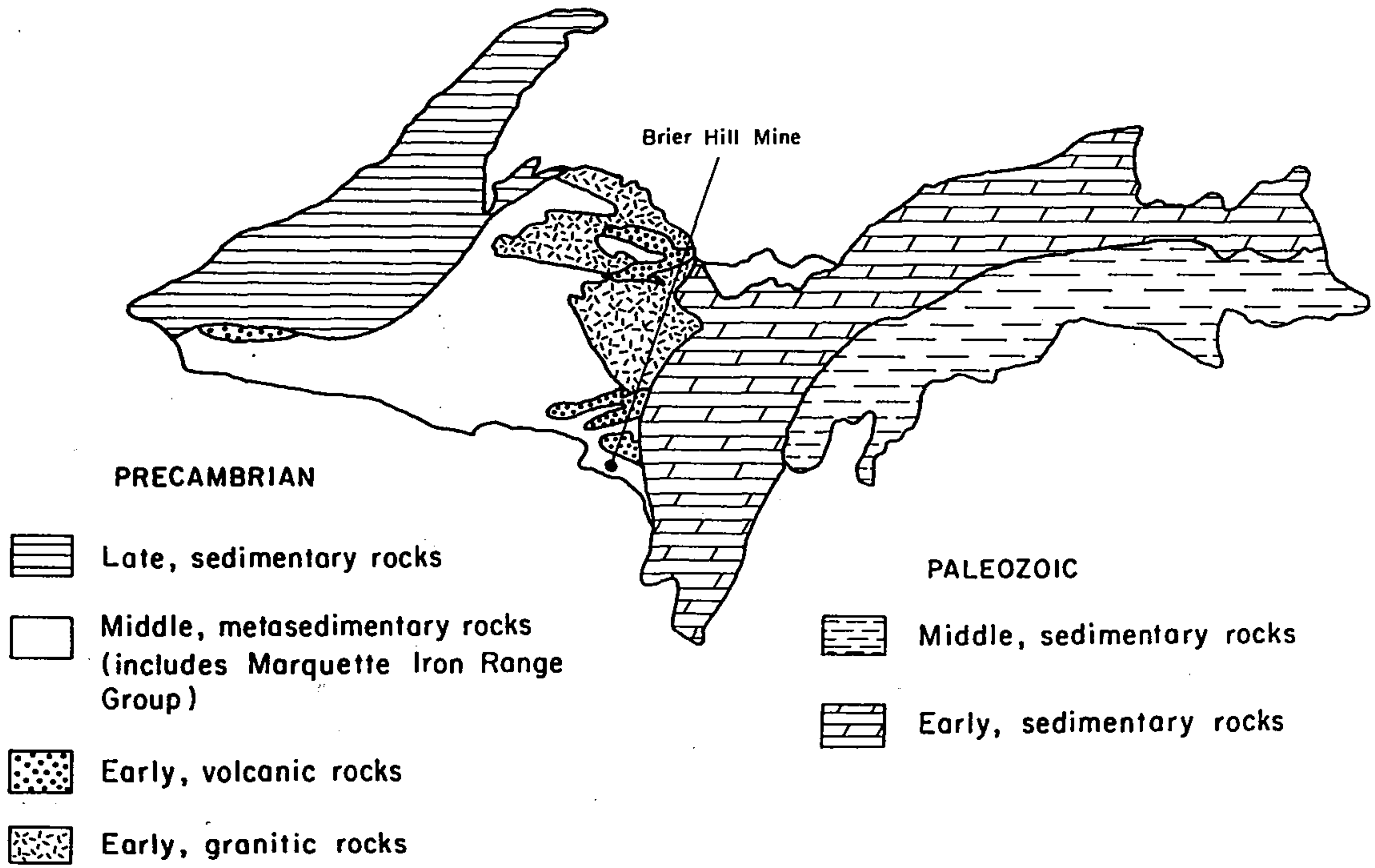

Figure 7.1 Location and regional geology, Brier Hill Mine, Michigan.

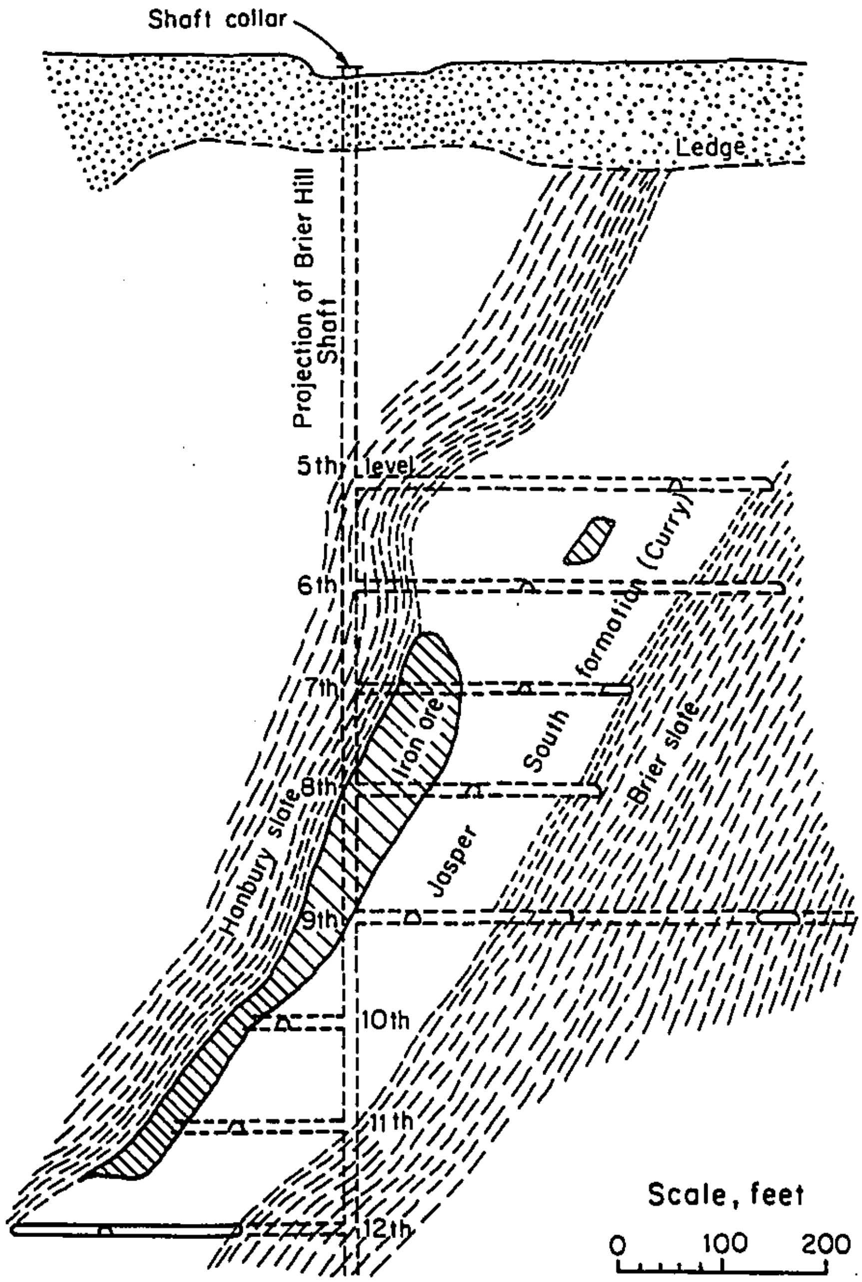

Figure 7.2 Geological cross-section, Brier Hill Mine [6].

for the recovery of pillars left behind by mining of primary stopes. Mine extraction stopped in 1923. The mine was owned by the Penn Iron Mining Co.

Primary extraction was performed by using cut-and-fill mining. Stopes of 7 m width were extracted to a height of about 10 m before filling with waste rock was performed. Pillars also of 7 m width were extracted after several rooms had been finished. Filling of these secondary stopes was performed only when the top of the pillar was reached.

By November 1913, primary stoping was finished down to the tenth level, with primary pillars still remaining between the seventh to ninth level. The pillars in the eighth and ninth levels having shown the effect of pressure, pillar recovery changed from overhand cut-and-fill to underhand cut-and-fill.

Chimneying disintegration occurred sometime between November 1913 and October 1916 as a result of a slate extraction area created in the hangingwall. The slate was used for stope fill. Mining below the tenth level had not begun by 1916.

No further information is available on the exact location of the slate extraction stope, nor on the results of visual or instrument monitoring of the progression of caving. The chimney worked its way up 275 m to surface in one year and left a conical pit on surface, 10 or 12 m deep.

7.3 SELECTION OF CASE STUDY

The Brier Hill mine represents the first known case of chimneying disintegration failure to have been described. It has been quoted in other publications [30][121] and is striking enough in its occurrence to be worthwhile back-analyzing.

In his comprehensive presentation of rock mass movements due to mining at the site, Rice [6] recounts the occurrence of the chimney over a deep but small opening 4.3 m x 8.5 m in the graphitic slate unit. The opening was meant to cave to supply slate as fill for cut-and-fill mining. The cave easily worked itself as a chimney reaching surface with approximately the same lateral dimensions, having cut across the 60° dipping slates.

The site is well described as far as geology and mine extraction is concerned. However, this early publication, and none have since described the conditions further, fails to provide any quantitative description of rock mass properties such as rock strength, in situ stress, modulus of elasticity, etc. Through the use of other references, representative values for these parameters will be obtained to study the cause(s) of this occurrence. The site represents a case of a well-developed slaty rock mass environment, Figure 1.3e.

7.4 NUMERICAL MODELLING

7.4.1 Numerical Model Selection

The Brier Hill orebody has been extracted over its 200 m longitudinal length, and the geological units are continuous over this distance with similar geometric relationships. In the case of the rock mass quality, no indication has been given of longitudinal change in properties. It will be assumed that no significant change occurs.

Therefore a 2-D approach can be justified. Furthermore, it will be assumed that the rock mass will behave elastically. Although slates vary in integrity and strength [122] these rock properties are normally considered to behave elastically in a rock mass away from openings [53]. As for jasper and jasper bound iron ore, no data has been found on lab tests or previous modelling work. However, jasper, a predominantly silica based rock, and iron ore when massive or continuous, are rock materials with integrity, supporting the possibility of elastic rather than non-elastic behaviour. The MSAP2D linear elastic numerical modelling code (Chapter 3.4) was adopted for this case study.

7.4.2 Geomechanical Properties

No geomechanical properties have been found related to this particular site. The basic modelling rock properties and rock mass strength were obtained by consideration of other sources and are meant to be representative approximations. Table 7.1 summarizes the properties selected.

The slate unit weight range is given by Hoek and Bray [76] as 0.025 to 0.029 MN/m^3. A value of 0.029 MN/m^3 was selected for hangingwall and footwall slate unit weight. Jasper is a quartz rich rock with a small amount of hematite concentrations. Hurlbut [123] provides a unit weight of 0.0269 MN/m^3 for jasper. The banded iron ore commonly has alternating bands of hematite and jasper. Therefore an average unit weight of 0.039 MN/m^3 was selected (hematite being 0.052 MN/m^3).

The modulus of elasticity values vary for slate depending on its state of alteration. Rodrigues [122] provides a range of 7.8 to 85 GPa for laboratory derived values. He also provides a range of 0.28 to 0.33 for Poisson's ratio. Because the slate was evaluated as weak by Rice, a field value of E = 4 GPa and υ = 0.29 were selected for the hangingwall. For the footwall which was rated as better than the hangingwall, values of E = 6 GPa and

Table 7.1 Selected Geomechanical Properties for the Brier Hill Mine Numerical Model

	γ_r (MN/m^3)	E (GPa)	υ	m	s	σ_c (MPa)
Hangingwall Slate	0.029	4.0	0.29	0.9	0.0006	85.0
Jasper	0.0269	16.0	0.25	2.8	0.02	150.0
Footwall Slate	0.029	6.0	0.28	1.3	0.001	60.0
Orebody	0.039	14.0	0.27	2.0	0.004	110.0

$\upsilon = 0.28$ were used. The hangingwall is known to have been easy to cave when unsupported over the Brier Hill Mine openings. A lower quality rock mass is thus apparent. Table 2.1 from Hoek and Brown [95] indicates that for a lower quality RMR ("fair" or worse) values of m less than 1.35 and s less than 0.002 should be used for slate. Hoek [53] uses a value of $m = 1.66$ and $s = 0.006$ for good quality slate.

For these reasons the hangingwall slate parameters are considered to be lower than these values, falling between fair and poor quality rock mass, Table 2.1. Values of $m = 0.9$ and $s = 0.0006$ were selected. For the footwall slate, a better quality slate, $m = 1.3$ and $s = 0.001$ were selected.

A value of 60 MPa was used as unconfined compressive strength for weak slate, 85 MPa for stronger slate based on values quoted by Lama and Vutukuri [112] for weak slates.

No point of reference exists for jasper properties, banded with hematite or otherwise. In this case, being fine grained sedimentary rock, it should be considered under the lithified rock classification of Hoek and Brown.

A good quality Hoek and Brown rock mass rating was assigned to the jasper, $m = 2.8$, $s = 0.02$, a fair quality rating to the banded ore, $m = 1.3$, $s = 0.002$, because the alternating laminations might weaken it in comparison to the purely jasper content. Respectively, 150 MPa and 110 MPa were used for uniaxial compressive strength, representative of siltstone, (a fine grained lithified argillaceous rock) [112]. As for modulus of elasticity, 16 GPa and 14 GPa were used respectively for the jasper and ore body. This was selected as a comparison to the slate moduli and the competence of the formations. The competent field elasticity modulus range is defined greater than 6 GPa

[112]. Because of the laminated nature of the ore, a weaker Poisson's ratio, 0.27, was used compared to that selected for jasper, 0.25.

The initial ground stress field existing at the site was not available. However, publications related to northern Michigan peninsula stress measurements were examined to provide this data.

Adams [124] indicates in his summary of North American ground stress trajectories, that measurements in a mine of the northern Michigan peninsula iron range return values of major principal stress that are oriented N110W to N75W. Aggson [125] obtained the following values of major principal stress for a depth of 975.4 m: using the overcoring method σ_1 = 31.9 MPa, σ_2 = 25.8 MPa, σ_3 = 18.6 MPa. The major principal stress was oriented at N82W.

This vertical stress value is lower than Herget's database [118], i.e. σ_v = 0.026 to 0.034 MPa/m.

However, Herget's ratios of minimum and maximum horizontal to vertical stress

$$\frac{\sigma_{hmax}}{\sigma_v} = \frac{253.87}{depth(m)} + 1.45 \qquad (7.1)$$

$$\frac{\sigma_{hmin}}{\sigma_v} = \frac{279.72}{depth(m)} + 0.88 \qquad (7.2)$$

for the depth at which these measurements were performed are close to the ratios of stress measured; therefore, the stress value to use for the model will follow the Herget load assumptions.

The orientation of the major principal stress in that area (N75°W to N82°W) is parallel with the orientation of the strike of the orebody. Therefore, the intermediate principal stress, usually horizontal in the Canadian Shield [27][118] and perpendicular to σ_1, is, in this case, orthogonal to orebody strike. The vertical stress follows the trend as the minor principal stress. Therefore, overlying weight can be used for σ_v in the model, and equations 7.1 and 7.2 can be used for the horizontal stress values.

7.4.3 The Brier Hill Mine Numerical Model

The central transverse section of the Brier Hill Mine orebody was used in modelling the rock mass response to mining using the MSAP2D modelling code, Figures 7.2 and 7.3. Although some pillars existed between footwall and hangingwall, from level 8 to level 9, the amount was not enough to show rock pillars in the model. Because loose rock fill was used to fill the extracted portions of the orebody, its contribution to stress transfer is expected to be negligible. Therefore, the model was run without backfill leaving the stope open as a worse case situation. The unextracted ore below level 10 was included in the model, Figure 7.3, as per conditions on site [6].

The stope dimension is 10 m wide on a 65° dip, located 150 m below surface. The stope was placed in the middle of a 530 m high by 830 m wide model. The finite element mesh selected is composed of 2937 elements, Figure 7.4. The size of the elements is smaller around the opening, about 1 m x 1 m, and in the hangingwall, where the chimney has occurred, to arrive at a good representation of the redistribution of stresses around the opening. In this fashion, a better definition of critical and failure areas could be afforded with the model's failure criteria and with the applications of the analytical equations. Because no information was given by Rice as to the exact location of the opening that caused the chimney, no provision was made to create this opening into

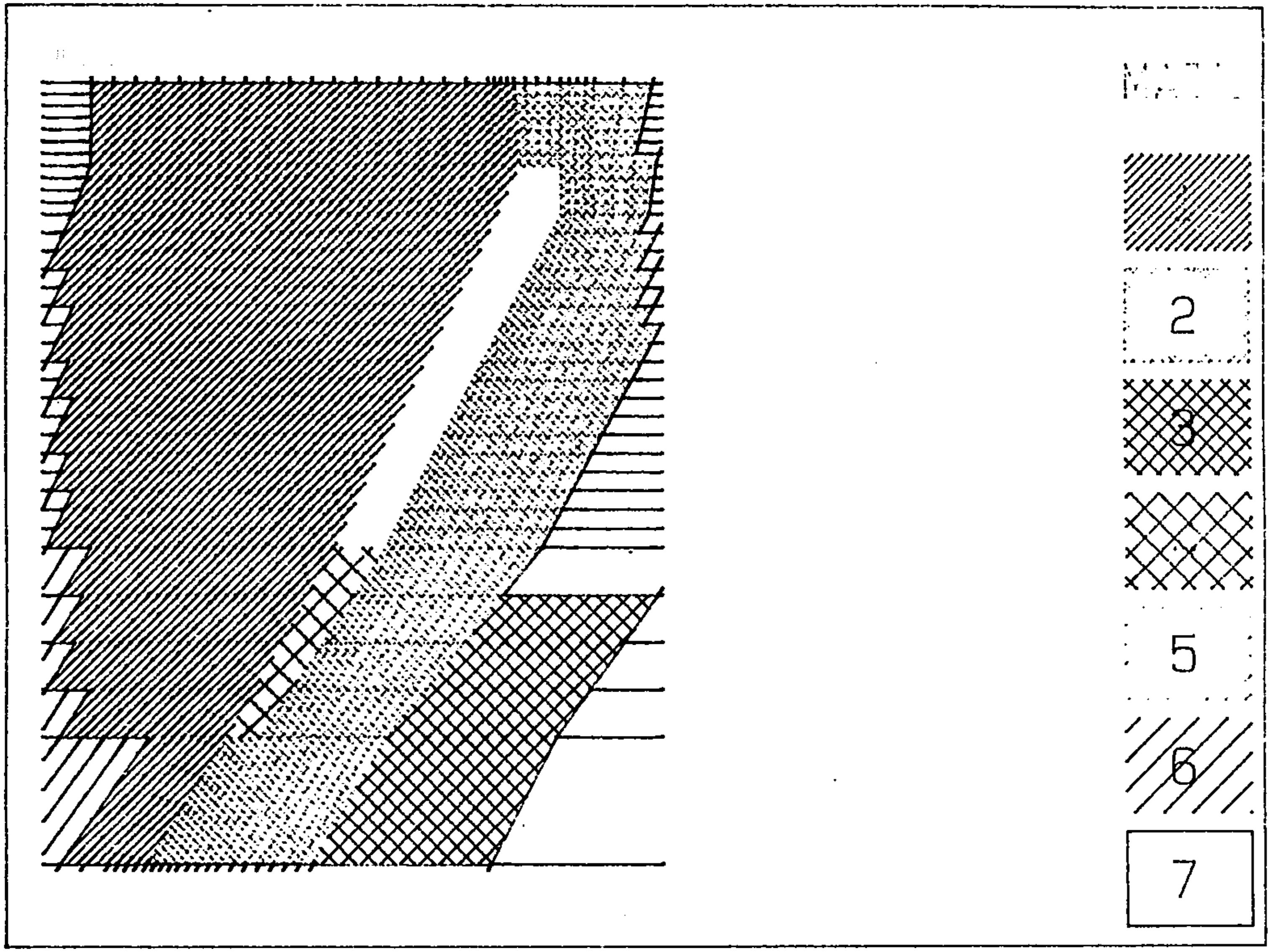

Figure 7.3 Model geology cross-section, Brier Hill Mine.

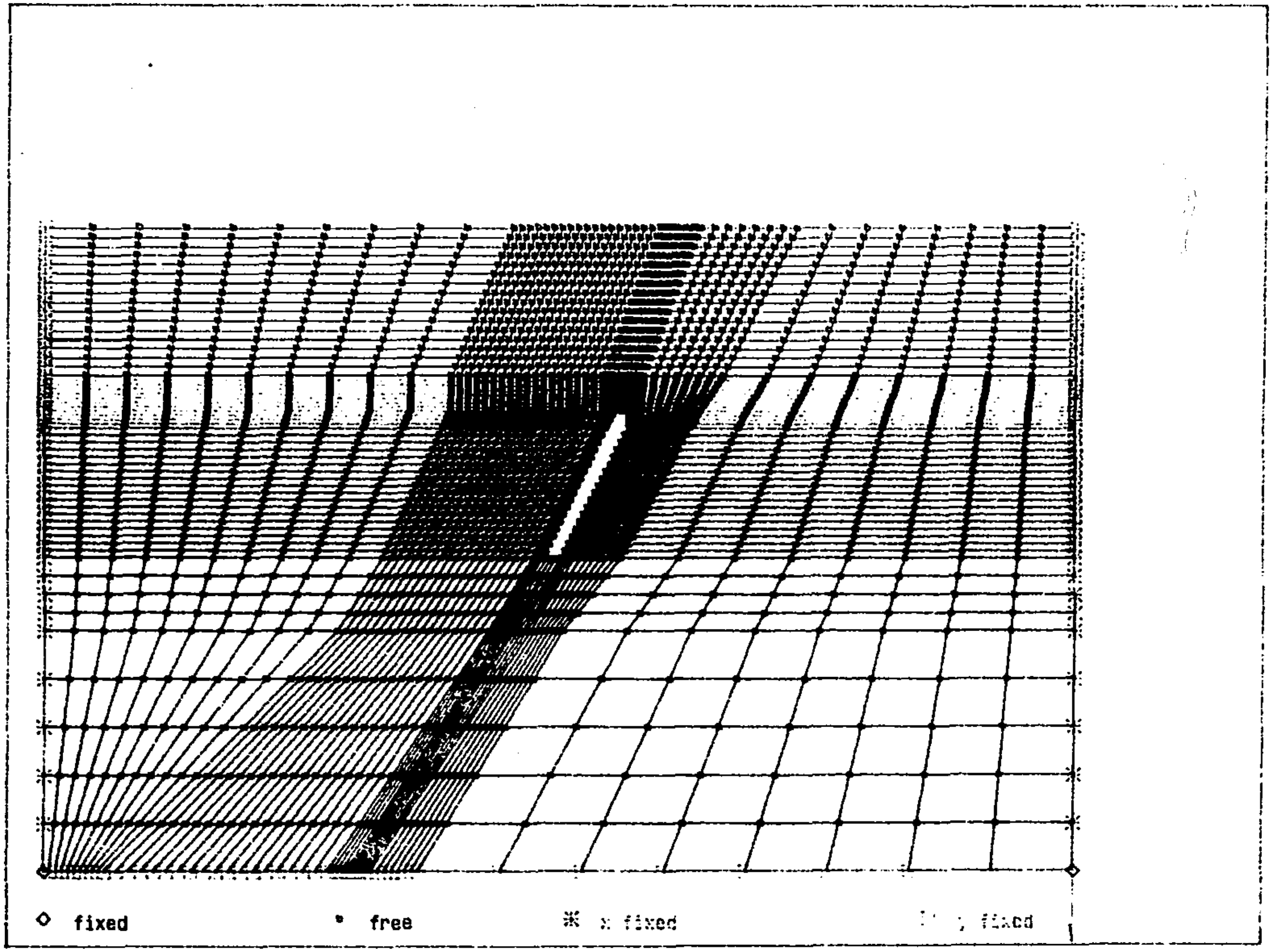

Figure 7.4 Brier Hill Mine numerical modelling mesh.

the model. However, it can be assumed that, for economic reasons, this opening was not placed far from the orebody.

7.4.4 Modelling Results

Displacement, imposed ground stresses, and evaluation of the safety levels for the modelled rock mass of the Brier Hill Mine were obtained from the application of MSAP2D.

Figure 7.5 shows an enlargement of the calculated displacements at the periphery of the stoped out area. A maximum displacement of 3.8 mm occurs in the hangingwall slate. The general rock mass movement is toward the opening.

Figures 7.6 and 7.7 show respectively the stresses in the rock mass surrounding the mined area and a close-up of the hangingwall, where chimneying has occurred. The immediate hangingwall has tensile radial stresses over its full height, and in the lower portion both tangential and radial stresses are tensile. The radial stresses decrease from 5.6 MPa to 0.06 MPa, tension, at higher locations up the hangingwall. The tensile tangential stresses reach a maximum of 0.15 MPa. The radial tensile stress zone is 4 m deep at the lower hangingwall and reaches a depth of 18 m into the upper hangingwall.

The lower and upper footwall are subjected to an 8 m thick zone of radial tensile stresses which are less than 0.4 MPa. The mid-height portion of the footwall is subjected to a 4 m thick zone of tensile tangential stresses ranging from 0.15 to 3.7 MPa.

Compressive radial and tangential stresses are found in the stope crown, the former ranging from 1.2 MPa to 8.8 MPa, the latter from 26 MPa to 31 MPa. Compressive radial and tangential stresses are also found beyond the immediate hangingwall and

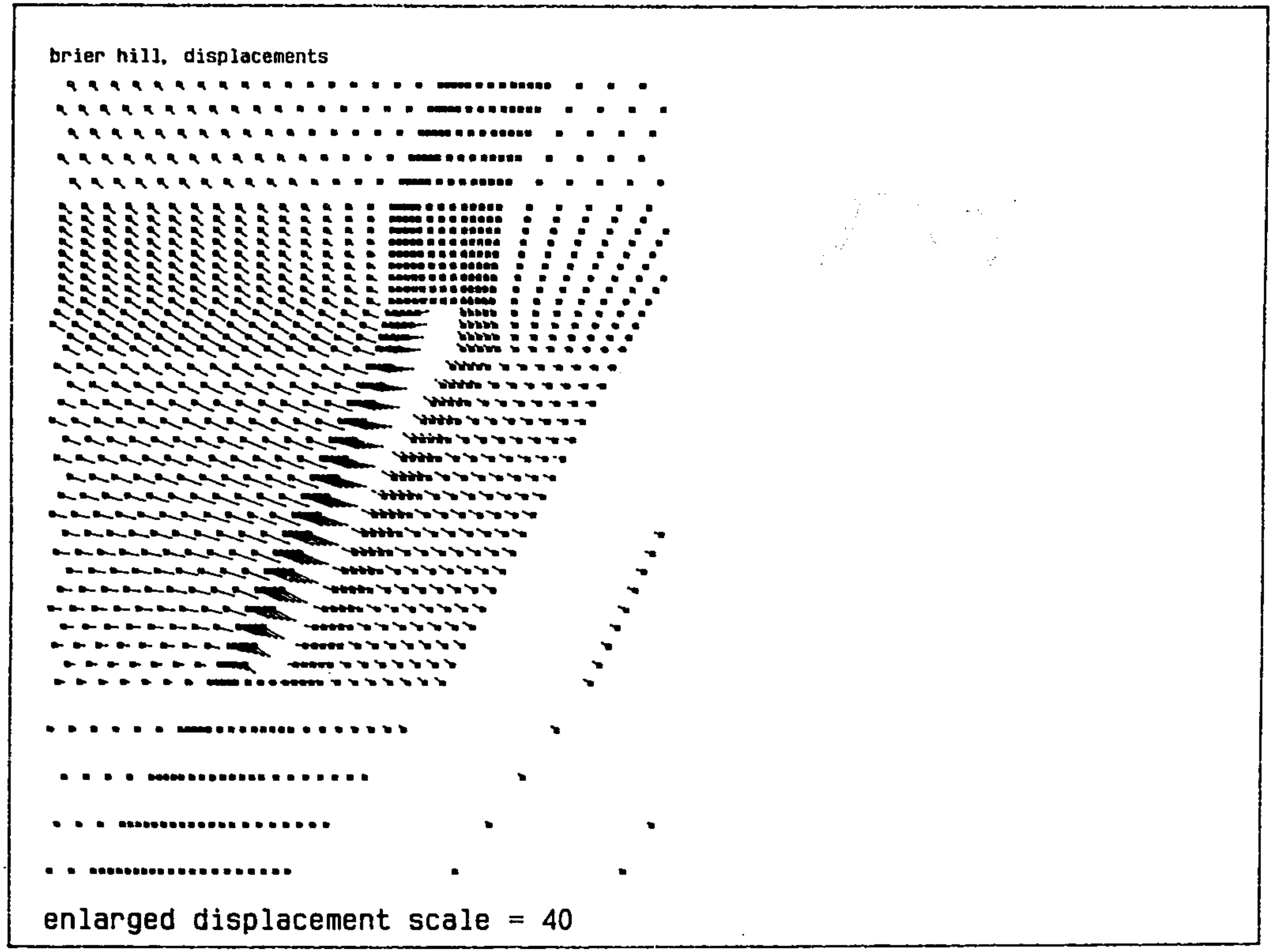

Figure 7.5 Rock mass displacements around the extracted area, Brier Hill Mine.

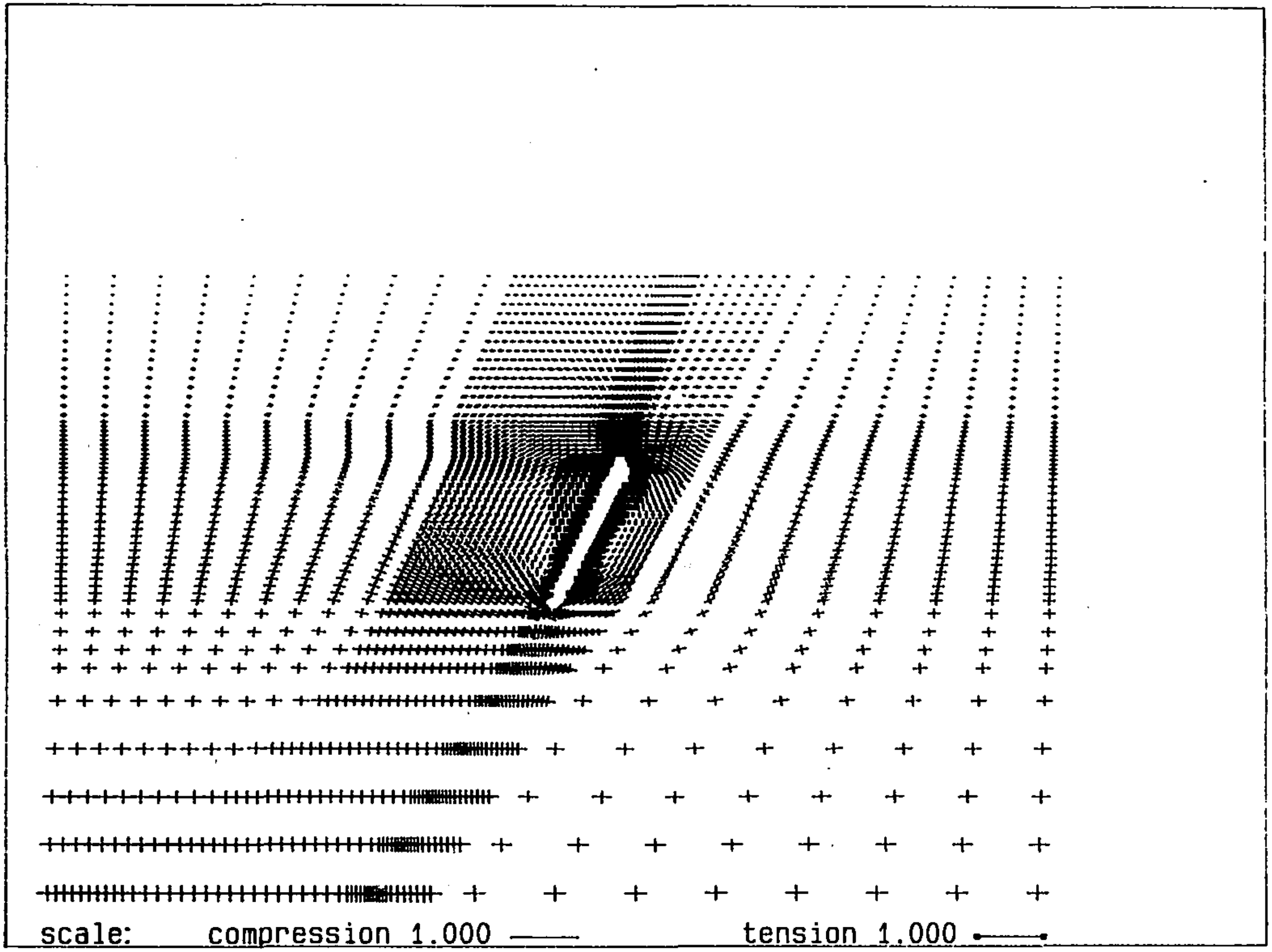

Figure 7.6 Stresses around extracted area, Brier Hill Mine.

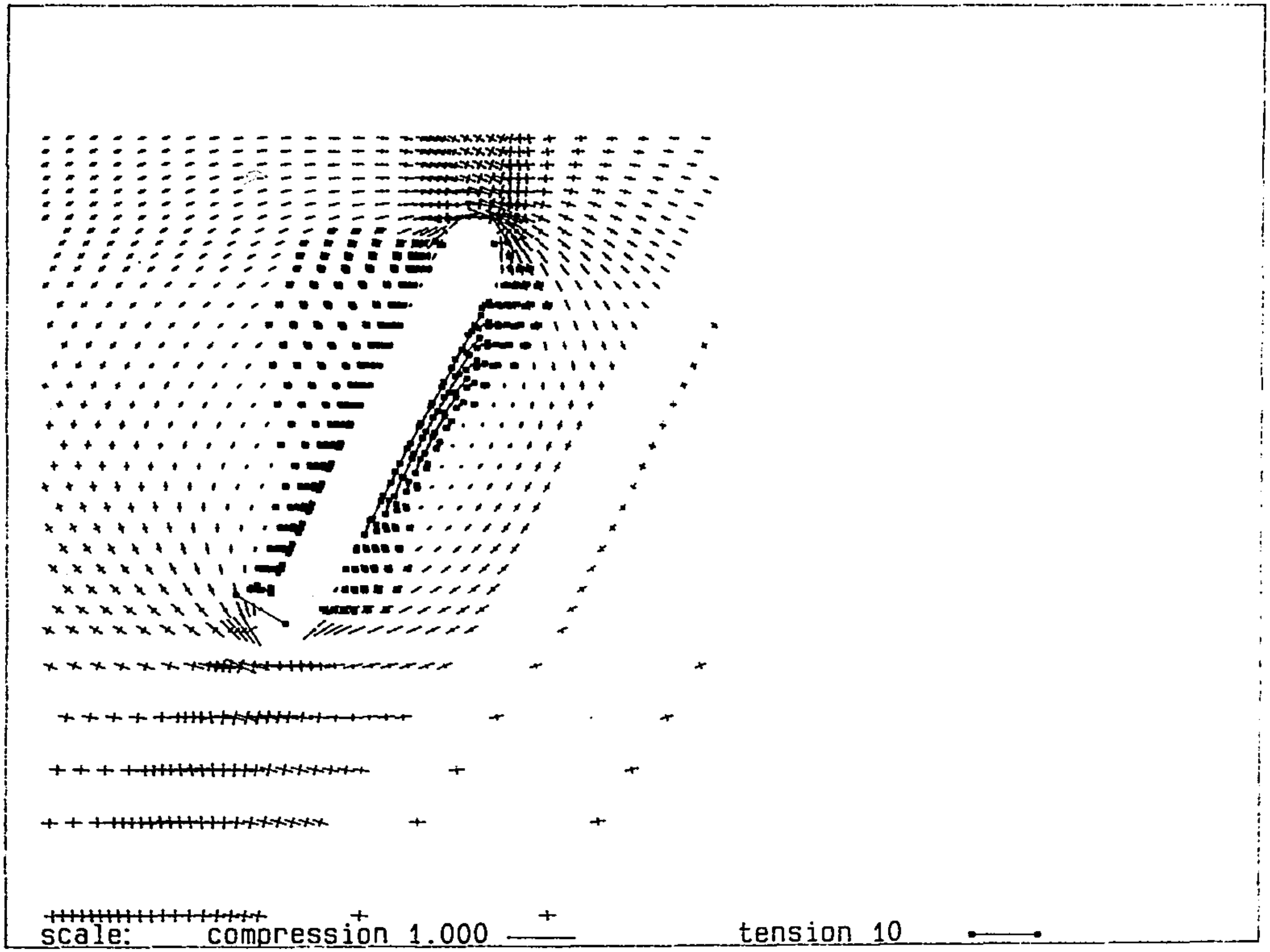

Figure 7.7 Enlargement of stresses around extracted area, Brier Hill Mine.

footwall.

The Hoek and Brown failure criterion available on MSAP2D was used to verify imposed stress conditions versus material resistance in the form of a Mohr envelope. The m and s parameters selected for the various geological units, Table 7.1, were applied to define the failure envelope.

The footwall jasper is indicated to have failed (F_s<1.0) where tangential stresses surpass the rock mass tensile strength calculated at 0.9 MPa (Appendix 5), Figure 7.8. The jasper rock mass has failed by compression over a limited portion of the crown periphery. The orebody below the modelled opening is safe (F_s > 1.4).

The hangingwall slate shows the most extensive failed and critical areas. Figures 7.6 and 7.8 indicate that tension is responsible for most of the immediate hangingwall failure, but that compression is responsible for the failure and critical areas at and above level 10 where chimneying disintegration started, and in the far-field hangingwall.

7.5 APPLICATION OF ANALYTICAL EQUATIONS

7.5.1 Chimneying Disintegration Failure

The Brier Hill Mine failure has been described by Rice [6] as a chimneying disintegration failure. Applications of the chimneying analysis has been performed in Appendix 5.

Equation 2.66 is used to describe the potential for the first rupture line above the opening. Although the opening which was subjected to failure was 4.3 m x 8.5 m in section, its location is not known in the hangingwall of level 10, but is assumed close to

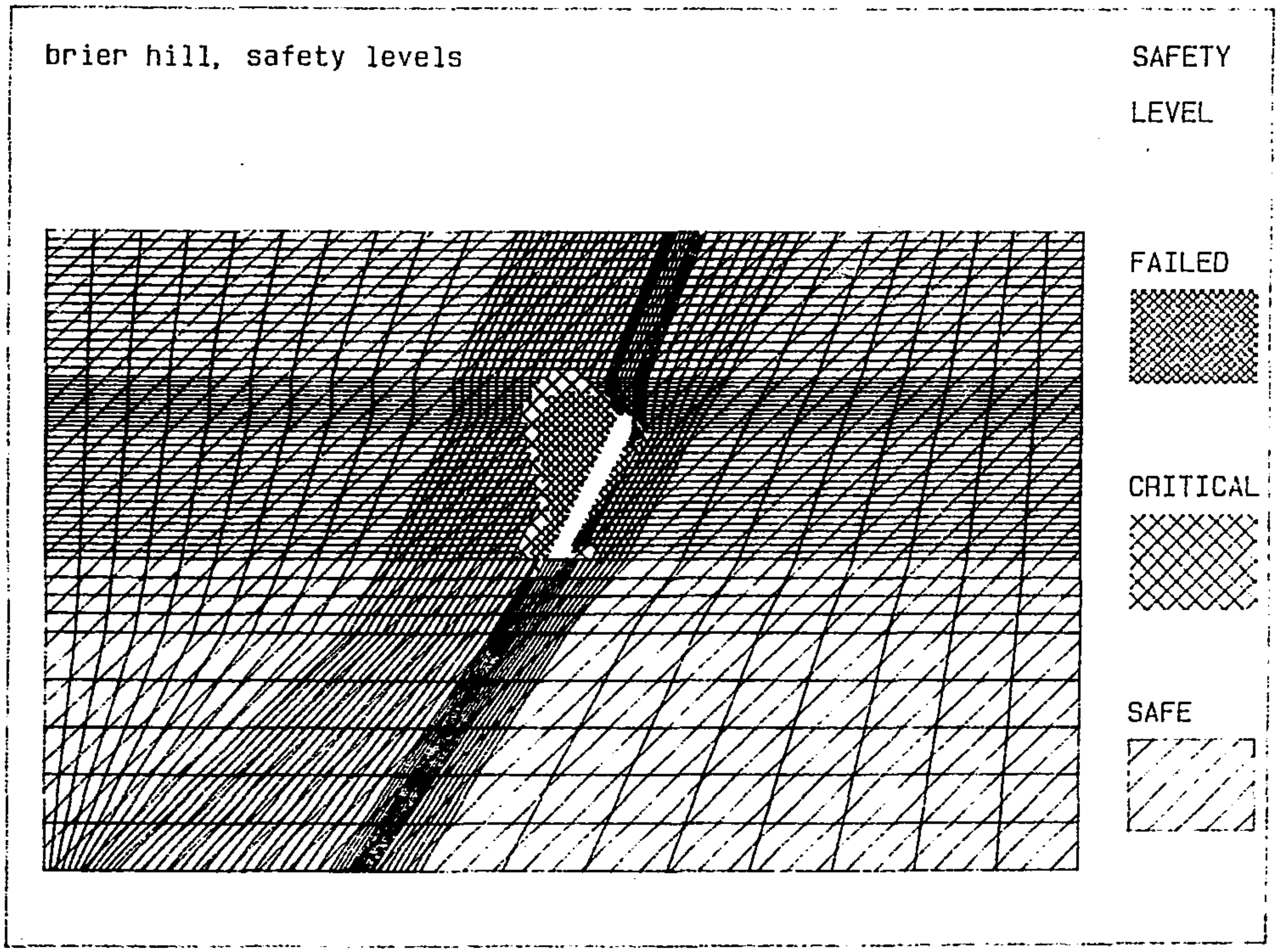

Figure 7.8 Hoek and Brown failure criterion safety levels for the rock mass around the extracted area, Brier Hill Mine.

the stope for economic reasons.

The factor of safety against chimneying disintegration using an 8.5 m width and the approximate values selected for intact strength is 1.6.

7.5.2 Block Caving Failure

The possibility exists that caving rather than chimneying occurred. Empirically, the Diering and Laubsher chart indicates that the opening could have caved if, for Q=0.32 (Appendix 5), a slate dip of 60° and a width of 8.5 m, the opening was very much wider than the 4.5 m it was. If block caving was to continue, the factor of safety for a stable arch forming is insufficient (F_s = 0.78) in the case of bulk failure of such an arch.

7.6 APPLICATION OF EMPIRICAL METHODS

An approximate value of Q = 0.32 was derived for the hangingwall slate. Lack of information with regards to the jasper rock mass precluded the application of the NGI, although from the site description a range of values of Q = 3 to 10 could be asserted using the rock mass elasticity modulus value used, translated to the Q value using the Serafim and Pereira [18] relationship between RMR and E_m (equation 4.1) and the conversion of RMR to Q using

$$RMR = 9 \ln Q + 44 \tag{7.1}$$

The surface crown pillar chart method (Appendix 5) (Figure 1.15) indicates C_s = 2.0 for the slate Q = 0.32 and C_s = 6.5 for the jasper Q = 4.7. The minimum thickness needed for rock above the slate opening is 13.1 m, that for the jasper is 1.1 m.

7.7 SUMMARY

Numerical modelling has shown that a large portion of the hangingwall slate has failed, given the selected approximate m and s input values. These same values, when used to calculate chimneying disintegration potential, provide a realistic factor of safety of 1.6, close to the value of the rock mass that has failed ($F_s < 1.0$). Chimneying disintegration is more likely for the small borrow stope as a failure than block caving, as indicated by empirical means. However, block caving is known to have occurred over much wider lengths, above the extracted orebody, a possibility indicated by the calculation showing the unlikeliness of stabilizing arches forming. The empirical surface crown pillar method only indicated 13.1 m for stability above the 4.3 m x 8.3 m opening, compared to the failure that developed from a depth of 275 m.

To reconcile the numerical modelling with the analytical equation results, lower values of m and/or s are required in order to provide lower c_m values. Depending on the effects of rock mass weakening of gouge and graphitic components, the m and s values could be lower affecting not only c_m for the analytical equation but also the extent of the failure zone predicted by the modelling. Alternatively, Hoek and Brown [95] provide lower m and s values for disturbed rock masses (Table 3.5) such as those that have failed and are in a residual strength condition. The failure does indicate that gravity rock mass failures to surface are likely to occur when geomechanical conditions allow for it, at deep as well as shallow levels.

CHAPTER 8

ATHENS MINE CASE STUDY

8.1 GENERAL GEOLOGY

The Athens Mine is located in the northern peninsula of the State of Michigan, Figure 8.1. It was one of the largest producers of sedimentary iron ore from the Marquette Formation of the Marquette iron range. Descriptive site elements were provided by Allen [5].

Like the Brier Hill Mine, the ore consists of inter-layered hematite and jasper bands, each less than a few centimeters thick from geologic formations of Precambrian age. The orebody plunges west at an angle of 15° and is bound on the north side by a 60 m wide diorite dyke, on the south side by what is described as a "fault" dyke, Figure 8.2, so called because of the horizontal displacement of the ore on either side, but no fault has been identified. The orebody thickness is fairly constant at 100 m, and the average width is close to 80 m. The orebody enters the east boundary of the property at a depth of about 480 m and reaches a depth of 800 m at the west boundary.

The dykes extend subvertically to surface. The portions of both dykes in contact with the orebody are composed of "soap rock" or fault gouge, and are planes of shearing weakness.

The orebody is capped by jasper and underlain by slate, which are not described in Allen's article. Sand and gravel covers part of the bedrock, up to a thickness of 45 m.

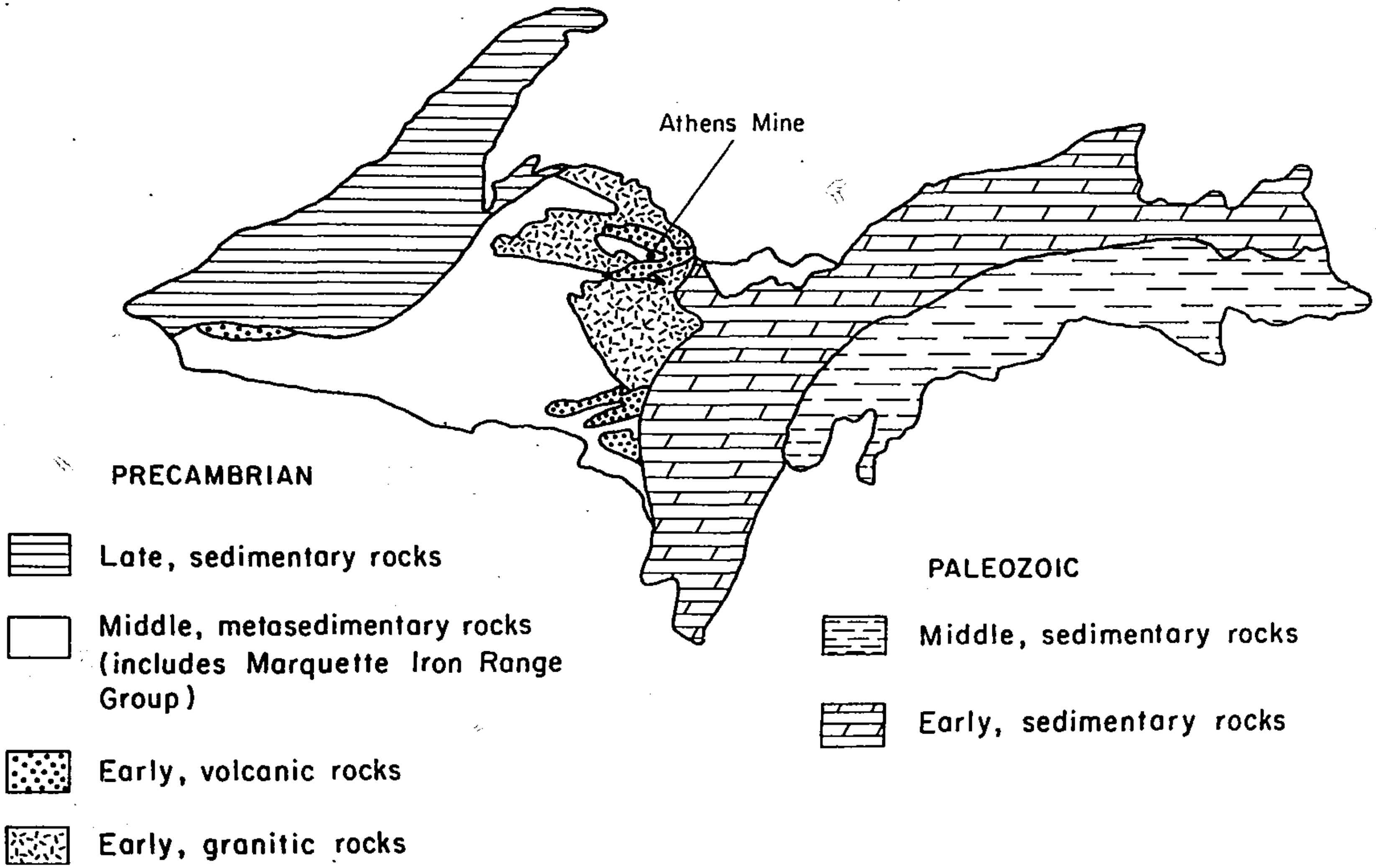

Figure 8.1 Location and regional geology, Athens Mine, Michigan.

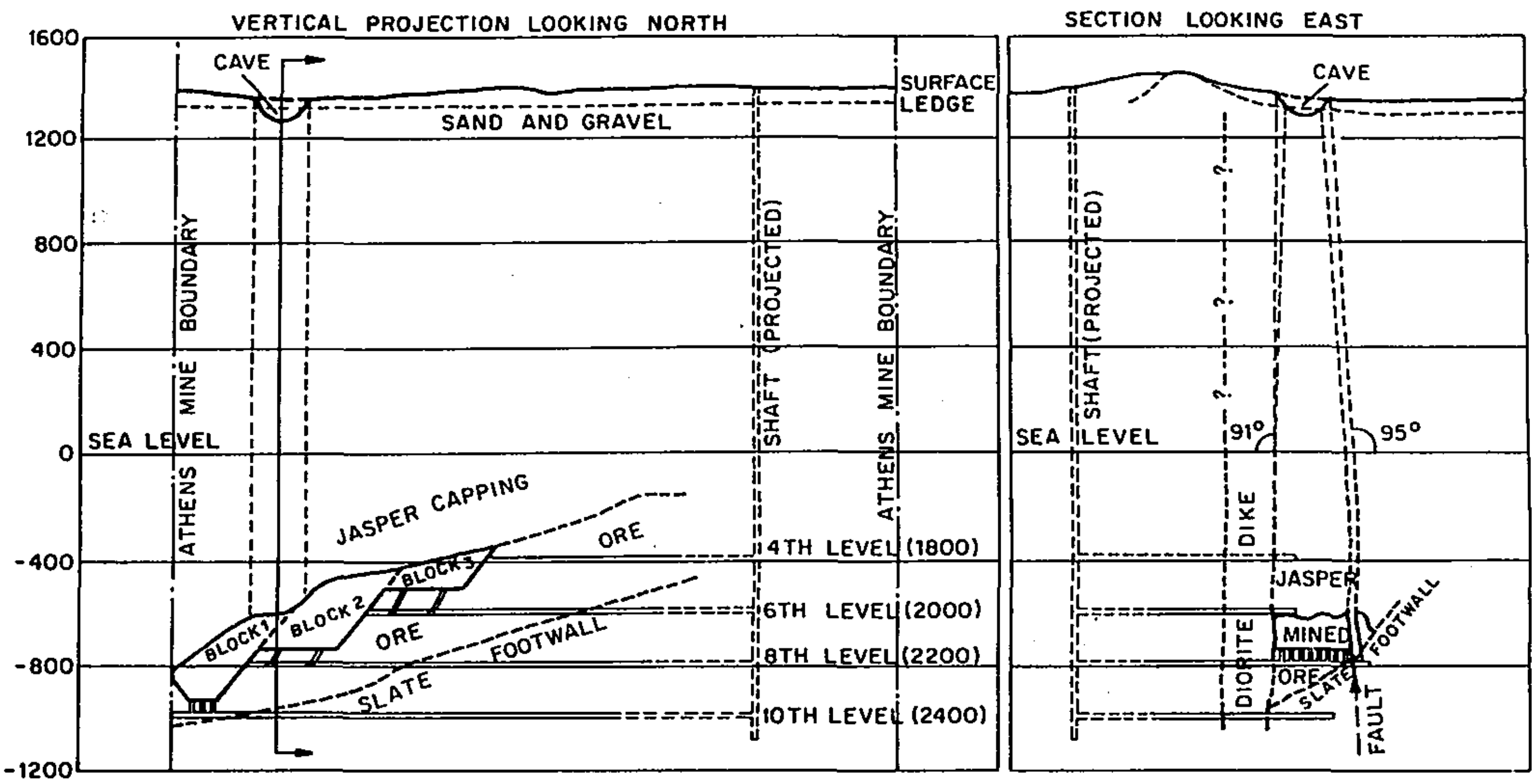

Figure 8.2 Geological longitudinal section (looking north) and cross-section (looking east), Athens Mine [5]. The East-West outline of the plug failure extrapolated by Allen [5] is shown as a dashed line; the dikes formed the North-South boundary.

8.2 MINING EXTRACTION

The Athens Mine was held under lease by the Athens Iron Mining Co., and was owned and operated by the Cleveland-Cliffs Iron Co., and the Pickands-Mather Co. The mine was opened in 1913 with activity ongoing at the time of the Allen article.

The orebody was divided into mining blocks which would be mined progressively from deep to shallow levels, Figure 8.2. The benefits of this progress were to delay the cave expected to reach surface above the mined out block and locate this eventual cave over a mined area below the working places. In this way, reports Allen, prohibitive ground pressures would be avoided, providing a saving in timber cost; dry working places (avoiding water inflow from surfaces) would increase efficiency and allow a saving in freight in shipping dry ore, as well as reduce pumping costs.

The mining method used was underhand cutting starting from the jasper hangingwall of each block. Each block was to be successively mined. The ore was reported to have a tendency to "swell" when newly developed.

After block 1 was extracted, blocks 2 and 3 were mined simultaneously. The considerable amount of water encountered in developing block 1 had reduced substantially by the time block 2 as mined. Figure 8.2 shows the outline of the excavated blocks when the failure of the stope occurred.

8.3 SELECTION OF CASE STUDY

The Athens Mine suffered a major plug subsidence in 1932 of a rock block overlying mining blocks 1 and 2, having a vertical dimension equal to the depth of the orebody, 660 m, a width of 80 m spanning the orebody between the dykes and length of 70 m. This is one of the few plug failures mentioned in the literature, and the only one to be well described in the context of a mining operation, even though no geomechanical information has since then been available.

Though the mining extraction at the Athens Mine was carried out at deeper horizons than that defined for shallow stopes, the case study becomes important to identify which geomechanical element(s) influenced the occurrence of the failure. A repeat of such conditions at shallow levels would be critical as confinement ground stress levels there would be less than deeper conditions, which in this case were insufficient to prevent failure. Furthermore, this failure shows that when conditions are propitious for gravity failure, deep openings can be affected.

The continuous structural feature usually associated with plug failure, Chapter 1.3, exists here as the bounding dikes.

The applied numerical modelling, while selected to represent site conditions, will be evaluated for its performance versus the analytical and empirical equations in predicting this particular type of failure that occurred.

Although geomechanical parameters are not available, sufficient description of site geology and ground control problems exist to select approximate but representative values for stability analysis.

8.4 EVENTS LEADING TO FAILURE

The mining strategy adopted, starting at lower levels and progressing upward, was meant to remove the effects of the expected caving of overlying jasper and water inflow that might ensue, by moving away from previously mined areas. Although a considerable amount of water was encountered in mining block 1, little water had been encountered in the working places of block 2.

In June of 1932 the plug bounded by the diorite dykes, spanning a distance of 80 m, 70 m in the longitudinal direction, and reaching surface from the mine opening (660 m), failed suddenly as a unit into the stopes of the open 1 and 2 blocks below. Some water inflow into the mine occurred, presumably from a surface source which amounted to approximately 1500 litres per minute. A slump in the 45 m thick overburden was observed, bounded by the vertical extent of the plug failure planes, Figure 8.2. No precursors to failure were noted.

The portion of both dykes in contact with the orebody and overlying jasper was described as "soap rock" or fault gouge. No information on joint families or faults was provided to explain the formation of the discontinuities bounding the other plug faces. Speculation by Allen led him to believe that the rock was unjointed, originally intact, which failed by double cantilever mode.

Observations by Allen [5] and Crane [126] of regional mines with similar geological distributions indicate that expressions of surface failures from the caving, or angles of draw, were found to be planar, and strike north-south with an 80° to vertical dip. Furthermore, these were found to segment the rock into portions which were arranged on strike in a step-like fashion. These breaks would follow the east-west advance of the mining extraction.

The possibility existed then that the block sides orthogonal to the dykes were planar and along discontinuities, at least in the upper portion, even if the bottom of the block failed by exceeding rock strength.

8.5 NUMERICAL MODELLING

8.5.1 Numerical Model Selection

The numerical code to model the mining blocks of the Athens Mine was selected based on the geometry of the excavation, the nature of the failure, and the behaviour of the rock mass components.

Although the mining blocks are successive, longitudinally spanning some 350 m, the vertical height of the extraction is variable and plunging. In this case a 2-D code which represents constant geometrical conditions in the third dimension would not be representative. And although the geological units are longitudinally consistent, they also are dipping. Furthermore, the plug failure mechanism had well defined cross dimensions rather than continuous longitudinal extension.

Therefore, a 3-dimensional modelling code would provide more representative results and provide the stress distribution on each plug surface for analysis of failure conditions. As for the approach taken in Chapter 7, jasper is expected to behave elastically, as is the diorite. In the case of the latter, the contact surface with the orebody is taken to be altered or infilled because of geological emplacement or movement.

However, the material was assumed to be integral.

The numerical code selected was the BMINES program, presented in Section 4.4.1. The 3-D finite element capability would allow the requirements of the geometry, elastic consideration, and failure mechanism to be met. Stress distribution and application of the Hoek and Brown failure criterion to generate factor of safety contours could be performed.

8.5.2 Geomechanical Properties

The material properties selected are presented in Table 8.1. Since no geomechanical properties have been found related to this site, the basic modelling input parameters were obtained by considering other sources and are meant to be representative approximations.

A simplified geological environment to meet the continuity requirements of BMINES was taken to be as follows: far-field jasper, diorite dykes, and jasper above and below the mined-out blocks. Although the immediate footwall of ore would not be represented, the failure originating from the hangingwall (crown) would require representative contact jasper properties.

In this case, the immediate jasper was given slightly lower rock mass elastic and strength values than the far-field owing to possible effects of dike emplacement or faulting and because caving was expected above mined-out blocks. The values selected were based on the premises outlined for the Brier Hill Mine, Table 7.1. The diorite dyke, composed of coarse grained igneous rock, was assumed to be of "fair" quality. As a conservative estimate, Table 2.1 of Hoek and Brown recommended values indicates values

Table 8.1 Geomechanical Properties Selected for the Athens Mine Modelling

	γ_r (MN/m^3)	E (GPa)	υ	m	s	σ_c (MPa)
Jasper Crown, Ore and Footwall Slate	0.027	10.0	0.26	2.0	0.004	120
Diorite Dykes	0.027	8.0	0.25	2.5	0.001	140
Far-Field Jasper	0.027	12.0	0.26	2.8	0.02	150

of m = 3.4 and s= 0.002 for such conditions. Slightly lower values were selected because of possible emplacement effects weakening, as reported by Crane [126], dykes in the iron range, or from faulting activity, and to take into consideration the weakness of its contact with the orebody.

This would reflect the "several sets of moderately weathered joints" accompanying the values under the Hoek and Brown fair quality designation.

The diorite rock mass elasticity value E=8.0 GPa is a translation using the RMR value of 45 associated with the m and s values of "fair rock" in Table 2.1, using Serafim and Perreira's empirical equation [111], equation 4.1. Poisson's ratio is a mid-range (between intact and weak) value for coarse grained igneous rocks.

The mine is also located in the northern Michigan peninsula; the initial ground stress field existing at the site is assumed to be the same as the Brier Hill Mine, discussed in Chapter 7.4.2. The major principal stress is approximated as east-west to coincide with the orebody longitudinal direction, orthogonal to and 1.47 times the intermediate principal stress; both are horizontal, the minor principal stress, 1.74 times less than the major principal stress, is vertical and represents the weight of the rock.

8.5.3 The Athens Mine Numerical Model

The longitudinal and cross section of the mine provided by Allen (Figure 8.2) was used in modelling the rock mass response to mining at the time of failure using the BMINES modelling code. Although some pillars existed the amount was not enough to show pillars in the model, and the stopes remained opened, timbering providing ground support. Thus, the model was run with the mining blocks left open as a worse case situation.

Given the restriction on the number of elements available and the shape of the mining extraction, the modelling mesh was constructed to yield a representative outline of the mining activity. Furthermore, densification of the mesh around the known plug failure surfaces was made to arrive at a good representation of the redistribution of stresses there. In this fashion, a better definition of critical and failure areas could be afforded with the model's failure criteria and with the applications of the plug failure analytical equation.

The extracted mining block, 175 m high by 365 m long and 80 m wide, was placed in the middle of the 1535 m high by 2795 m long and 840 m wide model. The finite element mesh selected is composed of 14,850 elements.

8.5.4 Modelling Results

Figures 8.3 and 8.4 respectively show the major and minor principal stresses in a central longitudinal section, Figures 8.5 and 8.6 the major and minor principal stresses on a cross section mid-way between the estimated east and west plug boundaries.

The crowns of the mining blocks are subjected to a compressive minor principal stress varying from 0.3 MPa to 11.7 MPa. The lowest value occurs at mid longitudinal and mid cross-section span in the area included in the plug failure. The footwall of the mining blocks are for the most part subjected to 2.6 to 11.7 MPa of compressive minor principal stress.

The major principal stress levels are 17 to 42 MPa, in the crown, the highest values recorded at the west side of the plug. In the footwall the values are less on

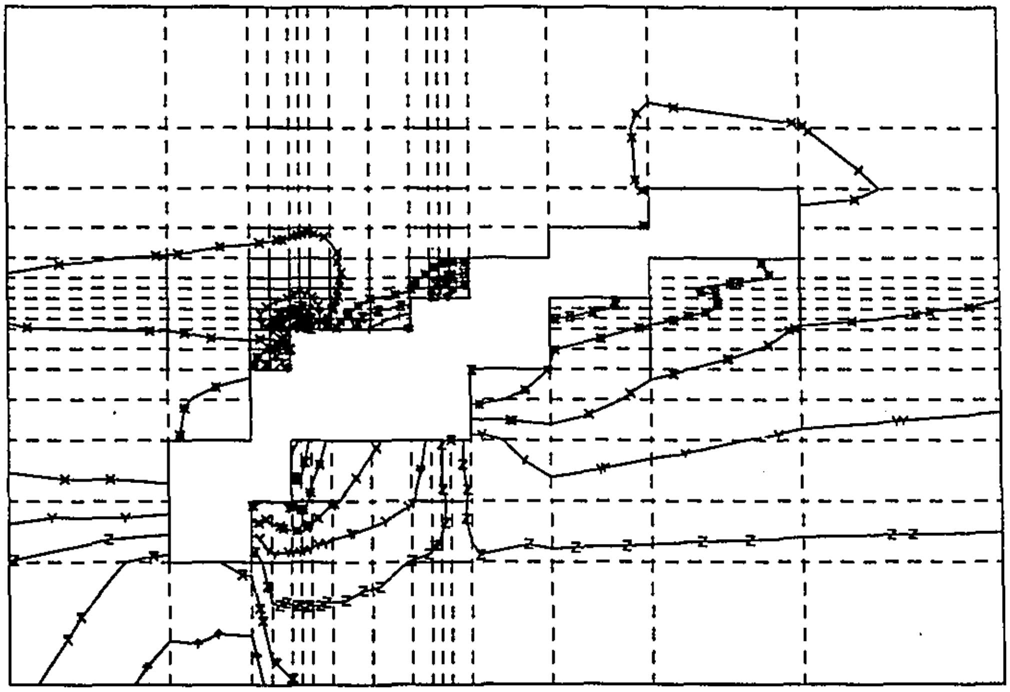

Stress Level
(MPa)
- compression
+ tension

O	-6.000 E1
▲	-5.643 E1
+	-5.286 E1
X	-4.929 E1
◇	-4.571 E1
↑	-4.214 E1
X	-3.857 E1
Z	-3.500 E1
Y	-3.143 E1
X	-2.786 E1
✱	-2.429 E1
X	-2.071 E1
I	-1.714 E1
●	-1.357 E1
⊡	-10.000 E0

Figure 8.3 Major principal stresses, Athens Mine, at the time of failure, longitudinal section.

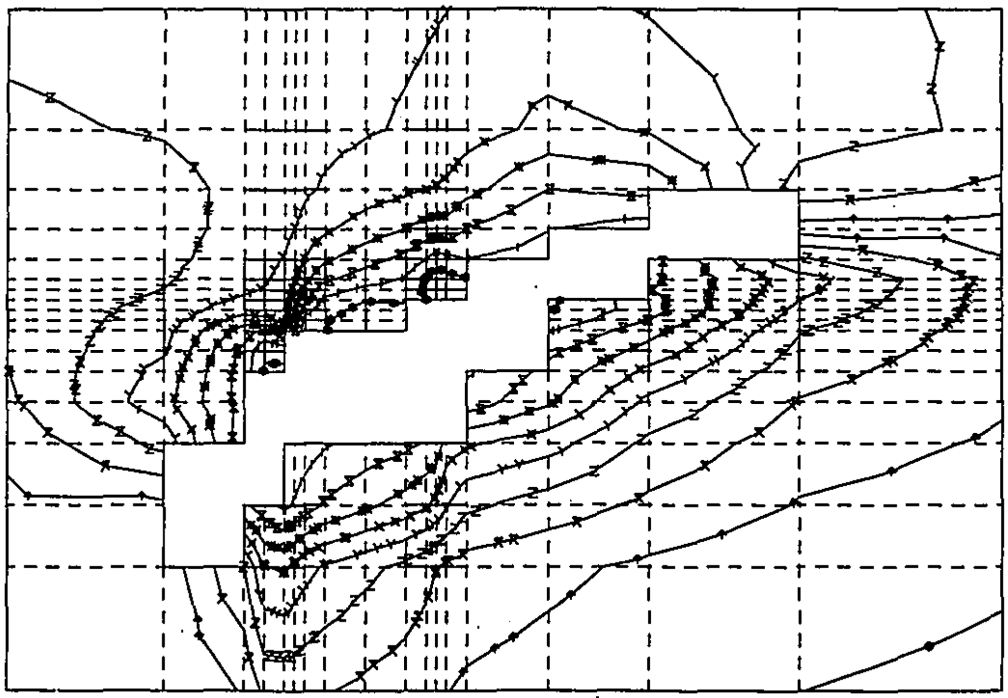

Stress Level
(MPa)
- compression
+ tension

⊙ -3.000 E1
△ -2.771 E1
\+ -2.543 E1
X -2.314 E1
◇ -2.086 E1
↑ -1.857 E1
X -1.629 E1
Z -1.400 E1
Y -1.171 E1
X -9.429 E0
✱ -7.143 E0
X -4.857 E0
I -2.571 E0
✱ -2.857 E-1
▣ 2.000 E0

Figure 8.4 Minor principal stresses, Athens Mine, at the time of failure, longitudinal section.

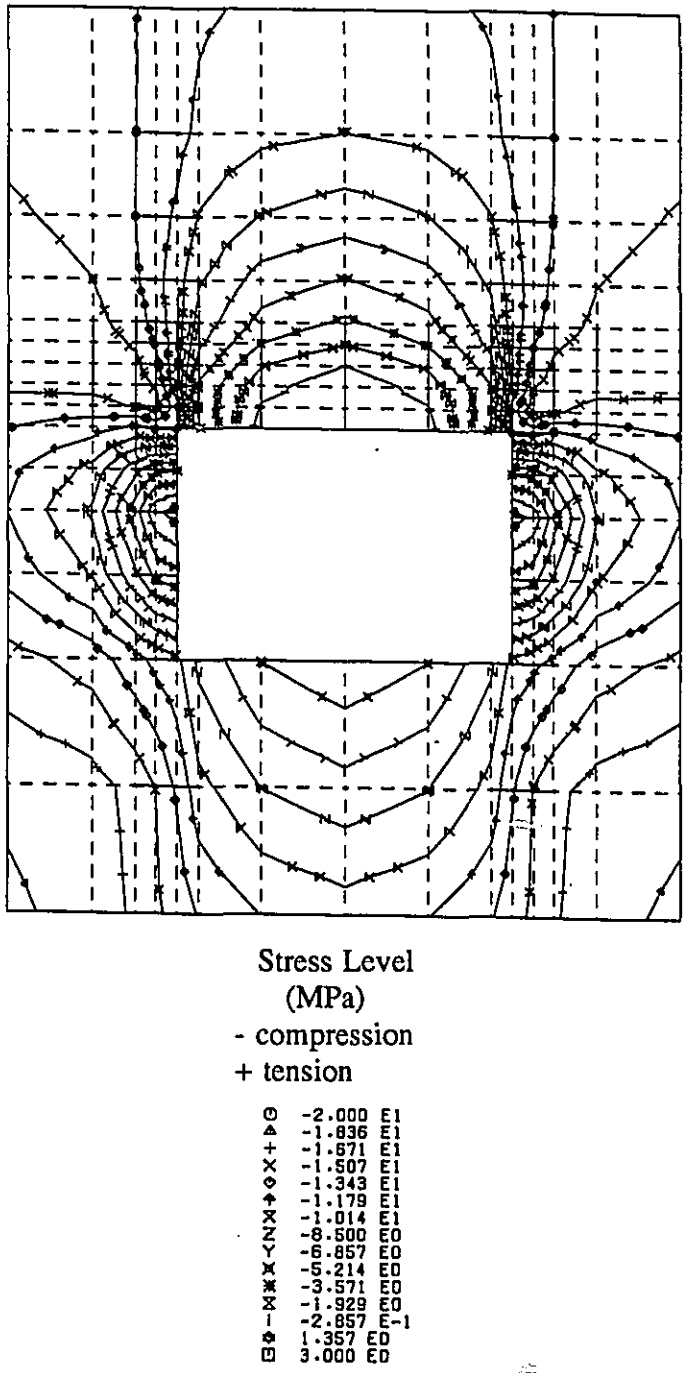

Figure 8.5 Major principal stresses, Athens Mine, at the time of failure, cross-section within the plug failure area.

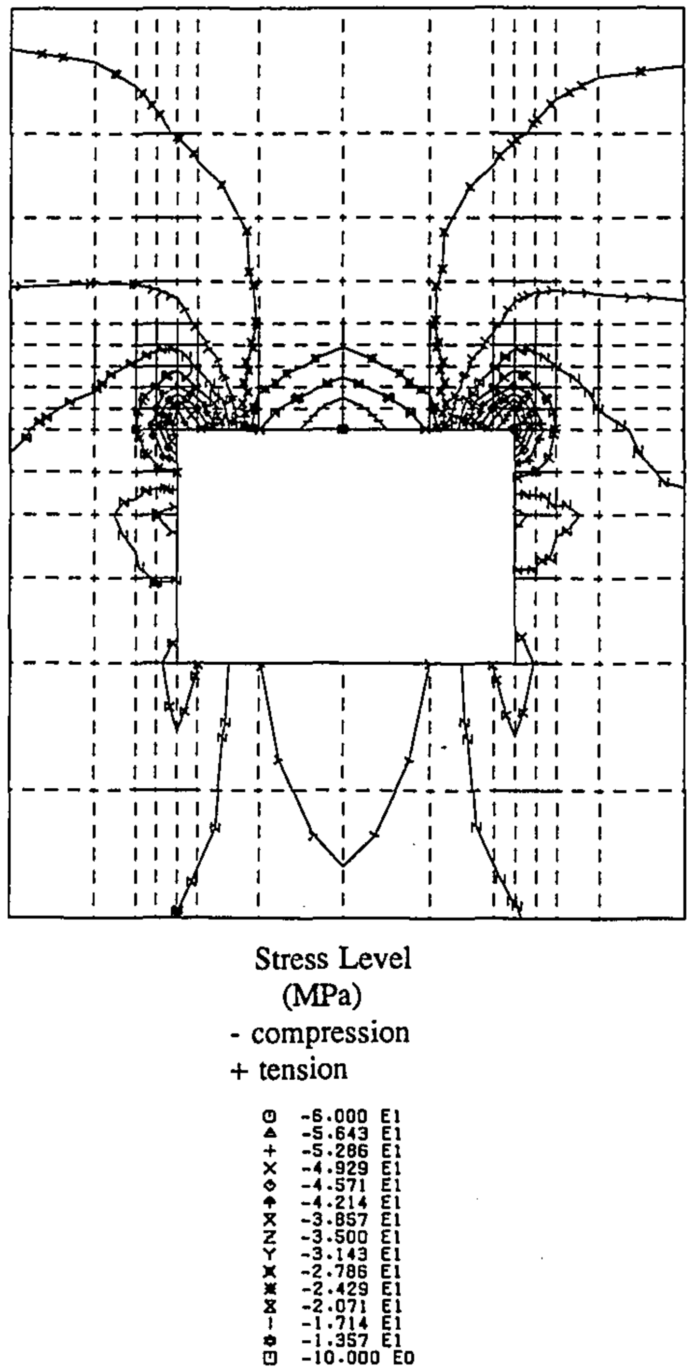

Figure 8.6 Minor principal stresses, Athens Mine, at the time of failure, cross-section within the plug failure area.

average but ranging from 20 to 39 MPa.

The cross sections, Figures 8.5 and 8.6, indicates that the upper stope corners have high concentrations of compressive stress and the stope sides low compressive (to tensile values) stresses. Application of the Hoek and Brown failure criterion, Figures 8.7, 8.8, indicate possible limit equilibrium areas in small portions of the footwall and areas of failure immediately in the crown and periphery of the mining block subjected to the plug failure.

The indication of partial failure in the crown was supported in Allen's publication, the capping immediately over the orebody breaking into relatively small masses of rock in the arching process above earlier mining operations. This broken rock is thought to have acted later as a cushion above the timber mat for the much larger mass released by the failure.

The factor of safety contours follow the outline of the diorite dykes but are always at a value of 1.7 or better there and in the overlying jasper, to surface.

8.6 APPLICATION OF ANALYTICAL EQUATIONS

8.6.1 Plug Failure

Allen has described the failure as the plug type which necessitated rupture through jasper crown as well as slippage along the weak dykes. This then implies that shearing in the jasper crown occurred and therefore that the plug weight was sufficient to exceed confinement from redistributed ground stress and the shear resistance of this jasper rock mass.

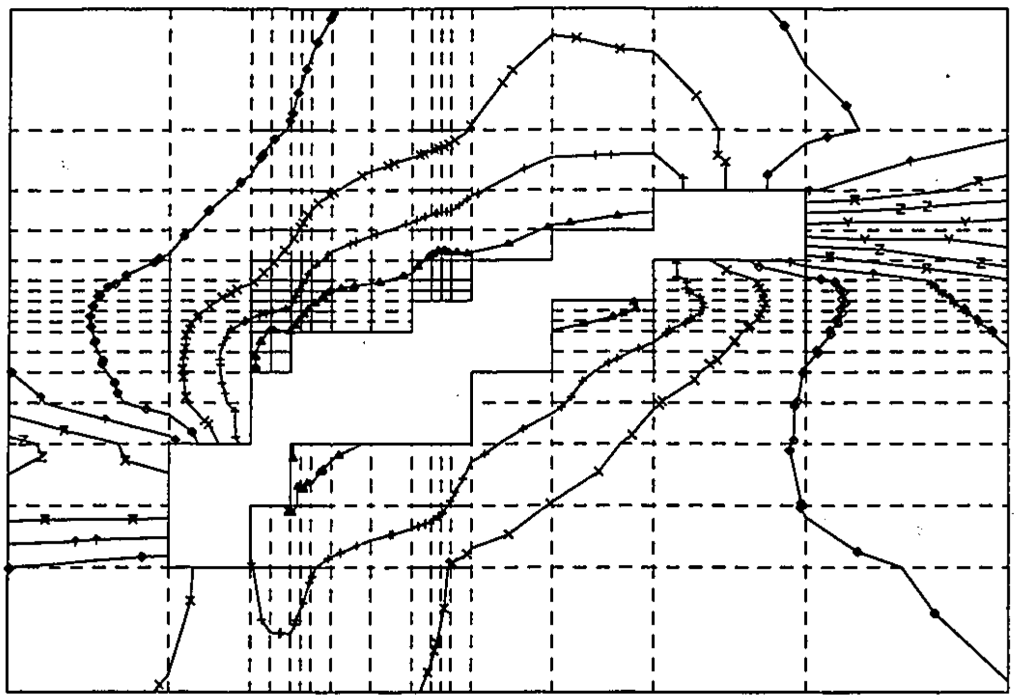

Factor of Safety

Figure 8.7 Application of the Hoek and Brown failure criterion to the Athens Mine at the time of failure, longitudinal section.

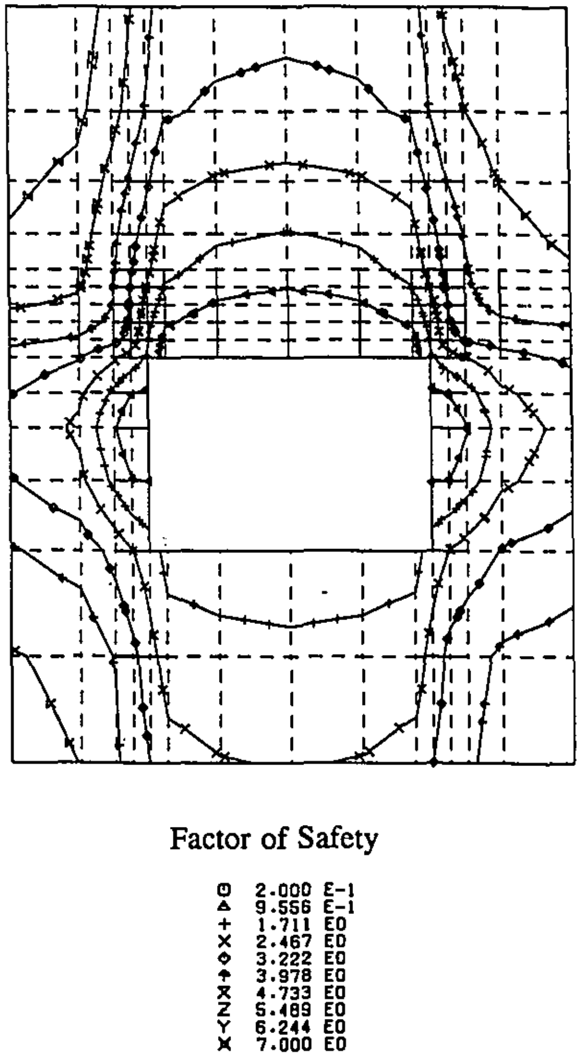

Figure 8.8 Application of the Hoek and Brown failure criterion to the Athens Mine at the time of failure, cross-section within the plug failure area.

The application of the developed analytical equation indicates that confinement was sufficient to resist plug failure, $F_s = 4.5$. The analysis was performed assuming effective vertical jointing in the jasper as well as the diorite dyke contact to define such a block. Crane [126] indicates that apart from horizontal bedding in the jasper, continuous vertical joints are the rule in the region's iron mines. Groundwater, the presence reported by Allen, was included in the analysis.

Because the boundary of the dykes has been described as weak "soap rock" by Allen, and generically so in the iron mines of this region by Crane, a low friction angle of 4° was adopted which reflects the Barton et al values [11], Table 1.5, for such conditions. A friction angle of 16° was adopted for the plane and smooth jasper joints.

The stresses were calculated using the normal component of the three principal stresses on 306 elements making up the boundary of the 3-D plug geometrically defined by Allen.

Since this calculated of safety is relatively high, the plug could not have developed by shearing through intact rock but more probably on discontinuities.

The value for the factor of safety being higher than limit equilibrium could reside in the orientation and value of the ground stresses used to numerically generated confining stresses. A change in orientation (which was approximated as E-W from a value approximately N82W) would reduce the effect of the major natural principal stress as it is currently normal to the jasper discontinuity and parallel to the weak dyke boundaries. The intermediate natural principal stress used in the model is also higher than that measured at other sites.

Furthermore, the stepped shape used in the model for approximating the actual shape of the extracted blocks could have concentrated stresses around such corners and thereby artificially increase confining compressive stresses.

8.6.2 Chimneying Disintegration Failure

Chimneying disintegration potential is important to consider as a starting mechanism which might have been followed by the plug failure.

Appendix 6 indicates that the 80 m width of the orebody would place the jasper crown at a factor of safety of 1.04 against chimneying. This assumes that the timbering used for ground support was insufficient to prevent rock mass mobilization. With the stope crown in the area of the plug failure shown by modelling to be locally failed, this might have weakened the rock mass to help chimneying disintegration develop or encourage block ravelling failure. Such chimneying however, would require that the Jasper rock mass can be sheared effectively which, from the Allen [6] or Crane [126] references is neither weak but rather blocky implying shearing of intact rock, which is probably not plausible. The possibility that chimneying disintegration in one or both dykes could have developed, and removed stresses in the lower plug areas, is plausible. This might have led to sufficient unconfinement and allowed the plug failure to develop.

8.6.3 Block Caving Failure

Appendix 6 outlines the calculations that show that a stabilization arch to block caving would not fail by internal block failure, but by bulk failure of a stabilizing arch if the height of the block cave is 180 m or more.

The Deiring and Laubsher chart Figure 1.19 indicates that this opening of hydraulic radius 15.4 m in a rock mass with RMR of 50, with a longitudinal dip of 15°, is in a transition stability mode, where dilution rather than caving occurs.

8.7 APPLICATION OF EMPIRICAL METHODS

A value of Q = 1.1 was approximated for the crown given the generic descriptions of Michigan iron mines jasper and diorite dykes structure by Crane [126] and the modulus of elasticity of rock mass, Appendix 6. This is in close agreement with the rock mass quality level at which the m and s values were chosen.

The NGI system indicates that support is required for this quality. Both the diorite dykes and the usual extensive vertical jointing in jasper [126] are very nearly vertical. With a strike length of 350 m covering blocks 1 to 3, a width of 80 m, the scaled critical span of 5 based on Q = 1.1 (Appendix 6) indicates that a thickness of 563 m would be required for limit equilibrium compared to 660 m that failed.

8.8 SUMMARY

The Athens Mine failure occurred rapidly and involved the downward displacement of an integral large rock block, a plug.

Approximate redistributed stress level and direction calculated from numerical modelling, along with plug friction properties return a factor of safety of 4.3 against failure of 3D plug. This value would be sensitive (lower) to changes in original stress direction as well as lower natural values.

The modelling used orientations and values that for the purpose of construction were slightly off that actually measured at one other Michigan minesite. Numerical modelling application of the Hoek and Brown failure criterion predicted only a limited failure of the crown, which might have been a prelude to plug failure, in the form of chimneying disintegration, ravelling or caving.

Chimneying disintegration calculations, $F_s = 1.04$ do not reflect the quality of the orebody rock mass which would not have lent itself to shearing thereby making this failure mechanism a remote possibility. It is likely, however, that chimneying disintegration could have occurred in one or both dykes thereby removing plug confinement and led to the plug failure. Block caving is not indicated empirically, and would be expected to stabilize itself at the onset, a caving height of 130 m above the stope required to prevent such a formation. The empirical surface crown pillar chart indicated a value of required thickness of 563 m compared to 660 m that actually failed.

CHAPTER 9

DISCUSSION

Common shallow hard rock mine environments have been described, as well as the nature of failures encountered at these levels. Failure specific equations have been developed to describe the failure process and the expected extent for the purpose of designing stable stopes.

The six case studies reviewed represent the typical rock mass environments of Canadian hard rock mines and the five common failure mechanisms.

From these cases four examples of failures of shallow stopes has been examined:

1) Destratification in part of the surface crown pillars at Niobec not resulting in failure to surface;
2) Chimneying disintegration and related block ravelling at Belmoral, leading to failure to surface;
3) Chimneying disintegration and block caving failures to surface at the Brier Hill Mine;
4) Plug failure to surface in the Athens Mine to surface, with a possible block ravelling or chimneying disintegration precursor.

These and other failed case studies [4] can yield information on the likelihood of stope failure to surface from the hangingwall, crown or footwall. Potential for hangingwall ravelling from the Pierre Beauchemin Mine and the Belmoral Mine indicate that without tensile stresses (usually localized), ravelling will not continue deep in the hangingwall. Hangingwall strata failures have a low probability of developing to surface unless the dip is low, since the resulting cavity is of limited depth into the hangingwall (analytical equation prediction and failure at Pierre Beauchemin, Niobec mines). One hangingwall failure was registered at the Brier Hill Mine from block caving over a very large, deep stope. The extent of the cavity from crown block falls increases with the dip of the discontinuities constituting block surfaces to the extent where vertically jointed rock masses, when lacking confinement, have failed to surface such as several mines within the wide regional mining of Cobalt [4]. Chimneying disintegration has developed in the crowns of stopes, at Belmoral, Brier Hill and Selbaic Mines, and continued to surface. No such stope hangingwall failure was recorded at the Brier Hill Mine, nor has such a footwall failure been reported. However, it is probable that the Bousquet 1 hangingwall failure adjoining the surface crown pillar was by chimneying disintegration. The back-analysis of the Pamour surface crown pillar failure [43] showed that in a generally foliated environment ravelling of thin slabs from the steep dipping stope periphery led to sill and surface crown pillar collapse.

It would appear, therefore, that the failure of shallow stopes is expected to occur within or very close to the surface crown pillar.

Examination of the failed and unfailed cases also provided data for the effect of geomechanics parameters on each type of failure.

Plug failure potential depends considerably on the distribution of stresses available to resist movement, and on the dip of the delimiting discontinuities. This is seen by examining the Pierre Beauchemin, Dumagami and Athens cases. For Dumagami, slight increases in compressive stresses are sufficient to increase the factor of safety significantly. For similar plug weights and resisting stress levels (Pierre Beauchemin mining step 3 and Dumagami step 2), the effect of a vertical plug failure versus a 40° inclined plug provides a factor of safety of 14.8 for the inclined block versus 6.7 for the vertical one (standardized to surface angle of friction of 35° in both cases).

Deep plugs, such as the Athens Mine (660 m high), are for the most part confined by natural stresses, only the bottom 150 m being affected by high, redistributed compressive stresses. In this case a 10% reduction in the values of the original stress field would only reduce the factor of safety from 4.5 to 4.0. Therefore these cases show that for the common shallow stopes, with depths to 50 m, the effects the original stress field value (and its proper measurement), the stope geometry, discontinuity dip and depth of stope are important.

The Athens Mine case study also indicated the effect of the friction properties on the factor of safety. With a reduction or increase in the surface angle of friction of 2° from the 4° used for "soapy" gouge, the factor of safety range is 4.1 to 5.3 compared to the 4.5 calculated. The difficulty also arises in defining an angle of friction for very weak material surfaces in situ, which if in the case of the Athens Mine dykes is as bad as it is described by Allen [5] may not contribute to shear resistance.

Similarly, resistance against plug failure would be greatly increased if part of the discontinuities on which a plug will fail was composed of rock or rock mass material to be sheared, i.e. the discontinuities were not uninterrupted to surface. A one meter length by 1 m wide area of intact rock interrupting the path of one of the block's discontinuities would provide from 10 MN to 60 MN of direct resistance to weight. This is based on cohesion of typical intact rock [104]. In this case of the Pierre Beauchemin Mine, this compares to a weight force of 2.5 to 7.1 MN for rock of average density (0.027 MN/m^3)

and respective plug heights of 6 m to 17 m.

Block sliding in the crown periphery has been considered in case studies where the sliding plane dipped from 41° to 85°. Even in the case of the highest dip, where block weight and size were also high, the required tangential compressive stress to maintain stability is less than 0.50 MPa. Compared to this requirement, crown periphery tangential stress has been compressive, varying approximately from 0.8 to 31 MPa for stope dips of 45° - 90°. The required compressive tangential stress was therefore available. These redistributed stresses, in a two-dimensional section, are based on natural horizontal stresses 1.5 to 3 times vertical stress and stope height to width ratios of at least one. When discontinuities are dipping, block falls will lead to a cavity after which block slides must occur for failure to continue. In this case the extent of the cavity caused by falling blocks becomes important versus available surface crown pillar thickness. In the case of vertically jointed rock masses development to surface without stoppage would occur if confining stresses are insufficiently compressive. Furthermore, it has been shown that when the dip of the block sides which are confined by ground stresses are less than the friction angle of that surface, block falls will occur irregardless of the imposed stress. Block ravelling failure in the surface crown pillar is therefore not anticiapted in the ϕ_r to ~ 80° dip range.

Depending on the geometry and stope size, portions of stope hangingwalls and/or footwalls of case studies are subjected to tensile tangential stresses. Hangingwall block slide failures are therefore possible as witnessed by the Belmoral case study, but may be limited to the local near-stope tensile areas. Low compressive stresses are needed for stabilization.

Stratified rock failures can lead to stable cavities. Only a limited load is expected from overlying strata because of load sharing. Progressively shorter stratas are expected to fail because of stratum thickness and variation in bending properties of rock.

In the Niobec Mine destratification case, where only bedding joints occurred, failures were of limited span, sometimes less than the stope span. The height of such failures were less than that calculated using the analytical equation, which predicts a developed cavity height approximately 25% the cavity width. This could be due to similar stope dimensions resulting in plate conditions which are more self-supportive than beam conditions used in the analysis.

The case studies indicate that chimneying disintegration to surface occurs in rock masses with low cohesion. The analytical equation developed has confirmed the known cases of failure which occurred in rock masses with cohesion less than 0.14 MPa. Figure 9.1 shows the calculated relationship between factor of safety and span for lower cohesion values.

The general correlation between stope span and rock mass cohesion values to define chimneying disintegration, at $F_s = 1$, is

$$L_{critical} = 100 \ c_m \tag{9.2}$$

where L is expressed meters and c_m in MPa. Insufficient numbers of case studies exist to indicate if this correlation should be used for rock mass cohesion greater than 0.14 MPa, but the Athens Mine case, indicating a factor of safety of 1.04 for a rock mass of $c_m = 0.8$, has shown that chimneying did not occur to surface.

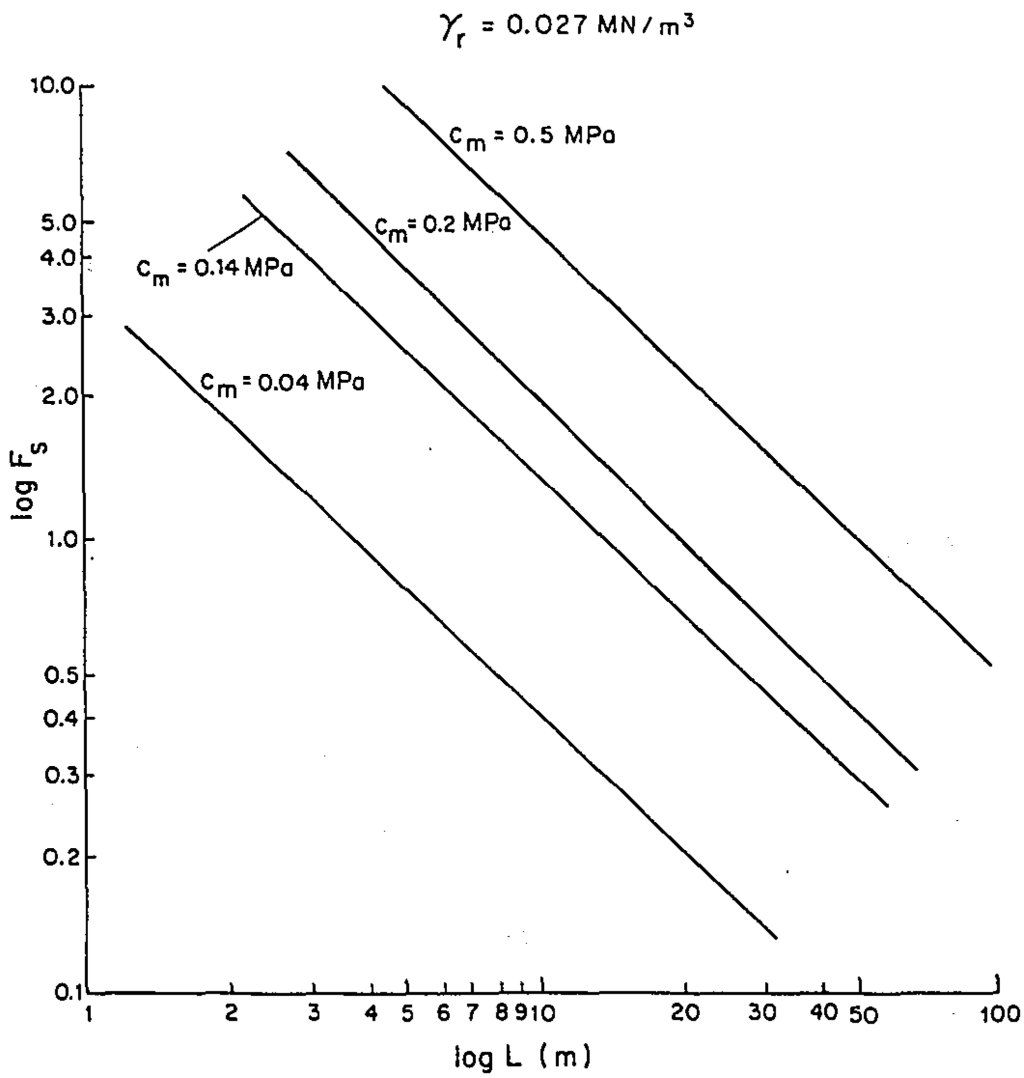

Figure 9.1 Relationships between stope span L, rock mass cohesion c_m and factor of safety F_s, chimneying disintegration failure analysis

In order to accommodate chimneying the failure arcs would have to incorporate the trace of the discontinuities. Contrary to the path of least resistance in degradable schist and altered rock that shear ruptures can take, blocks in a rock mass would in effect force a failure surface to go around the blocks involving large interlocking asperities which would imply shearing of intact rock. Therefore the boundary for chimneying disintegration could lie with the smallest size which the rock mass is broken down to and allow rockmass shearing to occur. In the case of schists and altered rock this can be a naturally existing small size, down to the particle size.

In the case studies, the effect of the imposed compressive failures brought about by redistributed stresses which accompany chimneying disintegration, is to break the rock mass. This has for effect not only to break down the mass but also to remove part or significant portion of its confinement thereby allowing gravity action to occur, the basis for the chimneying disintegration analysis.

Application of the equations to calculate the potential for stabilization of block caving rock masses has shown that at shallow levels caving would be difficult to stabilize itself. Stresses within a stabilizing arch would be sufficient to overcome integral bulk material strength. High lateral ground stresses would be required to develop compressive failures of individual caving material blocks. Block caving is known to have occurred to surface at the Brier Hill Mine in the hangingwall of a large extraction area. The immediate portion of this periphery was in tension. Stabilization with arching in this case was not indicated by the analytical equation.

The limit between potential for block caving versus potential for chimneying disintegration in poor rock would seem to depend on the stress conditions imposed and span of the opening. In the Brier Hill case where block caving has occurred in the hangingwall of the main 15 m wide, 150 m high stope, the chimneying disintegration occurred over a 4 m x 8 m (plan) borrow stope (with an estimated height of 2.5 m). These dimensions and Belmoral's 3.8 m wide by 3.8 m high 1-7 exploration drift where chimneying also occurred can be compared to the Diering and Laubscher caving potential chart, Figure 1.17. In the Brier Hill and Belmoral cases an adjusted RMR of 15 to 20 would require a hydraulic radius of 8 to 10 for block caving to occur. This would require a stope larger than the openings involving chimneying disintegration. The almost exhaustive extraction of the Brier Hill orebody, its main stope, provided this condition.

The case studies considered provided insight into several aspects of design. They confirmed the distribution of failure mechanisms and cause for instabilities outlined in Table 1.2. Two reviews can be made, Table 9.1: that most failures to surface will occur from the surface crown pillar and that chimneying disintegration is not seen as occurring because of a lack of clamping stress with contribution from compressive stresses sufficiently high to fail weak rock and reduce shear resistance. Two operational decisions permit such a failure to occur: too large a period of time before support is imposed, allowing for the weak mass to mobilize and start failing, and allowing for a space in which failed material (with low bulking factors) and failure proceed without the failure choking. Block slides which require little confinement are not expected to develop to surface within in the footwall.

With regards to Tables 1.2 and 1.3, the most expected failure mechanisms are ravelling and chimneying. Block fall ravelling has been shown to be possible in case studies (Pierre Beauchemin, Belmoral, and Athens) where blocks and structures are well

Table 9.1 Summary of Instability Element for Failures of Shallow Stopes of Hard Rock Mines

Type of Failure	Propitious Environments (Figure 1.3)	Mobilized Rock Mass	Lack of Ground Stress Clamping	Controlling Instability Elements
Rock fracturing	a	FW, CR, HW	No	Stress loading (p) (gravity or induced)
Plug failure	d, e, f	CR	Yes (s)	Near-vertical dipping continuous discontinuities (p); low friction properties (t)
Ravelling	b, e, f, g	CR, HW*	Yes (s)	Blocky rock mass (p); steep dipping joints (s)
Strata failure	f	CR, HW*	No	Stratification (p); stope span (s)
Chimneying disintegration	c, d, e, g	CR, HW	No+ (s)	Material of low cohesion (but not cohesionless (p)); small size rock mass particles
Block caving	b, e, g	CR, HW	Yes (s)	Well developed jointing and blocks (p); stope span (t); tensile rock mass failure

\+ overstressed
* shallow dipping

Order of Importance:
p primary
s secondary
t tertiary

defined, and chimneying disintegration in all case studies where the rock mass is weak because of strong metamorphic fabric such as graphitic slate or mica schist as well as in altered rock examples presented. Ravelling would account for the 20% failures of blocky rock masses and perhaps some of the 11% failures of stratified masses. Chimneying disintegration would probably account for most of the 5% failures of weak orebodies, 11% failures of weak walls, some of the 44% failures of the faulted and weak masses and some of the 17% failures of the generally foliated rock masses.

Although a limited cross-section of stope geometries (including sizes) were examined, failure based design of shallow stopes can be seen to depend on the level of imposed stress and the effectiveness and orientation of discontinuities. Stope size does dictate the level of imposed stope periphery stresses as shown in the Dumagami, Niobec and Athens Mine case studies. Specifically, vertically high stopes concentrate high compressive stresses in the crown when the major principal stress is orthogonal to the longitudinal direction compared to long extraction areas with stresses parallel to this direction which will have low stresses in the crown. The case studies examined were not representative of irregular geometries. The proximity of on-dip stopes seen in the Pierre Beauchemin, Dumagami and Belmoral cases indicate an effect on the nature and location of redistributed ground stresses. But the horizontal longitudinal proximity as at Niobec does not substantially reduce the crown stresses for the stopes in the center of such a sequence. Case studies with stopes distributed in both directions (e.g. grid) have been known to fail by block falls and plug failures [4][32].

Intact or poorly jointed rock environments are difficult to fail in the case of very large stopes (Niobec Mine) which reflects the few failures seen in this environment.

Conventional numerical modelling, although useful to provide stress distributions, was unsuccessful in providing the extent and development of known failures. Only where weak material was involved, was failure predictable but not indicated to reach surface.

The conventional NGI empirical method was only successful in predicting need for support. The dedicated empirical surface crown pillar method was successful in anticipating failures, but not to provide the minimum dimensions to avoid these. It commonly underestimated the required surface crown pillar thickness and in the case of weak rock, might provide widely varying answers for a small variation in the estimate of rock mass quality.

CHAPTER 10

STABILITY ANALYSIS PROCEDURE

Whether at the pre-extraction stage or when considering established shallow stope configurations, a standard methodology to evaluate the related stability should be followed as a reference point for decision making and communication purposes as well as to guide the necessary work with regards to data collection, analysis and application of analytical methods. This Chapter summarizes and places in perspective the elements involved in analysing the stability of shallow stopes of hard rock mines. A step-by-step procedure is defined for such stability evaluation, identical to that used in constructing the case studies of Chapters 3 to 8.

An overall design process was established by Bétournay [1], Figure 10.1. It retains the concept of following a step-by-step procedure, but is sufficiently generic to maintain a flexibility for various site configurations, Figure 1.1. It incorporates decision making and changes in mining strategy.

The stability analysis procedure defined here will provide details to the four related steps of this process: Identification of Deposit and Regional Characteristics, Geotechnical Investigations, Data Analysis, and Stability Analysis (Dimensioning). Ground control and monitoring aspects will also be discussed.

The shallow stope analysis procedure consists of following a decision flow chart which attempts to direct the analysis based on the rock mass environment in place (dependent on geological classification, evaluation of the predominant discontinuity and their disposition and intact material strength), the expected failure mechanism (s) and the

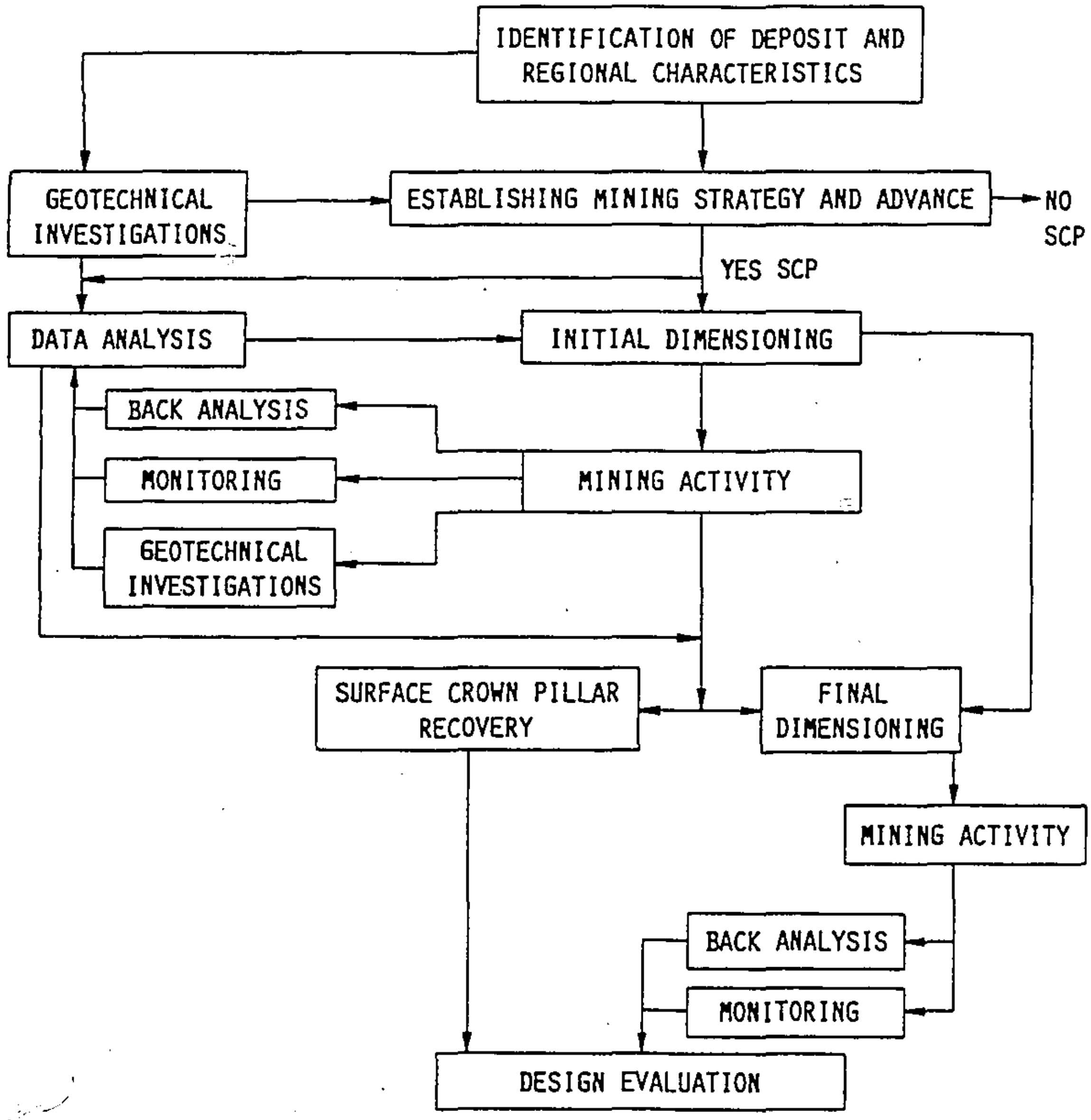

Figure 10.1 Surface crown pillar design process [1]

analytical methods applied to arrive at a stability evaluation. This is shown in Figure 10.2. In support of this analytical progression is Table 10.1, a catalogue containing the range of investigations, parameters and methods to select from for guiding the analysis with respect to the support work required and the order in which it should be performed.

The end result of this analysis will be the obtention of one or several factors of safety representing the cross section of possible failure mechanisms. In order to properly evaluate the most likely development of instability leading to failure (from one or a sequence of failure mechanisms), the way in which the safety factor was calculated as well as the limitations of each limit equilibrium equation must be understood.

Table 10.2 summarizes the Advantages of these analyses, Table 10.3 summarizes the limitations associated with the stability analysis equations (Chapter 2; Table 10.1). As mentioned in Chapter 2, these are limit equilibrium equations representing actual mechanical conditions of the common failure mechanisms.

Simplifications have been adopted to reduce the complexity of block to block interactions. In the case of ravelling equations, only peripheral activity is considered as representative of the gradual block dislocation process. Therefore, continuum stress distribution and no internal rock mass movement is considered. A simplification of the block size distribution (one size for each geomechanical unit) is also made for the benefit of less complex calculations and lab testing procedures.

A 2-D plane strain analysis is also adopted to significantly reduce the complexities of a third joint set out of the plane of analysis. This does, however, result in a more conservative stability evaluation, because the shear resistance provided by such a third side is not considered.

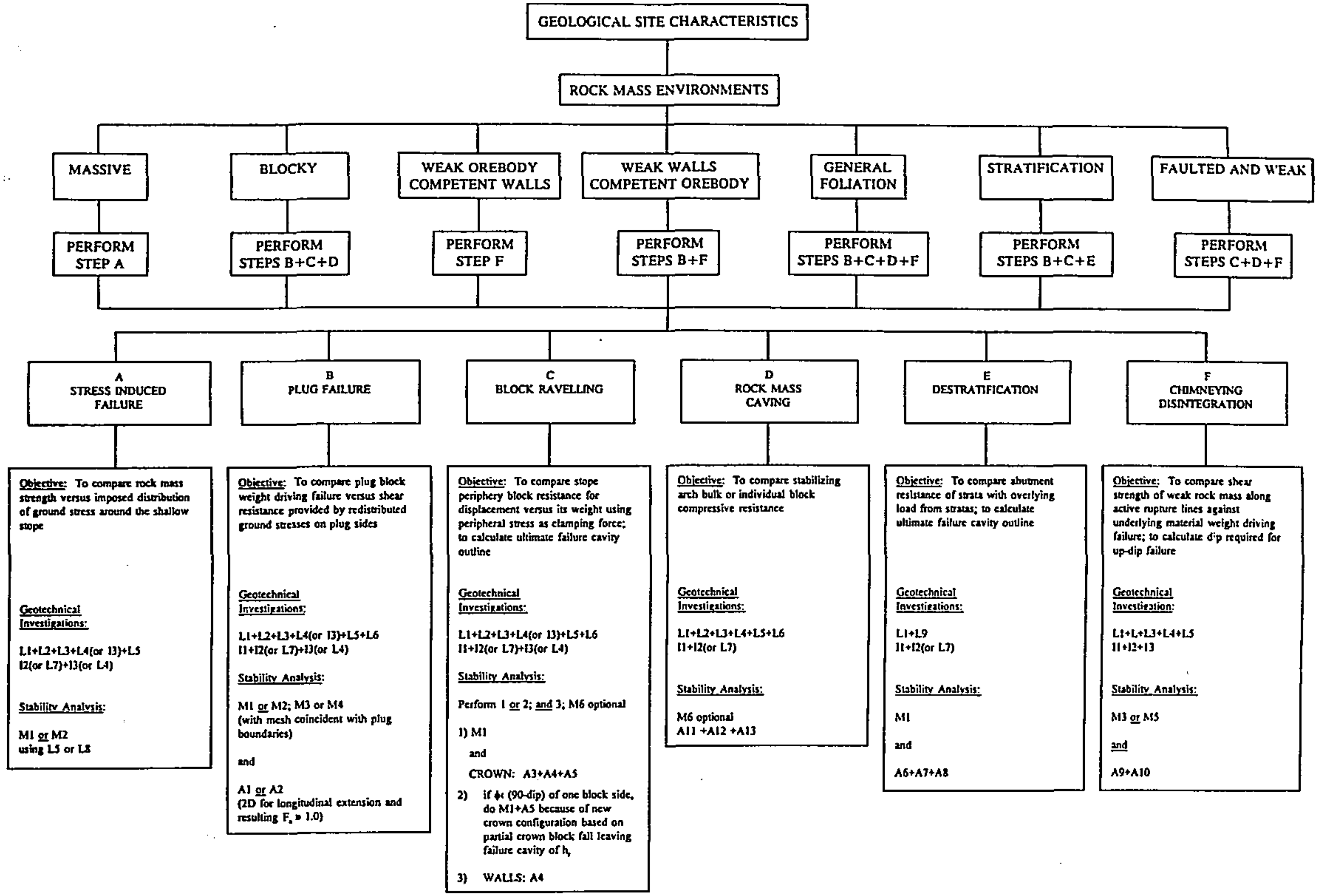

Figure 10.2 Stability analysis procedure for shallow stopes of hard rock mines.

Table 10.1 Compendium of Analysis Procedure Elements

Step	Class of Work	Element	Descriptive Element	Applied Equation (Reference Table)	Parameter(s) Obtained
Geotechnical Investigations	Laboratory	L1	Intact rock strength; tensile tests, uniaxial and triaxial compression tests		E, υ, σ_c, σ_t, ϕ (uniaxial)
		L2	Calculations of Hoekk and Brown intact strength Mohr envelope, using L1 data		m_{lab}
		L3	Discontinuity properties; roughness, alteration, orientation, spacing; rock core survey		
		L4	Calculation of rock core rock mass RQD and quality (CSIR or NGI) from L3 data		RQD, RMR or Q
		L5	Calculation of Hoek and Brown rock mass strength Mohr envelope, using L2 to L4 data	$m_{field} = m_{lab}\, e^{\frac{(RMR-100)}{28}}$ $s_{field} = e^{\frac{(RMR-100)}{9}}$ $\tau = (\cot\phi - \cos\phi)\frac{m_{field}\sigma_c}{8}$ $\phi = \arctan\frac{1}{\sqrt{4\,h\cos^2\theta - 1}}$ $\theta = 1/3\left[90 + \arctan\frac{1}{\sqrt{h^3 - 1}}\right]$ $h = 1 + \frac{16(m_{field}\,\sigma + s_{field}\,\sigma_c)}{3\,m_{field}^2\,\sigma_c}$	m_{field}, s_{field}, c_{mass} (τ at $\sigma_n = 0$), ϕ mass

Table 10.1 (continued)

		L6	Physical properties of discontinuity surface τ-σ relationship; shear test		k_n, k_s, c, ϕ_r
		L7	Empirical calculation of rock mass modulus of elasticity from L3 or I3	$E_m = 10^{\left(\frac{RMR-40}{10}\right)}$	E_m
		L8	Selection of Hoek and Brown rock mass strength parameter	Table 2.1	$m_{(field)}$, $s_{(field)}$
		L9	Beam tensile test; thickness of stratum		E_b, h_t, h_c, σ_t, t
	In situ	I1	Natural ground stress values and orientation; measurement of undisturbed natural ground stress at < 100 m.		Distribution and values of σ_1, σ_2, σ_3
		I2	Rock mass modulus of elasticity; dilatometer tests in boreholes at levels comparable to shallow stopes		E_m
		I3	Evaluation of rock mass RQD and quality (CSIR or NGI), groundwater	RQD = 115 - 3.3 J_v	RMR, Q, level of water table
Stability Analysis	Numerical Modelling	M1	2-D elastic finite element application, for stopes of extensive longitudinal dimension within a rock mass of elastic behaviour. Failure criterion: Hoek and Brown.		
		M2	3-D elastic finite element application, for stopes of limited longitudinal dimension, within a rock mass of elastic behaviour. Failure criterion: Hoek and Brown.		
		M3	2-D elasto-plastic finite element application, for stopes, of extensive longitudinal dimension, with a rock mass where one or more unit exists with non-elastic, irrecoverable strain. Failure criterion: c-ϕ.		
		M4	3-D elasto-plastic finite element application, for stopes of limited longitudinal dimension, within a rock mass where one or more unit exists with some non-elastic, irrecoverable strain. Failure criterion: c-ϕ.		

Table 10.1 (continued)

		M5	2-D large strain finite element application for stopes of extensive longitudinal dimension, with a rock mass where one or more units exists with large non-elastic, irrecoverable strain.		
		M6	2-D discontinuous, block, application for stopes of extensive longitudinal dimension, within a rock mass of effective block distribution.		
	Analytical Equation	A1	Uninterrupted discontinuities parallel and vertical, or dipping away from the stope (wedge shape), at or between extension of stopes walls, intersected by vertical cross discontinuities to form 3-D plug. Calculation of normal stress component to stope walls (plug surfaces) for each modelling element in contact with plug. Comparision to driving weight and stress imposed force in the direction of driving weight.	$F_s = \dfrac{\sum_{i=1}^{n} \left[c_i A_i + \left(\left[\sum_{j=1}^{m} \sigma_{nj} A_j \right] - \dfrac{\gamma_w (H_i - d)^2 b_i}{3} \right) \tan\phi_{ri} \right] \sin\psi_i}{V\rho g + \left[\sum_{i=1}^{m} \left[\sum_{j=1}^{m} \sigma_{nj} A_j \right] - \dfrac{\gamma_w (H_i - d)^2 b_i}{3} \right] \cos\psi_i}$	
		A2	Uninterrupted dipping parallel discontinuities at or between extension of stope walls, with intersecting cross vertical discontinuities to form 3-D plug. Calculation of normal stress component to stope walls (plug surfaces) for each modelling element in contact with plug. Comparision to driving weight and stress imposed force in the direction of driving weight.	$F_s = \dfrac{c_s A_s + \left[\left[\sum_{j=1}^{m} \sigma_{nsj} A_{sj} \right] + V\varrho g \cos\psi_s - \dfrac{\gamma_w (H_s - d)^2 b_s}{3} \right] \tan\phi_{rs}}{V\varrho g \sin\psi_s + \left[\sum_{j=1}^{m} \sigma_{n2j} A_{2j} - \dfrac{\gamma_w (H_s - d)^2 b_s}{3} \right] \sin(\psi_s - \psi_2)} +$ $\dfrac{c_2 A_2 + \left\{ \left[\left[\sum_{j=1}^{m} \sigma_{n2j} A_{2j} \right] - \dfrac{\gamma_w (H_s - d)^2 b_2}{3} \right] \cos(\psi_s - \psi_2) \right\} \tan\phi_{r2}}{V\varrho g \sin\psi_s + \left[\sum_{j=1}^{m} \sigma_{n2j} A_{2j} - \dfrac{\gamma_w (H_i - d)^2 b_i}{3} \right] \sin(\psi_s - \psi_2)} +$ $\dfrac{\sum_{i=3}^{4} \left[c_i A_i + \left(\left[\sum_{j=1}^{m} \sigma_{nij} A_{ij} \right] - \dfrac{\gamma_w (H_i - d)^2 b_i}{3} \right) \tan\phi_{ri} \right]}{V\varrho g \sin\psi_i + \left[\sum_{j=1}^{m} \sigma_{n2j} A_{2j} - \dfrac{\gamma_w (H_i - d)^2 b_i}{3} \right] \sin(\psi_s - \psi_2)}$	

Table 10.1 (continued)

		A3	Calculation of minimum normal force required for two supporting sides of a peripheral falling crown block to develop shear resistance for support (valid only if $\phi_r >$ (90-dip) of one or more block sides).	$W + \sum_{i=1}^{2} A_i \sigma_{avg} \cos^2\alpha_i \sin\alpha_i = \sum_{i=1}^{2} \left(c_i + \sigma_{avg} \cos^2\alpha_i \tan(\phi_n)\right) A_i \cos\alpha_i$	
		A4	Calculation of ultimate cavity height from crown block falls.	$h_r = \frac{L \sin(\psi_1 - \omega) \sin\psi_2}{\cos\omega \sin\left(180 - (\psi_1 + \psi_2)\right)}$	
		A5	Calculation of minimum normal force required to confine sides of a peripheral sliding block to develop shear resistance for support.	$W \sin\psi_s = 2cA_s + (2\sigma_{avg} A_s \cos^2\alpha_{sr} + W \cos\psi_s) \tan(\phi_n)$	
		A6	Calculation of minimum length (L_{j+1}) of a loaded stratum.	$T_s = \frac{p_{l+1} L_{j+1}^2 h_t \cos\theta}{4\left(\frac{E_c}{E_t} h_c^3 + h_t^3\right)} \Gamma - \sigma_e$	
		A7	Calculation of ultimate failure cavity height from consecutive stratum failure due to overlying load causing diagonal (shear) failure of strata at at abutment.	$H_c = \frac{L - L_{j+1}}{2 \tan(45° + \phi/2)}$	
		A8	Calculation of stable length for voussoir arching of failed strata.	$z_o = t(1-n)$ $f_c = \frac{1}{4}\frac{\gamma_r L^2}{n z_o}$ $f_{av} = \frac{1}{2} f_c \left(\frac{2}{3} + \frac{n}{2}\right)$ $A_L = L + \frac{16}{3}\frac{z_o^2}{L}$ $\Delta A_L = \frac{f_{av}}{E_m} A_L$	

Table 10.1 (continued)

				$z = \left[\frac{3L}{16}\left[\frac{16z_c^2}{3L} - \Delta A_L\right]\right]^{1/2}$	
		A9	Resistance of weak rock mass along active rupture lines versus mobilized weight, in chimneying disintegration.	$F_s = \frac{1}{\gamma_r\left[\frac{(45^\circ + \phi/2)\,\pi r^2}{360} - \frac{h_1 N}{2}\right]} \sum_{i=1}^{n} \frac{s}{\sin\left[\tan^{-1}\left[\frac{(h_{ik} + h_{(i+1)k})\,0.5}{N + (i-1/2)s}\right]\right]}$ $c_m \cos\left[\tan^{-1}\left[\frac{(h_{ik} + h_{(i-1)k})\,0.5}{N + (i-1/2)s}\right]\right]$	
		A10	Limiting conditions for chimneying disintegration to continue up-dip.	$1 \leq \frac{\Sigma\, T_i + W_T \cos\psi \tan\phi}{W_T \sin\psi}$	
		A11	Bulk resistance of block caving stabilizing arch versus internal stress imposed.	Table 2.1 $\sigma_1 = \sigma_3 + \sqrt{m\sigma_c\,\sigma_3 + s\sigma_c^2}$ (strength) $K_a = \frac{\sigma_1}{\sigma_3} = \frac{1 - \sin\phi}{1 + \sin\phi}$ $\sigma_1 = \gamma_r\, Z$ (stress) $F_s = \frac{\sigma_1 \text{ (strength)}}{\sigma_1 \text{ (stress)}}$	
		A12	Compression resistance of blocks within block caving stabilizing arch versus imposed stress.	Table 2.1 $F_s = \frac{\sigma_c}{\sigma_1}$	
		A13	Evaluation of caving potential with Diering and Laubscher chart.	Figure 1.19	

Table 10.2 Advantages of Analytical Equations

Plug	Ravelling	Destratification	Chimneying Disintegration	Block Caving
Representative of failure mechanisms	Representative of failure mechanisms	Representative of failure mechanism	Representative of mechanism	Considers stabilizing mechanism
	Simple	Simple	Simple	Simple
Accurate (exact conditions and mechanics considered)	Compares ultimate stable cavity outline versus location of surface	Considers overlying strata and axial loads	Provides minimum rock mass resistance required to avoid failure	
Allows for input of ground control effect	Allows for input of ground control effect	Compares ultimate stable cavity outline versus location of surface	Allows for input of ground control effect	
		Allows for input of ground control effect		

Table 10.3 Limitations of Analytical Equations

Plug	Ravelling	Destratification	Chimneying Disintegration	Block Caving
Preparation and computationally Intensive	Simplified 2-D Block distribution	Elastic unjointed Analysis	Pre-determined Failure	Assumes Arbitrary material strength
	No complex block motion	2-D	2-D	Assumes vertical cave walls
	Modelling intensive	May not represent thin strata		
	Continuum stress Distribution	Strata of identical properties		

The plug failure equation, precise in its representation of actual conditions, requires detailed preparation and computation work: numerical modelling with proper mesh distribution around the surface crown pillar, calculation of normal plug surface stress components from the modelling results, and calculation of total normal force on the plug surface.

The analysis of destratification is based on an elastic plane strain distribution of stresses, which may not be representative of crowns with similar longitudinal length and span. This avoids the complexities in considering each stratum as a clamped plate. The analysis, which considers the development of shear cracks away from the abutment, is dependent on identical strata properties with sufficient thickness to behave in this fashion rather than the case of thin strata expected to fail completely in shear at the abutment.

Chimneying disintegration considers a failure surface pre-determined with circular components and in 2-D to avoid complexities brought on by 3-D analysis and/or non-circular consideration. This parallels the general slope stability circular analysis. It may not be entirely representative in cases where material foliation thickness or mechanical behaviour variations occur within the rock mass.

Caved material strength, being used to examine the propensity for a stabilizing arch to develop, is based on bulk arch strength or block to block intact rock strength. In order to satisfy the Krynine principle of granular soil arching, the rock mass joints, and therefore block sides are assumed to be cohesionless. This may be a conservative approach to the self stabilization of such a rock mass, as block with cohesive surfaces cave poorly and readily form stabilizing arches [45].

A common limitation to several of these analyses relates to the bounds of applicability. As such, what is the boundary between ravelling and block caving, and chimneying disintegration and block caving? However, because the ravelling, chimneying disintegration and block caving incorporate simplifications which err on the side of underestimating stability, designs using these can effectively reduce the onset for such occurrences.

Ground control and monitoring aspects to consider vary according to the failure mechanism anticipated and the mining method practised but must nonetheless address the anticipated extent of failure and prevent failure from reaching surface.

Only plug failures occur rapidly, without appreciable movement to warn of need for artificial support. In this case, because the mass involved is potentially large, sufficient support may not be found, thereby placing the entire emphasis of such failure prevention on monitoring of changes in stabilizing and destabilizing parameters: variations in groundwater pressure, reduction in shear strength with time and clamping stress change. It must be anticipated that proximal mining activity will change the redistributed stress field. Removal of destabilizing forces include removing lower portions of a plug by blasting, such as Vertical Crater Retreat, if plug weight or removing all of a crown pillar is desirable, and lowering the groundwater table by well pumping.

Block caving and chimneying disintegration represent an uncontrollable and self progressive rock mass failure started at some point during the creation of a shallow stope. Ground control becomes a preventative measure in the sense of keeping the rock mass integral without allowing failure to begin and proceed beyond the operators' capability to apply support when failures develop rapidly. Mobilization of such a rock mass can be prevented if ground support such as cable bolting is pre-applied to areas of future extraction. In this fashion ground support would be present at the moment of and around newly created stope periphery.

Ravelling and destratification is another example of progressive failure, but has occurred reasonably slowly so that control of peripheral block movements can be achieved when peripheral and conventional support is applied during stope expansion. Areas not accessible, such as those created during bulk mining (longhole mining, blasthole mining, VCR, etc.) should consider installation of cable bolts from remote accessways.

The pattern and therefore mechanical contribution to the stabilizing forces against failure by artificial support can be calculated and input as forces in the analytical equations. In the case of block movements (plug, ravelling) the total contribution of the ground support opposing the direction of weight destabilization should be considered.

Against surface shear movement such as put forward for chimneying disintegration, the contribution to shear resistance at the failure surface, in the respective slice distribution, can be calculated. Practically, however, artificial ground support has not physically performed well in weak rock masses which offers poor anchoring capabilities [34][35][37].

In the case of stratified rock, ground support has the benefits of artificially stopping the inception of failure and creating strata (beam) of thickness corresponding to support length, thereby increasing the resistance to failure.

Generally, ground support can be applied so that transfer of load is allowed to fall to rock mass areas beyond the calculated extent of failure (ravelling, destratification, chimneying, block caving).

In most cases development of failure involves displacements in shear. Until recently, no displacement monitoring instrumentation was able to provide continuous indication of shear movement, extensometers, for example, providing displacement indication along its axis. Time Domain Reflectometry, originally used to locate breaks in transmission cables, is now regularly used with respect to shallow stope stability [127]128][129][130]. Using a grouted rigid co-axial cable in boreholes, the method provides for monitoring movements of shear, tensile or combination of displacements, at any point along the length of the cable which can be as long as 600 m. The method is also able to quantify the type of movement. Several cables placed around the periphery and in the surface crown pillar of a shallow stope can and have been able to delineate the growth of failure to surface with time as well as the type of failure mechanism developing.

All of the analysis and ground control approaches stress the importance of evaluating the geomechanical parameters which are required, especially in situ stress determination, of major importance as a stabilizing factor or initiator of failure. As discussed earlier, the sensitivity of solutions often depends on variation of input geomechanical parameters. For this reason, major efforts should be spent on evaluating the key failure parameters identified in Chapter 9.

The options open to a designer to represent the relative stability of a shallow stope are:

1) the use of a factor of safety (limit equilibrium method) calculated using one value for each parameter.

2) the general probability approach, comparing the statistical distribution of the resisting forces to that of the driving forces.

3) the probabilistic approach which allows for the statistical distributions for all parameters involved in a particular limit equilibrium calculation, based on a specific failure hypothesis.

4) the reliability approach, whereby event trees or rates of failures, for structural components, together with their respective probabilities of occurrence are defined and the probability of failure derived for a given period of service of the overall structure.

Design of mining structures in general are made for relatively short periods of time (e.g. up to 30 years) whereas the integrity of a shallow underground opening, if it is allowed to fail (progressively or suddenly), is of concern for current and future surface infrastructures and surrounding population. The design life is therefore very long. This, together with the fact that a low 12% rate of failure has been registered (Table 1.3), let alone several for each type of failure mechanism, would seem to preclude adopting a reliability approach.

The open ended factor of safety so far has been used as a reference point for desired level of protection against failure, and also as a "coefficient of uncertainty" where it can be arbitrarily factored to account for ignorance of the completeness or reliability of parametric inputs. This provides for a false sense of security. A failure can occur at a factor of 2 as well as one of 5. Furthermore, no standards exist to indicate what level should be adopted for a particular failure mechanism.

The factor of safety calculated on the single value of parameters does not reflect the natural variations encountered for each geomechanical parameter, especially in shallow underground environments where variations are wider than for deeper rock masses. Nor does it provide for missing field or lab tests or biased results.

The probability and probabilistic approach define the level of stability using definite bounds, 0 to 1, making it easy to provide a better evaluation of each design. Furthermore, the variability factor can be treated. The probability approach, Figure 11.3, compares the statistical distributions of the resisting factors with that of the loading factors.

Probabilistics enables the distribution of each parameter's values to be used within the equilibrium analysis, yielding a factor of safety that is also statistically distributed. The process is simplified if the parameters' values are assumed to be distributed normally, which yield a calculated quantity which is also normally distributed. Probabilistics also allows for factoring of levels of confidence on quality and quantity of data, as well as thoroughness of investigations.

However, the application of probabilistics, as for factor of safety, is hypothesis (failure mechanism) dependent, therefore reinforcing the notion that performing an integrated analysis of the problem, i.e. comparing results for several different failure mechanisms, is more representative.

The physical meaning that can be attributed to a certain factor of safety or probability of failure is not evident: what time span or how many similar situations would statistically fail given the same probability? Furthermore, each shallow opening is unique, if not in geomechanical properties, in geometry and size. To the extent that the

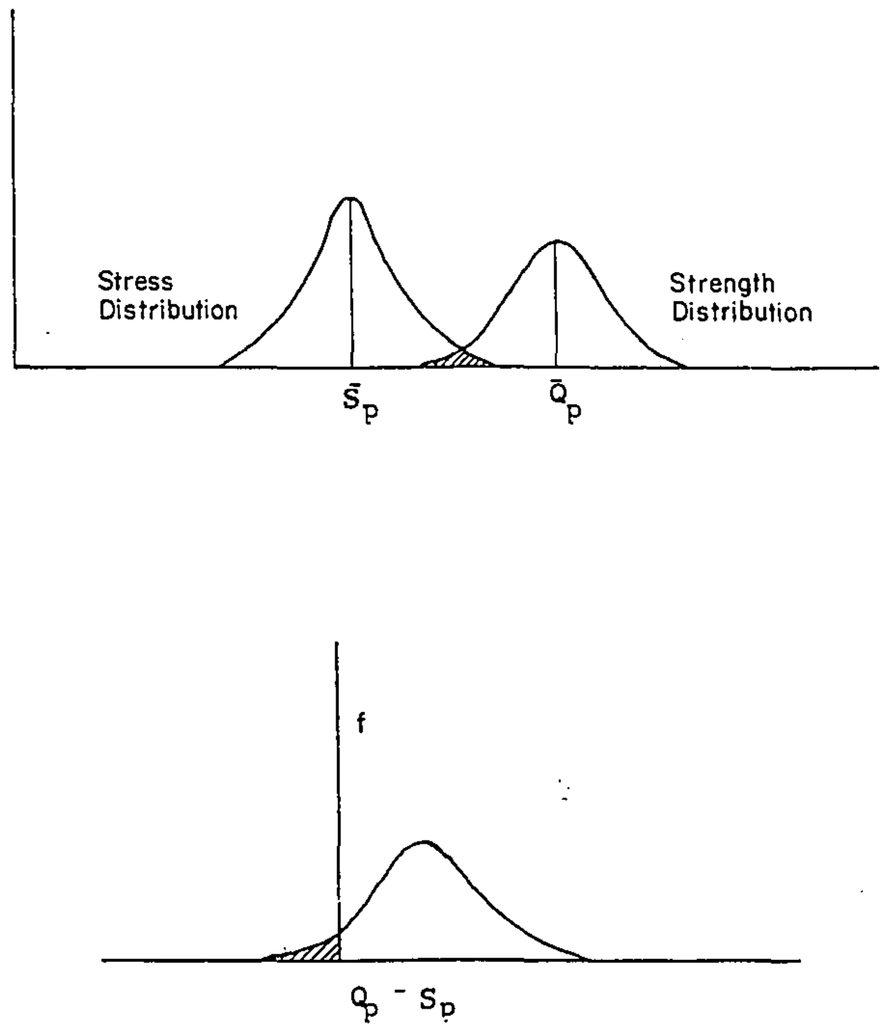

Figure 10.3 Effect of dispersion of stress and strength on probability of failure (represented by the hatched area) [45]

hypothesis for each failure mechanism is different, comparing levels of factor of safety may not be correct. It appears that both, the single value factor of safety and the probabilistic calculated factor of safety, have inadequacies. However, the application of probabilistics to the factor of safety has a lower degree of built-in uncertainties and could better reflect the variability in design of shallow underground openings.

Application of the probabilistic method involves the calculation of a probability of failure (or success) for a given factor of safety. The Monte Carlo technique randomly generates a value for each parameter used in the factor of safety calculation (each parameter is assumed to be normally distributed). A factor of safety is then calculated for each set of randomly generated equation parameters. This requires several hundred such calculations to be performed for statistical accuracy. It can be replaced by the Rosenbluth method [131] applicable to a function of two or more random variables, which uses only two values for each variable, at one standard deviation on either side of the mean. Therefore, 2^n factors of safety can be calculated, where n is the number of normally distributed variables involved in the limit equilibrium analysis.

The probability of failure for a given factor of safety is the area under the factor of safety distribution covered from 0 to this factor of safety, Figure 10.4.

Probabilistic designs have been used in geotechnical projects by Call et al [132] and Priest and Brown [133] for rock slope stability, by Nguyen and Chowdhury [134] for stability of soil slopes and by Hoek [21] for surface crown pillar plug failure analysis.

Nguyen and Chowdhury report insignificant differences in the calculation of probabilities between the two methods.

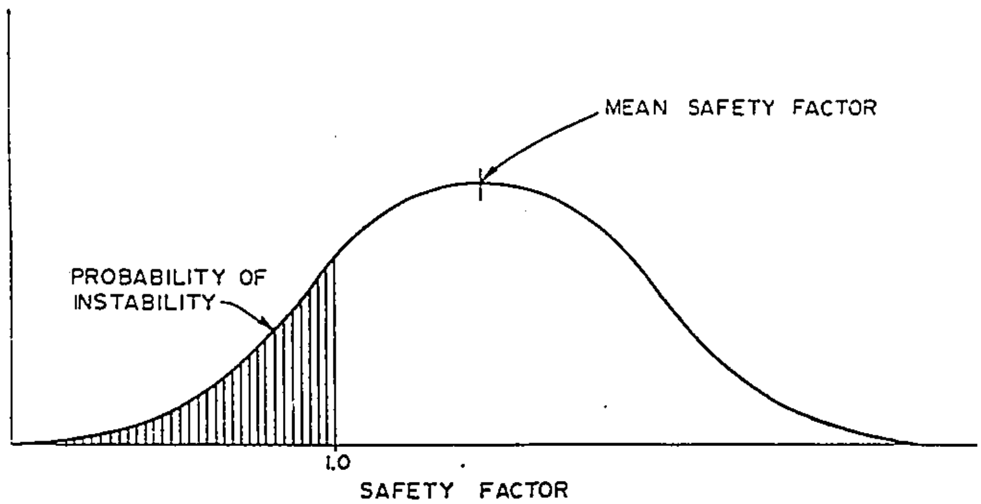

Figure 10.4 Example of a probabilistic distribution of safety factors used to calculate probability of instability

CHAPTER 11

CONCLUSIONS

This thesis has examined the conditions influencing the stability of shallow stopes of hard rock mines and the factors that control their stability. By having studied the mechanical behaviour of failures associated with these environments and examples of stable shallow stope cases, and the geomechanical parameters that effect stability, conclusions can be made on the following issues: occurrence of failures, evaluation of design methods, case studies and design approach for each type of rock mass setting.

11.1 OCCURRENCE OF FAILURES

i) Most Canadian hard rock mine settings can be described as moderately to poorly competent, affected by joints, faults, and rock alteration.

ii) Natural conditions existing at Canadian hard rock mines are such that gravity driven failures can be anticipated in many types of common geological settings.

iii) Failures that have occurred can be classified into five categories: plug, ravelling, destratification, chimneying disintegration, and block caving. A shallow stope failure involves caving to surface.

iv) Failures are not necessarily limited to start from the shallow stope surface crown pillars but could start from the stope hangingwall or footwall and most probably lead to failure within the surface crown pillar. The parameters controlling the stability/occurrence of failures are discontinuities (orientation, persistence), confining stress, stope span, rock mass cohesion but not pillar thickness. Design should therefore address the question "Which portion of the rock mass is mobilized in the failure to surface" rather than "what should be the thickness of the surface crown pillars?".

v) Plug failures occur in areas that are low in redistributed compressive stresses and are bounded by steep dipping through-going discontinuities with little or no intact rock interruptions and lower friction properties.

vi) Ultimate ravelling to surface is not expected to incorporate blocks sliding out of the rock mass into the underlying cavity, after ravelling from block falls. The latter, facilitated by blocks with sides dipping 0° to block surface angle of friction ϕ_r and approximately 90°, offers the most chance for such a failure to reach surface.

vii) Chimneying disintegration has occurred in weak rock masses with low cohesion over narrow openings, < 8 m, that have been brought to failure by compression. For low mass quality, openings several times these dimensions are required to cause block caving.

viii) Chimneying can develop at depths of up to 275 m and rapidly work itself to surface.

ix) Block caving can develop natural support arches, even when material angle of friction is low and cohesion absent.

x) Ravelling and chimneying are the most expected failure mechanisms for shallow stopes of hard rock mines.

xi) The distribution of natural ground stresses in the Precambrian Shield where most of Canada's underground mining occurs normally provides high confinement in the upper periphery of the shallow stope (surface crown pillar). Lower compressive stresses are present when the stope longitudinal direction, sequence of stopes is parallel to the major principal stress direction. Ravelling can locally occur at peripheries where tangential redistributed stresses are tensile but is not expected to lead to stope failure from there.

xii) A number of proximal shallow stopes distributed in a grid pattern could affect stress distribution thereby reducing considerably compressive stresses imposed to the rock masses in surface crown pillars, facilitating failures.

11.2 EVALUATION OF DESIGN METHODS

i) Conventional rock mechanics analytical equations will not indicate the nature or extent of failures of shallow stopes of hard rock mines.

The analytical equations developed to represent the mechanical behaviour of failure mechanisms provide realistic representation of failure potential and field behaviour as has been surveyed in several case studies.

ii) The analytical equations developed which described gravity movements of rock mass elements (blocks, plugs) require a representative distribution of stresses around the shallow stope to obtain a representative factor of safety against failure. Modelling is necessary to provide this distribution of stresses around shallow stopes which usually do not have simple geometries. Theoretical and existing surface crown pillar analytical formulas are not appropriate.

iii) The analytical equations developed which described the rupture of intact or rock mass material (destratification, chimneying disintegration) do not necessitate actual imposed stress as input values in designing. However, strata failures can be described more precisely with stress input obtained from modelling.

iv) Numerical modelling can only anticipate failures in weak rock masses around shallow stopes where chimneying has historically started, not to surface.

v) Conventional continuum modelling (e.g. finite elements, small strain) which are often used in mining cannot predict the nature nor the outline of shallow stope failures to surface.

vi) Although a discontinuum code was not available to evaluate as a design tool of discontinuous rock masses, the ravelling equation using continuum modelling codes was sufficient to represent actual field behaviour including hangingwall ravelling of a historical shallow stope failure.

vii) Conventional empirical methods provide only an indication of need for support. However, the use of the NGI system indicates that cases where failure occurred were all prescribed as needing support.

viii) The surface crown pillar chart successfully indicated the stability of non-failed cases but usually underestimated the depth of stope required to maintain stability. Furthermore, it may provide undependable dimensions in low quality rock masses.

ix) Shallow stopes of hard rock mines should be designed with the analytical equations developed in this research program, using continuum numerical modelling as stress input only. Empirical methods could provide an approximate indication of potential stability (stable vs unstable). Designs based solely on empirical methods and personal experience are not quantifiable nor successful in outlining the extent and location of failure.

x) Mine operators must perform sufficient field and lab tests in order to obtain the necessary geomechanical parameters for each type of failure mechanism anticipated. In particular, in situ stress measurements are necessary to obtain representative redistributed stresses which play an important role in all the failure mechanisms except for destratification. Representative shear resistance of weak rock masses are also necessary to fully evaluate the potential for chimneying disintegration, one of the most common failure mechanisms.

xi) Mine operators must perform a design based on the cross section of failure mechanisms anticipated and apply dedicated ground control and monitoring techniques accordingly.

11.3 CASE STUDIES AND DESIGN FOR ROCK MASS ENVIRONMENTS

i) The analytical equations developed in this research can be used as design tools to avoid complete shallow stope failures and to indicate relative stability.

ii) The Belmoral (Québec) failure of 1980 occurred as a result of chimneying disintegration in the schist ore zone to the contact with wet overburden. Hangingwall ravelling developed to surface following behind but not ahead of chimneying.

iii) The Brier Hill (Michigan) failure over a small opening occurred as a result of chimneying disintegration in the hangingwall graphite slate without caving being involved.

iv) The failure at the Athens Mine was probably a plug failure which occurred under the influence of low friction boundaries, water pressure and in situ major principal stress not aligned with the mining blocks' longitudinal direction. Initial crown block falls or chimneying disintegration in the bounding dykes, may have occurred to unconfine the lower plug portion.

v) These and other failures began in unsupported areas or developed after limited and undedicated ground support had been applied.

vi) Massive, poorly jointed rock masses fail when stresses are sufficiently high. Such failures are expected only when high-extraction large or multiple openings exist. In this case, conventional numerical modelling is required.

vii) Blocky, well-jointed rock masses may fail by ravelling or block caving. Conventional numerical modelling is required to assess background stress distribution. The ravelling equations developed here can be used effectively to design shallow openings; this offers a simpler and more rapid design tool.

Block caving analytical equations are not available. Empirical means are available, as a general design tool for caving potential, as are the block numerical programs. Conditions which would lead to inception of caving are still not well defined although tensile stresses might have contributed to the block caving of the Brier Hill Mine. The analytical formulations developed here for evaluating block caving stabilization have confirmed the development of caving activity around the main Brier Hill Mine stope.

viii) Rock mass environments with extensive discontinuities such as stratified and faulted terrains allow for several types of failures such as plug, ravelling, and strata failures. Analytical equations for these have been developed here which allow for the calculation of extent of expected failure; existing rock mechanics equations do not, irrespective of discontinuity orientation.

ix) Weak rock mass environments such as walls and orebodies are susceptible to chimneying disintegration which is a strength-related and not discontinuity-related failure. Design and stability evaluations can be performed using the analytical equation developed here. Numerical methods have potential application for predicting the development of failure only when several mining steps based on the removal of failed finite elements or large strain elements are used. The dedicated surface crown pillar empirical method has not been suitable for such cases.

x) In rock masses of low cohesion, ground support should be applied as soon as an opening is created to prevent the mobilization of the rock mass chimneying disintegration failure process. If chimneying disintegration has started, the chimney cavity should be sealed and filled. It should not be allowed to grow by allowing a void sufficiently large to prevent bulking from choking the failure. Bulking is low in materials subject to chimneying.

CHAPTER 12

RECOMMENDATIONS FOR FUTURE STUDY

The research performed for this doctoral program has initiated several new elements of rock mechanics as well as expanded upon others. Based on its findings, the following are recommended to be pursued with regards to the stability of shallow stopes of hard rock mines.

i) Some of the analytical equations would benefit from more applications to case studies of failures. This would define more closely rock mass parameters and allow for further evaluation of the analytical methods developed. In particular, the limiting span and conditions separating chimneying from caving potential, which is not well known at this point, would require identification.

ii) Similarly, verification by sophisticated numerical modelling should be considered. In particular, modelling of weak rock masses with a large strain program which can remove failed elements might parallel the development of chimneying disintegration as predicted here. Modelling for large scale plug failure, development of strata failure cavity as well as ravelling expectations, should be performed using discontinuum programs.

iii) The effects of several proximal stopes especially disposed in a grid pattern on the stress distribution within the surface crown pillars of central stopes are critical to understanding gravity ravelling and plug failures which have occurred in such settings.

iv) Refinement of data gathering techniques in regards to precision and depth of application becomes important to provide specific 3-D distribution of discontinuities and anomalous zones. Geophysical methods such as geotomography and ground penetrating radar have allowed for this and need to be applied more routinely. In this fashion, site specific ultimate failure mechanisms may be recognized at the design stage before extraction occurs.

v) Distribution of stresses around generic shallow stope geometries for various stress orientations and values would provide stress level curves/tables for hangingwall, footwall, and crowns which may be used with the analytical equations developed here.

vi) Development of field tests to quantify rock mass cohesion modulus of elasticity and unconfined compressive strength for weak rock masses are needed. Current sampling and testing methods are inadequate to provide useable values for analysis. With such a method, typical weak geological environments (schists, slates, shales) and degree of alteration of rock could be profiled.

vii) The development of analytical equation(s) to predict the onset of block caving are not yet available and are required not only as a stability evaluation method but also to help establish the boundary between chimneying disintegration and block caving.

viii) Close monitoring with instruments addressing failure-specific rock mass movements would confirm and quantify failure mechanisms, at sites with historical failures.

ix) Time dependent behaviour of discontinuity shear strength, from loss of strength and material degradation is important to evaluate in the context of structurally controlled failure mechanisms.

x) Incorporation of more case studies of low rock mass quality would make the surface crown pillar empirical chart more precise and address a comparison versus the analytical equation developed for chimneying disintegration.

REFERENCES

1. Bétournay, M.C., 1986. "A design process for surface crown pillars of hard rock mines"; 38th CIM Annual General Meeting, Montreal, paper 146.

2. Roche Associés, 1984. "Surface pillars"; Contract Report #26SQ23440-3-9005; CANMET, Energy, Mines and Resources, Canada.

3. Roche Associés, 1985. "Surface pillars, phase II"; Contract Report #26SQ23440-5-9014; CANMET, Energy, Mines and Resources, Canada.

4. Golder Associates, 1990. "Crown pillar stability back-analysis"; Contract Report #23440-8-9074/01-SQ; CANMET, Energy, Mines and Resources, Canada.

5. Allen, C.W., 1934. "Subsidence resulting from the Athens system of mining at Negaunee, Michigan"; Proceedings Am. Ins. Min. & Met. Eng.; 109; pp. 195-202.

6. Rice, G.S., 1934. "Ground movement from mining in Brier Hill Mine, Norway, Michigan"; Proceedings Am. Ins. Min. & Met. Eng.; 109; pp. 118-152.

7. Bétournay, M.C., Nantel, S. and Lessard, D., 1987. "Summary of 24 surface crown pillar case studies"; CIM Bulletin; 968 #8; pp. 31-37.

8. Queen's University, 1991a. "Seismic and radar characterization of discontinuities and anomalous rock quality within mine surface crown pillars using velocity and attenuation imaging"; Contract Report #23440-7-9153/01-SS; CANMET, Energy, Mines and Resources, Canada.

9. Queen's University, 1991b. "Application of seismic geotomography to the Sigma Mine surface crown pillars"; report to CANMET; CANMET, Energy, Mines and Resources, Canada.

10. Trow Ltd., 1988. "The determination of surface crown pillar mechanical and structural properties"; Contract Report #03SQ23440-8-9063; CANMET, Energy, Mines, and Resources, Canada.

11. Barton, N., Lien, R. and Lunde, J., 1974. "Engineering classification of rock masses for the design of tunnel support"; <u>Rock Mech.</u>; 6 #4; pp. 189-236.

12. Steffen Robertson and Kirsten, 1984. "Rock mechanics study, Thompson open pit"; Contract Report for INCO.

13. Biron, F. and Labrie, D., 1986. "Histoire du cas de la mine Chimo"; Proceedings Surface Crown Pillar Colloquium, Val d'Or; pp. 25-73.

14. Bétournay, M.C., Yu, Y.S. and Thiverge, S., 1987. "A case study of surface crown pillars: the Niobec mine"; Proceedings 28th U.S. Rock Mechanics Symposium, Tucson; pp. 1197-1204.

15. Sherritt Gordon Mines Ltd., 1987. "Ground stability evaluation with particular reference to an echelon lensed orebody"; Contract Report #14 sq23440-4-9147; CANMET, Energy, Mines and Resources Canada.

16. Bétournay, M.C., 1988. "Application of finite element modelling to shallow underground openings, Holt-McDermott Mine"; Divisional Report 88-82(TR); CANMET, Energy, Mines and Resources, Canada.

17. Bétournay, M.C. and Labrie, D., 1988. "La stabilité des chantiers supérieurs et leurs piliers de surface, Mine Eldrich: méthodes analytiques"; Divisional Report 88-17 (TR); CANMET, Energy, Mines and Resources, Canada.

18. Strata Engineering, 1987. "Weak rock mass model for support of surface crown pillars at Les Mines Selbaie. Phase II - numerical model development and calibration". CANMET Contract Report #15sq.23440-5-9017; CANMET, Energy, Mines and Resources, Canada.

19. Jacques, Whitford and Associates, 1991. "Stability of the Gays River Mine orebody hangingwall"; Contract Report #14SQ23340-9-9194; CANMET, Energy, Mines and Resources, Canada.

20. Bétournay, M.C., Mirza, C. and Lau, K.C., 1988. "Coring of soft soil-like rock materials"; Proceedings 2nd International Conference on Case Histories in Geotechnical Engineering, St. Louis; pp. 291-297.

21. Hoek, E., 1989. "A limit equilibrium analysis of surface crown pillar stability", Proceedings International Conference on Surface Crown Pillar Evaluation for Active and Abandoned Metal Mines, Timmins; pp. 3-13.

22. Gill, D.E., Fortin, M., Matte, S. and Papantonopoulos, C., 1989. "Application d'une méthode généralisée d'analyse à la rupture à l'évaluation des piliers de surface"; Proceedings International Conference on Surface Crown Pillar Evaluation for Active and Abandoned Metal Mines, Timmins; pp. 89-102.

23. Bétournay, M.C., 1987. "Éléments géomécaniques de récupération de piliers de surface"; Proceedings 3rd Quebec Mining Association Ground Control Colloquium, Val d'Or.

24. Bétournay, M.C., 1989. "What do we really know about surface crown pillars?"; Proceedings International Conference on the Evaluation of Surface Crown Pillars for Active and Abandoned Metal Mines, Timmins; pp. 17-33.

25. Herget, G., 1984. "Load assumptions for underground excavations in the Canadian Shield"; Divisional report 84-82(J); CANMET, Energy, Mines and Resources, Canada.

26. Arjang, B., 1990. "Pre-mining stresses at some hardrock mines in the Canadian Shield"; Proceedings 30th U.S. Rock Mechanics Symposium, Morgantown; pp. 545-551.

27. Herget, G., 1993. Personal communication.

28. Kanduth, H. and Germain, P., 1990. "In situ stress measurements in three of Noranda's mines using a novel borehole slotting method"; Proceedings Stresses in Underground Structures, Ottawa; pp. 50-59.

29. Labrie, D., 1991. Personal communication.

30. Brady, B.H. and Brown, E.T., 1985. "Rock mechanics for underground mining"; George Allen and Unwin, London; 527p.

31. Whittaker, B.N. and Reddish, D.J., 1989. "Subsidence: Occurrence, Prediction and Control"; Elsvier, Amsterdam; 528p.

32. Hoek, E., 1991. "Oral Presentation of the Müller Lecture, 7th International Congress on Rock Mechanics, Aachen.

33. Thivierge, S., 1992. Personal communication.

34. Picciaccia, L., 1989. Personal communication.

35. Bétournay, M.C., 1987. Field observations, Belmoral Mine.

36. Commission d'Enquête sur la Tragédie de la Mine Belmoral et les Conditions de Sécurité dans les Mines Souterraines, 1981. Volume 1: "Les Mines Belmoral Ltée, Causes et Prévisibilité de l'Effondrement".

37. Bétournay, M.C., 1988. Field observations, Selbaie Mine.

38. Timoshenko, S. and Winowski-Krieger, S., 1987. "Theory of plates and shells"; McGraw-Hill, New York; 580p.

39. Pandey, P. and Singh, D.P., 1986. "Deformation of a rock in different tensile tests"; Engineering Geology ; 22; pp. 281-292.

40. Evans, W.H., 1941. "The strength of undermined strata"; Trans Instn. Min. Met.; 50; pp. 475-532.

41. Sterling, R.L., 1977. "Roof design for underground openings in near-surface bedded rock formations"; Ph.D. Thesis, University of Minnesota.

42. Beer, G. and Meek, J.L., 1982. "Design curves for roofs and hangingwalls in bedded rock based on 'voussoir' beam and plate solutions"; Trans. Instn. Min. Met.; A91; pp. 18-22.

43. Pender, M.J., 1985. "Prefailure joint dilatancy and the behaviour of a beam with vertical joints"; Rock Mechanics; 18; pp. 253-266.

44. Morrison, R.G.K., 1976. "A philosophy of ground control"; McGill University; 182p.

45. Coates, D.F., 1981. "Principles of rock mechanics"; Monograph 874; CANMET, Energy, Mines, and Resources;

46. Heyman, J., 1969. "The safety of masonry arches"; Int. J. Mech. Sci.; 11; pp. 362-385.

47. Hackett, P., 1964. "The prediction of rock movements by elastic theory, compared with in situ measurements"; Eng. Geology Supp. I; pp.80-102

48. Széchy, K., 1973. "The art of tunnelling"; Akademiai Kiado, Budapest; 1097p.

49. Terzaghi, K., 1961. "Theoretical soil mechanics"; Wiley; 510p.

50. Denkhaus, H.G., 1964. "Critical review of strata movement theories and their application to practical problems"; J.S. Afr. Inst. Min. Met.; 64 #8; pp. 310-332.

51. Dhar, B.B., Geldart, L.P. and Udd, J.E., 1970. "Stresses at depth around elliptical and ovaloidal openings in an infinite elastic medium"; Trans Can. Inst. Min. Met.; 73.

52. Hoek, E. and Brown, E.T., 1980. "Underground excavations in rock"; Institution of Mining and Metallurgy, London; 290p.

53. Brown, E.T. and Hoek, E., 1988. Discussion on paper 20431 by R. Ucar. J. Geotech. Engineering; A.S.C.E; 114 #3; pp. 371-373.

54. Bieniawski, Z.T., 1973. "Engineering classification of rock masses"; Trans. South Afr. Inst. Civil Eng.; 15; pp. 335-344.

55. Hock, E., 1983. "Strength of jointed rock masses"; Géotechnique; 33#3; pp. 187-223.

56. Deere, D.U., 1964. "Technical description of rock cores for engineering purposes, rock mechanics and engineering geology"; 1; pp. 17-22.

57. Barton, N., 1976. "Recent experiences with the Q-System of tunnel support design"; Proceedings of the Symposium on Exploration for Rock Engineering, Johannesburg; pp. 107-117.

58. Bétournay, M.C., 1988. "Piliers de surface: soutènement naturel passif"; Divisional Report 88-38(OP); CANMET, Energy, Mines and Resources, Canada.

59. Bucky, P.B., 1956. "Fundamental considerations in block caving"; Q. Color. School Mines; 51 #3; pp. 129-146.

60. Kendorski, F.S., 1978. "The cavability of ore deposits"; Mining Engineering; 30 #6; pp. 628-631.

61. Mahtab, M.A. and Dixon, J.D., 1976. "Influence of rock fractures and block boundary weakening on cavability"; Trans. Soc. Min. Engrs.. Am. Inst. Min. Metall. Petrolm. Engrs; 260; pp. 6-12.

62. Laubscher, D.H., 1977. "Geomechanics classification of jointed rock masses - mining applications"; Trans. Instn. Min. Met.; 86; pp. A 1-8.

63. Diering, J.A.C. and Laubscher, D.H., 1987. "Practical approach to the numerical stress analysis of mass mining operations"; Trans. Instn. Min. Met.; 96; pp. A 179-188.

64. Janelid, I. and Kvapil, R., 1966. "Sublevel caving"; Int. J. Rock Mech. Sci.; 3; pp. 129-153.

65. Drucker, D.C. and Prager, W., 1952. "Soil mechanics and plastic analysis or limit state design"; Quarterly of Applied Mathematics; 10#2, pp.157-175.

66. Hedley, D.G.F., Herget, G., Miles, P. and Yu, Y.S., 1979. "CANMET's rock mechanics research at Kidd Creek mine"; Division Report 79-11(TR); CANMET, Energy, Mines and Resources, Canada.

67. Yu, Y.S., 1987. Unpublished CANMET Report.

68. Yu, Y.S., Bétournay, M.C., Thivierge, S. and Larocque, G., 1988. "Pillar and stopes stability assessment of the Niobec mine using the three-dimensional finite element techniques"; Proceedings 15th Canadian Rock Mechanics Symposium, Toronto; pp. 99-108.

69. Picciaccia, L., Bétournay, M.C. and Labrie, D., 1989. "Rock mechanics investigation and assessment of near-surface crown pillar stability at four Ontario and Quebec mines"; Proceedings International Conference on Surface Crown Pillar Evaluation for Active and Abandoned Metal Mines, Timmins; pp. 47-55.

70. Strata Engineering, 1988. "Recovery of the surface crown pillar through the control caving method at Les Mines Selbaie, Joutel, Quebec"; Contract Report #035sq23440-7-9195; CANMET, Energy, Mines and Resources, Canada.

71. Newland, P.L. and Allely, B.H., 1957. "Volume changes in drained triaxial tests on granular materials"; Géotechnique; V7; pp. 17-34.

72. Ladanyi, B. and Archambault, G., 1970. "Simulation of shear behaviour of a jointed rock mass", Proceedings 11th U.S. Symposium on rock mechanics, pp. 105-125.

73. Barton, N., 1976. "The shear strength of rock and rock joints", Int. J. Rock Mech. Min. Sci. and Geomech. Abstr.; V 13; pp. 255-279.

74. Barton, N. and Bakhtar, K., 1983. "Rock joint description and modelling for the hydrothermomechanical design of nuclear waste repositories"; Contract Report for CANMET, Energy, Mines and Resources, Canada.

75. Patton, F.D., 1966. "Multiple modes of shear failures in rock and related materials", Thesis University of Illinois, in Barton, N. and Bakhtar K., 1983, "Rock joint description and modelling for the hydrothermomechanical design of nuclear waste repositories".

76. Herget, G., 1988. "Stresses in rock"; A.A. Balkema, Rotterdam; 179 p.

77. Goodman, R.E. and Shi, G.H., 1985. "Block theory and its application to rock engineering"; Prentice Hall; 338p.

78. Wang, B.L., 1991. "A block-spring model for jointed rocks"; Ph.D. Thesis, University of Ottawa.

79. Bétournay, M.C., 1986. "Preliminary geomechanics assessment of the Montauban Mine"; CANMET Division Report 8 (TR), Energy, Mines and Resources, Canada.

80. Timoshenko, S. and Goodier, J.N., 1951. "Theory of elasticity"; McGraw-Hill, New York; 506p.

81. Wright, F.D. and Bucky, P.B., 1949. "Determination of room and pillar dimensions for the oil-shale mine at Rifle, Colorado"; Trans. Am. Inst. Min. Met. Eng.; 181; pp. 352-359.

82. Stephansson, O., 1971. "Stability of single openings in horizontal bedded rock"; Eng. Geol.; 5; pp. 5-71.

83. Fayol, M., 1985. "Sur les mouvements de terrain provoqués par l'exploitation des mines"; in Sterling, R.L., "Roof design for underground openings in near-surface bedded rock formation".

84. Shorey, P.R., 1975. "An approach to thick beam analysis for roof strata"; Int. J. Rock Mech. Min. Sci.; 12; pp. 373-379.

85. Walrod, G. and Adler, L., 1971. "Analyzing development of roof falls"; Coal Age; March; pp. 103-111.

86. Lambe, T.W. and Whitman, R.V., 1969. "Soil mechanics"; John Wiley and Sons, New York; 553p.

87. Hoek, E. and Bray, J.W., 1977. "Rock slope engineering"; Institution of Mining and Metallurgy, London; p402.

88. Bishop, A.W., 1955. "The use of the slip circle in the stability analysis of earth slopes"; Geotechnique; 5; pp. 7-17.

89. Oberg, E., Jones, F.D. and Horton, H.L., 1988. "Machinery's Handbook"; Industrial Press; 2511p.

90. Terzaghi, K., 1945. "Stability and stiffness of cellular cofferdams"; Trans. A.S.C.E.; 110; pp. 1083-1119.

91. Krynine, D.P., 1945. Discussion of "Stability and stiffness of cellular cofferdams"; Trans. A.S.C.E.; 110; pp. 1175-1178.

92. Handy, R.L., 1985. "The arch in soil arching"; J. Geotech. Eng.; 111 # 3; pp. 302-318.

93. Jenike, A.W., 1964. "Storage and flow of solids"; Bulletin #123; Utah Engineering Experiment Station; University of Utah.

94. Wilkins, J.K., 1972. "A revised theory for the shear strength of rock fill"; Austral. Geomech. J.; G2 #1; pp. 55-59.

95. Hoek, E. and Brown, E.T., 1988. "The Hoek & Brown failure criterion - a 1988 update"; Proceedings 15th Canadian Rock Mechanics Symposium, Toronto; pp. 31-38.

96. Newmark, N.M., 1967. "Effects of earthquakes on dams and embankments"; Fifth Rankine Lecture; Geotechnique; pp. 139-159.

97. Stagg, K.G. and Zienkiewicz, O.C., 1969. "Rock mechanics in engineering practice"; John Wiley and Sons, London; 442p.

98. Bray, D., 1987. "La géologie du gîte aurifère du projet Eldrich-Flavel"; Présentation, Journée, Minière de La Sarre; 21p.

99. Goodman, R.E., 1976. "Method of geological engineering in discontinuous rocks"; West Publishing.

100. Mitri, H., 1988. "Finite element applications in mining engineering"; McGill University, Professional Seminar Text.

101. Evdokimov, P.D., and Sapegin, D.D., 1967. "Stability, shear and sliding resistance, and deformation of rock foundations"; in Barton, N. and Bakhtar, K., 1983, "Rock joint description and modelling for the hydrothermomechanical design of nuclear waste repositories".

102. Monterval, 1987. "Rapport des essais pressiométriques, Mine Eldrich"; Geotechnical Report for Eldrich Mines.

103. Cording, E.J., Hendron, A.J. and Deere, D.U., 1971. "Rock engineering for underground caverns"; Proceedings Symposium Underground Rock Chambers, Phoenix; pp. 567-600.

104. Rocha, M., 1964. "Mechanical behaviour of rock foundations in concrete dams"; Transactions 8th Congress on Large Dams, Edinburgh; #44; pp. 785-732.

105. Gagnon, G. and Gendron, L.A., 1977. "The geology and current development of the St-Honoré niobium deposits"; Technical Paper, 79th CIM Annual General Meeting.

106. Thivierge, S., Roy, D.W., Chown, E.H. and Gauthier, A., 1983. "Evolution du complexe alcalin de St-Honoré (Québec) après sa mise en place"; Mineralium Depositae; 18; pp. 267-283.

107. Hamel, G., Closset, L. and Bétournay, M.C., 1991. "Simulation de la Mine Niobec: stabilité du troisième bloc minier"; Division Report MRL 91-87(TR); CANMET, Energy, Mines and Resources, Canada.

108. Agbagian Associates, 1981. "Modernization of the BMINES computer code. Volume One: Users guide"; contract report #0282022;U.S.B.M., U.S. Department of the Interior.

109. Yu, Y., Toews, N., Boyle, R. and Bétournay, M., 1992. "A preliminary mine stability assessment of the Dumagami Mine"; Division Report 92-03(TR); CANMET, Energy, Mines and Resources, Canada.

110. Vongpaisal, S., Udd, J. and Larocque, G., 1993. "Ground stability analysis of 0-15 ore zone Phase 2: mining block between 3215 and 3515 levels Sigma Mine, Val d'Or, Québec"; Division Report MRL 93-33(CL); CANMET, Energy, Mines and Resources, Canada.

111. Serafim, J.L. and Pereira, J.P., 1983. "Considerations in the geomechanical classification of Bieniawski"; Proceedings International Symposium on Engineering Geology and Underground Construction; Lisbon; V1 #2; pp 33-42.

112. Lama, R.D. and Vutukuri, V.S., 1978. "Handbook on mechanical properties of rock"; Volume II; Trans Tech Publication, Clausthal; 481p.

113. Morrison, R.G.K., 1976. "A philosophy of ground control"; Department of Mining and Metallurgical Engineering, McGill Univesity; 182p.

114. Yu, Y.S. and Toews, N.A., 1988. "PCEPFE user's guide - a 2-D elastic-plastic finite element stress analysis package using a personal computer"; Division Report 88-95(TR); CANMET, Energy Mines & Resources, Canada.

115. Vu, L., Darling, R., Béland, J. and Popov, V., 1987. "Structure of the Ferderber gold deposit, Belmoral Mines Ltd., Val d'Or, Quebec"; CIM Bulletin; 80 #907; pp. 68-77.

116. Brown, E.T. (editor), 1981. "Rock characterization, testing and monitoring, I.S.R.M. suggested Methods"; Pergamon Press; 211p.

117. Hassani, F.P., Scoble, M.J. and Whittaker, B.N., 1982. "Application of the point load under test to strength determination of rock and proposals for a new size correction chart"; Proceedings 21st U.S. Rock Mechanics Symposium, University of Missouri.

118. Herget, G., 1984. "Load assumptions for underground excavation in the Canadian Shield"; Division Report 84-82(J); CANMET, Energy, Mines and Resources, Canada.

119. Belie, J., 1992. Personal Communication.

120. Evans, A.M., 1987. "An introduction to ore geology"; 2nd Edition; Blackwell Scientific Publications; 358p.

121. Obert, L. and Duvall, W.I., 1976. "Rock mechanics and the design of structures in rock"; John Wiley and Sons; New York; 650p.

122. Rodrigues, F.P., 1970. "Anisotropy of rocks: most probable surfaces of the ultimate stresses and the moduli of elasticity"; Proceedings 2nd International Congress on Rock Mechanics, Belgrade; #1; pp. 133-142.

123. Hurlbut, C.S., 1971. "Dana's manual of mineralogy"; 18th Edition; John Wiley and Sons; 518p.

124. Bell, J.S. and Adams, J., 1990. "Mapping regional stress provinces in Canada - a progress report"; Proceedings Stresses in Underground Structures, Ottawa, pp. 3-12.

125. Aggson, J.R., 1970. "Report on in situ determinations of stresses; Mather Mine, Ishpening, Michigan"; U.S. Bureau of Mines; Progress Report DMRC 10006.

126. Crane, W.R., 1929. "Subsidence and ground movement in the copper and iron mines of the upper peninsula, Michigan"; U.S. Bureau of Mines, Bulletin 295.

127. Charette, F., 1993. "T.D.R. installation to evaluate the stability of surface crown pillars at the sides of the expanding Selbaie Mine pit operation". Personal Communication.

128. Charette, F., 1993. "Installation and monitoring of three abandoned mine crown pillar sites, Cobalt, Ontario"; Division Report MRL 92-095(CL); CANMET, Energy, Mines and Resources Canada.

129. Aston, T. and Charette, F., 1993. "Installation and monitoring of three abandoned mine crown pillar sites, Timmins, Ontario"; Division Report MRL 93-020(CL); CANMET, Energy, Mines and Resources, Canada.

130. Technical University of Nova Scotia, 1993. "Monitoring of surface crown pillar deformation at Goldenville, N.S., using time domain reflectometry"; Contract Report # 26SQ23440-0-9045; CANMET, Energy, Mines and Resources, Canada.

131. Rosenbluth, E., 1972. "Point estimates for probability movements"; Proc. Nat. Acad. Sci., USA; 10; pp. 3812-3814.

132. Call, R.D., Caldwell, J.A. and Larson, N.B., 1982. "Optimization of open pit angles from the probability of failure"; CIM 4th Open Pit Operators Conference, Edmonton; Paper #22.

133. Priest, S.D. and Brown, E.T., 1983. "Probabilistic stability analysis of variable rock slopes"; Trans. Instn. Min. Metall.; A 92; pp. A1-A12.

134. Nguyen, V.U. and Chowdhury, R.N., 1984. "Probablistic study of spoil pile stability in strip coal mines - two techniques compared"; Int. J. Rock Mech. Min. Sci. & Geomech. Abstr.; 21, #69 pp. 303-312.

135. Goodman, R.E., 1980, "Introduction to rock mechanics"; John Wiley and sons; 478p.

APPENDICES

APPENDIX 1

ANALYTICAL AND EMPIRICAL STABILITY CALCULATIONS

PIERRE BEAUCHEMIN MINE

APPENDIX 1

Table 1. Calculation of Rock Mass Rating for Pierre Beauchemin Mine Geological Materials

Unit	Rating Parameter						
	Strength	RQD	Joint Spacing	Joint Condition	Ground Water	Joint Orientation	Total
Diorite	7	17	20	25	10	- 5	74
Tonalite	12	13	20	25	10	- 5	75
Fault Zone	2*	0	10	0	10	-5	22

* Nominal, orthogonal to schist

Table 2. Calculation of Rock Mass Strength Envelope for Pierre Beauchemin Mine Geological Materials, Based on the Hoek and Brown Failure Criterion

Tonalite					
σ (MPa)	h	θ (degrees)	ϕ (degrees)	τ (MPa)	c_m (MPa)
0	1.015	55.9	62.4	5.8	5.8
5	1.050	52.8	53.8	13.8	7.0
10	1.083	50.8	49.5	20.0	8.3
15	1.118	49.3	46.5	25.3	9.5
20	1.153	48.0	44.1	30.5	11.1
25	1.187	46.9	42.2	35.2	12.5

$$\sigma_t = \frac{s\sigma_c}{m} = 2.2 \text{ MPa}$$

σ_c = 176.6 MPa

m = 4.42

s = 0.056

Table 2. (continued)

Diorite					
σ (MPa)	h	θ (degrees)	ϕ (degrees)	τ (MPa)	c_m (MPa)
0	1.096	50.2	48.3	3.6	3.6
5	1.337	43.4	36.5	7.5	3.8
10	1.579	40.1	31.3	10.8	4.6
15	1.821	38.0	28.0	13.7	5.7
20	2.062	36.6	25.7	15.89	6.2
25	2.301	35.5	23.9	18.6	7.5

$$\sigma_t = \frac{s\sigma_c}{m} = 2.0\ MPa$$

σ_c = 60.3 MPa

m = 1.83

s = 0.06

APPENDIX 1

Calculation of Plug Failure Factor of Safety, Pierre Beauchemin Mine

The potential plug failure would slide on the dipping N2SE 45SE joint; the opposite side is parallel to the sliding plane

2-D ANALYSIS (omitting sides 3 and 4)

$\psi_s = \psi_2 \;=\; 45°$

$\phi_{rs} \;=\; 35°$

$\phi_{r2} \;=\; 18°$ (Barton et. al. [11] recommend 6° to 24° for such a fault zone gouge)

$\gamma_r \;=\; 0.027 \text{ MN/m}^3$

$c_s \;=\; 0$

$c_2 \;=\; 0.25 \text{ MPa}$

Dry conditions, no water pressure

Mining Step 1

$$V\rho g = A_T \gamma_r$$

$$= 6 \text{ m} \; \frac{(43 \text{ m} + 40 \text{ m})}{2} \times 1 \text{ m (unit width)} \times 0.027 \text{ MN/m}^3$$

$$= 7.1 \text{ MN}$$

From equation 2.15

$$F_s = \frac{c_s A_s + \left(\left(\sum_{j=1}^{m} \sigma_{nsj} A_{sj} \right) + V\varrho g \cos\psi_s - \frac{\gamma_w (H_s - d)^2 b_s}{3} \right) \tan\phi_{rs}}{V\varrho g \sin\psi_s + \left(\sum_{j=1}^{m} \sigma_{n2j} A_2 j - \frac{(\gamma_w (H_s - d)^2 b_s}{3} \right) \sin(\psi_s - \psi_2)} +$$

$$\frac{c_2 A + \left(\left(\left(\sum_{j=1}^{m} \sigma_{n2j} A_2 j\right) - \frac{\gamma_w (H_s - d)^2 b_2}{3}\right) \cos\left(\psi_s - \psi_2\right)\right) \tan\phi_{r2}}{V\varrho g \sin \psi_s + \left(\sum_{j=1}^{m} \sigma_{n2j} A_2 j - \frac{\gamma_w (H_i\ d)^2 b_i}{3}\right) \sin\psi_s - \psi_2} +$$

$$\frac{\sum_{i=3}^{4} \left(c_i A_i + \left(\left(\sum_{j=1}^{m} \sigma_{nij} A_{ij}\right) - \frac{\gamma_w (H_i - d)^2 b_i}{3}\right) \tan\phi_{ri}\right)}{V\varrho g \sin\psi_i + \left(\sum_{j=1}^{m} \sigma_{n2j} A_{2j} - \frac{\gamma_w (H_i - d)^2 b_i}{3}\right) \sin\left(\psi_s - \psi_2\right)}$$

Element	σ_{nsj} (MPa)	τ_{sj}* (MPa)	A_{sj} (m)	Element	σ_{nj} (MPa)	τ_j (MPa)	A_j (m)
1	0.40	0.40	6	9	0.56	0.47	5 m
2	0.63	0.49	6	10	0.66	0.67	5 m
3	0.94	0.63	6	11	0.78	0.76	5 m
4	1.03	0.70	6	12	0.90	1.06	5 m
5	1.19	0.81	6	13	1.05	1.11	5 m
6	1.38	1.05	6	14	1.36	1.30	5 m
7	2.00	0.90	6	15	2.00	1.50	5 m
8	1.57	0.18	6	16	3.12	1.69	5 m

Sliding side: $\Sigma A_{sj} \sigma_{nsj} = 54.0$ MN   Side 2 $\Sigma A_{2j} \sigma_{n2j} = 52.2$ MN

(* τ_n is negative when directed against weight action)

$$F_s = \frac{(54.0 + 7.1\ (0.71))0.7 + (0.25\ (40) + (52.2)(0.32))}{7.1\ (0.71)}$$

$= 13.5$

<u>Mining Step 2</u>

$W = A_T \gamma_r$

$$= 6\left(\frac{(35 + 26)}{2}\right) \text{ x } 6 \text{ m x } 1 \text{ m (unit width) x } 0.027 \text{ MN/m}^3$$

= 4.8 MN

Element	σ_{nsj} (MPa)	τ_{sj} (MPa)	A_{sj} (m)	Element	σ_{nj} (MPa)	τ_j (MPa)	A_j (m)
1	0.50	0.68	4.0	11	0.92	-0.89	2.20
2	0.74	0.75	4.0	12	1.25	-0.94	2.20
3	1.02	0.84	4.0	13	1.41	-1.06	2.20
4	1.4	0.96	4.0	14	1.47	-1.26	2.20
5	1.58	1.09	4.0	15	1.55	-1.49	2.20
6	1.76	1.19	3	16	1.59	-1.69	3
7	1.79	1.26	3	17	2.00	-1.82	3
8	1.84	1.36	3	18	2.70	-2.24	3
9	1.99	1.16	3	19	4.12	-2.51	3
10	2.5	0.42	3	20	5.73	-.294	3

Sliding side: $\Sigma A_{sj}\sigma_{nsj} = 50.6$ MN

Side 2: $\Sigma A_{2j}\sigma_{n2j} = 62.9$ MN

$$F_s = \frac{(50.6 + 4.8(0.71))0.7 + (0.25(26) + (62.9)(0.32))}{4.8(0.71)}$$

= 18.9

Mining Step 3

$$W = A_T \gamma_r$$

$$= \left(\frac{20 + 11}{2}\right) m \ x \ 6 \ m \ x \ 1 \ m \ x \ 0.027 \ \mathrm{MN/m^3}$$

$$= 2.5 \ \mathrm{MN}$$

Element	σ_{nsj} (MPa)	τ_{sj} (MPa)	A_{sj} (m)	Element	σ_{nj} (MPa)	τ_j (MPa)	A_j (m)
1	0.49	0.35	4	6	0	-1.20	2.2
2	0.68	0.51	4	7	1.49	-0.97	2.2
3	1.17	0.41	4	8	1.82	-0.80	2.2
4	3.37	0.69	4	9	0	-1.15	2.2
5	1.05	0	4	10	0.93	0.91	2.2

Sliding Side: $\Sigma A_{sj} \sigma_{nsj} = 27.84 \ \mathrm{MN}$ Side 2: $\Sigma A_{2j} \sigma_{n2j} = 9.3 \ \mathrm{MN}$

$$F_s = \frac{(27.84 + 2.5(0.71))0.7 + (0.25(11) + (9.3)(0.32))}{2.5 \ (0.71)}$$

$$= 14.9$$

APPENDIX 1

Calculation of Required Tangential Roof Stress to Prevent Crown Block Fall, Pierre Beauchemin Mine

Such crown falls assume the periphery is horizontal (which is not the case).

The minimum tangential stress required to maintain blocks from falling out of the crown is given by equation 2.21:

$$W + \sum_{i=1}^{2} A_i \, \sigma_{tang} \cos^2\alpha_i \, \sin\alpha_i = \sum_{i=1}^{2} (c_i + \sigma_{tang} \cos^2\alpha_i \, \tan(\phi_{ri}) A_i \, \cos\alpha_i$$

$$c_1 = c_2 = 0$$

$$A_1 = \frac{0.25 \text{ m}}{\cos 4°} = 0.251 \text{ m}$$

$$\alpha_1 = 90° - 49° = 41°$$

$$(\phi_{ri})_1 = (\phi_{ri})_2 = 35°$$

$$\alpha_2 = 90° - 45° = 45°$$

$$A_2 = \frac{1.00 \text{ m}}{\cos 4°} = 1.002 \text{ m}$$

$$W = 0.25 \text{ m} \; x \; 1.00 \text{ m} \; x \; 1 \text{ m} \; x \; 0.0272 \text{ MN/m}^3$$

$$= 6.8 \; x \; 10^{-3} \text{ MN}$$

Equations 2.22 becomes

$$6.8\ x\ 10^{-3}\ \mathrm{MN}\ +$$

$$\left(0.251\ \mathrm{m}\ x\ 1\ \mathrm{m}\ x\ \sigma_{tang}(0.75^2)(0.66)\ +\ 1.002\ \mathrm{m}\ x\ 1\ \mathrm{m}\ \sigma_{tang}(0.71)^2(0.71)\right)\ =$$

$$\left(\sigma_{tang}(0.75)^2(0.70)\right)\left(0.251\ x\ 1\ \mathrm{m}\right)(0.75)\ +\ \left(\sigma_{tang}(0.71)^2(0.70)\left(1.019\ \mathrm{m}\ x\ 1\ \mathrm{m}\right)\right)(0.71)$$

$$6.8\ x\ 10^{-3}\mathrm{MN}\ +\ 0.45\ \mathrm{m}^2\sigma_{tang}\ =\ 0.33\ \mathrm{m}^2\sigma_{tang}$$

Since σ_{tang} will be calculated as negative, the analysis suggests that the block cannot be stabilized because of geometrical consideration, here α_1 and α_2 >(ϕ+i).

Ultimate height of block fall cavity

- assuming stope crown has a flat roof

$$h_r\ =\ \frac{L\ \sin\ (\psi_1\ -\ \omega)\ \sin\ \psi_2}{\cos\ \omega\ \sin\ (180\ -\ (\psi_1+\psi_2))}$$

$\omega\ = 0°$

$\psi_1\ = 45°$

$\psi_2\ = 50°$

$$L\ =\ \frac{4.5\ \mathrm{m}}{\sin\ 50°}\ =\ 7.0\ \mathrm{m}$$

$$h_r\ =\ \frac{4.1\ \sin\ 45\ \sin\ 50}{\sin\ (180-(95))}$$

$h_r\ = 3.8$ m

APPENDIX 1

Calculation of Required Tangential Stress to Prevent Crown Block Slide,

Pierre Beauchemin Mine

Such block slides assume the crown periphery is dipping. The minimum tangential stress required is given by equation 2.26:

$$W\sin\psi_s = 2cA_s + (2\sigma_{tang}A_s\cos^2\alpha_{ns} + W\cos\psi_s)\tan(\phi_{rs})_s$$

where

ψ_s = 45°

α_{ns} = 45°

A_s = 1.002 m

c_s = 0

(ϕ_{rs}) = 35°

W = 6.8×10^{-3} MN

The analysis becomes

$$6.8 \; x \; 10^{-3} \; \text{MN} \; (0.71) =$$

$$\left(2\sigma_{tang} \; x \; 1.002 \; \text{m} \; x \; 1 \; \text{m} \; x \; (0.71)^2 + 6.8 \; x \; 10^{-3} \; \text{MN} \; (0.71)\right) 0.7$$

$$\sigma_{tang} = 4.9 \; x \; 10^{-3} \; \text{MPa}$$

APPENDIX 1

Calculation of Required Tangential Stress to Prevent Hangingwall Block Slide, Pierre Beauchemin Mine

Although very few cross-joints (family N20E 50NW) occur in the hangingwall, for the purpose of completeness block slides will be analyzed using the smallest joint spacing surveyed.

The factor of safety existing for a potential sliding block is given by equation 2.26

$$W\sin\psi_s = 2c\,A_s + \left(2\sigma_{tang}A_s\cos^2\alpha_{ns} + W'\cos\psi_s\right)\tan\phi_{rs}$$

where

ψ_s = 50°

α_{ns} = 40°

A_s = 0.255 m

c_s = 0

$(\phi_{rs}) = \quad 35°$

$W \quad = \quad 6.8 \text{ x } 10^{-3} \text{ MN}$

The analysis becomes

$$6.8 \ x \ 10^{-3} \text{ MN } (0.65) =$$

$$\left(2\sigma_{tang} \ x \ 0.255 \text{ m } x \ 1 \text{ m } x \ (0.65)^2 + 6.8 \ x \ 10^{-3} \text{ MN } (0.75)\right) 0.7$$

$$\sigma_{tang} = 21.4 \ x \ 10^{-3} \text{ MPa}$$

APPENDIX 1

Calculation of Strata Failures and Cavity Height, Pierre Beauchemin Mine Hangingwall

The load imposed on a strata depends on the number of strata that have detached from the rock mass. Since the stresses imposed across the lower strata are tensile, according to the numerical model, to a depth of 36 m into the hangingwall, 36 m of strata load is assumed.

For the lowest stratum the load is given by 36 meters of 0.25 m thick strata, or 144 strata. As discussed in Chapter 2, the total load on the lowest stratum is

$$p_{j+1} = \gamma_r \, t \, \cos\theta \sum_{i=1}^{n-j} \frac{1}{i}$$

γ_r = 0.0272 MN/m^3

j = 0

L_j = 45 m

t = 0.25 m

n = 144

θ = 45°

ϕ = 46°

T_s = 12.8 MPa

$$h_c = \frac{t}{1+\sqrt{\frac{E_c}{E_t}}} = \frac{0.25}{1 + \sqrt{\frac{72.2}{42.6}}} = 0.11 \text{ m}$$

$$h_t = \frac{t}{1+\sqrt{\frac{E_t}{E_c}}} = \frac{0.25}{1 + \sqrt{\frac{42.0}{72.2}}} = 0.14 \text{ m}$$

p_{j+1} = 0.0272 MN/m^3 x 0.25 m (4.46)* x 1 m

= 0.030 MN/m

(* 4.46 is used because the sum of the series does not converge the increase in the sum becomes too small after 50 strata)

Using equation 2.44

$$T_s < \frac{p_{j+1}\, L_{j+1}^2\, h_t}{4\left(\frac{E_c}{E_t}\, h_c^3 + h_t^3\right)} - \sigma_a$$

Using σ_a = 0.8 MPa, the minimum tangential stress existing for the various spans

$$12.8 \text{ MPa} \leq \frac{0.30 \text{ MN} \left(L_{j+1}^2\right) (0.14 \text{ m})}{4\left(\frac{72.2}{42.6}(0.11)^3 + (0.14 \text{ m})^3\right)} - 0.8$$

L $_{j+1}$ = 5.2 m

In this case the height of a cavity is given by equation 2.46

$$H = \frac{L - L_{j+1}}{2 \tan\,(45° + \phi/2)}$$

For mining step 1, $L = 43$ m, $H = 7.6$ m; for mining step 2, $L = 50$ m, $H = 9.0$ m; for mining step 3, $L = 57$ m, $H = 10.5$ m.

APPENDIX 1

Calculation of Linear Arch Stability, Pierre Beauchemin Mine Hangingwall

The sequence of calculation to evaluate linear arch stability is given in Chapter 2. Applying first, equations 1.13 to 1.18 to evaluate f_c.

γ_r = 0.0272 MN/m^3

t = 0.25 m

E_m = 12,700 MPa

n = 0.25

Θ = 45°

(1) Iterating to find f_c with L

if f_c = 9.0 MPa, $L^4 + 26.7L^2 - 9{,}507 = 0$

L = 9 m

if f_c = 11.0 MPa, $L^4 + 48L^2 - 14{,}173 = 0$

L = 9.9 m

if f_c = 13.0 MPa, $L^4 + 80.4L^2 - 19{,}771 = 0$

L = 10.3 m

if f_c = 15.0 MPa, $L^4 + 123.4L^2 - 26{,}270 = 0$

L = 10.6 m

if f_c = 17.0 MPa, $L^4 + 179.7L^2 - 33{,}810 = 0$

L = 10.7 m

if f_c = 19.0 MPa, $L^4 + 250.9\ L^2 - 42{,}234 = 0$

$L = 10.75$ m

if $f_c = 21.0$ MPa, $L^4 + 338.8L^2 - 51{,}593 = 0$

$L = 10.7$ m

if $f_c = 23.0$ MPa, $L^4 + 445L^2 - 61{,}888.0 = 0$

$L = 10.5$ m

Therefore $f_c = 19$ MPa, providing maximum span of $L = 10.75$ m

(2) Comparing f_c to peak strength

Shear stress imposed at edges, from loading of voussoir

$$\tau = \frac{10.75 \text{ m} \times 0.0272 \text{ MN/m}^3 \times 0.25 \text{ m}}{2} = 0.036 \text{ MPa}$$

Using the peripheral compressive tangential stress of 0.8 MPa existing at the largest span.

$$\sigma_1 = \frac{19 + 0.8}{2} + \sqrt{\left(\frac{19 + 0.8}{2}\right)^2 + 0.036^2}$$

$$= 19.8 \text{ MPa}$$

$$\sigma_3 = \frac{19 + 0.8}{2} - \sqrt{\left(\frac{19 + 0.8}{2}\right)^2 + 0.036^2}$$

$$\approx 0$$

Therefore a state similar to unconfined compressive stress is imposed. Since the unconfined compressive strength according to Hoek and Brown calculations for diorite is 60.3 MPa,

$$F_s = \frac{60.3}{19.8} = 3.0$$

Therefore failure is by shear or buckling, not compression.

The shear factor of safety, considering a Mohr-Coulomb surface (*) is

(3) <u>Verification against block drop shear failure</u>

$$F_s = \frac{\sigma_n \tan\phi}{\tau} = \frac{f_c\ n\ t\ \tan\phi}{\tau}$$

$$= \frac{19.8 \text{ MPa } x\ 0.25\ x\ 0.25 \text{ m } x\ 1 \text{ m } \tan 35}{0.036}$$

$$= 24.1$$

Therefore since the factor of safety is greater against voussoir shear failure; failure would occur by buckling.

(* as per the block ravelling analysis, a $\phi = 35°$ is used)

APPENDIX 1

Calculation Against Chimneying Disintegration Failure, Pierre Beauchemin Mine

The requirements to calculate the factor of safety against chimneying disintegration are to sum the vertical component of shear forces and divide by the sum of the slice's weight.

The Pierre Beauchemin 105N-1 stope has a horizontal length of $\frac{5.4 \text{ m}}{\sin (40°)}$ or 8.4 m. Because the problem is symmetrical, only one half the span is required. Dividing the arc into six slices of 0.7 m width provides the vertical shear resistance given based on the following calculations:

c_{mass} = 3.6 MPa

ϕ_{mass} = 48.3

$\alpha/2$ = $45° + \phi/2$

s = 0.7 m

L = 8.4 m

calculation of first rupture:

$$r = \frac{0.5\ (8.4)}{[1 - \cos\ (45 + 24.2)]}$$

$$r = 6.5 \text{ m}$$

$$N = 6.5 - 4.2 = 2.3 \text{ m}$$

$l_1 = 0.5L = 4.2 \text{ m}$

$h_{1h} = \sqrt{4.2\ (2\ (6.5) - 4.2)}$ $\qquad \beta_1 = \tan^{-1}\left[\dfrac{(6.1 + 5.8)\ 0.5}{2.3 + 0.5\ (0.7)}\right]$

$= 6.1 \text{ m}$ $\qquad = 66.0°$

$l_2 = 0.5\ (8.4) - (2-1)\ 0.7$

$l_2 = 3.5 \text{ m}$

$h_{2h} = \sqrt{3.5\ (2\ (6.5) - 3.5)}$ $\qquad \beta_2 = \tan^{-1}\left[\dfrac{(5.8 + 5.3)\ 0.5}{2.3 + 1.5\ (0.7)}\right]$

$= 5.8 \text{ m}$ $\qquad = 59.0°$

$l_3 = 0.5\ (8.4) - (3-1)\ 0.7$

$l_3 = 2.8 \text{ m}$

$h_3h = \sqrt{2.8\ (2\ (6.5) - 2.8)}$ $\qquad \beta_3 = \tan^{-1}\left[\dfrac{(5.3 + 4.8)\ 0.5}{2.3 + 2.5\ (0.7)}\right]$

$h_{3h} = 5.3 \text{ m}$ $\qquad = 51.2°$

$l_4 = 0.5\ (8.4) - (4-1)\ 0.7$

$l_4 = 2.1 \text{ m}$

$h_4h = \sqrt{2.1\ (2\ (6.5) - 2.1)}$ $\qquad \beta_4 = \tan^{-1}\left[\dfrac{(4.8 + 4.0)\ 0.5}{2.3 + 3.5\ (0.7)}\right]$

$h_{4h} = 4.8 \text{ m}$ $\qquad = 41.5°$

$l_5 = 0.5\ (8.4) - (5-1)\ 0.7$

$l_5 = 1.4$ m

$h_{5h} = \sqrt{1.4\ (2\ (6.5) - 1.4)}$

$h_{5h} = 4.0$ m

$\beta_5 = \tan^{-1}\left[\frac{(4.0 + 2.9)\ 0.5}{2.3 + 4.5\ (0.7)}\right]$

$= 32.3°$

$l_6 = 0.5\ (8.4) - (6-1)\ 0.7$

$1_6 = 0.7$ m

$h_6 = \sqrt{0.7\ (2\ (6.5) - 0.7)}$

$= 2.9$ m

$\beta_6 = \tan^{1}\left[\frac{(2.9)\ 0.5}{2.3 + 5.5\ (0.7)}\right]$

$= 13.1°$

$h_{7h} = 0$

Slice	β	c_m (MPa)	ϕ	V_i (MN)
1	66°	3.6	48.3°	1.1
2	59°	3.6	48.3°	1.5
3	51.2°	3.6	48.3°	2.0
4	41.5°	3.6	48.3°	2.8
5	32.3°	3.6	48.3°	4.0
6	13.1°	3.6	48.3°	10.8
Σ				22.2

The weight is

$$W_T = A_T \gamma_r$$

$$A_t = \frac{\alpha/2}{360} \pi r^2 - \frac{h_{1h} N}{2}$$

$$A_T = \frac{45 + 48.3/2}{360} \pi (6.5)^2 - \frac{6.1 \ x \ 2.3}{2} = 18.5 \text{ m}^2$$

$$W_T = 18.5 \text{ m}^2 \ x \ 0.027 \text{ MN/m}^2$$

$$= 0.5 \text{ MN}$$

$$F_s = \frac{22.2}{0.5} = 44.4$$

Because no first rupture line is expected, a second rupture line and chimneying will not occur.

APPENDIX 1

Calculation of Arching Stability in Caving Above the Pierre Beauchemin Mine

Shallow Stope

$\gamma_r = 0.0272$ MN/m^3

L = 8.4 m

ϕ = 35°

c = 0 MPa

Z = 17 m

θ = 45° + ϕ/2

= 62.5°

Bulk failure of the arch

$$F_s = \frac{\text{strength available}}{\text{imposed stress}}$$

· Stress

$$\sigma_1 = \gamma_r Z$$

$$\sigma_3 = \gamma_r Z \left(\frac{1-\sin\phi}{1+\sin\phi}\right)$$

σ_1 = 17 m x 0.0272 MN/m^3 = 0.46 MPa

$$\sigma_3 = 0.46 \text{ MPa}\left(\frac{1-0.57)}{1+0.57}\right) = 0.12 \text{ MPa}$$

· <u>Strength</u>

From Table 2.1, for diorite

m_{field} = 0.025

s_{field} = 1 x 10^{-7}

$$\sigma_1 = \sigma_3 \sqrt{m \ \sigma_c \ \sigma_3 + s \ \sigma_c^2}$$

$$\sigma_1 = 0.12 + \sqrt{0.025 \ (58.8) \ 0.12 + 1 \ x \ 10^{-7} \ (58.8)^2}$$

$$= 0.55 \text{ MPa}$$

$$F_s = \frac{0.55}{0.46}$$

$$= 1.2$$

<u>Block Compression failure</u>

With equation 2.69

$$F_s = \frac{\sigma_c}{\sigma_1}$$

$$= \frac{58.8}{0.55}$$

$$= \quad 106.9$$

APPENDIX I

Calculation of NGI Rock Mass Quality Q, Pierre Beauchemin Mine

Surface Crown Pillar

· Material: diorite

RQD = 77.6

J_n = 6 (three joint sets and random)

J_r = 1.5 (planar, some irregularity)

J_a = 1.0 (unaltered, staining only)

J_w = 1.0 (dry excavation)

SRF = 5.0 (single weakness zone containing clay, < 50 m depth)

$$Q = \frac{77.6}{6} \; x \; \frac{1.5}{1.0} \; x \; \frac{1.0}{5.0} = 3.88$$

Hangingwall

· Material: diorite

RQD = 77.6

J_n = 6

J_r = 1.5

J_a = 1.0

J_w = 1.0

SRF = 1.5 (stress versus strength is low, but opening near surface)

(fault, zone below hangingwall, is excavated with opening)

$$Q = \frac{77.6}{6} \; x \; \frac{(1.5)}{1.0} \; x \; \frac{1.0}{1.5} = 12.93$$

APPENDIX 1

Calculation of Critical Crown Pillar Span, Pierre Beauchemin Mine

$Q = 3.88$

From Figure 1.15, the value for $F_s = 1$ $C_s = 7.3$ m

To calculate the minimum pillar thickness:

$$C_s = L\left[\frac{\gamma_r}{t\,(1 + L/S)\,(1 - 0.4\cos\psi)}\right]^{0.5}$$

$L = 8.4$ m

$\gamma_r = 2.72$ T/m^3

$\psi = 45°$

$S = 120$ m

$$7.3 = 8.4\left[\frac{2.7}{t\,(1 + 8.4/120)\,(1 - 0.4\,(0.707))}\right]^{0.5}$$

$t = 4.7$ m

APPENDIX 2

ANALYTICAL AND EMPIRICAL STABILITY CALCULATIONS

NIOBEC MINE

APPENDIX 2

Table 1. Calculation of Rock Mass Rating for Niobec Mine Geological Materials

Unit	Rating Parameter						
	Strength	RQD	Joint Spacing	Joint Condition	Ground Water	Joint Orientation	Total
Limestone	7	20	30	25	10	-10	82
Carbonatite	12	17	20	20	10	-10	69

APPENDIX 2

Table 2. Calculation of c_m and ϕ Values for the Niobec Mine Geological Materials

Limestone					
σ (MPa)	h	θ (degrees)	ϕ (degrees)	τ (MPa)	c_m (MPa)
0	1.007	57.2	66.9	3.5	3.5
5	1.041	53.4	55.2	12.3	5.1
10	1.075	51.3	50.4	18.8	6.7
15	1.108	49.7	47.3	24.1	7.9
20	1.142	48.3	44.7	29.6	9.9
25	1.176	47.2	42.7	34.5	11.4

$$\sigma_t = \frac{s\sigma_c}{m} = 1.07 \text{ MPa}$$

$\sigma_c = 92$ MPa

$m = 8.6$

$s = 0.1$

Table 2 (continued)

Carbonatite					
σ (MPa)	h	θ (degrees)	ϕ (degrees)	τ (MPa)	c_m (MPa)
0	1.004	57.9	69.9	2.5	2.5
5	1.034	54.0	56.9	11.8	4.2
10	1.063	51.9	51.8	18.9	6.2
15	1.093	50.4	48.6	25.3	8.3
20	1.123	49.1	46.1	30.4	9.6
25	1.152	48.0	44.1	35.3	11.0

$$\sigma_t = \frac{s\sigma_c}{m} = 0.65 \text{ MPa}$$

σ_c = 140.5

m = 6.4

s = 0.03

APPENDIX 2

Calculation of Strata Failures and Cavity Height, Niobec Mine Surface Crown Pillar

The load imposed on a strata depends on the number of strata that have detached from the rock mass. As indicated in Appendix 1 the sum of the load of each new stratum is significant only to the fiftieth strata (which adds 0.02 of its weight to the lowest strata).

In the case of the Niobec limestone forming the base of the surface crown pillar and roof of the stopes it is reasonable to assume that if the bedding joints were weak the strata could fail owing to non-support and the wide span of the single or large openings created once pillars are removed.

The limit span after several strata have failed would be (provided sufficient strata are still loading the first stable strata):

$\gamma_r = 0.027\ MN/m^3$

$t = 0.06\ m$

$n = 50$

$\theta = 0$

$\phi = 40°$

$T_s = 5.6\ MPa$

$E_c = 30\ GPa$

$E_b = 55.6\ GPa$

$E_t = 22.3\ GPa$

$\sigma_a = 0.8\ MPa$

$$h_c = \frac{t}{1 + \sqrt{\frac{E_c}{E_t}}}$$

$$h_c = \frac{0.06}{1 + \sqrt{\frac{30.0}{22.3}}}$$

$$h_t = \frac{t}{1 + \sqrt{\frac{E_t}{E_c}}}$$

$$h_t = \frac{0.06}{1 + \sqrt{\frac{22.3}{30.0}}}$$

$$p_{j+1} = 0.027 \text{ MN/m}^3 \; x \; 0.06 \text{ m } (4.46) \; x \; 1 \text{ m}$$
$$= 0.007 \text{ MN/m}$$

$$T_s \leq \frac{p_{j+1} \; L_{j+1}^2 \; h_t}{4\left(\frac{E_c}{E_t} \; h_c^3 + h_t^3\right)} - \sigma_a$$

$$5.6 \leq \frac{0.007 \; (L_{j+1}^2) \; (0.032)}{4\left(\left(\frac{30.0}{22.3}\right)(0.028)^3 + (0.032)^3\right)} - 0.8 \text{ MPa}$$

$L_{j+1} = 1.71$ m

if L = 75 m

$$H = \frac{75 - 1.71}{2 \tan (45 + 40/2)}$$

$= 17.0$ m

if L = 45 m

$$H = \frac{45 - 1.71}{2 \tan (45 + 40/2)}$$

$= 10.0$ m

APPENDIX 2

Calculation of Linear Arch Stability, Niobec Mine Surface Crown Pillar

$\gamma_r = 0.027$ MN/m^3

$t = 0.06$ m

$E_m = 15{,}000$ MPa

$n = 0.25$

$\theta = 0°$

$\phi = 35°$ (linestone joint, slightly rough and unaltered (Barton [11])

(1) Iterating to find f_c with L

if $f_c = 6$ MPa, $L^4 + 2.26L^2 - 123.1 = 0$

$L = 3.16$ m

if $f_c = 8$ MPa, $L^4 + 8.03L^2 - 219.0 = 0$

$L = 3.37$ m

If $f_c = 10$ MPa, $L^4 + 15.7L^2 - 342 = 0$

$L = 3.5$ m

If $f_c = 12$ MPa, $L^4 + 27.14L^2 - 493 = 0$

$L = 3.53$ m

If $f_c = 14$ MPa, $L^4 + 43.1L^2 - 671.8 = 0$

$L = 3.49$ m

Therefore f_c = 12 MPa, providing a maximum span of L = 3.53 m

(2) Comparing f_c to peak strength

Calculating the imposed shear stress at the voussoir block edge

$$\tau = \frac{3.53 \text{ m } x \ 0.027 \text{ MN/m}^3 \ x \ 0.06 \text{ m}}{2} = 0.002 \text{ MPa}$$

$\tau \approx 0$ MPa

Using the smallest tangential compressive stress of 0.8 MPa existing at that span

$$\sigma_1 = \frac{12 + 0.8}{2} + \sqrt{\left(\frac{12 + 0.8}{2}\right)^2 + 0}$$

$$= 12.8 \text{ MPa}$$

$$\sigma_3 = \frac{12 + 0.8}{2} - \sqrt{\left(\frac{12 + 0.8}{2}\right)^2 + 0}$$

$$= 0$$

Therefore a state similar to unconfined compressive strength is imposed. With lab test

σ_c = 92 MPa

$$F_s = \frac{92}{12.8} = 7.2$$

Therefore failure is by shear or buckling, not compression.

(3) Verification against shear (block drop) failure

$$F_s = \frac{\sigma_n \tan\phi}{\tau} = \frac{f_c \, nt \tan \phi}{\tau}$$

$$= \frac{12.8 \ x \ 0.06 \ x \ 0.25 \tan 35}{0.002}$$

$$= 67.2$$

Therefore failure would occur by buckling.

APPENDIX 2

Calculation Against Chimneying Disintegration Failure, Niobec Mine

The requirements to calculate the factor of safety against chimneying disintegration are to sum the vertical component of shear forces of failure arcs' slices and divide by the sum of the slices' weight.

Currently Niobec stopes are either 25 m x 25 m square in plan or longer in one direction. Furthermore, very long openings, with a width of 25 m will be created when support pillars are created. Therefore a width of 25 m will be used for the analysis. Because the problem is symmetrical, only one half of the span is required. Dividing this arc into six slices of 2.1 m provides the shear resistance given based on the following calculations:

$c_{mass} = 3.5$ MPa

$\phi_{mass} = 66.9°$

$\alpha/2 = 45° + \phi/2$

$s = 2.1$ m

$L = 25$ m

calculation of the first rupture

$$r = \frac{0.25\ (25)}{[1 - \cos\ (45 + 33.5)]}$$

$r = 15.6$ m

$N = 15.6 - 12.5 = 3.1$ m

$l_2 = 0.5L = 12.5$ m

$$h_{1h} = \sqrt{12.5\ (2\ (15.6) - 12.5)} = 15.2 \text{ m}$$

$$\beta_1 = \tan^{-1}\left[\frac{(15.2 + 14.7)\ 0.5}{10.4 + 0.5\ (2.1)}\right] = 52.6°$$

$$l_2 = 0.5\ (25) - (2-1)\ 2.1$$

$$= 10.4 \text{ m}$$

$$h_{2h} = \sqrt{10.4\ (2\ (15.6) - 10.4)} \qquad \beta_2 = \tan^{-1}\left[\frac{(14.7 + 13.8)\ 0.5}{10.4 + 1.5\ (2.1)}\right]$$

$$= 14.7 \text{ m} \qquad = 46.4°$$

$$l_3 = 0.5\ (25) - (3\text{-}1)\ 2.1$$

$$= 8.3 \text{ m}$$

$$h_{3h} = \sqrt{8.3\ (2\ (15.6) - 8.3)} \qquad \beta_3 = \tan^{-1}\left[\frac{(13.8 + 12.4)\ 0.5}{10.4 + 2.5\ (21)}\right]$$

$$= 13.8 \text{ m} \qquad = 39.9°$$

$$l_4 = 0.5\ (25) - (4\text{-}1)\ 2.1$$

$$= 6.2 \text{ m}$$

$$h_{4h} = \sqrt{6.2\ (2\ (15.6) - 6.2)} \qquad \beta_4 = \tan^{-1}\left[\frac{(12.4 + 10.5)\ 0.5}{10.4 + 3.5\ (2.1)}\right]$$

$$= 12.4 \text{ m} \qquad = 32.8°$$

$$l_5 = 0.5\ (25) - (5\text{-}1\ 2.1$$

$$= 4.1 \text{ m}$$

$$h_{5h} = \sqrt{4.1\ (2\ (15.6) - 4.1)} \qquad \beta_5 = \tan^{-1}\left[\frac{(10.5 + 7.6)\ 0.5}{10.4 + 4.5\ (2.1)}\right]$$

$$= 10.5 \text{ m} \qquad = 24.5°$$

$$l_6 = 0.5\ (25) - (6\text{-}1)\ 2.1$$

$$= 2.0 \text{ m}$$

$$h_{6h} = \sqrt{2.0\ (2\ (15.6) - 2.0} \qquad \beta_6 = \tan^{-1}\left[\frac{(7.6 + 0)\ 0.5}{10.4 + 5.5\ (2.1)}\right]$$

$$= 7.6 \text{ m} \qquad = 9.8°$$

$$h_{7h} = 0$$

Slice	β	c_m (MPa)	ϕ	V_i (MN)
1	52.6°	3.5	66.9°	5.6
2	46.4°	3.5	66.9°	7.0
3	39.9°	3.5	66.9°	8.8
4	32.8°	3.5	66.9°	11.4
5	24.5°	3.5	66.9°	16.1
6	9.8°	3.5	66.9°	42.6
Σ				91.5

The weight is

$W_T = A_T \gamma_r$

$$A_T = \frac{\alpha/2}{360} \pi r^2 - \frac{h_{1h} N}{2}$$

$$= \frac{45 + 18}{360} \pi (15.6)^2 - \frac{15.2 (3.1)}{2}$$

$$= 110.2 \text{ m}^2$$

$W_T = 110.2 \text{ m}^2 \times 0.027 \text{ MN/m}^2$

$= 2.98$ MN

$$F_s = \frac{91.5}{2.98} = 30.7$$

Because no first rupture line is expected, a second rupture line and chimneying will not occur.

APPENDIX 2

Calculation of NGI Rock Mass Quality Q,

Niobec Mine

Surface Crown Pillar

· Material : limestone

RQD = 92

J_n = 3 (one joint set plus random)

J_r = 2 (smooth, undulating)

J_a = 1.0 (unaltered)

J_w = 1.0 (dry, no inflow)

SRF = 1.0 (based on stress ratios in compression and tension for 60 m depth)

$$Q = \frac{92}{3} x \frac{2}{1.0} x \frac{1.0}{1.0} = 61.3$$

Stope Walls (vertical)

· Material : carbonatite

RQD = 87

J_n = 4 (two joint sets)

J_r = 1.5 (irregular planar)

J_a = 1.0 (unaltered at shallow depth)

J_w = 1.0 (dry, no inflow)

SRF = 1.0 (based on stress ratios in compression and tension for 60 m depth)

$$Q = \frac{87}{4} x \frac{1.5}{1.0} x \frac{1.0}{1.0} = 32.6$$

APPENDIX 2

Calculation of Critical Crown Pillar Span, Niobec Mine

Q = 61.3

From Figure 1.15, the value for F_s is C_s = 31

To calculate the minimum pillar thickness

$$C_s = L\left[\frac{\gamma_r}{t\ (1 + L/S)\ (1-0.4\ \cos\psi)}\right]^{0.5}$$

L = 25 m

γ = 2.7 T/m^3

ψ = 0

S = 75 m

$$31 = 25\left[\frac{2.7}{t\left(1 + \frac{25}{75}\right)(1-0.4)}\right]^{0.5}$$

t = 2.2 m

if S = 360 m

t = 2.9 m

APPENDIX 3

ANALYTICAL AND EMPIRICAL STABILITY CALCULATIONS

DUMAGAMI MINE

APPENDIX 3

Table 1. Calculation of Rock Mass Rating for Dumagami Mine Geological Materials

Unit	Rating Parameter						
	Strength	RQD	Joint Spacing	Joint Condition	Ground Water	Joint Orientation	Total
Mafic Tuff	12	8	10	20	10	-10	50
Schist	7	3	5	12	10	-12	25
Pyrite	7	20	30	25	10	-10	82
Footwall Rhyolite	7	17	10	20	10	-10	54
Rhyolite	7	13	10	20	10	-10	50

Table 2. Calculation of Rock Mass Strength Envelope for Dumagami Mine Geological Materials, Based on the Hoek and Brown Failure Criterion

Mafic Tuff Rhyolite					
σ (MPa)	h	θ (degrees)	ϕ (degrees)	τ (MPa)	c_m (MPa)
0	1.020	55.2	60.2	0.9	0.9
5	1.288	44.4	38.1	6.0	2.1
10	1.555	40.3	31.7	9.6	3.4
15	1.821	38.0	28.1	12.3	4.3
20	2.088	36.5	25.5	15.0	5.5
25	2.355	35.4	23.6	17.2	6.3

$$\sigma_t = \frac{s\ \sigma_c}{m} = 0.4 \text{ MPa}$$

σ_c = 100.2 (from Hoek and Brown intact rock regression)

m = 1.0

s = 0.004

Table 2 (continued)

Schist					
σ (MPa)	h	θ (degrees)	ϕ (degrees)	τ (MPa)	c_m (MPa)
0	1.033	54.2	57.2	0.2	0.2
5	2.700	34.3	21.6	3.2	1.2
10	4.367	32.1	16.4	4.8	1.8
15	6.033	31.3	13.8	6.2	2.5
20	7.700	30.9	12.1	7.4	3.1
25	9.367	30.7	11.0	8.2	3.3

$$\sigma_t = \frac{s\sigma_c}{m} = 0.1\text{MPa} \quad \text{(parallel to foliation)}$$

σ_c = 50 MPa

m = 0.4

s = 0.0001

Table 2 (continued)

Massive Pyrite					
σ (MPa)	h	θ (degrees)	ϕ (degrees)	τ (MPa)	c_m (MPa)
0	1.014	56.2	63.1	3.6	3.6
5	1.057	52.3	52.7	12.0	5.5
10	1.100	50.0	47.9	18.3	7.2
15	1.15	48.2	44.4	23.4	8.8
20	1.19	46.9	42.1	27.5	9.4
25	1.23	45.7	40.2	32.7	11.6

$$\sigma_t = \frac{s\sigma_c}{m} = 1.6 \text{ MPa}$$

σ_c = 83.0 (from Hoek and Brown intact rock regression)

m = 7.4

s = 0.14

Table 2. (continued)

Footwall Rhyolite					
σ (MPa)	h	θ (degrees)	ϕ (degrees)	τ (MPa)	c_m (MPa)
0	1.039	53.6	55.6	0.9	0.9
5	1.514	40.8	32.5	5.1	1.9
10	1.989	37.0	26.3	7.8	2.9
15	2.460	35.0	22.9	10.2	4.0
20	2.940	33.8	20.6	12.0	4.5
25	3.414	33.0	18.8	13.9	5.4

$$\sigma_t = \frac{s\sigma_c}{m} = 0.4 \text{ MPa}$$

σ_c = 62.4 (from Hoek and Brown intact rock regression)

m = 0.9

s = 0.006

APPENDIX 3

Calculation of Plug Failure Factor of Safety, Dumagami Mine

The potential plug failure would slide on an assumed vertical schist-orebody and orebody-foliated rhyolite boundary, as well as joints crossing the orebody.

2-D ANALYSIS

ψ = 90°, approximation from 85° to simplify calculations

ϕ_{ri} = 25°

γ_r = 0.05 MN/m^3

c_i = 0

Dry conditions, no water pressure

Mining Step 1

$$V\rho g = A_T \gamma_r$$

$$= 9 \text{ m x } 140 \text{ m x } 1 \text{ m x } 0.05 \text{ MN/m}^3$$

$$= 63 \text{ MN}$$

$$F_s = \frac{\sum_{i=1}^{n}\left(c_i A_i + \left(\left(\sum_{j=1}^{m} \sigma_{nj} A_j\right) - \frac{\gamma_w (H_i - d)^2 b_i}{3}\right)\tan\phi_{ri}\right)\sin\psi_i}{V\rho g + \left(\sum_{i=1}^{m}\left(\sum_{j=1}^{m} \sigma_{nj} A_j\right) - \frac{\gamma_w (H_i - d)^2 b_i}{3}\right)\cos\psi_i}$$

Element	σ_{nj} (MPa)	τ_j (MPa)	A_j (m)	Element	σ_{nj} (MPa)	τ_j (MPa)	A_j (m)
1	0.8	0	4	36	0.6	0	4
2	1.6	0	4	37	1.3	0	4
3	2.5	0	4	38	2.4	0	4
4	2.75	0	4	39	2.58	0	4
5	3.0	0	4	40	3.0	0	4
6	3.5	0	4	41	3.5	0	4
7	3.9	0	4	42	3.75	0	4
8	4.25	0	4	43	4.42	0	4
9	4.6	0	4	44	4.7	0	4
10	4.8	0	4	45	4.9	0	4
11	5.1	0	4	46	5.25	0	4
12	5.4	0	4	47	5.5	0	4
13	5.7	0	4	48	5.75	0	4
14	6.2	0	4	49	6.28	0	4
15	7.1	0	4	50	6.78	0	4
16	7.4	0	4	51	7.14	0	4
17	7.8	0	4	52	7.55	0	4
18	8.3	0	4	53	7.85	-0.3	4
19	8.45	0	4	54	7.9	-1.12	4
20	8.6	0	4	55	7.95	-1.74	4
21	8.9	0	4	56	7.96	-2.0	4
22	9.71	0	4	57	8.6	-1.83	4
23	10.2	0	4	58	8.76	-2.2	4
24	10.0	0	4	59	8.9	-2.25	4
25	10.5	0	4	60	9.6	-2.5	4
26	11.6	0	4	61	10.0	-2.69	4
26	11.8	0	4	62	10.38	-2.74	4
28	12.6	0	4	63	10.64	-2.87	4
29	13.6	0	4	64	10.95	-3.03	4
30	14.2	0	4	65	11.8	-2.8	4
31	15.8	0	4	66	12.8	-2.15	4
32	16.2	0	4	67	14.4	-2.2	4
33	17.6	0	4	68	15.8	-1.67	4
34	18.4	0	4	69	17.83	-0.85	4
35	20.0	0	4	70	19.0	0	4

Side 1: $\Sigma A_j \sigma_{nj}$=1211 MN

Side 2: $\Sigma A_j \sigma_{nj}$ = 1465 MN

$$F_s = \frac{(112+1465)\ 0.47}{63}$$

$$= 20.0$$

APPENDIX 3

Mining Step 2

$W = A_T \gamma_r$

$= 9 \text{ m} \times 20 \text{ m} \times 1 \text{ m} \times 0.05 \text{ MN/m}^3$

$= 9 \text{ MN}$

Element	σ_{nj} (MPa)	τ_j (MPa)	A_j (m)	Element	σ_{nj} (MPa)	τ_j (MPa)	A_j (m)
1	0.82	0	4	6	0.91	0	4
2	1.25	0	4	7	1.35	0	4
3	2.02	0	4	8	2.54	0	4
4	3.05	0	4	9	2.94	0	4
5	3.32	0.25	4	10	3.39	0	4

Side 1: $\Sigma A_j \sigma_{nj} = 41.8$ MN

Side 2: $\Sigma A_j \sigma_{nj} = 44.5$ MN

$$F_s = \frac{(41.8 + 44.5)\ 0.47}{9}$$

$$= 4.5$$

Mining Step 3

$W = A_T \gamma_r$

$= 9 \text{ m} \times 20 \text{ m} \times 1 \text{ m} \times 0.05 \text{ MN/m}^3$

$= 9 \text{ MN}$

Element	σ_{nj} (MPa)	τ_j (MPa)	A_j (m)	Element	σ_{nj} (MPa)	τ_j (MPa)	A_j (m)
1	1.0	0	4	6	1.0	0	4
2	3.0	0	4	7	3.0	0	4
3	4.0	0.23	4	8	4.0	0	4
4	4.7	1.0	4	9	4.63	0	4
5	5.4	1.1	4	10	5.75	0	4

Side 1: $\Sigma A_j \sigma_{nj} = 56.4$ MN   Side 2: $\Sigma A_j \sigma_{nj} = 73.5$ MN

$$F_s = \frac{(56.4 + 73.5)\ 0.47}{9}$$

$$= 6.8$$

Mining Step 4

Element	σ_{nj} (MPa)	τ_j (MPa)	A_j (m)	Element	σ_{nj} (MPa)	τ_j (MPa)	A_j (m)
1	1.3	-0.12	4	6	1.4	0.14	4
2	2.5	0.21	4	7	2.6	0.23	4
3	3.8	0.5	4	8	4.49	0.55	4
4	4.7	1.85	4	9	4.7	1.02	4
5	5.5	1.43	4	10	5.95	0.7	4

Side 1: $\Sigma A_j \sigma_{1j} = 71.2$ MN   Side 2: $\Sigma A_j \sigma_{2j} = 76.6$ MN

$$F_s = \frac{(71.2 + 76.6)\ 0.47}{9}$$

$$= 7.7$$

Mining Step 5

Element	σ_{nj} (MPa)	τ_j (MPa)	A_j (m)	Element	σ_{nj} (MPa)	τ_j (MPa)	A_j (m)
1	1.5	-0.30	4	6	1.6	0.27	4
2	3.0	0.19	4	7	3.2	0.55	4
3	4.4	0.57	4	8	4.8	0.80	4
4	6.0	1.06	4	9	6.3	0.96	4
5	7.3	1.60	4	10	7.9	0.59	4

$\Sigma A_j \sigma_{1j} = 88.8$ $\Sigma A_j \sigma_{2j} = 95.2$ MN

$$F_s = \frac{(88.8 + 95.2)\ 0.47}{9}$$

$$= 9.6$$

Mining Step 6

Element	σ_{nj} (MPa)	τ_j (MPa)	A_j (m)	Element	σ_{nj} (MPa)	τ_j (MPa)	A_j (m)
1	3.1	-1.19	4	6	4.9	0.64	4
2	5.2	-0.4	4	7	8.7	1.84	4
3	7.25	0	4	8	6.8	2.25	4
4	8.8	1.56	4	9	8.3	1.7	4
5	9.3	2.6	4	10	13.0	3.0	4

Side 1: $\Sigma A_j \sigma_{nj} = 134.6$ Side 2: $\Sigma A_j \sigma_{nj} = 166.8$ MN

$$F_s = \frac{(134.6 + 166.8)\ 0.47}{9}$$

$$= 15.7$$

Mining Step 7

Element	σ_{nj} (MPa)	τ_j (MPa)	A_j (m)	Element	σ_{nj} (MPa)	τ_j (MPa)	A_j (m)
1	4.3	-2.13	4	6	9.6	0	4
2	7.8	-1.54	4	7	10.2	1.38	4
3	10	0	4	8	9.7	4.5	4
4	13.8	+2.5	4	9	11.4	4.6	4
5	11.4	+4.8	4	10	16.4	4.1	4

Side 2: $\Sigma A_j \sigma_{nj} = 189.2$ MN

Side 1: $\Sigma A_j \sigma_{nj} = 229.6$ MN

$$F_s = \frac{(189.2 + 229.6)\ 0.47}{9}$$

$$= 21.4$$

APPENDIX 3

Calculation of Required Tangential Roof Stress to Prevent Crown Block Slide.

Dumagami Mine

Using equation 2.26, the minimum tangential stress required is given by

$$W\sin\psi_s = 2cA_s + (2\sigma_{tang}A_s\cos^2\alpha_{ns} + W\cos\psi_s)\tan(\phi_{rs})$$

α_{ns} = 5°

ψ_s = 85°

$A_s = \dfrac{5\ \text{m}}{\cos 5°} = 5.02$ m

c_s = 0

(ϕ_{rs}) = 25°

γ_r = 0.05 MN/m^3

W = $A_T\,\gamma_r$

= 9 m x 5 m x 1 m x 0.05 MN/m^3

= 2.25 MN

The analysis becomes:

$$2.25\ \mathrm{MN}\ (0.99) =$$

$$\left(\sigma_{tang}\ x\ 5.02\ \mathrm{m}\ x\ 1\ \mathrm{m}\ x\ (0.99)^2 + 2.25\ \mathrm{MN}\ (0.087)\right)\ 0.47$$

$$\sigma_{tang} = 0.93\ MPa$$

APPENDIX 3

Calculation Against Schist Chimneying Disintegretion Failure. Dumagami Mine

The Dumagami Mine has no openings, except cross-cuts, in the hangingwall schist, 4 m wide. An opening of this dimension and of a larger size, 8 m, will be calculated:

L = 4 m

γ_r = 0.027 MN/m^3

c_{mass} = 0.2

ϕ_{mass} = 57.2°

$\alpha/2$ = 45° + $\phi/2$ = 73.6°

n = 5

s = 0.4

L = 4 m

Calculation of the first rupture line

$$r = \frac{0.5(4)}{[1 - \cos\ (73.6)]}$$

$$= 2.79 \text{ m}$$

N = 2.79 - 2 = 0.79

$l_1 = 0.5L + 2\ \text{m}$

$h_{1h} = \sqrt{2\ (2(2.79) - 2)}$ $\qquad \beta_1 = \tan^{-1}\left[\dfrac{(2.7 + 2.5)\ 0.5}{0.79 + 0.5\ (0.4)}\right]$

$= 2.70\ \text{m}$ $\qquad \beta_1 = 67.8°$

$l_2 = 0.5\ (4) - (2-1)\ (0.4) = 1.6\ m$

$h_{1h} = \sqrt{1.6\ (2(2.79) - 1.6)}$ $\qquad \beta_2 = \tan^{-1}\left[\dfrac{(2.5 + 2.3)\ 0.5}{0.79 + 1.5\ (0.4)}\right]$

$= 2.50\ \text{m}$ $\qquad = 60.0°$

$l_3 = 0.5(4) - (3-1)\ 0.4 = 1.2$

$h_{3h} = \sqrt{1.2\ (2(2.79) - 1.2)}$ $\qquad \beta_3 = \tan^{-1}\left[\dfrac{(2.3 + 1.95)\ 0.5}{0.79 + 2.5\ (0.4)}\right]$

$= 2.30\ \text{m}$ $\qquad = 49.9°$

$l_4 = 0.5\ (4) - (4-1)\ 0.4 = 0.8$

$h_{4h} = \sqrt{0.8\ (2\ (2.79) - 0.8)}$ $\qquad \beta_4 = \tan^{-1}\left[\dfrac{(1.95 + 1.43)\ 0.5}{0.79 + 3.5\ (0.4)}\right]$

$= 1.95\ \text{m}$ $\qquad = 37.7°$

$l_5 = 0.5\ (4) - (5-1)\ 0.4 = 0.4$

$h_{5h} = \sqrt{0.4\ (2(2.79)\ -0.4)}$

$= 1.43$ m

$\beta_5 = \tan^{-1}\left[\dfrac{(1.43)\ 0.5}{0.79 + 4.5\ (0.4)}\right]$

$= 15.4°$

$h_{6h} = 0$

Slice	β	c_m (MPa)	φ (degrees)	V_i (MN)
1	67.8°	0.2	57.2	0.030
2	60.0°	0.2	57.2	0.046
3	49.9°	0.2	57.2	0.068
4	37.7°	0.2	57.2	0.104
5	15.4°	0.2	57.2	0.290
Σ				0.538

$$F_s = \frac{0.538}{0.027\left[\dfrac{(73.6)\ \pi\ 2.79^2}{360} - \dfrac{2.7\ (0.79)}{2}\right]} = 5.1$$

<u>L = 8 m</u>

$\gamma_r = 0.027$ MN/m^3

$c_{mass} = 0.2$

$\phi_{mass} = 57.2°$

$\alpha/2 = 45° + \phi/2 = 73.6°$

n = 5

s = 0.8 m

L = 8 m

Calculation of the first rupture line

$$r = \frac{0.5\ (8)}{[1 - \cos\ (73.6)]}$$

$$= 5.57\ \text{m}$$

$$N = 5.57 - \frac{8}{2} = 1.57$$

$$l_1 = 0.5L$$

$$l_1 = 4\ \text{m}$$

$$h_{1h} = \sqrt{4\ (2\ (5.57) - 4)} \qquad \beta_1 = \tan^{-1}\left[\frac{(5.3 + 5.0)\ 0.5}{1.57\ 0.5\ (0.8)}\right]$$

$$= 5.3\ \text{m} \qquad = 69.1°$$

$$l_2 = 0.5\ (8) - (2-1)(0.8)$$

$$= 3.2\ \text{m}$$

$$h_{2h} = \sqrt{3.2\ (2\ (5.57) - 3.2} \qquad \beta_2 = \tan^{-1}\left[\frac{(5.0 + 4.6)\ 0.5}{1.57 + 1.5\ (0.8)}\right]$$

$$= 5.0\ \text{m} \qquad = 60.0°$$

$$l_3 = 0.5\ (8) - (3-1)\ (0.8)$$

$$= 2.4$$

$$h_{3h} = \sqrt{2.4\ (2\ (5.57) - 2.4)} \qquad \beta_3 = \tan^{-1}\left[\frac{(4.6 + 3.9)\ 0.5}{1.57 + 2.5\ (0.8)}\right]$$

$$= 4.6 \text{ m} \qquad = 50°$$

$$l_4 = 0.5\ (8) - (4-1)\ (0.8)$$

$$= 1.6 \text{ m}$$

$$h_{4h} = \sqrt{1.6\ (2\ (5.57) - 1.6)} \qquad \beta_4 = \tan^{-1}\left[\frac{(3.9 + 2.9)\ 0.5}{1.57 + 3.5\ (0.8)}\right]$$

$$= 3.9 \text{ m} \qquad = 37.9°$$

$$l_5 = 0.5\ (8) - (5-1)\ (0.8)$$

$$= 0.8 \text{ m}$$

$$h_{5h} = \sqrt{0.8\ (2\ (5.57) - 0.8)} \qquad \beta_5 = \left[\frac{(2.9)\ 0.5}{1.57 + 4.5\ (0.8)}\right]$$

$$= 2.9 \text{ m} \qquad = 15.7°$$

$$h_{6h} = 0$$

Slice	β	c_m	ϕ	V_i
1	69.1°	0.2	57.2	0.06
2	60.0°	0.2	57.2	0.09
3	50.0°	0.2	57.2	0.13
4	37.9°	0.2	57.2	0.21
5	15.7°	0.2	57.2	0.56
Σ				1.059

$$W = A_T \gamma_r$$

$$A_T = \frac{(45 + 57.2/2)\ \pi\ 5.57^2}{360} - \frac{1.57(5.3)}{2}$$

$$= 15.8\ m^2$$

$$W = 0.43\ MN$$

$$F_s = \frac{1.059}{0.43} = 2.49$$

Because, in either size opening, the first rupture line is not anticipated, a second rupture line will not develop.

APPENDIX 3

Calculation Against Massive Pyrite Chimneying Disintegration Failure, Dumagami Mine

γ_r = 0.05 MN/m^3

c_{mass} = 3.6 MPa

ϕ_{mass} = 63.1°

$\alpha/2$ = 45° + $\phi/2$ = 76.5°

n = 5

s = 0.9

L = 9 m

Calculation of the first rupture line

$$r = \frac{0.5\ (9)}{[1 - \cos\ (76.5)]} = 5.87\ \text{m}$$

$$N = 5.87 - 4.5 = 1.37$$

$$l_1 = 0.5\ (9) = 4.5\ \text{m}$$

$$h_{1h} = \sqrt{4.5\ (2\ (5.87) - 4.5)}$$

$$= 5.7\ \text{m}$$

$$\beta_1 = \tan^{-1}\left[\frac{(5.7 + 5.4)\ 0.5}{1.37 + 0.5\ (0.9)}\right]$$

$$= 71.8°$$

$l_2 = 0.5\ (9) - (2-1)\ 0.9 = 3.6\ \text{m}$

$h_{2h} = \sqrt{3.6\ (2\ (5.87) - 3.6)}$ $\beta_2 = \tan^{-1}\left[\dfrac{(5.45 + 4.9)\ 0.5}{1.37 + 1.5\ (0.9)}\right]$

$= 5.4\ \text{m}$ $= 62.2°$

$l_3 = 0.5\ (9) - (3-1)\ 0.9 = 2.7\ \text{m}$

$h_{3h} = \sqrt{2.7\ (2\ (5.87) - 2.7)}$ $\beta_3 = \tan^{-1}\left[\dfrac{(4.9 + 4.2)\ 0.5}{1.37 + 2.5\ (0.9)}\right]$

$= 4.9\ \text{m}$ $= 51.5°$

$l_4 = 0.5 - (4.1)\ 0.9 = 1.8\ \text{m}$

$h_{4h} = \sqrt{1.8\ (2\ (5.87) - 1.8)}$ $\beta_4 = \tan^{-1}\left[\dfrac{(4.2 + 3.1)\ 0.5}{1.37 + 3.5\ (0.9)}\right]$

$= 4.2\ \text{m}$ $= 38.9°$

$l_5 = 0.5\ (9) - (5-1)\ 0.9 = 0.9\ \text{m}$

$h_{5h} = \sqrt{0}.9\ (2\ (5.87) - 0.9)$ $\beta_5 = \tan^{-1}\left[\dfrac{(3.1)\ 0.5}{1.237 + 4.5\ (0.9)}\right]$

$= 3.1\ \text{m}$ $= 16.0°$

$h_{6h} = 0$

Slice	β (degrees)	c_m (MPa)	ϕ (degrees)	V_i (MN)
1	71.8	3.6	63.1	1.06
2	62.2	3.6	63.1	1.70
3	51.5	3.6	63.1	2.57
4	38.9	3.6	63.1	4.02
5	16.0	3.6	63.1	11.3
Σ				20.6

$$W = A_T \gamma_r$$

$$= 0.05 \left[\frac{(45 + 63.1/2)\ \pi\ 5.87^2}{360} - \frac{5.7\ (1.37)}{2} \right]$$

$$= 0.95 \text{ MN}$$

$$F_s = \frac{20.6}{0.95} = 21.6$$

Because the first rupture line is not anticipated, a second rupture line will not develop.

APPENDIX 3

Calculation of Arching Stability in Caving Schist, Dumagami Mine

γ_r = 0.027 MN/m^3

ϕ = 16°

c = 0 MPa

θ = 45° + ϕ/2 = 53°

Against intact block compression failure:

Z = 135 m

$$\sigma_h = \sigma_1 \cos^2\theta + \sigma_3 \sin^2\theta$$

$$\sigma_1 = \gamma_r Z$$

$$\sigma_3 = \gamma_r Z \left(\frac{1-\sin\phi}{1+\sin\phi}\right)$$

$$\sigma_1 = 135 \text{ m} \times 0.0272 \text{ MN/m}^3 = 3.67 \text{ MPa}$$

$$\sigma_3 = 3.67 \text{ MPa} \left(\frac{1-0.28}{1+0.28}\right) = 2.08 \text{ MPa}$$

$$F_s = \frac{\sigma_c}{\sigma_1}$$

$$F_s = \frac{40}{3.67}$$

$$= 10.9$$

<u>Z = 20 m</u>

$$\sigma_1 = 20 \text{ m} \times 0.0272 \text{ MN/m}^3 = 0.54 \text{ MPa}$$

$$\sigma_3 = 0.54 \text{ MPa} \left(\frac{1-0.28}{1+0.28}\right) = 0.30 \text{ MPa}$$

$$F_s = \frac{40}{0.54} = 74.1$$

<u>Against bulk material failure:</u>

<u>Z = 135m</u>

$$F_s = \frac{\text{strength available}}{\text{imposed stress}}$$

<u>· Stress</u>

$$\sigma_1 = 3.67 \text{ MPa}$$

$$\sigma_3 = 2.08 \text{ MPa}$$

· Strength

From Table 3.5, for volcanic rock,

$m_{field} = 0.017,\ s_{field} = 1\ x\ 10^{-7}$

$$\sigma_1 = \sigma_3 + \sqrt{m\sigma_c\ \sigma_3 + s\sigma_c^2}$$

$$= 2.00 + \sqrt{0.017\ (40)\ (2.08) + 1\ x\ 10^{-7}\ (40)^2}$$

$$= 3.27$$

$$F_s = \frac{3.27}{3.67} = 0.89$$

Z = 20 m

· Stress

$\sigma_1 = 0.54$ MPa

$\sigma_3 = 0.30$ MPa

· Strength

$$\sigma_1 = 0.3 + \sqrt{0.017\ (40)\ (0.3) + 1\ x\ 10^{-7}\ (40)^2}$$

$$= 0.75$$

$$F_s = \frac{0.75}{0.54}$$

$$= 1.39$$

APPENDIX 3

Calculation of Arching Stability in Caving Pyrite, Dumagami Mine

$\gamma_r \quad = \quad 0.05 \ \mathrm{MN/m^3}$

$\phi_r \quad = \quad 25°$

$c \quad = \quad 0 \ \mathrm{MPa}$

$\theta \quad = \quad 45° + \phi/2 = 57.5°$

Against intact block compression failure:

Z = 135 m

$$\sigma_h = \sigma_1 \cos^2\theta + \sigma_3 \sin^2\theta$$

$$\sigma_1 = \gamma_r Z$$

$$\sigma_3 = \gamma_r Z \left(\frac{1-\sin\phi}{1+\sin\phi}\right)$$

$$\sigma_1 = 135 \ \mathrm{m} \ x \ 0.05 \ \mathrm{MN/m^3} = 6.75 \ \mathrm{MPa}$$

$$\sigma_3 = 6.75 \ \mathrm{MPa} \left(\frac{0.58}{1.42}\right) = 2.75 \ \mathrm{MPa}$$

$$F_s = \frac{\sigma_c}{\sigma_1}$$

$$= \frac{86}{6.75}$$

$$= 12.7$$

<u>Z = 20 m</u>

σ_1 = 20 m x 0.05 MN/m^3 = 1.0 MPa

$$\sigma_3 = 1 \text{ MPa} \left(\frac{0.58}{1.42}\right) = 0.41 \text{ MPa}$$

$$F_s = \frac{86}{1.0}$$

$$= 86.0$$

<u>Against bulk material failure:</u>

<u>Z = 135m</u>

$$F_s = \frac{\text{strength available}}{\text{imposed stress}}$$

<u>· Stress</u>

σ_1 = 3.67 MPa

$2\sigma_3$ = 2.08 MPa

<u>· Strength</u>

From Table 3.5, for fine grain crystalline rock (approximation for massive pyrite),

$m_{field} = 0.017,\ s_{field} = 1 \ x \ 10^{-7}$

$$\sigma_1 = \sigma_3 + \sqrt{m\sigma_c \ \sigma_3 + s \ \sigma_c^2}$$

$$\sigma_1 = 2.08 + \sqrt{0.017 \ (86) \ (2.08) + 1 \ x \ 10^{-7} \ (86)^2}$$

$$= 3.82$$

$$F_s = \frac{3.82}{3.67}$$

$$= 1.04$$

<u>Z = 20 m</u>

<u>· Stress</u>

$\sigma_1 = 0.54$ MPa

$\sigma_3 = 0.30$ MPa

· Strength

$$\sigma_t = 0.3 + \sqrt{0.017\ (86)\ 0.3 + 1\ x\ 10^{-7}\ (86)^2}$$

$$= 0.96$$

$$F_s = \frac{0.96}{0.54}$$

$$= 1.78$$

APPENDIX 3

Calculation of NGI Rock Mass Quality Q, Dumagami Mine

Surface Crown Pillar

· Material: massive pyrite

RQD = 82

J_n = 6 (perpendicular to orebody, sub horizontal, random parallel to orebody)

J_r = 2.0 (smooth undulating)

J_a = 1.0 (unaltered)

J_w = 1.0 (dry excavation)

SRF = 1.0 (medium stress)

$$Q = \frac{82}{6} \; x \; \frac{2.0}{1.0} \; x \; \frac{1.0}{1.0} = 2.73$$

Hangingwall

· Material: schist

RQD = 17

J_n = 6 (parallel to orebody (schistosity), sub horizontal, random perpendicular to orebody)

J_r = 1.0 (smooth planar)

J_a = 4.0 (talc coating)

J_w = 1.0 (medium inflow)

SRF = 1.0 (dry excavation)

$$Q = \frac{17}{6} x \frac{1.0}{4.0} x \frac{1.0}{1.0} = 0.71$$

Footwall

· Material: foliated rhyolite

RQD = 66

J_n = 6 (foliation, vertical, random)

J_r = 1.0 (smooth planar)

J_a = 4.0 (talc coating)

J_w = 1.0 (dry excavation)

SRF = 1.0 (medium stress)

$$Q = \frac{66}{6} x \frac{1}{4} x \frac{1.0}{1.0} = 2.75$$

APPENDIX 3

Calculation of Scaled Crown Span, Surface Crown Pillar Empirical Method, Dumagami Mine

Q = 18.0, using worse rock around the stope

From Figure 1.15, C_s = 12.0

θ = 85°

L = 9 m

γ_r = 5t/m3

ψ = 85°

S = 125 m

$$12.0 = 9\left[\frac{5}{t\ (1+9/125)\ (1-0.4\ (0.09))}\right]^{0.5}$$

t = 2.8 m

APPENDIX 4

ANALYTICAL AND EMPIRICAL STABILITY CALCULATIONS

BELMORAL MINE

APPENDIX 4

Table 1. Calculation of Rock Mass Rating for Belmoral Mine Geological Materials

Unit	Rating Parameter						
	Strength	RQD	Joint Spacing	Joint Condition	Ground water	Joint Orientation	Total
Granodiorite (far-field)	7	17	20	25	10	0	79
Granodiorite (altered)	7	13	10	25	10	-12	53
Schist	0	3	5	10	10	-12	16

Table 2. Calculation of Rock Mass Strength Envelope for Belmoral Mine Geological Materials, Based on the Hoek and Brown Failure Criterion

Altered Granodiorite					
σ (MPa)	h	θ (degrees)	ϕ (degrees)	τ (MPa)	c_m (MPa)
0	1.007	57.1	66.5	0.5	0.5
5	1.227	45.8	40.4	5.9	1.6
10	1.460	41.5	33.5	9.6	3.0
15	1.709	38.8	29.4	12.8	4.3
20	1.943	37.2	26.7	15.6	5.6
25	2.177	36.0	24.8	17.9	6.4

$$\sigma_t = \frac{s\sigma_c}{m} = 0.16$$

σ_c = 60.4

m = 1.9

s = 0.005

Table 2 (continued)

Schist					
σ (MPa)	h	θ (degrees)	ϕ (MPa)	τ (MPa)	c_m (MPa)
0	1.003	58.3	71.8	0.04	0.04
3	5.571	31.45	14.3	1.30	0.54
5	8.619	30.75	11.4	1.78	0.77
10	16.238	30.29	8.3	2.58	1.12
15	23.857	30.16	6.8	3.23	1.44
20	31.476	30.11	5.9	3.80	1.73
25	39.095	30.08	5.3	4.28	1.96

$$\sigma_t = \frac{s\ \sigma_c}{m} = 0.002\ \text{MPa}$$

σ_c = 10 MPa

m = 0.35

s = 0.00008

Table 2. (continued)

Far-Field Granodiorite					
σ (MPa)	h	θ (degrees)	ϕ (degrees)	τ (MPa)	c_m (MPa)
0	1.023	55.0	59.6	5.6	5.6
5	1.071	51.5	50.9	12.7	6.6
10	1.119	49.2	46.4	18.3	7.8
15	1.166	47.5	43.3	23.3	9.1
20	1.215	46.1	40.9	27.8	10.5
25	1.263	44.9	38.9	32.1	11.9

$$\sigma_t = \frac{s\sigma_c}{m} = 2.43$$

σ_c = 116.4

m = 4.8

s = 0.1

APPENDIX 4

Calculation of Required Tangential Stress to Prevent Hangingwall Block Slides,

Belmoral Mine

The geometry of the problem is defined in Figure 6.73, the analysis is the same for a block sliding from the crown. The minimum tangential stess required is given by equation 2.26

$$W \sin\psi_s = 2cA_s + (2\sigma_{tang} A_s \cos^2\alpha_{ns} + W\cos\psi_s)\tan(\phi_{rs})$$

ψ_s = 45°

α_{ns} = 45°

A_s = 0.5 m

c_s = 0

(ϕ_{rs}) = 16°

W = 0.5 m x 0.5 m x 0.0274 MN/m^3

= 6.85 x 10^{-3} MN

$$6.85 \times 10^{-3}\ (0.71) = \left(2\sigma_{tang}\ (0.5)\ (0.71)^2 + 6.85 \times 10^{-3}\ (0.71)\right) 0.20$$

σ_{tang} = 0.04 MPa

<u>Calculation of Required Tangential Stress to Prevent Crown Block Falls, Belmoral Mine</u>

$c_1=c_2 \quad = \quad 0$

$\alpha_1 \quad = \quad 45°$

$\alpha_2 \quad = \quad 45°$

$A_1=A_2 \quad = \quad 0.5 \text{ m}$

$W \quad = \quad 0.5 \text{ m} \; x \; 0.5 \text{ m} \; x \; 1 \text{ m} \; x \; 0.0274 \text{ MN/m}^3 = 0.00685 \text{ MN}$

The minimum tangential stress required to maintain blocks from falling out is given by

equation 2.21:

$$W + \sum_{i=1}^{2} A_i \, \sigma_{tang} \cos^2\alpha_i \, \sin\alpha_i = \sum_{i=1}^{2} A_i \, (c_i + \sigma_{tang} \cos^2\alpha_i \, \tan\phi_{ri}) \cos\alpha_i$$

Since $\phi < \alpha$, the block will not be able to be supported irrespective of imposed stress, i.e. a negative value is returned for σ_{tang}:

$$0.00685 \text{ MN} + 2 \; (0.5) \; \sigma_{tang} \; (0.71)^2 \; (0.71) = 2 \; (0.5) \; (\sigma_{tang} \; (0.71)^2 \; (0.29)) \; (0.71)$$

$$0.00685 + 0.25\sigma_{tang} = 0$$

Ultimate height of block fall cavity

$$h_r = \frac{L \sin(\psi_1 - \omega) \sin \psi_2}{\cos \omega \sin(180 - (\psi_1 + \psi_2))}$$

$\omega = 0$

$\psi_1 = 45°$

$\psi_2 = 45°$

$$L = \frac{3.0}{\cos 65} = 3.8$$

$$h_r = \frac{3.3 \sin 45 \sin 45}{\sin(180 - 90)}$$

$= 1.8$ m

APPENDIX 4

Calculation Against Schist Chimneying Disintegration Failure, Belmoral Mine

$L \quad = \quad 3.8 \text{ m}$

$\phi_{mass} \quad = \quad 71.8°$

$c_{mass} \quad = \quad 0.04 \text{ MPa}$

$s \quad = \quad 0.38 \text{ m}$

$n \quad = \quad 5$

$\gamma_r \quad = \quad 0.028 \text{ MN/m}^2$ (assumed)

$$r = \frac{0.5\ (3.8)}{[1 - \cos\ (45 + 71.8/2)]}$$

$$= 2.26 \text{ m}$$

$$N = 0.26 - (0.5)\ (3.8)$$

$$= 0.36 \text{ m}$$

$l_1 = 0.5\ L$

$= 1.9\ \text{m}$

$h_{1h} = \sqrt{1.9\ (2\ (2.26)\ -1.9)}$

$= 2.23\ \text{m}$

$\beta_1 = \tan^{-1}\left[\dfrac{2.23\ +\ 2.13)\ 0.5}{0.36\ +\ 0.5\ (0.38)}\right]$

$= 75.8°$

$l_2 = 0.5\ (3.8)\ -\ (2-1)\ 0.38$

$= 1.52$

$h_{2h} = \sqrt{1.52\ (2\ (2.26)\ -\ 1.52)}$

$= 2.13\ \text{m}$

$\beta_2 = \tan^{-1}\left[\dfrac{(2.13\ +\ 1.96)\ 0.5}{0.36\ +\ 1.5\ (0.38)}\right]$

$= 65.5°$

$l_3 = 0.5\ (3.8)\ -\ (3-1)\ 0.38$

$= 1.14\ \text{m}$

$h_{3h} = \sqrt{1.14\ (2\ (2.26)\ -\ 1.14)}$

$= 1.96\ \text{m}$

$\beta_3 = \tan^{-1}\left[\dfrac{(1.96\ +\ 1.69)\ 0.5}{0.36\ +\ 2.5\ (0.38)}\right]$

$= 54.3°$

$$l_4 = 0.5\ (3.8)\ -\ (4-1)\ 0.38$$

$$= 0.76\ \text{m}$$

$$h_{4h} = \sqrt{0.76\ (2\ (2.26)\ -\ 0.76}$$

$$\beta_4 = \tan^{-1}\left[\frac{[1.169\ +\ 1.25]\ 0.5}{0.36\ +\ 3.5\ (0.38)}\right]$$

$$= 1.69\ \text{m}$$

$$= 41.0°$$

$$l_5 = 0.5\ (3.8)\ -\ (5-1)\ 0.38$$

$$= 0.38\ \text{m}$$

$$h_{5h} = \sqrt{0.38\ (2\ (2.26)\ -\ 0.38)}$$

$$\beta_5 = \tan^{-1}\left[\frac{(1.25)\ 05}{0.36\ +\ 4.5\ (0.38)}\right]$$

$$= 1.25\ \text{m}$$

$$= 16.8°$$

$$h_{6h} = 0$$

Slide	β	c_m (MPa)	ϕ (degrees)	V_i (MN)
1	75.8°	0.04	71.8	0.004
2	65.5°	0.04	71.8	0.007
3	54.3°	0.04	71.8	0.010
4	41.0°	0.04	71.8	0.017
5	16.8°	0.04	71.8	0.050
Σ				0.088

$$W_T = A_T \gamma_r$$

$$A_T = \frac{(45 + \phi)\pi r^2}{360} - \frac{h_{1h} N}{2}$$

$$= 3.2 \text{ m}^2$$

$$W_T = 3.2 \ x \ 1 \text{ m} \ x \ 0.028 \text{ MN/m}^3$$

$$= 0.0897 \text{ MN}$$

$$F_s = \frac{0.088}{0.0897} = 0.98$$

Continuation up-dip

$\sigma_t \approx 0$ MPa

$\Sigma T_i \approx$ MPa

$\psi = 65°$, footwall surface $\phi = 16°$

Since $\psi > \phi$, failure will continue up-dip

APPENDIX 4

Calculation of Arching Stability in Caving Hangingwall Altered Granodiorite, Belmoral Mine

$\gamma_r = 0.0274 \text{ MN/m}^3$

$\phi = 16°$

$c = 0 \text{ MPa}$

$Z = 40 \text{ m}$

$\theta = 45° + \phi/2 = 53°$

Against intact block compression failure:

$$\sigma_h = \sigma_1\cos^2\theta + \sigma_3\sin^2\theta$$

$$\sigma_1 = \gamma_r Z$$

$$\sigma_3 = \gamma_r Z\left(\frac{1-\sin\phi}{1+\sin\phi}\right)$$

$$\sigma_1 = 40 \text{ m} \times 0.0274 \text{ MN/m}^3 = 1.1 \text{ MPa}$$

$$\sigma_3 = 1.1 \text{ MPa}\left(\frac{0.72}{1.28}\right) = 0.62 \text{ MPa}$$

$$F_s = \frac{\sigma_c}{\sigma_1}$$

$$= \frac{60.4}{1.1}$$

$$= 54.9$$

Against bulk material failure:

$$F_s = \frac{\text{strength available}}{\text{imposed stress}}$$

· Stress

σ_1 = 1.1 MPa

σ_3 = 0.62 MPa

· Strength

From Table 3.5, using lithified rock values to represent the schistocity,

$m_{field} = 0.01 \; s_{field} = 1 \; x \; 10^{-7}$

$$\sigma_1 = \sigma_3 + \sqrt{m\sigma_3 \; \sigma_c + s\sigma_c^2}$$

$$= 0.62 + \sqrt{0.01 \; (0.62) \; (10) + 1 \; x \; 10^{-7} \; (10)^2}$$

$$= 0.87$$

$$F_s = \frac{0.87}{1.1} = 0.79$$

APPENDIX 4

Calculation of NGI Rock Mass Quality Q. Belmoral Mine

Surface Crown Pillar

· Material: schist

RQD = 10 (nominal value of 10 is used if RQD < 10 [10])

J_n = 6 (schistosity, sub horizontal, random)

J_r = 0.5 (schistosity)

J_a = 8.0 (gouge, < 5 mm)

J_w = 1.0 (dry)

SRF = 10 (multiple weakness zones)

$$Q = \frac{10}{6} x \frac{0.5}{8.0} x \frac{1.0}{10} = 0.01$$

Hangingwall

· Material: schistose granodiorite (in contact with schist)

RQD = 60

J_n = 12 (heavily jointed - blocky)

J_r = 3 (rough, irregular)

J_a = 4 (softening mineral)

J_w = 1.0 (dry)

SRF = 1.5 (stress versus strength is low, but opening near surface)

$$Q = \frac{60}{12} x \frac{3}{4} x \frac{1}{1.5} = 2.5$$

APPENDIX 4

Calculation of Scaled Crown Span, Surface Crown Pillar Empirical Method, Belmoral Mine

$Q = 0.01$

$\gamma_r = 2.8\ T/m^3$

$\psi = 65°$

$L = 3.8\ m$

$S = 60\ m$

$C_s = 0.45$

$$C_s = L\left[\frac{\gamma_r}{t\,(1 + L/S)\,(1 - 0.4\cos\psi)}\right]^{0.5}$$

$t = 226\ m$

APPENDIX 5

ANALYTICAL AND EMPIRICAL STABILITY CALCULATIONS

BRIER HILL MINE

APPENDIX 5

Table 1. Calculation of Rock Mass Mohr Envelope for Brier Hill Geological Materials, Based on the Hoek and Brown Failure Criterion

Hangingwall Slate					
σ (MPa)	h	θ (degrees)	ϕ (degrees)	τ (MPa)	c_m (MPa)
0	1.004	57.9	69.9	0.14	0.14
5	1.500	41.0	32.7	4.8	1.59
10	1.992	36.9	26.3	7.6	2.66
15	2.481	34.9	22.8	9.8	3.53
20	2.975	33.7	20.4	11.8	4.38
25	3.469	33.0	18.7	13.5	5.04

$$\sigma_t = \frac{s\sigma_c}{m} = 0.04 \text{ MPa}$$

σ_c = 60 MPa

m = 0.9

s = 0.0006

Table 1 (continued)

Footwall Slate					
σ (MPa)	h	θ (degrees)	ϕ (degrees)	τ (MPa)	c_m (MPa)
0	1.003	58.2	71.3	0.23	0.23
5	1.260	45.0	39.0	6.0	1.9
10	1.516	40.8	32.4	9.5	3.2
15	1.773	38.4	28.6	12.4	4.3
20	2.029	36.7	26.0	15.0	5.2
25	2.285	35.6	24.0	17.3	6.2

$$\sigma_\tau = \frac{s\sigma_c}{m} = 0.06 \text{ MPa}$$

$$\sigma_c = 80 \text{ MPa}$$

$$m = 1.3$$

$$s = 0.001$$

Table 1 (continued)

Jasper					
σ (MPa)	h	θ (degrees)	ϕ (degrees)	τ (MPa)	c_m (MPa)
0	1.014	56.2	63.1	2.4	2.4
5	1.090	50.5	48.8	9.5	3.8
10	1.166	47.5	43.3	14.6	5.2
15	1.242	45.1	39.7	19.1	7.6
20	1.316	43.8	36.6	25.5	8.2
25	1.395	42.5	35.0	26.6	9.1

$$\sigma_t = \frac{s\sigma_c}{m} = 0.89 \text{ MPa}$$

σ_c = 125 MPa

m = 2.8

s = 0.02

Table 1 (continued)

Banded Iron Ore					
σ (MPa)	h	θ (degrees)	ϕ (degrees)	τ (MPa)	c_m (MPa)
0	1.005	57.7	68.8	0.7	0.7
5	1.127	48.9	45.8	7.6	2.4
10	1.242	45.4	39.7	12.0	3.7
15	1.364	43.0	35.8	15.8	5.0
20	1.485	41.2	33.0	19.8	6.8
25	1.606	39.8	30.9	22.4	7.4

$$\sigma_t = \frac{s\sigma_c}{m} = 0.22 \text{ MPa}$$

σ_c = 110 MPa

m = 2.0 MPa

s = 0.004

Calculation Against Slate Chimneying Disintegration Failure, Brier Hill Mine

$$\phi_{mass} = 69.9°$$

$$c_{mass} = 0.14 \text{ MPa}$$

$$s = 0.85 \text{ m}$$

$$L = 8.5 \text{ m}$$

$$n = 5$$

$$r = \frac{0.5\ (8.5)}{\left[1 - \cos\left(45 + \frac{69.9}{2}\right)\right]}$$

$$= 5.14$$

$$N = 5.14 - (0.5)\ (8.5)$$

$$= 0.90$$

$$l_1 = 0.5 \text{ L}$$

$$= 4.25 \text{ m}$$

$$h_{1h} = \sqrt{4.25\ (2\ (5.14) - 4.25)}$$

$$= 5.06$$

$$\beta_1 = \tan^{-1}\left[\frac{(5.06 + 4.83)\ 0.5}{0.9 + 0.5\ (0.85)}\right]$$

$$= 75.0°$$

$$l_2 = 0.5\ (8.5) - (2-1)\ 0.85$$

$$= 3.4 \text{ m}$$

$$h_{2h} = \sqrt{3.4\ (2\ (5.14) - 3.4)} \qquad \beta_2 = \tan^{-1}\left[\frac{(4.83 + 4.44)\ 0.5}{0.9 + 1.5\ (0.85)}\right]$$

$$= 4.83 \text{ m} \qquad = 64.9°$$

$$l_3 = 0.5\ (8.5) - (3-1)\ 8.5$$

$$= 2.55 \text{ m}$$

$$h_{3h} = \sqrt{2.55\ (2\ (5.14) - 2.55)} \qquad \beta_3 = \tan^{-1}\left[\frac{(4.44 + 3.8)\ 0.5}{0.9 + 2.5\ (0.85)}\right]$$

$$= 4.44 \text{ m} \qquad = 53.7°$$

$$l_4 = 0.5\ (8.5) - (4-1)\ 0.85$$

$$= 1.7 \text{ m}$$

$$h_{4h} = \sqrt{1.7\ (2\ (5.14) - 1.7)} \qquad \beta_4 = \tan^{-1}\left[\frac{(3.8 + 2.83)\ ).5)}{0.9 + 3.5\ (0.85)}\right]$$

$$= 3.8 \text{ m} \qquad = 40.5°$$

$$l_5 = 0.5\ (8.5) - (5-1)\ 0.85$$

$$= 0.85 \text{ m}$$

$$h_{5h} = \sqrt{0.85\ (2\ (5.14) - 0.85)} \qquad \beta_5 = \tan^{-1}\left[\frac{(2.83)\ 0.5}{0.9 + 4.5\ (0.85)}\right]$$

$$= 2.83 \text{ m} \qquad = 16.7°$$

$$h_{6h} = 0$$

Slice	β	c_m (MPa)	ϕ (degrees)	V_i (MN)
1	75.0°	0.14	69.9	0.03
2	64.9°	0.14	69.9	0.06
3	53.7°	0.14	69.9	0.09
4	40.5°	0.14	69.9	0.14
5	16.7°	0.14	69.9	0.41
Σ				0.73

$$W_T = A_T \gamma_r$$

$$A_T = \frac{(45° + \phi/2)\ \pi r^2}{360} - \frac{h_{1h}\ \mathrm{N}}{2}$$

$$= 16.16 \text{ m}^2$$

$$W_T = 16.16 \times 1 \text{ m} \times 0.028 \text{ MN/m}^3$$

$$= 0.45 \text{ MN}$$

$$F_s = \frac{0.73}{0.45}$$

$$= 1.6$$

APPENDIX 5

Calculation of Arching Stability in Caving Slate, Brier Hill Mine

$\gamma_r = 0.028 \text{ MN/m}^3$

$\phi = 16°$

$c = 0 \text{ MPa}$

$Z = 275 \text{ m}$

$\theta = (45° + \phi/2) = 53°$

Against intact block compression failure:

$$\sigma_h = \sigma_1 \cos^2\theta + \sigma_3 \sin^2\theta$$

$$\sigma_1 = \gamma_r\, z$$

$$\sigma_3 = \gamma_r\, z \left(\frac{1-\sin\phi}{1+\sin\phi}\right)$$

$$\sigma_1 = 0.028 \text{ MN/m}^3 \; x \; 275 \text{ m} = 7.7 \text{ MPa}$$

$$\sigma_3 = 7.7 \left(\frac{0.724}{1.276}\right) = 4.4 \text{ MPa}$$

$$F_s = \frac{\sigma_c}{\sigma_1}$$

$$= \frac{60}{7.7}$$

$$= 7.8$$

<u>Against bulk material failure</u>

$$F_s = \frac{\text{strength available}}{\text{imposed stress}}$$

<u>· Stress</u>

$\sigma_1 = 7.7$ MPa

$\sigma_3 = 4.4$ MPa

<u>· Strength</u>

From Table 2.1, using lithified rock values,

$m_{field} = 0.01$, $s_{field} = 1 \ x \ 10^{-7}$

$$\sigma_1 = \sigma_3 + \sqrt{m \ \sigma_3 \ \sigma_c + s \ \sigma_c^2}$$

$$\sigma_1 = 4.4 + \sqrt{0.01 \ (4.4) \ (60) + 1 \ x \ 10^{-7} \ (60)^2}$$

$$= 6.0 \text{ MPa}$$

$$F_s = \frac{6.0}{7.7}$$

$$= 0.78$$

APPENDIX 5

Calculation of NGI Rock Mass Quality Q, Brier Hill Mine +

Hangingwall Slate

RQD = 35 (weak slate, graphitic near stope)

J_n = 9 (three joint sets: slaty cleavage, foliation commonly occurring in slates [117] and a third perpendicular to these to allow free caving)

J_r = 1.0 (smooth planar - slaty cleavage)

J_a = 4.0 (graphitic coating)

J_w = 0.66 (some water inflow, as quoted by Rice [6])

SRF = 2.0 (medium ground stress, based on depth vs strength)

$$Q = \frac{35}{9} \; x \; \frac{1}{4.0} \; x \; \frac{0.66}{2.0} = 0.32$$

Jasper Crown

E_m = 16 GPa

$$E_m = 10^{\left(\frac{RMR - 10}{40}\right)}$$

RMR = 58

RMR = 9 lnQ + 44

Q = 4.7

+ approximated from site description, due to lack of geomechanical data

APPENDIX 5

Calculation of Scaled Crown Span, Surface Crown Pillar Empirical Method, Brier Hill Mine

Hangingwall Slate

$Q = 0.32$

$L = 4.3$ m

$\gamma_r = 2.9$ T/m^3

$\psi = 60°$

$S = 8.5$ m

$C_s = 2$ m

$$C_s = L\left[\frac{\gamma_r}{t\ (1+L/S)\ (1-0.4\ \cos\psi)}\right]^{0.5}$$

$$t = \frac{4.3^2\ (2.9)}{(2)^2\ (1\ +\ 4.3/8.5)\ (1-0.4\ (0.5))}$$

$t = 13.05$ m

Jasper Crown

$Q = 4.7$

$\gamma_r = 2.69$ T/m^3

$\psi = 60°$

$L = 8\ m$

$S = 200\ m$

$C_s = 5.5\ m$

$$t = \frac{8.3\ (2.69)}{5.5^2\ (1 + 4.3/8.5\ m)\ (1 - 0.4\ (0.5))}$$

$$= 1.36\ m$$

APPENDIX 6

ANALYTICAL AND EMPIRICAL STABILITY CALCULATIONS

ATHENS MINE

APPENDIX 6

Table 1. Calculation of Rock Mass Mohr Envelope for Brier Hill Geological Materials, Based on the Hoek and Brown Failure Criterion

Far-Field Jasper					
σ (MPa)	h	θ (degrees)	ϕ (degrees)	τ (MPa)	c_m (MPa)
0	1.014	56.2	63.1	2.88	2.88
5	1.077	51.2	50.2	10.1	4.1
10	1.141	48.4	44.9	15.6	5.6
15	1.204	46.4	41.4	20.3	7.0
20	1.268	44.8	38.8	24.5	8.4
25	1.331	43.5	36.7	28.3	9.7

$$\sigma_t = \frac{s\sigma_c}{m} = 1.1 \text{ MPa}$$

$\sigma_c = 150$ MPa

$m = 2.8$

$s = 0.02$

APPENDIX 6

Table 1 (continued)

Crown Jasper					
σ (MPa)	h	θ (degrees)	ϕ (degrees)	τ (MPa)	c_m (MPa)
0	1.005	57.6	68.6	0.8	0.8
5	1.116	49.3	46.6	7.8	2.5
10	1.228	45.8	40.3	12.5	4.0
15	1.339	43.4	36.5	16.4	5.3
20	1.450	41.6	33.8	20.0	6.6
25	1.561	40.3	31.6	23.1	7.7

$$\sigma_t = \frac{s\sigma_c}{m} = 0.24 \text{ MPa}$$

$\sigma_c = 120$

$m = 2.0$

$s = 0.04$

Table 1. (continued)

Diorite Dykes					
σ (MPa)	h	θ (degrees)	ϕ (degrees)	τ (MPa)	c_m (MPa)
0	1.001	59.0	75.7	0.3	0.34
5	1.077	51.2	50.2	8.5	2.5
10	1.153	47.9	44.0	13.8	4.1
15	1.229	45.7	40.2	18.3	5.6
20	1.305	44.0	37.5	22.3	7.0
25	1.381	42.7	35.4	26.0	8.2

$$\sigma_t = \frac{s\sigma_c}{m} = 0.06 \text{ MPa}$$

σ_c = 140 MPa

m = 2.5

s = 0.01

APPENDIX 6

Calculation of Plug Failure Factor of Safety, Athens Mine

The plug failure is analysed based on a block defined as per Allen [5]: 80 m between the dyke boundaries, a 70 m span longitudinally in the crown and the height from the mining block to the surface of 660 m.

West Face						East Face					
Element	σ_a (MPa)	A (m_2)	Element	σ_a (MPa)	A (m^2)	Element	σ_a (MPa)	A (m^2)	Element	σ_a (MPa)	A (m^2)
208	3.6	750	4366	27.4	75	362	3.6	750	4520	27.1	75
209	3.6	2250	4367	26.8	225	363	3.6	2250	2521	27.6	225
210	3.6	3000	4368	26.8	300	364	3.6	3000	4522	24.9	300
211	3.6	3000	4369	27.4	300	365	3.6	3000	4523	27.4	300
212	3.6	2250	4370	27.9	225	366	3.6	2250	4524	29.5	225
213	3.6	750	4371	28.4	75	367	3.6	750	2525	30.3	75
802	10.7	750	4960	28.0	50	956	10.7	750	5114	24.1	50
803	10.7	2250	4961	26.7	150	957	10.7	2250	5115	18.9	150
804	10.7	3000	4962	27.0	200	958	10.7	3000	5116	18.9	200
805	10.7	3000	4963	28.0	200	959	10.7	3000	5117	18.3	200
806	10.7	2250	4964	28.7	150	960	10.7	2250	5118	29.3	150
807	10.7	750	4965	29.2	50	961	10.7	750	5119	31.9	50
1396	16.6	500	5554	28.6	25	1550	16.6	500	5708	19.3	25
1397	16.6	1500	5555	27.5	75	1551	16.6	1500	5709	10.4	75
1398	16.6	2000	5556	27.5	100	1552	16.6	2000	5710	10.4	100
1399	16.6	2000	5557	28.6	100	1553	16.6	2000	5711	19.4	100
1400	16.6	1500	5558	29.5	75	1554	16.6	1500	5712	27.7	75
1401	16.6	500	5559	29.9	25	1555	16.6	500	5713	32.9	25
1990	21.2	500	6148	29.3	25	2144	21.4	500	6302	13.2	25
1991	21.2	1500	6149	28.1	75	2145	21.4	1500	6303	3.6	75
1992	21.2	2000	6150	28.1	100	2146	21.4	2000	6304	3.6	100
1993	21.2	2000	6151	29.4	100	2147	21.4	2000	6304	13.2	100
1994	21.2	1500	6152	30.3	75	2148	21.3	1500	6306	29.7	75
1995	21.2	500	6153	30.7	25	2149	21.3	500	6307	34.7	25
2584	24.7	300	6742	30.9	25	2738	24.9	300			
2585	24.7	900	6743	29.6	75	2739	24.8	900			
2586	24.6	1200	6744	29.6	100	2740	24.8	1200			
2587	24.6	1200	6745	31.0	100	2741	24.9	1200			
2588	24.7	900	6746	31.9	75	2742	24.9	900			
2589	24.8	300	6747	31.9	25	2743	25.0	300			
3178	26.3	150	7336	33.1	25	3332	26.3	150			
3179	26.1	450	7337	32.1	75	3333	25.9	450			
3180	26.1	600	7338	32.1	100	3334	25.9	600			
3181	26.2	600	7339	33.2	100	3335	26.3	600			
3182	26.4	450	7340	34.0	75	3336	26.7	450			
3183	26.6	150	7341	34.1	25	3337	27.0	150			
3772	27.0	100	7930	51.3	25	3926	26.9	100			
3773	26.6	300	7931	54.3	75	3927	26.0	300			
3774	26.6	400	7932	54.3	100	3928	26.0	400			
3775	26.9	400	7933	51.5	100	3929	27.0	400			
3776	27.2	300	7934	49.6	75	3930	27.7	300			
3777	27.6	100	7935	39.5	25	3931	28.2	100			
$\Sigma\sigma_a A$ = 822,212 MN						$\Sigma\sigma_a A$ = 763,375 MN					

North Face						South Face					
Element	σ_n (MPa)	A (m^2)	Element	σ_n (MPa)	A (m^2)	Element	σ_n (MPa)	A (m^2)	Element	σ_n (MPa)	A (m^2)
235	2.5	750	4393	20.5	75	228	2.5	750	4386	20.6	75
257	2.5	1500	4415	20.4	150	250	2.5	1500	4408	20.6	150
279	2.5	3000	4437	20.2	300	272	2.5	3000	4430	20.3	300
381	2.5	3000	4459	20.0	300	294	2.5	1500	4452	20.1	300
323	2.5	1500	4481	19.8	150	316	2.5	1500	4474	19.9	150
345	2.5	750	4503	19.8	75	338	2.5	750	4496	20.0	75
809	7.3	750	4987	20.9	50	822	7.3	750	4980	21.0	50
851	7.3	1500	5009	20.7	100	844	7.3	1500	5002	20.8	100
873	7.3	3000	5031	20.4	200	866	7.3	3000	5024	20.5	200
895	7.3	3000	5053	20.3	200	888	7.3	3000	5046	20.4	200
917	7.3	1500	5075	20.3	100	910	7.3	1500	5068	20.3	100
939	7.3	750	5097	20.1	50	932	7.3	750	5090	20.3	50
1423	11.4	500	5581	21.3	25	1416	11.4	500	5574	21.4	25
1445	11.4	1000	5603	21.0	50	1438	11.4	1000	5596	21.1	50
1467	11.4	2000	5625	20.5	100	1460	11.4	2000	5618	20.6	100
1489	11.4	2000	5647	20.9	100	1482	11.4	2000	5640	21.0	100
1511	11.4	1000	5669	22.1	50	1504	11.4	1000	5662	22.2	50
1533	11.4	500	5691	22.0	25	1526	11.4	500	5684	22.2	25
2017	14.7	500	6175	21.7	25	2010	14.7	500	6168	21.8	25
2039	14.7	1000	6197	21.4	50	2032	14.7	1000	6190	21.6	50
2061	14.7	2000	6219	20.5	100	2054	14.7	2000	6212	20.7	100
2083	14.7	2000	6241	21.9	100	2076	14.7	2000	6234	22.1	100
2105	14.7	1000	6263	25.9	50	2098	14.7	1000	6256	26.0	50
2127	14.7	500	6285	26.4	25	2120	14.7	500	6278	26.3	25
2611	17.5	300	6769	22.3	25	2604	17.5	300	6762	22.4	25
2633	17.5	600	6791	22.0	50	2626	17.5	600	6784	22.1	50
2655	17.5	1200	6813	20.9	100	2648	17.5	1200	6806	21.0	100
2677	17.5	1200	6835	22.6	100	2670	17.5	1200	6828	22.8	100
2699	17.5	600				2692	17.5	600			
2721	17.5	300				2714	17.5	300			
3205	19.1	150	7363	24.4	25	3198	19.1	150	7356	24.4	25
3227	19.1	300	7385	24.2	50	3220	19.1	300	7678	24.3	50
3249	19.1	600	7407	23.4	100	3242	19.1	600	7400	23.4	100
3271	19.1	600	7429	27.9	100	3264	19.1	600	7422	25.2	100
3293	19.0	300				3286	19.0	300			
3315	19.0	150				3308	19.0	150			
3799	19.9	100	7957	25.6	25	3792	19.9	100	7950	25.6	25
3821	19.9	200	7979	26.5	50	3814	19.9	300	7972	26.3	50
3843	19.8	400	8001	26.8	100	3836	19.8	400	7994	26.7	100
3865	19.7	400	8023	28.2	100	3858	19.8	400	8016	27.8	100
3887	19.6	200				3880	19.7	200			
3909	19.6	100				3902	19.6	100			
$\Sigma\sigma_n A$ = 498,071 MN						$\Sigma\sigma_n A$ = 498,050 MN					

The analytical equation to calculate the plug stability is equation 2.14

$$F_s = \frac{\sum_{i=1}^{n}\left(c_i\,A_i+\left(\left(\sum_{j=1}^{m}\sigma_{nj}\,A_j\right)-\frac{\gamma_w\,(H_i-d)^2 b_i}{3}\right)\tan\phi_{ri}\right)\sin\psi_i}{V\rho g+\left(\sum_{i=1}^{m}\left(\sum_{j=1}^{m}\sigma_{nj}\,A_j\right)-\frac{\gamma_w\,(H_i-d)^2\,b_i}{3}\right)\cos\psi_i}$$

The numerical modelling assumed the dykes to be vertically dipping, rather than the 85° - 80° of the plug-dyke contact sides, the plug will be analysed with vertical walls. Water was still reported to originate from the plug boundaries.

$b_{i\ north}$ = $b_{i\ south}$ = 70 m

$b_{i\ west}$ = $b_{i\ east}$ = 80 m

H_i = 660 m (water table at bottom of overburden)

d = 0

ϕ_{north} = ϕ_{south} = 4° (Table 1.5; Allen details the contact as weak "soap rock", and Crane [126] mentions intrusive dykes are often weak and disintegrated at contacts from emplacements; this addresses both the low friction mineral coating and "no rock contact when sheared"

ϕ_{west} = ϕ_{east} = 16° (unaltered joint in jasper crown, smooth, planar)

c_{north} = c_{south} = c_{west} = c_{east} = 0

γ_r = 0.027 MN/m³

γ_w = 0.01 MN/M³

V = 660 m x 80 m x 70 m - 15 m x 15 m x 80 m

= 3,678,000 m³

$$F_s = \frac{55{,}440 + 389{,}540}{99{,}306}$$

$$= 4.5$$

APPENDIX 6

Calculation Against Hangingwall Jasper Chimneying Disintegration Failure, Athens Mine

γ_r = 0.027

c_{mass} = 0.8

ϕ_{mass} = 68.6

$\alpha/2$ = 45° + $\phi/2$ = 79.3°

n = 5

s = 8 m

L = 80 m

Calculation of the first rupture line

$$r = \frac{0.5\ (80)}{[1 - \cos\ (79.3°)]}$$

$$= 49.1$$

N = 49.1 - 40 = 9.1

$$l_1 = 0.5\ (80) = 40$$

$$h_{1h} = \sqrt{40\ (2\ (49.1) - 40)}$$

$$= 48.2 \text{ m}$$

$$\beta_1 = \tan^{-1}\left[\frac{(48.2 + 46.0)\ 0.5}{10.3 + 0.5\ (8)}\right]$$

$$= 73.1°$$

$l_2 = 0.5\ (80)\ -\ (2-1)\ 8\ =\ 32\ \text{m}$

$h_2 = \sqrt{32\ (2\ (49.1)\ -\ 32)}$ $\beta_2 = \tan^{-1}\left[\dfrac{(46.0\ +\ 42.2)\ 0.5}{10.3\ +\ 1.5\ (8)}\right]$

$= 46.0\ \text{m}$ $= 63.2°$

$l_3 = 0.5\ (80)\ -\ (3-1)\ 8\ =\ 24\ \text{m}$

$h_3 = \sqrt{24\ (2\ (49.1)\ -\ 24)}$ $\beta_3 = \tan^{-1}\left[\dfrac{(42.2\ +\ 36.3)\ 0.5}{10.3\ +\ 2.5\ (8)}\right]$

$= 42.2\ \text{m}$ $= 52.3°$

$l_4 = 0.5\ (80)\ -\ (41-1)\ 8\ =\ 16\ \text{m}$

$h_4 = \sqrt{16\ (2\ (49.1)\ -16)}$ $\beta_4 = \tan^{-1}\left[\dfrac{(36.3\ +\ 26.9)\ 0.5}{10.3\ +\ 3.5\ (9)}\right]$

$= 36.3\ \text{m}$ $= 37.1°$

$l_5 = 0.5\ (80)\ -\ (5-1)\ 8\ =\ 9\ \text{m}$

$$h_5 = \sqrt{8\ (2\ (49-1)\ -\ 8)} \qquad \beta_5 = \tan^{-1}\left[\frac{(26.9)\ 0.5}{10.3\ +\ 4.5\ (8)}\right]$$

$$= 26.9 \text{ m} \qquad = 16.2°$$

$h_6 = 0$

Slice	β (degrees)	c_m (MPa)	ϕ (degrees)	V_i (MN)
1	73.1	0.8	68.6	1.90
2	63.2	0.8	68.6	3.23
3	52.3	0.8	68.6	4.95
4	37.1	0.8	68.6	8.46
5	16.2	0.8	68.8	22.03
Σ				40.6

$W = A_T\ \gamma_r$

$$W = 0.027\left[\frac{(45\ +\ 68.6/2)\ \pi\ 49.1^2}{360} - \frac{48.2\ (9.1)}{2}\right]$$

$= 39$ MN

$$F_s = \frac{40.6}{30}$$

$= 1.04$

APPENDIX 6

Calculation of Arching Stability in Caving Jasper Crown, Athens Mine

$\gamma_r = 0.027$ MN/M^3

$\phi = 16°$

c = 0 MPa

z = 660 m

$\theta = (45° + \phi/2) = 53°$

Against intact block compression failure

$$\sigma_h = \sigma_1 \cos^2 \theta + \sigma_3 \sin^2 \theta$$

$$\sigma_1 = \gamma_r Z$$

$$\sigma_3 = \gamma_r Z \left[\frac{1 - \sin \phi}{1 + \sin \phi}\right]$$

$$\sigma_1 = 0.027 \text{ MN/m}^3 \ x \ 660 \text{ m} = 17.8 \text{ Mpa}$$

$$\sigma_3 = 17.8 \left[\frac{0.724}{1.276}\right] = 10.2 \text{ MPa}$$

$$F_s = \frac{\sigma_c}{\sigma_1}$$

$$= \frac{120}{17.8}$$

$$= 6.75$$

Against bulk material failure with jasper boundaries

Z = 20 m (based on modelling failure contour)

Stress

σ_1 = $\gamma_r Z = 0.41$ MPa

σ_3 = 0.23 MPa

Strength

From Table 2.1 using lithified rock values

m_{field} = 0.01, $s_{field} = 1 \times 10^{-7}$

$$\sigma_1 = \sigma_3 + \sqrt{m\sigma_3\ \sigma_c + s\sigma_c^2}$$

$$\sigma_1 = 0.41 + \sqrt{0.01(0.23)(120) + 1x10^{-7}(120)^2}$$

$$= 0.94 \text{ MPa}$$

$$F_s = \frac{0.94}{0.41}$$

$$= 2.3$$

Z = ?, for $F_s = 1$

$$1 = \frac{0.027(Z)(0.57) + \sqrt{0.01(0.027)Z(0.57)\ 120 + 1x10^{-7}(120)^2}}{0.027(Z)}$$

Z = 130 m

APPENDIX 6

Calculation of NGI Rock Mass Quality Q, Athens Mine +

Jasper Crown

E_m = 10 GPa

$$E_m = 10^{\frac{(RMR - 10)}{40}}$$

RMR = 50

RMR = 9 lnQ + 44

Q = 2

This compares with Q = 1 to 10 for the m and s values selected from Table 2.1.

Because the vertical geological contacts can act as weak joints Q should be reduced. It is assumed that, as per the jasper of Michigan iron mines [126], three families of joints exist, with irregular planar surfaces. The addition of a fourth (contact) family with a zone of soft minerals reduces J_n from 9 to 12 and J_r 1.5 to 1, and therefore, Q to 1.1 (equation 1.47).

+ Approximated from site description, due to lack of geomechanical data

APPENDIX 6

Calculation of Critical Crown Pillar Span, Athens Mine

Q = 1.1

From Figure 1.115, the value for F_s = 1 is C_s = 5

$$C_s = L \left[\frac{\gamma_r}{t\ (1 + L/S)\ (1 - 0.4 \cos \phi)} \right]^{0.5}$$

L = 80 m

γ = 2.7 T/m^3

ψ = 90°

S = 350 m

$$5 = 80 \left[\frac{2.7}{t\ (1 + 80/350)\ (1 - 0.46)} \right]$$

t = 563 m